QUASI-ANALYTICAL MODELLING AND OPTIMISATION TECHNIQUES FOR TRANSPORT AIRCRAFT DESIGN

by

Askin T. Isikveren

Doctoral Thesis
Report 2002-13

intentionally blank

Preface

This document constitutes a dissertation of research work for eligibility of a PhD Degree from the Department of Aeronautics (Flygteknik), Royal Institute of Technology (KTH), Stockholm, Sweden.

This accomplishment is not only a product of one's ability to conceive and investigate topics under the guidance of the pedagogical process, but such a formulation of ideas or even the notion of approaching the conceptual aircraft design problem from an alternate perspective simply would not have be possible without accumulating a wide-ranging skill set in industry. In conjunction with a welcome professional association with Williams International, it is with great fortune I have had the opportunity to be employed by such companies as Hawker de Havilland Ltd, Saab Aircraft AB, American Airlines and Bombardier Aerospace.

Expressions of gratitude are forwarded to my supervisor Professor Arthur Rizzi for his invaluable advice and insight during the course of this degree. As a student, I affiliate myself with the Royal Institute of Technology with honour. The institution's progressive attitude towards selection of research topics and innovative approach to contemporary tertiary education will serve to perpetuate its unqualified prestige.

A final word of profound thanks goes to my family, my wife Carina and daughter Emma, for the untold amount of patience, understanding and support exhibited by them during the protracted period of accomplishing this milestone on a part-time basis.

Montreal, Quebec, Canada
May 2002

Askin T. Isikveren

Nota bene: The reader is advised that the data of known aircraft used in this document have intentionally not been labelled in the multitude of charts and plots presented herein. This act is to ensure the security of sometimes highly confidential information, and ensures the author does not violate any current non-disclosure agreements.

intentionally blank

Abstract

The research work presented here focuses on the subject of transport aircraft design at the pre-design or conceptual level. The primary topics addressed are: (1) generation of a vast array of new quasi-analytical expressions to permit a conceptual treatment of commercial and business transport aircraft with adequate sensitivity for more advanced trade studies; (2) review and adoption of a method to predict stability and control characteristics (using the Mitchell method); (3) a study of the relative merits between various methods in facilitating an expedient and robust constrained multi-objective optimisation result within the context of traditional conceptual design problems (Genetic Algorithms and Nelder-Mead Simplex search); (4) creation of a software package as a new and unique conceptual tool that permits the generation of design proposals in an accurate yet expeditious manner; and, (5) practical demonstration of the new conceptual design software package by undertaking some actual aircraft design proposals.

The design problem is addressed using mostly closed form solutions but transcendental expressions with much simplified numerical scheme algorithms have also been adopted for sake of accuracy. Various new models have been proposed for atmospheric properties, geometry, gas-turbine engine performance, low-speed and high-speed aerodynamic characteristics, minimum control speed limited balanced field estimation, asymmetric flight, and, en route performance characteristics including definition of operationally permissible speed schedules and flight techniques for payload-range/fixed sector profiles optimised in terms of maximum specific air range, minimum fuel, minimum time, minimum direct operating cost and maximum profit/return on investment. The work was extended further to include issues relating to the impact of vehicular attributes to pricing the market is willing to absorb. Useful information regarding how these individual computational elements of the methodology may be integrated for the purpose of constructing coherent modular sub-spaces and formulation of a basic inter-disciplinary coupling is also presented. The mathematical foundations derived in this work have lead to an array of tangible conclusions that aid the conceptual designer via implicit guidelines to achieve truly balanced design concepts.

In an explicit demonstration of methodology effectiveness and relative simplicity, a software package called QCARD or Quick Conceptual Aircraft Research and Development was created in the MATLAB environment. The new software system was developed to assist the designer in predicting, visualising and optimising conceptual aircraft designs in a much more interactive and far-reaching manner than what is afforded with contemporary applications whilst emphasising speed and economy of effort.

The methodology and software was employed for a 19 passenger turbofan commuter transport design using the cost effective Williams International FJ44-2 engines. To complement this, a fuselage stretch version of the baseline vehicle designed to accommodate 31-34 passengers was also undertaken utilising a growth version of the original FJ44 power plant. The minimum goal for both of these concepts was to afford unparalleled comfort through speed and spaciousness with a competitive edge against turboprops in terms of economics and field performance. The final design effort involved proposal of a Trans-Atlantic high-performance executive transport employing an unconventional Twin Oblique Lifting Surfaces, or, TOLS configuration. The intent here was to produce a new super-large business jet able to operate up to low supersonic speeds with field performance, en route fuel burn efficiency and cost comparable to that of contemporary business aircraft for this market segment.

intentionally blank

Quasi-analytical modelling and Optimisation Techniques for Transport Aircraft Design

intentionally blank

Dissertation

The thesis embodies a synopsis of research work undertaken for this degree and four related technical papers. A list of all the technical papers are itemised as thus,

Paper I
Methodology for Conceptual Design and Optimisation of Transport Aircraft
Askin T. Isikveren,
Paper 98-7.8.2. Presented at 21st ICAS Congress, Melbourne, Australia, September 1998.

Paper II
Design and Optimisation of a 19 Passenger Turbofan Regional Transport
Askin T. Isikveren,
Paper 1999-01-5579. Presented at 1999 World Aviation Congress and Exposition, San Francisco, USA, October 1999.

Paper III
High-Performance Executive Transport Design Employing Twin Oblique Lifting Surfaces
Askin T. Isikveren,
Paper 2001-01-3031. Presented at 2001 World Aviation Congress and Exposition, Seattle, USA, September 2001.

Paper IV
Identifying Economically Optimal Flight Techniques of Transport Aircraft
Askin T. Isikveren,
Paper C-9699. Submitted to AIAA Journal of Aircraft, status “accepted for publication”, issue pending in 2002.

intentionally blank

Table of Contents

1 Introduction 1

1.1 What is Conceptual Design 1

1.2 Basis and Protocol for Conceptual Aircraft Design Prediction 3
1.2.1 First Order Minimalism 4
1.2.2 Advanced Higher Order Iterative Algorithms 4
1.2.3 Quasi-analytical Algorithms – A Compromise Between Economy of Effort and Higher Order Accuracy 5

1.3 Operational Criteria Placed On Contemporary Transport Aircraft 6
1.3.1 Present-Day Air Traffic Control and Route Structure 6
1.3.2 Operationally Permissible Flight Control Techniques 7

1.4 Stability and Control 7

1.5 Multi-disciplinary Design Optimisation 8

1.6 Computer Aided Engineering in Conceptual Design 9

1.7 Decision Support Systems 11

1.8 Objectives, Scope and Thesis Structure 11

2 Formulation of a New Project Design Specifications 15

2.1 Establishing the Value of Performance and Amenities 15

2.2 Constructing the Airframer Paradigm 16

3 Mathematical Foundations: Concept of an Impulse Function 19

3.1 Mathematical Formulation and Governing Rules of Operation 19

3.2 Identification of Maxima and Minima Using the Impulse Function Approximation 20

3.3 Exponential Interpolation for Integrated Computations 20

4 The International Standard Atmosphere 23

4.1 Nomenclature Describing Atmospheric Properties 23

4.2 Modelling Temperature Variation 23

4.3 Density 24

4.4 Coefficient of Viscosity 24

5 Geometric Definitions 25

5.1 An Overview of Equivalent Reference Wing Conventions 25
5.1.1 Weighted Mean Aerodynamic Chord Method 25
5.1.2 ESDU Method 26
5.1.3 Simple Trapezoid or Net Method 27
5.1.4 Ancillary Wing Conventions 28
5.1.5 Fundamental Parametric Relationships for the Reference Wing 29

5.2 Quasi-analytical Methods for Fuselage Geometric Description 30
5.2.1 Fuselage Centre-Section: Cross Section Definition 31
5.2.2 Forward and Aft Fuselage Sections: Three-dimensional Definition 33

5.3 Analytical Method for Wing-to-Fuselage Fairing Geometric Description 36

5.4 Quasi-analytical Method for Turbofan Nacelle and Miscellaneous Power Plants Geometric Description 37
5.4.1 Nacelle Three-dimensional Definition 37
5.4.2 The Nacelle Geometric Design Variables 38

5.5 Estimating the Wetted Area of Primary Components 40
5.5.1 Centre Fuselage External Area 40
5.5.2 Forward and aft Fuselage External Area 40
5.5.3 Wing-Fuselage Fairing 42
5.5.4 Wing, Empennage and Other Streamlined Surfaces 42
5.5.5 Nacelle Surfaces 44
5.5.6 Sample Computations of Wetted Area Using Actual Aircraft Data 46

5.6 Estimating the Volume for Living Space and Fuel 47
5.6.1 Approximating the Cabin Volume 47
5.6.2 Estimating the Fuel Capacity of Integral Fuel Tanks in Wing 49
5.6.3 Estimating the Fuel Capacity of Centre Tanks 51
5.6.4 Estimating the Fuel Capacity of Forward and Aft Wing-Fuselage Fairing Conformal and Aft Auxiliary Tanks 52

6 Predicting the Weight of Major Constituents 55

6.1 Overview of Deriving Weight Estimating Relationships 55

6.2 The First Functional Weight Group 55
6.2.1 The Advanced Technology Multiplier 56
6.2.2 Wing Weight Estimating Relationship 56
6.2.3 Winglet Weight Estimating Relationship 58
6.2.4 Fuselage Weight Estimating Relationship 59
6.2.5 Undercarriage Weight Estimating Relationship 61
6.2.6 Horizontal Tail Weight Estimating Relationship 62
6.2.7 Vertical Tail Weight Estimating Relationship 62
6.2.8 Dorsal and Ventral Fin Weight Estimating Relationship 63

6.3 The Second Functional Weight Group 63
6.3.1 The Constant Weight Passenger Coefficient 63
6.3.2 Systems and Fixed Equipment Weight Estimating Relationship 65
6.3.3 Power Plant Installation Weight Estimating Relationship 65
6.3.4 Completion Allowance and Paint Weight Estimating Relationship 67
6.3.5 Crew Weight Estimation 68
6.3.6 Unusable Fuel Weight Estimating Relationship 68
6.3.7 Operating Items Weight Estimating Relationship 68

6.4 The Third Functional Weight Group 69
6.4.1 Estimation of Fuel Capacity 69
6.4.2 Maximum Payload-OWE Contingency Allowance 69

6.5 Defining the Complete Array of Design Weights 69
6.5.1 Green Manufacturer's Empty Weight 69
6.5.2 Basic Empty Weight or Delivered Manufacturer's Empty Weight 70
6.5.3 Basic Operating Weight or Operational Weight Empty 70
6.5.4 Maximum Payload Weight 70
6.5.5 Maximum Zero-Fuel Weight 71
6.5.6 Defining the Maximum Takeoff Weight – Utilising the Maximum Fuel Decrement Design Variable 71
6.5.7 Defining the Maximum Ramp Weight or Maximum Taxi Weight 72
6.5.8 Defining Maximum Landing Weight of a Vehicle 72

6.6 Sample Prediction of Weights against Actual Aircraft Data 73

7 Predicting Low-Speed and High-Speed Aerodynamic Attributes 75

7.1 Low-Speed Aerodynamics: Lift 75
7.1.1 Clean Wing Lift Attributes and Maximum Lift 75

7.1.2 Maximum lift Generated by Trailing and Leading Edge High-Lift Devices 77
7.1.3 Establishing the Accuracy of Clean Wing and High-Lift Prediction 79

7.2 Zero-Lift Drag Estimation – The Equivalent Length Method 80
7.2.1 Derivation of the Equivalent Characteristic Length Method 80
7.2.2 Gauging the Robustness of the Equivalent Characteristic Length Method 84

7.3 Vortex-Induced Drag at Subsonic Speeds 86

7.4 Three Dimensional Effects and Ancillary Drag Contributors 87

7.5 Total Incremental Drag due to One Engine Inoperative Condition 88
7.5.1 The General One Engine Inoperative Drag Constituent 89
7.5.2 Drag Generated by Windmilling Engines 91

7.6 Compressibility or Wave Drag 93
7.6.1 Derivation of the Incremental Drag due to Compressibility 94
7.6.2 Quantifying Wave Drag due to Volume and Lift 95

7.7 Quantifying the Aerodynamic Impact of Winglets 96
7.7.1 Quantifying the Drag Reduction of Winglet Devices 97
7.7.2 Proficiency of Drag Reduction due to Winglet Prediction 100

7.8 Validation of the Total Aerodynamic Drag Model 101

8 Modelling the Performance of Gas Turbine Engines 105

8.1 Performance Degradation for Non-Standard Ambient Conditions 105

8.2 De-rated Engine Performance and Other Variations in Rating 105

8.3 Thrust Reverse 106

8.4 Thrust Performance for Low to Intermediate Speeds 106

8.5 Thrust Performance for High Speed 106

8.6 Thrust Specific Fuel Consumption 107
8.6.1 The General Model and Baseline Calibration 107
8.6.2 Examining the Sensitivities of Thrust Specific Fuel Consumption with By-Pass Ratio 108

9 Formulation and Prediction of Optimal Field and En route Performance Control 109

9.1 Takeoff Performance 109
9.1.1 Balanced Field Length Prediction 110
9.1.2 Identification of Minimum Control Speed 112

9.2 Landing Field Performance 112

9.3 Comparison between Estimated and Actual Aircraft Data for Field Length Performance 114

9.4 All Engines and One Engine Operational Optimal Climb Control 115
9.4.1 Energy-Height Approximation for Accelerated Climbing Flight 115
9.4.2 Further Refinements for Optimal Climb Speed Formulation 120
9.4.3 Energy-Height Approximation for Accelerated Climbing Flight with One Engine Inoperative 121

9.5 Discussion and Synopsis of Climb Optima Differential Derivatives 122

9.6 Optimal Cruise Control Identification 122

9.7 An Iterative Scheme to Solve for Operational Performance 126

10 En route Operational Performance Control and Flight Profile Optimisation 133

10.1 Operational Climb Control 133
10.1.1 Approximating the Optimal Climb Trajectory Speeds Locus 133
10.1.2 Formulating Coherent Climb Control Techniques 135
10.1.3 Merits of Faster Climb Control Techniques – Cruise Soaking 135

10.2 Descent Control 137

10.3 Defining En route Operational Limitations – Flight Envelope 138

10.4 Flight Technique and Profile Optimisation 139
10.4.1 Quasi-analytical Construction of Conceptual Performance Dataset 139
10.4.2 Basic Structure of the Optimum Trajectory-Profile Algorithm 143

10.5 Comparison Between Estimated and Actual Aircraft Data for Integrated En route Performance 146

11 Stability and Control 149

11.1 Methods and Criteria for Empennage Sizing 149

11.2 The Mitchell Computer Program 150
11.2.1 Aerodynamic Derivatives 151
11.2.2 Moments of Inertia 151
11.2.3 Assumptions when Solving the Equations of Motion 151
11.2.4 Conversion to the MATLAB Platform 153

11.3 Assessing the Suitability of Aircraft Design Candidates 155
11.3.1 Longitudinal Short Period Mode 155
11.3.2 Phugoid Mode 159
11.3.3 Dutch-Roll Mode 159
11.3.4 Roll Mode 161

12 Direct Operating Cost, Profit-Return on Investment and Associated Optimal Flight Techniques 163

12.1 Formulation of Models Adhering to a Continuous Function Concept 163

12.2 Solving for Optimal Flight Techniques 166

12.3 Operational Flexibility Index 167

12.2 An Alternative to the Traditional Long Range Cruise Speed Schedule Definition 168

12.2 Merit Functions to Measure Relative Profit and Return on Investment 170

13 A Survey of Constrained Multi-objective Optimisation Methods 173

13.1 Fundamentals of Multi-disciplinary Optimisation 173
13.3.1 Design variables 174
13.3.2 Constraints 174
13.3.3 Synthetic Functions 175

13.2 Selecting Optimisers Appropriate for the Conceptual Aircraft Design Problem 175
13.2.1 Evolutionary Computing – “GAOTv5” in MATLAB 176
13.2.2 Melder-Mead – “fminsearch” in MATLAB 179
13.2.3 Running a Sample Problem using a Cocktail Combination of GAOTv5 and fminsearch 180

13.3 Fashioning Non-linear Multi-objective Optimisation Problems into Manageable Forms **181**
13.3.1 Kreisselmeier-Steinhauser Function 181
13.3.2 Utility Function Formulation 183
13.3.3 Global Criteria Formulation 184

14 Aircraft Design Software Synthesis **185**

14.1 Introduction and Advantages of MATLAB **185**

14.2 The QCARD System **187**
14.2.1 Launching the QCARD System 187
14.2.2 Geometric Definition 189
14.2.3 Total Drag 189
14.2.4 Maximum Lift 190
14.2.5 Propulsion 190
14.2.6 Weight 190
14.2.7 Performance Definitions 192
14.2.8 Stability and Control 192
14.2.9 Economics 192
14.2.10 Constrained Multi-objective Optimisation 196

15 Aircraft Design Projects - Practical Demonstration of Prediction Methods and QCARD-MMI Software Package **197**

15.1 PD340-2 **197**
15.1.1 PD340-2 Specifications 197
15.1.2 PD340-2 Synopsis of Trade Studies and Optimisation 198
15.1.3 PD340-2 Design Description 198
15.1.4 PD340-2 Predicted Performance and Design Review 201

15.2 PD340-3X **205**
15.2.1 PD340-3X Specifications 206
15.2.2 PD340-3X Synopsis of Trade Studies and Optimisation 206
15.2.3 PD340-3X Design Description 208
15.2.4 PD340-3X Predicted Performance and Design Review 209

15.3 TOLS-X **210**
15.3.1 TOLS-X Specifications 212
15.3.2 TOLS-X Synopsis of Trade Studies and Optimisation 212
15.3.3 TOLS-X Design Description 215
15.3.4 TOLS-X Predicted Performance and Design Review 218

16 Conclusions **223**

17 Bibliography **225**

Appendix A – Abstract of Papers and Technical Papers **235**

Paper I: *Methodology for Conceptual Design and Optimisation of Transport Aircraft* 237

Paper II: *Design and Optimisation of a 19 Passenger Turbofan Regional Transport* 257

Paper III: *High-Performance Executive Transport Design Employing Twin Oblique Lifting Surfaces* 275

Paper IV: *Identifying Economically Optimal Flight Techniques of Transport Aircraft* 297

Nomenclature: Symbols

A	=	area; coefficient of proportionality
$\tilde{A}$	=	convergence augmenter
AR	=	aspect ratio
a	=	speed of sound; Fourier Series Expansion coefficient
B	=	takeoff field length
b	=	span; coefficient of proportionality
C	=	circumference
C_D	=	drag coefficient
C_{DOCS}	=	direct operating cost per sector and given flight technique
C_L	=	lift coefficient
$C_{L\alpha}$	=	3D lift curve slope
$C_{l\alpha}$	=	2D lift curve slope
C_{MAIN}	=	maintenance cost per sector and given flight technique
c_f	=	skin friction coefficient
c_{main}	=	flight time dependent maintenance cost denoting theoretically most efficient work practise
c	=	local chord; coefficient of proportionality; thrust specific fuel consumption
c_R	=	root chord
(c'/c)	=	effective chord ratio
c^{ε}_f	=	equivalent skin friction coefficient
c^{I}_{main}	=	flight time related maintenance cost component
c^{II}_{main}	=	fixed maintenance cost component
D	=	drag force
d	=	diameter; coefficient of proportionality; distance
d_{wf}	=	local fuselage chord
e	=	Oswald Span Efficiency Factor
f	=	coefficient of proportionality
g	=	acceleration due to gravity
h	=	flight level; height
h_e	=	energy-height
h_{cab}	=	maximum cabin height
j	=	convergence augmenter factor
K_o	=	Kuchemann correction factor for wave drag
K_g	=	gust alleviation factor
k	=	coefficient of proportionality
k_{main}	=	constant depicting fraction of maintenance cyclic to maintenance flight time dependent cost
L	=	lift force
l	=	length
l_{ε}	=	equivalent characteristic length
M	=	Mach number
N_R	=	Reynolds number
N_S	=	number of sectors completed per reference time frame
n	=	load factor; wave drag exponent
P	=	arbitrary point in productivity index plot; pressure; profit or return on investment attributable to flying services for given sector mission and reference time frame
PI	=	productivity index
P_S	=	specific excess power; pre-optimum profit or return on investment rise rate
P_{SS}	=	post-optimum profit or return on investment decay rate
p_f	=	price of fuel per unit weight
p_{ss}	=	maximum roll acceleration
q	=	dynamic pressure
R	=	flare arc radius; range
R_{LRC}	=	range at LRC while carrying standard passenger complement
r	=	local radius
S	=	surface or wetted area
S_{cab}	=	cabin slenderness ratio given by cabin length divided by the addition of cabin width and cabin height
s_{dec}	=	reference sector distance where the post-optimum profit or return on investment decay rate is measured
S_W	=	wing area
s	=	circumferential length; distance; sector distance for given mission
s_{be}	=	break-even sector distance where profit or return on investment is zero
s_i	=	initial estimate for break-even sector distance numerical scheme
s_{opt}	=	sector distance where profit or return on investment global maximum occurs
s_{ref}	=	reference sector distance used for yield modelling
T	=	temperature; thrust
t	=	collective tank; time; block time for given sector and flight technique
t/c	=	thickness to chord ratio
t_{man}	=	time allowance for start-up, taxi-out and taxi-in
$t_{min\text{-}max}$	=	optimum block time
$t_{mintime}$	=	lowest possible block time required to complete a sector mission
t_n	=	block time equal to the upper applicable threshold of a regressed maintenance cost model
t_o	=	block time equal to lower applicable threshold of a regressed maintenance cost model
t_R	=	time constant
$\mathbf{u}$	=	unit vector

V = volume; forward speed
V_{cab} = gross cabin volume; from cockpit divider to aft cabin
V = empennage volume coefficient
V_2 = second segment safety speed
W = weight
W_G = gross weight
$W_{f,minfuel}$ = lowest possible block fuel required to complete a sector mission
$W_{f,mintime}$ = block fuel required to complete a sector mission in the lowest possible block time
W_{fuel} = block fuel required to complete a sector mission for a given flight technique
w = coefficient of proportionality
w_{cab} = maximum cabin width
Y_{SEC} = total revenue for a given sector mission
y = arbitrary spanwise location; coefficient of proportionality
α = lowest angle in a sector arc; coefficient of proportionality; angle of attack
α_{main} = constant coupling maintenance flight hour cost to segment flight time
β = highest angle in a sector arc; coefficient of proportionality; flap deflection angle; sideslip angle
β_{main} = potential regression parameter accounting for segment flight time influence on maintenance flight hour cost
χ = coefficient of proportionality
Δ = increment; differential
ΔISA = international standard atmosphere
δ = static pressure ratio; coefficient of proportionality; control surface deflection angle
ε = length to diameter ratio; error ratio; absolute error
Φ = impulse function
Φ_α = linear sector distance gradient coefficient in profit or return on investment response model
Φ_β = linear sector distance constant in profit or return on investment response model
Φ_χ = exponential constant in profit or return on investment response model
Φ_δ = exponential sector distance coefficient on profit or return on investment response model
Φ_ε = coefficient representing the asymptotic behaviour in the profit or return on investment response model
ϕ = angular sweep from displaced origin; bank angle
Γ = aircraft price; dihedral
γ = coefficient of proportionality
η = correction which accounts for effects of viscosity; correction factor
η_{act} = Reynolds number adjustment parameter
η_τ = manoeuvring efficiency
ϑ_{cab} = partial differential operator for cabin metrics
φ = down-sweep; coefficient of proportionality; form factor
κ = special correlation coefficient for Dutch Roll damping criteria
Λ = sweep angle
λ = taper ratio; corrected box ratio; passenger load factor for given sector mission
μ = coefficient of viscosity; mass parameter
μ' = corrected coefficient of friction
ν = kinematic viscosity
Π = linear factor; residual function
Θ = partial differential operator of PI; objective function algebraic model
θ = temperature ratio; arc angle
ρ = density
σ = density ratio
τ = flap effectiveness factor
υ = modified geometric model coefficient
ς = scaling factor
ϖ = pressure; adjusted cost differential with respect to block time or profit differential with respect to number of sectors completed per reference time frame
ω = shield-sweep; coefficient of proportionality
ξ = non-dimensional placement parameter
∇ = gradient operator

Nomenclature: Subscripts

A	=	aeroplane; airborne
ATM	=	advanced technology multiplier
AV	=	average
a.c.	=	aerodynamic centre
adj	=	adjusted
aero	=	complete aerofoil
afe	=	aft fuselage engine mount
auxf	=	auxiliary fuel tank
avn	=	avionics
BR	=	braking
b	=	body
bpax	=	business aircraft outfitting
CR	=	critical
Cfe	=	power plant configuration
Cfg	=	configuration
Cvt	=	vertical tail configuration
Cw	=	wing design
c	=	cross-section; critical condition; compressibility; climb
cab	=	cabin
c.g.	=	centre of gravity
centf	=	centre fuel tank
comp	=	interior completion including paint; compressibility
cons	=	consumables and other provisions
cfuse	=	centre fuse body
co	=	wing placement
DD	=	drag divergence
DR(1)	=	assumed de-rate level
d	=	coefficient; ambient conditions
de	=	
decr	=	fuel decrement
des	=	design flag
dia	=	diameter
dslot	=	double slotted
duct	=	S-duct or straight-duct
EAS	=	equivalent airspeed
ecab	=	equivalent cabin
eff	=	effective
elec	=	electrical
em	=	coefficient of proportionality for engine weight
eng	=	engine
equiv	=	equivalent
f	=	fuselage
fair	=	fairing
fairf	=	fairing fuel
fatt	=	cabin attendants
fcnt	=	flight controls
fcrew	=	flight crew
flr	=	floor
fowl	=	Fowler flap
furn	=	green furnishings
fus	=	fuselage
fuse	=	fuselage
fusu	=	unusable fuel
fwd	=	forward
GR	=	ground roll
gbd	=	gross fuselage
geo	=	flap constant of proportionality
gm	=	geometric mean
Hchd	=	half chord
h	=	horizontal; horizontal tail
hcut	=	cut-off altitude
ht	=	horizontal tail
htail	=	horizontal tail
hyd	=	hydraulics
i	=	vortex-induced
ib	=	inboard
id	=	idle
inc	=	representative incidence
ind	=	induced
inst	=	instrumentation
L	=	lift
LE	=	leading edge
LD	=	landing
LOF	=	lift-off
LRC	=	long range cruise
lam	=	laminar flow
lg	=	landing gear
lgt	=	length
MC	=	minimum control
MD	=	minimum drag
MCRZ	=	maximum cruise
MO	=	maximum operating
MRC	=	maximum range cruise
MU	=	minimum unstick
m	=	mean
mf	=	mixed flow
max	=	maximising
min	=	minimising; minimum
misc	=	miscellaneous
nac	=	nacelle
nos	=	
ntyp	=	nacelle type
o	=	initial condition; coefficient; maximum static, ISA, sea level; zero-lift
oL	=	zero lift
ob	=	outboard
op	=	operating, operational
oper	=	operational items
opt	=	optimum
orig	=	original
ow	=	on-wing
pax	=	passengers
pay	=	maximum payload
pow	=	power plant
prop	=	propeller
pwr	=	power; power plant installation type
pyl	=	pylon

Qchd	=	quarter chord
R	=	root; rudder; rotation
REF	=	reference condition
ref	=	reference condition
regs	=	airworthiness regulations
res	=	residual
rev	=	revised
sls	=	sea level standard
S	=	stall
SR	=	sector region
s	=	suggested value;
sec	=	upper/lower airofoil
sp	=	spar; spoiler
sys	=	systems
T	=	tip; transition
TD	=	touch down
TE	=	trailing edge
TO	=	MTOW
TRANS	=	transiton
t	=	block time
tr	=	thrust reverser
tot	=	total
tm	=	most outboard
trop	=	tropopause
turb	=	turbulent
uflr	=	underfloor tank
ult	=	ultimate
v	=	vertical; vertical tail
vt	=	vertical tail
vtail	=	vertical tail
W	=	wing
WL	=	winglet
w	=	wing
wet	=	wetted area
wingf	=	wing fuel tank
wlet	=	winglet
wf	=	wing-fuselage juncture
wm	=	windmilling
XS	=	cross-section
x	=	vertical location; longitudinal location
θ	=	due to ambient conditions

Acronyms and Abbreviations

AAA	Advanced Aircraft Analysis
ACSYNT	AirCraft SYNThesis
AEA	Association of European Airlines
AEO	All Engines Operational
AIAA	The American Institute of Aeronautics and Astronautics
APC	Aircraft-Pilot Coupling
APR	Automatic Power Reserve
APU	Auxiliary Power Unit
ASTROS	Automated STRuctural Optimisation System
ATC	Air Traffic Control
ATM	Advanced Technology Multiplier
AUW	All-Up Weight
BES	Bombardier Engineering Systems
BEW	Basic Empty Weight
BFL	Balanced Field Length
BGA	Binary Genetic Algorithm
BPR	By-Pass Ratio
CAD	Computer-Aided Design
CAP	Control Anticipation Parameter
CAS	Calibrated Air Speed
CDM	Combined Drag Model
CFD	Computational Fluid Dynamics
CI	Cost Index
CLB Mode	Climb Mode; L – Low, I – Intermediate, H – High
CPU	Central Processor Unit
CRC	Conceptual Research Corporation
DOC	Direct Operating Cost
DSS	Decision Support System
ECLM	Equivalent Characteristic Length Method
ELRC	Economical Long Range Cruise
ER	Extended Range
ECS	Environmental Control System
ESDU	Engineering Science Data Unit
ETOPS	Extended Twin Operations
EVS	Enhanced Vision System
FAR	Federal Aviation Regulations
FC	Flight Controls
FCS	Flight Control System
FGA	Float Genetic Algorithm
FIR	Flight Information Regions
FL	Flight Level
FMC	Flight Management Computer
FPS	Flight Planning System
FRP	Fuselage Reference Plane
GA	Genetic Algorithms
GAOT	Genetic Algorithms for Optimisation Toolbox
GASP	General Aviation Synthesis Program
HSC	High Speed Cruise
ICAO	International Civil Aviation Organisation
IGW	Increased Gross Weight
IFR	Instrument Flight Rules
ISA	International Standard Atmosphere
JAR	Joint Airworthiness Regulations
KS	Kreisselmeier-Steinhauser function
KTH	Royal Institute of Technology, Stockholm, Sweden
LRC	Long Range Cruise
MAC	Mean Aerodynamic Chord
MCRZ	Maximum Cruise
MDO	Multi-disciplinary Design Optimisation
MFLW	Minimum FLight Weight
MFW	Minimum Fuel Weight
MIDAS	Multi-disciplinary Integration of Deutsche Airbus Specialists
MLW	Maximum Landing Weight
MRC	Maximum Range Cruise
MRW	Maximum Ramp Weight
MTOT	Maximum Takeoff [Power] Thrust

MTOW	Maximum Takeoff Weight
MTOGW	Maximum Takeoff Gross Weight
MVO	Multi-Variate Optimisation
MZFW	Maximum Zero-Fuel Weight
NBAA	National Business Aircraft Association
NTOT	Normal Takeoff [Power] Thrust
OEI	One Engine Inoperative
OWE	Operational Weight Empty
OFI	Operational Flexibility Index
OPR	Overall Pressure Ratio
OPTIM	Optimisation Toolbox in MATLAB
OTPA	Optimum Trajectory Profile Algorithm
OWE	Operational Weight Empty
PAX	Passenger
PEH	Performance Engineer's Handbook
PIANO	Project Interactive ANalysis and Optimisation
PIO	Pilot Involved Oscillation
PEH	Performance Engineer Handbook
P-ROI	Profit/Return on Investment
QCARD	Quick Conceptual Aircraft Research and Development
RoC	Rate of Climb
RoD	Rate Of Descent
ROI	Return On Investment
SAE	Society of Automotive Engineers
SAR	Specific Air Range
SAS	Stability Augmentation System
SBW	Strut-Braced Wing
SQP	Sequential Quadratic Programming
STD	Standard
TET	Turbine Entry Temperature
TOFL	Take-off Field Length
TOGW	Takeoff Gross Weight
TOLS	Twin Oblique Lifting Surfaces
TSC	Typical Speed Cruise
TSFC	Thrust Specific Fuel Consumption
VLM	Vortex-Lattice Method
WER	Weight Estimating Relationship
WPEBS	Wing-Pylon-Engine Bracing Structural Systems
YEIS	Year of Entry into Service

List of Figures

Figure 1. Illustration of the conceptual design process segmented into two tiers: the initial or “pre-design” and refined baseline configuration definitions. 2

Figure 2. Chart indicating the value of performance and amenities for business aircraft using a parametric productivity index. 16

Figure 3. Sensitivity study of next available price in relation to maximum range and cabin length for Gulfstream Aerospace business jets. 18

Figure 4. The idealised unit step function compared to a mathematical approximation. 20

Figure 5. Equivalent reference wing geometric definition using the Weighted MAC method. 26

Figure 6. Equivalent reference wing geometric definition using the ESDU method. 27

Figure 7. Equivalent reference wing geometric definition using the Simple Trapezoid or Net method. 28

Figure 8. Equivalent reference wing geometric definition using the Airbus Gross and Boeing Wimpress methods. 29

Figure 9. Illustration of displace origin for fuselage cross-section geometric definition. 31

Figure 10. Comparison between actual geometry and model for the Embraer 170 typical fuselage cross-section. 32

Figure 11. Comparison between Saab 2000 and Saab 340 actual and modelled forward fuselage geometric definition. 34

Figure 12. The generic elliptic paraboloid comprises a series of ellipse sections varying in relative size in accordance with a parabolic progression. 36

Figure 13. General representation of swept surface resulting from revolution of curve AB about the x-axis. 38

Figure 14. Parameters of arbitrary parabolic curve used to compute arc length. 43

Figure 15. The area of the surface swept out by revolving arc AB about the axis shown. 45

Figure 16. Prediction accuracy of presented methods to estimated wetted area of major constituents and accumulated vehicular result for select transport aircraft. 46

Figure 17. Primary working parameters required in estimating the cabin volume of both circular and ovoid cross-sections. 47

Figure 18. Prediction accuracy of method to estimate cabin volume of any transport aircraft. 49

Figure 19. Example geometric layout of integral fuel tanks within the wing structure that caters to tank span discontinuity. 50

Figure 20. Dimensioning of the centre fuel tank for volume prediction (forward view). 52

Figure 21. Conceptual turbofan dry engine WER based on data gathered from Aviation Week , Janes and Svoboda. 66

Figure 22. Prediction accuracy of presented method to estimate the weight of major constituents and accumulated vehicular result for selected transport aircraft. 73

Figure 23. Predicting the lift characteristics of a clean finite wing using quasi-analytical techniques (1-g stall concept shown). 76

Figure 24. Prediction accuracy of algorithm to compute C_{Lmax} using quasi-analytical techniques. High-lift devices set to neutral and maximum deflection shown. 79

Figure 25. The premise of mixed laminar and turbulent flow used to derive an augmented realistic skin friction coefficient. 82

Figure 26. Resilience of ECLM accuracy for a given error in vehicular characteristic length and en route Reynolds number based on vehicular characteristic length. 85

Figure 27. Simplifications of forces and geometric considerations during the asymmetric thrust condition. 89

Figure 28. Benchmarking predicted windmilling drag using the imaginary skin friction method against actual engine windmilling data; ISA, sea level conditions. 92

Figure 29. Definitions for the transonic mixed flow regime and indication of speed thresholds for certain drag escalation attributes. 93

Figure 30. Definition of working parameters to compute drag due to lift in supersonic flight. 96

Figure 31. Resolving local lift and drag forces generated by the winglet into the direction of freestream. 98

Figure 32. Comparison between flight-test derived and predicted improvement in block fuel for B737-800 commercial transport. 100

Figure 33. CDM prediction effectiveness inspected for the Saab 2000 high-speed turboprop regional transport. 101

Figure 34. CDM prediction effectiveness inspected for the Learjet 60 midsize turbofan business aircraft. 102

Figure 35. CDM prediction effectiveness inspected for the Global Express ultra long range turbofan business aircraft. 102

Figure 36. CDM prediction effectiveness inspected for the B737-800 narrow-body commercial transport; note that $\tau_{act} = 1.30$ used in generating the reference condition. 103

Figure 37. Takeoff reference speeds and general requirements for civil transport aircraft. 109

Figure 38. Model of the landing approach and flare path for prediction purposes. 113

Figure 39. Prediction accuracy of algorithms to compute the BFL and LFL (or LD) for a select array of regional, narrow-body and business aircraft. 114

Figure 40. Specific excess power and specific energy contours for identifying minimum time to climb flight paths. 116

Figure 41. Available power (or thrust) and required power (or drag) interaction showing potential for infinite looping together with a suggested procedure for speed optima convergence. 127

Figure 42. Demonstration of how the traditional optimal climb trajectory plot may be transformed (flight below the tropopause). 133

Figure 43. Elucidating the concept of cruise soaking due to faster CAS/Mach climb speed schedules; TOC = top of climb, and, BOD = beginning of descent. 136

Figure 44. Identification of V_{MO} / M_{MO} flight envelope boundary using the “20-80” rule. 138

Figure 45. Geometric interpretation of transforming the independent AUW parameter into a dependent variable using logarithmic correlation. 141

Figure 46. Geometric interpretation of transforming the fuel expended and time elapsed parameters into dependent variables being a function of distance traversed. 142

Figure 47. Flight profile as defined by Association of European Airlines (AEA). 143

Figure 48. Flow chart depicting the algorithm construct of OTPA catering to both payload-range and fixed sector mission premise. 145

Figure 49. Comparison between known data and predicted ISA still air range performance of in-service aircraft using the conceptual operational control methods and OTPA algorithm. 146

Figure 50. Basic geometric definition of aircraft required by Mitchell Code; reproduced from a sketch congruous with the originally drafted version. 152

Figure 51. Flow chart depicting the algorithm construct of SCMITCH code for analysing stability and control attributes of an aircraft design candidate. 154

Figure 52. Qualitative pilot assessment rating of flying characteristics (Cooper-Harper). 156

Figure 53. Longitudinal Short Period oscillation pilot opinion contours taken from ESDU. 157

Figure 54. Short Period frequency characteristics, CAP evaluation; Category C Flight phase. 158

Figure 55. ICAO recommended Short Period mode characteristics. 158

Figure 56. ICAO recommended Phugoid mode characteristics; key: zeta = damping ratio, omega = undamped natural frequency. 159

Figure 57. Minimum values of natural frequency and damping ration for Dutch Roll oscillation. 160

Figure 58. Dutch Roll damping criteria as stipulated by SAE; key: k = κ, phi = ϕ and beta = β. 160

Figure 59. Roll response pilot opinion boundaries; lines of constant Cooper-Harper pilot ratings also indicated. 161

Figure 60. DOC and P-ROI computation and identification of corresponding optimal flight techniques procedure flowchart. 164

Figure 61. Typical block time-fuel summary for a given sector distance and mission. 165

Figure 62. Degradation in SAR assuming traditional LRC (1% reference line) and ELRC compared to datum of MRC (fixed AUW, ISA, still air). 169

Figure 63. Typical sector distance response of P-ROI model assuming an hourly-based reference time frame utilisation. 171

Figure 64. Objective function topography used to bench-test the MATLAB GAOTv5 and fminsearch cocktail optimiser algorithm. 180

Figure 65. Example of KS function characteristics for various scalar multiplier, or ρ values. 182

Figure 66. QCARD-MMI design synthesis system core subspace contributors. 186

Figure 67. The QCARD-MMI introductory splash-screen when launching the system. 187

Figure 68. Definition of the aerofoil section for a wing in the QCARD synthesis system. 188

Figure 69. Inspection of the reference wing definition for a given design candidate. 188

Figure 70. Rudimentary DSS through inspection of generalised nacelle location chart. 189

Figure 71. Gauging the relative aerodynamic merits of a chosen design candidate. 190

Figure 72. Maximum lift prediction for high-lift device deflection neutral or otherwise. 191

Figure 73. QCARD interface (executing) to predict the constituents' weight breakdown. 191

Figure 74. Instantaneous BFL estimation according to given flap and ambient conditions. 193

Figure 75. Examining and contrasting CLB Mode L against the optimal schedule results. 193

Figure 76. Flight envelope (including performance control) formulation and visualisation. 194

Figure 77. Example payload-range for maximum SAR and maximum block speed. 194

Figure 78. Examining the longitudinal Short Period contours for an aircraft design. 195

Figure 79. Predicting the maximum profit of an aircraft design using the QCARD system. 195

Figure 80. QCARD interface for constrained multi-objecitve optimisation analysis. 196

Figure 81. Final simplified selection process for PD340-2 turbofan commuter concept. 199

Figure 82. Artist's impression of the PD340-2 19 PAX regional turbofan transport. 199

Figure 83. General arrangement of the PD340-2 19 PAX turbofan commuter aircraft. 200

Figure 84. Fuselage structural arrangement and assemblies common to Saab 340 vehicle. 201

Figure 85. Payload-range envelope for PD340-2 19 PAX commuter turbofan transport. 202

Figure 86. Direct Operating Cost per seat-nm comparison of PD340-2 to competition. 204

Figure 87. Annual operating profit comparison of PD340-2 to competition (50% load factor). 204

Figure 88. Trade study and final configuration selection for PD340-3X STD tri-jet regional transport. 207

Figure 89. PD340-3X 31-34 PAX regional transport general arrangement. 208

Figure 90. Payload-range envelope for PD340-3X STD and PD340-3X ER 31-34 PAX regional turbofan transports. 210

Figure 91. Introducing the Twin Oblique Lifting Surfaces (TOLS) configuration. 211

Figure 92. Simplified representation of final selection for TOLS-X design. 214

Figure 93. The TOLS-X high-performance executive transport general arrangement. 216

Figure 94. Cross-section area development plot of TOLS-X configuration at sonic speed compared to contemporary high-speed business aircraft. 217

Figure 95. Historic correlation of wave drag sourced from Jobe, and, Saltzman and Hicks compared to TOLS-X concept. 218

Figure 96. Payload-range envelope for TOLS-X business jet transport. 219

List of Tables

Table 1. FAA and JAA sanctioned standard crew weights; data also includes hand baggage allowance. 68

Table 2. FAA and JAA sanctioned standard passenger and baggage weights; applicable for narrow-bodies and larger aircraft only. 70

Table 3. FAA and JAA sanctioned standard passenger and baggage weights; applicable for all regional and JAA aircraft less than 20 seats. 71

Table 4. Synopsis of performance partial derivative coefficients for climbing flight. 123

Table 5. Weight and geometry data for PD340-2 19 PAX turbofan commuter. 200

Table 6. Parametric review of PD340-2 commuter against contemporary turboprops. 203

Table 7. Leading particulars for PD340-3X STD and PD340-3X ER commuter turbofan concept. 209

Table 8. Design weights, merit values and geometry data for TOLS-X vehicle. 215

Table 9. Parametric review of TOLS-X against contemporary large and super-large business jets. 220

Quasi-analytical Modelling and Optimisation Techniques for Transport Aircraft Design

An Introduction

Askin T. Isikveren

This treatise focuses on the formulation of many new algorithms intended for use in pre-design and conceptual aircraft design sizing studies and associative measure of capability. Fundamentally, emphasis is placed on the development of simple algebraic models. In the absence of maintaining a harmonious interaction between the various design parameters, a reliance on statistical datasets of actual aircraft is considered, but where practical, applied using a quasi-analytical mindset. By producing a software package encompassing these ideas, it is the intention of the author to convey the notion that a visually interactive ensemble, imbued with capabilitie of conducting a sophisticated level of objective function analysis whilst ensuring consistent sensitivity, and, complemented by some basic decision support tools to assist the designer during the conceptual process can be produced without resorting to very large, convoluted and cumbersome digital codes.

1 Introduction

Today, early indications are emerging that the aerospace sector is undergoing some changes with respect to how vehicles are designed, built and operated. It appears that the analytical tools currently available for conceptual design engineers to conduct feasibility studies that "push the envelope" in terms of minimising development costs and creating shifts in operational paradigms are not suitable due to the predominant philosophy of simply utilising and coding existing, sometimes outdated handbook methods. Many new methodologies that approach the conceptual design problem from a different perspective are to be reviewed in this body of work. Together with the main focus of generating theories more compatible in applicability and scope for requirements stipulated by contemporary design offices, they are also devised expressly for the purpose of being utilised to investigate the more seriously contemplated concepts currently gathering momentum, such as progenitive highly synergised family concepts, and, high transonic and/or supersonic commercial flight.

1.1 What is Conceptual Design?

Throughout the aerospace industry and academic institutions this question is open to many interpretations, and frequently, quite distinct viewpoints. It is therefore prudent to address this issue from the outset in order to set the theme of this dissertation, thus allaying any chance for misinterpretation.

The entire aircraft design process can be categorised into three distinct phases: (1) conceptual definition; (2) preliminary definition; and, (3) detailed definition. Depending on the requirements of time and resources deemed appropriate by the airframe manufacturer, the conceptual definition phase itself cannot be branded as adhering to one type of mindset. In fact as exemplified by Figure 1, there exist two tiers under this phase, one aimed at establishing a very quick (time-scale can be from one to a few weeks) yet technically consistent feasibility study some call pre-design, and the other would be a protracted and labour intensive effort involving more advanced first-order trade studies to produce a refinement in defining the minimum goals of a candidate project. During the preliminary

definition, product design is still undergoing a somewhat fluid process and indeed warrants some element of generalist-type thinking, but can be thought of essentially as a constrained exercise because the minimum goals of the project have already been established during the conceptual definition phase and the aim is to meet these targets using methods that do not necessarily reflect the conventional wisdom established during the conceptual definition phase. Furthermore, the participants in this working group are mostly genuine specialists in each respective discipline. As the status of a project is well within the preliminary design phase, assuming the manufacturer has confidence in the potential for a new product line and has established a development cost it is willing to absorb, the detailed definition phase would begin after the project is formally launched. This phase is, as a literal interpretation would yield, design of the individual details, sub-assemblies and assemblies that constitute the aerospace vehicle.

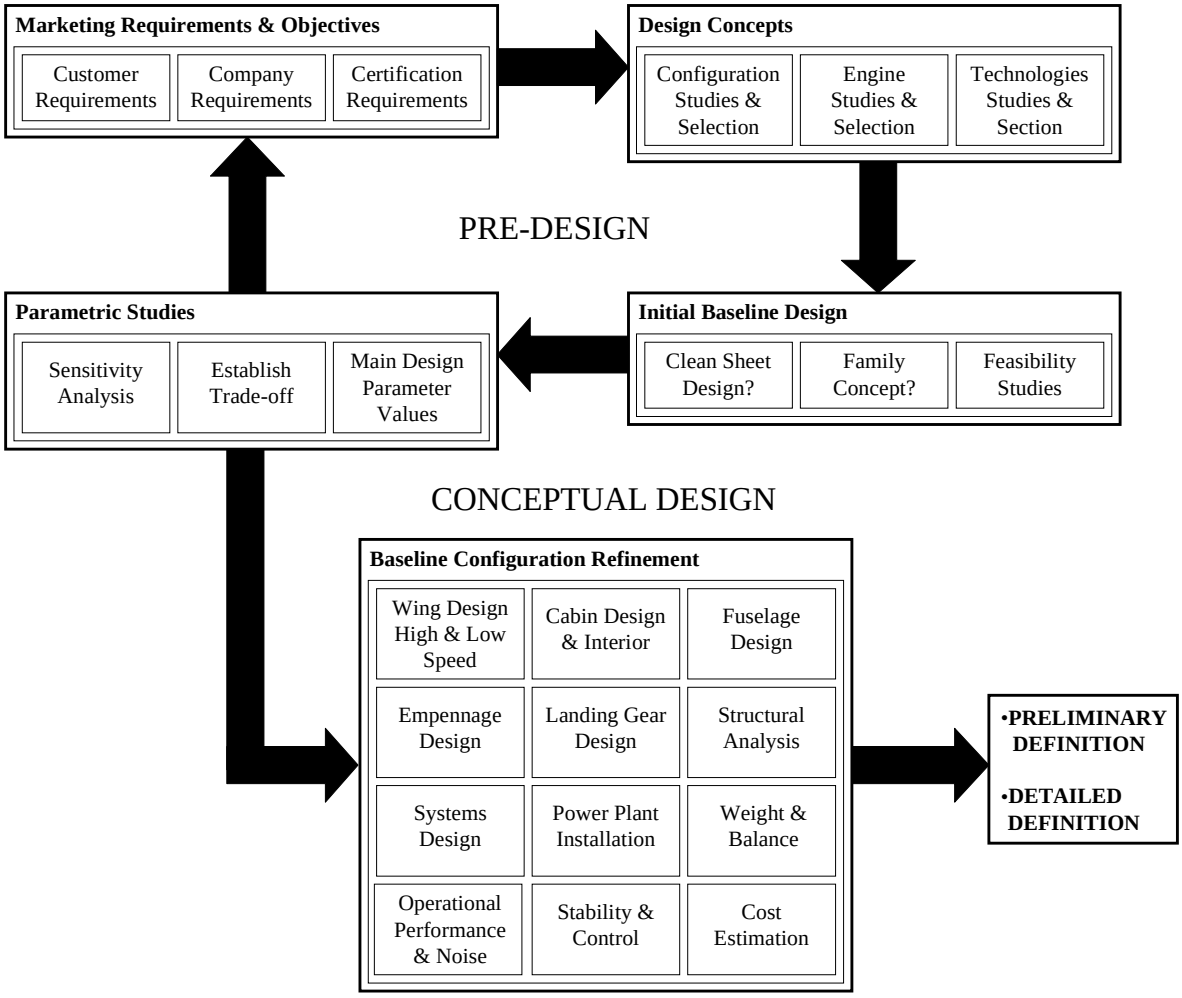

Figure 1. Illustration of the conceptual design process segmented into two tiers: the initial or “pre-design” and refined baseline configuration definitions.

More specifically, a transport aircraft pre-design and conceptual design, which is the concentration of this research, may be defined as a very tentative engineering proposal, which meets the requirements of a current (or envisioned) market niche with facility for accommodating perceived future needs constrained by the realities of contemporary and foreseeable economic forces. Disciplines of structures, weights, thermodynamics and

aerodynamics must be traded with each other in order to produce a balanced design candidate, which not only conforms to airworthiness and operational requirements, but also, if it is destined to be a commercial transport, gives wide scope of revenue potential. The analytical processes that aid in bringing a conceptual design into fruition are primarily based on methods that are simple to at most moderately high in complexity. Notwithstanding, interactions between multitudes of free variables that go into defining a configuration commonly result in a rather complex array of objective functions. These criteria are subsequently inspected via sensitivity studies in order to foster an optimised vehicle layout. The focal point that coalesces from quantifying the weight, lift, drag and power plant characteristics of a vehicle candidate is performance. For coherent aircraft critical appraisals, this aspect is considered crucial because it is used as a fundamental comparison basis not only in an absolute sense but also when considered in the transformed Direct Operating Cost (DOC) and Maximum Profit/Return on Investment (P-ROI) functional form.

1.2 Basis and Protocol for Conceptual Aircraft Design Prediction

As described by Torenbeek[1] and Bil[2], conceptual design is primarily a search process whereby the goal is to formulate a set of design variable quantities, which in consort produces a vehicle that at least fulfils a devised list of minimum requirements. The mechanism behind this search is mathematics and the core utilities required to conduct the design process can be itemised as:

- Design specifications – a set of minimum requirements that define the success of any aircraft design candidate. The specifications are categorised into two groups: those that are hard specifications and those that are soft. The hard specifications stipulate no compromise in delivering compliance according to the target values, whereas, soft specifications permit some element of freedom in violating the original target.
- Design parameters – are a set of abscissa values intentionally selected such that they collectively describe the vehicular characteristics of with regards to compliance, performance and profitability. These independent variables not only define the aeroplane in a physically tangible sense, but can also be expressed as special ratios or parametric functional relationships known to demonstrate direct correlation to a desired outcome.
- Dependent variables – are the ordinate values produced from the collective outcome of the design parameters. They are also known as objective functions because they demonstrate functional relationships to the design parameters through physical principles or statistical correlation.
- Figures of merit – are special ratios and mathematical expressions that demonstrate a strong functional proportionality to a given dependent variable without resorting to the length of actually computing the value. They are characteristically expressed as a combination of design parameters in order to reduce the number of steps in computing them, thereby simplifying the problem of establishing what level of sensitivity a particular design parameter has with respect to the dependent variable outcome.
- Prediction methods – are expressions that explicitly define the physical relationship between the design parameters and dependent variables. These functions vary greatly in complexity and accuracy of the methods relies on the amount and fidelity of the input information.

- Design space – is a collection of vehicular candidates that completely, partially, or not even fulfil the design specifications. Occasions where several design candidates fulfil the design specifications, another arbitrary rule, such as examination of a given figure of merit, can be used to establish the best candidate.

Conceptual aircraft design has been the subject of parametric studies albeit in limited scope since the mid portion of this century. It is can be said that two distinct levels of analysis are available to modern designers: first order minimalism predominated by the closed form edict, or, higher order techniques that draw heavily upon complex mathematics and numerical methods.

1.2.1 First Order Minimalism

Originally borne out of industrial necessity, this approach limits the knowledge of mathematics to an elementary level by employing first order analytical techniques in conjunction with empirical databases and established handbook methods[1,3,4,5]. The tools utilised are commonly of a closed form and adopt greatly simplified critical assumptions in an effort to reduce the amount of work to be expended.

For example, a first order maximum range calculation may use a linear control factor to represent climb, a closed form analytical representation for cruise at constant Mach number whereupon the descent is assumed to be equal to the fuel used during cruising flight over the same distance. This supposition totally neglects the transversality condition which is additive between climb, cruise and descent phases, and, does not take into account appropriately the quantities of fuel necessary for manoeuvring, reserves or other contingencies. In keeping with the simplification tact, ambient conditions are routinely fixed to an idealised scenario of ISA and atmospheric properties showing no indication of the vehicle's attributes in more realistic operational circumstances.

This is not to detract from the relevance of a first order assumption, especially during the pre-design stages of a new conceptual design project since they provide fast and reasonably accurate tools for prediction. However, the entire process is dominated by an implicit minimum goal success philosophy, which makes for a highly subjective basis susceptible to a sometimes quite optimistic result when utilised by the uninitiated.

1.2.2 Advanced Higher Order Iterative Algorithms

The design prediction method in this instance is increased in complexity somewhat via the introduction of techniques based on finite element theory and calculus of variations[6,7,8]. In essence, this approach reflects a natural shift of the design process where more detailed analyses replace older approximations. The primary intent here is to skip the traditional conceptual step and view it more as a preliminary design problem from the outset. As a result, each discipline is identified as a subspace open to individual optimisation prior to attempts made for global objective function convergence.

A typical example is the methodology for wing design. The analysis can be upgraded from the conceptual approach of statistical regression functions for wing weight approximation based on various geometries and loadings of actual data from a variety of past and present commercial aircraft to a wing structure subspace problem including structural/stress analysis and weight optimisation based on finite element techniques. The design variables are expanded to include skin, rib and web thickness and main spar geometry. Through an iterative process where hundreds of stress constraints are considered, the function returns a wing weight that is optimum for specific wing geometries (aspect ratio, taper ratio, thickness and sweep).

The two major advantages associated with this approach are the effects of biased decision making can be avoided, and, it is most useful for non-conventional configurations. However, the computational resources required tend to become excessive including additional problems that arise because of programming and debugging. Also, since a more detailed slant is considered, there are many occasions where the method must rely on simplified analytical techniques in order to fulfil the requirements of complete variable definition before the algorithms are permitted to proceed. An issue of inconsistency with respect to this method's formulation of the critical assumptions may therefore be raised: first order expressions commonly used as a basis for complex analysis techniques does not seem to justify a marked increase in complexity when tackling the design problem.

1.2.3 Quasi-analytical Algorithms – A Compromise Between Economy of Effort and Higher Order Accuracy

One approach in calculating objective functions is to predict the most basic and integral element(s) using an analytical technique and then apply adjustments by way of factors, penalties and increments to better model the specific problem at hand. This method is termed as a quasi-analytical approach because the predictions are based on analytically derived intermediary estimates that are then correlated against known empirical or actual data. Application of this method originates from work conducted by Burt[9] and Shanley[10] who examined ways in which prediction of wing weight can be based on elementary strength and stiffness considerations with supplementary adjustments incorporated according to experimental and statistical data. The main thrust of their respective methods was a fundamental willingness to rely on a collocation of computational procedures, namely analytical, numerical and statistical operations, strategically applied to each functional component that contributes to the objective function.

To elucidate the method clearly, consideration can be given to one of the more sophisticated algorithm exemplars used in practise, such as, a sequence of operations to conduct wing structural weight estimation[11,12]. The optimum bending shear and torsion carrying structural box beam weight would be estimated by a station cut analysis that considers materials, their properties, the construction type, the specific geometry, the loads either supplied or assumed by some test-based data for compression stability evaluation. The total wing weight estimate would then be accomplished by applying a series of analytical and statistically based increments to this basic estimate to account for non-optimum weights such as fasteners, cut-outs, wing fold, splices and joints, fuselage attachment, fuel containment, and all other unique features of the aircraft wingbox under analysis. To complete the exercise, the control surfaces weights, fixed edges, etc. would be estimated in isolation using statistical methods.

One salient observation is that higher-end quasi-analytical procedures do require an elaborate array of input data than the traditional statistically based methods. Nonetheless, if approached in a thoughtful manner, a sizable scope in reducing the complexity can be realised. This is achievable through the formulation of suitable default assumptions and accumulation of knowledge that instils a genuine appreciation of the physical cues regarding sensitivity of each engineering parameter to the final objective function. When adopting this approach and placing such an emphasis on economy of effort, the methodology offers greater versatility in terms of retaining accuracy for contemporary technology vehicles. Furthermore, the main advantage over the purely statistical based methods (irrespective of increasing complexity when constructed in the analytical form) is an ability to retain some semblance of accuracy in extrapolating outside the parameter dataset range. Moreover, a possibility now arises in maintaining this accuracy level during

trade-studies and departures in the contemporary technology level and eventually leads to a much surer assessment of the feasibility of unconventional configurations.

1.3 Operational Criteria Placed On Contemporary Transport Aircraft

Trajectories computed using more refined methods like calculus of variations are characterised by continuously varying airspeeds during climb and descent phases with the throttle setting assumed to be a continuous function of time for the entire flight. In contrast, a succinct overview of both Air Traffic Control (ATC) and route structure to follow demonstrate the difficulties associated when attempting to adhere to precision a planned profile with respect to route, flight level* and time. Also, it is customary to predict performance for new conceptual designs of transport aircraft based on techniques which model the idealised scenario. The onus is placed on the designer to ensure that new conceptual designs should abide by the rules and practises in accordance with modern day operational criteria. In essence, the performance specification should be defined by taking increasingly demanding airworthiness regulations into account, which proves to be an especially arduous undertaking when attempting to produce commercially viable designs.

1.3.1 Present-Day Air Traffic Control and Route Structure

The ATC service is responsible for the "…provision of a safe, orderly and expeditious flow of air traffic…"[13] and is one of the more important air navigation services originally conceived by the International Civil Aviation Organisation (ICAO). For each specific region, subdivisions known as Flight Information Regions (FIR) are designated. These in turn, consist of two elements, namely, the airspace division and the route structure. Within each FIR, airspace can be distinguished as controlled and uncontrolled – the controlled airspace being under ATC's jurisdiction. Primarily, ATC determines aircraft position and subsequently applies this information in assessing the minimum safe distance required for separation between aircraft. Combined with an additional task of reacting to potentially dangerous situations, these standards, amongst others, determine the maximum number of aircraft, which can use a certain volume of airspace in a certain period of time. Procedural allocation of airspace also depends on the specific flight phase an aircraft is undergoing because relative speed between vehicles must be taken into consideration as well.

Route structure is defined in a horizontal plane in terms of a series of reference points determined by the location of radio navigation beacons. These reference points, commonly referred to as waypoints, are connected by straight line segments which also have a dual property being a series of pre-designated vertical planes or available flight levels the vehicle may traverse. These flight paths are structured into special zones due to many reasons, some of which usually pertain to undesirable terrain profile avoidance, purposes of noise abatement, or even to segregate civil transports from military traffic. Furthermore, each airway segment defined by the two-waypoint nodes characteristically, through both the local regulatory body as well as ATC compliance, permit aircraft the ability of utilising a distinct airspeed and flight level from previous ones. Route structure can be divided into two categories: ones approved by the local regulatory agency which incidentally must be used at all practicable times, and, company designated routes only to be used occasionally when extenuating circumstances arise.

* The term flight level is a common operational parlance. This quantity is the altitude expressed in units of hundreds of feet, e.g. FL 250 is equivalent to 25000 ft.

1.3.2 Operationally Permissible Flight Control Techniques

Current airline operational practise utilises simplified control techniques comprising of a constant calibrated airspeed (CAS) which transitions to a constant Mach number. This technique is referred to as the CAS/Mach speed schedule and is employed for climb and descent phases. Climbing flight commences with a speed schedule of CAS and then proceeds with constant Mach number usually at a maximum climb throttle setting. Conversely, descent is mostly conducted at an idle throttle and begins with a constant Mach with subsequent transition to constant CAS.

Some flexibility to cruise is afforded since speed and flight level are permitted to vary for each waypoint along the route. This translates into possibilities of adhering to optimal flight plans provided ATC and route structure do not impose any restrictions. Although available thrust may theoretically allow an aircraft to fly continuously at Maximum Range Cruise (MRC) speeds, this procedure is not usually selected in practise. Instead, a speed schedule called Long Range Cruising (LRC) is adopted which is a trade between the fuel penalty for time saved due to faster cruise speed. This value is commonly defined as 98-99% of maximum specific air range and is derived based on schedules at the initial condition of flight which allows the vehicle to remain close to the maximum Specific Air Range target (SAR) whilst still affording a significant measure of speed increase. For flights where delays must be soaked or the mission requirement is of short distance, a larger fuel penalty can be accepted when the aircraft is flown at the Maximum Cruise (MCRZ) rating and at lower flight levels.

1.4 Stability and Control

The very concept of stability and control is concerned with the provision of permitting sustained authority over the aircraft at any point within the vehicular flight envelope. This requirement extends to a control system that promotes ease and effectiveness of aeroplane response acquiescent with the pilot's commands. As it has been proven repeatedly[14], and sometimes with spectacular results, inadequate appreciation with respect to stability and control fundamentals can catastrophically cause the demise of any projects – even those showing unequivocal promise from the outset. One truism in the aerospace industry is the fact that almost all aircraft projects have experienced flying qualities problems at some stage during the flight-testing process. Even if handling and control present no problems when the vehicle is operated in the nominal mode, one aspect like very poor control in manual reversion mode may for instance become the source of major consternation because of the fundamental design minimum goals potentially being compromised.

The basic concept for stability[14,15,16,17] is simply a stable aircraft has a tendency to restore itself to its original condition whenever a force or moment disturbs the flight – this property of the vehicle is referred to as static stability. The disturbance is indicative of random fluctuations that arise from the atmosphere, such as from gusts. The concept of dynamic stability involves an appreciation of the vehicle characteristics as a result of a disturbance from an equilibrium condition. There exist two distinct categories of response: (1) dynamically stable, which in-turn is sub-divided into those situations where a gentle resumption back to original condition occurs, or, a damped oscillation where resumption back to the original condition occurs with overshoots; and, (2) dynamically unstable, which is also sub-divided into undamped oscillations of constant amplitude usually referred to as neutral dynamic stability, forced oscillations where the amplitude increases over time, and finally, a statically unstable situation typified by divergence from the equilibrium condition after a disturbance. It is quite evident that the aircraft should not possess any statically unstable properties in any dynamic mode, or at the very least, the divergence that results

from such instability is not so rapid the pilot can reasonably apply a correction. If the aircraft exhibits any dynamically unstable oscillatory behaviour, the oscillations need to be either totally eliminated or damped sufficiently to reduce the frequency through passive or active means.

Aircraft control is concerned with the response of the vehicle after control mechanisms have been intentionally manipulated to deviate from a given equilibrium condition. Aerodynamic control is achieved through basically three sets of dedicated surfaces: elevators in pitch; ailerons in primary roll and secondary yaw; and, the rudder in primary yaw and secondary roll. Control is a different problem from that of stability. The aircraft control system should possess a characteristic response to a control action such that it is in the same sense and control reversal is avoided entirely. The sensitivity of control displacements should also be calibrated such that a statically stable aircraft is not "too stable". Also, the magnitude of the force to manipulate the control should steadily increase with the control displacement and correspondingly reflected in the magnitude of the aircraft response, and little or negligable time lag should prevail in the aircraft response to a control input. These requirements not only apply to aerodynamic control but also the engine throttle, and hence speed.

In view of the foregoing discussions, in conjunction with the notion simplified methods in assessing handling qualities are not tenable, and the fact gross inefficiencies would result from manual calculation procedures, it is quite evident a requirement now exists in developing and integrating some sort of dedicated software system. This utility should permit rapid and economical estimations of aerodynamic stability and control qualities from data available in the conceptual design stage. Two candidates that can conduct stability and control analysis are the Digital Datcom[18] and Mitchell[15] computer programs. The Digital Datcom for all intensive purposes is a translation (with some minor differences) of the Datcom methods into a computer program. The greatest drawback of Digital Datcom is the methods are geared more towards preliminary design operations and therefore raises questions of inconsistency between formulation of critical assumptions for complex analysis techniques. In contrast, the Mitchell code most advantageously works from a more simplified numerical description of the external geometry, and from that basis, can compute the aerodynamic derivatives, moments of inertia, characteristics of the fixed-stick stability modes, the lateral response to control inputs and disturbances, and some low-speed limitations.

1.5 Multi-disciplinary Design Optimisation

Due to the austere nature of skills for implementation, the lack of an extensive array of constraints imposed by airworthiness regulations, an absence of issues dictated by operational performance protocols and loose adherence to customer sponsored performance guarantees, the aircraft design process was considerably less complex in the past. As technological development has compounded the intricacy to the point where many specialists now participate in the design process, even though the specialists can find the best technological solution within the realm of their respective discipline, it does not necessarily mean the best global design will result. Accumulated experience within the aerospace industry draws one to the conclusion that philosophically an interdisciplinary approach to aircraft conception is paramount if significant breakthroughs are to be realised. One method in addressing this issue is to create a formalised design strategy and examples are the so-called Multi-disciplinary Integration of Deutsche Airbus Specialists (MIDAS)[19] and the Bombardier Aerospace Bombardier Engineering System (BES)[20] initiative.

Apart from spelling out the phases, milestones and processes in an aircraft design cycle, scope must be given to optimise each stage and this can only be achieved with multi-disciplinary design and optimisation practises. The American Institute of Aeronautics and Astronautics (AIAA) defines Multi-disciplinary Design Optimisation (MDO) as "…a technology that synergistically exploits the interaction among disparate disciplines to improve performance, lower cost and lower product design cycle time…". A variety of techniques whether they are based on the premise of mathematical programming or evolution methods are available today as numerical tools in searching for an optimum solution. One successful commercial application of this design philosophy is the Automated STRuctural Optimisation System (ASTROS)[21] finite element based software system developed to assist the preliminary design of aerospace structures.

The intention of this particular research was to establish some sort of framework for multi-disciplinary design functionality at the conceptual design level. Investigative work conducted by Van der Velden[22] reveals feasibility in utilising evolution and Nelder-Mead Simplex methods for not only simplified Multi-variate Optimisation (MVO) problems, but also for the more complex hyper-dimensional (greater than 20 design variables) MDO problem formulation as well.

1.6 Computer Aided Engineering in Conceptual Design

The use of software to conduct aircraft conceptual design and optimisation has been around for well over a decade. Even though significant strides have been made in relation to interactive graphics capability, computer aided engineering systems for conceptual design have not established a pivotal role. Reasons for apprehension in extensively integrating such systems stem from the fact that the conceptual design process is not strictly a logical and sequential series of events, thus coming into conflict against the rigid structure dictated by computer programming. Another reason is the plain fact the programs and algorithms producing the prediction during minimum goal formulation are not totally transparent, therefore the results are tacitly accepted or met with great scepticism such that more time is expended in justifying the result than the time it took to conduct the original analysis. This suspicion becomes even more pronounced whenever multi-parametric sensitivity studies take place. Owing to the quite complex interaction between the multitudes of design variables, the physical relationships between disciplines become difficult to comprehend. The final difficulty lies with the feeling the software is "designing" the aircraft as opposed to the designer because the perception is the tool requires minimal input from the human in the loop and the final vehicular design is deemed immediately invalid. This phenomenon is sometimes ignominiously referred to as the "black-box" solution.

Notwithstanding these foibles, computer aided aircraft conceptual design can produce significant benefits. These include greater throughput of design feasibility studies for a given period, an ability to dramatically expedite the response time for projects that emerge unexpectedly, an ability to generate a marked improvement in design quality and the number of concurrent design projects undertaken for given resource level, possibility in promoting a reduction in development cost for the project as it matures, and the likelihood of undertaking a more sophisticated larger scale design problem is not possible with the traditional greatly simplified handbook methodologies. For this reason, significant energy is expended in developing new software packages that can deliver these tangible benefits whilst avoiding the pitfalls discussed earlier. At this moment in time, a number of conceptual design codes are commercially available, however, the frequency of competing software platforms is not vast since airframe manufacturers have a propensity to develop

their own algorithms in–house. In order to serve as a benchmark indicating the level of sophistication currently available to designers, a synopsis of contemporary commercially available software is presented below.

PIANO

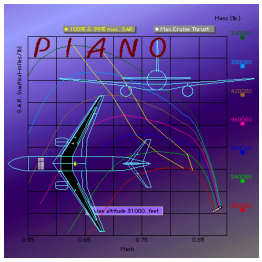

Developed by Simos[23] and distributed by Lissys Ltd., the Project Interactive ANalysis and Optimisation software package is publicised as being a complete aircraft design program. The scope for analysis includes geometry, weights, aerodynamics and a somewhat broader (yet still simplified) range of performance estimation capability compared to other products. The basic theme for PIANO is the conventional commercial transport adhering to FAR Part 25 certification; however, business aircraft can be designed if other sources are utilised for missing information or analysis capability. Currently, the software's clientele list is not extensive, yet includes well-known airframe manufacturers, engine manufacturers, and governmental and research institutions. One major drawback is that PIANO only executes on the Apple Macintosh and is currently not portable to any other platform.

AAA

The origins of DARcorporation's Advanced Aircraft Analysis stem from the multi-volume and quite comprehensive texts, Airplane Design, Parts I-VIII[5] and Airplane Flight Dynamics Parts I and II, authored by Roskam. AAA incorporates and coordinates the methods, statistical databases (now quite dated), formulas, and relevant illustrations and drawings from these references. The AAA program allows the design engineer to rapidly evolve an aircraft configuration from early weight sizing, through open loop and closed loop dynamic stability and sensitivity analysis, while working within regulatory and cost constraints. The software applies to civil and military aircraft including unconventional configurations.

RDS-Professional

RDS marketed and supported by Conceptual Research Corporation (CRC) is an aircraft design, sizing and performance software package with very basic drafting functions. An emphasis is placed on conducting very rapid feasibility studies. In fact the author claims it allows the development, assessment, and optimisation of a new notional design concepts in as little as a day. The algorithm methods reflect primarily the widely used textbook by Raymer[4], Aircraft Design: A Conceptual Approach. The package is adequate for early design and requirements trade studies, and has a number of automated capabilities for producing key graphs and figures documenting the trade study results. The program facilitates cost analysis, as well as airline economics.

ACSYNT

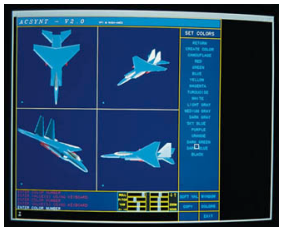

Available from Phoenix Integration, Inc., this code is intended for aircraft sizing and optimisation/mission analysis[24]. Working closely with airframe and engine manufacturers, Ames formulated the basic AirCraft SYNThesis tool. In 1987, Ames and the Virginia Polytechnic Institute CAD Laboratory began to design and code a Computer-Aided Design (CAD) system for ACSYNT. The product of this collaboration is a high-end aircraft design tool that provides a three-dimensional computer-aided design environment coupled with detailed analysis capabilities. An aircraft concept can be modelled in the CAD interface, and then analysed using a suite of multi-disciplinary modules representing aerodynamic, propulsion, and mission performance parameters. ACSYNT has been successfully applied to high-speed civil transport configurations, subsonic transports, and supersonic fighters. The entire package does offer a vast array of functionality, but necessitates a significant investment in time and effort to use it effectively. In view of this characteristic, ACSYNT is not a software platform for all aircraft designers.

1.7 Decision Support Systems

There are examples of work done in the field of Decision Support Dystems (DSS) for engineering design and much of the work is focused on presenting design axioms or advice to designers on how to design[25]. These approaches require the investment of considerable time to capture the knowledge into forms that can be accessed and subsequently provide the designer with suitable advice. A sophisticated study conducted by Eaglesham[26] has extended the conventional DSS concept for engineering and added the further dimension of costs related to the manufacturing of advanced composite components, thus providing a means to access the information that companies already have, but have in the past found difficult to use in meaningful ways during the design selection process.

Ideally, even a rudimentary design decision support systems should take advantage of the data a given airframe manufacturer has accumulated about the various aerospace disciplines. It is this type of information most companies attempt to purchase “off-the-shelf” with commercially available conceptual design packages. It comes as no surprise they find the application somewhat short of expectations because various methodologies and design driver philosophies are not necessarily reflected in the package, and as is commonly the case, in direct conflict with the manufacturers perception of what is appropriate. The key to successfully fulfilling this requisite is to integrate engineering design knowledge into a format similar to how contemporary business information systems deal with knowledge discovery, i.e. statistical correlation and visual cues indicating zones relevance or consequence.

A suitable amount of effort should be expended in establishing some semblance of a DSS infrastructure to permit possibilities of incorporating more elaborate functionalities with relative ease in the future. Apart from addressing issues of “error-trap” type messages and warnings that simply instruct the designer of an impending questionable basis for the analysis, a minimum goal should be at least imparting to the designer information showing how the aircraft fits in the historical trend and what room for pragmatic improvement is available compared to their own preconceptions of what is valid.

1.8 Objectives, Scope and Thesis Structure

The fundamental research questions are: How can existing methods for conceptual design prediction and limited optimisation be significantly improved upon, and, to what

extent could an improved aircraft design be produced thereafter?

Based on the posed questions, a number of principal aims were generated to serve as solidifying the purpose of the research. The core research objectives can be summarised as such:

To assess the needs of aircraft designers and produce new and improved algorithms by analysing the scope of analysis tools necessary for them to execute contemporary conceptual design analysis objectives in an effective and expedient manner. To propose new aircraft design proposals in an attempt to highlight new market niche possibilities; this task also has the dual purpose of demonstrating a software package developed from the conceptual design theoretical work.

This initial aim was to completely re-examine the type of analytical tools utilised in predictions during conceptual design of aircraft. This was mostly realised by exploring the merits of an alternative analytical basis for the calculation of atmospheric properties, weights, power plant performance, aerodynamics, operational performance, and, DOC and P-ROI prediction. Emphasis was also placed on deriving a unified analytical treatment not only to demonstrate relevance in the computed result, but also accommodate a deeper insight into the design problem at hand. The goal was to gain an understanding that would implicitly orientate the designer to achieving a truly balanced aircraft conceptual design. To complement this effort, a follow-on objective was to verify the accuracy of the above-mentioned new techniques against published results of contemporary vehicles. A focus is placed on turbofan regional aircraft in the ensuing discussions, however, it should be highlighted that all presented research is generally applicable for any gas-turbine based propulsion systems with propeller power or jet thrust output as well as any size class of transport vehicle. A strong mathematical basis has been identified as the mainstay to achieving the intended result, with an onus placed on converting traditionally discrete analytical expressions by continuous differentiable functions open to solution for conditions of optimality. This unique approach gives facility to transform the typical conceptual design optimisation problem from the interaction of a sometimes esoteric array of merit functions to definitions of feasibility using tangible dependent variables having a physical meaning.

The next milestone of this research was to produce a new and unique conceptual aircraft design tool that emphasises the designer’s role during the synthesis process. By virtue of setting this ultimate goal meant the selection of an appropriate software environment to work in. The software system requirements also include a modular and robust construct to ensure future development with relative ease, and possibly as the most important consideration, revolves around issues of portability as well.

The third and final goal was to demonstrate the speed and effectiveness of the software package that embodies the theory developed in this work by conducting actual conceptual design studies of two regional and one business transport aircraft examples.

These core objectives can subsequently be itemised into a series of sub-objectives, namely,

- Review of the various new models developed for atmospheric properties, geometry, weights, gas-turbine engine performance, aerodynamic characteristics and operational performance qualities coupled to DOC/ P-ROI objective functions;

- Include discussion of Quick Conceptual Aircraft Research and Development (QCARD) software package as a new and unique design tool, and a brief overview of the concept behind hidden and explicit design DSS framework in the QCARD system;
- Implementation of methods to predict stability and control characteristics (Mitchell code) and to subsequently couple this subspace into the QCARD system;
- Facility to support constrained multi-objective optimisation using Genetic Algorithms (GA), or, Nelder-Mead Simplex search, or, a strategic combination of both in QCARD system; and,
- To draw together all the published theories, principles and design software package and conduct practical design examples ideally targeting market segments that are quite broad and distinct from one another.

This PhD thesis consists of a comprehensive introductory note concerning the development and rationale behind new conceptual design prediction methodologies and systematically expounds the theories themselves, including an explanation of scope and applicability therein. The intention is for this body of text to act as a precursor to a summary of four selected papers that focuses on an overview of the methodology, practical application of the developed methods on three conceptual design exercises and a comprehensive examination of objective functions related to costs and profitability with respect to flight technique formulation of commercial transports.

Paper I, “Methodology for Conceptual Design and Optimisation of Transport Aircraft”, introduces the notion of an impulse function used to produce differentiable continuous expressions out of normally discrete processes, and, to construct maximising and minimising functions. In addition, new prediction methods for atmospheric properties, gas-turbine engine performance, high and low speed aerodynamic characteristics, and, operational performance qualities coupled to DOC and maximum P-ROI objective functions were also presented. A discussion of methods to identify optimal performance and subsequently formulate operationally permissible climb, cruise and descent control techniques was expounded, including a review of the Optimum Trajectory Profile Algorithm (OTPA) borne from a collection of work discussed above. Coupled to this was an introductory note to a new method for DOC and P-ROI optimisation with respect to predicted operational performance. It was rounded-off with a presentation of the PD340-3X, a 31-34 PAX commuter turbofan aircraft conceptual design.

Paper II entitled, “Design and Optimisation of a 19 PAX Turbofan Regional Transport”, solely covers the conceptual design of the PD340-2, a new 19 PAX turbofan commuter aircraft. The PD340 project design study was conducted for Williams International with support from Saab AB, Karlebo Aviation AB and KTH. The technical paper had a dual purpose of detailing the viability of targeting a new market niche and to act as a demonstration of the author’s initial array of prediction methods’ inherent capabilities. The conceptual design utilised Williams-Rolls Inc. FJ44-2A small turbofan engines and adhered to maximum commonality with Saab Aerospace Saab 340 aircraft. The design ended up with competitive field performance and comparable reference speeds to turboprops and was set a minimum goal of climbing to altitudes at least 10000 ft higher than contemporary turboprops with reasonable time-to-climb to initial cruise altitude. In conjunction with cruise at speeds targeted to be around 50% faster than turboprops, a potential to generate around three times the maximum profit at optimal stage length was also found.

Paper III, “High-Performance Executive Transport Design Employing Twin Oblique Lifting Surfaces”, entails a description of TOLS-X aircraft conceptual design, a new Trans-Atlantic 19 PAX executive transport able to cruise up to low supersonic speeds. Here, the concept of Twin Oblique Lifting Surfaces (TOLS) configuration was first introduced, and preliminary evidence was given to motivate the aerodynamic suitability for high-transonic and low-supersonic operation. Owing to the unique nature of such configurations, a new method to quantify vortex-induced drag factor for TOLS type configurations was presented. Also proposed was the concept of the BR-71X engine: a modified BMW Rolls-Royce BR-715 power plant suitable for operation up to low super-sonic speeds. The TOLS-X vehicle minimum goals were characterised by the largest cabin volume compared to contemporary large and smaller super large business jets, and TOLS-X was found to possess a similar SAR efficiency to the Gulfstream GIV-SP yet at much faster speeds while having an ability to operate out of typical corporate airfields.

The final manuscript, Paper IV, “Identifying Economically Optimal Flight Techniques of Transport Aircraft”, details a comprehensive treatment of how to identify optimal flight techniques with respect to DOC and P-ROI for given sector mission criteria and assumed reference time frame utilisation. A series of new models used to accurately simulate maintenance and material costs, block fuel expenditure and revenue were introduced. One salient conclusion from the theory was hourly-based utilisation results in faster block speeds tending towards the minimum block time threshold, whereas, the fixed departures scenario yields a slower yet congruous flight technique optima requirement for DOC and P-ROI objectives. As an alternative for optimality, a new speed schedule definition called Economical Long Range Cruise (ELRC) was created to replace the traditional 99% maximum SAR LRC speed. To complement this, a new merit function called Operational Flexibility Index (OFI) was derived to enable transparency of what en route operational qualities a given aircraft exhibits. Merit parameters that give rise to the ability of sub-optimising for more desirable P-ROI characteristics were also presented, and details were given showing how the methodology may be integrated to facilitate the optimisation of conceptual aircraft designs. To complete the paper, worked examples for 50 PAX regional aircraft, namely, two turbofans and one high-speed turboprop were also discussed.

2 Formulation of a New Project Design Specifications

One of the most difficult tasks in the competitive environment of aircraft manufacturing and sales is to produce a vehicle that employs a particular mix of design specifications, i.e. amenities, performance, efficiency and flexibility, at a price the market is willing to absorb. Rather than the questionable approach of a technology-driven edict solely dictating what makes sound economic sense, there exists a vital requirement that some sort of impartial methodology can be utilised such that both engineering and strategic product development departments can plan for new design proposals with some confidence. It should not be disputed that the market sets the price of all aircraft products. Factors such as reliability, maintainability, utility, perceived safety, efficiency, operating costs, brand name loyalty and aesthetics affect the propensity for a customer to purchase an aircraft. In addition, it is erroneous for one to postulate that costs associated with research, design, testing, manufacturing and certification play a significant role in setting price; in the long run it is the market that dictates price.

2.1 Establishing the Value of Performance and Amenities

A significant amount of effort has been expended in addressing the issue of aircraft price and value. Work conducted by Timmons[27] through the so-called "Comfort Index", defined as the cabin volume multiplied by maximum range, was one of the first attempts and can be considered the basis for a contemporary need in using analytical and statistical techniques in understanding the economic advantage of aircraft. Norris[28] introduced an alternative figure of merit suited more for commercial transports called the "Value Factor" to observe trends against aircraft price. This parameter is defined as the product of vehicle daily productivity, available passenger space and passenger headroom divided by the amount of expended fuel per day.

Narrowing the list to those parametric expressions that exhibit the best qualities to perform a thoughtful prediction analysis, Killingsworth and Wolz[29] showed a correlation between the price of business jets and a productivity index defined as the product of speed, range and cabin volume. A notable contribution also includes investigations conducted by Moghadam and Farsi[30]. They examined the cost of performance for multi-engine gas-turbine business aircraft and established a trend exists between aircraft price and their own parametric construct coined "Performance Index" that represents a market-based measure of aircraft performance. This parametric expression is defined as the cabin volume multiplied by maximum fuel range, maximum fuel speed and maximum fuel payload divided by the Takeoff Field Length (TOFL).

After reviewing the array of suggested methods that map market trends, an adequately descriptive parametric productivity index (PI) was found to be an equation first proposed by Allied Signal Aerospace[31]

$$PI = \frac{M_{LRC}\, R_{LRC}\, V_{cab}}{B} \tag{1}$$

where M_{LRC} is the aircraft typical LRC Mach number, R_{LRC} represents the maximum achievable range at LRC speed and carrying the aircraft standard PAX complement, V_{cab} is the cabin volume, or alternatively expressed as the product of cabin cross-sectional area (A_{cab}) and cabin length (l_{cab}), and B equals the TOFL. This parametric equation promotes suitable trend progression and by virtue of this characteristic, can be utilised to identify

pockets of coverage not currently serviced by contemporary aircraft. This also includes the possibility of more dramatically, identifying new market niche opportunities. Based on known business aircraft data, Figure 2 elucidates the potential this methodology offers for prediction work.

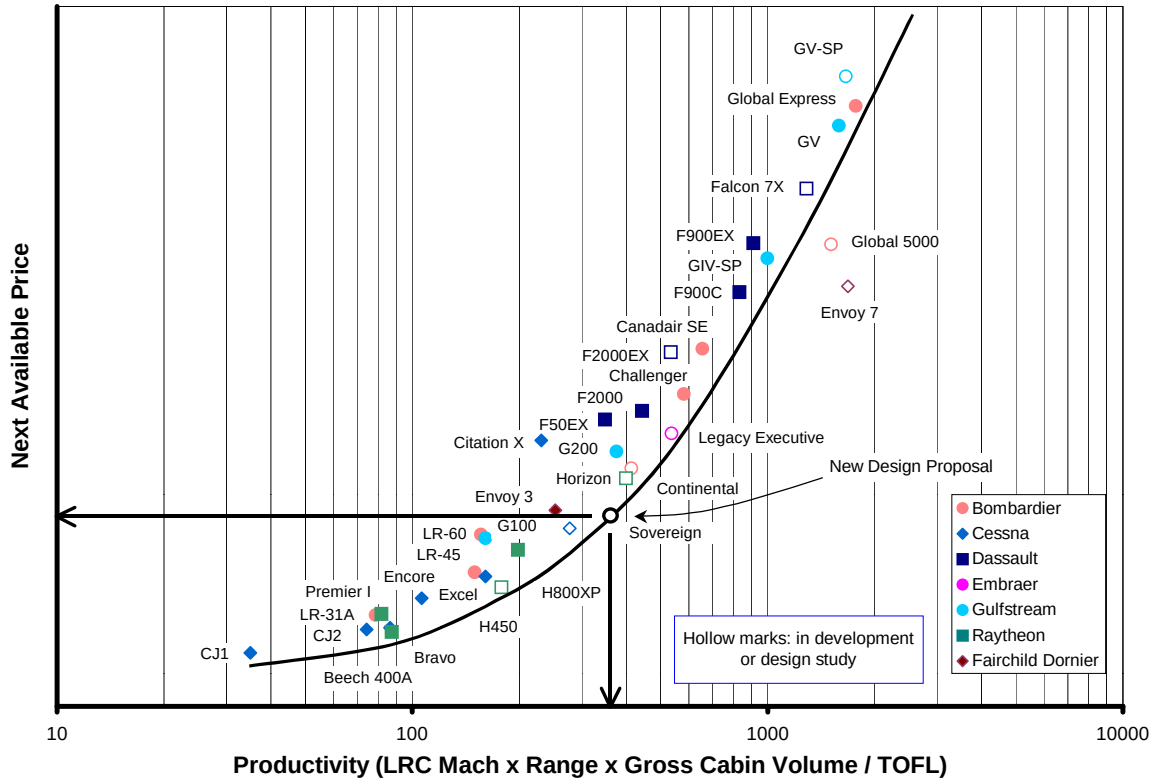

Figure 2. Chart indicating the value of performance and amenities for business aircraft using a parametric productivity index.

2.2 Constructing the Airframer Paradigm

As a complementary toolkit for the market niche identification equation given by Eq. (1), the next step requires finding a method where price can be quantified based on a given combination of design specifications with suitable assurance. One way this task can be accomplished is through the use of Geometric Programming. First discovered by Claurence Zener of Westinghouse in 1961, the original goal of Geometric Programming was to permit a computationally convenient non-linear optimisation technique, which even in a restricted form would offer a number of advantages over conventional techniques based on classical calculus. Zener noted that the sum of component costs of a process sometimes can be minimised almost by inspection provided these costs are functions of the product of the variables involved in each cost term, with each of the variables raised to arbitrary real exponents. One example of the method's success is cited based on McMasters'[32] work of using this mathematical technique in finding solutions to various optimisation problems related to aircraft performance.

In order to exploit the potential benefits of adopting the Zener approach, a new primal objective function construct known hereon as the Airframer Paradigm was created in an effort to ascertain how much a given set of design specifications are worth to the market. Recognising that a given aircraft manufacturer intrinsically defines its own unique primal objective function (in this instance referring to aircraft price), a multivariate model based

on the build-up and summation of component "costs" of an assembly (or macroscopic aircraft design objective functions) can be constructed. Through experimentation one suggested form that showed promise was

$$\Gamma = f_1 \, R_{LRC}^{w_1} + f_2 \, B^{w_2} + f_3 \, V_{cab}^{w_3} + f_4 \, S_{cab}^{w_4} + f_5 \, M_{MCRZ}^{w_5} \tag{2}$$

Γ is the aircraft price, S_{cab} represents the cabin slenderness ratio given by cabin length divided by the addition of cabin width and cabin height, or $S_{cab} = l_{cab} / (w_{cab} + h_{cab})$, and, M_{MCRZ} is the maximum cruise Mach number.

As a general curiosity, it would be of interest to examine the sensitivity of the paradigm equation assuming various combinations of design specifications. A more insightful investigation could be identification of what direction in its domain Γ increases most rapidly at a given design variable combination $P_o(R_{LRCo},B_o,V_{cabo},S_{cabo},M_{MCRZo})$. The importance of this posed question becomes quite evident if one considers point P_o in the domain represents a known baseline aircraft design. If the partial derivatives of the primal objective function $\Gamma(R_{LRC},B,V_{cab},S_{cab},M_{MCRZ})$ are defined at $P_o(R_{LRCo},B_o,V_{cabo},S_{cabo},M_{MCRZo})$, then the gradient of Γ at P_o is the vector

$$\nabla\Gamma = f_1 \, w_1 \, R_{LRC}^{w_1-1} \, \underline{i} + f_2 \, w_2 \, B^{w_2-1} \, \underline{j} + \vartheta_{cab} \, \underline{k} + \Theta_{cab} \, \underline{l} + f_5 \, w_5 \, M_{MCRZ}^{w_5-1} \, \underline{m} \tag{3}$$

and is obtained by evaluating the partial derivatives of Γ at P_o. Recalling the partial derivatives for cabin volume and cabin slenderness are themselves compound functions of cabin metrics, a series of conditional partial derivatives need to be defined, thus giving some freedom in electing what design variables shall be observed for sensitivity studies.

Initially one can examine the partial differential

$$\vartheta_{cab} = \Gamma_{V_{cab}} = f_3 \, w_3 \, V_{cab}^{w_3-1} \tag{4}$$

for an independent V_{cab}, otherwise,

$$\vartheta_{cab} = \Gamma_{l_{cab}} = f_3 \, w_3 \, A_{cab}^{w_3} \, l_{cab}^{w_3-1} + f_4 \, w_4 \, \frac{l_{cab}^{w_4-1}}{\left(w_{cab} + h_{cab}\right)^{w_4}} \tag{5}$$

for an independent l_{cab}. Furthermore,

$$\Theta_{cab} = \Gamma_{S_{cab}} = f_4 \, w_4 \, S_{cab}^{w_4-1} \tag{6}$$

for an independent S_{cab}, or, $\Theta_{cab} = 0$ for an independent l_{cab}.

In order to appreciate how much the function Γ changes for excursions from point P_o to a another point, the rate change of Γ is calculated by multiplying the directional derivative of Γ by **u**, which is the direction of the tendency away from P_o. The direction of the tendency towards another point from baseline P_o is algebraically described by the unit vector $\mathbf{u} = \nabla F / | \nabla F |$.

As an example of the perceptive power the Airframer Paradigm can produce, a sensitivity study of Gulfstream Aerospace's product range of G100, G200, GIV-SP, GV

and GV-SP business jets was conducted in order to establish the design specification drivers typified by Gulfstream aircraft in the business jet market place. Assuming Gulfstream Aerospace produce derivative and clean sheet aircraft proposals using the GIV/GV fuselage cross-section, the most influential parameters to an equipped aircraft price the market is willing to absorb is chiefly a function of range and cabin length. Figure 3 illustrates this sensitivity, and as a validation exercise, an equipped aircraft price for the new GV-SP business jet was predicted. As annotated in the chart, a prediction of USD 43.0 million, subsequently incremented in price for Enhanced Vision System (EVS) to be equipped as standard, and incorporating an adjustment to reflect 2003USD (GV-SP entry-into-service planned for fourth quarter 2003) produces a total of around USD 45.0 million. This figure appears to mimic the currently quoted price found in aviation media[33].

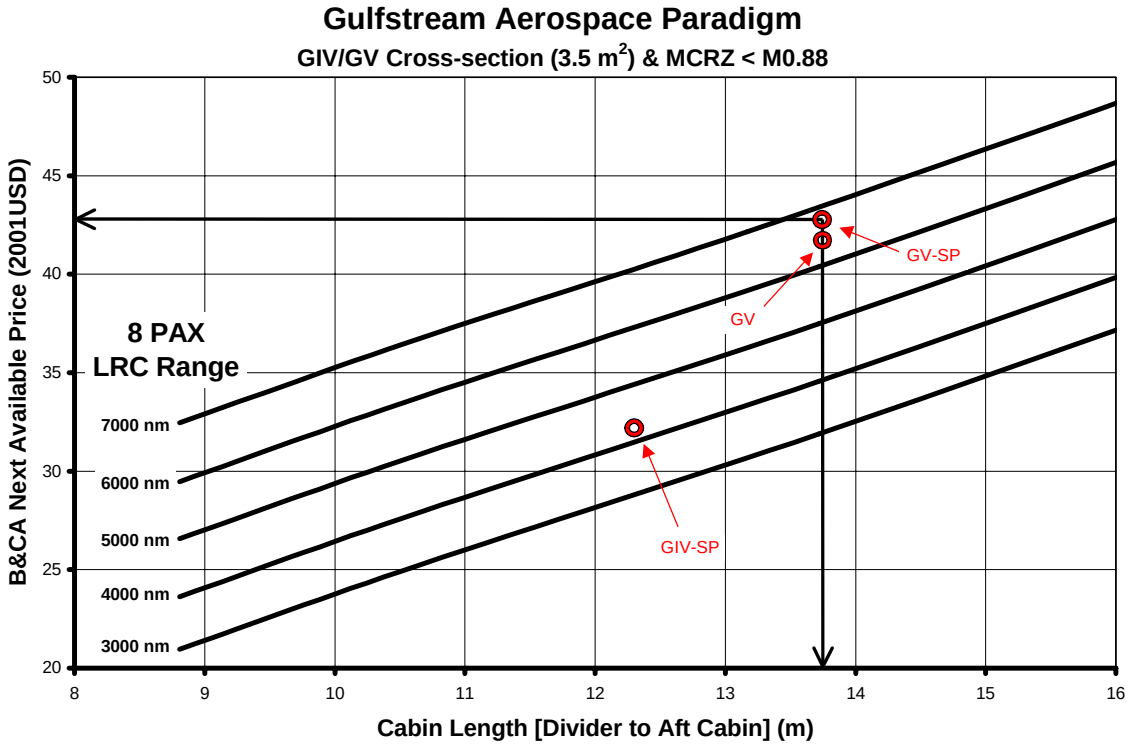

Figure 3. Sensitivity study of next available price in relation to maximum range and cabin length for Gulfstream Aerospace business jets.

By combining the market niche identification method with paradigm prediction, the possibility now arises in finding a sequence of design specifications that meet both a targeted PI and aircraft price. Although the presented methods have been illustrated using business aircraft data, this does not exclude validity for commercial transports as well. In lieu of a more suitable parametric association, the PI given by Eq. (1) can still be used for commuters, regionals, narrow-bodies and wide-bodies as a tool for market niche identification. Furthermore, the Airframer Paradigm given by Eq. (2) and the accompanying protocol for sensitivity studies can be considered as being universally applicable for all transport aircraft types.

3 Mathematical Foundations: Concept of an Impulse Function

A traditional conceptual study revolves around analysis that is predominately discrete in nature. This can become quite cumbersome and impractical especially when typical conceptual design performance assessments even at the most elementary level can consist of hundreds or even thousands of point calculations, each requiring an instantaneous estimate. Additionally, this philosophy denies the possibility of conducting analytical performance optima identification via single expression algorithms, thereby, in an effort to reduce complexity; it compels the use of coarser numerical integration procedures or closed form approximations prone to large errors.

3.1 Mathematical Formulation and Governing Rules of Operation

By introducing the concept of an impulse function or unit step, normally discrete procedures of analysis can be transformed into continuous differentiable equations. The step input function represents a jump discontinuity and the idea is to promote an instantaneous change in the reference analytical expression according to specific requirements. The mathematical representation of a step function is

$$f(x) = \begin{cases} 1 & \forall\, x > 0 \\ 0 & \forall\, x < 0 \end{cases} \quad \text{or} \quad f(x) = \Phi_x \tag{7}$$

where $\Phi_x = \Phi(x,x_s)$ is the impulse function and the function is not defined at $x = 0$. A mathematical approximation of the jump discontinuity can be proposed as

$$\Phi(f, f_s) = k_1 + k_2 \tanh[k_3(f - f_s)] \tag{8}$$

where the coefficients k_n represent values which assist in modelling an idealised unit step, and, the variables f and f_s are the tested and critical values respectively. Suitable values for these constants were found to be $k_1 = 0.5$, $k_2 = 0.5$ and $k_3 = 110$. Figure 4 illustrates the concepts behind both the idealised jump discontinuity and its analytically approximate counterpart. As an example of this impulse function utility, consider the operator $\Phi(10,20)$, which results in 0, or conversely, $\Phi(20,10)$ is 1.

It can be discerned the approximate unit step expression does invoke some degree of error with respect to the idealised function. This phenomenon is taken to be an advantageous occurrence because instead of modelling an abrupt change in characteristics, properties are more realistically resolved as a transition. This notion can be exemplified by modelling of the atmosphere where transition in flight level between the troposphere and the tropopause takes place. The progression between a linear temperature ratio lapse to a constant one is not surmised to happen instantaneously but rather is intuitively expected to occur progressively. The impulse function or approximate unit step aids in simulating this intuitive analogy.

The rules of differentiation concerning the impulse function are assumed to conform approximately to standard results produced by the derivative of a constant

$$\frac{d\Phi_x}{dx} \cong 0 \quad \text{and} \quad \frac{d}{dx}(\Phi_x x) \cong \Phi_x \tag{9}$$

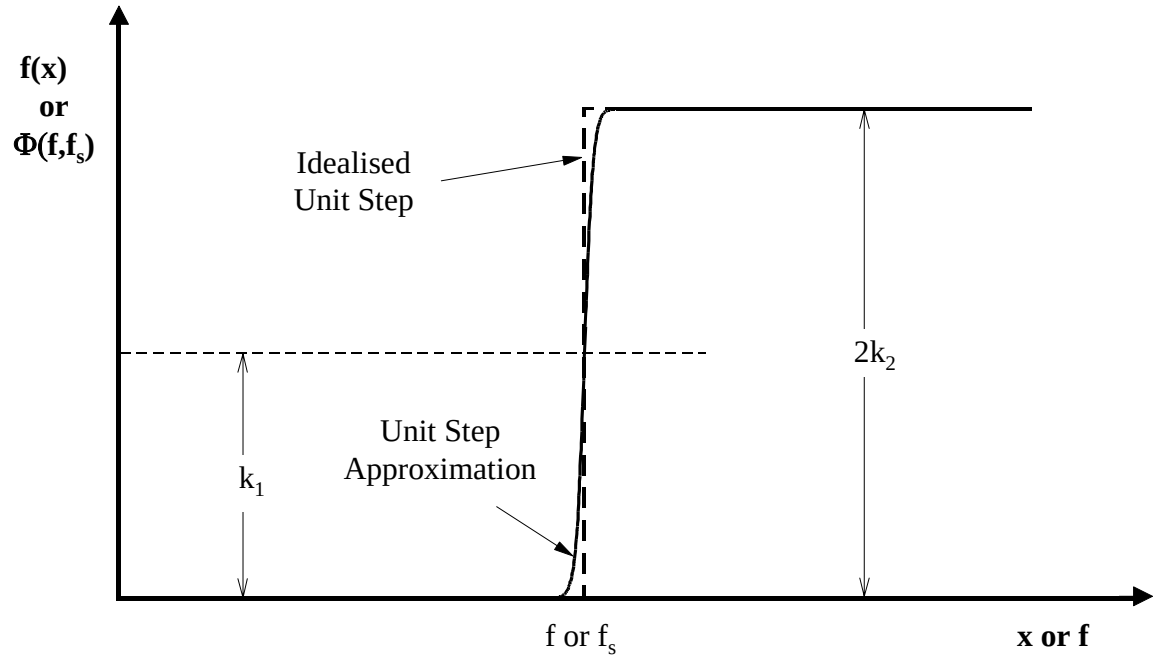

Figure 4. The idealised unit step function compared to a mathematical approximation.

3.2 Identification of Maxima and Minima Using the Impulse Function Approximation

Many instances arise in conceptual prediction that necessitates identification and subsequent introduction of maxima and minima values for the end result. This aspect hinders adherence to the continuous function edict because expressions already geared to accommodate continuous properties may lose this status by becoming discretised during the identification process. Fortunately, the aforementioned approximate unit step philosophy can be extended for identification of maxima or minima between quantities as well. A maximising function Φ_{max} can be produced via the associative rule

$$\Phi_{max}(a,b) = a\,\Phi(a,b) + b\,\Phi(b,a) \tag{10}$$

whereas, a minimising function Φ_{min} between the tested values a and b is of the form

$$\Phi_{min}(a,b) = a\,\Phi(b,a) + b\,\Phi(-b,-a) \tag{11}$$

3.3 Exponential Interpolation for Integrated Computations

A third and final utility produced by the unit step function operator is the ability to conduct interpolation or extrapolation of results using exponential curve fitting. This can be considered as a very powerful tool especially when a number of discrete calculations are produced from a series of step sizes and an integrated solution which lies within a particular interval is desired. A closed form expression capable of delivering such an integrated solution with accuracy was achieved by combining exponential interpolation with unit step functions, the latter basically “switching” on or off intervals of relevance. If one considers a number of intervals (i) bounded by discrete independent quantities n_{i-1}, n_i, n_{i+1}, n_{i+2}….., with corresponding computed results of m_{i-1}, m_i, m_{i+1}, m_{i+2},….., respectively,

a general system of equations for this series of i intervals using the premise of exponential regression can be constructed, i.e.

$$m_{i-1} = j_i e^{k_i n_{i-1}} \quad i = 1,2,3,..... \tag{12}$$

$$m_i = j_i e^{k_i n_i} \quad i = 1,2,3,..... \tag{13}$$

By solving for the coefficients of proportionality, j_i and k_i, an interpolated estimate of the integrated solution, say at $n_{i+1/2}$, would be given by the formula

$$\begin{aligned} m_{i+1/2} = & \left\{ \Phi\left(n_{i+1/2}, n_{i-1}\right)\Phi\left(n_i, n_{i+1/2}\right) m_{i-1}\left(\frac{m_i}{m_{i-1}}\right)^{\left(\frac{n_{i+1/2}-n_{i-1}}{n_i-n_{i-1}}\right)} \right\} \\ & + \left\{ \Phi\left(n_{i+1/2}, n_i\right)\Phi\left(n_{i+1}, n_{i+1/2}\right) m_i\left(\frac{m_{i+1}}{m_i}\right)^{\left(\frac{n_{i+1/2}-n_i}{n_{i+1}-n_i}\right)} \right\} \\ & + \left\{ \Phi\left(n_{i+1/2}, n_{i+1}\right)\Phi\left(n_{i+2}, n_{i+1/2}\right) m_{i+1}\left(\frac{m_{i+2}}{m_{i+1}}\right)^{\left(\frac{n_{i+1/2}-n_{i+1}}{n_{i+2}-n_{i-1}}\right)} \right\} + ... \end{aligned} \tag{14}$$

with the final solution found from a rationalised form of Eq. (14)

$$m_{i+1/2} = m_i\left(\frac{m_{i+1}}{m_i}\right)^{\left(\frac{n_{i+1/2}-n_i}{n_{i+1}-n_i}\right)} \tag{15}$$

This occurs because interval boundaries that fall outside a coupled boundary constraint of i and i+1 for an i+1/2 estimate produce unit step operator results of zero. It can be observed that $\Phi(n_i,n_{i+1/2}) = 0$ for interval i-1 and i, and, $\Phi(n_{i+1/2},n_{i+1}) = 0$ for interval i+1 and i+2. In contrast, a factored result between $\Phi(n_{i+1/2},n_i) = 1$ and $\Phi(n_{i+1},n_{i+1/2}) = 1$ is equal to one thereby defaulting the interpolation for interval i and i+1 only. A practical example of a closed form expression that produces estimates of integrated results would be the calculation of climb time, fuel and distance to specified flight level. If for instance, the analyst wishes to estimate these dependent variables at service ceiling, a chained equation in the form of Eq. (14) can be constructed for each separate dependent variable assuming an All-Up Weight (AUW) with service ceiling flight level as the input parameter alone, hence, giving scope to estimate the integrated solution.

intentionally blank

4 The International Standard Atmosphere

A fictitious set of values established by international agreement postulated to be representative of the variation with altitude of physical properties of air is known as the International Standard Atmosphere (ISA). The atmosphere's chaotic behaviour does not permit the ISA model to adequately predict actual conditions anywhere at any given time, but contemporary performance presentations of aircraft at a given altitude are always quoted with respect to the Standard Atmosphere.

4.1 Nomenclature Describing Atmospheric Properties

Atmospheric properties of major importance for the scope of this study include the variation of temperature (T), pressure (ϖ), density (ρ), speed of sound (a), coefficient of viscosity (μ) and kinematic viscosity (ν) with height above the Earth's surface. When quantifying these properties it is useful to refer to relative values which in each case are local values divided by the sea level value. Sea level standard values are denoted by the suffix sls.

The static pressure ratio $\delta = \varpi/\varpi_{sls}$ is related to temperature and density variation in the following manner

$$\delta = \theta\,\sigma \tag{16}$$

where $\theta = T/T_{sls}$ is defined as the absolute temperature ratio and $\sigma = \rho/\rho_{sls}$ the corresponding density ratio at given flight level. The coefficient of viscosity is defined by measuring the kinematic viscosity of a gas to its density

$$\mu = \nu\,\rho \tag{17}$$

The parameter ν is equal to 1.46×10^{-5} m^2/s at sea level standard conditions. Local sonic velocity variation is related to temperature lapse rate by the following formula

$$a = a_{sls}\,\theta^{1/2} \tag{18}$$

where a_{sls} is the speed of sound value at sea level standard conditions.

As an addendum, operational concerns dictate that adequate modelling of these properties should be permitted not only for the idealised Standard Atmosphere, but more poignantly, for any subsequent temperature deviations from this reference.

4.2 Modelling Temperature Variation

It has been demonstrated[34] temperature decreases linearly with flight level. This premise holds true within the troposphere, and when surpassed, temperature remains approximately constant with increasing flight level up to about FL 700 or the lower part of the stratosphere. This altitude can be considered as an upper threshold of flight level well in excess of those frequented by contemporary subsonic transport aircraft. A continuous function concept for temperature variation is quite difficult to achieve with contemporary methods of representation due to the existence of a tropopause discontinuity. By incorporating an impulse function to mimic commencement of the tropopause, i.e. $\Phi_{trop} =$

Φ(h,FL 361), the lapse rate for temperature ratio (θ) as a function of flight level (h) and International Standard Atmosphere temperature deviation (ΔISA) is proposed here as

$$\theta = 1 + \frac{\kappa \Phi_{trop} \left(k_1^{\theta} h + k_2^{\theta} \right) + k_3^{\theta} \Delta ISA - h}{\kappa} \qquad [FL\ 0,\ FL\ 700] \qquad (19)$$

where the coefficients k_1^{θ} = 6.900 x 10^{-4} per FL, k_2^{θ} = -0.2480, k_3^{θ} = 5.046 FL/^{o}C and κ = 1454 per FL would be used in order to model the International Standard Atmosphere or any given temperature deviations from ISA.

4.3 Density

For the standard atmosphere, the atmospheric hydrostatic relation[34] equates density ratio lapse as some exponential function of temperature ratio. By introducing the influence of the tropopause, variation of density ratio for ISA can be expressed as

$$\sigma_{ISA} = \theta_{ISA}^{4.2561} + \Phi_{trop} \left(k_1^{\sigma} \ln h + k_2^{\sigma} \right) \qquad (FL\ 0,\ FL\ 700] \qquad (20)$$

By facilitating this with an enhancement that accounts for any arbitrary temperature deviation from ISA, the density ratio is therefore given by

$$\sigma = \frac{\theta_{ISA}\ \sigma_{ISA}}{\theta} \qquad (FL\ 0,\ FL\ 700] \qquad (21)$$

where the coefficients k_1^{σ} = -0.4398 and k_2^{σ} = 2.583 and κ = 1454 per FL would be used in order to model the International Standard Atmosphere or any given temperature deviations from ISA.

4.4 Coefficient of Viscosity

A physical quantity important for the calculation of Reynolds number used for drag prediction is the coefficient of viscosity (μ) at given flight level. This property increases with temperature thus falls steadily with flight level until the tropopause is reached and becomes constant in the stratosphere. Various formulae have been produced and a useful one was found to be Sutherland's[35] empirical expression which models the variation of flight level with temperature ratio.

$$\frac{\mu}{\mu_{sls}} = \frac{1.383}{\theta + 0.383} \theta^{3/2} \qquad [FL\ 0,\ FL\ 700] \qquad (22)$$

The parameter μ_{sls} is equal to 1.79 x 10^{-5} kg/ms at sea level standard conditions. The formula given by Eq. (22) is a continuous function and is applicable for all ambient temperatures up to and including 2500 K.

5 Geometric Definitions

For all aircraft design proposals, a good deal of importance must be placed on an accurate definition and subsequent analysis of geometric attributes. This statement is supported by the basic fact the entire scope of intermediary and final objective function evaluations, i.e. design weights, aerodynamics, performance, etc., stem from a fundamental geometric description leading to a physically tangible outcome. In view of this circumstance, it becomes crucial to have some semblance of accuracy with respect to geometric description and analysis even at the conceptual design level of engineering analysis. This particular section not only presents a review of the best practises and conventions in terms of geometry, but also offers alternate methodologies in describing complex assemblies with greater accuracy than has been achievable using the traditional handbook approach. The new algorithms do appear to employ a step up in level of sophistication compared to the traditional approach, but this is deceptive since the increase in sophistication is dependent upon an addition of some previously ignored general set of design variables.

5.1 An Overview of Equivalent Reference Wing Conventions

The equivalent wing concept is a representation of actual cranked wings by a fictitious planform that extends towards the fuselage centre-line. For the sake of simplifying the array of main design parameters that need to be considered for sizing and optimisation, the overall aerodynamic characteristics of a vehicular configuration with cranks or notches in the planform geometry are replaced by a suitable representative, namely, an equivalent trapezoid. All aerodynamic computations are non-dimensionalised with respect to the reference wing area and associative aerodynamic design parameters. Since each semi-wing geometry is simplified into a straight-tapered trapezoidal shape with no crank (constant sweep), the complexity of design variables is somewhat rationalised into a more manageable and therefore comprehensible level. The basic parameters for all reference lifting surfaces, i.e. wing and empennage, can be itemised as: the wing area (S_W); leading edge sweep (Λ_{LE}) and quarter-chord sweep (Λ_{Qchd}); aspect ratio (AR); taper ratio (λ); dihedral (Γ) and the mean thickness to chord ratio $(t/c)_m$.

The sections to follow, in order of preference, will offer a succinct explanation of the three most recognised reference wing definition methodologies. All the conventions described below require projecting the body and the wing onto the same horizontal plane, such that vertical positioning of the wing becomes redundant. Furthermore, the reference wing is considered to have an identical (maximum) span to that of the original wing. The span does not include additional length due to wingtip devices, like for instance winglets; this aspect is treated separately both from a geometric and aerodynamic viewpoint, and is discussed extensively in Section 7.7.

5.1.1 Weighted Mean Aerodynamic Chord Method

The initial task is to project the exposed inboard trapezoidal panel leading and trailing edge lines (at the fuselage-wing juncture) through the fuselage to the aircraft plane of symmetry as shown in Figure 5. The reference wing planform area is then obtained by summing each trapezoidal panel area. Recognising each panel possesses an intrinsic Mean Aerodynamic Chord (MAC) magnitude and location, the supposition is an equivalent reference wing would have an MAC equal in magnitude and location to the collective influence of all panels – obtained using the superposition of each panel constituent MAC weighted on the basis of individual areas.

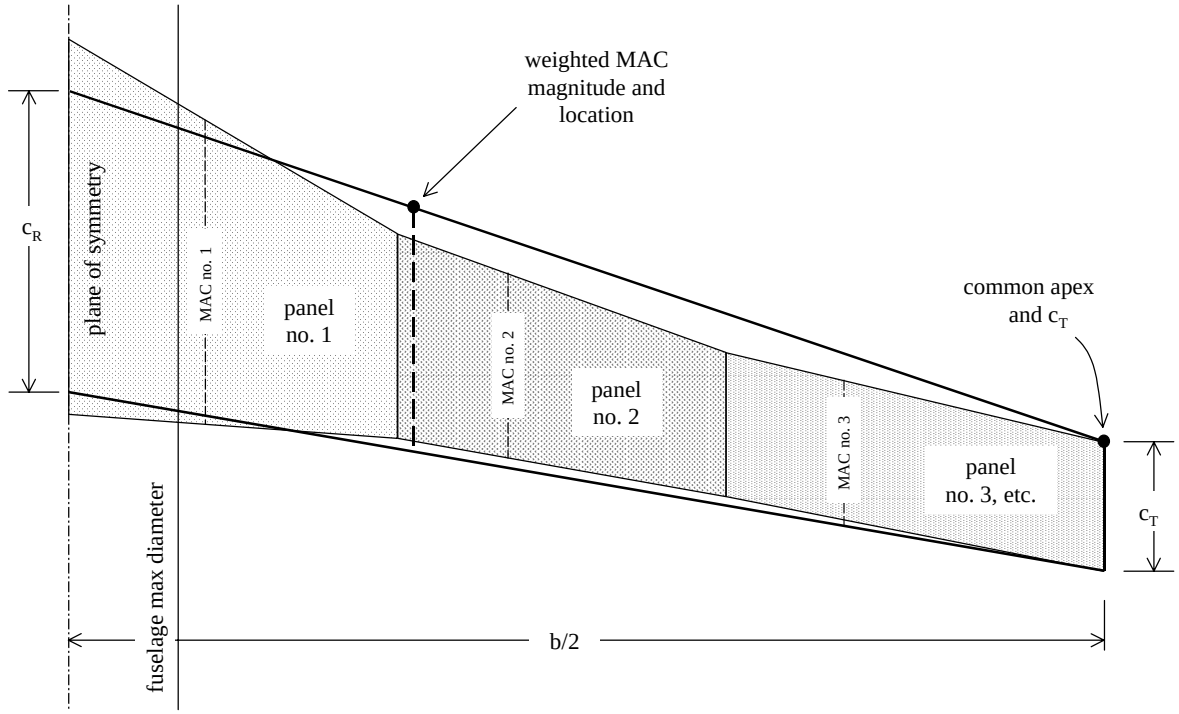

Figure 5. Equivalent reference wing geometric definition using the Weighted MAC method.

Assuming the reference wing shares a common apex point at the original wing tip chord leading edge, the leading edge sweep of the reference wing can be quantified by projecting a line through the tip chord apex and leading edge of the weighted MAC towards the aircraft centre-line. This operation identifies the reference wing root chord apex at the plane of symmetry. Since the reference wing area has been tallied, the root chord length is then derived using the original wingspan and tip chord. The main advantage of the weighted MAC method is that it produces a reference wing area at least equal[†] to the original wing (projected to the plane of symmetry) planform area. This does however mean a slightly more conservative representation of the equivalent reference wing in an aerodynamic sense compared to other conventions. The very notion the MAC location is based on weighted areas means that there is a tendency to draw the MAC more inboard, thus generating a slight larger mean wing thickness. Also, since the reference wing planform area is at least equal to the original wing area, a smaller AR is produced as well (recall $AR = b^2 / S_W$). Regardless of these observations, this method of defining the equivalent reference wing is considered to be the most apt representation of the original wing.

5.1.2 ESDU Method

The concept of the ESDU equivalent wing planform[36] (Figure 6) was first published in 1976, since that time, it has been employed with a growing popularity and has become a standard in numerous academic institutions and airframe manufacturers. Fundamentally, the methodology works off the exposed original wing planform area with some inherent geometric elements as a basis for generating the final projected equivalent reference wing.

[†] By virtue of projecting a collinear line through the wing tip chord and weighted MAC leading edges, in some instances, the reference wing area can become marginally larger than the original planform area.

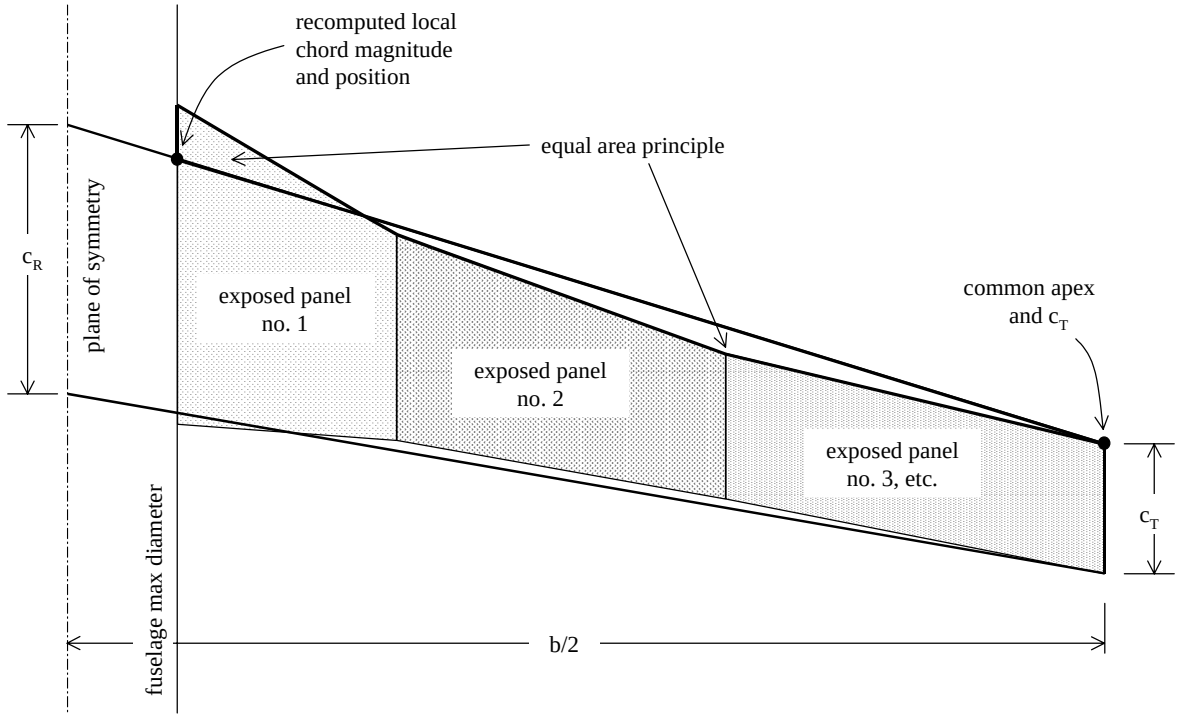

Figure 6. Equivalent reference wing geometric definition using the ESDU method.

The exposed planform area of the original wing is calculated by summing the areas of each exposed trapezoidal panel. Assuming the residual span measured from the fuselage maximum diameter (henceforth recognised as the fuselage-wing juncture) datum to the wingtip, the chord at the projected fuselage-wing juncture is computed using the original wingtip chord and the recently computed exposed planform area. The leading edge of the fuselage-wing juncture chord is then calculated using the equal area principle – which can be thought of as a line projecting towards the aircraft plane of symmetry from the wingtip and when intersecting the original cranked planform Λ_{LE} angles forms transversal zones of equal area. Concurrently, the angle at which this geometric congruity occurs is designated as the equivalent reference wing Λ_{LE} angle. Using the trigonometric property of similar triangles and projecting from the original wing wingtip chord and the recently computed fuselage-wing chord magnitude and location, the reference wing root chord is quantified with the corresponding equivalent reference planform area.

The ESDU equivalent reference wing is typified by smaller planform area and higher AR compared to the original planform. Since there is a tendency to draw the location of the MAC outboard in relation to the Weighted MAC method, the wing $(t/c)_m$ is smaller therefore advantageous from an aerodynamics perspective.

5.1.3 Simple Trapezoid or Net Method

The most basic of equivalent reference wing conventions, the process requires simply projecting both the leading and trailing edge lines of the most outboard trapezoidal panel towards the aircraft centre-line as depicted in Figure 7. The implication is the reference wing inherits the most outboard panel's Λ_{LE} angle, which can be undesirable for multiple cranked planform geometries where an appreciable difference occurs between each panel Λ_{LE} angle. In conjunction with qualities that promotes a propensity for lower values of S_W compared to the original planform and higher AR compared to the ESDU method, it is suggested this convention be utilised only for single wing planform breaks (one crank)

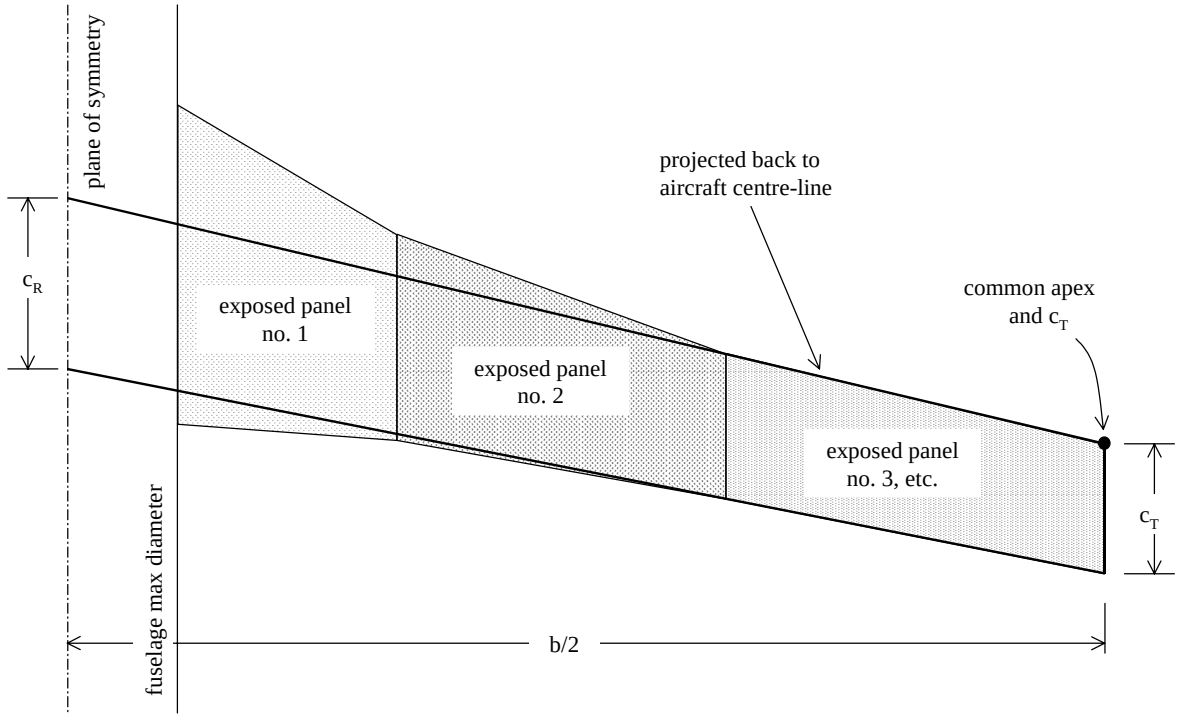

Figure 7. Equivalent reference wing geometric definition using the Simple Trapezoid or Net method.

where both panels share a common Λ_{LE} angle. In this way, the simple trapezoid will produce a better representation model of the original planform as opposed to employing this methodology for more complicated wing with multiple cranks.

5.1.4 Ancillary Wing Conventions

Airframe manufacturers are usually inclined to conceiving unique in-house developed technical methodologies and conventions for purposes of tailoring to their respective design philosophies. Accordingly, there exist other reference wing definition conventions and two notable examples are the Airbus Gross[37] and Boeing Wimpress[38], and it can be stated that the method of definition is quite distinct from the Weighted MAC, ESDU and Net approaches. The Airbus Gross method assumes the total wing area comprises the exposed wing area (up to the wing-fuselage juncture) and the rectangular area across the fuselage cross-section in plan-view bounded by the leading and trailing edges where wing-fuselage juncture occurs. The Boeing Wimpress employs a slightly more complicated approach – the simple trapezoid area is tallied with the remaining exposed wing area and a contribution produced by a weighted residual area within the fuselage.

Irrespective of the Airbus Gross and Boeing Wimpress conventions, the equivalent trapezoidal geometric details, i.e. root chord, magnitude and location of MAC, sweep angles, etc., are subsequently derived from the basic assumption of tip chord congruity with the original planform. Although the two most recognised airframe manufacturers adopt these reference wing definition conventions, they are customised for all too common planform geometries with no leading edge cranks and generally one trailing edge break. One fortuitous bi-product of adopting a unique reference wing convention for an airframe manufacturer is some form of security can be maintained, especially those occasions where correlation between aircraft design parametric associations and vehicular aerodynamic attributes are examined.

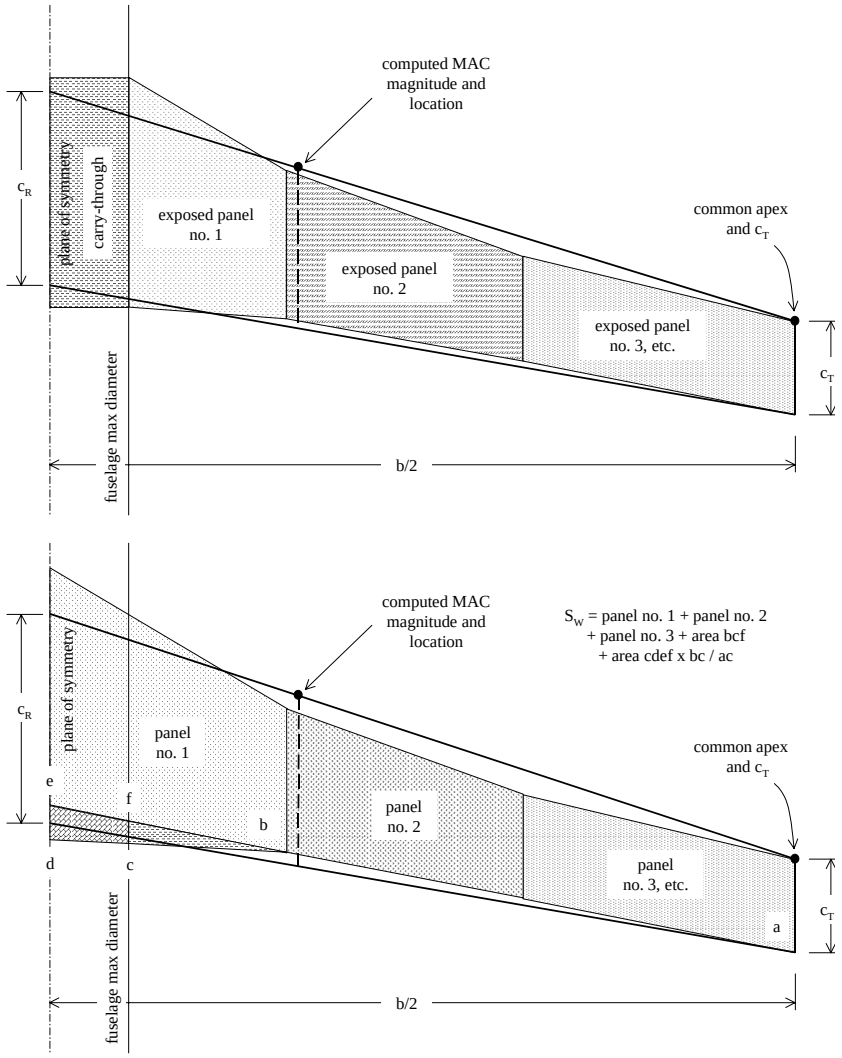

Figure 8. Equivalent reference wing geometric definition using the Airbus Gross (above) and Boeing Wimpress (below) methods.

5.1.5 Fundamental Parametric Relationships for the Reference Wing

Once the reference wing convention has been chosen, arrays of basic geometric and parametric measures are required for a complete definition of the lifting surface planform. These expressions are well established relationships and covered extensively in the literature[1,2,3,4,5,39], and as a precursor to the derivations to follow are reviewed briefly here. These parameters relate to the constraint-free condition where the designer considers an arbitrary S_w, AR and λ, and hence would like to quantify the resulting c_R. Utilising the customary equation for wing geometric definition

$$AR = \frac{b^2}{S_w} \tag{23}$$

and recalling the definition of trapezoidal area

$$S_w = \frac{b}{2} c_R (\lambda + 1) \tag{24}$$

and by re-arranging Eq. (23), then substituting the result into Eq. (24), the root chord may be solved for by the expression

$$c_R = \frac{2}{(1+\lambda)}\sqrt{\frac{S_W}{AR}} \tag{25}$$

This result is important since S_w, AR and λ can now be considered as independent design variables, which is conducive for any generalised optimisation methodology. To finalise the array of fundamental analytical relationships that can be utilised in the design process, the chord distribution of a linearly tapered wing[34] is given by

$$c = c_R\left[1+(\lambda-1)\frac{2y}{b}\right] \tag{26}$$

where y is any span-wise location.

5.2 Quasi-analytical Methods for Fuselage Geometric Description

At the conceptual design level, the traditional approach is to assume a fuselage body consisting of the main cabin, deemed to be a right circular cylinder, with the pilot's compartment, nose and tail cones attached accordingly. Each component is generally assumed to be axially symmetric, though the nose and tail cones are not strictly considered to be conical, but are assumed to be quadric slightly prolate circular hyperboloids with fineness ratios obtained from length and diameter determined earlier by baseline fuselage geometric definitions[1,4,5,39].

To obviate the loss of precision, one suggested method is to employ conic lofting[2,4]. The principal toolkit for lofting is a second-degree all-purpose curve known as the "conic"; thus allowing for individual cross-sections to be described by geometric constructs like the circle, ellipse, parabola and hyperbola. In geometric terms, the operation involves identifying a start point, end point, and, a control point to which a shape parameter is varied until the desired curve is achieved. From each cross-section, the local circumference and area are computed numerically, giving scope to yield an estimate of both wetted area and volume. Conic lofting is an advantageous process when issues of accuracy in reproducibility are concerned because a unique mathematical definition describes each of the curves that collectively compose the entire body. However, this marked improvement in accuracy comes at the behest of time expended in defining the individual cross-sections. This is a quite difficult proposition when the designer is confronted with a "clean-sheet" exercise because there is no real preconceived (let alone elaborate) notion of what the body shall look like.

To find a middle ground between the extremes of simplistic yet expedient empirical estimation and more elaborately defined conic lofting, an alternative utilising analytical techniques is to be presented. Before proceeding with the method, the fundamental assumptions that need to be considered include:

- The fuselage is taken to be a three-segment body: the nose; the centre; and, the aft.
- The centre body is assumed to have a constant cross-section with the singular constraint of symmetry about the x-z plane.

5.2.1 Fuselage Centre-Section: Cross-Section Definition

The fuselage cross-section geometry, as depicted in Figure 9, consists of upper and lower lobes with a stipulation of symmetry about the x-z plane imposed. One can assume a basic circular geometry can be distorted into an ovoid shape by displacing the original origin by some proportion (henceforth designated as the distortion coefficient, or, ξ_x) of the maximum cross-section height (d_v), i.e. a circular geometry distortion coefficient would be $\xi_x = 0.50$, and all others would fall between, $0 < \xi_x < 1$, zero corresponding to the upper or positive z-direction.

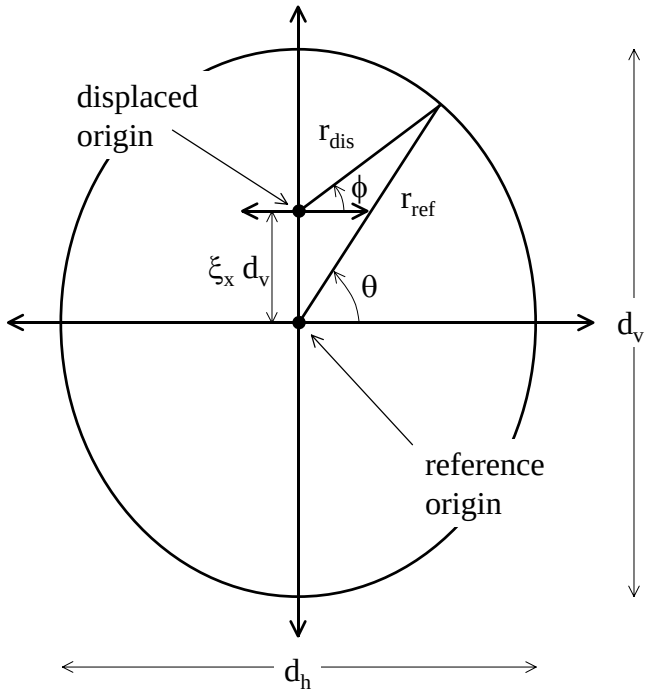

Figure 9. Illustration of displaced origin for fuselage cross-section geometric definition.

Since an association can be established between the radius and angular sweep, the Fourier Series Expansion[40] can satisfactorily represent this functional relationship as an infinite sum of sine and cosine terms. Due to stipulation of symmetry about the x-z plane and placing an emphasis on compactness, a sufficiently accurate model of any continuous fuselage cross-section geometry can be obtained using an abridged form

$$r(\phi) = a_o + a_1 \cos 2\phi + b_1 \sin \phi \tag{27}$$

The coefficients a_o, a_1 and b_1 can be evaluated using a numerical integration procedure like Simpson's rule[41], or alternatively evaluated with non-linear regression techniques such as the Levenberg-Marquardt method[42,43].

As a demonstration of the presented method, consider a model of the Embraer 170 typical fuselage cross-section. This geometry is fashioned as a double-bubble arrangement and has dimensions of $d_v = 3.35$ m and $d_h = 3.01$ m. Using a supplied schematic in brochure documentation[44], the distortion coefficient was estimated to be $\xi_x = 0.651$, or alternatively stated, the distance from the cross-section vertical axis midpoint to the beginning of the lower lobe semi-circle was estimated to be approximately 0.505 m. Upon substitution of the main data and recognising four points can be compiled to constitute the

model dataset, conducting analysis using Eq. (27) as the template, an estimate of the Embraer 170 cross-section described in metres is given by the expression

$$r(\phi) = 1.5698 - 0.10520\cos 2\phi + 0.33504\sin\phi$$

To appreciate the accuracy of this result, Figure 10 compares the Embraer 170 actual geometry to that of the model. It is evident that the model does not adequately trace the zone of geometric transition between the upper and lower lobe juncture, nonetheless, a qualitative assessment shows the model to be generally in good agreement with the actual cross-section.

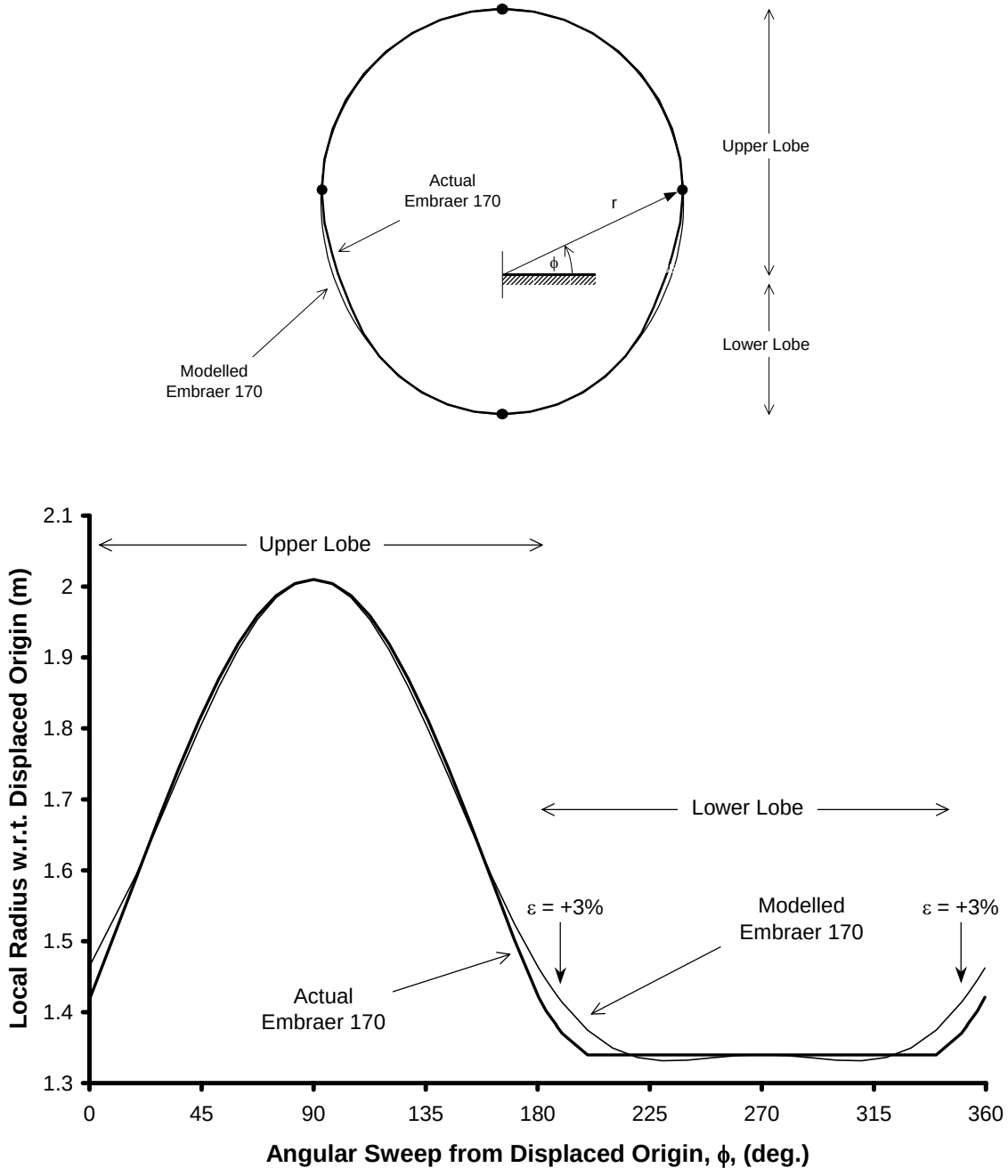

Figure 10. Comparison between actual geometry and model for the Embraer 170 typical fuselage cross-section.

If one focuses on the upper and lower lobe junction points, a maximum error of approximately +3% occurs, otherwise the remainder of the geometry appears to be adequately modelled. The lower lobe geometry does pose some problems for the model since the actual geometry calls for a constant radius for given angular sweep. This generates some oscillatory behaviour from the Fourier Series Expansion, however, the error can be considered to be quite minor considering the coarser level of accuracy deemed acceptable for conceptual design predictions.

The area within a sector region (A_{SR}) bounded by rays $\phi = \alpha$, $\phi = \beta$ and the curve $r = f(\phi)$ reads as[45]

$$A_{SR} = \int_{\alpha}^{\beta} \frac{1}{2} r^2 \, d\phi \qquad \alpha \le \phi \le \beta \tag{28}$$

Recognising the cross-section geometry is only symmetric about the x-z plane, two distinct values of A_{SR}, namely for the upper and lower lobes need to be computed. Collectively, the area of the fuselage cross-section, A_{XS}, becomes

$$A_{XS} = \frac{\pi}{2}\left(2a_o^2 + a_1^2 + b_1^2\right) \tag{29}$$

The length differential equation of a sector region bounded by rays $\phi = \alpha$, $\phi = \beta$ and the curve $r = f(\phi)$ is defined as[45]

$$ds^2 = r^2 d\phi + dr^2 \qquad \alpha \le \phi \le \beta \tag{30}$$

Attempts to integrate Eq. (30) between the appropriate limits of ϕ becomes a difficult proposition owing to the form of $r(\phi)$ as presented in Eq. (27). Instead, an equivalent method exists wherein the average radius (r_{AV}) characteristic of the function can be utilised to generate a sufficiently accurate estimate of the arc length. The average value of r over the curve $r = f(\phi)$, $\alpha \le \phi \le \beta$, with respect to ϕ is the value of the integral[45]

$$r_{AV} = \frac{1}{\beta - \alpha} \int_{\alpha}^{\beta} r(\phi) \, d\phi \qquad \alpha \le \phi \le \beta \tag{31}$$

Recognising the cross-section geometry is symmetric about the x-z plane, two distinct values of r_{AV}, namely for the upper and lower lobes, need to be computed to generate an accurate approximation of the circumference. Recalling the length of an arc of constant radius is $C = 2\pi r$, collectively, the circumference of the fuselage cross-section, C_{XS}, becomes

$$C_{XS} = 2\pi a_o \tag{32}$$

5.2.2 Forward and Aft Fuselage Sections: Three-dimensional Definition

The intention here was to create a quasi-analytical process whereby both the fuselage forward and aft bodies can be geometrically described as slightly prolate, circular, hyperboloid surfaces with an offset vertex. The first requisite is a level of accuracy better than those produced using traditional empirical methods[1,4,39]. An additional and quite

important objective is the ability to analytically estimate the wetted area of the body from the initial geometry description process. A fundamental assumption is that the fuselage forward and aft body geometry will be modelled using a template exponential function in the x-z plane. The body shell is then produced via a surface of revolution about the x-axis generated between the region of $z = f(x)$, $a \leq x \leq b$, and the x-axis. The final step is to offset the axis-symmetric surface of revolution in the z-direction by applying a vertical coordinate increment/decrement at each body station. This adjustment is effected using a linear function related to both body station and down-sweep or up-sweep.

As presented in Figure 11, each section is partitioned into two segments delineated by a sweep line (down-sweep denoted by φ) originating from the body apex or extremity to the fuselage centre-section vertical midpoint (at Fuselage Reference Plane or FRP). A

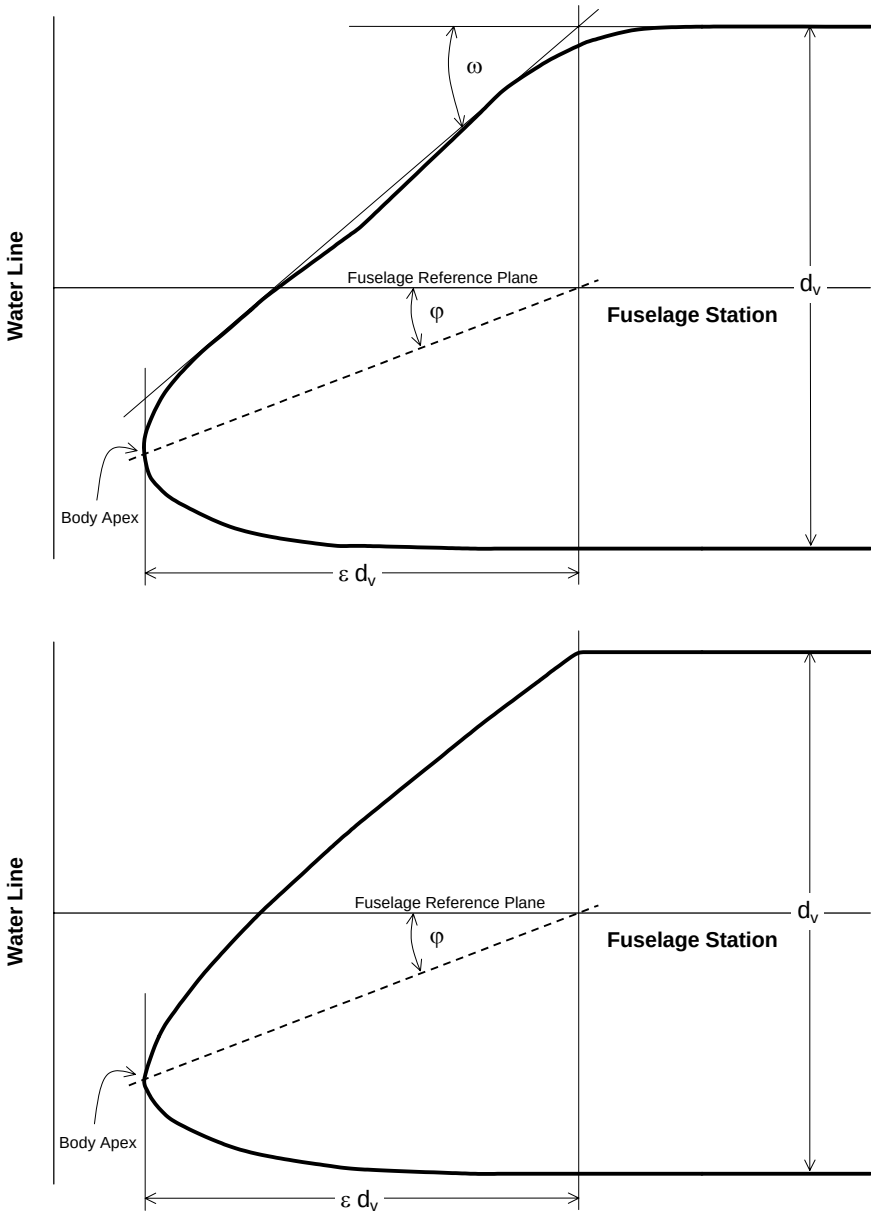

Figure 11. Comparison between Saab 2000[46] and Saab 340[47] actual (above) and modelled forward fuselage geometric definition.

supplementary parameter designated as the shield-sweep, ω, is also introduced and is essentially a measure of the angle of the body frontal face in the x-z plane. The convention discussed for the forward fuselage example is equally applicable for the aft fuselage body as well. Instead of down-sweep, generally an up-sweep would be considered, and the shield-sweep would be replaced by tail-sweep of the body lower portion, both measured anti-clockwise with respect to the FRP.

Recalling the objective is to describe upper and lower segments using very simple analytical models whilst retaining a suitable level of accuracy, a review of plane curves revealed an adequate representation of geometry in side view could be obtained by using the algebraic model

$$z = \alpha\, x^{\beta} \tag{33}$$

where z denotes the vertical axis or water-line and x represents the longitudinal or fuselage station. The β coefficient is derived empirically and based on correlation to known aircraft fore and aft bodies, investigations have shown that the potential coefficient is a trigonometric function of φ and ω.

$$\beta = 0.54 + 0.1\tan(\omega - \varphi) \tag{34}$$

The α coefficient is simply found by equating Eq. (33) with the fuselage vertical radius corresponding to fuselage station [ε d_v] from the body apex. The parameter ε is used to define the body length to diameter ratio.

$$\alpha = \frac{d_v}{2}\frac{1}{(\varepsilon\, d_v)^{\beta}} = \frac{d_v^{(1-\beta)}}{2\,\varepsilon^{\beta}} \tag{35}$$

Invoking a geometric constraint of z(x = [ε d_v]) = d_v/2 ± [ε d_v]tan(φ), where the axis convention dictates –[ε d_v]tan(φ) to denote observance of the upper body and +[ε d_v]tan(φ) the lower. A geometric description of the each upper and lower body segment as a function of body station is therefore given by

$$z(x) = \begin{cases} +\dfrac{d_v^{(1-\beta)}}{2}\left(\dfrac{x}{\varepsilon}\right)^{\beta} + (\varepsilon\, d_v - x)\tan\varphi & \forall\ x \text{ above body apex} \\ -\dfrac{d_v^{(1-\beta)}}{2}\left(\dfrac{x}{\varepsilon}\right)^{\beta} - (\varepsilon\, d_v - x)\tan\varphi & \forall\ x \text{ below body apex} \end{cases} \tag{36}$$

To re-iterate, the ordinate values generated by Eq. (36) adhere to the axis convention defined by the body down-sweep or up-sweep depending on whether the forward or aft fuselage are being considered respectively. Sweeping out a surface then generates the three-dimensional geometry of a forward or aft fuselage assembly by revolving around the longitudinal axis or the fuselage station axis. A vertex offset is subsequently imposed by adjusting each z value through a geometry augmenter (see structure of Eq. (36) for increment/decrement) that is a linear function of body station and body down-sweep.

5.3 Analytical Method for Wing-to-Fuselage Fairing Geometric Description

There exists a growing popularity, particularly when it concerns business jets, in utilising multiple fuel storage cells within the wing-fuselage fairing body as exemplified by in-service aircraft like the Bombardier Aerospace CL-604 Challenger[48], Embraer Legacy[49] and ERJ 145XR[50], Dassault Aviation Falcon 2000EX[51] and Falcon 900EX[52], and Gulfstream Aerospace G200[53] to name a few. These tanks are normally saddle and underfloor tanks located either well forward and aft, or, even just forward and aft of the wing torsion box structure. Furthermore, there is also a propensity in the industry to incorporate conformal fuel tanks, i.e. more amorphous-looking tanks defined by tracing the fairing geometry rather than installation of a series of box-like cells. For this reason, a requirement now arises calling for a relatively accurate assessment of fairing volume; the most expedient method would be use of an appropriate member from the quadric surface family of cylinders.

The wing-fuselage fairing geometry is taken to be a quadric surface, namely, a body whose equations combine linear constants with quadratic terms to describe the outer shell. Characteristics displayed by elliptic paraboloids appear well suited in modelling the way wing-fuselage fairings are fashioned on contemporary aerospace vehicles. As shown in Figure 12, the cross-sections perpendicular to the x-axis forward of the y-z plane are ellipses, whereas, the cross-sections in the plane that contain the x-axis are parabolas.

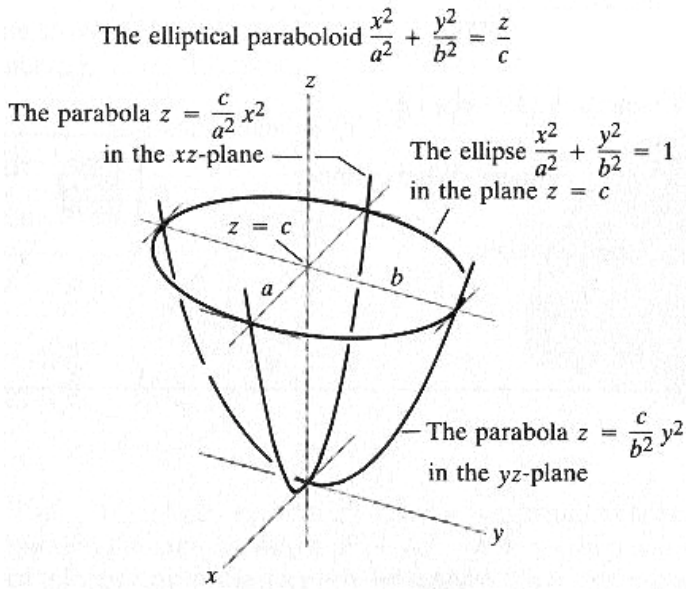

Figure 12. The generic elliptic paraboloid comprises a series of ellipse sections varying in relative size in accordance with a parabolic progession[45].

In the context of traditional aircraft axes, the generic elliptic paraboloid is given by the Cartesian equation[45]

$$\frac{x}{c} = \left(\frac{z}{a}\right)^2 + \left(\frac{y}{b}\right)^2 \tag{37}$$

and is symmetric with respect to the y and z planes. Now, considering a forward or aft wing-fuselage fairing having a length from the wing front or rear spar of l_{fair}, a base width equal to the local fuselage chord, d_{wf}, and designated fairing height, t_R, in order to generate the entire surface, the z values are computed for given x, and y correspondingly computed at given x

$$z = \frac{\tilde{z}}{\tilde{y}}\left(\tilde{y}^2 - y^2\right)^{1/2} \tag{38}$$

where the ellipse operator is

$$\tilde{y} = \left(\frac{d_{wf}^2}{4 l_{fair}} x\right)^{1/2} \tag{39}$$

and the parabolic function reads as

$$\tilde{z} = \left(\frac{t_R^2}{4 l_{fair}} x\right)^{1/2} \tag{40}$$

where $y = \tilde{y}\ i / n$ for i = 1, 2, 3, ….., n, for given station x. The parameter, n, is used for spacing y values according to the number of segments deemed satisfactory; a selection of n = 12 segments would produce adequate results.

5.4 Quasi-analytical Method for Turbofan Nacelle and Miscellaneous Power Plants Geometric Description

Many methods exist which allow for the prediction of nacelle wetted area for gas turbine engines, unfortunately, a detailed array of information is also required to utilise these geometric expressions and this becomes impractical at the conceptual level since much of the dimensioning is open to conjecture. The idea is to develop a simple yet effective empirical expression, which requires a minimum of subjective work on the part of the designer. The aim is to construct a generic nacelle model fashioned to be a quadric surface representing constituents of fan cowling, gas generator cowling and plug in the hot flow; the body can be explicitly thought of as an ellipsoid with pieces cut by perpendicular planes on both ends.

5.4.1 Nacelle Three-dimensional Definition

An adequate method is to describe such geometries by utilising the flexibility exhibited by parametric equations[45] (see Figure 13). Here, the coordinates of the x and z are expressed as functions of a third variable or parameter, t, and by a pair of parametric equations, namely, x = f(t) and z = f(t).

Usually, the functions for x and z are trigonometric in form, and after some experimentation, the most appropriate system of equations was found to be

$$x = \varsigma_{lgt}\, l_{nac}\, e^{\frac{\pi}{2}t} \sin\frac{\pi}{2} t \tag{41}$$

$$z = \varsigma_{dia}\, d_{nac}\left(1 + e^{\frac{\pi}{2}t}\cos\frac{\pi}{2}t\right) \tag{42}$$

where t = i / n for i = 1, 2, 3, ….., n, l_{nac} and d_{nac} are the nacelle length and maximum diameter respectively. The scaling factors, ς_{lgt} and ς_{dia}, are derived based on the properties inherent to each trigonometric function; their respective values are ς_{lgt} = 0.2079 and ς_{dia} = 0.2028. The parameter, t, can be thought of as a spacing variable and its purpose is to generate each x and z coordinates according to the number of segments deemed satisfactory. For example, investigations have shown a sufficiently consistent representation of any nacelle body can be achieved using a total of n = 12 segments.

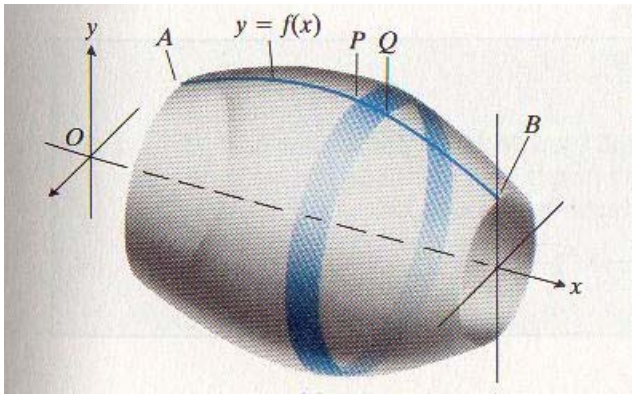

Figure 13. General representation of swept surface resulting from revolution of curve AB about the x-axis[45].

5.4.2 The Nacelle Geometric Design Variables

This sequence of analysis requires the correlation between a tangible global design variable such as the maximum static thrust of an engine (T_o) and the fall-out or associative geometric design parameters. Thrust is a driver variable because it is one of the primary determinates in any aircraft sizing process. As a result, a departure from the algebraic process needs to occur, and statistical methods are enlisted in defining the dependent variables.

A strong logarithmic correlation between engine equivalent diameter (d_{eng}) and engine weight may be described by an expression of the form[54]

$$d_{eng}^2 = \left(k_{d1}\ln T_o\right) - k_{d2} \tag{43}$$

where k_{d1} and k_{d2} are regression coefficients. Substituting an empirical equation for engine weight[54] and subsequently expanding Eq. (43) leads to

$$d_{eng} = \left(k_{d1}k_{em2}\ln T_o + k_{d1}\ln k_{em1} - k_{d2}\right)^{1/2} \tag{44}$$

This result indicates that the predicted equivalent diameter of any gas turbine engine can be taken to be a monotonic function of the T_o potential at ISA, sea level conditions. As a supplementary note for turboprop installations, a good initial rule in quantifying propeller diameters (d_{prop}) is to factor d_{eng} by 3. This simulates an equivalent by-pass ratio increase

due to the presence of propeller or larger fan diameter for given equivalent maximum static thrust rating.

Even though Eq. (44) estimates the equivalent diameter of arbitrary gas turbine engines, the corresponding equivalent nacelle diameter is of interest when attempting to calculate the external wetted area. An extensive review of nacelle layouts have shown an additional 250 mm (10 in.) increase in d_{eng} would account for the enshrouding structure's geometry. Quantifying Eq. (44)'s coefficients of proportionality using data given in Aviation Week[55], Janes[56] and data compiled by Svoboda[57], and incrementing the structural allowance criterion, the equivalent diameter of any gas turbine nacelle is then given approximately by

$$d_{nac} = \left(4 - \Phi_{lg}\right)\left[0.0625 + \frac{1}{4\sqrt{2}}\left(1.730 \ln T_o - \pi\right)^{1/2}\right] \qquad \forall\ T_o > 8.5 \text{ kN} \tag{45}$$

where T_o is in kN and d_{nac} is given in metres. The impulse function operator $\Phi_{lg} = \Phi(s,1)$ denotes presence of an on-wing nacelle-undercarriage integration and is invoked for values of $s = 1$, otherwise is zero for $s < 1$.

Caution should be exercised when quantifying d_{eng} and d_{nac} during the design process. If the intention is to not consider a rubber-engine approach to sizing, then the metrics produced by Eq. (45) relates to engine and nacelle sizing based on an engine T_o quoted at the maximum practical[‡] or even thermodynamic limit. If a particular engine designation is to be employed, the designer must be mindful that the geometric design variables must be based on a T_o quoted as the maximum practical or thermodynamic limit, and then de-rate the engine accordingly before proceeding with any ensuing analysis.

Prediction of nacelle total length (l_{eng}) can be derived based on the same premise used for d_{nac}. There exists a correlation between the total volume encased by engine geometry for given T_o, and when this association is empirically derived[54], l_{eng} in metres can be determined trivially via

$$l_{eng} = \frac{4V_{eng}}{\pi d_{eng}^2} = \frac{4k_{ev1}T_o^{k_{ev2}}}{\pi\left(k_{d1}k_{em2}\ln T_o + k_{d1}\ln k_{em1} - k_{d2}\right)} \tag{46}$$

The arbitrary total l_{nac} any pitot installation is approximately related to l_{eng} by some correction factor k_{ntyp}. The correction is equal to $k_{ntyp} = 5/3$ for short duct nacelles and $k_{ntyp} = 2.0$ for long duct installations. It is also common practise to integrate the gas turbine engine nacelle and wing structure through an on-wing installation layout for many high or low wing turboprop configurations. The total nacelle length for on-wing installations ($l_{nac,ow}$) can be estimated by summation of l_{eng} and local wing chord length at the spanwise powerplant location y_{eng}. The final scenario concerns powerplant installations as an S-duct integrated into the fuselage body, or a straight duct usually integrated structurally with the vertical tail assembly. The revised nacelle length is then taken to be 25% longer than a comparable long duct pitot installation. It would be ideal to combine the myriad of isolated algorithms that predict nacelle length conforming to a given power plant installation philosophy; such a task produces the algorithm for nacelle length prediction to look like

[‡] This upper limit in thrust is sometimes defined as the lowest permissible flat rating temperature the engine manufacturer has made available to the market, and a commercial version of the engine operating at the thermodynamic limit is simply not a pragmatic consideration.

$$l_{nac} = \left(5 + \Phi_{ntyp} + \frac{7}{4}\Phi_{duct}\right)\frac{T_o^{0.9839}}{6\pi\left(1.730 \ln T_o - \pi\right)} + \Phi_{lg}\, c_R \left[1 - (1-\lambda)\frac{2y_{eng}}{b}\right] \quad \forall\ T_o > 8.5 \text{ kN} \tag{47}$$

Invoking the concept of an impulse function assists this endeavour with incorporation of operators such as, $\Phi_{ntyp} = \Phi(s,1)$ representing the assumption of a long ducted nacelle, and, $\Phi_{duct} = \Phi(s,1)$ calling for an additional adjustment of the nacelle length by virtue of the installation being either an S-duct or straight duct type. All operators are invoked for values of s =1, otherwise is zero for s < 1.

5.5 Estimating The Wetted Area of Primary Components

The total exposed surface area of an aircraft is defined as the area of external parts that contribute to the friction drag. For conceptual design, primary constituents can be identified as wing, empennage, fuselage, engine nacelles including pylons, dorsal intakes (S-duct), propellers, or, miscellaneous contributions due to additional fairings and appendages such as fuselage mounted undercarriage pods, winglets as well as ventral and dorsal fins. A wide selection exists in literature[1,4,5,39] for the prediction of wetted area of aircraft, and it can be said that they vary in the level of detail required for input as well. To follow is a synopsis of the suggested methodology when estimating conceptual wetted area. As it shall be seen, this section comprises entirely of recently conceived alternative methods for each of the major constituents discussed above. The emphasis is to improve the prediction accuracy of not only the global objective, namely the vehicular wetted area, but to ensure a better major constituent calculation. This is of importance to all subsequent drag calculations since it is fundamental to the component build-up method, which crucially defines the Equivalent Characteristic Length Method reference condition to be presented in Section 7.2.

5.5.1 Centre Fuselage External Area

The fuselage is divided into a nose section including pilots' compartment, cabin, and aft section, each of which is sized separately and then combined to yield the total fuselage wetted area. The cabin is housed within the centre fuselage structure, and this major assembly is assumed to be a right cylinder, i.e. constant cross-section throughout. The total exposed surface area of the centre fuselage is simply

$$S_{wet,cfuse} = C_{XS}\, l_{cfuse} \tag{48}$$

where C_{XS} is given by Eq. (32), and l_{cfuse} is the length of the entire [centre] fuselage segment. It should be remembered that corrections to the fuselage total wetted area must be incorporated to account for the presence of lifting surface junctions, nacelle or fairing cutouts, etc. on the fuselage body.

5.5.2 Forward and Aft Fuselage External Area

In view of the forward and aft fuselage section geometry three-dimensional description methodology outlined in Section 5.2.2, the quasi-analytical model given by Eq. (36) permits the opportunity of now deriving the associative wetted area of the body as well. If z = f(x) and dz / dx are continuous functions of x, it can be shown the value of the integral[45]

$$S_{wet} = \int_a^b 2\pi z \sqrt{1+\left(\frac{dz}{dx}\right)^2}\, dx \qquad a \le x \le b \tag{49}$$

will define the total area of the surface swept out by revolving z = f(x), a ≤ x ≤ b about the x-axis. This integral is produced by substitution of Eq. (33) and its derivative into Eq. (49), and the evaluation of it appears to be a non-trivial problem. To find an alternative action other than attempting to complete this complex definite integral expression, an equivalent form looks something like

$$S_{wet} = \int_0^{\varepsilon d_v} 2\pi\alpha \sqrt{x^{\vartheta} + \kappa x^{\tau}}\, dx \tag{50}$$

where $\vartheta = 2\beta$, $\kappa = \alpha^2\beta^2$ and the exponential coefficient $\tau = 4\beta\text{-}2$. Upon examination of Eq. (50), one insightful observation may be recognition that the algebraic function within the definite integral mimics geometric progression characteristics of the exponential expression $z = \upsilon x^{\gamma}$. The supposition is this method of simplification can be incorporated, thus paving the way for an adequate approximation of the original integral. Taking into consideration the terms within the square root segment of the function, and assuming congruity through geometric similarity, and rearranging such that x^{γ} becomes the subject

$$x^{\gamma} \equiv \frac{\left(x^{\vartheta} + \kappa x^{\tau}\right)^{1/2}}{\upsilon} \tag{51}$$

Taking the natural logarithm of each side, and then introducing the body length quantity [εd_v], thence solving for γ

$$\gamma = \frac{\left\{\ln\left(\varepsilon^{\vartheta} d_v^{\vartheta} + \kappa \varepsilon^{\tau} d_v^{\tau}\right)\right\} - \ln \upsilon}{\ln \varepsilon d_v} \tag{52}$$

By choosing two suitable points on the body, for example, $x = \varepsilon d_v/4$ and $x = \varepsilon d_v$, two simultaneous equations are produced with the solution for υ given as

$$\upsilon = \frac{\ln\left[\left(\frac{\varepsilon d_v}{4}\right)^{\vartheta} + \kappa\left(\frac{\varepsilon d_v}{4}\right)^{\tau}\right] - \left(1 - \frac{\ln 4}{\ln \varepsilon d_v}\right)\ln\left[(\varepsilon d_v)^{\vartheta} + \kappa(\varepsilon d_v)^{\tau}\right]}{\frac{\ln 4}{\ln \varepsilon d_v}} \tag{53}$$

The definite integral problem posed by Eq. (50) can now be analysed using an equivalent expression with an adequate amount of accuracy

$$S_{wet,sec} = \frac{2\pi\alpha\upsilon}{1+\gamma}(\varepsilon d_v)^{\gamma+1} \tag{54}$$

where $S_{wet,sec}$ represents the forward or aft fuselage body wetted area.

5.5.3 Wing-Fuselage Fairing

It was earlier discussed in Section 5.3 that the fairing geometry would be suitably described by an elliptic paraboloid analytical representation. The purpose of this approach was to find a more consistent method in firstly drafting the fairing assembly, and then more importantly, to produce an analytical expression in predicting the maximum volume of fuel that can be stored for given fairing station length. One extension to these two basic requirements could possibly include the notion of quantifying the incremental contribution the fairing makes to the fuselage wetted area. The amount of work and algorithm complexity in fulfilling this particular requirement was considered to quite excessive compared to the relative magnitude of influence typical fairing assemblies impose upon the global wetted area result, i.e. around 6-8% is an upper limit. The key inference to this method is there exists a direct correlation between the increment in wetted area due to fairing and the length fraction of the fairing with respect to overall fuselage length. Using known aircraft data, one useful association to predict fairing wetted area ($S_{wet,fair}$) was found to be

$$S_{wet,fair} \cong \frac{3\chi_{fair}}{4} S_{wet,gbf} \tag{55}$$

where $S_{wet,gbf}$ is the total gross fuselage wetted area (addition of forward, centre and aft fuselage bodies) not augmented according to the masked area due to presence of the fairing assembly. The parameter, χ_{fair}, represents the fraction of fairing length in relation to the total fuselage length, namely,

$$\chi_{fair} = \frac{l_{fwd,fair} + l_{aft,fair}}{l_{fuse}} \tag{56}$$

The subscripts fwd and aft define the forward and aft fairings respectively. It is highlighted that both $l_{aft,fair}$ and $l_{aft,fair}$ exclude the local wing chord at the aircraft wing-fuselage juncture, i.e. the forward fairing length is equal to the distance between the most forward point on the fairing and the wing-fuselage juncture wing chord leading edge, and, similarly for the aft fairing, but working from the wing-fuselage juncture wing chord trailing edge. Now, to establish the total net fuselage wetted area, an empirical assessment found that the fuselage body area masked by the fairing assembly is approximately equal to 80% of the fairing wetted area. Alternatively, based on this supposition, one can then argue that the fuselage total wetted area (including the fairing) is approximately equal to the summation of $S_{wet,gbf}$ and 20% of the estimated fairing wetted area. In view of this and recalling the relation given by Eq. (55), thus, a revision of the total fuselage wetted area due to presence of a wing-fuselage fairing assembly becomes

$$S_{wet,fuse} = S_{wet,gbf}\left(1 + \frac{3\chi_{fair}}{20}\right) \tag{57}$$

5.5.4 Wing, Empennage and Other Streamlined Surfaces

The fundamental aim is to develop an all-purpose method whereby the wetted area of all lifting surfaces such as the wing and empennage can be estimated with adequate accuracy. An ancillary stipulation is the algorithm should be robust enough to cover streamlined appendages with very high fineness ratios; this includes assemblies like engine

pylons, winglets, ventral fins and dorsal fins. The arc length of a parabola can be computed using the catenary[58]

$$s_{par} = l_{par}\left[1 + \frac{2}{3}\left(\frac{2d_{par}}{l_{par}}\right)^2 - \frac{2}{5}\left(\frac{2d_{par}}{l_{par}}\right)^4 + ...\right] \tag{58}$$

where the working parameters are given by Figure 14

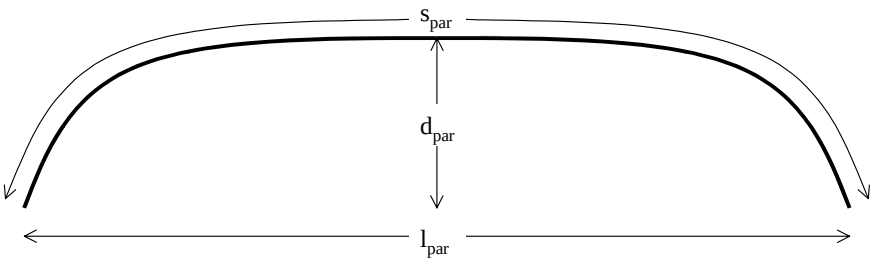

Figure 14. Parameters of arbitrary parabolic curve used to compute arc length.

If d_{par} is relatively small in comparison to l_{par}, Eq. (58) can be used as a basis to formulate a general expression to approximate the arc length of any aerofoil section. For each of the aerofoil upper or lower surfaces, a sufficiently accurate generic model is proposed as

$$s_{sec} = c\left[1 + \Theta_{sec}\left(\frac{t}{c}\right)^2\right] \tag{59}$$

The coefficient Θ_{sec} represents a factor that accounts for both the geometric scaling of chord c to produce the arc length s_{sec}, and has a dual function of serving as a relative thickness-chord partition parameter. Whenever a symmetric profile is not employed, the height of an aerofoil upper surface with respect to the chord line is not equal to that of the lower surface. By applying Eq. (59) to the lower and upper aerofoil section curves separately, and then combining both in order to produce the total circumferential length (s_{aero}) of any aerofoil

$$s_{aero} = c\left[2 + \Theta_{aero}\left(\frac{t}{c}\right)^2\right] \tag{60}$$

A suggested value for the scaling factor Θ_{aero} is 9.0. The thickness distribution (t/c) for given wing buttock line is assumed to be for all intensive purposes a variation based on geometric similarity between the root $(t/c)_R$ and tip $(t/c)_T$

$$\left(\frac{t}{c}\right) = \left(\frac{t}{c}\right)_R\left[1 + \left(\lambda^* - 1\right)\frac{y}{y_{max}}\right] \tag{61}$$

where, $\lambda^* = (t/c)_T / (t/c)_R$, is the thickness taper ratio. Based on the structure of Eq. (60), squaring Eq. (61) and subsequently neglecting the smaller term produces

$$\left(\frac{t}{c}\right)^2 \cong \left(\frac{t}{c}\right)_R^2 \left[1 + \left(\lambda^* - 1\right)\frac{2y}{y_{max}}\right] \tag{62}$$

Now, the surface area differential equation for any body of length, a, characterised by a varying cross-section, hence, corresponding circumference, s(y), reads as[45]

$$dS_{wet} = s\,dy \qquad 0 \le y \le a \tag{63}$$

To modify Eq. (63) and produce a definite integral equation requires recognition of limits between the inboard side of a trapezoidal panel to the outboard and subsequent substitution of Eq. (26), Eq. (60) and Eq. (52). Upon evaluation of the definite integral and factorising the result, a formula to estimate one trapezoidal panel wetted area for all types of planform geometries, including, dorsal fins, engine pylons and vertical stabiliser bullets[§] reads as

$$S_{wet,wing} = \frac{c_R\, y_{max}}{2}\left\{(1+\lambda)\left[2 + \Theta_{aero}\left(\frac{t}{c}\right)_R^2\right] + \frac{2\Theta_{aero}}{3}\left(\frac{t}{c}\right)_R^2 \left(\lambda^* - 1\right)(1+2\lambda)\right\} \tag{64}$$

If the entire wing is a straight tapered trapezoid, by simply substituting $y_{max} = b$, Eq. (64) can compute the entire surface area of the planform (disregarding the fuselage cut-out). In order to generate a more accurate result, Eq. (64) can be used in a cumulative fashion, i.e. to reflect a more specific thickness distribution and for multiple crank wing layouts, the surface area formula would be applied to each exposed (span less fuselage cut-out) trapezoidal panel with appropriate measurement for local span, panel taper ratio and thickness taper ratio incorporated. The total surface area estimate would then be produced upon summation of each of these constituents. As a final note, it is recommended that the wing area masked by on-wing nacelle installations be deducted from the wing wetted area computational procedure; similarly, the masked area can be taken to be a trapezoidal panel with a lateral length equal to that of the nacelle local diameter.

5.5.5 Nacelle Surfaces

Earlier in Section 5.4.1, a parametric system of equations in order to define three-dimensionally any nacelle installation was presented. Using these mathematical descriptors as a basis, the goal here is to derive an analytical expression for a resultant wetted area. Another form of the integral formula presented by Eq. (49) includes instances where the curve is given in parametric form and sweeps out a surface. With x and z as functions of a third variable t that varies from a to b, then S_{wet} is computed using[45]

[§] This assembly is found on aircraft configurations employing a T-tail layout. The vertical stabiliser bullet can be thought as a localised fairing to minimise interference drag effects between the horizontal tailplane and vertical stabiliser. It also has a beneficial effect in reducing localised buffeting and vibration.

$$S_{wet} = \int_a^b 2\pi\rho \sqrt{\left(\frac{dx}{dt}\right)^2 + \left(\frac{dz}{dt}\right)^2}\, dt \qquad a \le x \le b \qquad (65)$$

where ρ is the distance from the axis of revolution to the element of arc length (see Figure 15) and is expressed as a function of t.

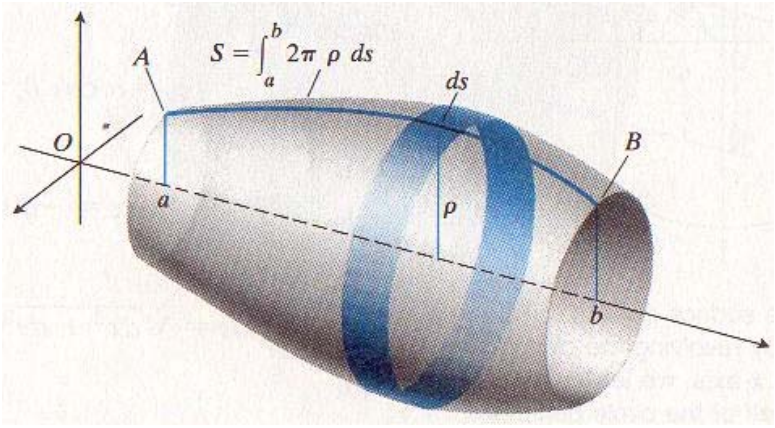

Figure 15. The area of the surface swept out by revolving arc AB about the axis shown[45].

After substituting the derivatives of x and z in conjunction with Eq. (45) into the surface area formula for parametric equations given by Eq. (65), expanding out the results and then recognising the trigonometric identity sin 2θ = 2 sin θ cos θ, the integral problem now can be posed thus

$$S_{wet,nac} = 2\pi^2\, \varsigma_{dia}\, d_{nac} \int_0^1 \left(e^{\frac{\pi}{2}t} + e^{\pi t} \cos\frac{\pi}{2} t \right) \sqrt{\varsigma_{lgt}^2\, l_{nac}^2 \left(1+\sin\pi t\right) + \varsigma_{dia}^2\, d_{nac}^2 \left(1-\sin\pi t\right)}\ dt \qquad (66)$$

Eq. (66) is a non-trivial integral expression; nonetheless, it can be solved analytically. After some algebraic manipulation and quantifying the constant terms, the wetted area of any nacelle is proposed here as

$$S_{wet,nac} = 2\pi^2\, \varsigma_{dia}\, d_{nac} \left\{ \left(0.2057\, l_{nac}^2 + 0.04661\, d_{nac}^2\right)^{1/2} + \left(0.1853 l_{nac}^2 + 0.07557\, d_{nac}^2\right)^{1/2} - \left(0.005077\, l_{nac}^2 + 0.01611\, d_{nac}^2\right)^{1/2} - \left(0.01651 l_{nac}^2 + 0.03666\, d_{nac}^2\right)^{1/2} \right\} \qquad (67)$$

Eq. (67) can be used for podded configurations including both short and long duct, as well as straight duct installations. The equation is equally proficient at producing an equivalent S-duct type installation estimate providing an equivalent nacelle length is derived. By virtue of the power plant integrations being mostly an on-wing type of configuration, turboprop installations require an additional step to the wetted area algorithm given above. In this instance, the nacelle wetted area would comprise the estimate yielded from Eq. (67) in addition to a combined surface area computed assuming two rectangular panels d_{nac} / 2 in height and l_{nac} in length.

5.5.6 Sample Computations of Wetted Area Using Actual Aircraft Data

When combining all the major constituent contributions detailed thus far, a wetted area algorithm can be established for the entire vehicle. As an affirmation of the presented methods, Figure 16 plots the estimation error (ε = predicted – actual) for major constituents as well as the collective vehicular result against available manufacturer quoted values.

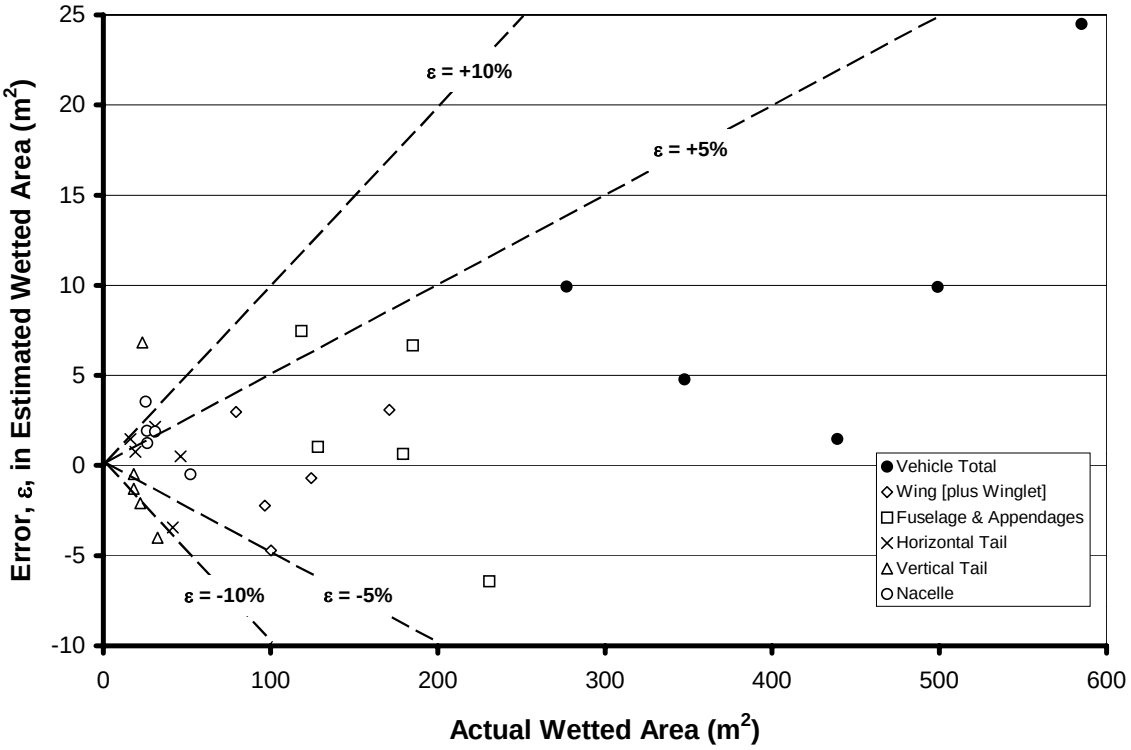

Figure 16. Prediction accuracy of presented methods to estimated wetted area of major constituents and accumulated vehicular result for select transport aircraft.

Known aircraft data involved a collection of business and regional jets as well as turboprops. The vehicles examined include: Bombardier Aerospace CL-604 Challenger[59], Global Express[60], CRJ200[61] and CRJ700[62]; Fokker Aircraft BV Fokker 100[3]; and, Saab Aerospace Saab 340[47] and Saab 2000[46].

Unfortunately, the level of major constituents' prediction accuracy cannot be regarded as being universally consistent. The more enhanced methodology created for both wing and fuselage (including fairing, dorsal fins, engine pylons, etc.) bodies, which typically constitutes approximately 75-80% of the total wetted area, has translated into an appreciable improvement in accuracy, i.e. mostly within an acceptable ±5% splay the as shown in Figure 16. For the remaining major constituent bodies such as the horizontal tail, vertical tail and nacelles, the error splay opens out to a maximum error of ±10% for almost all bodies that were analysed; nonetheless, it must be recognised that each of these constituents is characterised by a wetted area that is an order of magnitude smaller than that of the entire vehicle. The global vehicular result indicates the likelihood of producing a wetted area prediction with an error bandwidth of ±5% is quite high. This is an encouraging outcome and can be explained by both a concentrated focus of improving the major constituent estimate. Additionally, the effect of self-cancelling errors prevails to some extent as well, combining to assist in improving wetted area prediction accuracy.

5.6 Estimating the Volume for Living Space and Fuel

The physical property of volume is quite an important working parameter for all aircraft design proposals. Usable volume for cabin has a direct correlation to how amenable (or not) the living space will be perceived by passengers when the mission is being undertaken. In the context of commercial transports where a known number of passengers predetermines the cabin length, the living volume really means a sufficient amount of headroom or possibly seat width resulting from a more generous cross-sectional area. For business aircraft, cabin volume means an ability to stand up and walk comfortably from one end of the cabin to the other. Establishing an accurate estimate of the maximum volume to house fuel is another important prerequisite. It can be appreciated that since the fuel volume is one of the integral working quantities that help define the MTOW and thus performance capability, efficiency, etc., due consideration should given to improving prediction algorithms where they are found wanting.

5.6.1 Approximating the Cabin Volume

This parameter is one of the fundamental metrics used in assessing the competitiveness of one cabin over another. Owing to the nature of geometry associated with cabin cross-sections, i.e. the living space is usually fashioned by the removal of a circular segment from the fuselage lower portion; computation of this objective function has been more often than not neglected. The following is a simple procedure in approximating the gross cabin volume of any type of cross-section, whether circular or ovoid in shape. The method works off the premise, firstly, that the cross-section is uniform throughout, and the designer has already quantified the primary working parameters, namely, the maximum cabin height, h_{cab}, the maximum cabin width, w_{cab}, the cabin floor width, w_{flr}, and the length of the cabin, l_{cab}. Figure 17 provides a schematic representation of the physical problem being analysed.

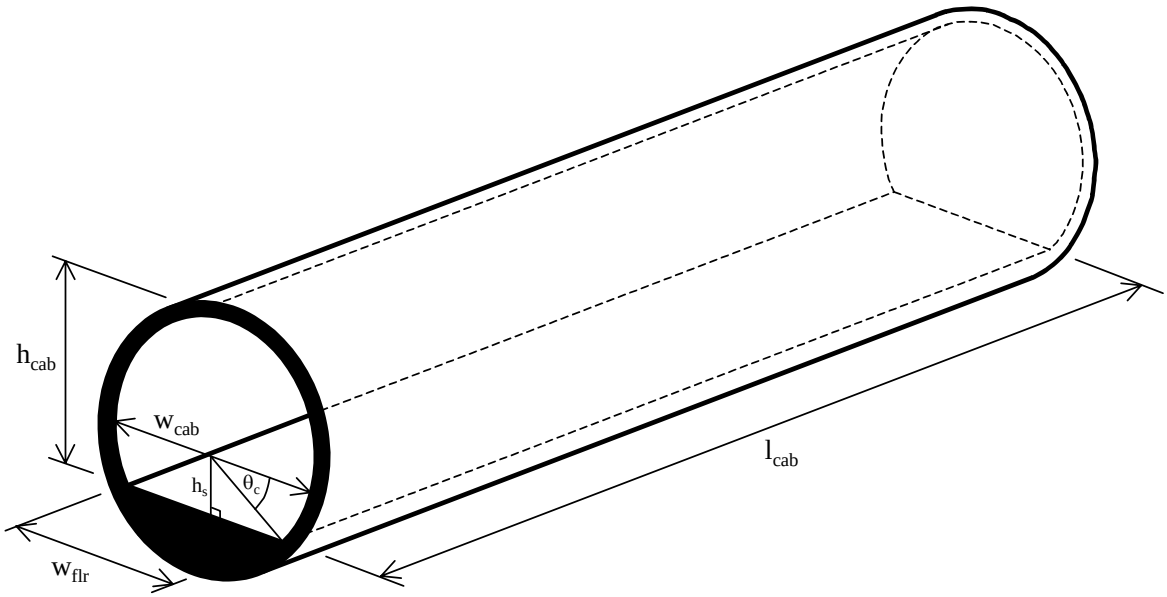

Figure 17. Primary working parameters required in estimating the cabin volume of both circular and ovoid cross-sections.

Assuming the maximum cabin radius remains approximately constant from the maximum width line to the floor, the residual height from the fuselage cross-section vertical axis mid-point to the floor, h_s, is found simply from

$$h_s \cong \frac{1}{2}\sqrt{w_{cab}^2 - w_{flr}^2} \tag{68}$$

The angle θ_c for any fuselage cross-section is given using basic trigonometry, thus

$$\theta_c = \tan^{-1}\frac{2h_s}{w_{flr}} \tag{69}$$

The value of θ_c in Eq. (69) becomes an approximation since the distance h_s using Eq. (68) will always be an estimate, however, with the introduction of some consistent key parametric assumptions to follow, the final algorithm for cabin volume is expected to yield a sufficiently accurate result. To continue, an estimate of the cabin upper cross-sectional area bounded by vertical and lateral axes with quadrant measurements of $(h_{cab} - h_s)$ and $w_{cab} / 2$ respectively, can be produced by associating the closed shape to that of a half-ellipse.

$$A_1 \cong \frac{\pi w_{cab}^2}{4}\left(h_{cab} - h_s\right) \tag{70}$$

The sector swept-out by angle θ_c can be thought of as equivalent to a circular arc with radius approximately equal to $w_{cab} / 2$. The area estimate within this sector, doubled to acknowledge both left and right hand side contributions, is given by

$$A_2 \cong \frac{\theta_c w_{cab}^2}{4} \tag{71}$$

A final account of the total cabin cross-sectional area is made by computing the isosceles triangle with measurements of w_{flr} and h_s for base and height respectively

$$A_3 = \frac{h_s\, w_{flr}}{2} \tag{72}$$

The total volume of the cabin is found by taking the product of cabin length, l_{cab}, and summation of the cross-section area constituents, namely, $A_1 + A_2 + A_3$. Combined with some algebraic manipulation, the final result reads as

$$V_{cab} = \frac{l_{cab}}{4}\left[w_{cab}\left(\pi h_{cab} + \theta_c w_{cab}\right) + h_s\left(2w_{flr} - \pi w_{cab}\right)\right] \tag{73}$$

To establish the applicability of Eq. (73) in estimating the cabin volume of transport aircraft, Figure 18 plots the estimation error (ε = predicted – actual) against manufacturer quoted values. As it can be seen, the method mostly produces results within a ±5% splay, with occasional excursions outside this bound, but generally not exceeding ±10%.

Aircraft cabin volume data used in this validation exercise consisted of cabins drafted

in the CATIA CAD environment. The list included: Airbus A319 Corporate Jetliner; Boeing B717-200, B737-600, and, BBJ1 and BBJ2 business jets; Bombardier Aerospace Learjet 31A, Learjet 45, Learjet 60, Continental, CL-604 Challenger, Global 5000, Global Express, CRJ200, CRJ700, CRJ900; Cessna Citation CJ2, Citation Bravo, Citation Encore, Citation Excel, Citation Sovereign and Citation X; Dassault Aviation Falcon 50EX, Falcon 2000EX, Falcon 900EX and Falcon 7X; Embraer Legacy, ERJ 135, ERJ 140, ERJ 145, Embraer 170, Embraer 175, Embraer 190 and Embraer 195; Fairchild Dornier 328JET, 728 and 928; Gulfstream Aerospace G100, G200, GIV-SP and GV-SP; Raytheon Premier I, Beech400A, Hawker 450, Hawker 800XP and Hawker Horizon.

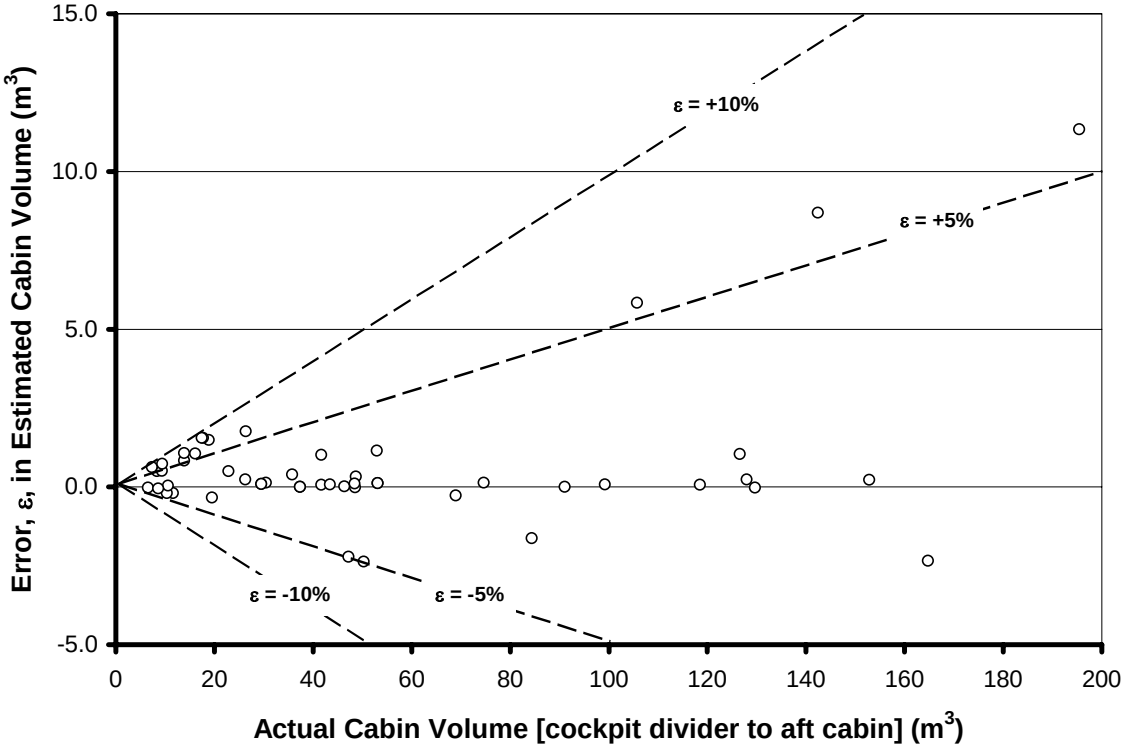

Figure 18. Prediction accuracy of method to estimate cabin volume of any transport aircraft.

5.6.2 Estimating the Fuel Capacity of Integral Fuel Tanks in Wings

For contemporary transport aircraft, it is common practise to store fuel using integral tanks. These tanks are created by sealing the airframe wing structure and are partitioned via segments comprising the fore and aft bulkheads, wingbox and any discontinuities imposed within wing structure (i.e. cut-out due to engine and tanks limited by wing span). Figure 19 presents an example layout of integral wing tanks for equipment with power plant layout configured as underwing podded or on-wing assemblies. In this instance, the forward and aft spars have been assumed to be continuous, and a volume cut-out has been incorporated in recognition of engine nacelle placement. The greatest advantage integral tanks have compared to other philosophies is that fuel volume can be maximised within the wing geometry. From this perspective, it is reasonable to assume that the wing structure geometry may be used for calculating available volume for fuel with adjustments made for structure.

The estimation of wing tank volume is partitioned into two classifications: calculation of the maximum volume for a wing free of nacelle placement, and, a decrement in volume due to a structural cut-out accounting for presence of power plant. The maximum volume estimate relies on the premise that each tank is continuous and is trapezoidal in plan view and they collectively extend out to a nominated maximum span chosen by the designer. The tank maximum span is typically around 70% of wing semi-span, however, additional fuel increments may be considered for extended/long-range performance by increasing the maximum span past this conventional value. Figure 19 demonstrates that each tank is bounded by dimensions of local tank chords at inboard and outboard tank spans, and, terminates at the maximum tank span. All the tank chords are quantified using the property of geometric similarity as given by Eq. (26) either for the complete wing, or, if the wing is cranked, separately for each designated trapezoidal panel. A pragmatic tank width is to assume the dimensions are bounded structurally by fore and aft wing spars, and typically, the two spars are spaced at a non-dimensional distance of l_{SP}.

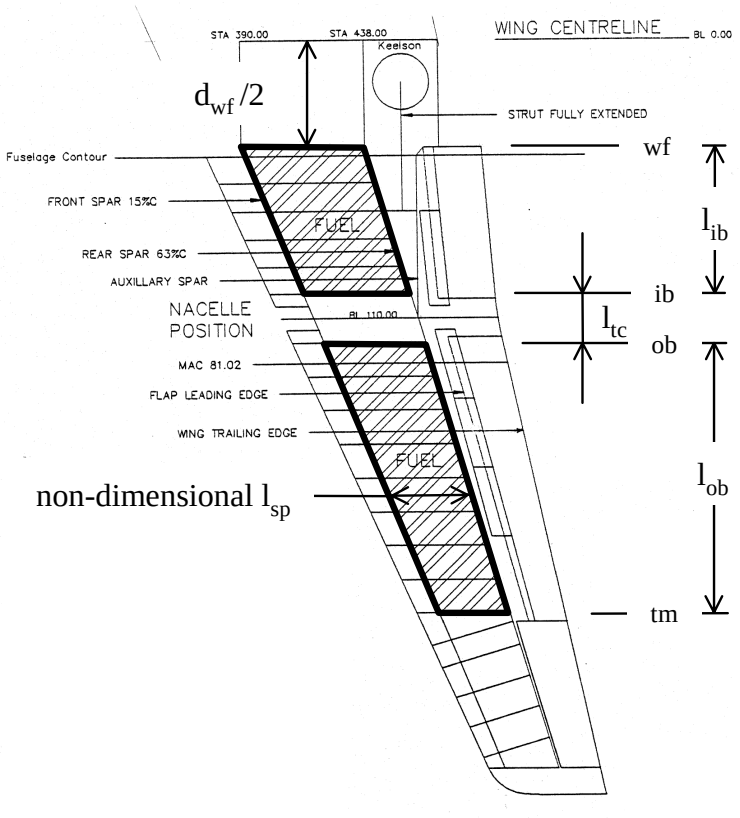

Figure 19. Example geometric layout of integral fuel tanks within the wing structure that caters to tank span discontinuity.

Volume encased by the each tank is more precisely described by an elliptical cylinder with pieces cut by perpendicular planes on both ends representing a discontinuity imposed by both the forward and rear wing spars. In an effort to economise complexity, this volume may be adequately described by a truncated pyramid geometry with rectangular cross-section[1]. Based on the example given in Figure 19, the simplest and most direct expression to compute the total wing fuel volume is

$$V_{wingf} = 2\frac{k_{adj}\, b_t}{3}\left[(t/c)_{tm} l_{sp,tm}\, c_{tm}^2 + (t/c)_{wf} l_{sp,wf}\, c_{wf}^2 + \sqrt{(t/c)_{tm} l_{sp,tm}\, c_{tm}^2 (t/c)_{wf} l_{sp,wf}\, c_{wf}^2}\,\right] - 2\frac{k_{adj}\, l_{tc}}{3}\left[(t/c)_{ob} l_{sp,ob}\, c_{ob}^2 + (t/c)_{ib} l_{sp,ib}\, c_{ib}^2 + \sqrt{(t/c)_{ob} l_{sp,ob}\, c_{ob}^2 (t/c)_{ib} l_{sp,ib}\, c_{ib}^2}\,\right] \quad (74)$$

where the collective tank span, b_t, is equal to

$$b_t = l_{ib} + l_{tc} + l_{ob} \quad (75)$$

The parameter c is the local wing chord, and the subscripts wf, ib, ob and tm denote the wing-fuselage juncture, inboard tank outer locale, outboard tank inner locale and maximum tank span wing stations respectively. Since each of the parallel end faces were taken to be rectangular in shape (as opposed to something like two catenaries or ellipse), an adjustment must be incorporated to reconcile the over-estimated volume. The correction has been approximated to equal 4%. Additionally, an account should be made to represent loss of available volume due to presence of structure. Torenbeek[1] indicates that this loss is around 4%. Combining both these corrections in the form of a linear factor results in k_{adj} = 0.92. The relative spar spacing l_{sp} can be obtained from a conceptual wing structure layout, or, in the absence of such dimensioning, an empirically derived value of $l_{spar} \approx 0.48$ can be employed. The wing thickness at any wing station can be found according to the premise outlined by Eq. (61).

Even though the above example tank layout assumed continuous forward and rear spars and the gross volume operation was conducted in one step, a more accurate assessment can be produced if the designer partitions the tank computations into multiple panels. Eq. (74) would then be applied to each tank and the total tank volume estimate would then be produced upon summation of each of these constituents.

5.6.3 Estimating the Fuel Capacity of Centre Tanks

In many instances, variants from a basic equipment type specification will be performed with particular scope given to cater for enhanced performance capabilities as the design matures in the market. One common option is to allow for extended range (ER) or long-range performance by the introduction of a centre tank that enables supplementary fuel quantities, or, on some occasions outboard wing tanks may be employed. A good transport aircraft conceptual design should always give scope for increased gross weight variants of the basic vehicle in order to fulfil new niche service required by operators in the future. The basic design should not only meet the original specifications from the outset, but further trade studies should be conducted to surmise the impact of Increased Gross Weight (IGW) variants.

A centre fuel tank volumetric calculation involves appreciation of the wing-fuselage junction locale, or, more specifically where wing fillets interface with fuselage geometry. The fillets are incorporated to avoid premature flow separation, buffet and drag, and, also serve as delineation between centre and the inboard wing tanks. As a basic rule, it is proposed that the fillet structure meets fuselage curvature at a vertical position of approximately $3t_R / 2$ (where t_R is equal to the maximum wing thickness at mid-span) from which the centre wing chord line is offset by distance $\xi_w\, d_h$ radially from the fuselage lower segment. From this fundamental assumption, the total length of the tank can be derived using simple trigonometry as exemplified by Figure 20.

After some algebraic manipulation, the fuselage geometric chord d_{wf}, which represents the centre tank length, is derived by the equation

$$d_{wf} = \sqrt{4\xi_w (1-\xi_w) d_h^2 + 6(1-2\xi_w) d_h \, c_R (t/c)_R - 9 c_R^2 (t/c)_R^2} \tag{76}$$

where ξ_w a factor between 0 and 1, d_h is the fuselage horizontal diameter, c_R is the wing root chord and $(t/c)_R$ is the wing thickness ratio at wing semi-span b / 2. Now that the location of the wing-fuselage juncture has been identified, the centre tank width must be calculated. A pragmatic tank width is to assume the dimensions are bounded structurally by fore and aft wing spars, and typically, the two spars are spaced at a non-dimensional distance of l_{sp}. Since the tank length has been calculated, this information together with the property of geometric similarity can be utilised to dimension local chord length at the wing-fuselage juncture c_{wf} using Eq. (26).

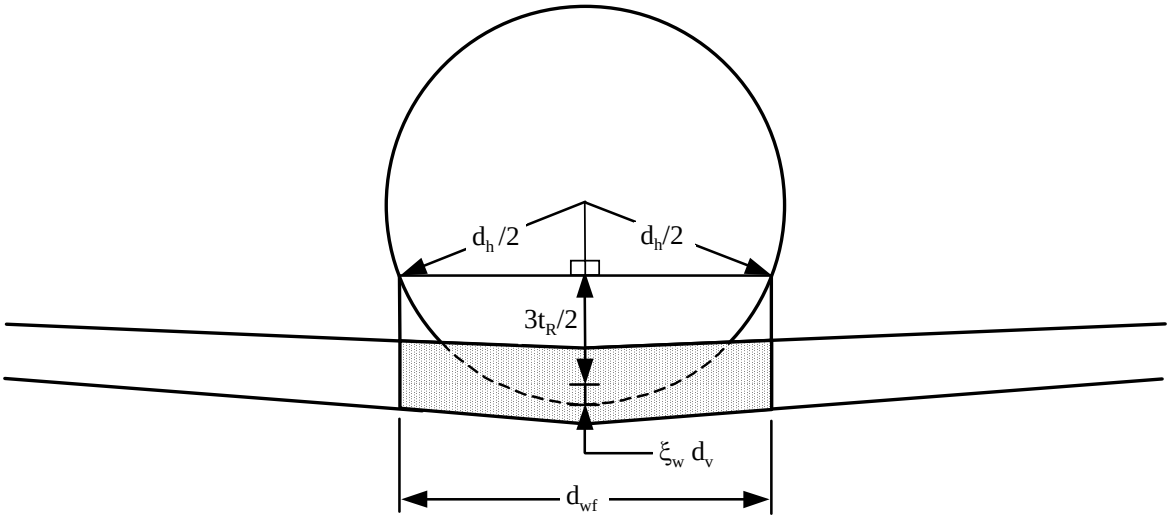

Figure 20. Dimensioning of the centre fuel tank for volume prediction (forward view).

As for the wing fuel tank(s), the volume encased by the centre tank would be adequately described using a truncated pyramid geometry with rectangular cross-section and corrections made for structure and actual geometry

$$V_{centf} = \frac{k_{adj} d_{wf}}{3} \left[(t/c)_{wf} l_{sp,wf} c_{wf}^2 + (t/c)_R l_{sp,R} c_R^2 + \sqrt{(t/c)_{wf} l_{sp,wf} c_{wf}^2 (t/c)_R l_{sp,R} c_R^2} \right] \tag{77}$$

5.6.4 Estimating the Fuel Capacity of Forward and Aft Wing-Fuselage Fairing, Conformal and Aft Fuselage Auxiliary Tanks

The total volume for any under floor and wing-fuselage fairing conformal tank configuration involves the addition of volume housed by a cylinder with base area equal to the lower fuselage cross-section circular segment, and, volume stored in fairings that adhere to an elliptic paraboloid geometric description. As elucidated earlier, elliptic paraboloids more accurately describe volume encased by the forward and aft fuselage fairing and saddle tanks. The aft fuselage auxiliary tank is simply predicted assuming a cylinder with segment cutout bounded by the circular cross-section and chord.

Using Eq. (29) and Eq. (73) as a basis, the circular segment cylinder or under floor tank volume (V_{uflr}) is given as

$$V_{uflr} = k_{adj} l_{uflr} \left[A_{XS} - \frac{d_h}{8} \left(\pi d_v \left[2\xi_x + 1 \right] + 2\Theta_c d_h \right) + \frac{\xi_x d_v}{4} \left(2d_{flr} - \pi d_h \right) \right] \tag{78}$$

for tank length l_{uflr}, geometric chord d_{flr} established at the cabin floor water-level or double-bubble upper and lower lobe juncture point, and the angle Θ_c for any fuselage cross-section is given using basic trigonometry

$$\Theta_c = \tan^{-1} \frac{2\xi_x d_v}{d_{flr}} \tag{79}$$

The volume of an elliptic paraboloid[45] is given as half the body's base, which is an ellipse, multiplied by the height. If the volume analysis is put into context of an aircraft design problem, the maximum volume enshrouded by the fairing, either forward or aft, is equal to a half-body elliptic paraboloid

$$V_{fairf,tot} = \frac{\pi k_{adj}}{8} (t/c)_R \, c_R \, d_{wf} \, l_{fair} \tag{80}$$

Presumably, it will be more common to utilise a conformal faring tank that is some proportion as opposed to the entire length of the body. In such cases, a body of volume needs to be removed from the total permissible given by Eq. (80), and this should be defined as space between the body apex to the residual length produced when deducting the chosen body length for usable fuel from the entire body length. Working off Eq. (80) as a basis, a more flexible expression to compute total fuel stored in either the forward or aft fairing assuming some proportion of the body used as storage is presented here as

$$V_{fairf} = \frac{\pi k_{adj}}{8} l_{fair} \left[(t/c)_R \, c_R \, d_{wf} - 2a_{res} \, b_{res} \left(1 - k_{res} \right) \right] \tag{81}$$

The constant k_{res} represents the fraction of fairing to be designated as a conformal fuel tank. The parameters a_{res} and b_{res}, which are the values of height and width (of the elliptic paraboloid half-body) respectively at fairing body station (1 - k_{res}) l_{fair}, are computed using the geometric description algorithm detailed previously, and more specifically defined by Eq. (38) through Eq. (40).

Another common approach in storing fuel is to utilise an aft fuselage auxiliary tank. Examples of such installations can be found in the Bombardier Aerospace Canadair SE[63] (less centre aisle thoroughfare) and Global Express[64], Embraer Legacy[49] and Gulfstream Aerospace G200[48] business jets. These tanks are generally located aft of the aft cabin bulkhead and can be taken to be congruous with the constant cross-section that defines the cabin living volume. Using the formula that predicts cabin volume as a guide, the total volume possible for storage in the aft fuselage with tank length l_{auxf}, is approximated to be

$$V_{auxf} = \frac{k_{adj} l_{auxf}}{4} \left[w_{cab} \left(\pi h_{cab} + \theta_c w_{cab} \right) + h_s \left(2w_{flr} - \pi w_{cab} \right) \right] \tag{82}$$

intentionally blank

6 Predicting the Weight of Major Constituents

Conceptual aircraft empty weight functional sensitivity of design parameters are commonly expressed as having an exponential relationship based on statistics and empiricism. As is the case with most weight prediction methods in literature[1,2,4,5,39], more refined estimates based on statistical equations through sophisticated regression analysis become transcendental algorithms characterised by relatively small and partially self cancelling errors with an accuracy of the order of 5-10%. Investigations have shown this to be somewhat true for specific methods but were found to be wanting in many instances when adequate objective function sensitivity for rather advanced trade studies are desired. For the purposes of optimisation, it is of utmost importance that an adequate parametric representation of the relationship between applied loads, geometric shape and configuration choice are achieved.

6.1 Overview of Deriving Weight Estimating Relationships

The final weight estimation algorithm adopted involves a hybrid transcendental approach using Linnell's[65] parametric description suitably modified for major components in conjunction with additional methods that supply fidelity from more specific parameters related to performance and geometry. Moreover, by adopting Scott and Nguyen's[66] notion of two functional weight groups, a basis can be laid for derivation of the aircraft Operational Weight Empty[††] (OWE). Since the sum of fuel and payload, or combined to constitute the so-called useful load, can be regarded as both a variable to optimise and the objective function, a third functional weight group is now introduced - leading to a combination of all three for Maximum Takeoff Weight (MTOW).

The second functional group designated as fixed equipment weight are estimated using a variation of the method given by Scott and Nguyen. The fixed weight is referred by Scott and Nguyen to be a "constant weight" because it is assumed to be related to passenger capacity, and hence, constant during the conceptual sizing process. The variation of a linear constant weight coefficient models the impact of fuselage size to fixed equipment and it can be quickly surmised that this parameter is specific to each respective manufacturer, therefore requires some measure of augmentation. The third and final function group consists of weights characterised by ancillary geometric and philosophical considerations. These encompass estimation of available fuel weight with or without a centre and auxiliary tanks, and, contingency design maximum payload-OWE allowances. A philosophical decision of artificially increasing the desired maximum payload by some factor to create a contingency buffer for unexpected OWE penalties incurred during preliminary design is often considered in practise and is therefore also facilitated. To round off these functional groups, an advanced technology multiplier to account for weight reduction possibilities of aircraft empty weight is also available.

6.2 The First Functional Weight Group

The first functional weight group comprises wing including winglet, fuselage, landing gear and empennage constituents. All of the weight estimating relationships (WER) describing these components are expressed as functions of the MTOW, and therefore represent a transcendental disposition of the complete vehicular WER algorithm.

[††] The equivalent of OWE for business jets is the BOW. This weight comprises the summation of the green aircraft weight (MEW equivalent), completion allowance and paint, and operating items, which includes the flight crew.

6.2.1 The Advanced Technology Multiplier

This parameter, first proposed by Scott and Nguyen[66], postulates the potential for weight reduction in the future based on observed trend data covering the last forty years. The dataset of statistical information from which the Scott and Nguyen Advanced Technology Multiplier (ATM) is derived relates primarily to the so-called constant weight group. The constant weight category is proportional to passenger capacity and includes items such as APU, instruments, electrical, avionics, furnishings and equipment, ECS and any fixed useful load. Scott and Nguyen highlight the constant weight group has declined by about 0.15% per year. Using the premise that an average entry-into-service year is 1975 as a reference, and introducing a refinement over Scott and Nguyen's originally derived improvement in weight reduction over time, a new redefined ATM (Π_{ATM}) is suggested as

$$\Pi_{ATM} = e^{2.965-0.001525\,YEIS} \tag{83}$$

where the year of entry into service of the aircraft design being analysed is represented by the variable YEIS. It should be noted that Eq. (83) is intended only for the constant weight group. Scott and Nguyen also propose an ATM applicable for the variable or first functional weight group, namely, wing, empennage, fuselage and landing gear. Scott and Nguyen indicate ATMs of about 0.85 have been estimated for very advanced transports. This value is considered to be quite optimistic within the more pragmatic realm of contemporary transport aircraft design and manufacturing, so, by utilising the more conservative operator given by Eq. (83), the designer is able to account for a certain element of optimism in setting the minimum goal for weight without incurring unnecessarily high amount of risk.

6.2.2 Wing Weight Estimating Relationship

A pragmatic wing WER (W_{wing}), formula proposed by Linnell[65] has the exponential form

$$W_{wing} = \Pi_{ATM}\,\alpha_w\,\Pi_{Cw}\left[\frac{W_G\,n_{ult}\,S_w\,AR^{\beta_w}\left(\chi_w + \lambda/2\right)\tau_S^{\delta_w}}{\Pi_{t/c}\cos^{\varepsilon_w}\Lambda_{Qchd}}\right]^{\phi_w} \tag{84}$$

W_G is the vehicle design weight or MTOW (kg) for the candidate being analysed, S_w the vehicle's reference wing area (m^2), AR is the reference wing aspect ratio, λ the reference wing taper ratio, and, Λ_{Qchd} is the reference wing quarter chord sweep (deg.). The exponents found in Eq. (84) are equal to ϕ_w = 0.656 and $\beta_w = \delta_w = \varepsilon_w$ = 1.5 with associative constants given as α_w = 0.0328 and χ_w = 1.1. The coefficient α_w represents a departure from Linnell's original trend coefficient value in keeping with a more contemporary aircraft weights database.

Based on experience, aeroplanes are certified to withstand limit load factors so that structure does not begin yielding until a certain threshold is surpassed. JARs and FARs require factors of safety of 1.5 to be administered during the sizing process. Since the certification requirements do not permit manoeuvring load factor for any speed up to V_D (design dive speed) to be less than 2.50, a fixed quantity of ultimate load = factor of safety x limit load, or, n_{ult} = 1.5 x 2.50 = 3.75 is typically assumed. This value is appropriate for large transport aircraft, however, for vehicles of smaller size the most critical case may be attributable to gust loads, thus, altering the nature of the wing's root bending moment

sensitivity[12]. The gust limit load factor on an aeroplane predominates when operating at lower AUWs. Assuming the design cruising speed $V_c = V_{MO}$ is critical for the gust load case, the load factor[67] is

$$n_{gust} = 1 + K_g \, C_{L\alpha A} \, \rho \, U_{de} \, V_c \, \frac{S_W}{2W} \tag{85}$$

The gust alleviation factor, K_g, is given as an empirical function of the so-called mass parameter μ

$$K_g = \frac{0.88\mu}{5.3 + \mu} \tag{86}$$

where

$$\mu = \frac{2}{g \, c_{gm} \, \rho \, C_{L\alpha A}} \frac{W}{S_W} \tag{87}$$

and the geometric mean chord is found by the relation, $c_{gm} = S_W/b$. Torenbeek[12] indicates that the critical situation occurs for W = Maximum Zero Fuel Weight (MZFW) and suggests examining a standard scenario of flight at an altitude of FL 200 and a high-speed gust velocity of U_{de} = 15.2 m/s (50 fps) taken from the FAR airworthiness standards[68].

For straight tapered wings, the vehicular lift-curve slope, $C_{L\alpha A}$, can be approximated using the Helmbold equation[34] adjusted for sweep and incorporating the Prandtl-Glauert compressibility correction, namely, $\beta = (1\text{-}M^2)^{1/2}$,

$$C_{L\alpha A} \cong \frac{C_{l\alpha} AR}{\frac{C_{l\alpha}}{\pi} + \sqrt{\left(\frac{AR}{\cos \Lambda_{Hchd}}\right)^2 + \left(\frac{C_{l\alpha}}{\pi}\right)^2 - AR^2 \, M^2}} \tag{88}$$

where Λ_{Hchd} is the reference wing half chord sweep (deg.). Assuming a thin airfoil, section lift-curve slope of $C_{l\alpha}$ = 0.11 per deg. (2π per rad) is given theoretically, however, it was found an average of 0.088 per deg. (5.04 per rad) taken from Abbott and Von Doenhoff[69] yields more realistic predictions.

Now that the gust limit load factor is quantified, the next step is to choose the most limiting scenario between manoeuvre and the gust cases. This is achieved via an impulse function that identifies the maximum between tested values (see Eq. (10) for details).

$$n_{ult} = 1.5 \, \Phi_{max}\left(n_{gust}, 2.5\right) \tag{89}$$

Π_{Cw} is a design factor that exhibits dependence on aeroplane configuration, i.e. low-wing versus high-wing layout, spoilers, undercarriage placement, and is given by the derived constituent expression

$$\Pi_{Cw} = k_{co} \, k_{sp} \, k_{lg} \tag{90}$$

The k_{co} parameter flags wing installation philosophy and is equal to 1.17 for low-wing vehicles, whereas, k_{co} = 1.25 would simulate a high-wing option. Assuming a linear variation, the contribution expressed as a function wing placement per fuselage cross-section non-dimensional height is

$$k_{co} = 1.17 + 0.08\xi_w \tag{91}$$

The configuration choice is further sub-divided into consideration given for the presence of spoilers, i.e. k_{sp} = 1.02 when $\Phi_{sp} = \Phi(s,1) = 1$ (otherwise unity when s < 1)

$$k_{sp} = 1 + 0.02\Phi_{sp} \tag{92}$$

and, whether the undercarriage is to be integrated as an on-wing installation or not

$$k_{lg} = 1.03 - 0.015\,\Phi_{lg} \tag{93}$$

When s = 1, the impulse function, $\Phi_{lg} = \Phi(s,1)$, introduces an additional correction due to an on-wing nacelle-undercarriage integration otherwise is zero for s < 1.

By incorporating all the constituents given by Eq. (91) through Eq. (93) into Eq. (90), and neglecting the small terms, the correction due to aircraft configuration reads as

$$\Pi_{Cw} = 1.2051 + 0.08240\xi_w + 0.02410\,\Phi_{sp} - 0.01755\Phi_{lg} \tag{94}$$

τ_S is a measure of structural stiffness, which is hypothesised to vary with dynamic pressure and limit loads. This contribution is described by

$$\tau_s = 1 + 1.31\left(\frac{0.5\rho_{sls}\,V_{MO}^2}{1000g}\right)^2 \frac{1}{n_{ult}^3} \tag{95}$$

where V_{MO} is the maximum operating speed at sea level standard conditions expressed in units of m/s and ρ_{sls}/g is equal to 0.125 kg s^2/m^4.

$\Pi_{t/c}$ is a wing thickness factor expressed as a trigonometric association given by

$$\Pi_{t/c} = 16.5 \sin 2\pi\left(\frac{t}{c}\right)_m \tag{96}$$

6.2.3 Winglet Weight Estimating Relationship

The winglet device WER is segmented into two contributions: the first is simply the constituent weight contribution due to the assemblies, and the second pertains to a structural consequence to the wing itself. The first contribution relies on the notion of structural design congruity with the wing structural system, and quantifying this involves the assumption of similarity in structural efficiency exemplified by weight per unit surface area. It is commonly appreciated that the reduction in vortex-induced drag due to presence of winglet devices varies in proportion to the amount of additional loading seen outboard of the wing towards the tips. This refashioned span load distribution comes with a penalty epitomised by increasing wing root bending moments[70,71]. Predicting the weight increase

due to correspondingly increasing local bending moments is not one easily open to simplification. Nonetheless, a basic algorithm can be constructed using experimental results as the guideline. Based on the winglet height and cant angle parameter sensitivity studies conducted by Ishimitsu[70], experimentation indicates the rate increase in wing root bending moment is proportional to the rate reduction in vortex-induced drag. When examining a given winglet dimensional configuration, the variation of the rate reduction in vortex-induced drag was found to vary almost linearly with instantaneous lift coefficient. In view of these observations, it is conceivable that a plausible inference could be that an increase in wing weight assuming the presence of a winglet device would be linearly proportional to the potential for reduction in the vortex-induced drag.

The final algorithm for predicting the total winglet weight is found by incorporating the two contributions, namely component or assembly weight, and collective wing structural augmentation. Neglecting a weight contribution due to flutter ballast (to meet certification requirements of demonstrating flutter free flight up to $1.15V_D$ and $1.15\ M_D$ dive speeds), the incremental weight for a given winglet device dimensional configuration is proposed here as

$$\Delta W_{wlet} = \frac{W_{wing}}{2}\left(\frac{S_{wet,wlet}}{S_{wet,wing}} + 0.7\,\partial\frac{dC_D}{dC_L^2}\right) \tag{97}$$

The wetted area constituents $S_{wet,wing}$ and $S_{wet,wlet}$ which represent the wing and winglet respectively, can be computed using Eq. (64). The parameter $\partial d^2C_D/C_L{}^2$ represents a fractional change operator for the vortex-induced drag factor, and is quantified by comparing the original wing planform and an equivalent wing planform with winglets canted as some angle off the vertical. Details of how this operation is computed is presented in Section 7.7.1.

6.2.4 Fuselage Weight Estimating Relationship

The fuselage weight formula primarily exhibits functional sensitivity to dimensional and body slenderness parameters together with influences attributable to maximum cabin differential pressure, design load factor, dynamic pressure and heavy masses mounted directly to the structure. The fuselage WER is of the form

$$W_{fuse} = \Pi_{ATM}\left[\alpha_f\, k_{\Delta P}\, \Pi_{Cfg}\, l_{fuse}^{\beta_f+\chi_f}\, d_{equiv}^{\chi_f-\beta_f}\left(\frac{n_{ult}}{\delta_f}\right)^{\varepsilon_f} W_{Gs}^{\phi_f}\left(\frac{V_{MO}}{\varphi_f}\right)^{\gamma_f} + \Pi_{Cfe}\right] \tag{98}$$

The parameter W_{Gs} represents the candidate's MTOW less wing weight and other heavy masses mounted directly to the wing structure. The exponent values are $\beta_f = 0.50$, $\chi_f = 0.75$, $\varepsilon_f = \phi_f = 0.40$ and $\gamma_f = 0.30$; the factors are equal to $\alpha_f = 0.585$, $\delta_f = 3.75$ and $\varphi_f = 298$. The variable l_{fuse} is the fuselage length (m), and d_{equiv} is a fictitious equivalent fuselage external diameter and is found by taking into account the fuselage vertical and horizontal diameters

$$d_{equiv} = \frac{2d_v + d_h}{3} \tag{99}$$

The influence of differential cabin pressure requires special treatment here. Linnell[65] had originally presented a table correlating correction factors for cabin pressurisation against a given design's maximum pressure differential. The onus was then on the designer to introduce this correction in a discrete manner. To accommodate a continuous function concept, an adequate account for the fuselage weight versus pressure relationship was obtained by fitting to an exponential expression. The pressure relationship ($k_{\Delta P}$) reads as

$$k_{\Delta P} = 1.066\, e^{0.002959 \Delta P} \tag{100}$$

where the pressure differential ΔP is expressed in units of kPa.

Π_{Cf} is a design factor that takes into account the presence of cut-outs, such as doors and windows, considered as a fixed value of 1.10. The design factor also signifies the impact of landing gear integration. If the landing gear is to be mounted in the fuselage, a dependence algorithm expressed as a function of landing gear installation philosophy, Φ_{lg}, in conjunction with wing vertical placement, $\Phi_{\xi w}$, needs to be addressed. The fuselage mounted landing gear correction factor is given as 1.03 and this value is invoked only if an on-wing integrated nacelle installation is not considered and the wing vertical placement is greater than $0.25d_v$, or $\Phi_{\xi w} = \Phi(\xi_w, 0.25)$. Combining both these aspects into a single operation becomes

$$\Pi_{Cfg} = 1.1 + 0.033 \Phi_{\xi w} \left(1 - \Phi_{lg}\right) \tag{101}$$

Eq. (98) represents a default vehicular configuration where the engines are installed as under-wing nacelles with pylons, and is hence considered to be a reference configuration layout. An additional fuselage weight penalty is imposed through introduction of ancillary support structure to house aft-fuselage mounted power plants. Torenbeek[1] indicates increased fuselage bending moments may be generated on touchdown for such engine installations - implying an incremental weight contribution to sustain structural integrity for such circumstances. A calculation method is presented by Torenbeek that correlates a weight penalty proportional to the longitudinal distance between engine mounts and the extended rear spar line at the reference wing mid-span wing chord locale referred to fuselage diameter in plan view and the maximum takeoff gross weight of the vehicle.

$$W_{afe} = k_{afe} \frac{l_{eng}^2}{d_{wf}} W_G \tag{102}$$

W_{afe} is the fuselage structural weight increment due to presence of aft mounted engines, k_{afe} is a constant, l_{eng} is the longitudinal distance between aft engine mounts and the extended rear spar line at the reference wing mid-span wing chord locale.

Upon examination of a variety of aft-fuselage mounted configurations, Torenbeek's mathematical premise was employed but using a variant more accommodating to a conceptual first approximation of physical scale. It had been empirically observed that a relationship between the constituent fuselage structure and geometric modules, i.e. forward and cabin sections, the total fuselage length, and, where the wing semi-span chord apex is located can be established empirically to produce an initial guess for l_{eng}. It was found that the reference wing apex point is situated at a mean location of $0.4l_{fuse}$, and in conjunction with a nominal rear spar of $0.65c_R$, a WER which accounts for the influence of aft-mounted engines can be derived to be

$$W_{afe} = k_{afe} \frac{\left[l_{nos} + l_{cab} - 0.4l_{fuse} - 0.65c_R\right]^2}{d_{wf}} W_G \tag{103}$$

with $l_{nose} = \varepsilon\, d_v$ and the constant of proportionality $k_{afe} = 5/3$.

An alternative to both under-wing podded and aft-fuselage mounted approaches for power plant installations may involve an idea to integrate engines as an on-wing configuration where the entire nacelle synergistically enshrouds engine, local wing structure and facilitates the main landing gear through introduction of fairings extending from the basic nacelle to fulfil requirements of permitting adequate space and sound aerodynamic practise. This premise has an implication of potential weight reduction since the fuselage does not require ancillary support structure and wheel bays to house the retractable main landing gear. The main landing gear bay weight is assumed to be a linear function of the vehicle MTOW and by considering this correlation as a fuselage weight decrement whenever an on-wing combined with landing gear power plant installation is employed, it can be quantified as

$$W_{owe} = k_{owe} W_G \tag{104}$$

where W_{owe} is the potential fuselage weight reduction upon removal of both main gear bays and k_{owe} is a constant equal to 3.31×10^{-3}.

Combining both Eq. (103) and Eq. (104) to create a mathematical expression for contribution of power plant installation philosophy with respect to fuselage weight becomes

$$\Pi_{Cfe} = \left[\Phi_{afe} k_{afe} \frac{\left[l_{nos} + l_{cab} - 0.4l_{fuse} - 0.65c_R\right]^2}{d_{wf}} - \Phi_{lg} k_{owe} \right] W_G \tag{105}$$

When s = 1, the impulse function, $\Phi_{afe} = \Phi(s,1)$, introduces a correction due to aft-fuselage mounted power plant installation, otherwise is zero for $s < 1$.

6.2.5 Undercarriage Weight Estimating Relationship

Landing gear weight formula is based on Linnell's[65] original premise of coupling vehicular gross weight, landing gear strut length, landing touch down speed and tyre inflation pressure. This description was subsequently generalised into a landing gear WER indicating solely a monotonic relationship to the maximum gross weight.

$$W_{lg} = \Pi_{ATM}\, \alpha_{lg} \left(\frac{W_G}{\beta_{lg}} \right)^{\chi_{lg}} \tag{106}$$

The coefficient values are $\beta_{lg} = 1.40 \times 10^4$, $\chi_f = 1.05$, and the factor, α_{lg} is given by the expression

$$\alpha_{lg} = 587 - 153\left(\Phi_{pwr} + \Phi_{\xi w} - \Phi_{\xi w}\Phi_{lg}\right) \tag{107}$$

The algorithm given by Eq. (107) works off the reference configuration of an under-wing podded engine installation, and introduces corrections due to wing placement and

landing gear type. An additional impulse function for power plant installation type, i.e. not an under-wing podded, is given as $\Phi_{pwr} = \Phi(s,1)$; $s < 1$ denotes the reference under-wing podded condition, otherwise, for $s \geq 1$ represents aft fuselage mounted, S-duct and straight duct integration.

6.2.6 Horizontal Tail Weight Estimating Relationship

Linnell[65] focuses on the horizontal tail as the reference for an ensuing vertical fin estimate. The WER of the tailplane is presented as similar form to that of wing weight prediction methodology

$$W_{ht} = \Pi_{ATM}\, \alpha_{ht} \left[\frac{W_G\, n_{ult}\, S_{ht}^2\, AR_{ht}}{\beta_{ht} S_w (t/c)_{ht,m} \cos^{\chi_{ht}} \Lambda_{ht,Qchd}} \right]^{\delta_{ht}} \tag{108}$$

Eq. (108) includes contribution due to elevators and any mass balancing. The factors values are equal to $\alpha_{ht} = 4.40$ and $\beta_{ht} = 10^4$, with the exponents defined to be $\delta_{ht} = 0.56$ and $\chi_{ht} = 1.8$. The variable S_{ht} is the vehicle's reference horizontal tail planform area (m^2), AR_{ht} is the reference horizontal tail aspect ratio, $(t/c)_{ht,m}$ is the representative relative thickness for the horizontal tail expressed as a decimal, and, $\Lambda_{ht,Qchd}$ is the reference horizontal tail quarter chord sweep (deg.).

6.2.7 Vertical Tail Weight Estimating Relationship

The vertical tail WER[65], including the rudder and mass balance, relies on the notion of structural design congruity with the horizontal stabiliser. This is achieved by assuming mathematical similarity of structural efficiency combined with an appreciation of geometric form

$$W_{vt} = \Pi_{ATM}\, \Pi_{Cvt}\, \frac{W_{ht}}{S_{ht}} S_{vt}\, \frac{(t/c)_{ht,m} \cos\Lambda_{ht,Qchd}}{(t/c)_{vt,m} \cos\Lambda_{vt,Qchd}} \tag{109}$$

S_{vt} is the reference vertical tail planform area (m^2), $(t/c)_{vt,m}$ is the representative relative thickness for the horizontal tail expressed as a decimal, and, $\Lambda_{vt,Qchd}$ is the reference vertical tail quarter chord sweep (deg.).

A design factor representing the choice whether or not synergy is to exist between the horizontal and vertical tails is denoted by the parameter Π_{Cvt}. Here, the impact of integration ranging from the conventional fuselage mounted horizontal tail to cruciform or the extreme of T-tail installation is modelled using a linear variation precept. Assuming a conventional tailplane installation is approximately in-line with the FRP, the horizontal tail vertical placement non-dimensionalised with respect to the fuselage maximum vertical diameter is defined as being $\xi_{ht} = 0$. In keeping with this convention, a T-tail arrangement would be ξ_{ht} = (vertical tail tip water-line minus FRP water-line) / d_v; it is evident that the ξ_{ht} parameter can have values greater than unity. To proceed, the design factor to account for empennage synergy is presented here as

$$\Pi_{Cvt} = 0.893 + 0.651\xi_{ht} \tag{110}$$

One conclusion readily drawn from examination of Eq. (109) is the notion that the algorithm does not work for aeroplane design candidates free of a tailplane surface. If a horizontal tail is not selected, an equivalent method is required to predict the vertical tail weight based on the above methodology. The idea is to employ the horizontal tail weight equation given by Eq. (108) on the vertical tail and then use the normalised weight-planform area relationship for the final vertical tail result.

6.2.8 Dorsal and Ventral Fin Weight Estimating Relationship

Here, the premise of structural design congruity with the vertical tail is assumed. Scaling the dorsal and ventral fin weight to that of the vertical tail weight per unit surface area produces

$$W_{fins} = \frac{W_{vt}}{S_{wet,vt}} S_{wet,fins} \tag{111}$$

where $S_{wet,fins}$ is the total dorsal and/or ventral fins wetted area and $S_{wet,vt}$ is the vertical tail wetted area; all the surface area measurements are predicted using Eq. (64).

6.3 The Second Functional Weight Group

The weight of the second function group is assumed as being influenced by required engine and fuselage size, where the latter is related to passenger capacity and/or cabin volume. Scott and Nguyen[66] refer to this component as the constant weight group because it is taken to be constant during the sizing process. Fundamentally, the second functional weight group is predicted using a linear relationship with passenger accommodation. This premise albeit useful, requires the incorporation of some additional operations in order to attain required fidelity depending on the type of aeroplane being considered, i.e. commercial transport or business jet.

6.3.1 The Constant Weight Passenger Coefficient

Extensive investigations were conducted in an attempt to reconcile both categories of transport aircraft, commercial and business vehicles, into a single weight prediction procedure. It was found that this goal could be accomplished with the proviso specific constant weight passenger coefficients are derived for the two distinct classifications: one dedicated to commercial transports, and the other, pertaining to business aircraft only. If one examines commercial transport aircraft, Scott and Nguyen's[66] procedure of simply using a coefficient of proportionality (hereon identified as k_{pax}) was found to be valid up to a certain point.

For commercial transports, the only problem that needs to be addressed is the question of how a continuous function concept can be generated between transports utilising a varying number of seats abreast and whether a single or multiple aisle concept is employed. Scott and Nguyen do not distinguish according to number of seats abreast and suggest a discontinuous change in value for the constant weight passenger coefficient between short-range narrow-body 2-class interior, and, long-range wide-body 3-class interior layouts. The final augmented Scott and Nguyen method incorporates an adjustment of the k_{pax} parameter according to increasing accommodation size. It is conceivable that an increase in the constant weight group efficacy, i.e. a reduction in the magnitude of k_{pax}, would exist in proportion to an increasing number of passengers. A multiple aisle premise is introduced into the prediction process by invoking additional adjustment to the k_{pax}

parameter for passenger accommodations greater than 180 passengers. For commercial transports carrying PAX number of passengers, one useful definition of this coefficient was derived to be

$$k_{cpax} = 55.168 + 10.344N_{abs} + 13.952\Phi_{pax} + 2.6160\Phi_{pax}N_{abs} - 3.9865PAX^{0.3494} \tag{112}$$

The major advantage of constructing the prediction algorithm of Eq. (112) in the form shown is an ability for the designer to gauge the sensitivity of primary drivers such as number of seats abreast (N_{abs}) and influence of a multiple aisle premise (adhering to $\Phi_{pax} = \Phi(PAX,181)$ impulse function). It is evident a coupled and cumulative influence to k_{pax} occurs for commercial transports with multiple aisles for given number of seats abreast, as exemplified by the $\Phi_{pax}N_{abs}$ component in Eq. (112).

Business aircraft require a completely different approach when it concerns the constant weight group estimate. Unlike commercial transports, supporting systems and interior completions are a function of not only the standard interior accommodation, but perhaps more importantly, proportional to the mission role defined for the aircraft. Even though the chief aim of designing a cabin living volume is to accommodate the standard number of passengers comfortably, the physical dimensioning of the cross-section and cabin length are also a function of mission duration. For example, long-range aircraft would stipulate a stand-up cabin philosophy with corresponding impression of greater freedom of movement within the living volume as opposed to short-range small business aircraft. Also, long-range business aircraft would need to house a crew rest area including additional lavatory compared to smaller aircraft. As a result, the k_{pax} coefficient represents a smaller contribution related directly to the standard passenger accommodation and more to the physical scaling of the living volume itself.

Driver parameters that demonstrate functional relationship to interior completion and systems weight were found to be the cabin volume and slenderness. Since it has been established that cabin living volume dimensioning can be considered as a consistent indication of mission duration and hence maximum range capability, no requirement arises to introduce a special functional representation for allowances such as crew rest area. Once the basic form of the algorithm had been established, the constant weight passenger coefficient operator for business aircraft was derived statistically to be

$$k_{bpax} = 15.651 + 38.270\frac{V_{cab}}{PAX} + 4297.1\frac{d_{ecab}}{PAX}\left(1 - \frac{4.7923}{l_{cab}}\right) \tag{113}$$

Similar to Eq. (99), the parameter d_{ecab} is a fictitious equivalent cabin internal diameter and is found by taking into account the cabin maximum height and width

$$d_{ecab} = \frac{2h_{cab} + w_{cab}}{3} \tag{114}$$

To complete the final prediction algorithm, both the commercial and business aircraft constant weight passenger coefficient operations are combined into one all encompassing expression

$$k_{pax} = k_{cpax} + \Phi_{acsel}\left(k_{bpax} - k_{cpax}\right) \tag{115}$$

6.3.2 Systems and Fixed Equipment Weight Estimating Relationship

The complete systems group comprises fuel (W_{sfuel}), flight controls (W_{fcnt}), APU (W_{apu}), instrumentation (W_{inst}), avionics (W_{avn}), hydraulics (W_{hyd}), electrical (W_{elec}), ECS (W_{ecs}), green furnishings (W_{furn}) and miscellaneous (W_{misc}) weights. Written out in algebraic form, the total systems weight (W_{sys}) group is

$$W_{sys} = W_{sfuel} + W_{fcnt} + W_{apu} + W_{inst} + W_{avn} + W_{hyd} + W_{elec} + W_{ecs} + W_{furn} + W_{misc} \tag{116}$$

The constituent weights for each system component can be estimated using methods detailed by Torenbeek[1] and Raymer[4]. Owing to the inherent difficulty in appreciating what constitutes each of these system components, the chances of producing adequate constituent estimates and subsequent combined systems prediction becomes mostly an elusive task. Instead, the Scott and Nguyen[66] constant weight passenger coefficient is thought to be more of a sound basis for conceptual weight prediction of the total systems group. Statistical correlation demonstrates that irrespective of aircraft classification as commercial or business transport, the total systems weight is approximately 60% of the entire constant weight group. Since the basis of the constant weight group is to assume linear variation with passenger accommodation, and introducing the derived notion that systems constitute around 60% of the total, a simpler estimate for total systems weight is proposed here to be

$$W_{sys} = 0.6\,\Pi_{ATM}\,k_{pax}\,PAX \tag{117}$$

where PAX denotes the standard or design number of passengers accommodated by the aeroplane candidate.

6.3.3 Power Plant Installation Weight Estimating Relationship

The weight summation of any conceptual propulsion and associated structural group[‡‡] consists of the basic gas turbine engine (W_{eng}), nacelle (W_{nac}), pylon weight (W_{pyl}), and where applicable, the addition of propellers (W_{prop}).

$$W_{pow} = W_{eng} + W_{prop} + W_{nac} + W_{pyl} \tag{118}$$

The power plant and installation weight including contributions made by nacelles and pylons is based on an exponential statistical regression. The sample size covered 60 different gas turbine engines produced by 7 manufacturers and each varying in maximum sea level static thrust capability between 8.5 kN (1900 lb.f) to 100 kN (22470 lb.f). Figure 21 demonstrates the correlation of engine dry weight to maximum sea level thrust (T_o) capability for existing turbofans using the data given in Aviation Week[55] and Janes[56] publications, and, data compiled by Svoboda[57]. As indicated in the statistical correlation shown in Figure 21, a useful prediction algorithm to quantify the engine dry weight in

[‡‡] Even though the propulsion group is commonly referred to as propulsion installation or engine installation, the most appropriate categorisation is propulsion system. This means any subsequent weight estimation should be tallied as part of the systems group total.

kilograms would look like

$$W_{eng} = 0.0177\left(1 + 0.2\Phi_{prop}\right)T_o^{1.0572} \tag{119}$$

where the impulse function $\Phi_{prop} = \Phi(s,1)$ invokes a 20% increase in weight due to addition of a reduction gearbox and propeller pitch control unit necessary for turboprop power plants.

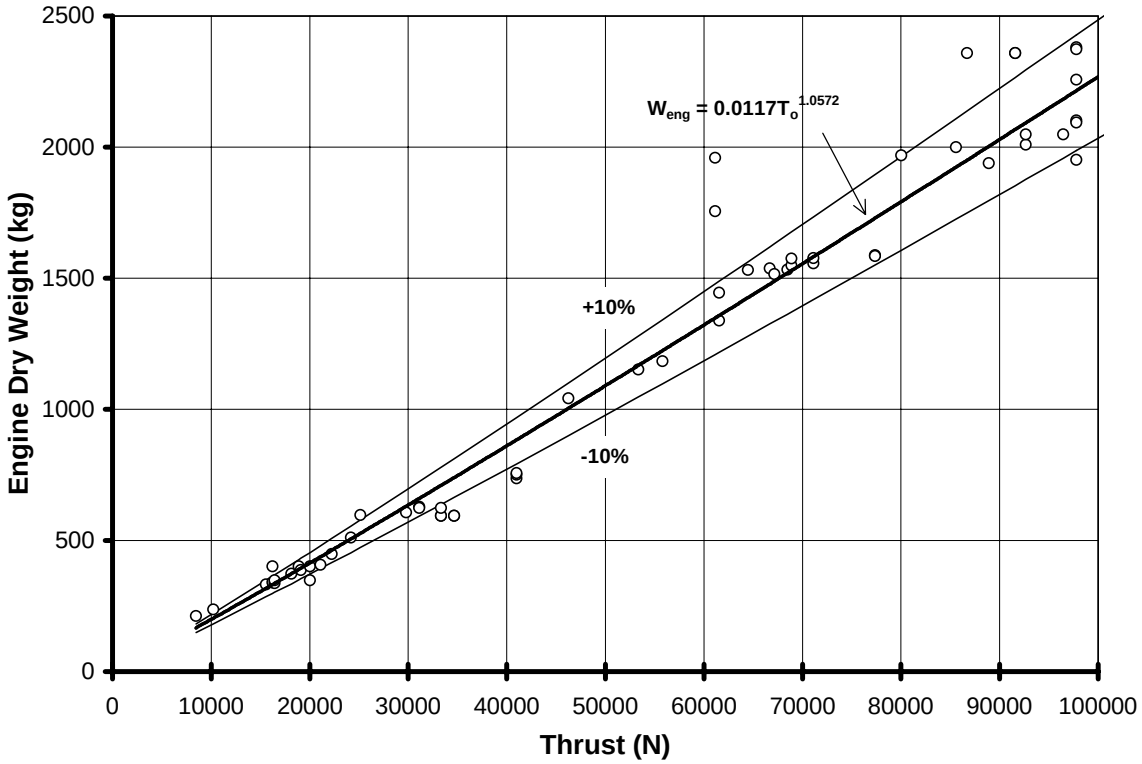

Figure 21. Conceptual turbofan dry engine WER based on data gathered from Aviation Week[55], Janes[56] and Svoboda[57].

It was established earlier that the engine diameter, d_{eng}, could be derived assuming a logarithmic correlation to T_o as exemplified by Eq. (44). It was subsequently stated that an adequate estimate for propeller diameter would simply involve multiplying the engine diameter by a factor, algebraically given as $d_{prop} = 3\, d_{eng}$. When one inspects the method in which W_{eng} is derived, i.e. through an exponential association with T_o, it may be reasonable to conclude that in keeping with the propeller diameter premise, the weight of the propeller will exhibit the same fundamental statistical correlation to T_o as did W_{eng}. Studies have show that a simple linear relationship between W_{prop} and T_o occurs, and a good prediction can be obtained from

$$W_{prop} = 6.13\Phi_{prop}\, T_o \tag{120}$$

The nacelle structural weight is commonly assumed as being related to geometric parameters such as nacelle width and length, and nacelle wetted area. Additionally, further refinements may be obtained by accounting for the engine dry weight in conjunction with the inlet capture cross-sectional area. These parametric relationships are valid whenever

detailed weight analyses are required. Unfortunately, some degree of structural design must be attempted first for a salient prediction to happen. It is desirable however, during the pre-design or conceptual design stage that rudimentary dimensioning be effected from a rather simple fundamental assumption, i.e. sourced from absolute or relative T/W inferences made by the designer producing some value of T_o. Pylon weight is considered to be proportional to the gas turbine engine and nacelle weight sub-units and this constituent is subsequently described with an exponential correlation.

Previously, motivation was given to a concept where the predicted nacelle diameter or length of any gas turbine engine installation can be is expressed as a function of T_o. In view of this information, it is reasonable to assume that a conceptual nacelle and pylon WER can be created which solely depends on variation with T_o. Furthermore, since it was earlier highlighted that engine dry weight can be expressed as a monotonic function of T_o, it is reasonable to assume that a simplified nacelle WER expressed as a factor to engine dry weight would display good associative properties. Supplementary corrections need to be introduced to account for the influence of the particular type of inlet ducting (traditional pitot versus S-duct or long duct), the type of propulsion being considered (turbofan versus turboprop), and the utilisation of thrust-reversing capability. The impulse function can be employed to signify the influence any of these attributes may have on the final nacelle weight. Using the basic form of from GASP[39], the nacelle weight (W_{nac}) algorithm looks like

$$W_{nac} = 0.345\,\Pi_{ATM}\left(1+\Phi_{duct}\right)\left(1-0.53\Phi_{prop}\right)\left(1+0.18\Phi_{tr}\right)W_{eng} \tag{121}$$

Values corresponding to s = 1 invoke corrections due to ducting, $\Phi_{duct} = \Phi(s,1)$, and, incremental weight due to presence of thrust-reverser outfitting, $\Phi_{tr} = \Phi(s,1)$. Otherwise for s < 1, the default estimate is for a turbofan, pitot installation without facility for thrust-reverse. The weight correction due to thrust-reverse outfitting was taken from Torenbeek[1]. The adjustment for revising nacelle weight for turboprops was produced based on known data for the Saab 340A[72] and Saab 2000[73] vehicles. The S-duct and straight duct corrections were based on crafting a typical geometric layout.

By adhering to a congruous theme, the pylon weight is of an exponential form dependent upon engine and nacelle weight

$$W_{pyl} = 0.574\left(1-\Phi_{duct}\right)\left(1-\Phi_{prop}\right)W_{eng}^{0.736} \tag{122}$$

6.3.4 Completion Allowance and Paint Weight Estimating Relationship

Similar to the system weight prediction method, an estimate of interior completion allowance is derived by taking a fraction of the constant weight group quantity. To complement the fraction established for the total systems weight, statistical correlation has found that this constituent is approximately 40% of the constant weight group. Again, this fraction is assumed to be applicable for both commercial and business aircraft. It is general practise to assume that weight of paint is included to produce the delivered MWE, hence, is taken as being combined with the completion allowance. The weight due to paint is predicted by multiplying the vehicular wetted area with a known factor expressed as weight per unit area – a typical value was found to be 0.120 kg/m^2. Applying these principles, the total for completion and paint becomes

$$W_{comp} = 0.4k_{pax}\,PAX + 0.12S_{wet} \tag{123}$$

6.3.5 Crew Weight Estimation

Standard crew weights for conceptual design purposes are gleaned from FAA[74] and JAA[75] statistical data. Table 1 presents the standard crew weights as sanctioned by the FAA and JAA.

	FAA		JAA	
Gender	Flight Crew (kg)	Flight Attendant (kg)	Flight Crew (kg)	Flight Attendant (kg)
Male	90.7	72.5 (1)	85.0 (1)	75.0 (1)
Female	68.0			

(1) weighted average value

Table 1. FAA and JAA sanctioned standard crew weights; data also includes hand baggage allowance.

The JAA stipulates the highest, and therefore, the most conservative value for flight crew and flight attendant standard weights. In view of this, it is suggested that a design assumption for flight crew and flight attendants be declared as W_{fcrew} = 85 kg (188 lb) and W_{fatt} = 75 kg (165 lb) respectively.

6.3.6 Unusable Fuel Weight Estimating Relationship

Unusable fuel alludes to any trapped fuel that cannot for all intensive purposes be used for any operational performance. It is considered to be a fixed quantity for all aircraft, and hence, taken to be a permanent feature of the vehicle OWE. The best method in quantifying this value is to employ statistical techniques and the most economical yet suitable procedure is to assume it to be some proportion of the Maximum Fuel Weight (MFW). For the purposes of initial conceptual design work, one suggested algorithm is

$$W_{fusu} = 0.02 W_{fuel} \tag{124}$$

6.3.7 Operating Items Weight Estimating Relationship

Operating items essentially permit derivation of the OWE when tallied with the delivered MWE. This group includes contributions of flight and cabin crew including accompanying baggage, galley inserts, galley supplies, consumables, potable water, toilet chemicals and lavatory supplies, unusable fuel, engine oil, flight manuals, over-water provisions, tow bar, ladder and any miscellaneous equipment (W_{misc}) required for operation.

$$W_{oper} = W_{fcrew} + W_{fatt} + W_{cons} + W_{fusu} + W_{misc} \tag{125}$$

In the absence of any actual data, the weight of flight crew and cabin attendants are gauged from Table 1, unusable fuel from Eq. (124), and, the consumables and other provisions (W_{cons}) in units of kg can be estimated using

$$W_{cons} = 18.0 + 5.4\,PAX \tag{126}$$

6.4 The Third Functional Weight Group

This categorisation of weight reflects contributions of the useful load fraction due to fuel and any weight contingency allowances deemed necessary by the designer. The third functional group does not reflect any direct association with an instantaneously computed MTOW, however, as it will be seen can becomes an additional component that promotes transcendental behaviour in the complete vehicular WER algorithm.

6.4.1 Estimation of Fuel Capacity

The weight of fuel is simply computed using the volumetric estimation methods detailed in Section 5.6.2 through 5.6.4. The most crucial assumption in this particular analysis involves what constitutes a pertinent value for fuel density. Aircraft manufacturers generally assume either of two densities: 0.802 kg/m^3 (6.70 lb/USG) or 0.809 kg/m^3 (6.75 lb/USG); the lower density value is utilised because it produces a more conservative maximum fuel weight result. In keeping with a comprehensive statistical survey conducted by the U.S Department of Energy (DOE) and data provided to Boeing by a major international airline for worldwide fuel surveys[38], a fuel density of 0.809 kg/m^3 (6.75 lb/USG) is recommended as the appropriate choice during conceptual design exercises.

6.4.2 Maximum Payload-OWE Contingency Allowance

To ensure that a reasonable margin exists in delivering the minimum performance goals laid out for a new design candidate, one practise is to introduce a definition of maximum payload in excess of the originally intended or final value. Experience has shown that the OWE of an aircraft typically increases by up to 5% during the course of preliminary design, detailed design and flight-testing. By assuming an inflated maximum payload capability from the outset, any weight penalties incurred during the development phases can be offset by a reduced payload capability, hence assisting to avoid the violation of minimum performance goals. This margin is usually introduced as a relative quantity, i.e. as a percentage of the OWE, and accordingly becomes another contributor to the transcendental nature of the complete vehicular WER algorithm. Although the notion of an OWE contingency allowance is considered prudent, an element of caution should be exercised when utilising this concept. By virtue of incorporating a higher weight than actually required produces a situation where the MTOW and AUW become inflated, and if the contingency is set too conservatively, the designer is running the risk of unnecessarily penalising the aircraft concept by unwittingly sponsoring operational inefficiencies.

6.5 Defining the Complete Array of Design Weights

The purpose of this section is to familiarise the reader with fundamental terminology associated with the discipline of weights, and to present algebraically how the array of essential design weights are defined for any pre-design or conceptual aircraft design exercise.

6.5.1 Green Manufacturer's Empty Weight

This MEW summation comprises the airframe structure, systems including propulsion group, green furnishings, miscellaneous contributions and any additional manufacturer's tolerances.

$$MEW = W_{wing} + W_{fus} + \Delta W_{wlet} + W_{lg} + W_{ht} + W_{vt} + W_{fins} + W_{sys} + W_{pow} \tag{127}$$

6.5.2 Basic Empty Weight or Delivered Manufacturer's Empty Weight

The Basic Empty Weight (BEW) consists of the MEW and interior completion allowance including paint.

$$BEW = MEW + W_{comp} \tag{128}$$

6.5.3 Basic Operating Weight or Operational Weight Empty

The weight of the aeroplane less payload and fuel is designated as the OWE. Alternatively, one can think of the OWE as the summation of the BEW and the total operational items, which includes the crew, consumables, unusable fuel, engine oil and other provisions.

$$OWE = BEW + W_{oper} \tag{129}$$

6.5.4 Maximum Payload Weight

The standard average passenger weights are derived from extensive surveys of many airliners throughout the world. The FAA and JAA subsequently issue the statistical data compiled from such efforts with the intention of providing methods and procedures for developing and running an operational weight and balance control system. In the absence of an intentional maximum payload target set by the designer, this statistical information can be employed and some semblance of relevance can thus be ensured. The FAA[74] and JAA[75] do not publish a congruous array of standard passenger and baggage weights. This arises because a different ratio of male to female mix[§§] is considered and the JAA specifies an accuracy of 0.1% whereas the FAA does not. Both dataset sources include contributions due to lower values for aircraft operated by regional carriers. It is highlighted that different weight values are assumed depending on the time of year as well.

For aircraft larger than regionals, i.e. narrow-bodies and larger generally equivalent to 100+ PAX, standard passenger and baggage weights are quoted as

	FAA		JAA	
Time of Year	Adult (kg)	Baggage (kg)	Adult (kg)	Baggage (kg)
Summer	81.6	11.3 (1)	84.0	11.0 (1)
Winter	83.9	13.6 (2)	84.0	15.0 (2)

(1) domestic flights (2) international flights

Table 2. FAA and JAA sanctioned standard passenger and baggage weights; applicable for narrow-bodies and larger aircraft only.

To find out an adequate assumption for these classifications of aircraft, the most conservative weights should be taken. Using this criterion, a combined total of 95 kg (≈209 lb) per PAX for domestic operation and 99 kg (≈218 lb) per PAX become suitable assumptions.

The JAA values presented in Table 2 are only valid for aircraft with a capacity of 30+ seats. Regional aircraft and JAA aircraft with less than 20 seats adhere to a unique set of weights. Table 3 itemises these values below.

[§§] This ratio is 60:40 assuming FAA guidelines and 80:20 for JAA aircraft.

	FAA		JAA	
Time of Year	Adult (kg)	Baggage (kg)	Adult (kg)	Baggage (kg)
Summer	77.1	11.3	92.0 (1)	11.0
Winter	79.4		74.0 (2)	

(1) male passengers (2) female passengers

Table 3. FAA and JAA sanctioned standard passenger and baggage weights; applicable for all regional and JAA aircraft less than 20 seats.

The JAA sanctioned values are the most conservative, hence, is recommended as an adequate basis for design analysis work. Using the JAA male to female ratio of 80:20, the combined standard weight assumption becomes 99.5 kg (220 lb) per PAX. This quantity is a value commonly adopted by contemporary regional aircraft manufacturers.

Even though the National Business Aircraft Association (NBAA) prefers to use 90.7 kg (200 lb) per PAX as a weight allowance for one passenger and baggage when comparative type exercises are conducted between business jets, it is suggested a more conservative value equal to 99.5 kg (220 lb) be used from the outset. This will act as a contingency or margin ensuring minimum performance goals of the given business jet candidate are still met in case the mature design suffers from excessive weight penalties later on.

6.5.5 Maximum Zero-Fuel Weight

The MZFW is the OWE plus the maximum payload. This design weight must be chosen with care such that it is sufficiently high to avoid any payload restrictions when actual operations dictate higher than specification OWE.

$$\mathrm{MZFW} = \mathrm{OWE} + W_{\mathrm{pay}} \tag{130}$$

where W_{pay} is the maximum payload weight.

6.5.6 Defining the Maximum Takeoff Weight – Utilising the Maximum Fuel Decrement Design Variable

The MTOW is the maximum weight authorised at brakes release. As discussed earlier, quantifying the MTOW involves the summation of all three functional weight groups. The primary problem is identifying a weight summation algorithm that produces the most beneficial definition of MTOW. One method in addressing this matter is to recognize the fact that one of the integral components will become a designated quantity of fuel intended to complement each dynamically computed MZFW. When this predetermined amount of fuel is added to the MZFW, a minimum goal for the MTOW can then be produced. In keeping with this edict, the algorithm for predicting MTOW becomes

$$\mathrm{MTOW} = \mathrm{MZFW} + W_{\mathrm{fuel}} - \Delta W_{\mathrm{decr}} \tag{131}$$

The interesting consequence of Eq. (131) is the possibility of the fuel decrement parameter ΔW_{decr} being considered as a design variable, which also means a sensitivity analysis can be performed using this parameter as well. By ensuring ΔW_{decr} is part of the global MVO or MDO process, a better probability of identifying the true optimum would

occur because the resulting design MTOW would indeed reflect the lowest gross weight that completes a given mission specification.

6.5.7 Defining the Maximum Ramp Weight or Maximum Taxi Weight

The ramp increment is an allotted quantity of fuel specifically expended during taxi and other ground operations prior to takeoff. Even though this quantity of fuel is not used directly for any purpose relating to field or en route performance, it is good practise to deduct the ramp increment from the maximum usable fuel before proceeding with any maximum range prediction for all aircraft design candidates. An adequate estimate of what constitutes an appropriate amount reserved for ramp increment can be obtained using regression techniques. One such model is proposed here as

$$\Delta W_{ramp} = \rho_{fuel}\left(71\left[\ln V_{fuel}\right] - 476 - 38\,\Phi_{des}\right) \tag{132}$$

ρ_{des} is the fuel density and V_{fuel} is the total volume of fuel to be housed in the aircraft being considered. The prediction given by Eq. (132) has the dual purpose of catering for commercial transports and business jets. This is achieved via an impulse function, $\Phi_{des} = \Phi(s,1)$, that is dependent upon the design type being considered; the expression defaults to a commercial transport assumption. To finalise the estimation process, it is common practise to round the ramp fuel weight increment to the nearest 50 or 100.

The Maximum Ramp Weight (MRW) is simply given as the summation of MTOW and the ramp increment computed above

$$MRW = MTOW + \Delta W_{ramp} \tag{133}$$

6.5.8 Defining Maximum Landing Weight of a Vehicle

Maximum Landing Weight (MLW) appears to be an elusive design parameter when conducting conceptual predictions in the sense that no direct or even quasi-analytical methods are discussed in literature. One published method presents the use of statistical equations that take into account MTOW, MZFW and design range parameters in order to derive a conceptual result for MLW[1]. This approach suffers from the ability of distinguishing MLW definition according to how the vehicle is to be utilised. For instance, smaller vehicles may have scope to fulfil all designated mission requirements with a MLW slightly lower than or even equal to MTOW. For short haul aircraft, where multi-hop capability is considered essential, a relatively high MLW is desirable. Alternatively, for larger transport vehicles and business aircraft, approach and landing climb requirements may be excessively compromised thereby necessitating a MLW definition that is much lower in proportion to MTOW. Additional considerations concern the operational flexibility of a chosen MLW for emergency situations. A MLW definition, which is too low, may in some instances necessitate the crew to land over-weight for situations of mission duress. If this procedure is completed successfully, in accordance with regulatory requirements, a costly inspection procedure must ensue which is financially detrimental to any operator.

In view of the issues discussed, therefore, a new formal methodology requirement exists which can aid the conceptual designer to reconcile often conflicting specifications with regards to landing weight and associative performance. The proposed method is to assume a hypothetical mission where the vehicle completes a pre-designated sector distance and completes this sector using minimum fuel flight techniques from MTOW at

brakes release. The sector distance can be established as the shortest distance the aircraft will in all probability be utilised. Once the mission has been completed, the gross weight at which landing is conducted, may be for the interim, taken to be a viable MLW candidate. A series of fixed sector distances can then be considered for the primary aim of allowing a designer to visualise the functional sensitivity of MLW to issues of multi-hop capability, landing speeds and distance maxima adherence, etc.

6.6 Sample Prediction of Weights against Actual Aircraft Data

When combining all the detailed major constituent contributions, a weight prediction algorithm can be established for the entire vehicle. As an affirmation of the presented methods, Figure 22 plots the estimation error (ε = predicted – actual) for major constituents as well as the collective vehicular result against manufacturer quoted values. It should be noted that the results presented for vehicle empty weights prediction relate to the specification OWE and not a typically outfitted aircraft.

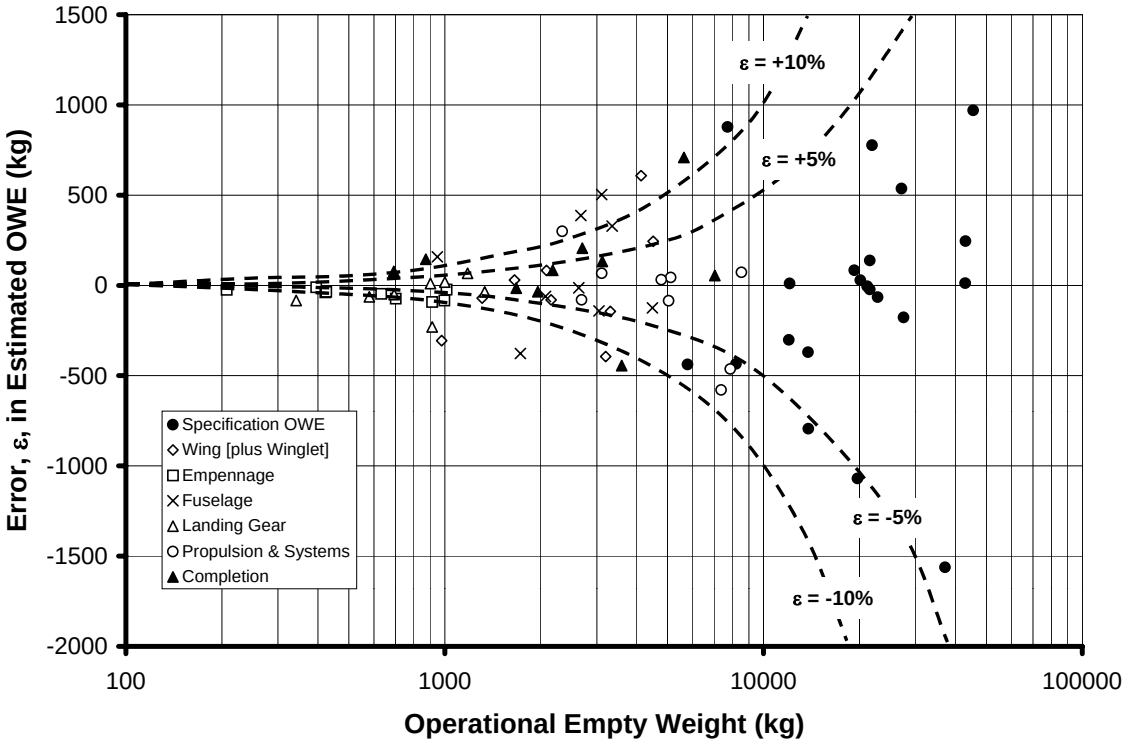

Figure 22. Prediction accuracy of presented method to estimate the weight of major constituents and accumulated vehicular result for select transport aircraft.

Available aircraft data involved a collection of regional, narrow-body and business jets as well as turboprops. The vehicles examined include: Boeing BBJ1[76], BBJ2[76], B737-600[77] and B737-800[77]; Bombardier Aerospace Learjet 45[78], Challenger CL-604[51], Global Express[64], CRJ200[79], CRJ700[80] and CRJ900[81]; Cessna Citation Excel[82] and Citation Sovereign[83]; Embraer ERJ 145[84], Embraer 170[44], Embraer 175[85] and Embraer 195[86]; Fairchild Dornier 728[87] and 928[88]; Gulfstream Aerospace GIV-SP[89] and GV-SP[90]; and, Saab Aerospace Saab 340B[91] and Saab 2000[92]. This list of aircraft used for validation purposes was strategically selected in order to capture widely divergent philosophies with regards to airframe design, mission roles and vehicular performance capabilities. Note that

all aircraft assuming specification OWE data points are displayed in Figure 22; data pertaining to major constituents is shown where the original manufacturer information was available.

For the major constituents such as wing, empennage, fuselage, landing gear, systems including propulsion package and interior completions, the general tendency is to remain within a relative error of between ±5-10%. However, a sufficiently high frequency exists where the splay opens out to a maximum error of greater than ±10%. Concurrently, in an absolute sense, the maximum does not appear to exceed approximately ±500 kg. Although the error tolerance has been compromised for these major constituents, the precept of self-cancelling errors generally produces an OWE result within an acceptable ±5% bandwidth; excursions outside this threshold can be considered as infrequent, and even then appears to not exceed approximately ±10%. In light of the widely held belief that a difficulty exists in generating more precise predictions when airframe designs of several manufacturers are considered concurrently, the presented weight estimation algorithm demonstrates adequate predictive qualities. As demonstrated by this retention of accuracy for aircraft varying in size and capability, it is reasonable to conclude satisfactory objective function sensitivity would be produced as well.

7 Predicting Low-Speed and High-Speed Aerodynamic Attributes

The importance of predicting low-speed and high-speed aerodynamic qualities of aircraft cannot be understated. The implication to vehicular definition relates to an initial appreciation of how the flight envelope will look as well as being one of the integral components in formulating the aeroplane's operational performance attributes. The main aim is to develop methodologies where the designer has an ability to approach the design solution in a more sophisticated manner; not only in terms of departing from the usual more simplified approach premise, but an account of the impact a technological decision makes to the end result. These two primary goals must also be tempered by an appreciation for reduction in the analysis complexity. This is surmised as being achievable by first of all soliciting the designer's philosophical requirements and translating this notion into single all-encompassing algorithms that provide visibility to the designer. Secondly, the methodologies must be impervious to stoppage when key information required on the part of the designer is found to be lacking.

7.1 Low-Speed Aerodynamics: Lift

To consistently support design studies of not only quite complex conventional planforms (with multiple cranks, dihedral, etc.), but also of more exotic layouts such as multi-surface and non planar wings, it was recognised the algorithm to compute maximum lift attributes adhere to a quasi-analytical philosophy. This task can be achieved by concurrent utilisation of dedicated software to quantify the fundamental parameter of clean wing lift-curve slope with well-established empirical methodologies.

7.1.1 Clean Wing Lift Attributes and Maximum Lift

The clean wing maximum lift can be computed for any original multi-surface or non-planar planform geometric definition using a three-dimensional Vortex-Lattice Method[93] (VLM), which calculates aerodynamic properties of multi-wing designs that are swept (symmetric or otherwise skewed), tapered, cambered, twisted and cranked with dihedral. Unlike what is offered by classical VLM approaches, one particular approach models the wake coming off the trailing edge of every lifting surface as flexible and changing shape according to the flight state considered. With a distorting wake, non-linear effects such as the interaction of multiple surfaces can be simulated more consistently. The source of the basic theory for the VLM with flexible wake is cited as Moran[94], and an exemplar of software embodying these principles is one authored by Melin[95]. Succinctly, the classical "horse-shoe" arrangement of other VLM programs has been replaced with a "vortex-sling" arrangement. It basically works in the same way as the "horse-shoe" procedure with the exception that the legs of the shoe are flexible and consist of seven (instead of three) vortices of equal strength. Since the primary assumption of any VLM is linearity, two seed computations are conducted for the lifting surface system at angles of attack (AoA or α) where collinearity is likely as depicted in Figure 23 and labelled as Step 1; two such candidates are suggested as $\alpha = 0°$ and $+4°$.

Following the protocol mapped out in Figure 23, the next step is to identify the zero-lift AoA (α_{oL}); this is found by extrapolating the lift-curve slope ($dC_L/d\alpha$) back to the point at which $C_L = 0$. The slope $dC_L/d\alpha$ itself is quantified by comparing the computed VLM lift at the two seed AoA VLM calculations. Wing lift carry-over into the fuselage body can be accounted for by factoring the original (wing only) $dC_L/d\alpha$ with a calibrated variation of

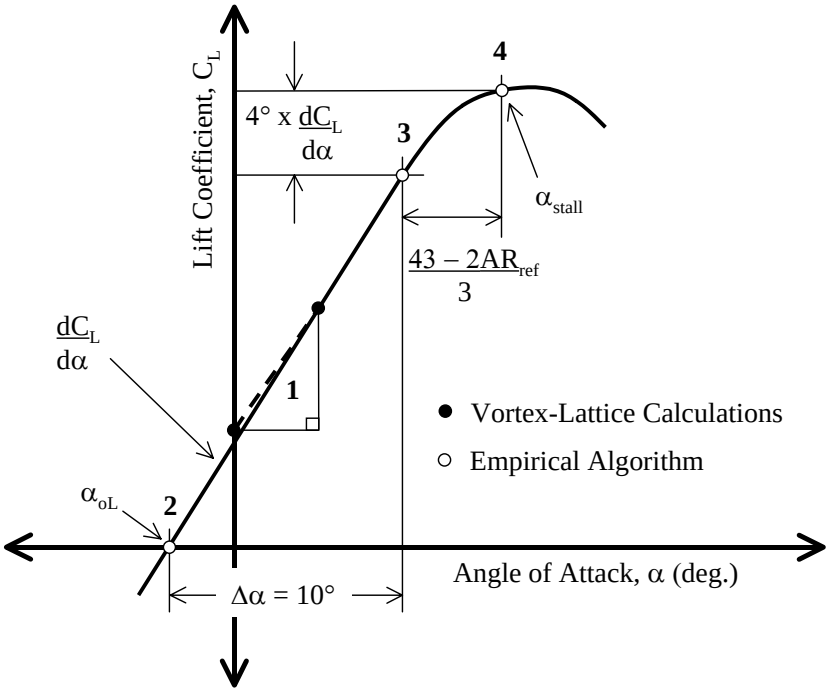

Figure 23. Predicting the lift characteristics of a clean finite wing using quasi-analytical techniques (1-g stall concept shown).

a method given by Pitts et al[96]

$$\left.\frac{dC_L}{d\alpha}\right|_{vehicle} = \xi \left.\frac{dC_L}{d\alpha}\right|_{wing} \tag{134}$$

where

$$\xi = \left(1 + \varsigma \frac{d_h}{b}\right)\frac{S_{net}}{S_{gross}} + \frac{\pi}{2\,dC_L/d\alpha\big|_{wing}}\frac{d_h^2}{S_{gross}} \tag{135}$$

is related to the fuselage external maximum width (d_h), the net or exposed wing planform area (S_{net}) and the gross wing planform area (S_{gross}). The parameter ς is a calibration constant and was derived to equal 3.2. As a final point, Pitts et al stipulates that the use of Eqn. (135) is only applicable for wing-body configurations not violating the constraint of $d_h / b < 0.2$.

From known data[3,97-101], Step 3 involves an AoA increment of $\Delta\alpha = 10°$ to yield an estimate of the cessation of the linear portion of the curve (usually around $\alpha = 8°$) or the beginning of non-linear lift leading eventually to stall. The final step involves adding 4° times the vehicular $dC_L/d\alpha$ to the now corrected C_L computed for Point 3 in Figure 23 to predict the clean wing C_{Lmax} adhering to a 1-g stall concept, or, simply given as

$$C_{L\,max} = 14^{\circ}\left(1 + 0.064\,\Phi_{regs}\right)\frac{dC_L}{d\alpha} \tag{136}$$

When s = 1, the impulse function, $\Phi_{regs} = \Phi(s,1)$, introduces a multiplier derived from information presented by Obert[3], otherwise is zero for s < 1. An appropriate parameter value is invoked in accordance with the analysis being conducted, i.e. under the premise of a power-off 1-g stall concept (s = 0), or, the minimum speed in a stall manoeuvre in accordance with FARs (s = 1) respectively.

If the value is of interest, the corresponding AoA for stall (α_{stall}) can be estimated as well. A suggested empirically derived method based on the same data[3,97-101] quoted earlier. Working off the equivalent reference wing aspect ratio as the only independent variable for analysis, α_{stall} is found by incrementing the AoA at Point 3 shown in Figure 23 by (43 - $2AR_{ref}$) / 3, or alternatively put, by combining all the steps detailed above can be simplified to read

$$\alpha_{stall} = \alpha_{oL} + \frac{73 - 2\,AR}{3} \tag{137}$$

Eqn. (137) is taken to be applicable for the 1-g stall concept only. Since the AoA for stall will differ between the 1-g stall break and minimum speed in a stall manoeuvre, it is suggested that Eqn. (137) be incremented by an additional $\Delta\alpha \approx 1.0°$ to model the minimum speed (FARs) in stall manoeuvre AoA.

7.1.2 Maximum Lift Generated by Trailing and Leading Edge High-Lift Devices

High-lift produced by flap and slat deflection is estimated based on methods presented by Young[102]. This reference uses empirical correlation from assorted accumulated data and predicts with adequate accuracy the aerodynamic characteristics of high lift devices. The methods are not explained in great detail here; however, the salient features will be appropriately noted. A similar and more detailed working account may be found in a design review done by Pazmany[103] and Isikveren et al[104].

Making allowances for effective chord, flap incidence and part span, the increment due to the presence of any trailing edge flap is given by

$$\Delta C_{L\,flaps} = \left[\Delta C'_L (c'/c) \frac{F(AR)}{F(6)} + C_{L\,max\,W} (c'/c - 1) \right] f(\Lambda) \tag{138}$$

where (c´/c) is the effective chord ratio; F(AR) is the function relating the vehicular $dC_L/d\alpha$ and the aspect ratio, and this is standardised to an AR = 6.0; C_{LmaxW} is the maximum clean wing lift attainable, f (Λ) is a correction to the lift increment for a swept wing, and

$$\Delta C'_L = \left[\lambda_1 (c_{f1}/c)\, \lambda_2 (\beta_1) + \lambda_1 (c_{f2}/c)\, \lambda_{22} (\beta_{22}) \right] \left[\lambda_3 (b_{f22}/b) - \lambda_3 (b_{f21}/b) - \lambda_3 (b_{f12}/b) + \lambda_3 (b_{f11}/b) \right] \tag{139}$$

$\lambda_1(c_f/c)$ is a function of effective chords**,** $\lambda_2(\beta)$ is a function of the flap angle and is determined from experimental data (varies from one flap to another). The subscript 22 denotes the influence of an auxiliary flap or vane if applicable. The operation [$\lambda_3(b_{fx2}/b)$ -

$\lambda_3(b_{fx1}/b)]$ is a part span correction factor, and, x = 2 and 1 define the outboard and inboard (due to a central cut-out) ends respectively.

The first task is to take Eqn. (138), it's coupled constituent Eqn. (139), and introduce not only the fixed functional values related to design intent supplied by Young, but a parameter to account for the stall concept adopted per chosen airworthiness regulations. Additionally, by incorporating supplementary simplifications for sake of brevity, i.e. linear sensitivity to AR, an all-purpose fixed quantity for effective chord, introduction of a continuous functional form for the f (Λ) correction parameter, the final algorithm describing change in lift due to trailing edge device deflection is proposed here as

$$\Delta C_{L\text{flaps}}\Big|_{TE} = \left(\frac{20 + \Phi_{\text{dslot}} + 5\Phi_{\text{fowl}}}{20}\right) k_{\text{geo}}\, \beta_{\text{flap}}\, AR\left(3\, b_{\text{flap}} - 1\right)\cos^3 \Lambda_{\text{Qchd}} \tag{140}$$

The two design related impulse functions, $\Phi_{\text{dslot}} = \Phi(s,1)$ and $\Phi_{\text{fowl}} = \Phi(s,1)$, represent the relative increase in lift compared to the default single-slotted flap prediction assuming double slotted of Douglas type and Fowler flapping arrangements respectively. The constant k_{geo} is equal to 2.183×10^{-3} and is universally applicable for all (chord extending) flaps considered. The flap deflection angle in degrees is denoted by β_{flap} with b_{flap} defining the part-span flap including fuselage carry-through, expressed as fraction of total reference wingspan.

A series of fixed flap settings corresponding with deflection optima based on experimental results given in literature[1,3-5,39] for given high-lift device types have been pre-selected for field calculations. Single slotted flaps tentatively have pre-designated deflection optima of 7^o, 15^o and 35^o for intermediate takeoff, maximum takeoff and landing configurations respectively. For double slotted flaps of Douglas type, initial guesses for optimal flap deflections have been assumed to be approximately 10^o, 20^o for intermediate and maximum takeoff, and 45^o for landing. Congruous with the double slotted premise, the Fowler assumes 10^o, 20^o and 45^o for intermediate takeoff, maximum takeoff and landing configurations respectively. Although optimal flap deflection is dependent upon a given vehicular configuration and ambient conditions in which the aircraft operates, these selected values were found to be very close to actual deflections used on contemporary aircraft and hence adopted for simplicity. Regardless of this directive, the algorithm used to determine C_{Lmax} given above permits an opportunity to truly optimise flap setting for the operational performance scenario considered; providing an extension is made to allow cubic interpolation of C_{Lmax} for the given intermediary flap setting.

These trailing edge high-lift devices may also be complemented by the introduction of leading edge slats. Occasions where a slat lift increment is desired, a tentative maximum deflection of 20^o is assumed based on experimentation and actual examples[64,97,105]. The increment in lift due to slat is only introduced for maximum lift prediction, i.e. maximum optimal flap deflection usually pertaining to landing configuration. Furthermore, an upper permissible boundary of $C_{Lmax} = 3.50$ which is universally applicable to all devices has been artificially set in keeping with conclusions drawn from surveys presented by Obert[3]. Young[102] suggests a rather simplified expression relating lift increment due to slat to the slat wing chord fraction. In the end, a more consistent approach exhibiting functional similarity with Eqn. (140) was chosen to be a more accurate model

$$\Delta C_{L\text{flaps}}\Big|_{LE} = k_{\text{geo}}\, AR\, b_{\text{flap}}\, \cos^3 \Lambda_{\text{Qchd}} \tag{141}$$

where all other parameters retain the previously given definitions, except for k_{geo}, now taken to be 0.0470, and b_{flap} is the slat part-span fraction.

To complete the entire prediction exercise, a trimmed lift coefficient needs to be produced. As outlined by McCormick[34] a complete treatment involves augmenting untrimmed vehicular lift coefficient according to the relative distance between vehicular centre of gravity (x_{cg}) and aerodynamic centre (x_{ac}) locations, and then incrementing contributions due to generated moment coefficient about the aerodynamic centre and the moments created because of increase in drag due to trim. Such an approach requires a detailed array of information; to simplify matters, sufficient accuracy can be achieved by dropping the terms dependent upon moment coefficient and increase in drag.

$$C_{L\text{trim}} = C_{L\,\max}\left[1 + \frac{\text{MAC}}{l_t}\left(x_{cg} - x_{ac}\right)\right] \tag{142}$$

Many aircraft manufacturers adopt the simplified functional form given by Eqn. (142) in their respective aerodynamic data handbooks. Default values for the non-dimensional relative MAC distance ($x_{cg} - x_{ac}$) can be assumed as -0.05 for aft-fuselage mounted vehicles, otherwise equal to approximately -0.15 for all other configurations.

7.1.3 Establishing the Accuracy of Clean Wing and High-Lift Prediction

Once each of the analytical and empirical constituents is combined to form the final algorithm, a wide-ranging analysis has shown predictions are relatively consistent with actual aircraft lift data. Using a generic supercritical profile as a basis for this investigation, namely the MS(1)-0313, Figure 24 elucidates this by demonstrating a typical bandwidth of

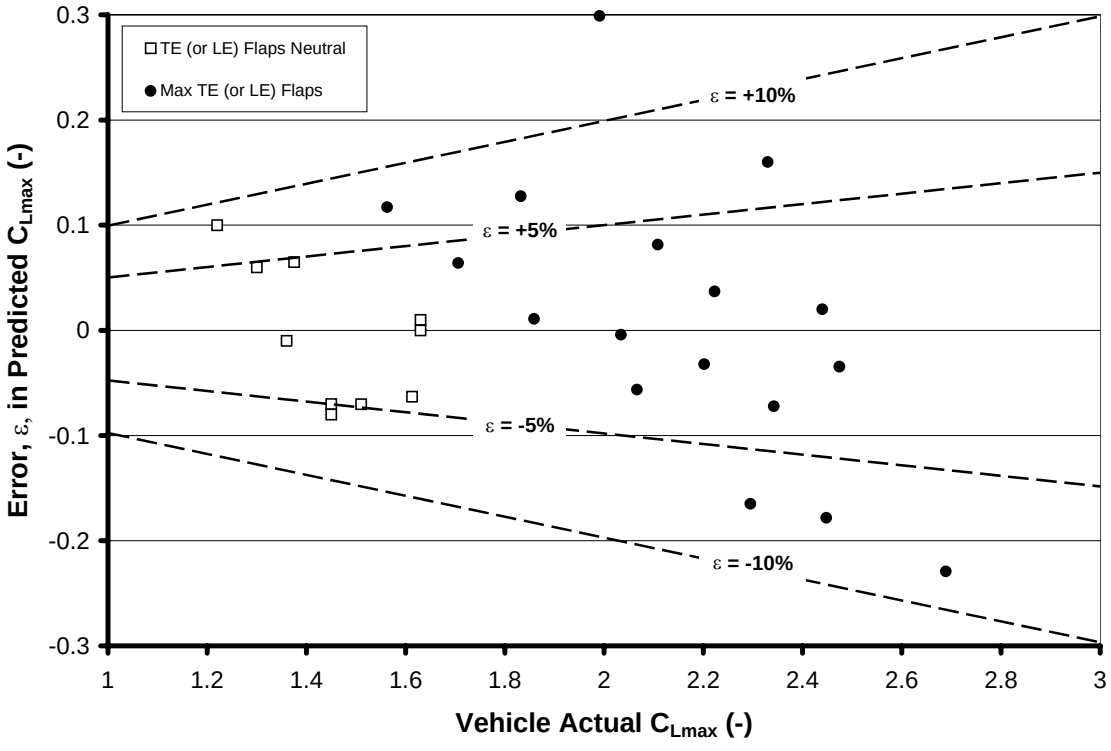

Figure 24. Prediction accuracy of algorithm to compute C_{Lmax} using quasi-analytical techniques. High-lift device set to neutral and maximum deflection shown.

error (ε = predicted – actual) with respect to manufacturer quoted values falls within a ±5% splay. More saliently, the study indicates there exists a good likelihood maximum lift predictions will not exceed an error of around ε = ±0.15 irrespective of flap deflection.

The benchmarking data comprised either known aerodynamic performance or was derived from vehicular stalling speeds. The aircraft used for this validation exercise were: Boeing BBJ1[76]; Bombardier Aerospace Learjet 45[78], Learjet 60[106], Challenger CL-604[51], Global Express[64], CRJ200[79], CRJ700[80] and CRJ900[81]; Cessna Citation Excel[82]; Dassault Aviation Falcon 2000[107] and Falcon 900[53]; Embraer ERJ 135[108], ERJ 140[109], ERJ 145[84]; Fokker Aircraft Fokker 70[110] and Fokker 100[111]; Gulfstream Aerospace GIV-SP[89] and GV-SP[90]; PD340-2 19 PAX regional jet conceptual design study[112]; and, Saab Aerospace Saab 340[113] and Saab 2000[114]. Note that all aircraft assuming maximum flap deflection data points are displayed in Figure 24; data pertaining to neutral flap deflection is shown where the original manufacturer information was available.

7.2 Zero-Lift Drag Estimation - The Equivalent Length Method

A common method for determining the zero-lift drag (C_{Do}) of aircraft components is an assumption that the constituent's friction drag is equivalent to a flat plate having the same wetted area and characteristic length. In this way, a very preliminary assessment of the complete vehicular zero-lift drag estimation may be accomplished by summation of these individual components. By creating a hybrid approach where the component build-up method is benchmarked against a standardised closed form expression, economy of effort can be achieved without incurring excessive degradation in predictive powers. A tool for estimating zero-lift drag is the friction coefficient equation based on experimentation done by Eckert[115], which accounts for fully turbulent flow and compressibility effects. By assuming an appropriate reference condition of Mach number and flight level, the component build-up method may be employed and a characteristic equivalent length for the entire vehicle can be derived from its equivalent skin friction coefficient - a quantity commonly used for aircraft comparison exercises. This equivalent characteristic length may in turn be reintroduced into Eckert's equation and solved for any other Mach number and flight level combinations the aeroplane encounters.

7.2.1 Derivation of The Equivalent Characteristic Length Method

Assuming the boundary layer is fully turbulent and accommodating effects due to compressibility on skin friction, the friction coefficient ($c_{f\ turb}$) according to Eckert based on wetted area is given by

$$c_{f\ turb} = \frac{A}{\left(\log N_R\right)^b \left(1 + cM^2\right)^d} \tag{143}$$

where M is the instantaneous Mach number, constants A = 0.455, b = 2.58, c = 0.144 and d = 0.58 are coefficients of proportionality derived by Eckert, and, the Reynolds number (N_R) in atmospheric flight at given speed and flight level can be expressed as

$$N_R = \frac{\rho_{sls}}{\mu_{sls}} \frac{\sigma}{\mu/\mu_{sls}} V l_b \tag{144}$$

The identity ρ_{sls}/μ_{sls} is approximately equal to approximately 6.9×10^4 s/m^2, and l_b is any specified representative length of the body.

The results obtained by an approximate turbulent theory such as the one given by Eq. (143) assumes a smooth adiabatic flat plate. In actual flight conditions, typical values of skin friction exceed the predicted value significantly. This circumstance does not necessarily invalidate the use of Eckert's equation, but rather, raises the requirement of additional adjustments to reflect actual physical observations. The first correction calls for account of an equivalent sand roughness. The traditional method utilises the concept of a cut-off Reynolds number[4], which is determined using the characteristic length and skin roughness derived from a table of values presented for different surfaces. Other sizable contributions to the final value of skin friction includes dissimilar boundary layer development and velocity profiles between streamlined shapes and the flat plate analogy, and, pressure effects due to frontal area. Instead of relying on a sequence of discretised computations, the aim here is to formulate a single-step prediction procedure for skin friction coefficient that can incorporate these adjustments.

Examination of Eq. (143) reveals the theoretical turbulent skin friction coefficient is primarily a function of Reynolds number with a supplementary account of compressibility effects. In view of this situation, any adjustment that takes into account actual-flight corrections should be expressed as being proportional with Reynolds number, or, algebraically incorporated into the $(\log N_R)^b$ term. With this idea in mind, Eq. (143) would be modified to read as

$$c_f = \frac{A}{\left[\log\left(\eta_{act} N_R\right)\right]^b \left[1 + cM^2\right]^d} \tag{145}$$

where the parameter $\eta_{act} = 1$ produces a skin friction result synonymous with Eckert's original theory, otherwise, for values $\eta_{act} \neq 1$ constitutes an additional correction to represent equivalent sand roughness, pressure and interference effects. Based on an elaborate amount of experimentation done in wind tunnel and flight-testing, Poisson-Quinton[116] was able to quantify the difference between actual values of skin friction and theoretical turbulent friction assuming a smooth adiabatic flat plate. The results showed a simple linear proportionality between c_f and $c_{f\,turb}$, namely,

$$c_f = \tau_{act}\, c_{f\,turb} \tag{146}$$

By initially equating Eq. (145) with a factorised Eq. (146) using the binomial construct, solving for the constant of proportionality, τ_{act}, and then re-arranging the interim result such that η_{act} becomes the subject, the Reynolds number adjustment parameter becomes

$$\eta_{act} = 10^{\left(\tau_{act}^{-1/b} - 1\right)\log N_R} \tag{147}$$

Assuming an actual flight Reynolds number of around 20×10^6 where τ_{act} was found to equal approximately 1.45 as cited in Poisson-Quinton's results[116], produces a correction of $\eta_{act} = 0.105$, which would then be introduced into the modified Eckert's equation given by Eq. (145). The Reynolds correction coefficient of $\eta_{act} = 0.105$ can be thought of as a "mean curve" adjustment, representative of conventional technology/manufacturing

levels[‡‡], and therefore has been presented as the basis for establishing predictions at the very initial design stage. Consideration must also be given to the fact a practical lower limit of $\tau_{act} = 1.30$ (or potential C_{Do} reduction of up to 10% from the mean curve) has been derived when analysing some narrow bodies and larger aircraft types from data supplied by Obert[3], and this factor is in turn synonymous with a Reynolds correction coefficient of $\eta_{act} = 0.197$.

Eq. (143) represents a condition where fully turbulent flow exists. It would be prudent to give scope in accommodating mixed laminar and turbulent flow, hence permit the designer to set a minimum goal of what proportion laminar flow shall occur over the characteristic length of the body constituent in question. Since an algorithm to quantify a realistic turbulent skin friction coefficient has been established with Eq. (143), this can be used as a basis to formulate an extension such that a realistic skin friction assuming mixed flow is produced. Working off a basic assumption that momentum thickness at given transition point is synonymous for both laminar and turbulent flows (see Figure 25), the final skin friction can be produced by summing the friction coefficients for partly laminar and turbulent flow[2].

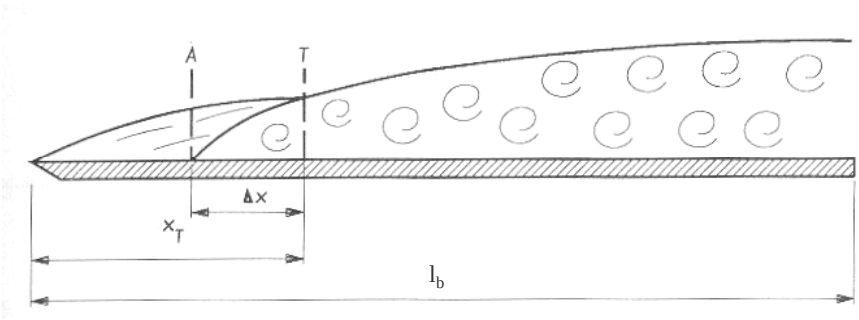

Figure 25. The premise of mixed laminar and turbulent flow used to derive an augmented realistic skin friction coefficient[2].

Matching the momentum thickness of the laminar and fully turbulent boundary layer at transition point T gives

$$c_{f\ lam}\, x_T = c_{f\ turb}\, \Delta x \tag{148}$$

where $c_{f\ lam}$ is the skin friction coefficient for laminar flow, x_T is the point along the body characteristic length where flow transition occurs and Δx is a distance ahead of the transition point where fictitiously the onset of fully turbulent flow takes place. It can be shown[34] the total flat plate friction coefficient for a mixed laminar and turbulent flow is calculated from

$$c_f = c_{f\ turb} - \frac{x_T}{l_b}\left(c_{f\ turb} - c_{f\ lam}\right) \tag{149}$$

In this equation, $c_{f\ turb}$ is computed assuming a Reynolds number based on a body characteristic length starting from the fictitious onset of turbulent flow to the end of the

‡‡ The aircraft surface can have many irregularities. These include gaps and steps, protruding flush rivet heads, and, surface waviness due to airframe construction, dynamic distortion and cabin pressurisation.

body, and, $c_{f\ lam}$ is calculated based on the entire length of assumed laminar flow, or distance x_T. Substitution of Eq. (148) into Eq. (149) can produce an alternate form

$$c_f = \left(1 - \frac{x_T + \Delta x}{l_b}\right) c_{f\ turb} \tag{150}$$

Since $c_{f\ turb}$ also depends on Δx, an iterative procedure is required to solve for Δx in Eq. (150). A valid form of simplification is in order here. Introducing a presumption the fictitious distance Δx consistently exhibits linear proportionality with x_T for low to mid-range values of $\Delta x / l_b$, scope can be given to dispense with the transcendental nature of Eq. (150), hence permit a reduction in complexity. Investigations found that for x_T / l_b values less than approximately 0.40, the total skin friction coefficient for mixed laminar and turbulent flow can alternatively be expressed as

$$c_f = \left(1 - \chi_{mf} \frac{x_T}{l_b}\right) c_{f\ turb} \tag{151}$$

The constant of proportionality, χ_{mf}, assists in ascertaining what proportion of the completely turbulent flow premise imparts an influence on the mixed flow result. Experimentation has found a useful value for this parameter is approximately $\chi_{mf} = 0.74$ for all $x_T / l_b < 0.40$. The upper boundary of assumed laminar flow fraction is a reasonable one for design prediction purposes since an example of the most successful flight testing of combined passive and active laminar flow control technology achieved laminar flow up to 30% of wing chord[117]. In addition, experimentation conducted in a more operationally pragmatic sense commonly produces transition at 15% wing chord[117].

The component build-up method for zero-lift drag at given Mach number and flight level is given as

$$C_{Do}\big|_{M,h} = \frac{\sum_{i=1}^{I} c_f^i S_{wet}^i}{S_W} \tag{152}$$

where the product $c_f^i S_{wet}^i$ is the drag area of each component i. By choosing an appropriate reference condition of Mach number and altitude[§§], an equivalent skin friction coefficient representative of the entire vehicle can be produced with the congruent relation

$$c_f^{\varepsilon} \sum_{i=1}^{I} S_{wet}^i \equiv \sum_{i=1}^{I} c_f^i S_{wet}^i \tag{153}$$

The parameter c_f^{ε} is the equivalent skin friction for the sum of all constituent wetted areas produced using the equivalent flat plate analogy representing the entire aeroplane. It

[§§] The reference condition for Mach and flight level is open to the designer's willingness to trade larger errors in low speed for more accurate high-speed zero-lift drag or visa versa. Experimentation has found that a speed near the final vehicle MRC or LRC at an altitude 4000 ft lower than the intended certified ceiling are good reference conditions for a balanced error distribution.

is now proposed that this notion of equivalence can be extended to quantify a characteristic length as well. Since the entire vehicle has been replaced by the flat plate premise with a corresponding value for c_f^{ε}, by rearranging Eckert's equation, Eq. (143) can be solved for an equivalent characteristic length (l_ε) given by the identity

$$l_\varepsilon = \frac{10^{\left(\frac{A}{c_f^{\varepsilon}}\right)^{1/b}\left[1+cM^2\right]^{-d/b}}}{\frac{\rho_{sls}}{\mu_{sls}}\frac{\sigma}{\mu/\mu_{sls}}V} \tag{154}$$

Reintroducing this relation to Eckert's equation, and assuming the error in N_R due to a now fixed equivalent characteristic length (i.e. independent of Mach number or flight level effects) is small, a general zero-lift drag equation, designated hereon as the Equivalent Characteristic Length Method (ECLM), which accounts for all variations of Mach number and flight level can be given approximately as

$$C_{Do}\big|_{M,h} \cong \frac{A}{\left[\log\left\{\frac{\rho_{sls}}{\mu_{sls}}\frac{\sigma}{\mu/\mu_{sls}}Vl_\varepsilon\right\}\right]^b\left[1+cM^2\right]^d}\frac{S_{wet}}{S_W} \tag{155}$$

For a detailed analytical treatment of en route performance, drag is an integral parameter and has the primary requirement of being differentiable with respect to the airspeed V for all cases. Eq. (155) appears to be in a form that is quite complex, and more poignantly, not configured for a more in-depth calculus treatment. It was identified that this problem may be avoided via the use of logarithmic differentiation. By utilising the relation $x = e^{\ln x}$, Eq. (155) can be alternatively expressed as

$$c_f^{\varepsilon} = A\left[\ln 10\right]^b \exp\left\{-b\ln\left[\ln\left\{\frac{\rho_{sls}}{\mu_{sls}}\frac{\sigma}{\mu/\mu_{sls}}Vl_\varepsilon\right\}\right]-d\ln\left(1+c\frac{V^2}{a_{sls}^2\theta}\right)\right\} \tag{156}$$

which is in a form ready for differentiation albeit the complexity has not been reduced.

7.2.2 Gauging the Robustness of the Equivalent Characteristic Length Method

An interesting question is to what extent the equivalent characteristic length assumption is compatible to the exact component build-up method, and, more importantly what is the upper threshold of relative errors the designer may expect. In an effort to theoretically gauge the magnitude of inherent errors produced by this approach, the ECLM expression was reconfigured as an error function with respect to the exact component build-up method. The most expedient way to observe this would be the comparison of resultant equivalent skin friction errors analytically and do so for a range of contemporary regional transport and business jet Reynolds number regimes based on complete vehicular characteristic lengths. If Eckert's general equation is partitioned into Reynolds number and compressibility dependent constituents, in conjunction with some algebraic manipulation, Eq. (143) then becomes

$$c_f = \frac{\varpi_1}{\varpi_2\left[1+\dfrac{\log l_b}{\varpi_2}\right]^b} \tag{157}$$

where the compressibility term is described by

$$\varpi_1 = \frac{A}{\left[1+cM^2\right]^d} \tag{158}$$

and the Reynolds number dependent constituent is defined as

$$\varpi_2 = \log\left[\frac{\rho_{sls}}{\mu_{sls}}\frac{\sigma}{\mu/\mu_{sls}}V\right] \tag{159}$$

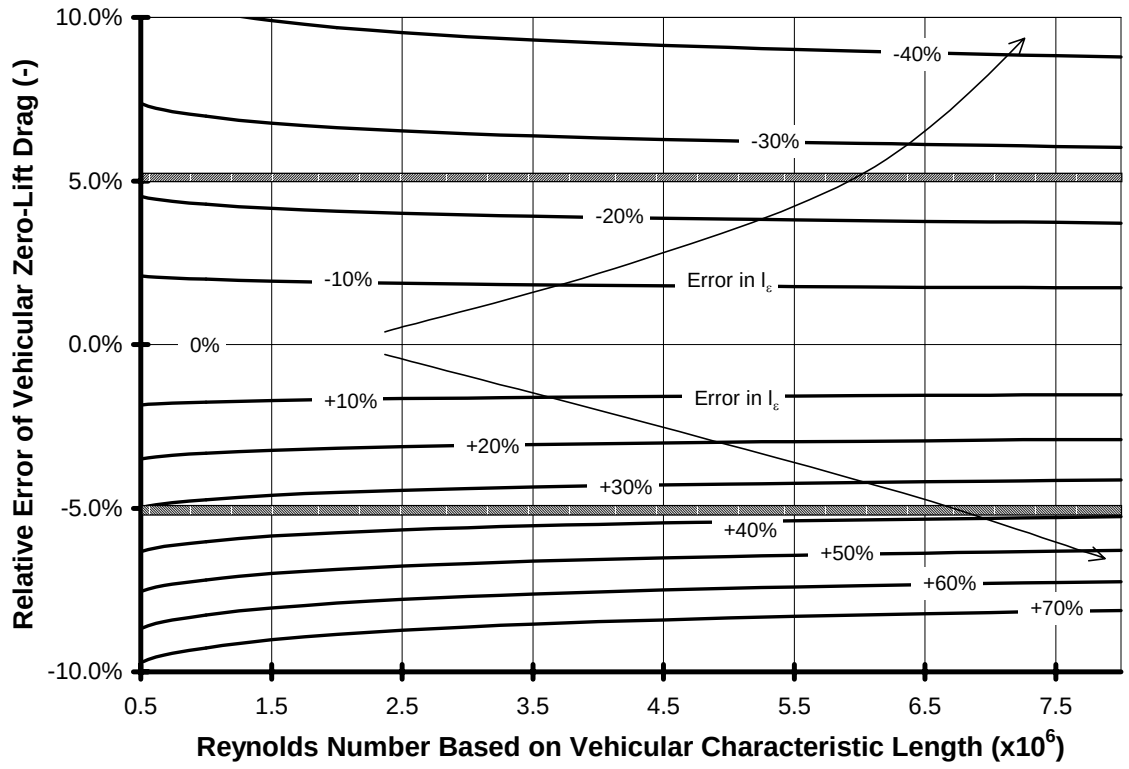

Figure 26. Resilience of ECLM accuracy for a given error in vehicular characteristic length and en route Reynolds number based on vehicular characteristic length.

Now, by introducing the notion of error factor defined as the ratio of the fixed vehicular characteristic length quantity derived from a reference Mach and flight level to the exact value of vehicular characteristic length, or $\varepsilon_l = l_\varepsilon/l_{exact}$, the relative error of an equivalent characteristic length assumption can be gauged by considering deviations from the exact value of $c_{f_{exact}}$ through a fractional comparison

$$\frac{c_f^{\varepsilon}}{c_{f_{exact}}} = \left[1 + \frac{\log \varepsilon_l}{\log N_R}\right]^{-b} \tag{160}$$

Figure 26 (previous page) shows the variation of resultant prediction error compared to the exact vehicular equivalent skin friction of zero-lift drag with Reynolds number based on vehicular characteristic length whilst assuming various errors in the ε_l ratio. To put Reynolds number based on vehicular characteristic length into context, small business jets typically operate at around $N_R = 10^6$, regional aircraft and larger business jets between $N_R = 1.5 \times 10^6$ and 2.0×10^6, and larger regional and narrow-body aircraft from $N_R = 3 \times 10^6$ and higher. For a typical en route Reynolds number of 1.5×10^6 based on vehicular characteristic length for regional transports, an error of -24% in l_ε compared to l_{exact} corresponds to a +5% overestimation of equivalent skin friction or total zero-lift drag. Conversely, for the same Reynolds number, a -5% underestimation of zero-lift drag is tolerated by a +33% error in equivalent characteristic length from the exact value. This result demonstrates the resilience of ECLM.

7.3 Vortex-Induced Drag at Subsonic Speeds

Many methods exist in quantifying this phenomenon and the most simplest of them is the Oswald Span Efficiency Method which assumes the vortex-induced drag coefficient of three dimensional wings with an elliptical lift distribution equals the square of the lift coefficient divided by the product of the aspect ratio and π. Additional drag produced by non-elliptical lift distributions is made by using the Oswald Span Efficiency Factor (e), which effectively reduces the aspect ratio. The vortex-induced drag factor[35] is given as

$$\left(\frac{dC_D}{dC_L^2}\right) = \frac{1}{\pi AR e} \tag{161}$$

Numerous estimation methods for e have been developed but they mostly tend to produce optimistically high values compared values of real aircraft. Obert[3] offers an empirically derived equation for the vortex-induced drag factor applicable for Mach numbers greater than about 0.40, based on actual aircraft regardless of power plant installation, assuming typical centre of gravity locales, inclusion of wing twist effects, and compressibility effects neglected.

$$\left(\frac{dC_D}{dC_L^2}\right)_{clean} = \frac{1.05}{\pi AR} + 0.007 \tag{162}$$

Eq. (162) does not appear to account for the distinction of power plant installation philosophy, i.e. clean wing, underwing podded or on-wing nacelle configurations, and the direct impact this has on span loading distribution. As an exercise, Eq. (162) was compared to Eq. (161) and Oswald span efficiency factor solved for a variety known e values of equipment with different power plant installation philosophies not covered by the statistical survey. Interestingly, the continuous functional form offered by Obert seemed to match the values for these known examples with an adequate degree of accuracy. This leads the author to believe a correlation between aspect ratio and power plant installation

philosophy must exist, hence Obert's regression analysis inherently accounted for this association.

For field performance where Mach numbers typically range between 0.15-0.25, it is apparent that a change in vortex-induced drag factor will take place due to a change in the span-wise lift distribution due to flaps extending and deflecting[118]. Literature demonstrates this variation is proportional to wing geometry, non-ellipticity of the span-wise lift distribution of the basic wing, the effect of flap cut-out and lift carry over by the fuselage[1]. Concurrent to this circumstance, there is also an additional physical effect that needs to be addressed. There is a reduction in the vortex-induced drag factor with increasing flap deflection, or alternatively, as flap deflection is increased, a reduction in the vortex-induced drag for given C_L occurs. This is attributable to an increasing benefit generated by the slot-effect at greater deflections and amounts to a measure of boundary layer control thus preventing separation. In order to acknowledge these known phenomena, the implication is an incremental change in the vortex induced-drag factor needs to be introduced to Eq. (163). Such a model is proposed here to be

$$\begin{aligned}\left(\frac{dC_D}{dC_L^2}\right) &= \left(\frac{dC_D}{dC_L^2}\right)_{clean} + \Delta\left(\frac{dC_D}{dC_L^2}\right)_{flaps} \\ \left(\frac{dC_D}{dC_L^2}\right) &= \frac{1.05 + 0.271\Phi_{flap}}{\pi AR} - 0.000487\beta_{flap} + 0.007\end{aligned} \tag{163}$$

The impulse function, $\Phi_{flap} = \Phi(\beta_{flap},1)$, invokes a correction to the vortex-induced drag factor to signify an irregularity in the lift distribution due to deployment of high-lift devices. Studies comparing the vortex-induced drag estimate generated using Eq. (163) to low-speed drag polars of the Saab 340[113] and Saab 2000[114] aircraft found the correlation to be quite adequate. This means the maintenance of sufficient accuracy can be expected using the one algorithm in predicting the vortex-induced drag regardless of flaps neutral or extended.

7.4 Three Dimensional Effects and Ancillary Drag Contributors

Five form factors that account for three-dimensional effects, ancillary interference, and excrescences are reviewed here. These values are computed based on thickness-chord ratios of the wing, horizontal and vertical tails, and, the fineness ratios of the fuselage and nacelle. All of the form factors itemised below were derived from original expressions developed for GASP[39] and subsequently modified to suit known data more appropriately.

The modified wing form factor reads as

$$\varphi_{wing} = 0.421\left[2 + 4\left(\frac{t}{c}\right)_m + 240\left(\frac{t}{c}\right)_m^4\right] \tag{164}$$

with the horizontal tail surface re-defined to be

$$\varphi_{htail} = 1 + 0.1\left(1 - 0.893\xi_{ht}\right)\left[2 + 4\left(\frac{t}{c}\right)_m + 240\left(\frac{t}{c}\right)_m^4\right] \tag{165}$$

The ξ_{ht} parameter represents horizontal tail placement non-dimensionalised by d_v with respect to the vertical tail tip and FRP water-line. Similarly with the wing, the vertical tail form factor was amended to read as

$$\varphi_{vtail} = 0.5\left[2 + 4\left(\frac{t}{c}\right)_m + 240\left(\frac{t}{c}\right)_m^4\right] \tag{166}$$

The fuselage form factor is predicated by body slenderness ratio. Assuming a streamlined fuselage without a blunt nose

$$\varphi_{fuse} = 1 + 0.0025\left(\frac{l_{fuse}}{d_v}\right) + 60\left(\frac{d_v}{l_{fuse}}\right)^3 \tag{167}$$

and finally, the nacelle form factor is based on the premise of slenderness as well

$$\varphi_{nac} = 1.17\left[1 + 0.35\left(\frac{d_{nac}}{l_{nac}}\right)\right] \tag{168}$$

The prediction of a low-speed drag polar for field performance requires account of contributions due to extended undercarriage and high-lift devices. In the absence of detailed undercarriage sizing, the drag due to extension of undercarriage can be quantified with adequate accuracy using statistical correlation from known data. Based on information gleaned from McCormick[34], a useful linear regression equation was derived to be

$$\Delta C_{D\,LG} = \frac{1}{S_W}\left(2.85\,x\,10^{-5}\,W_{TO} + 0.294\right) \tag{169}$$

The total aircraft drag of a configuration geared for field operation is also affected by a profile drag contribution from extended flaps and slats. Assuming a given trailing edge (and/or accompanying leading edge) high-lift device has been deployed, an approximation for the incremental drag is suggested as

$$\Delta C_{Do\,flap} = \frac{1}{S_W}\left(5.268\,x\,10^{-4}\,\beta_{flap}^2 - 0.005339\,\beta_{flap} + 0.0416\right)\left(\frac{c_f}{c}\right)\left(\frac{MAC}{b\,b_{flap}}\right)\cos^2\beta_{flap} \tag{170}$$

and typical values for the relative flap chord fraction of $c_f / c = 0.26$ and $c_f / c = 0.15$ for trailing edge and leading edge devices respectively are suggested as initial estimates.

7.5 Total Incremental Drag due to One Engine Inoperative Condition

The One Engine Inoperative (OEI) condition appears to be mostly disregarded in conceptual design literature. It is usually classified as a preliminary design problem[1,4] because yawing and rolling considerations become rather complex in nature since these

must be trimmed out by primarily the rudder and then aileron. Drag due to engine wind-milling, airframe sideslip, incremental changes in normal force vortex-induced and profile drag from control surface deflection, asymmetric slipstream effects and lift distribution reconfiguration producing independent vortex-induced contributions all combine to complicate matters. By examining the exact approach, a number of valid simplifications may be incorporated in order to reduce the scope of detailed information required whilst retaining strong predictive powers and objective function sensitivity with respect to the design variables. Studies have shown that many of these constituent contributors can be neglected with the exception of vortex-induced and profile drag generated by rudder deflection.

7.5.1 The General One Engine Inoperative Drag Constituent

If one considers the OEI asymmetric condition, studies have shown that many of these constituent contributors can be neglected with the exception of vortex-induced and profile drag generated by rudder deflection. Figure 27 demonstrates the pertinent forces and moments once this simplification is introduced. By assuming the vertical tail utilises a symmetric profile and all rudder deflections during asymmetric flight will be below stall, equilibrium is achieved via,

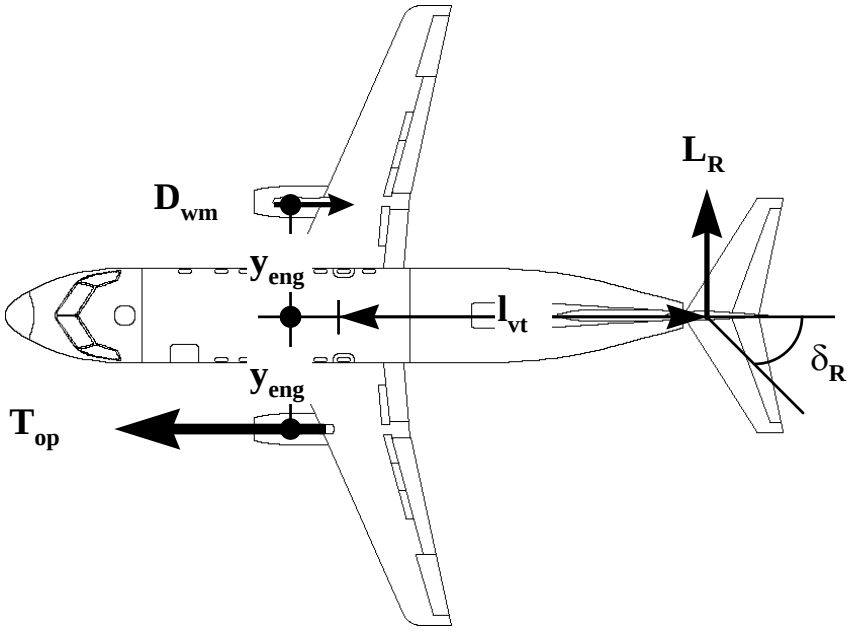

Figure 27. Simplifications of forces and geometric considerations during the asymmetric thrust condition.

$$L_R l_{vt} = y_{eng}\left(D_{wm} + T_{op}\right) \tag{171}$$

where y_{eng} is the moment arm from fuselage centre line to the critical and windmilling engines, D_{wm} is the drag produced by the wind-milling engine, T_{op} is the instantaneous available thrust produced by the critical engine at instantaneous velocity V and l_{vt} is the vertical tail moment arm. The instantaneous lift (L_R) generated by the flapped vertical tail is[34]

$$L_R = q\, S_{vt}\, C_{L\alpha,vt}\, \tau\, \eta\, \delta_R \tag{172}$$

with q denoting the dynamic pressure, S_{vt} the vertical tail reference area, τ a flap effectiveness factor, and η, a correction which accounts for the effects of viscosity.

The functions τ and η are generally derived empirically since they behave in a non-linear fashion with chord fraction (c_f / c) and rudder deflection angle (δ_R). If a simplification is sought, McCormick[34] demonstrates that thin airfoil theory can be utilised to produce adequate results but the functions are still represented by dependent variables. Assuming a typical c_f / c value for the flapped vertical tail of around 0.3, an estimate of τ = 0.66 may be derived using Weissinger's approximation[34***]. Furthermore, McCormick shows at an upper deflection of δ_R = 30°, a value of η = 0.74 would be appropriate. By assuming some level of conservatism for smaller deflections, an overall flap effectiveness of $\tau\eta$ = 0.49 applicable to the complete range of angles would result. This figure can be substantiated against Torenbeek's[1] presentation of overall effectiveness factors derived from experimental data for plain flaps.

The lift-curve slope characteristics ($C_{L\alpha,vt}$) can be estimated by the Helmbold equation[34] based on an approximate lifting surface theory with the effects of sweep ($\Lambda_{vt,Qchd}$) accounted for by a first order cosine relation given by Torenbeek[1].

$$C_{L\alpha,vt} = C_{l\alpha,vt}\left(\frac{AR_{vt}}{2+\sqrt{4+AR_{vt}^2}}\right)\cos\Lambda_{vt,Qchd} \tag{173}$$

Assuming a thin airfoil, section lift-curve slope of $C_{l\alpha,vt}$ = 0.110 per deg. (2π per rad) is given theoretically, however, it was found an average of 0.088 per deg. (5.04 per rad) taken from Abbott and Von Doenhoff[69] yields more realistic predictions. Thus, from linear thin airfoil and lifting surface theory, the rudder deflection required for equilibrium of the OEI asymmetric condition is given by

$$\delta_R = \frac{y_{eng}\left(D_{wm} + T_{op}\right)}{q\, S_{vt}\, C_{L\alpha,vt}\, \tau\, \eta\, l_{vt}} \tag{174}$$

From this basis, the possibility of accounting for the influence of minimum control speed limitations on field length and initial climb performance can be introduced at the conceptual level, and, methods to predict these quantities with respect to operational performance will be addressed in the takeoff field performance discussion of this report.

Since the geometric characteristics for equilibrium of asymmetric thrust has been quantified, the next step should be an appreciation of to what extent performance shall be degraded. By summing the forces and moments in Figure 27, and equating these to represent contributions of vortex-induced and profile drag due to rudder deflection, the total incremental drag contribution produced by an OEI asymmetric condition (ΔC_{DOEI}) is approximated by[39]

$$\Delta C_{DOEI} = \frac{D_{wm} + \left[D_{wm} + T_{op}\right]\frac{y_{eng}}{l_{vt}}\tan\delta_R}{q\, S_w} \tag{175}$$

*** Two point vortices represent the airfoil and this function is dependent upon c_f / c ratio.

This relation is not only applicable for low speed field performance, it can also be utilised for climb out analysis as well; specifically in relation to OEI maximum attainable flight level and drift-down net level off height proficiency trade studies at ISA and more importantly off-ISA conditions.

7.5.2 Drag Generated by Windmilling Engine

For multi-engine aircraft with engines not buried in the fuselage, the OEI performance will be influenced by additional drag due to a windmilling engine during the equilibrium condition of asymmetric flight. Torenbeek[1] proposes a conceptual method to estimate the magnitude of the drag increment by considering this quantity to be a function of engine frontal area, bypass ratio and internal configuration. Unfortunately, the method is rather esoteric because the procedure employs the momentum theorem, which requires an estimation of mean flow velocity in the nozzle exit together with the windmilling mass flow. Typical values for the ratio of these speeds are offered but they are specific to engine type thus not allowing for a continuous function concept. As an alternative, a more simplified approach is proposed which assumes the windmill drag component can be accounted for by representing it as an equivalent flat plate problem with an associated skin friction value which is imaginary and independent of Reynolds number variation or associative compressibility effects.

The notion of a "cut-off Reynolds number" can be useful in helping to quantify the drag produced by a windmilling engine in this respect. Raymer[4] discusses the merits of employing a cut-off Reynolds number parameter to account for expected higher skin friction coefficients in conventional zero-lift drag estimation when the surface of a body is relatively rough. By comparing the ratio of characteristic length and a skin-roughness value (l/k), the cut-off Reynolds number ($N_{R\ cut\text{-}off}$) is then determined by

$$N_{R\,cut-off} = a\left(\frac{l}{k}\right)^{b} \tag{176}$$

where a and b are constants of proportionality and $N_{R\ cut\text{-}off}$ varies monotonically with l/k for subsonic speeds.

Assuming a windmilling engine is essentially the nacelle but influenced by some degree of imaginary roughness on the body in this condition, i.e. analogous to an internal drag contribution, then a pre-designated cut-off Reynolds number would be independent of Mach number variation for subsonic flight[†††] and atmospheric conditions because as indicated by Raymer, there is a strong correlation to relative roughness alone. It is evident that the internal drag generated is related to maximum static engine thrust potential, which also may be postulated to be a function of engine size. This would mean the imaginary value for k would increase proportionately with nacelle physical dimensions, therefore, the imaginary relative roughness can be taken as approximately constant. In view of this, the imaginary cut-off Reynolds number can be considered independent of nacelle size or characteristic length as well. When the imaginary cut-off Reynolds number is quantified empirically and substituted into Eckert's equation for skin friction given by Eq. (143), neglecting compressibility effects and hence adopting the Prandtl-Schlichting form, the equivalent flat plate skin friction that simulates an imaginary roughness condition for a windmilling engine would be given as

[†††] OEI flight regime is considered predominately as a subsonic problem. This premise may not hold true for extended range and in some instances driftdown operations.

$$c_f^{wm} = \frac{A}{\left[\log N_{R\,cut-off}^{wm}\right]^b} \tag{177}$$

where A is equal to 0.455 and b = 2.58. Once the windmilling engine representative skin friction is quantified, an incremental contribution to drag in the OEI asymmetric condition is therefore given by

$$\Delta C_D^{wm} = \frac{c_f^{wm} S_{wet,nac}}{S_W} \tag{178}$$

In order to derive the value for imaginary skin friction, known windmill drag properties for the BAe 146-200[119] were used and the results were tested against other installed aircraft engines. The suggested values for conceptual analysis were found to be $N_{R\,cut-off}^{wm} = 9.3x10^4$, or corresponding imaginary skin friction of $c_f^{wm} = 0.007274$. Using this information in conjunction with the nacelle wetted area estimation methodology described previously, predictions of ΔC_D^{wm} were computed and subsequently compared to known windmill drag data for both the Williams International FJ44-2A[120] small turbofan rated at 10.2 kN (2400 lb.f) and the CFM56-7B26[121] engine rated at 118 kN (26400 lb.f) used on the B737-800 narrow-body commercial transport. Figure 28 demonstrates the level of accuracy generated using the imaginary skin friction method; the results were found to be quite encouraging, more so due to the fact the nacelle wetted area was not calibrated to any known data before computing the final result.

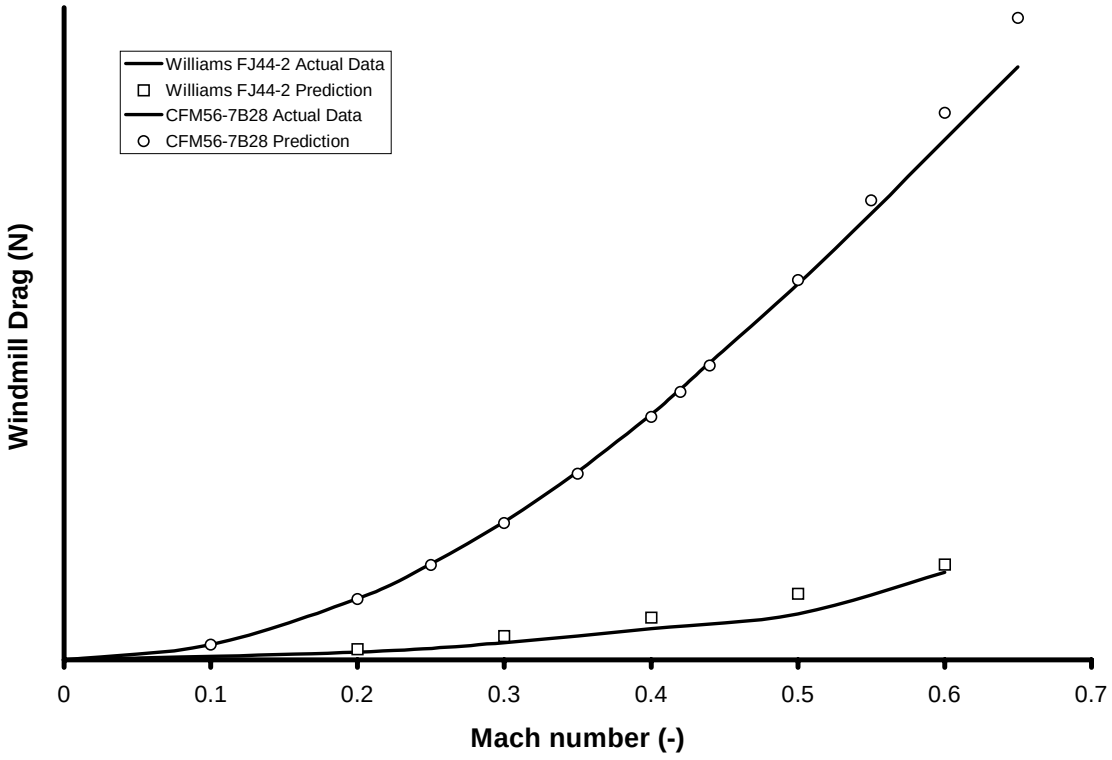

Figure 28. Benchmarking predicted windmilling drag using the imaginary skin friction method against actual engine windmilling data; ISA, sea level conditions.

Additionally, it is recommended that the drag contribution for turboprop engines using this method should be obtained by factoring the equivalent turbofan result by 3. This accounts for a simulated by-pass ratio increase due to the presence of propeller or larger fan diameter contribution for given maximum static thrust rating or nacelle size. One should recall the method is based upon the generic pitot nacelle, therefore, the actual nacelle wetted area for a turboprop (or even S-duct and straights ducts) power plant installation must be disregarded and the generic pitot introduced into the prediction process. Inspection of the Saab 2000's one engine inoperative drag assuming a propeller in the auto-feathered condition[114] produced an estimation error of –2.8%.

7.6 Compressibility or Wave Drag

Compressibility is a drag increment caused by an increase in free stream Mach number above a critical point where locally accelerated speeds increase sufficiently to reach Mach numbers of unity and above. The free stream Mach number at which this first occurs is called the critical Mach number, denoted here as M_{CR}, and can be thought of as the lower limit of the transonic flow regime. Steadily increasing values of free stream Mach number above M_{CR} are characterised by regions of supersonic flow terminated by normal shock waves shifting aft and increasing in strength. The formation of shocks in the transonic flow condition affects the drag up to the drag divergent Mach number (M_{DD}), thereafter the drag rise rate increases substantially as shown in Figure 29.

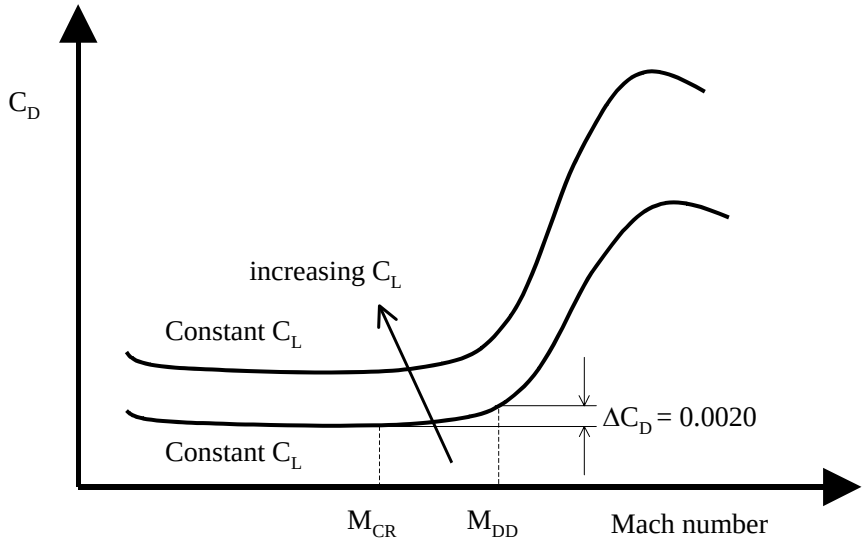

Figure 29. Definitions for the transonic mixed flow regime and indication of speed thresholds for certain drag escalation attributes.

The definition of what particular Mach number constitutes M_{DD} is open to several options. The most common is the Boeing definition where M_{DD} is the speed at which an incremental increase in viscous drag influenced by drag rise is equal to 20 counts (or ΔC_{DD} = 0.0020). Additionally, M_{DD} is a function of lift coefficient since shock formation and strength directly relates to increases in airflow velocity. Typically, for an initial analysis the drag rise is graphically estimated using a few rules of thumb rather than a more comprehensive appreciation of the dependence of M_{DD} on parameters like instantaneous operating lift coefficient, quarter chord sweep, mean wing thickness ratio and type of airfoil geometry employed as exemplified by Raymer[4]. Notwithstanding, this assumption

does not necessarily invalidate this first order estimate's predictive powers - but a wide range of information exists which aid in predicting compressibility drag characteristics for given set of design parameters adequately. Therefore, it would be deemed prudent in attempting to derive a closed form expression that describes the mixed flow regime simultaneously neglecting highly non-linear terms but having a stronger basis to set more realistic goals.

7.6.1 Derivation of the Incremental Drag due to Compressibility

Much of what is known about this flow regime are largely experimental hence are described by many different empirical models. Torenbeek[122] offers a variation of Korn's equation[123] to quantify the limits of wing section performance for given vehicle wing thickness, sweep and typical operating lift coefficient envelope

$$M_{REF} = M_{DD}\cos\Lambda_{Qchd} + \frac{1}{10}\left(\frac{C_L}{\cos^2\Lambda_{Qchd}}\right)^{3/2} + \frac{(t/c)_m}{\cos\Lambda_{Qchd}} \tag{179}$$

where M_{REF} is a wing section technology factor. Torenbeek suggests values of M_{REF} = 0.935 for supercritical aft loaded, and, M_{REF} = 0.87 for conventional peaky sections. Here, a modification of this premise with an empirical fit more akin to the actual performance produced by contemporary regional and business jet vehicles is proposed: a customary technology factor of M_{REF} = 0.850 for supercritical aft loaded sections is suggested as a more pragmatic value with an occasional upper limit not exceeding M_{REF} = M0.90.

By rearranging Torenbeek's version of the modified Korn's equation so that M_{DD} is the subject

$$M_{DD} = \frac{1}{\cos\Lambda_{Qchd}}\left[M_{REF} - \frac{1}{10}\left(\frac{C_L}{\cos^2\Lambda_{Qchd}}\right)^{3/2} - \frac{(t/c)_m}{\cos\Lambda_{Qchd}}\right] \tag{180}$$

Torenbeek[1] offers an arbitrary mathematical representation of the condition where drag rise is terminated (at speed M_{DD}) and an increased drag rise rate begins

$$\Delta C_{Dcomp} = \Delta C_{DD}\left[1 + \left(\frac{M - M_{DD}}{\Delta M}\right)\right]^n \tag{181}$$

where the symbols n = 2.5 and ΔM = 0.05 are given by Torenbeek; they have no physical significance but are derived from experimental data. As a consequence, Eq. (181) implicitly relates M_{CR} to M_{DD} as

$$M_{DD} = M_{CR} + \Delta M \tag{182}$$

This information can be used in conjunction with Eq. (180), thereby, allowing the definition of M_{CR} to be given as

$$M_{CR} = \left\{ \frac{1}{\cos\Lambda_{Qchd}} \left[M_{REF} - \frac{1}{10} \left(\frac{C_L}{\cos^2 \Lambda_{Qchd}} \right)^{3/2} - \frac{(t/c)_m}{\cos \Lambda_{Qchd}} \right] \right\} - \Delta M \qquad (183)$$

Now, by introducing the concept of an impulse function or approximate unit step that is critical Mach number dependent, i.e. $\Phi_{Mcr} = \Phi(M,M_{CR})$, and incorporating Eq. (182) and Eq. (183) into Eq. (181) yields

$$\Delta C_{Dcomp} = \Phi_{M_{CR}} \Delta C_{DD} \left[1 + \Phi_{M_{CR}} \left(\frac{M - M_{CR}}{\Delta M} - 1 \right) \right]^n \qquad (184)$$

which then leads to a closed form expression for the total compressibility drag contribution including the concept of initial and supplementary drag rise and the final equation conforms to the presupposed condition of differentiability with respect to airspeed V.

7.6.2 Quantifying Wave Drag due to Volume and Lift

As expounded by Torenbeek[124], the wave drag of wings and slender bodies is frequently related to the theoretical minimum wave drag of pointed optimum bodies. Even though the implicit assumption involves smooth bodies in inviscid flow, by utilising linearised theory as Mach number tends to unity from below[125], the relative merits of differing configurations can be compared as a guide to drag-rise behaviour. These optimum bodies can be represented by the von Karman ogive, Sears-Haack or Adams optimum either in isolation, as composite area distributions in pairs, or even all three in consort. Correcting for deviations from the optimum by a factor, K_o, as stipulated by Kuchemann[126] and introducing an empirical wave drag efficiency factor[4], η_{opt}, representing the ratio between actual wave drag and that of the optimum body, the wave drag due to volume for given body volume V_b reads as

$$\Delta C_{Dcomp}\Big|_{M_{sREF}} = \eta_{opt} K_o \frac{128}{\pi S_W} \frac{V_b^2}{l_b^4} \qquad (185)$$

The product $\eta_{opt} K_o$ can be estimated from values quoted by Raymer[4] and Torenbeek[124]. This is accomplished by initially choosing a reference Mach number that is slightly faster than sonic speed; and one suggested reference is $M_{sREF} = 1.05$. Raymer and Torenbeek indicate a combined factor of approximately 2.5 for $\eta_{opt} K_o$ is adequate. Although this value reflects supersonic designs displaying a relatively poor volume distribution, analysis of actual subsonic aircraft (even those catering to M_{MO} speeds up to M0.90) found $\eta_{opt} K_o = 4.0$ is more appropriate. Once the wave drag due to volume has been quantified for the reference condition, the next step is to build the wave drag model according to the operating parameters dictated by given flight conditions. Taking the logarithm on both sides of Eq. (181) and solving for the exponent n produces

$$n = \frac{\log\left(\frac{\Delta C_{Dcomp}\big|_{M_{sREF}}}{\Delta C_{DD}}\right)}{\log\left(\frac{M_{sREF} - M_{CR}}{\Delta M}\right)} \tag{186}$$

Eq. (186) is then substituted back into Eq. (181), hence, an estimate of the wave drag due to volume can be computed dynamically for an instantaneous operating lift coefficient, or alternatively, for a given critical Mach number premise.

The drag due to lift of surfaces at supersonic speeds ($\Delta C_{Di\ wave}$) with streamwise and spanwise elliptical pressure load distributions is quantified by Jones'[127] classical though not universally accepted relation describing the lower bound

$$\Delta C_{Di\,wave} = K_W \frac{\beta}{\pi} C_L^2\, r\, \lambda_{cbox} \tag{187}$$

where the working dimensions are shown in Figure 30. K_W is a deviation from the theoretical minimum and recommended as being equal to 1.25[124], $\beta = (M^2 - 1)^{1/2}$, $r = S_W / (b\ l_W)$ is a shape parameter, and, the so-called corrected box ratio is defined as $\lambda_{cbox} = \beta\ b / (2\ l_W)$. The fundamental assumption here is that the fuselage nose and tail do not contribute to lift.

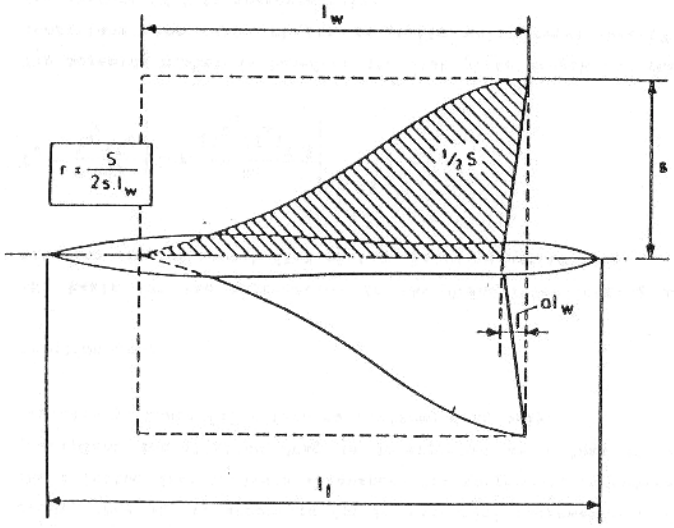

Figure 30. Definition of working parameters to compute drag due to lift in supersonic flight[124].

7.7 Quantifying the Aerodynamic Impact of Winglets

With greater emphasis being placed on improving aircraft cruise efficiency winglet devices appear to offer the most attractive combination of drag reduction and aesthetic appeal. It is therefore not surprising many existing aircraft types have been outfitted with winglets as part of an overall enhancement package and many kits are offered to retrofit in-service aircraft. The conventional winglet ($AR_{WL} \cong 1.5$) approach is now being replaced by

so-called blended winglets[128]; typified by a high aspect ratio ($AR_{WL} \cong 3.5$) and integrated by way of pronounced filleted transition geometry between the wing and winglet structures.

Regardless of the design philosophy, the known benefits of winglets can be itemised as follows:

- Decreased fuel burn and increased payload range attributes – achieved through an aerodynamic performance improvement, i.e. net vehicular drag reduction;
- Higher cruise altitude and OEI driftdown ceiling – due to a net vehicular drag reduction enabling a greater amount of specific excess power at given altitude and speed;
- Improved takeoff performance – higher effective OEI lift-to-drag and therefore higher second segment climb gradient for given reference speed; allows for higher TOGWs;
- Reduced engine maintenance – the option of retaining the original takeoff performance levels prior to installation of winglets promotes a reduced thrust concept;
- Lower airport noise levels – exploiting the reduced thrust concept.

All of these enhancements may not necessarily come to fruition concurrently; the designer should expect a combination of a few at best. Nonetheless, it is evident if appropriately designed and integrated with the main wing, the devices will translate into a some sort of a direct economic benefit for the operator.

Many examples of winglet performance prediction and design optimisation is available in literature[34,70,71,129-131]. In general, winglet configurations are analysed using the VLM to establish optimal planform attributes, cant, camber and twist in achieving maximum reduction of vortex-induced during cruise. A non-planar, three-dimensional potential flow panel method is subsequently employed to evaluate the configuration under takeoff and landing operating conditions, thereby gauging the possibility of adverse low speed characteristics. The revised span load is examined referenced to the ultimate wake in a Trefftz plane analysis in order to determine the induced drag and bending moment distribution. The final step in the design cycle is to weigh the economic feasibility of adding winglets to the aircraft; ideally, a revised (and re-optimised) performance estimate would entail consideration of the change in aerodynamic qualities and the change in aircraft empty weight. To alleviate the need for excessive effort, only a relative drag is quoted at given operating lift coefficient and change in OWE due to a wing bending moment increase. For conceptual design studies, one suggestion is to adopt these percentages and empirically adjust the design prediction accordingly with no due regard given to winglet design variable sensitivity. Unfortunately, as one would intuitively expect this approach is susceptible to inconsistencies. Therefore, a requirement now arises for a quasi-analytical method to quantify the change in vehicular drag due to winglets.

7.7.1 Quantifying the Drag Reduction of Winglet Devices

As depicted in Figure 31, by summing the forces in the direction of freestream and adhering to the sense convention indicated, the total force of the local system can be quantified to be

$$\sum F_x = D_{WL} \cos \alpha_{ind} - L_{WL} \sin \alpha_{ind} \tag{188}$$

where α_{inc} is the winglet representative incidence and α_{ind} is the spanwise induced angle of attack instantaneously generated by the wing.

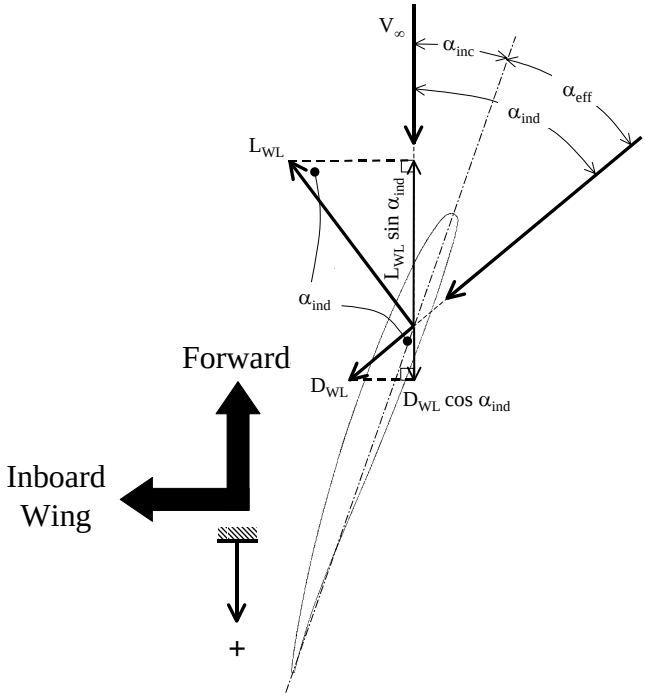

Figure 31. Resolving local lift and drag forces generated by the winglet into the direction of freestream.

A key requirement is to now formulate a semi-empirical expression for α_{ind}. Fundamentally, the trailing vortex shed at each wing-tip induces not only a downward velocity in the region of the wing itself, but the circulatory motion also generates induced velocities in a spanwise direction. When the freestream velocity is vectorially added to the spanwise induced velocity component in plan-view, the resulting vector produces an angle of attack α_{ind}. Prandtl's lifting-line theory stipulates the downward induced angle of attack generated by finite wings is proportional to the operating C_L and inversely proportional to the wing AR[132]. Working off this premise and introducing a coefficient of proportionality (η_{ind}) to represent a scaling factor between the downward and spanwise induced velocities towards the tips, then

$$\alpha_{ind} = \eta_{ind} \frac{C_L}{\pi AR} \tag{189}$$

A suggested scaling factor η_{ind} = 7.2 was empirically derived from flow visualization experiments undertaken by Head[133].

Since the true goal is to quantify a relative vehicular drag, Eq. (188) should be examined in the non-dimensionalised form, i.e. divided by qS_W. To this end, the instantaneous lift coefficient produced by the winglet ($C_{L\,WL}$) is given by

$$C_{L\,WL} = C_{L\alpha\,WL}\left(\alpha_{eff} - \alpha_{oL}\right) \tag{190}$$

where the effective angle of attack α_{eff} is found by taking the difference between α_{ind} and the winglet representative incidence angle α_{inc}. An account of the zero lift angle of attack α_{oL} is assumed here to be approximately $\alpha = -3°$ for 3% cambered aerofoil sections commonly used for winglet devices. The lift-curve slope characteristics ($C_{L\alpha\ WL}$) can be estimated using the Helmbold equation[34] modified for compressibility correction as given by Eq. (88).

The total winglet drag is determined by summing the winglet zero-lift ($C_{Do\ WL}$) and vortex-induced ($C_{Di\ WL}$) drag. The $C_{Do\ WL}$ contribution is derived using the component build-up method with an adjustment for interference as outlined earlier. It is highlighted that the incremental zero-lift drag due to presence of winglets must be considered in isolation from the vehicular characteristic length and the ECLM drag prediction algorithm. In this context, the winglet device is taken to be an add-on to an existing vehicle wing planform, and therefore, is not deemed to be a constituent in deriving the vehicular characteristic length.

Upon substitution of Eq. (189) and Eqn.(190) into Eqn.(188) now expressed in an equivalent non-dimensionalised form, the total incremental drag due to presence of winglets is determined by summing the resolved local winglet lift and drag force components, the change in drag due to compressibility if the winglet pre-empts the wing in generating super-velocities, and a reduction in the wing vortex-induced drag. Recognising an adjustment required to conform to the reference wing convention

$$\begin{aligned}\Delta C_D &= \frac{2}{qS_W}\left(-L_{WL}\sin\alpha_{ind} + D_{o\,WL}\cos\alpha_{ind} + D_{i\,WL}\cos\alpha_{ind}\right) + \Delta C_{D\,comp} + \Delta C_{Di} \\ &= 2\frac{S_{WL}}{S_W}\left(C_{Do\,WL}\cos\alpha_{ind} + C_{Di\,WL}\cos\alpha_{ind} - C_{L\,WL}\sin\alpha_{ind}\right) + \Phi_{M_{CR}}\Delta C_{D\,comp} + \Delta C_{Di}\end{aligned} \tag{191}$$

with the $\Delta C_{D\ comp}$ component considered to be greater than zero if the winglet M_{CR} has been exceeded by the freestream Mach number. By virtue of attaching winglets to the tips of a wing, one would expect an alteration to the spanwise lift distribution and the trailing vortex system downstream since circulation along the wingspan changes accordingly. In an attempt to quantify the relative reduction in vortex-induced drag due to presence of winglets (ΔC_{Di}) in the flow field, a useful basis is to refer to the fractional change in the vortex-induced drag factor used to augment the original ΔC_{Di} denoted by the subscript "orig"

$$\Delta C_{Di} = \mathbf{0}\frac{dC_D}{dC_L^2}C_{Di}\Big|_{orig} \tag{192}$$

The fractional change operator for the vortex-induced drag factor, namely $\mathbf{0}dC_D/dC_L{}^2$, is quantified by comparing the original wing planform and an equivalent wing planfom with winglets canted as some angle Γ_{WL} off the vertical. By incorporating the vortex-induced drag factor derived by Obert[3] and given by Eq. (162) the operator becomes

$$\mathbf{0}\frac{dC_D}{dC_L^2} = \frac{\Delta\left(dC_D/dC_L^2\right)}{\left(dC_D/dC_L^2\right)_{orig}} = \frac{AR_{orig} - AR_{rev}}{AR_{rev}\left(1 + \dfrac{\pi}{150}AR_{orig}\right)} \tag{193}$$

where for winglet span (or height) and root chord of h_{WL} and c_{WL} respectively the revised aspect ratio (AR_{rev}) is defined purely on the basis of geometry

$$AR_{rev} = \frac{\left(b + 2\,h_{WL}\tan\Gamma_{WL}\right)^2}{S_W + h_{WL}\,c_{R\,WL}\left(1+\lambda_{WL}\right)\tan\Gamma_{WL}} \tag{194}$$

7.7.2 Proficiency of Drag Reduction due to Winglet Prediction

Figure 32 shows a comparison of the calculated and actual improvement in block fuel for a Boeing B737-800 narrow-body transport. Actual data derived from flight-testing was taken from results published by Dees and Stowell[71]. With regards to the exercise of predicting a change in block fuel due to presence of winglets, a calibrated drag model assuming no wing tip device was created from information generated by Boeing[121] and subsequently contrasted against an assumption of winglets installed. Some precision is lost for short-range missions, i.e. 500 nm and less, which are characterised by lower operating lift coefficients (C_L < 0.5); nonetheless, the agreement for the B737-800 appears to be mostly a good one.

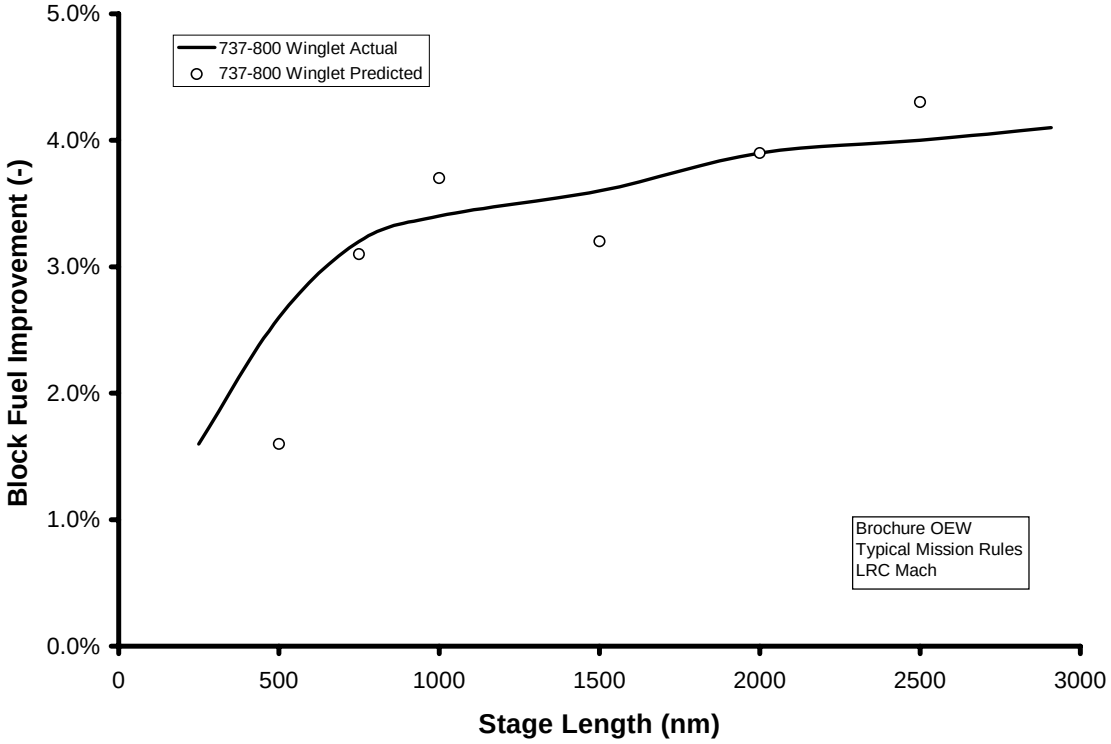

Figure 32. Comparison between flight-test derived[71] and predicted improvement in block fuel for B737-800 commercial transport.

One undesirable feature of this method is the fact ΔC_{Di} approaches zero with decreasing Γ_{WL}; this analytical sensitivity does not parallel the winglet parametric study results presented by Ishimitsu[70]. The problem can be allayed by stipulating an accepted design protocol of winglet integration not violating a minimum cant angle or lower threshold of Γ_{WL}. Cant angles less than approximately 15° are not permissible because it is indicative of a less pronounced rate change improvement in C_{Di} with respect to wing root

bending moment, and of equal importance, it gives less scope to provide aerodynamic interference relief between wing and winglet and is detrimental in delaying the formation of shock waves on the winglet upper surface.

7.8 Validation of the Total Aerodynamic Drag Model

The aerodynamic performance characteristics of known contemporary aircraft were available to validate the predictive powers of the methods discussed – henceforth referred to as the Combined Drag Model (CDM). Figure 33, Figure 34, Figure 35 and Figure 36 show the agreement between predictions using CDM and flight test drag polars for the Saab AB Saab 2000[114], Bombardier Aerospace Learjet 60[134], Bombardier Aerospace Global Express[135] and Boeing B737-800[121] respectively. Each chart indicates two zones of prediction effectiveness: "Infrequent Excursions" alludes to operating points within the certified aircraft flight envelope that are seldom impinged during typical operation, i.e. very low and very high operating lift coefficients, whereas, the inner boundary labelled "Core Predictions" are points that will always need to be considered during the course of examining the viability of a design candidate from an operational performance perspective. By virtue of conducting a validation exercise that encompasses aircraft of varying size, mission role and even power plant installation philosophy, the results indicate there exists a good likelihood that CDM will produce predictions well within ±10%, and it is discernable that core predictions will stay within an acceptable ±5% error bandwidth.

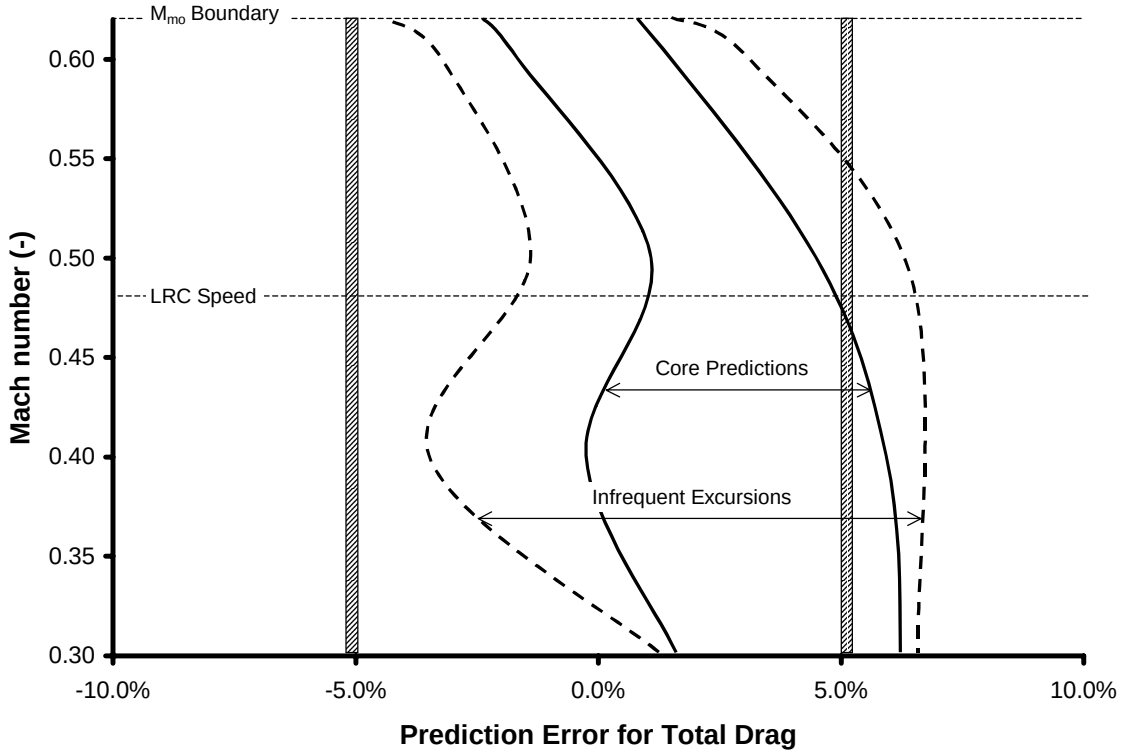

Figure 33. CDM prediction effectiveness inspected for the Saab 2000 high-speed turboprop regional transport.

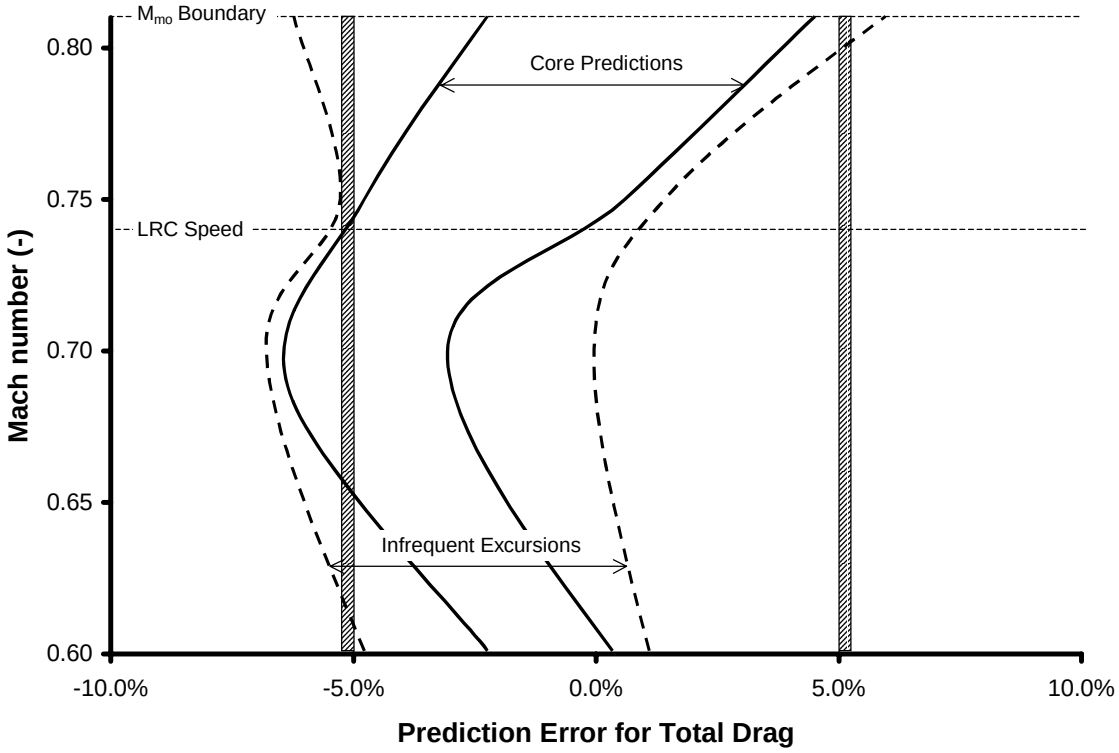

Figure 34. CDM prediction effectiveness inspected for the Learjet 60 midsize turbofan business aircraft.

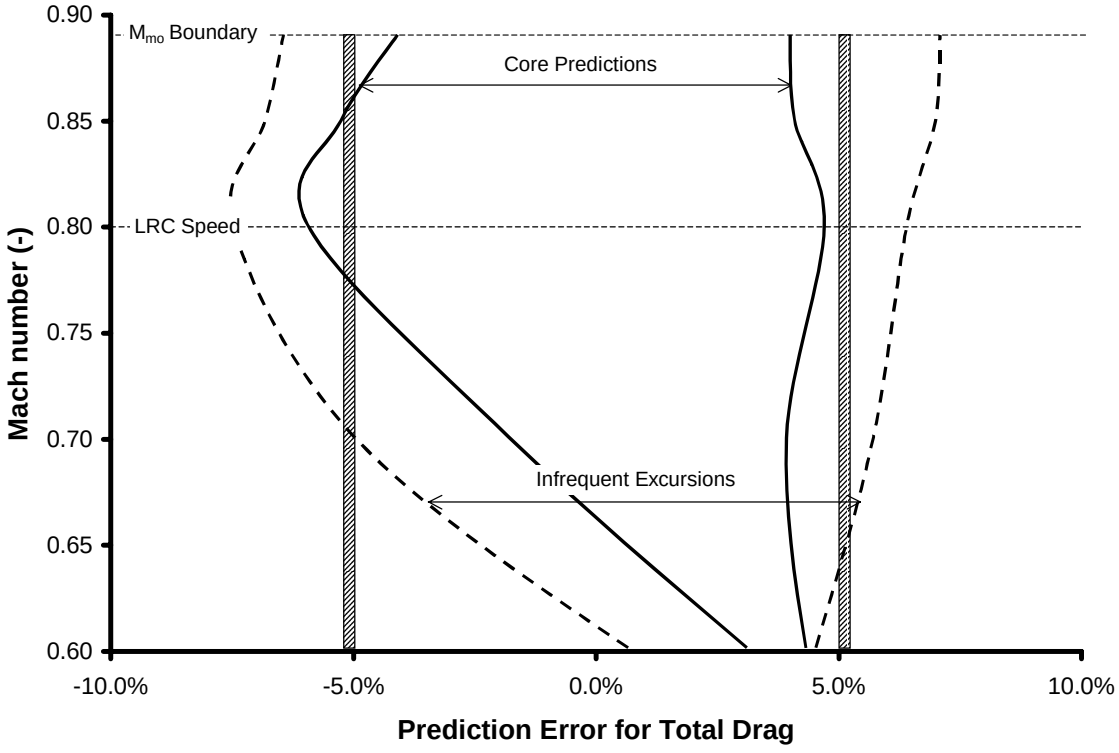

Figure 35. CDM prediction effectiveness inspected for the Global Express ultra long range turbofan business aircraft.

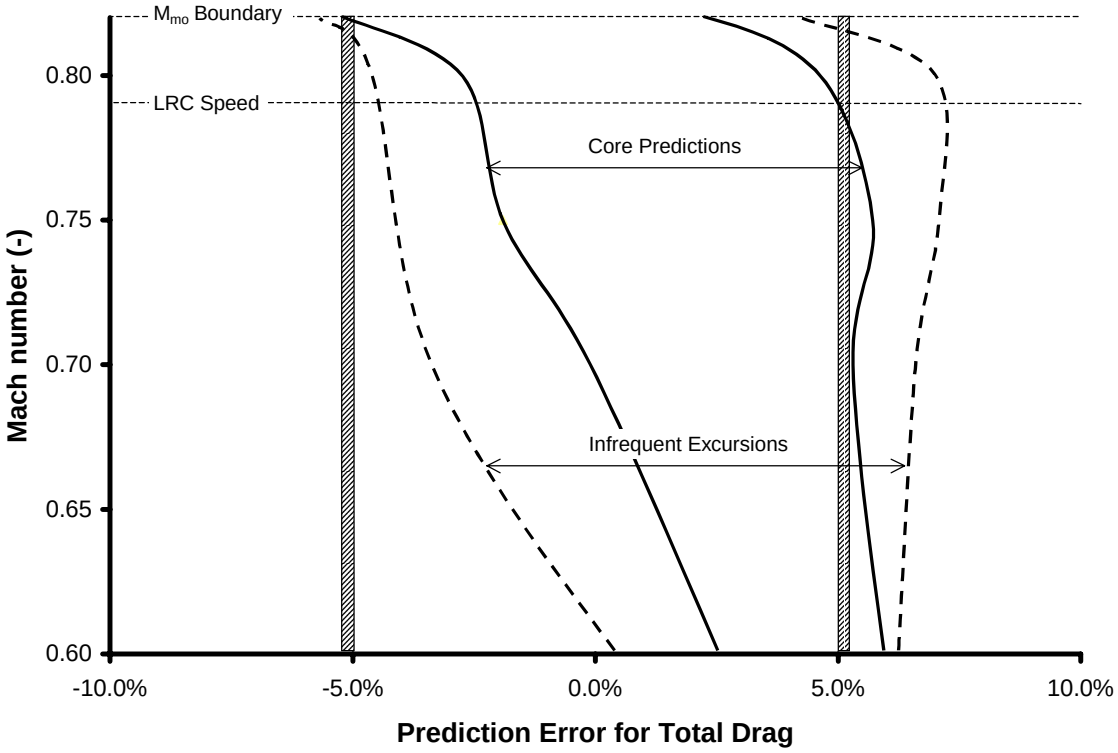

Figure 36. CDM prediction effectiveness inspected for the B737-800 narrow-body commercial transport; note that $\tau_{act} = 1.30$ used in generating the reference condition.

intentionally blank

8 Modelling the Performance of Gas Turbine Engines

The attributes of a gas turbine power plant are primarily dependent upon the effect of pressure ratio, altitude and free-stream velocity. The instantaneous production of thrust relies generally upon an engine's thermal efficiency in conjunction with variations in disc loading. The compression ratio is achieved partly by the inlet (ram pressure) generated by elevated mass flow at increased velocities but mostly through the compressor itself thus making pressure ratio engine specific. It is common practise to compare the corrected net thrust to the maximum static takeoff thrust for ISA, sea level and use this correlation to predict performance for any deviations from standard conditions.

The expressions to follow do not permit direct sensitivities to pressure ratio or turbine entry temperature because such a facility was deemed too detailed for this level of analysis. Investigations have shown that adequate representation of these parameters are produced through correlation of lapse coefficients to the maximum static thrust rating of a given engine because these are usually traded off against each other. However, owing to the availability of simple yet sufficiently accurate expressions, a By-Pass Ratio (BPR) to Thrust Specific Fuel Consumption (TSFC) functional sensitivity construct has been adopted. In this manner, generic turboprop and turbojet models can be created through regression thereby giving good representation of expected overall power plant efficiency without altering the inherent structure of the model itself. A generic model derived with statistical regression would possess the inherent capability of being utilised as a rubber engine for comprehensive sensitivity studies. Also, these functional forms are differentiable via logarithmic differentiation with respect to independent parameters that have a direct physical consequence i.e. flight level and velocity, thus allowing for a rather comprehensive scope of performance optimisation possibilities.

8.1 Performance Degradation for Non-standard Ambient Conditions

A linear performance deterioration model (k_θ) to account for the effects of temperature deviations from ISA (T_d) when calculating instantaneous available thrust, or even TSFC may be incorporated via

$$k_\theta = 1 \mp k_1 \Phi\left(T_d, T_c\right) \tag{195}$$

where T_c is the critical ISA deviation for flat rating or standard reference temperature for the basic model, and $k_1 = k_{Tcor}$ $(T_d\text{-}T_c)$ is the variation of reduction in thrust or thrust specific fuel consumption once this threshold or reference has been surpassed. The linear performance model is expected to be less than unity for thrust performance modelling, whilst, greater than unity when accounting for TSFC degradation. No thrust and TSFC credit is given for deviations below the reference temperature upon which the basic model has been constructed.

8.2 De-rated Engine Performance and Other Variations in Rating

Many aeroplanes employ thrust setting schedules which are less than full maximum static rating afforded by the engine. The lower thrust setting schedules are referred to as "de-rates" and the primary objective of administering such a constraint is for the sake of improving engine reliability, improving aeroplane dispatch reliability and reducing engine operating costs. De-rates take the form of some fixed percentage reduction (k_{DR1}) below

maximum thrust, and require an alteration of the engine's thermal properties thus changing performance characteristics for given speed and flight level compared to the baseline. A linear model to account for this is proposed as

$$k_{DR} = 1 \mp k_{DR1} \tag{196}$$

This expression can also be fortuitously utilised for "up-rating" the standard turbofan performance model in order to simplify definitions for other pertinent ratings. For example, a thrust regression model for Normal Takeoff [Power] Thrust (NTOT) may be created and appointed as a reference for simulating Maximum Takeoff [Power] Thrust (MTOT) commonly used as a boost of extra thrust to ensure a margin of reserve during one engine inoperative field performance. This rating is usually referred to as some fixed percentage increase over the NTOT available thrust and it can be reasonably surmised that the reference thrust model may be factored accordingly as well.

8.3 Thrust Reverse

The main function of thrust reverse is to reduce the ground roll distance providing an extra element of safety independent from wheel brakes or spoilers. Obert[3] offers data demonstrating the influence of BPR on thrust reverse effectiveness. It establishes a good correlation between the thrust produced by reversers and the engine's maximum static thrust potential for a variety of bypass ratios ranging from 3.0 to 12.0. Even though this data advocates a distinct increasing trend in fraction of maximum static thrust available for thrust reverse with BPR, a universally applicable estimate of $T_{reverse}$ / T_{max} = 0.30 independent of BPR was finally chosen for sake of simplicity. Since the magnitude of thrust reverse has been reasoned to be a linear factor of the maximum static rating, this feature can considered to be equivalent to de-rating an engine since the thrust magnitude characteristics are diminished for given forward speed. Hence, Eq. (196) would be used with the k_{DR1} value equal to 0.7.

8.4 Thrust Performance for Low to Intermediate Speeds

By assuming this lapse rate decays exponentially, an approximation of instantaneous thrust is proposed as

$$T = T_o\left[1 + \exp\left\{-\left(k_1 + k_2 h\right)T_o\right\}\right] k_\theta \, k_{DR} \, k_3 \exp\left\{-\left(k_4 h + k_5 V \exp\left[-k_6 h\right]\right)\right\} \tag{197}$$

where T is the instantaneous net thrust and, k_n are constants of proportionality. Eq. (197) is applicable for normal takeoff, maximum takeoff with Automatic Power Reserve (APR), maximum climb and maximum continuous thrust ratings. For the purposes of modelling any gas turbine (or rubber) engine with environmental control system engine bleed activated and anti-ice off, coefficients of k_1 = 0.259 per N, k_2 = 2.20 x 10^{-4} per FL.N, k_3 = 0.9936, k_4 = 2.87 x 10^{-3} per FL, k_5 = 1.44 x 10^{-3} s/m and k_6 = 1.80 x 10^{-3} per FL should be used in the absence of detailed data for regression. The above equation using these coefficients produces values of thrust in units of Newtons.

8.5 Thrust Performance for High Speed

A distinct maximum cruise thrust prediction method was also developed and is of the form

$$T = T_o\left[1+\exp\left\{-\left(k_1+k_2 h\right)T_o\right\}\right]k_\theta\, k_{DR}\, k_3 \exp\left\{-\left(k_4 h + V\left[k_5 + k_6\exp\left\{-k_7 h\right\}\cos\left(\frac{\pi}{4}+k_8 h\right)\right]\right)\right\} \quad (198)$$

It can be observed that incorporation of an engine rating parameter for universal modelling which accommodates both takeoff/climb/maximum continuous and maximum cruise has been dispensed with. Takeoff/climb/maximum continuous ratings are usually associated with lower vehicular subsonic speeds whereas maximum cruise with considerably higher ones, and because present day gas turbine overall power plant efficiencies exhibit strong variation with Mach number particularly with transonic performance[136], i.e. free-stream Mach numbers greater than approximately 0.65, this condition denies adequate regression qualities, and therefore compels distinction from one another. Furthermore, Eq. (198) need not be in an easily differentiable form for steady cruise analysis, whereas as it will be demonstrated later for climb, Eq. (197) must. For the purposes of modelling any gas turbine (or rubber) engine with environmental control system engine bleed activated and anti-ice off, coefficients of k_1 = 0.259 per N, k_2 = 2.20 x 10^{-4} per FL.N, k_3 = 1.781, k_4 = 4.00 x 10^{-3} per FL, k_5 = 2.00 x 10^{-3} s/m, k_6 = 1.60 x 10^{-3} s/m, k_7 = 2.00 x 10^{-4} per FL and k_8 = -0.0101 per FL should be used in the absence of detailed data for regression. The above equation using these coefficients produces values of maximum cruise thrust in units of Newtons.

8.6 Thrust Specific Fuel Consumption

TSFC (or c) is also a function of overall power plant efficiency[136] and Mach number. Scope was given for the creation of a unified analytical treatment of instantaneous TSFC prediction so a single expression that accounts for not only Mach number but also variations in engine ratings was pursued.

8.6.1 The General Model and Baseline Calibration

Assuming a baseline gas-turbine engine of a given BPR, the TSFC can be estimated using the construct

$$c = k_\theta\left\{k_1 h^{-k_2}\left(\frac{T}{T_o}\right)^{(k_3 h+k_4)} M + \left(k_5 h + k_6\right)\left(\frac{T}{T_o}\right) + k_7 h + k_8\right\} \quad (199)$$

For the purposes of modelling any gas turbine (or rubber) engine with environmental control system engine bleed activated and anti-ice off, coefficients of k_1 = 1.586 lb/lb.hr, k_2 = -0.303, k_3 = 8.40 x 10^{-4} per FL, k_4 = -0.760, k_5 = 5.45 x 10^{-4} lb/lb.hr.FL, k_6 = -0.307 lb/lb.hr, k_7 = -9.54 x 10^{-5} lb/lb.hr.FL and k_8 = 0.694 lb/lb.hr should be used in the absence of detailed data for regression. The above equation using these coefficients is calibrated for an engine for commercial use with takeoff BPR of approximately 5.2 and produces values of TSFC in units of lb/lb.hr. As a supplementary note for turboprop installations, a good initial rule in quantifying operating TSFC is to factor the turbofan equivalent result by 0.65. This simulates an equivalent by-pass ratio increase due to the presence of propeller or larger fan diameter for given equivalent maximum static thrust rating.

8.6.2 Examining the Sensitivities of Thrust Specific Fuel Consumption with By-Pass Ratio

BPR imparts a significant influence on variation of TSFC. When intake and exhaust losses are taken into consideration, increasing BPR usually accompanies with it decreasing TSFC until a minimum TSFC threshold is reached[1]. The suggested parameter values for the gas turbine TSFC model presented above is quoted for a reference engine, in this instance the BPR being equal 5.2. One method in producing an adequate representation of the functional sensitivity of TSFC for given BPR is to utilise regression analysis conducted by Svoboda[57]. Among the key parametric associations examined by Svoboda includes an analytical description of BPR and cruise TSFC that varies monotonically with T_o. This is a fortuitous circumstance because it signifies a simple extension to the reference prediction algorithm given by Eq. (199). The correlation between BPR and takeoff thrust is given as[57]

$$\mathrm{BPR} = 3.2 + 0.15\mathrm{T}_o^{1/2} \tag{200}$$

with the TSFC at cruise trend derived to be[57]

$$\mathrm{c} = 0.80 - 0.0144\mathrm{T}_o^{1/2} \tag{201}$$

In order to permit the introduction of BPR sensitivity into the global prediction process, the fractional change operator is invoked for TSFC, namely $\delta\mathrm{c}$. Using Svoboda's statistical equations as the source, the fractional change of TSFC reads as

$$\delta\mathrm{c} = \frac{\Delta\mathrm{c}}{\mathrm{c}_{\mathrm{orig}}} = \frac{\mathrm{BPR}_{\mathrm{orig}} - \mathrm{BPR}_{\mathrm{rev}}}{11.53 - \mathrm{BPR}_{\mathrm{orig}}} \tag{202}$$

and recognising the adjusted value of TSFC for a given assumed value of BPR is simply produced by the product of the fractional operator and the originally computed TSFC

$$\mathrm{c}_{\mathrm{rev}} = (1 + \delta\mathrm{c})\mathrm{c}_{\mathrm{orig}} = \frac{11.53 - \mathrm{BPR}_{\mathrm{rev}}}{11.53 - \mathrm{BPR}_{\mathrm{orig}}}\mathrm{c}_{\mathrm{orig}} \tag{203}$$

where $\mathrm{c}_{\mathrm{orig}}$ denotes the originally computed TSFC based on the reference engine, or Eq. (199).

9 Formulation and Prediction of Optimal Field and En route Performance Control

Takeoff and landing field length prediction is a unique problem to solve since relatively accurate results can be achieved using either a very simple parametric expression[3], or quite complex if one approaches the problem via integral methods[1,4]. Many alternatives for the estimation of field performance exist in current literature. Rather than opt for completely new algorithms, existing methods found in literature were utilised but with some enhancements introduced.

9.1 Takeoff Performance

A summary and explanation of takeoff for a transport category certified aeroplane is presented in Figure 37. Commencing from brakes release point, the vehicle is accelerated at normal takeoff [power] thrust whereupon the speed will exceed the stalling speed V_S. The aeroplane continues to accelerate during ground roll until minimum control speed V_{MC} is attained. If a critical engine fails at V_1, the average pilot could safely elect to continue with takeoff (accelerate-go) or conversely decided to come to a complete stop (accelerate-stop). At the takeoff rotation speed V_R, the attitude of the vehicle is pitched up but the pilot continues to accelerate to V_{MU}, the minimum unstick speed. At this speed, the aeroplane is able to lift-off even with OEI, however, to provide an additional margin of safety, the aeroplane is permitted to accelerate to the lift-off speed V_{LOF} at which point the vehicle becomes airborne. After lift-off, acceleration is continued up to V_2 (commonly referred to as the second segment). This takeoff climb speed is one attained at an imposed screen height above the ground.

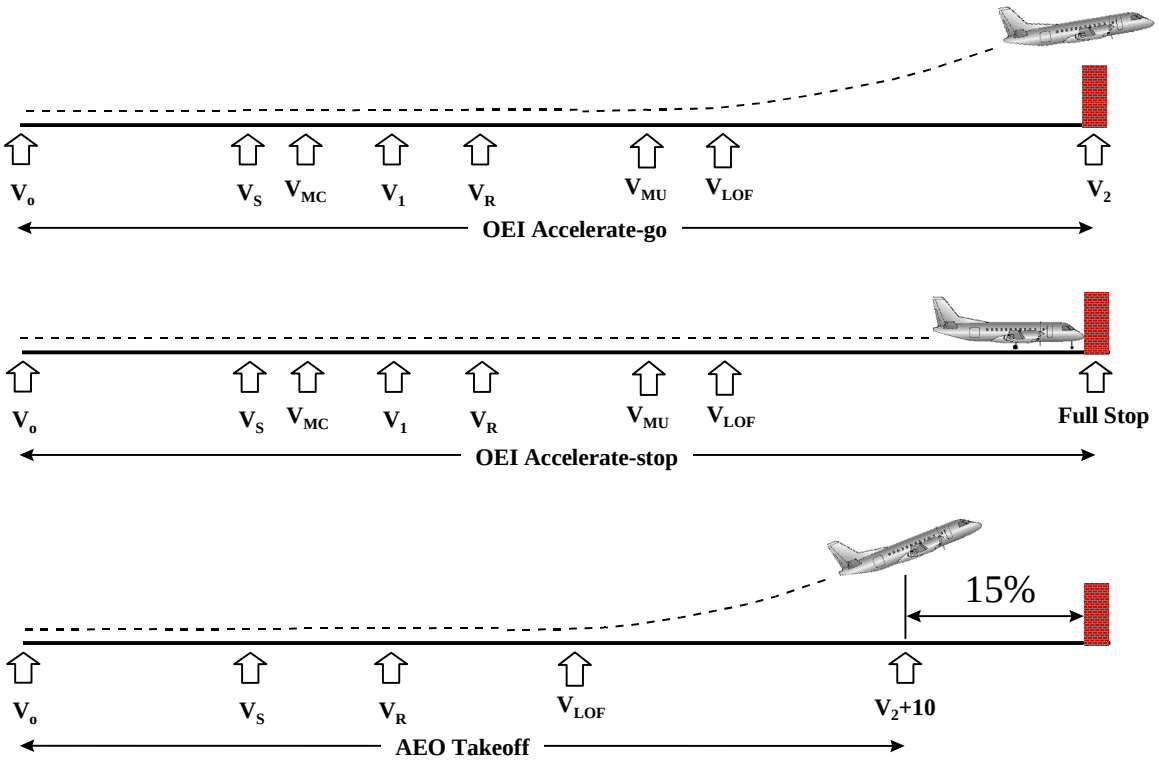

Figure 37. Takeoff reference speeds and general requirements for civil transport aircraft[137].

An array of margins has been set for the relationship of these reference speeds to one another. For both FAR[138] and JAR[139] certification, V_1 must be 5% higher than V_{MC}, V_{LOF} at least 10% greater than all-engines operational (AEO) V_{MU} or 5% higher than OEI V_{MU}. After lift-off, the vehicle must clear a 10.7 m (35 ft) obstacle and V_2 must be greater than $1.13V_S$ or $1.2V_S$ depending on the type of stall definition accepted by the regulations, i.e. 1g versus minimum aerodynamic stall respectively. A final common stipulation is that the takeoff climb speed must be the greater of the stall speed factored $(V_2 / V_S)_{min}$ speed and $1.1V_{MC}$. The AEO screen speed is the takeoff climb speed reached at the imposed obstacle height and must be greater than V_2. Typically this is defined as $V_3 = V_2 + 10$ KCAS (or up to +25 KCAS depending on the vehicle size).

9.1.1 Balanced Field Length Prediction

The Balanced Field Length (BFL) is defined as one where the distance to continue the takeoff following recognition of engine failure is equal to the distance required to stop if the takeoff should be aborted. An additional requirement states that final field length must be the greatest of OEI accelerate-go, OEI accelerate-stop, or 115% of the AEO distance to the screen height. Many alternatives for the estimation of field performance exist in current practise. They range in scope from the use of rather involved iterative numerical integral methods[39] to application of a simple parametric expression based on statistical methods[3] that do not exhibit any functional sensitivity to limiting conditions. Rather than opt for new algorithms, existing methods were utilised but with some enhancements introduced by the author. Torenbeek[1] offers a useful equation in functional form that correlates the field length performance of similar aircraft and this serves as an adequate first order approximation.

$$BFL = \left(\frac{0.863}{1 + 2.30\Delta\gamma_2}\right)\left(\frac{W_{TO}/S_W}{\rho g C_{L_2}} + h_{TO}\right)\left(\frac{1}{T/W_{TO} - \mu'} + 2.70\right) + \frac{\Delta s_{TO}}{\sqrt{\sigma}} \qquad (204)$$

$\gamma_2 = T/W - C_D/C_L$ is the instantaneous OEI climb gradient of the vehicle at the 10.7 m (35 ft) screen height threshold (h_{TO}), $\Delta\gamma_2$ is γ_2 less the minimum second segment climb gradient permitted by airworthiness authorities, W_{TO} / S_w is the wing loading at Takeoff Gross Weight (TOGW), T / W_{TO} is root mean square thrust-weight for the takeoff run, C_{L2} is the instantaneous lift coefficient at the stall speed factored speed (V_2), μ' is the coefficient of friction during acceleration and Δs_{TO} = 200 m (655 ft) is the inertia distance. The asymmetric lift-drag ratio (C_L / C_D) is calculated based on the most limiting condition when V_2 and the minimum control (V_{MC}) speeds are taken into consideration with the appropriate margins considered as dictated by airworthiness regulations.

Since the second segment climb gradient needs to be quantified in order to proceed with the prediction, it can be concluded that consideration of $(V_2 / V_S)_{min}$ should be introduced. Recalling that the takeoff climb speed must be the greater of the stall speed factored $(V_2 / V_S)_{min}$ speed and $1.1V_{MC}$, scope should be given to account for this scenario. A situation could arise whenever thrust loading is quite large or prevailing ambient conditions for given aeroplane configuration may invoke V_{MC} speed limitations as opposed to the common conceptual critical assumption of the $(V_2 / V_S)_{min}$ speed. The most limiting speed between V_2 and V_{MC} can be identified using the maximising function operator $\Phi_{max}(V_{2min}, k_{MC}V_{MC})$ where $V_{2min} = k_S V_S$, $k_S = (V_2 / V_S)_{min}$ and k_{MC} is the minimum control speed margin. Identification of a conceptual V_{MC} for given vehicle configuration and ambient conditions is treated more in-depth following this section. The instantaneous climb

gradient, γ_2, must be estimated at the screen height threshold where the vehicle has reached the greater of V_{2min} or $k_{MC}V_{MC}$. It is highlighted that C_L is taken to be equal to C_{L2} and is calculated by the relationship $C_{L2} = (1 / k_S)^2 C_{Lmax}$ at given flap setting. Using this supposition in consort with vortex-induced drag estimation methods, combined with estimates for zero-lift drag, incremental zero-lift constituent due to flap and/or slat deflection and drag due to undercarriage, the total low speed drag C_D can be derived.

The coefficient of friction during acceleration μ' is given by Torenbeek[1] as

$$\mu' = \mu + k_\mu \left(\frac{C_D}{C_L} \right) \tag{205}$$

derived from the momentary acceleration constituents $-[\mu + (C_D - \mu C_L)qS_W/W_{TO}]$, which assists in degrading T/W_{TO} potential during takeoff ground roll. In the absence of more detailed information, $\mu = 0.02$ is suggested for concrete; and the factor $k_\mu = 0.072$ was chosen to be an appropriate choice.

As analytically demonstrated by Torenbeek, the third product term in parentheses accounts for the accelerate-stop characteristics of the vehicle. Departing from the original form shown in Eq. (204), a more suitable functional form for BFL is proposed here as

$$\mathrm{BFL} = \left(\frac{0.863}{1 + 2.30\Delta\gamma_2} \right) \left(\frac{W_{TO}/S_W}{\rho g C_{L_2}} + h_{TO} \right) \left(\frac{1}{T/W_{TO} - \mu'} + \Delta_{Vx} \right) + \frac{\Delta s_{TO}}{\sqrt{\sigma}} \tag{206}$$

with the Δ_{Vx} term representing a cumulative deceleration of the vehicle at root mean square of engine failure recognition speed ($V_1/\sqrt{2}$). It expands out to read

$$\Delta_{Vx} = \left. \frac{1}{D_{OEI}/W_{TO} + \Phi_{tr}(T_{tr}/W_{TO}) + \Phi_{sp}(D_{sp}/W_{TO}) + \mu_{br}(1 - L_{op}/W_{TO})} \right|_{V_1/\sqrt{2}} \tag{207}$$

Fundamental parameters that quantify this contribution relates to the vehicular OEI drag (D_{OEI}) and the influence of maximum braking via the braking coefficient of friction (μ_{br}) the magnitude of which is adjusted for residual operating lift (L_{op}) yielding a combined mean value of around 0.32 for hard, dry surfaces and assuming maximum anti-skid effectiveness. For improved performance, the influence of spoiler actuation (denoted by the impulse function Φ_{sp}) or thrust reversing (denoted by the impulse function Φ_{tr}) is enabled with two additional parametric terms. Spoiler actuation may be introduced through a parasitic drag contribution (D_{sp}) derived using simple geometric analysis techniques in conjunction with an empirical drag coefficient based on frontal area similar in scope to how extended flap and slats are computed using Eq. (170). As a consequence, total lift dumping (i.e. complete suppression of lift) should be assumed in the calculations. It is stressed that any validity of accounting for thrust reverser usage for takeoff performance prediction must be established through interpretation of airworthiness regulations. FARs currently do not permit OEI thrust reverser effects to be assumed, whereas, JARs allow such a premise for turboprop aircraft.

9.1.2 Identification of Minimum Control Speed

The minimum control speed is a common limitation that degrades operational field performance flexibility for scenarios widely different to that of reference ISA, sea level standard conditions commonly scrutinised during conceptual design studies. An ability to adequately predict the influence of this constraint to vehicular performance for less idealised ambient conditions, or occasionally, design candidates which employ unnecessarily high thrust ratings is paramount to achieving a well balanced design with regards to field performance. At this speed, if a critical engine fails, the manufacturer must demonstrate that the aeroplane is able to maintain straight flight with zero yaw or with a bank angle of less than 5°. The following definition for V_{MC} revolves around the notion of maintaining a straight path with zero yaw regardless of being on the ground roll or in flight.

Identification of a conceptual V_{MC} can be achieved by rearranging Eq. (174) and solving for the instantaneous velocity generated when maximum permissible rudder deflection occurs ($\delta_R = \delta_{Rmax}$).

$$V_{MC} = V\left\{\frac{y_{eng}\left(D_{wm} + T_{op}\right)}{q_n S_{vt} C_{L\alpha,vt} \tau \eta l_{vt} \delta_{R\max}}\right\} \tag{208}$$

where the modified form solves for minimum control speed on the ground which is also treated as an approximation of minimum control speed in the air. In this way, an objective function sensitivity with engine thrust line location as well as thrust generation potential to BFL performance can be established, and hence, locate any stationary point thresholds. Obert[3] indicates a maximum rudder deflection of $\delta_{Rmax} = 30°$ would be an upper limit to maintaining linearity of hinge moments. This is not only important for addressing issues of promoting acceptable control forces, but also defines an upper boundary of validity for the simplified prediction methods presented in this study. The resulting transcendental equation appears to be in a form which facilitates convergence via simple iteration i.e. x = F(x); this is actually a misleading hypothesis. The basic equation has tendencies of strongly diverging from the solution up to a certain iteration threshold upon which subsequent estimates neither converge nor diverge, and loop endlessly. To deal with this problem, an iterative scheme*** that modifies the original transcendental expression into a stable form guaranteeing convergence and solved via simple iteration needs to be formulated.

9.2 Landing Field Performance

The landing segment can be separated into three portions of operation: approach, flare and the ground roll (Figure 38). The method presented by McCormick[34] offers an opportunity of not only producing reliable predictions but is comprehensive enough for adequate objective function sensitivity.

The flare is assumed to be a circular arc and approach speed is constant throughout the flare. Assuming $\theta_D = 3^o$ is the glide-slope angle, the total airborne distance, s_A, is given by

$$s_A = \frac{15.24}{\tan\theta_D} + \frac{R\tan\theta_D}{2} \tag{209}$$

*** A more comprehensive explanation of this philosophy and implementation is offered in Section 9.7

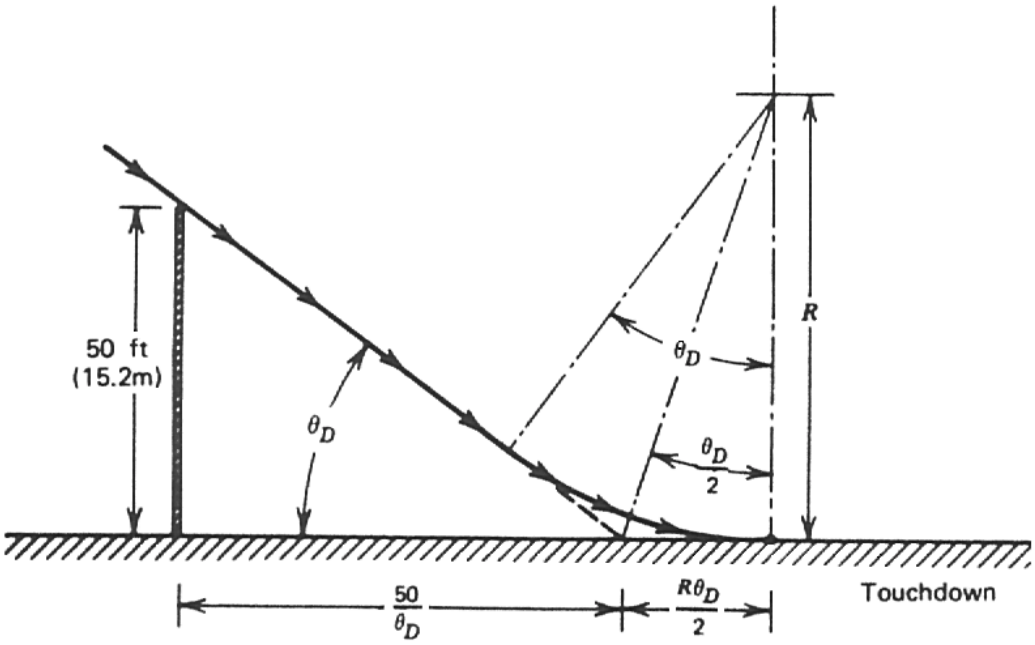

Figure 38. Model of the landing approach and flare path for prediction purposes[34].

The value 15.24 m represents a 50 ft screen height that must be cleared, and R is the flare radius. The flare radius for steady approach is

$$R = \frac{V_{REF}^2}{g\left[\left(C_{L\max}/C_{LREF}\right)-1\right]} \tag{210}$$

with the REF subscript denoting a stall speed factored reference speed according to airworthiness regulations.

After touchdown, delay time allowances are made for reconfiguring the vehicle from landing to braking. A 4 second delay is allowed for transition from landing to braking configuration. During this period, the vehicle changes speed from V_{REF} to V_{TD}, hence

$$s_{TRANS} = 4\,\frac{(V_{REF}+V_{TD})}{2} \tag{211}$$

and the touch down speed is defined as approximately $0.94V_{REF}$ and was derived empirically.

Ground roll is simply defined as a continuous deceleration whereupon the magnitude of all relevant variables are evaluated at the root mean square of touch down speed ($V_{TD}/\sqrt{2}$). A single step Euler numerical integration is employed at $V_{TD}/\sqrt{2}$, the instantaneous deceleration ($\dot{V}_{GR}$) is calculated using Eq. (212)

$$\dot{V}_{GR} = g\left[\frac{T_{id}}{W_{LD}} - \frac{D_{op}}{W_{LD}} - \Phi_{tr}\left(\frac{T_{tr}}{W_{LD}}\right) - \Phi_{sp}\left(\frac{D_{sp}}{W_{LD}}\right) - \mu_{br}\left(1-\frac{L_{op}}{W_{LD}}\right)\right]\Bigg|_{V_{TD}/\sqrt{2}} \tag{212}$$

T_{id} is the instantaneous thrust at idle throttle setting, i.e. $T/T_o \cong 0.03$, D_{op} is the total drag and W_{LD} is the landing weight.

By considering the M^{c}Cormick's rationale that the inverse of deceleration is a linear function of the square of the velocity, an approximate measure of the ground roll (s_{GR}) is then given by

$$s_{GR} = \frac{V_{TD}^2}{2\dot{V}_{GR}} \tag{213}$$

The total landing distance (LD), which is for all intensive purposes an estimate of the yet to be determined flight-tested landing distance, is then computed by the additional of s_A, s_{TRANS} and s_{GR}. The LD is usually only quoted for business aircraft, however, commercial transports must adhere to operational rules governed by FAR Part 121. In such a case, FAR part 121 stipulates that the LD should be factored by 1.667 in order to produce the landing field length (LFL).

It is highlighted that approach and landing climb minimum control speed thresholds have been disregarded in this instance since these scenarios are usually not limiting at ISA, sea level conditions although exceptions may occur where positive engine thrust levels are significant in some vehicles.

9.3 Comparison between Estimated and Actual Aircraft Data for Field Length Performance

Figure 39 plots the estimation error (ε = predicted – actual) for both BFL and LFL (or

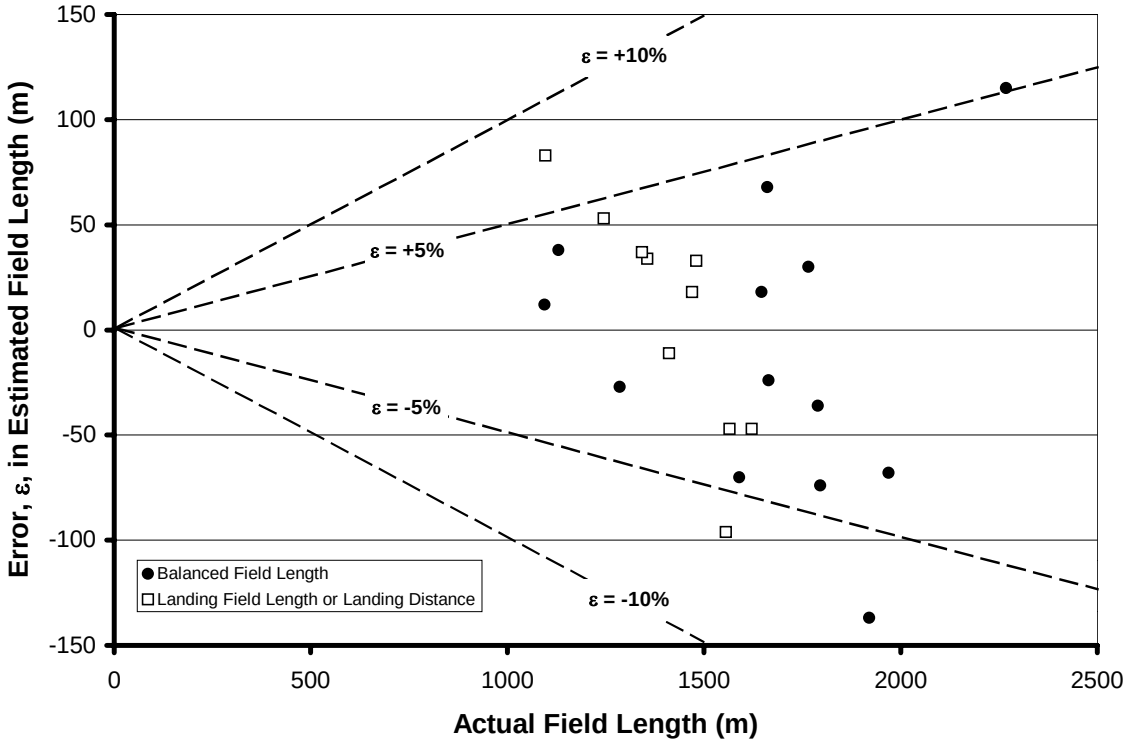

Figure 39. Prediction accuracy of algorithms to compute the BFL and LFL (or LD) for a select array of regional, narrow-body and business aircraft.

LD) results against manufacturer quoted values. Available aircraft data involved a collection of regional, narrow-body and business jets as well as turboprops. The vehicles examined include: Boeing B737-600[77]; Bombardier Aerospace Learjet 60[106], Challenger CL-604[51], Global Express[64], CRJ200[79], CRJ700[80] and CRJ900[81]; Cessna Citation Excel[82]; Dassault Aviation Falcon 900EX[53]; Embraer ERJ 145LR[84]; Gulfstream Aerospace GIV-SP[89] and GV-SP[90]; and, Saab Aerospace Saab 340B[91] and Saab 2000[92].

Figure 39 demonstrates that the presented methodologies for BFL and LFL (or LD) will generally fall within a ±50 m (±165 ft) bandwidth. Some excursions by as much as 50-100 m (165-330 ft) can be expected, but as a general rule, will not exceed 100 m. These absolute values are equivalent to predictions remaining within an acceptable relative error of ±5%.

9.4 All Engines and One Engine Operational Optimal Climb Control

Neglecting flight path-angle dynamics and effects of wind, the point mass equation of motion for accelerated flight in the vertical plane for given altitude is

$$\frac{dh}{dt} = \frac{(T - D)V}{\left[1 + \frac{V}{g}\frac{dV}{dh}\right]W} \tag{214}$$

where dh/dt is the instantaneous climb rate, T, D, and W are instantaneous available thrust, total drag and AUW at forward velocity V, and the final component V / g dV / dh accounts for accelerated climbs. This equation can be utilised to address two distinct premises for climbing flight, namely the acceleration-free and accelerated assumptions, and from the latter, an approximation to the actual accelerated trajectory may be generated for optimal climb speed schedule identification.

9.4.1 Energy-Height Approximation for Accelerated Climbing Flight

The acceleration-free scenario is indicative of a steady state solution where the component V / g dV / dh in Eq. (214) is taken to be zero. There is little error associated with this supposition when examining slower speed climbs, however, with higher performance gas turbine aircraft, the excess available thrust over the total drag may be considerable, hence giving rise to an acceleration component which may contribute to the climb profile. By defining a so-called energy-height as the complete exchange of kinetic energy into potential energy in addition to the vehicle's potential by virtue of its current altitude it then follows that the relationship between flight level and energy balance would be given by

$$h = h_e - \frac{V^2}{2g} \tag{215}$$

where h_e is the energy-height. The time required to go from one energy level to another will be given by

$$\Delta t_{1\to 2} = \int_{t_1}^{t_2} \frac{1}{P_s} dh_e \tag{216}$$

The quantity P_s is the specific excess power that can now be used for climbing, accelerating or turning. The path to minimise Δt at any flight level and airspeed will be the one that gives maximum rate change of h_e for a given P_s value. This condition is achieved by minimising the integral on the right and side of Eq. (216). When the partial derivative with respect to V of the integrand, $1 / P_s$, evaluated at given flight level is zero, the conditions of flight which produces a climb trajectory for minimum time can be defined as

$$\left(\frac{\partial P_s}{\partial V}\right)_{h_e} = 0 \tag{217}$$

It is common practise to solve this equation by means of a graphical procedure where contours of constant h_e and constant P_s values are plotted as a function of flight level and forward speed, the path for minimum time being the locus of points for which the contours are parallel as demonstrated by Figure 40. As an alternative, the aim is to produce a method that solves Eq. (217) analytically for all ambient conditions.

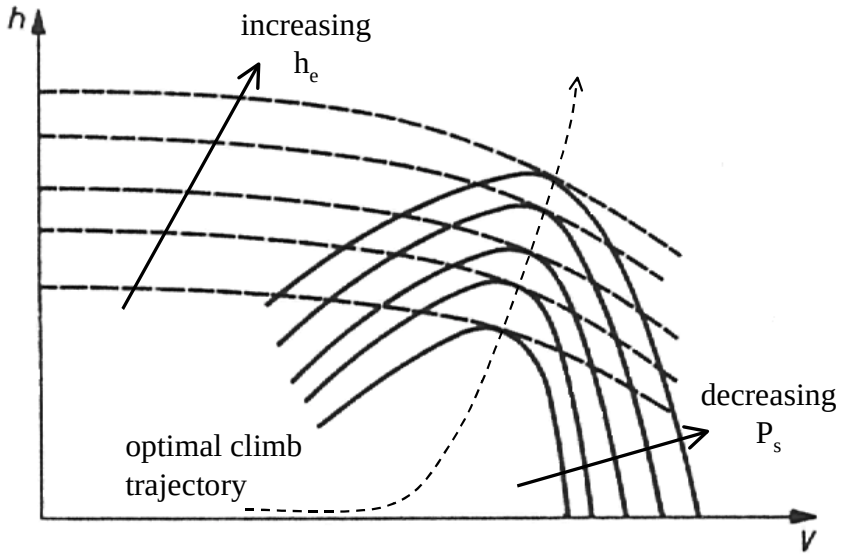

Figure 40. Specific excess power and specific energy contours for identifying minimum time to climb flight paths.

Before any unified analytical method can be undertaken, it must be identified that the optimal climb forward speed identification will not be quite accurate by virtue of employing a complete energy-height transformation premise. Use of Eq. (215) is not sufficient enough for final optimal trajectory definition because it assumes that potential and kinetic energy can be interchanged instantaneously and without loss thereby yielding speed schedules with optimistically higher velocities. In order to correct for this physical phenomenon, a modified energy-height balance relationship can be proposed as

$$h = h_e - \eta_\tau \left(\frac{V^2}{2g}\right) \tag{218}$$

where η_τ is designated as the "manoeuvring efficiency" which represents a measure of the total amount of kinetic energy which readily transforms into a potential equivalent. A value of $\eta_\tau = 1$ denotes the aircraft is infinitely manoeuvrable and that potential energy and kinetic energy can be interchanged instantaneously without loss. Factors less than unity can be used in order to simulate a more a reduced propensity for manoeuvring at given speed thereby resulting in a partial energy exchange with associative losses. Investigations have shown that $\eta_\tau = 0.5$ gives an adequate representation and it is stressed this assumption is valid exclusively for subsonic civilian transport category aircraft.

Eq. (214) gives measure of the instantaneous excess power, i.e. $P_s = (T - D)\,V$, delivered at velocity for some AUW. By choosing an arbitrary constant energy-height, substituting Eq. (215) into Eq. (214), and assuming the angle of climb is small enough for the straight and level flight drag characteristics to be still valid, it follows that rate of climb (RoC) will be a maximum when P_s is a maximum

$$\frac{\partial P_s}{\partial V} = \frac{\partial}{\partial V}\left\{(T - D)\,V\right\} = 0 \tag{219}$$

The partial derivative condition arises because P_s maxima are sought discretely for given flight level. Eq. (219) can be expanded and expressed as a collection of partial derivative constituents of available and required power components, thus, the condition

$$\frac{\partial P_s}{\partial V} = \frac{\partial}{\partial V}(TV) - \frac{\partial}{\partial V}(D_o V) - \frac{\partial}{\partial V}(D_i V) - \frac{\partial}{\partial V}(D_{WL} V) - \frac{\partial}{\partial V}(D_c V) = 0 \tag{220}$$

The total drag, $D = D_o + D_i + D_{WL} + D_c$, is a summation of zero-lift, vortex-induced, winglet (where applicable) and compressibility (where applicable) contributions. The partial derivative of available power is given by the source expression that quantifies maximum climb, namely, Eq. (197)

$$\frac{\partial}{\partial V}(TV) = \left(\frac{1}{V} + \eta_\tau\left(\frac{V}{g}\right)\left[\frac{k_2 e^{-(k_1+k_2 h)T_o}}{1+e^{-(k_1+k_2 h)T_o}} + k_4\right] - k_5\left[1 + k_6\eta_\tau\frac{V^2}{g}\right]e^{-k_6 h}\right)TV \tag{221}$$

At this juncture of the derivation, an important issue must be addressed. The fundamental assumption of employing an energy-height premise invokes through the physical appreciation of ambient atmospheric properties, constituent differentials with respect to forward speed V. These contributions can be categorised as ancillary effects due to temperature, density, coefficient of viscosity, and, compressibility – which uniquely imparts a dual influence to skin friction as well as drag rise and divergence characteristics.

Substitution of the energy-height balance equation, or Eq. (215), into the temperature ratio expression given by Eq. (19), the derivative with respect to V becomes

$$\tilde{\theta} = \frac{d\theta}{dh}\frac{\partial h}{\partial V} = \eta_\tau\left(\frac{V}{g}\right)\left(\frac{1}{\kappa} - \Phi_{trop}\,k_1^\theta\right) \tag{222}$$

where $\tilde{\theta}$ represents the temperature effect and is congruous with the full temperature ratio differential. It may at first glance, seem not so glaringly obvious to how an atmospheric property like temperature ratio can possibly vary with forward speed. The key is to develop an appreciation of the fact pressure altitude is now considered to be a function of forward speed for a fixed energy-height premise. Since temperature ratio and forward speed optima vary for each successive flight level, it is therefore plausible to construct a differential relationship between θ and V. This result is considered to be quite important because it is this basic relationship that shall be used to derive effects imparted by the remaining atmospheric parameters.

The density differential is obtained using Eq. (21) and is applicable for any arbitrary temperature deviation from ISA. The form of the density equation appears well suited to logarithmic differentiation in keeping with method compatibility to the full drag power derivatives to follow.

$$\begin{aligned}\frac{\partial}{\partial V}\sigma = \frac{\partial}{\partial V}e^{\ln\sigma} &= \frac{\partial}{\partial V}\exp\left(\ln\theta_{ISA} + \ln\sigma_{ISA} - \ln\theta\right)\\ &= \left(\frac{1}{\theta_{ISA}}\frac{\partial\theta_{ISA}}{\partial V} + \frac{1}{\sigma_{ISA}}\frac{\partial\sigma_{ISA}}{\partial V} - \frac{1}{\theta}\frac{\partial\theta}{\partial V}\right)\sigma\end{aligned} \tag{223}$$

The above can be expanded to include all terms; hence the coefficient of density effect in subsequent factorised form can be derived to be

$$\tilde{\sigma} = \frac{1}{\sigma}\frac{d\sigma}{dh}\frac{\partial h}{\partial V} = \left(\frac{1}{\theta_{ISA}} + 4.2561\frac{\theta_{ISA}^{3.2561}}{\sigma_{ISA}} - \frac{1}{\theta}\right)\tilde{\theta} - \eta_\tau\left(\frac{V}{g}\right)\frac{\Phi_{trop}k_1^\sigma}{h\sigma_{ISA}} \tag{224}$$

One pre-supposes that $\tilde{\sigma}$ will influence predominately the dynamic pressure as well as to a lesser extent Reynolds number dependent constituent derivatives.

As exemplified by Sutherland's formula given by Eq. (22), the coefficient of viscosity is dependent upon temperature ratio. By utilising again logarithmic differentiation

$$\begin{aligned}\frac{\partial}{\partial V}\left(\frac{\mu}{\mu_{sls}}\right) &= \frac{\partial}{\partial V}\exp\left(\ln 1.383 + 3/2\ln\theta - \ln\left[\theta + 0.383\right]\right)\\ &= \left(\frac{3}{2\theta}\frac{\partial\theta}{\partial V} - \frac{1}{\theta + 0.383}\frac{\partial\theta}{\partial V}\right)\left(\frac{\mu}{\mu_{sls}}\right)\end{aligned} \tag{225}$$

and expanding upon this by introducing the temperature ratio differential yields the coefficient of viscosity effect $\tilde{\mu}$, which is projected to have an impact on the instantaneous Reynolds number.

$$\tilde{\mu} = \left(\frac{1}{\mu/\mu_{sls}}\right)\frac{d\left(\mu/\mu_{sls}\right)}{dh}\frac{\partial h}{\partial V} = \left(\frac{3}{2\theta} - \frac{1}{\theta + 0.383}\right)\tilde{\theta} \tag{226}$$

The temperature ratio requires further inspection since it is integral to definition of instantaneous Mach number. The expression M = V / a indicates temperature effect must

be considered since local sonic velocity is proportional to $\theta^{1/2}$. When the drag constituent equations are reviewed, it is evident that the speed parameter of Mach number plays a role when calculating compressibility for skin friction, as depicted in Eq. (143), and identification of instantaneous critical Mach number used for wave drag, given by Eq. (184). Initially, as a measure of the impact temperature effect has on Mach number in Eq. (143), a parameter proposed here as the skin friction compressibility effect is now introduced

$$\tilde{\vartheta} = \frac{\partial}{\partial V}\left(\frac{1}{\theta}\right) = \frac{\partial}{\partial V} e^{(\ln 1 - \ln \theta)} = -\frac{\tilde{\theta}}{\theta} \tag{227}$$

Note that $\tilde{\vartheta}$ is negative and the magnitude demonstrates proportionality with M^2. This condition arises because the local sonic velocity acts as a divisor for the calculation of Mach number squared within the compressibility sub-unit of Eq. (143).

The drag rise and divergence effect essentially describes to what extent temperature ratio influences the compressibility drag differential of Eq. (220). This parameter requires the simultaneous inspection of instantaneous Mach number and critical Mach number. From Eq. (184), the relation [M - M_{CR}] may be singled out and differentiated with respect to V. Upon substitution of the modified Korn's equation, or Eq. (183) for M_{CR}

$$M - M_{CR} = \frac{V}{a_{sls}\theta^{1/2}} + \left(\frac{1}{10}\right)\left(\frac{1}{\sigma^{3/2}}\right)\left(\frac{1}{V^3}\right)\left(\frac{2W}{\rho_{sls} S_W}\right)^{3/2}\left(\frac{1}{\cos^4 \Lambda_{Qchd}}\right) - \left\{\frac{1}{\cos\Lambda_{Qchd}}\left[M_{REF} - \frac{(t/c)_m}{\cos\Lambda_{Qchd}}\right]\right\} + \Delta M \tag{228}$$

Now, by introducing equivalent exponential expressions where appropriate and upon differentiation

$$\tilde{\varsigma} = \frac{\partial}{\partial V}\left[M - M_{CR}\right] = \frac{1}{a}\left(1 - \frac{\tilde{\theta}}{2\theta}\right) - \frac{0.3 C_L^{3/2}}{\cos^4 \Lambda_{Qchd}}\left(\frac{\tilde{\sigma}}{2} + \frac{1}{V}\right) \tag{229}$$

where $\tilde{\varsigma}$ is defined as the drag rise and divergence effect.

In this fashion, the atmospheric property effects of $\tilde{\theta}$, $\tilde{\sigma}$, $\tilde{\vartheta}$ and $\tilde{\varsigma}$ can be viewed as supplementary contributors to the identification of optimal climb trajectories.

Since an energy balance is now introduced to flight plan formulation, the zero-lift contribution can be alternatively expressed as

$$\frac{\partial}{\partial V}\left(D_o V\right) = \frac{\partial}{\partial V}\left\{\frac{\rho_{sls}}{2} S_{wet} A \left[\ln 10\right]^b \exp\left(\ln \sigma + 3\ln V - b \ln\left[\ln N_R\right] - d \ln\left[1 + cM^2\right]\right)\right\} \tag{230}$$

Closer examination of Eq. (230) reveals the Reynolds effect and compressibility components can be distinguished from one another.

Upon differentiation and grouping, these all combine to define the complete required power zero-lift partial differential component as

$$\frac{\partial}{\partial V}\left(D_o V\right)=\left(\tilde{\sigma}+\frac{3}{V}-\left[\tilde{\sigma}-\tilde{\mu}+\frac{1}{V}\right]\frac{b}{\ln N_R}-\left[\tilde{\vartheta}+\frac{2}{V}\right]\frac{cdM^2}{1+cM^2}\right)D_o V \tag{231}$$

Now, converting the vortex-induced drag power contribution using the energy-height assumption yields

$$\frac{\partial}{\partial V}\left(D_i V\right)=\frac{\partial}{\partial V}\left\{\frac{2W^2}{\rho_{sls}S_W}\left(\frac{dC_D}{dC_L^2}\right)\exp\left(-\ln\sigma-\ln V\right)\right\}=-\left[\tilde{\sigma}+\frac{1}{V}\right]D_i V \tag{232}$$

The incremental drag power differential due to presence of winglets is treated, with validity, approximately equivalent to an instantaneous parasitic drag contribution for sake of simplicity

$$\frac{\partial}{\partial V}\left(D_{WL} V\right)=\frac{\partial}{\partial V}\left(\frac{\rho_{sls}}{2}S_W C_{DWL}\exp\left[\ln\sigma+3\ln V\right]\right)=\left[\tilde{\sigma}+\frac{3}{V}\right]D_{WL} V \tag{233}$$

and the constituent partial differential accounting for drag rise and divergence effects where pertinent is

$$\begin{aligned}\frac{\partial}{\partial V}\left(D_c V\right)&=\frac{\partial}{\partial V}\left\{\frac{\rho_{sls}}{2}S_W\,\Phi_{M_{CR}}\,\Delta C_{DD}\,\exp\left(\ln\sigma+3\ln V+n\ln\left[1+\Phi_{M_{CR}}\left(\frac{M-M_{CR}}{\Delta M}-1\right)\right]\right)\right\}\\&=\left(\tilde{\sigma}+\frac{3}{V}+\tilde{\varsigma}\frac{\Phi_{M_{CR}}\,n}{\Delta M}\left[1+\Phi_{M_{CR}}\left(\frac{M-M_{CR}}{\Delta M}-1\right)\right]^{-1}\right)D_c V\end{aligned} \tag{234}$$

9.4.2 Further Refinements for Optimal Climb Speed Formulation

As a general note to round off climb control formulation, it should be highlighted that the energy equations give an opportunity to construct climb trajectories that minimise fuel. By defining fuel specific energy as change in energy-height per unit weight change in fuel, i.e. $f_s = dh_e / dW_f$, and after substituting this with $P_s = dh_e / dt$ together with the identity $W_f = c\,T$, a condition for minimum fuel consumption reads as

$$\Delta W_{f\,1\to2}=\int_{h_{e1}}^{h_{e2}}\frac{cT}{P_s}dh_e \tag{235}$$

Scope was given by the closed form equations previously presented to minimise the integral on the right and side of Eq. (235), however, investigations have shown for transport aircraft generally fuel optimal climb trajectories are not particularly distinct from the accelerated minimum time to climb profile. It was therefore decided that the increase in complexity in order to offer solutions for fuel optimal procedures were not justified.

9.4.3 Energy-Height Approximation for Accelerated Climbing Flight with One Engine Inoperative

Of interest for OEI flight is the level of required power generated by this condition and how it influences the total required power partial derivative for climb rate and climb gradients. It was shown previously the condition for accelerated climb optimal forward speed identification is given by maximising specific excess power. Recalling that RoC will be a maximum when P_s is a maximum, the condition given by Eq. (219) still must be satisfied, but in this instance, the available power must be adjusted due to the loss of an engine and the total drag requires revision to account for influences imparted by an OEI windmilling/auto-feathered (or locked rotor) engine in combination with yawing drag. The collective drag now becomes $D = D_o + D_i + D_{WL} + D_c + D_{OEI}$, and is a summation of zero-lift, vortex-induced, winglet (where applicable), compressibility (where applicable) and OEI incremental contributions respectively. Eq. (220) can be expanded and expressed as a collection of partial derivative constituents of available and required power components, thus, the condition for OEI climb speed optima identification becomes

$$\frac{\partial P_s}{\partial V} = \frac{\partial}{\partial V}(TV) - \frac{\partial}{\partial V}(D_o V) - \frac{\partial}{\partial V}(D_i V) - \frac{\partial}{\partial V}(D_{WL} V) - \frac{\partial}{\partial V}(D_c V) - \frac{\partial}{\partial V}(D_{OEI} V) = 0 \tag{236}$$

where the individual constituents are identical to those given earlier with the exception of

$$D_{OEI} = D_{wm} + \left[D_{wm} + T_{op} \right] \frac{y_{eng}}{l_{vt}} \tan\delta_R \tag{237}$$

which is a bi-product of Eq. (175) converted from its original non-dimensional form into one with a tangible physical significance and T_{op} signifies thrust produced by the remaining operational engine(s).

Now, by delineating the asymmetric OEI drag force component in Eq. (237) into separate windmilling and yaw effects, converting each constituent into a required power, and, finally differentiating with respect to V produces

$$\begin{aligned} \frac{\partial}{\partial V}(D_{OEI} V) &= \frac{\partial}{\partial V}(D_{wm} V) + \frac{y_{eng}}{l_{vt}} \frac{\partial}{\partial V} \left\{ \left(D_{wm} + T_{op} \right) V \tan\delta_R \right\} \\ &= \frac{\partial}{\partial V}(D_{wm} V) + \frac{y_{eng}}{l_{vt}} \left\{ \left[\frac{\partial}{\partial V} \left(D_{wm} V + T_{op} V \right) \right] \tan\delta_R + \frac{\partial \delta_R}{\partial V} \left(D_{wm} + T_{op} \right) V \sec^2 \delta_R \right\} \end{aligned} \tag{238}$$

The constituent partial differential due to windmilling engine is given by

$$\frac{\partial}{\partial V}(D_{wm} V) = \left[\tilde{\sigma} + \frac{3}{V} \right] q V S_{wet,nac} c_f^{wm} \tag{239}$$

and the estimated contribution of incremental drag power due to the asymmetric thrust ($D_{yaw} V$) condition is

$$\frac{\partial}{\partial V}\left(D_{wm}V + T_{op}V\right) = \left[\tilde{\sigma} + \frac{3}{V}\right] qV\, S_{wet,nac}\, c_f^{wm} + \left(\frac{1}{V} + \eta_\tau\left(\frac{V}{g}\right)\left[\frac{k_2 e^{-(k_1+k_2 h)T_o}}{1+e^{-(k_1+k_2 h)T_o}} + k_4\right] - k_5\left[1 + k_6\eta_\tau\frac{V^2}{g}\right]e^{-k_6 h}\right) T_{op} V \tag{240}$$

Ancillary consideration must be given to the effect of rudder deflection with respect to forward speed. This is a dynamic consequence that ensures the vehicle minimises sideslip (goal of maintaining a straight path with zero yaw) during the asymmetric thrust condition, thus rudder deflection which counterbalances the yawing effect is represented by

$$\frac{\partial \delta_R}{\partial V} = -\frac{y_{eng}\left(\frac{2}{V} + \tilde{\sigma} - \eta_\tau\left(\frac{V}{g}\right)\left[\frac{k_2 e^{-(k_1+k_2 h)T_o}}{1+e^{-(k_1+k_2 h)T_o}} + k_4\right] + k_5\left[1 + k_6\eta_\tau\frac{V^2}{g}\right]e^{-k_6 h}\right) T_{op}}{qS_{vt}C_{l\alpha,vt}\left(\frac{AR_{vt}}{2+\sqrt{4+AR_{vt}^2}}\right)\tau\,\eta\, l_{vt}\cos\Lambda_{vt,Qchd}} \tag{241}$$

It is evident the rudder deflection differential for OEI flight is negative in sense and will decrease in magnitude with increasing forward speed. This can be qualitatively justified by interpretation of the relationship between forward speed, the available power from the engine(s) and lift generated by the rudder. With increasing speed at fixed flight level, instantaneous available power will tend to decrease, whilst increasing dynamic pressure will promote a larger magnitude of lift force for given rudder deflection, thus collectively, the condition for equilibrium will require less rudder deflection.

9.5 Discussion and Synopsis of Climb Optima Differential Derivatives

Based on the presented derivation of available and required power differentials, it can be discerned influences on excess power from thrust lapse due to airspeed, and, the zero-lift constituent with respect to Reynolds number are two principal contributors. Furthermore, the height-energy assumption for specific excess power shows additional influences due to ambient conditions and thrust lapse due to flight level have a significant effect on the ability of the vehicle to conduct climbing flight in an optimal sense. These results reinforce the philosophy that more refined thrust and drag modelling techniques are required for an adequate en route performance prediction regardless of the fact an overall initial assumption of conceptual first order minimalism has been introduced. Table 4 presents a synopsis of the derived theoretical results covered by Eq. (220) through Eq. (241). Each constituent partial differential is exhibited in coefficient form (k_X) since the available and required power derivatives are universally of the form $\partial / \partial V$ (FV) = k_X FV.

9.6 Optimal Cruise Control Identification

Optimal cruise performance has received considerable attention from theoretical and numerical analysts. The intention is to derive a rather comprehensive conceptual optimal cruise (maximum range) condition for constant altitude flight. The added requirement is to produce a theoretical expression consistent with conclusions drawn by authors like

	Accelerated Climb *(Energy-Height with Manoeuvre Efficiency Premise)*
Thrust Power Coefficient $k_T = \frac{1}{TV}\frac{\partial(TV)}{\partial V}$	$\frac{1}{V} + \eta_\tau\left(\frac{V}{g}\right)\left[\frac{k_2 e^{-(k_1+k_2 h)T_o}}{1+e^{-(k_1+k_2 h)T_o}} + k_4\right] - k_5\left[1 + k_6\eta_\tau\frac{V^2}{g}\right]e^{-k_6 h}$
Zero-Lift Drag Power Coefficient $k_{D_o} = \frac{1}{D_o V}\frac{\partial(D_o V)}{\partial V}$	$\tilde{\sigma} + \frac{3}{V} - \left[\tilde{\sigma} - \tilde{\mu} + \frac{1}{V}\right]\frac{b}{\ln N_R} - \left[\tilde{\vartheta} + \frac{2}{V}\right]\frac{cdM^2}{1+cM^2}$
Vortex-Induced Drag Power Coefficient $k_{D_i} = \frac{1}{D_i V}\frac{\partial(D_i V)}{\partial V}$	$-\left[\tilde{\sigma} + \frac{1}{V}\right]$
Winglet Drag Power Coefficient $k_{D_{WL}} = \frac{1}{D_{WL} V}\frac{\partial(D_{WL} V)}{\partial V}$	$\left[\tilde{\sigma} + \frac{3}{V}\right]$
Compressibility Drag Power Coefficient $k_{D_c} = \frac{1}{D_c V}\frac{\partial(D_c V)}{\partial V}$	$\tilde{\sigma} + \frac{3}{V} + \tilde{\zeta}\frac{\Phi_{M_{CR}} n}{\Delta M}\left[1 + \Phi_{M_{CR}}\left(\frac{M - M_{CR}}{\Delta M} - 1\right)\right]^{-1}$
OEI Windmill Drag Power Coefficient $k_{D_{wm}} = \frac{1}{D_{wm} V}\frac{\partial(D_{wm} V)}{\partial V}$	$\left[\tilde{\sigma} + \frac{3}{V}\right]$
OEI Yaw Drag Power Coefficient $k_{D_{yaw}} = \frac{1}{D_{yaw} V}\frac{\partial(D_{yaw} V)}{\partial V}$	$k_{D_{wm}}\left(\frac{D_{wm}}{D_{wm} + T_{op}}\right) + k_T\left(\frac{T_{op}}{D_{wm} + T_{op}}\right)$
OEI Yaw Drag Power Derivative $\frac{\partial \delta_R}{\partial V}$	$-\frac{y_{eng}\left(\tilde{\sigma} + \frac{3}{V} - k_T\right)T_{op}}{qS_{vt}C_{L\alpha,vt}\tau\eta l_{vt}\cos\Lambda_{vt,Qchd}}$

Table 4. Synopsis of performance partial derivative coefficients for climbing flight.

Torenbeek[136] and Page[140], in particular, with regards to occasions where the optimum cruise Mach number may reside in the drag rise.

The Breguet equation for cruise range (R) in integral form[35] is

$$R = \int_{W_i}^{W_f} \frac{V}{cD} dW \tag{242}$$

where W_i is the initial cruise weight, W_f is the final cruise weight. By applying logarithmic differentiation of the Breguet equation with respect to speed at given flight level, h, as proposed by Miller[141], the condition for optimal cruise reads

$$\frac{1}{V} - \frac{1}{c}\left(\frac{\partial c}{\partial V}\right)_h - \frac{1}{D}\left(\frac{\partial D}{\partial V}\right)_h = 0 \tag{243}$$

Miller originally assumed that specific fuel consumption c to be a minimum and a function of Mach number and flight level. However, this critical assumption indicates specific fuel consumption is independent of throttle setting. Since the thrust specific fuel consumption model structure presented in Eq. (199) facilitates such a dependency on throttle setting, Miller's original derivation can be expanded to account for the derivative of c with respect to V as well as accounting for contributions due to throttle (T/T_o)

$$\left(\frac{\partial c}{\partial V}\right)_h = \left(\frac{\partial c}{\partial M}\right)_h \left(\frac{\partial M}{\partial V}\right)_h + \left(\frac{\partial c}{\partial \left[T/T_o\right]}\right)_h \left(\frac{\partial \left[T/T_o\right]}{\partial V}\right)_h \tag{244}$$

The derivative of throttle setting can be determined a priori and incorporated in the following manner

$$\left(\frac{\partial \left[T/T_o\right]}{\partial V}\right)_h \equiv \left(\frac{\partial \left[D/T_o\right]}{\partial V}\right)_h \equiv \frac{1}{T_o}\left(\frac{\partial D}{\partial V}\right)_h \tag{245}$$

Hence through algebraic manipulation, the generalised condition for maximum specific air range speed (V_{MRC}) at flight level h was found to be

$$V_{MRC} = \frac{1}{\frac{1}{c}\left(\frac{\partial c}{\partial M}\right)_h \left(\frac{\partial M}{\partial V}\right)_h + \left[\frac{1}{cT_o}\left(\frac{\partial c}{\partial \left[T/T_o\right]}\right)_h + \frac{1}{D}\right]\left(\frac{\partial D}{\partial V}\right)_h} \tag{246}$$

where

$$\left(\frac{\partial c}{\partial M}\right)_h = \left(\frac{11.53 - BPR_{rev}}{11.53 - BPR_{orig}}\right) k_\theta \, k_1 h^{-k2} \left(\frac{T}{T_o}\right)^{(k_3 h + k_4)} \tag{247}$$

$$\left(\frac{\partial M}{\partial V}\right)_h = \frac{1}{a} \tag{248}$$

$$\left(\frac{\partial c}{\partial\left[T/T_o\right]}\right)_h = \left(\frac{11.53 - BPR_{rev}}{11.53 - BPR_{orig}}\right) k_\theta \left\{ k_1 h^{-k2}\left(k_3 h + k_4\right)\left(\frac{T}{T_o}\right)^{(k_3 h + k_4 - 1)} M + \left(k_5 h + k_6\right)\right\} \tag{249}$$

and the constants of proportionality k_n are related to regression coefficients for the TSFC model given earlier in Eq. (199). The total drag and derivative with respect to speed V is

$$D = D_o + D_i + D_{WL} + D_c \tag{250}$$

and

$$\frac{\partial D}{\partial V} = \frac{\partial D_o}{\partial V} + \frac{\partial D_i}{\partial V} + \frac{\partial D_{WL}}{\partial V} + \frac{\partial D_c}{\partial V} \tag{251}$$

respectively with constituents defined by zero-lift, vortex-induced, winglet and wave or compressibility drag with corresponding derivatives given by

$$D_o = \frac{A\left[\ln 10\right]^b}{\left[\ln N_R\right]^b\left[1 + cM^2\right]^d} q S_{wet} \tag{252}$$

$$\frac{\partial D_o}{\partial V} = \left(\frac{2}{V} - \frac{1}{V}\frac{b}{\ln N_R} - \frac{2}{V}\frac{cdM^2}{1 + cM^2}\right) D_o \tag{253}$$

$$D_i = \frac{W^2}{qS_W}\left(\frac{dC_D}{dC_L^2}\right) \tag{254}$$

$$\frac{\partial D_i}{\partial V} = -\frac{2}{V} D_i \tag{255}$$

$$D_{WL} = q S_w C_{D\,WL} \tag{256}$$

$$\frac{\partial D_{WL}}{\partial V} = 2\frac{D_{WL}}{V} \tag{257}$$

$$D_c = q S_W \Phi_{M_{CR}} \Delta C_{DD}\left[1 + \Phi_{M_{CR}}\left(\frac{M - M_{CR}}{\Delta M} - 1\right)\right]^n \tag{258}$$

$$\frac{\partial D_c}{\partial V} = \left(\frac{2}{V} + \frac{\Phi_{M_{CR}}\, n}{\Delta M}\left(\frac{1}{a} - \frac{0.3C_L^{3/2}}{V\cos^4\Lambda_{Qchd}}\right)\left[1 + \Phi_{M_{CR}}\left(\frac{M - M_{CR}}{\Delta M} - 1\right)\right]^{-1}\right) D_c \tag{259}$$

respectively, and, the local sonic velocity as well as dynamic pressure given by $a = a_{sls}\,\theta^{1/2}$ and $q = 1/2\,\rho\,V^2$.

The presented solution is applicable only for instances where the maximum range cruise speed is identified and analysed for payload-range calculations. It is suggested V_{MRC} be used as a conceptual substitute of LRC which should be determined later as the design progresses into maturity. This is a reasonable supposition since there are occasions where operators would prefer to fly at a vehicle's maximum range cruise where useful load limitations make faster speed schedules prohibitive, and additionally, the designer may gain some insight into the maximum range capabilities of a final vehicle candidate. Nonetheless, if this arbitrary speed schedule is desired, traditionally, LRC has been understood to be 99% (sometimes even 98%) of MRC SAR towards the faster end of the curve[3,38,136,141]. This practise is employed to trade increased speed capability for what is considered to be a relatively small penalty in fuel consumption rate.

9.7 An Iterative Scheme to Solve for Operational Performance

In formulating the predicted optimal field and en route performance control, it is quite evident that in order to achieve a suitable level of accuracy with an emphasis placed on decreasing complexity, operational performance cannot be evaluated solely using the closed form solution process. The transcendental algorithms presented for minimum control speed, optimal climb control, optimal cruise control, and, identification of holding speed schedule and maximum cruise speed typify this conclusion. The task here is to create an iterative formula or scheme that can be universally applied to any operational performance problem. Also, the process should characteristically be robust enough to avoid divergence and can circumvent entering an endless loop whereby the process neither convergences or diverges.

A large class of iterative methods for the solution of $f(x) = 0$ is based upon rewriting into an equivalent form $x = F(x)$. Providing an initial estimate x_o solution has been found, a sequence of values (x_n) in principle could be computed from this relationship, thereby converging to a final solution. This basic scheme is known as simple iteration. For example, when Eq. (220) is applied to All-Engines Operational (AEO) climb and rearranged so that an initial estimate V_o of the climbing airspeed solution has been found, then a sequence of values (V_n) in turn could be computed which theoretically would allow convergence to V_c, such that

$$V_c = V_n \left\{ \frac{\left.\frac{\partial}{\partial V}(TV)\right|_{V_n} - \left.\frac{\partial}{\partial V}(D_i V)\right|_{V_n} - \left.\frac{\partial}{\partial V}(D_\phi V)\right|_{V_n} - \left.\frac{\partial}{\partial V}(D_c V)\right|_{V_n}}{\left.\frac{\partial}{\partial V}(D_o V)\right|_{V_n}} \right\} \tag{260}$$

Eq. (260) appears to be a basic scheme requiring only simple iteration for convergence. In reality, Eq. (260) initially diverges from the solution at an accelerated rate, comes to a certain point, and then continues endlessly neither converging nor diverging in the process. In practise, if one were to adopt this approach for all of the presented transcendental equations that solve for speeds or define optimal speeds with respect to field minimum control, climb-out and cruise, reliable behaviour that is indicative of simple iteration convergence simply does not occur. This is a common characteristic of the

transcendental equations presented in this study because they are algorithms dominated by fundamental instabilities due to the interaction of instantaneous available power (or thrust) and required power (or drag) differentials with respect to forward speed. For instance, at given flight level, a faster forward speed guess would reduce the available power differential and simultaneously increase the required power differential thus leading to a resulting slower speed estimate assuming the sum of both differentials is greater than zero. Conversely, slower speed guesses result in higher forward speed estimates due to a considerable difference in available and required power differentials. Figure 41 gives a typical illustration of the progression between estimate and end result: an input guess (V_o) results in an estimate (marked by lines A and B) which diverges considerably from the actual solution regardless of the initial speed estimate being slow or fast.

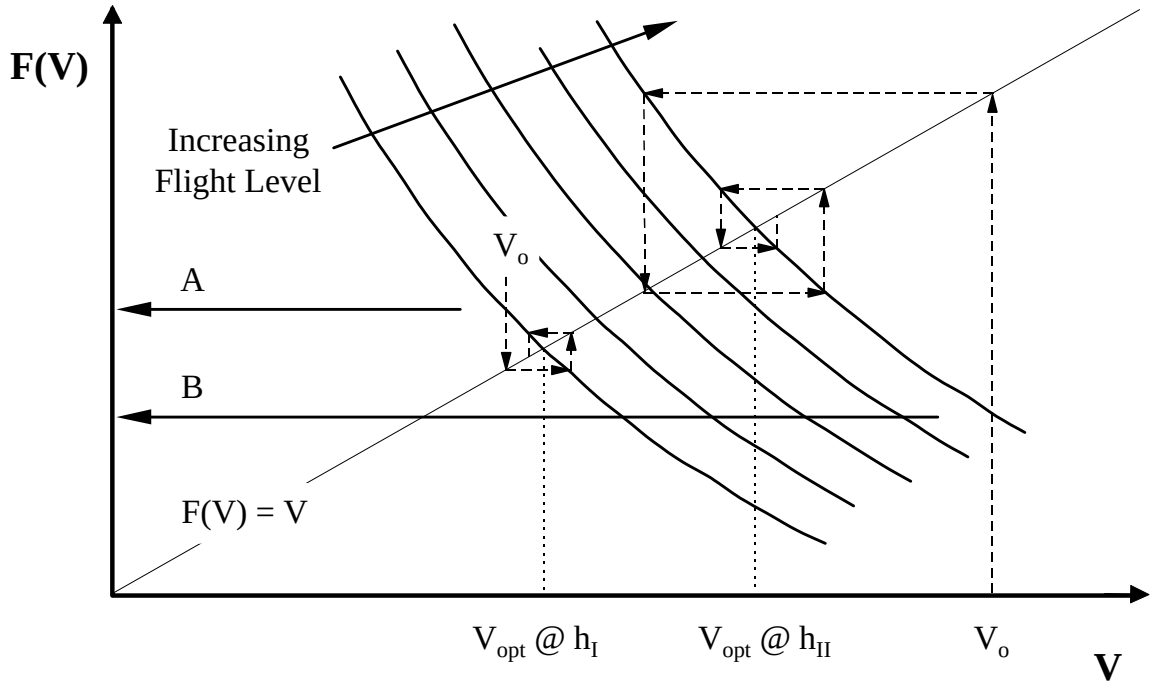

Figure 41. Available power (or thrust) and required power (or drag) interaction showing potential for infinite looping together with a suggested procedure for speed optima convergence.

The apparent failure of simple iteration premise does not signify a solution using this philosophy is always inappropriate. It was identified that convergence may be guaranteed if successive iterations are conducted with the method of interval halving between both initial and designated intermediary estimates. If an initial guess V_o and first simple iteration estimate produces $F(V_o) = V_i$, a new estimate for optimal climb speed, namely V_{i+1}, can be produced from interval halving between these bounded values.

$$V_{i+1} = \frac{1}{2}\left(V_o + V_i\right) \tag{261}$$

Proceeding to another estimate requires interval halving to be performed between a now fixed V_o and recently derived V_{i+1}

$$V_{i+2} = \frac{1}{2}\left(V_o + V_{i+1}\right) = \frac{1}{2}\left(V_o + \frac{V_o}{2} + \frac{V_i}{2}\right) = \frac{1}{4}\left(3V_o + V_i\right) \tag{262}$$

thus continuing until a sufficiently low number of iterations will allow convergence to the required tolerance. Since it is evident that this iterative technique requires the input of an initial guess, now generically assumed to be V_n, and first iterated estimate V_{n+1}, a general scheme can be constructed for V_{n+2} as follows

$$F(V) = V_{n+2} = \frac{1}{2^m}\left[\left(2^m - 1\right)V_n + V_{n+1}\right] \tag{263}$$

where $m \geq 1$ denotes the number of interval halving steps (with the V_n boundary always fixed) to be conducted for the (n+2)th result. Fortunately, this information can be simply expressed in terms of an initial estimate in conjunction with the equation to be solved. Since $V_{n+1} = F(V_n)$, and V_{n+1} is normally given by a transcendental expression of the form presented in Eq. (220), the interval halving method discussed above can be utilised to create an iterative scheme which actually converges and advantageously displays accelerated characteristics for a specific set of convergence augmenters. If the numerator excluding the estimate of this equation is assumed to be represented by Ω and the denominator is $\tilde{A}$, a more manageable succinct form of Eq. (263), i.e. $V_{n+1} = V_n\ (\Omega/\tilde{A})$ can be produced. Upon substitution of this association combined with some algebraic manipulation

$$F(V) = V_n\left\{\frac{\left(2^{2m} - 2^m\right)\tilde{A} + 2^m\Omega}{2^{2m}\tilde{A}}\right\} \equiv V_n\left\{\frac{\Omega + \left(2^m - 1\right)\tilde{A}}{2^m\tilde{A}}\right\} \tag{264}$$

By letting a residual function be defined as $\Pi = \Omega - \tilde{A}$, and, introduction of convergence augmenters designated $j^* = 2^m$, $j = 2^m$ and $\tilde{A}$, an iterative scheme to solve for optimal speed would look something like

$$F(V) = V_n\left\{\frac{\Pi + j^*\tilde{A}}{j\tilde{A}}\right\} \tag{265}$$

If the condition for optimality is given by an order one and degree one partial differential or any transcendental equation, i.e. $F(x) = f(x) + g(x) + h(x) + i(x)$, the convergence augmenter $\tilde{A}$ is assigned to be a constituent function, say g(x), which yields a relatively large result in magnitude compared to other contributors in the residual function. The operator $\Pi = F(x)$ in this instance being the optimising function for each successive iteration. Experimentation is required to find values for j* and j which exhibit the best trade-off between speed and propensity for convergence: as a general rule, when $j^* = j = 8$ (or $m = 3$) solutions should be obtained at the quickest rate.

In order to elucidate how the given iterative scheme works, consider formulation of an AEO optimal climb speed algorithm from the basic criterion presented in Eq. (220). Since the equation is a partial differential equation of order and degree one, the residual function

is equivalent to the optimising function, or, $\Pi = \partial P_s / \partial V$. The convergence augmenter $\tilde{A} = \partial(D_o V) / \partial V$ is identified since the zero-lift drag power differential generates values greatest in magnitude compared to other drag constituents. If three interval halving steps are assumed, i.e. m = 3, for the final iterative scheme, therefore, values of the ancillary convergence augmenters result in j* = 8 and j = 8. Upon substitution of these relations into Eq. (265), a modified form of the original transcendental expression would look like

$$V_c = V_n \left\{ \frac{\dfrac{\partial}{\partial V}(TV)\Big|_{V_n} + 7\dfrac{\partial}{\partial V}(D_o V)\Big|_{V_n} - \left[\dfrac{\partial}{\partial V}(D_i V)\Big|_{V_n} + \dfrac{\partial}{\partial V}(D_{WL} V)\Big|_{V_n} + \dfrac{\partial}{\partial V}(D_c V)\Big|_{V_n} \right]}{8\dfrac{\partial}{\partial V}(D_o V)\Big|_{V_n}} \right\} \tag{266}$$

requiring simple iteration for each successive value.

As another example, for identification of maximum range cruise Eq. (243) must be satisfied. Upon examination of the condition for optimality, one can conclude that this is a partial differential equation of order and degree one, and assuming that three interval halving steps ensure accelerated convergence, initially the convergence augmenters j* = 8 and j = 8 are defined. Further inspection of Eq. (243) shows the drag differential is greatest in magnitude compared to the TSFC derivative. In view of this, the convergence augmenter and associative residual functions are designated as

$$\tilde{A} = \frac{1}{D}\left(\frac{\partial D}{\partial V}\right)_h\Big|_{V_n} \tag{267}$$

and

$$\Pi = \frac{1}{V_n} - \frac{1}{c}\left(\frac{\partial c}{\partial V}\right)_h\Big|_{V_n} - \frac{1}{D}\left(\frac{\partial D}{\partial V}\right)_h\Big|_{V_n} \tag{268}$$

respectively. Upon substitution of all these variables into the generic iterative scheme given by Eq. (265), the final algorithm that solves for maximum range cruise speed becomes

$$V_{MRC} = V_n \left\{ \frac{\dfrac{1}{V_n} - \dfrac{1}{c}\left(\dfrac{\partial c}{\partial V}\right)_h\Big|_{V_n} + 7\left(\dfrac{1}{D}\right)\left(\dfrac{\partial D}{\partial V}\right)_h\Big|_{V_n}}{8\left(\dfrac{1}{D}\right)\left(\dfrac{\partial D}{\partial V}\right)_h\Big|_{V_n}} \right\} \tag{269}$$

for given AUW and flight level.

The identification of minimum drag speed used typically for holding fuel reserve calculations at given flight level and time duration can be accomplished by assuming $\Pi =$

dD / dV, where, $D = D_o + D_i + D_\phi + D_c$ from Eq. (250), and the convergence augmenter is chosen as $\tilde{A} = dD_o / dV$. Similar in scope to an optimal climb speed solution, but without consideration of an instantaneous available power derivative, the iterative scheme can be expressed as

$$V_{MD} = V_n \left\{ \frac{7\left.\frac{dD_o}{dV}\right|_{V_n} - \left[\left.\frac{dD_i}{dV}\right|_{V_n} + \left.\frac{dD_{WL}}{dV}\right|_{V_n} + \left.\frac{dD_c}{dV}\right|_{V_n}\right]}{8\left.\frac{dD_o}{dV}\right|_{V_n}} \right\} \tag{270}$$

Maximum cruise speed at given flight level and AUW is simply a transcendental equation assuming equilibrium of forces in horizontal flight, i.e. $T = D_o + D_i + D_\phi + D_c$.

$$V_{MCRZ} = V_n \left\{ \frac{T|_{V_n} + 7\,D_o|_{V_n} - D_i|_{V_n} - D_{WL}|_{V_n} - D_c|_{V_n}}{8\,D_o|_{V_n}} \right\} \tag{271}$$

For transcendental functions in quotient form or F(x) = f(x) / g(x), a variation of the basic iterative scheme constituents definition is required. Eq. (265) assures convergence, however, the rate of convergence deteriorates with increasing number of intermediary estimates produced by interval halving used for the next guess. Studies have shown that one interval halving step or m = 1 gives the best convergence rate. Hence, upon inspection of Eq. (264), in contrast to the linear optimising function approach, the convergence augmenters become simply equivalent to j* = 1 and j = 2 with the denominator g(x) designated as a convergence augmenter, $\tilde{A}$, and residual function defined as $\Pi = f(x)$.

To create an algorithm for the solution of minimum control speed for field performance calculations, the basic transcendental equation for minimum control speed is given by Eq. (208). Since the function is of the form F(x) = f(x) / g(x), hence,

$$\tilde{A} = g(x) = q_n\, S_{vt}\, C_{La}\, \tau\, \eta\, l_{vt}\, \delta_{Rmax} \tag{272}$$

and

$$\Pi = y_{eng}\left[D_{wm} + T_{op}\right]\Big|_{V_n} \tag{273}$$

Furthermore, the ancillary convergence augmenters are identified as j* = 1 and j = 2 because Eq. (208) is in quotient form. Upon substitution of all these variables into the generic iterative scheme given by Eq. (264), the final algorithm that solves for minimum control speed becomes

$$V_{MC} = V_n \left\{ \frac{y_{eng}\left[D_{wm} + T_{op}\right]\Big|_{V_n} + q_n S_{vt} C_{L\alpha}\, \tau\, \eta\, l_{vt}\, \delta_{R\,max}}{2 q_n S_{vt} C_{L\alpha}\, \tau\, \eta\, l_{vt}\, \delta_{R\,max}} \right\} \tag{274}$$

The number of iterations required for identifying field minimum control speed, optimal climb speed, optimal cruise speed control, minimum drag speed and maximum cruise speed solutions was found to be typically around 5-10 steps assuming an error tolerance of less than 1 knot (0.5 m/s). The outstanding advantage of the above iterative scheme is that it is guaranteed to work in all cases, but it does not necessarily mean that convergence is resilient to inappropriate first guesses. Investigations have shown the initial estimate must fall within a forward speed interval that does not yield solutions where the difference between instantaneous available power (or thrust) and the modified required power (or drag) differential is less than zero. A suggested first guess of 120 m/s regardless of vehicle size, flight level and ambient conditions will ensure convergence in almost all instances.

intentionally blank

10 En route Operational Performance Control and Flight Profile Optimisation

Now that the theoretical foundations for definition of optimal en route performance control have been presented, the next step involves analysis of a three-phase flight in which interactions between climb, steady cruise and descent are considered to allow for inspection of objective function sensitivities against the collective influence imposed by a general set of design variables.

10.1 Operational Climb Control

In order to generate operationally permissible climb control speed techniques, a fundamental requirement is to generate the optimal climb trajectory speeds locus. Although the main goal is to create a climb control speed technique analogous to the optimal trajectory climb, there are instances where additional climb modes will need to be generated in order to cater for objectives other than minimum time and minimum fuel expended to climb to given altitude. This section presents a computationally inexpensive method and corresponding model to assist in identifying the optimal climb trajectory speed locus and describe it using a closed form expression. This basic knowledge is then extended by suggestion of some important and philosophically distinct objectives for climb control, and discusses procedures in how operational permissible climb control speed techniques can be defined.

10.1.1 Approximating the Optimal Climb Trajectory Speeds Locus

If speed profile is plotted as an optimal climb trajectory is generated, the resultant locus shows strong hyperbolic tendencies with flight level. This circumstance requires an integral approach or its common approximate numerical alternative for a range of discrete flight level intervals. Conversely, if flight level can be regarded as a free variable against optimal forward speed, it is evident that this transformation promotes an approximate exponential progression to mimic the profile. This notion is illustrated in Figure 42. Consequently, if two reference flight levels can be selected which minimise the error incurred when weight loss due to fuel burn is neglected, i.e. rate change of speed with respect to flight level does not vary greatly between each reference flight level, an adequate approximation for the locus of forward speed for an optimal climb trajectory covering the entire flight level envelope can be constructed.

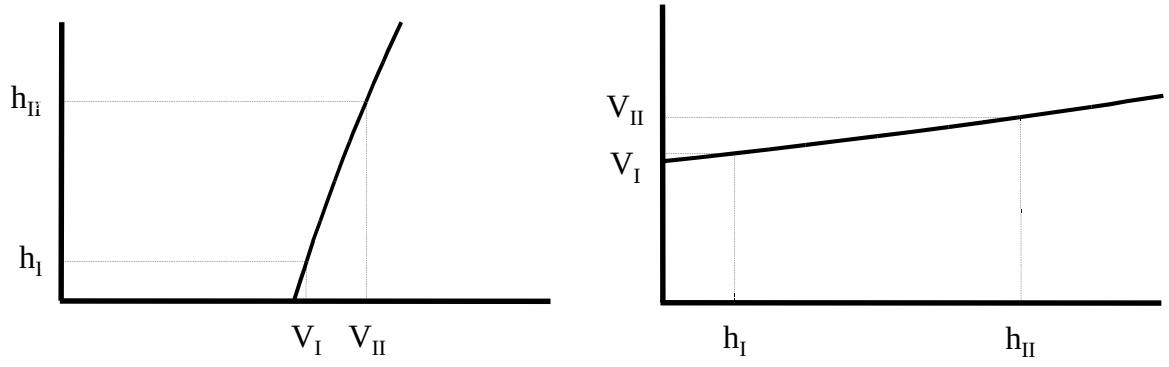

Figure 42. Demonstration of how the traditional optimal climb trajectory plot may be transformed (flight below the tropopause).

This curve geometry in the transformed trajectory is suited to an expression of the form

$$V = k_1 e^{k_2 h} \tag{275}$$

Assuming two points, i.e. speed at given energy–heights for example equal to 2500 m (8200 ft) and 7500 m (24600 ft) for AEO climb, are calculated using Eq. (220) and Eq. (266), it is then possible to construct a simple system of equations

$$V_I = k_1 e^{k_2 h_I} \qquad\qquad V_{II} = k_1 e^{k_2 h_{II}} \tag{276a \& b}$$

Now by rearranging Eq. (276a) to make k_1 the subject, and substituting this into Eq. (276b), the coefficient of proportionality k_2 is given by

$$k_2 = \frac{\ln\left(\frac{V_{II}}{V_I}\right)}{h_{II} - h_I} \tag{277}$$

Introducing this expression into Eq. (276a) leads to

$$k_1 = V_I \left(\frac{V_{II}}{V_I}\right)^{-\left(\frac{h_I}{h_{II}-h_I}\right)} \tag{278}$$

The identity $a^x = e^{x\ \ln a}$ can then be utilised in order to derive the instantaneous approximate optimal airspeed for climb with respect to flight level

$$V_h = V_I \left(\frac{V_{II}}{V_I}\right)^{\left(\frac{h-h_I}{h_{II}-h_I}\right)} \tag{279}$$

It is highlighted that optimal climb speed locus construction using Eq. (279) is only permissible for flight levels up to the tropopause. Owing to the temperature ratio being constant above this altitude threshold, a requirement arises where climb speed optima identification for higher flight levels using Eq. (220) and the corresponding iterative scheme given by Eq. (266) must be employed. Otherwise, a good approximation can be produced if one of the reference climb speed optima are estimated at or near the tropopause (V_{III}) and ensuing flight levels above this height are assumed to have constant climb speed optima thereafter.

$$V_h = \left(1 - \Phi_{trop}\right) V_I \left(\frac{V_{II}}{V_I}\right)^{\left(\frac{h-h_I}{h_{II}-h_I}\right)} + \Phi_{trop}\, V_{III} \tag{280}$$

If one elects to account for a decrease in instantaneous AUW due to fuel expended during the climb profile, a suggested procedure is to make an initial run-through set of calculations, then construct a fuel burn continuous function proportional to flight level.

This can be achieved by using the impulse function utility where the formulation of closed form expressions can be accomplished to describe integrated solutions as detailed by Eq. (14) and Eq. (15). The generated model can then be introduced into the final optima identification process as an approximation of fuel expended effects on optimal climb speed identification.

10.1.2 Formulating Coherent Climb Control Techniques

Operational conventions dictate a definition of initial cruise altitude or service ceiling that gives reasonable measure of maximum operating height potential for an aircraft whilst simultaneously fulfilling legitimate considerations of attaining this height in reasonable time. A well tempered conceptual climb control formulation for any prospective aircraft should therefore weigh the attributes of maximum rate of climb and minimum time to climb optimal trajectories and create a final approximate trajectory which would be used for the definition of a maximum service ceiling or flight envelope upper threshold.

It is common practise to assign at least two distinct climb modes, or more specifically, two different speed schedules for climb control each comprising of a fixed CAS and Mach speeds. The advantages with faster speed schedules are that they create possibilities in conducting further time, cost or profit function optimisation. More importantly opportunities in constraining previously unconstrained optima compared to single speed schedules because faster climb speed schedules (designated here as CLB Mode H) encourage “cruise soaking” or the exchange of cruise distance for climb which leads to significant block time reductions - this especially being the case for regional type sector missions. Furthermore, a slower climb speed schedule (CLB Mode L) enables closer adherence to fuel optimal procedures during climb thereby enhancing range capability. In this way, CLB Mode L and CLB Mode H speed schedule definitions are formulated with respect to optimal climb trajectory profile state and time function adherence and designated divergence criteria respectively.

Experimentation has produced a simple yet relatively robust procedure in defining a fixed CAS/Mach speed schedule that approximates the optimal climb trajectory for minimum time to altitude. Once the optimal trajectory speed schedule has been constructed, initially, the fixed CAS can be established by finding the equivalent calibrated airspeed at FL 200 and rounding down the result to the nearest 5 KCAS. The fixed Mach is subsequently identified by computing an equivalent Mach speed from the optimal climb trajectory trace at the target initial cruise altitude and rounded down to the nearest M0.01. Some care should be observed for fixed CAS schedules that could possibly produce a minimum RoC violation at an altitude well below the target initial cruise altitude. Such circumstances arise when the specific excess power degrades rapidly with increasing true airspeed and generally coincide with an altitude where the fixed CAS and Mach crossover occurs.

10.1.3 Merits of Faster Climb Control Techniques - Cruise Soaking

As demonstrated by the author[143,144], sector distance is a parameter in the transformed minimum DOC or maximum P-ROI function where optimal flight techniques depend on identification of a predetermined Mach/CAS schedule for climb and descent with corresponding optimal cruise determined from either maximum SAR or MCRZ speed at given flight level. For cruise fractions[†††] less than around 0.80 (or equivalently ≤ 1000 nm), the author has shown cost and profit optimal flight techniques generally tend towards the

[†††] Cruise fraction is defined as the distance traversed during cruise divided by the total sector distance.

threshold of minimum time (maximum block speed) schedules because the sensitivity of time related costs is proportionately higher than the fuel expended. In view of this, any enhancements to the technique that further reduce the block time for transport aircraft completing such sector missions would be advantageous and it appears there is scope afforded by manipulating climb mode definitions for prospective aircraft design candidates.

Figure 43 shows a typical collection of flight paths parameterised by a fixed stage length. Trajectory A illustrates a minimum fuel flight plan assuming CLB Mode L or pre-determined fixed climb speed schedule emulating an optimal climb trajectory proceeded by a maximum SAR cruise at LRC. Implementation of a slightly faster climb schedule say an intermediate climb or CLB Mode I and complemented by the goal of achieving a minimum time technique (Trajectory B) forces the flight level down since the cruise fraction has been exchanged or "soaked" by increased climb distance at given flight level. Similarly, a further increase in CAS/Mach (Trajectory C) or CLB Mode H will magnify cruise soak rate and may in many instances be complemented by a simultaneous reduction in climb time (hence block time) due to further reductions in flight level. In this way, an exchange between the cruise and climb fractions, or alternatively, the rationalisation of the cruise segment, may permit a block time reduction via the implementation of faster CAS/Mach speed schedule for climb.

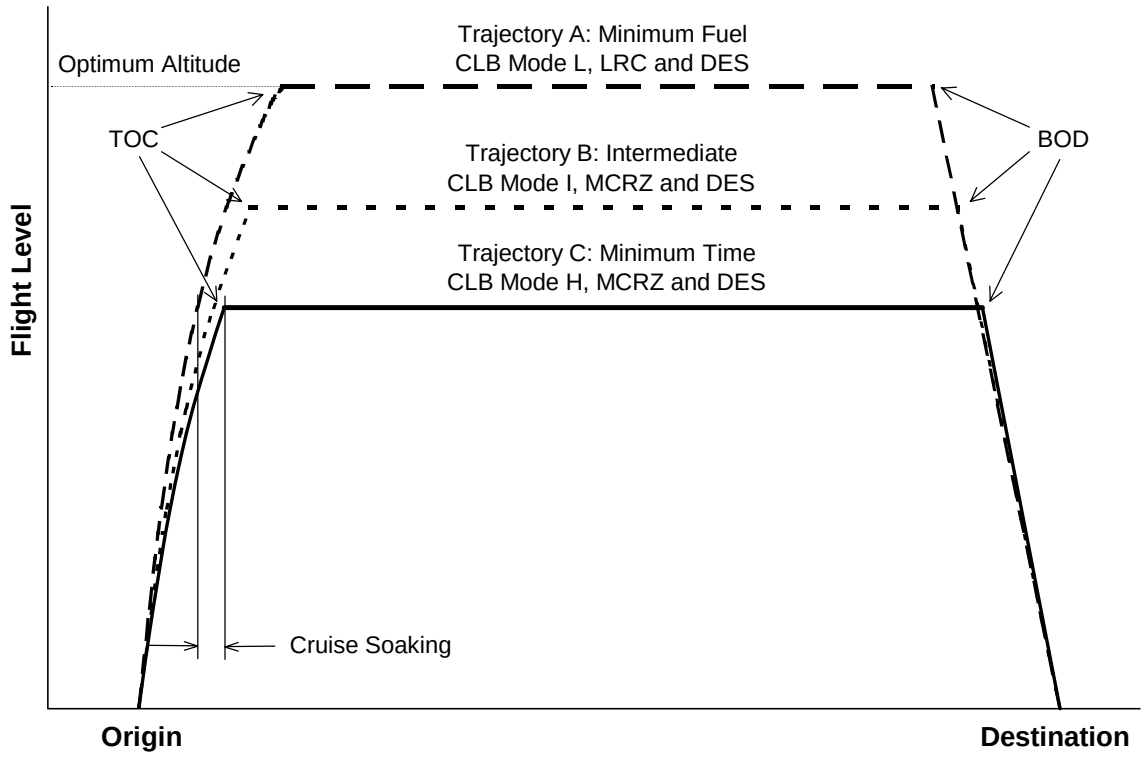

Figure 43. Elucidating the concept of cruise soaking due to faster CAS/Mach climb speed schedules; TOC = top of climb, and, BOD = beginning of descent.

This approach to speed schedule formulation would frequently promote a significant lowering of the minimum time threshold, thereby allowing scope for rationalisation of time related cost, or, possibility of further maximising the P-ROI through a simultaneous cost

magnitude reduction and equipment productivity increase. It must be noted that reduction in block time through continual reduction in flight level will reach a minimum and begin to increase henceforth if either the CAS/Mach speed crossover flight level junction is attained or a minimum cruise fraction threshold is surpassed. An added advantage which complements the faster schedule edict is that improvements in passenger comfort are available since the climb angle reduces with speed.

It must be noted certain operational criteria must be adhered to in order to justify a valid definition of CLB Mode H. Primarily, there should be a sufficient level of maximum available climb power to not only clear flight level with appropriate margins but do so along the entire trajectory path for prevailing ambient conditions. Also, the speed schedule could be inappropriate if cruise fraction minima inequality constraints defined primarily for passenger comfort are violated, and a reasonable degree of operational flexibility (in view of ATC or route structure restrictions) should be ensured with the identified optimal flight level. Most importantly, a significant block time reduction is associated with it an increased block fuel penalty - the designer should inspect for scenarios where fuel divergence due to a faster schedule begins to overshadow the simultaneous cost of time and subsequently try to justify adopting it as the faster climb control technique.

A minor contribution in cruise distance soaking may in some instances be afforded by the descent schedule. Some scope of block time improvement is evident but studies have shown the magnitude is not necessarily significant enough to warrant further manipulation.

10.2 Descent Control

Normally, one would formulate speed schedules for descent much in the same way as was previously done for climb control. Three options are usually available to the designer: Rate of Descent (RoD) as a control variable, a Mach/CAS schedule as the control variable, and, Mach/CAS speed schedule as the control variable with RoD used as the ancillary constraint. Work done by Erzberger and Lee[7] show RoD-controlled profiles yield results closer to the mathematical optimum than Mach/CAS speed schedules alone. The Mach/CAS schedule creates a condition in which idling predominates and therefore the aircraft descends at near maximum lift-to-drag condition in order to minimise energy loss thus resulting in a flight path that is roughly constant. In contrast, RoD-controlled profiles have the undesirable characteristics of steeper flight path angles as the aircraft descends - which is unsuitable for passenger comfort, and, this criterion for a control variable in descent proves to be dangerous due to no restrictions being placed on speed. A compromise commonly adopted by manufacturers is the combination of Mach/CAS with an additional limitation of a pre-selected maximum RoD. The maximum RoD threshold has additional constraints of not only conforming to a vehicle's maximum permissible but cabin RoD dictated by the environmental control system's envelope. Typical values for maximum cabin RoD generally vary between 300-500 fpm; the upper value being a more extreme system requirement.

For new conceptual aircraft design proposals, it is suggested that descent speed schedule definitions should be approached in mostly the same way as climb is with Mach/CAS, but with an ancillary consideration of maximum permissible vehicular as well as cabin RoD as the control variables. Generally, when the descent mode is not assumed as being congruous with the climb mode speed schedule, a slightly faster Mach (+M0.02 to +M0.05) and fixed speed (+30 KCAS to +50 KCAS) would be adopted. In this instance, multiple descent modes are disregarded in favour of one descent mode (designated as DES Mode) owing to small differences in the state and time variables. This approach also has the advantage of expediting ensuing mission analyses.

10.3 Defining En Route Operational Limitations - Flight Envelope

Appropriate formulation of the flight envelope is essential for maximising the en route performance capabilities of any respective aircraft and many regulatory guidelines exist for its definition[1]. The problem here is to create a set of simplistic rules that allow accurate envelope construction without unduly restricting the vehicle's unconstrained predicted performance. The flight envelope usually consists of four distinct boundaries, three of which are defined by speed thresholds related to stall (V_S), buffeting and emergency dive (M_{MO}), and, a combined consideration of manoeuvre-gust loads and maximum dynamic pressure (V_{MO}). The remaining boundary is an upper threshold of flight level derived from simultaneous appreciation of climb thrust limitations, maximum cabin pressure differential, and on some occasions, buffeting. The derivation of these boundaries is commonly performed using extrapolated wind tunnel data to full-scale and subsequently verified with flight-testing.

Initial prediction methods can become mathematically quite extensive which do not easily lend themselves to simplification or otherwise lose significant precision in the process. For example buffeting is characterised by breaks in C_L-α, c_m-α, or, c_x-α curves and emergence of pressure divergence on any of the lifting surfaces or fuselage. This poses a daunting challenge from the analytical point of view. By tackling the problem through a basic conceptual design philosophy of implicit minimum goal success, a useful empirical method was developed that adequately defines the flight envelope without the need for more esoteric aerodynamic modelling. This approach uses the information already available from an investigated vehicle's unconstrained predicted performance and correlates this to a database of previous observations collected from known designs.

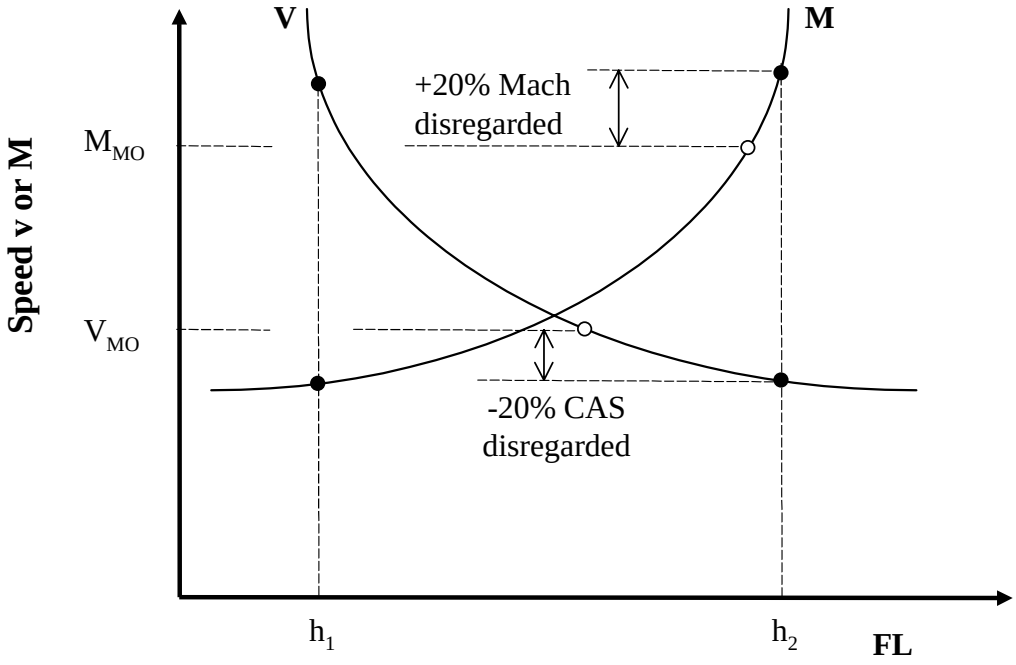

Figure 44. Identification of V_{MO} / M_{MO} flight envelope boundary using the "20-80" rule.

V_{MO} and M_{MO} speeds are set using known MCRZ thrust limited performance for a pre-designated Minimum Flight Weight (MFLW) vehicle configuration with adjustments incorporated from statistical bias. The MFLW can be defined by assuming around 65% of

the vehicle's MTOW, and this figure was obtained from comparisons made with Performance Engineer Handbooks (PEH) of other known designs or equivalently estimated by assuming an AUW equal to the sum of OWE and 25% of the Maximum Fuel Weight (MFW). Thereafter, the MCRZ speed threshold can be obtained assuming equilibrium of forces in horizontal flight for given MFLW at a specified interval of flight levels assumed to be between FL 150 and FL 350 in order to maximise en route performance flexibility. This speed variation with flight level is in fact hyperbolic, however, a transformation of speed as an exponential function of flight level can be introduced and appropriate limit speeds can then be predicted based on statistical regression from a database derived from other aircraft.

When MCRZ speed for varying flight levels assuming MFLW are investigated, it is evident that Mach number tends to increase with increasing flight level whereas CAS increases with reduction in flight level. By considering these curves as potential M_{MO} and V_{MO} candidates respectively and introducing the "20-80" rule, the vehicle's V_{MO} / M_{MO} boundary can be predicted. The 20-80 rule is an interval which disregards 20% of the slower CAS and faster Mach portions of MCRZ thrust limited speeds in the investigated flight level interval and was derived empirically (see Figure 44 above for illustration). The method does not facilitate a multiple V_{MO} / M_{MO} boundary definition, however, the approach is simple, promotes synergistic utilisation of primary conceptual calculation algorithms and validation has shown it to be relatively accurate.

10.4 Flight Technique and Profile Optimisation

The computation of range is an iterative, complicated and computationally intensive exercise, yet it is the one of the fundamental objective functions and therefore must be estimated with adequate accuracy. In the problem formulation, not only should the integrated three-phase flight be analysed, but also the requirements imposed by reserve and contingency fuels need to be accounted for. During occasions where a reserve is stipulated as being proportional to the trip fuel or time, a further layer of iterative looping compounds the amount of work that needs to be expended. Yet another layer for this numerical integration exercise is the issue of unconstrained (or otherwise) optimisation to produce objectives of maximum SAR and maximum block speed for both maximum payload-range as well as fixed sector distance missions. A further-reaching analysis would even include flight technique coupling and subsequent optimisation for minimum DOC and maximum P-ROI. It can be appreciated that these requirements for flight technique and profile optimisation with respect to range and the transformed economic objective functions can become daunting and indeed are the focus of large and cumbersome dedicated operational performance codes. The challenge here is to create a significantly compact, robust, fast-executing and modular method/system of flight technique and profile optimisation analysis that emulates in many respects the more sophisticated functionalities discussed above.

10.4.1 Quasi-analytical Construction of Conceptual Performance Datasets

Dedicated en route operational performance algorithms commonly employ the use of pre-defined aerodynamic coefficients and engine performance decks tabulated digitally which are both aircraft and configuration specific. Data in these arrays may be dependent upon more than one parameter and interpolation techniques can range from the basic linear, to quadratic or even cubic polynomial algorithms. Although these interpolation routines are relatively simple and demonstrate some degree of flexibility, a number of disadvantages exist which proves prohibitive for applications aimed solely at expediting

conceptual design performance prediction whilst retaining good accuracy. Problems to be overcome include:

- Algorithm calculation speeds hindered by the use of sequential tabular search methods. More sophisticated search engines not delivering an acceptable trade of calculation speed versus complexity; and
- A focus on minimal memory size allocation compromises the prediction accuracy through an emphasis on information compactness for solutions within tabular boundaries.

The idea is to create a series of tables where each describes accurately disseminated constituent performance sub-units that are then adequately described algebraically thence introduced for ensuing integrated performance optimisation calculations. For example, candidates for performance sub-units include climbing for both AEO and OEI conditions, and descent. The cruise performance control aspect is not considered for this categorisation since an algorithm to identify optimal and maximum cruise speeds is available as an iterative scheme and hence can be designated as an appended algorithm to the master performance optimisation routine.

An initial step requires the construction of performance tables for climbing and descending flight. Normally for given ambient ISA deviation and operational mode, two independent variables namely AUW and flight level are required for the estimation of state and time variables for a given flight phase. For the purposes of conceptual design performance calculations of time elapsed, fuel expended and distance traversed, numerical integration techniques such as the popular trapezoidal rule with a course step size for flight level exhibit rather accurate predictive powers. The trapezoidal rule integration formula for function f(x) assuming a step size, h, and respective truncation error is given as[41]

$$\int_{x_0}^{x_1} f(x)dx = \frac{h}{2}\left(f_0 + f_1\right) - \frac{h^3}{12} f^{(ii)}(\xi) \tag{281}$$

The construction of an integrated table calculation procedure begins with identification of the pertinent speed technique, i.e. fixed CAS/Mach schedule defined specifically for CLB Mode L, CLB Mode H, or DES Mode, employed for the appropriate flight phase. Assuming a numerical integration step size of FL 50 (5000 ft) is sufficient for an adequate calculation tolerance, for given ISA deviation and AUW, a one-dimensional array may be constructed to produce state and time variable estimates based on closed form thrust and drag prediction techniques detailed earlier. It is highlighted that in this methodology, the reference AUW for all calculations are actually the gross weight of the vehicle at the beginning of a given (climbing or descent) flight phase and not instantaneous values at given flight level. Recalling the impulse function operator utility mentioned previously, a closed form expression capable of delivering integrated results can then be utilised to calculate performance instantaneously. Since each of these integrated performance arrays must be constructed for given ISA deviation, AUW at initiation of flight phase and operational mode, it would be prudent to investigate additional avenues where the requirements for reference tables are minimised. This is of primary concern because the goal is to reduce the amount of information (memory) and increase calculation speed of any new performance optimisation package. Further simplification can be achieved via a transformation function - or a fundamental expression that is identified as being congruous

with some basic algebraic relationship exhibited by the ordinate and abscissa. One important example was found to be the transformation of dependent state and time variables for given independent variables of ISA deviation, AUW at initiation of flight phase, operational mode and flight level into dependent variables of AUW, fuel expended and time elapsed being a function of ISA deviation, operational mode and flight level, or, indirectly distance traversed.

Initially, AUW may be converted from an independent to dependent variable by means of a logarithmic transformation with respect to distance traversed. Figure 45 geometrically elucidates the validity of using this premise. It can be concluded that the information requirements for integrated performance whether climbing or descending stipulate the construction of only two arrays for independent variables. These are designated as MFLW and MTOW of the conceptual design proposal for given ISA deviation, operational mode and altitude interval from sea level to service ceiling. The fundamental algebraic expression is of the form

$$\mathrm{TOGW}_h = k_h^{(i)}\left[\ln d_h\right] + k_h^{(ii)} \tag{282}$$

A logarithmic correlation ensures that for given flight level (h) and distance traversed (d_h) there exists only one TOGW (TOGW_h). A pertinent observation is that the correlation coefficients $k_h^{(i)}$ and $k_h^{(ii)}$ vary with flight level. This seemingly discrete progression can be fortuitously converted into a continuous function using the impulse function operator utility in conjunction with exponential interpolation presented in Section 3.3 so that appropriate coefficient of proportionality combinations are employed for given flight level.

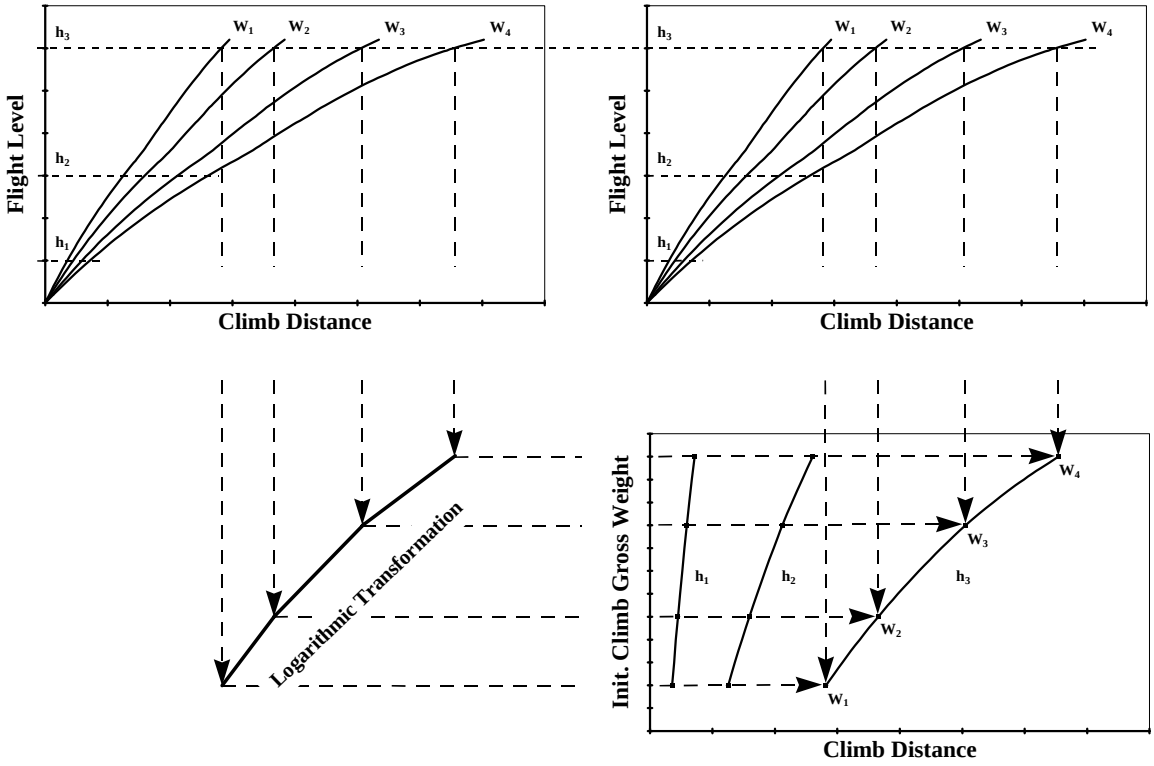

Figure 45. Geometric interpretation of transforming the independent AUW parameter into a dependent variable using logarithmic correlation.

Using a similar methodology to the TOGW transformation presented above, the fuel expended and time elapsed to climb or descend can be expressed as flight level and distance traversed dependent parameters. As depicted in Figure 46, the sole difference is that the transformation function was found to be linear in nature. The fundamental algebraic expression now becomes

$$\Theta_h = k_h^{[i]} d_h + k_h^{[ii]} \tag{283}$$

where for given d_h and h there exists a unique estimate of fuel expended or time elapsed (Θ_h), and, the associated correlation coefficients $k_h^{[i]}$ and $k_h^{[ii]}$ are flight level specific. Again, discrete correlation coefficients can be linked via an impulse function operator in conjunction with exponential interpolation so that appropriate coefficient of proportionality combinations are employed for given flight level. Since d_h is assumed to be the independent variable here, both of the state and time objectives can be expressed as monotonic functions of TOGW; this circumstance comes about when Eq. (282) is rearranged

$$d_h = \exp\left\{\frac{\text{TOGW} - k_h^{(ii)}}{k_h^{(i)}}\right\} \tag{284}$$

and substituted into Eq. (283).

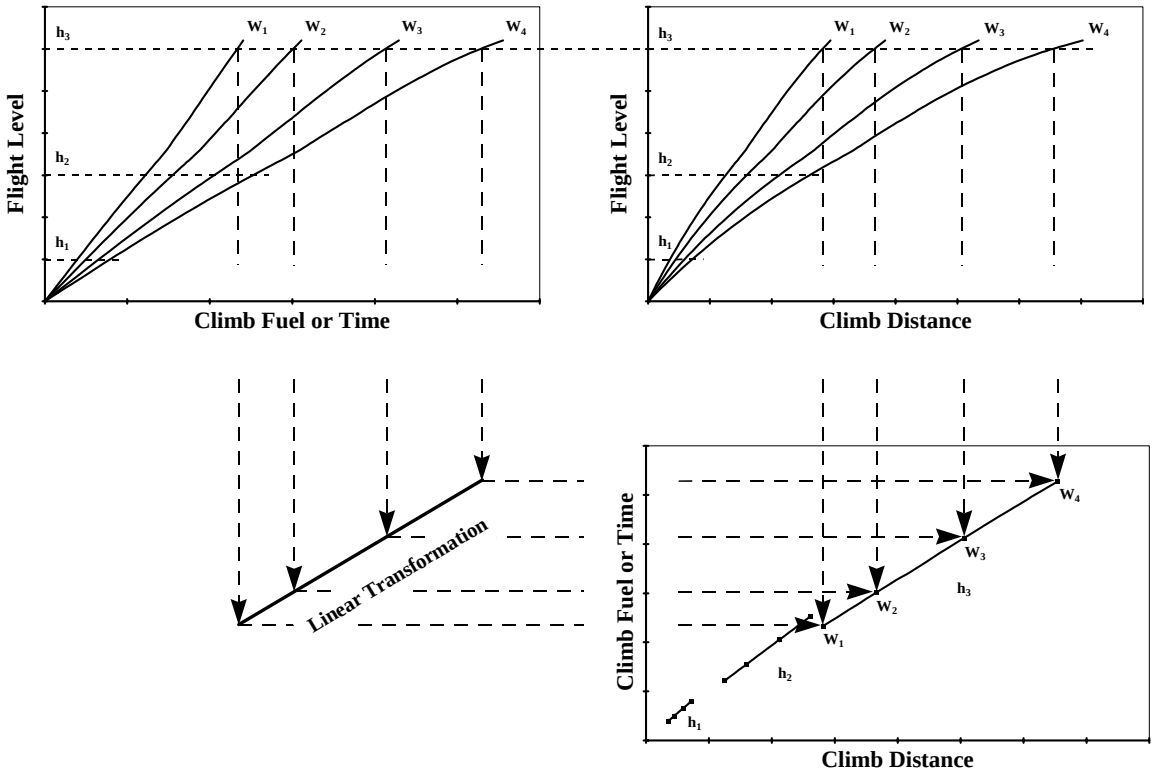

Figure 46. Geometric interpretation of transforming the fuel expended and time elapsed parameters into dependent variables being a function of distance traversed.

10.4.2 Basic Structure of the Optimum Trajectory-Profile Algorithm

A true trajectory optimisation algorithm analyses three-phase flight in which interactions between climb, steady cruise and descent are considered with each segment subject to transversality conditions which are additional and depend upon the end point constraints of state variables[7] as shown in Figure 47. Thus, the entire flight must be analysed as a global problem wherein the links between all the phases are considered concurrently. Unique and constant values of CAS, or Mach number, for corresponding throttle setting are indicative of each phase with strategic switches in CAS/throttle effected during the flight in accordance with procedures detailed in a flight plan.

A sector mission is the operation of an aircraft from the end of initial climb to the end of descent, with both nodes corresponding to a height of 1500 ft pressure altitude. Flight time and flight fuel include allowances required for takeoff, initial climb, approach and landing. The block time and block fuel includes additional allowances for start-up, taxi-out and taxi-in. The notion of flight and block definitions does not include any distance credit. Each sector mission analysis will have with it an associated reserve fuel that is carried to destination. Reserve fuel is a contingency allocation usually consisting of: an alternate or diversion flight over a designated distance; operation in a holding pattern for a specified duration and given altitude; possibly a contingency fuel proportional to the flight fuel expended to complete the sector mission; and where required, contingency fuel to cater for an extended flight of given duration and flight technique.

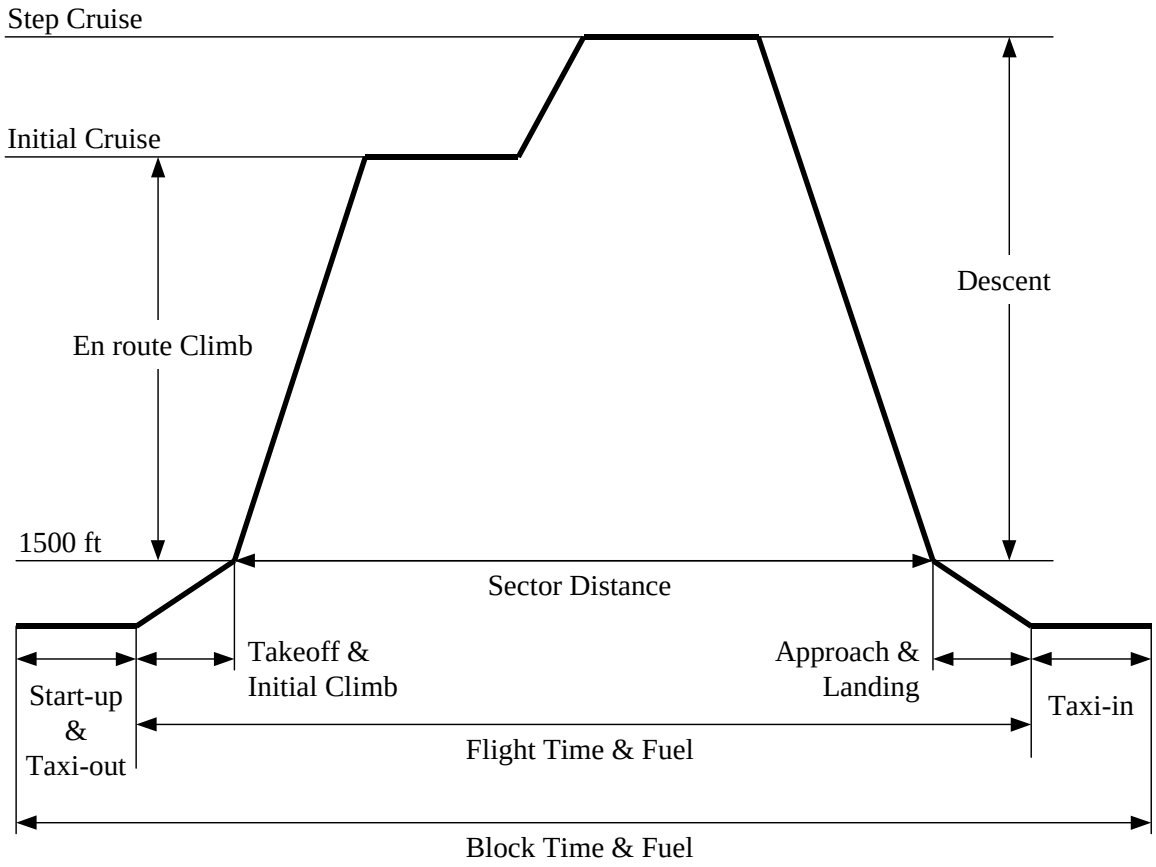

Figure 47. Flight profile as defined by Association of European Airlines (AEA)[145].

The OTPA utilises an interval halving numerical scheme to evaluate the primary objective functions of distance (where required), block fuel expended and block time elapsed for payload-range and fixed sector distance missions. A comprehensive overview of the entire algorithm's construct has been condensed into a simplified flow chart and can be found in Figure 48. TOGW, thus climb distance, is taken to be the free variable for given flight level - an upper and lower climb distance interval at flight level can be derived when MTOW and MFLW are assumed respectively. Based on this premise, other pertinent parameters such as the fuel expended to clear flight level and time elapsed to climb are quantified using the derived expression of Eq. (283).

The entire sector mission is partitioned into [a suggested] minimum of six nodes (five segments), with the initial segment devoted to climb, the intermediary ones accommodating cruise (including possibility to step cruise if elected to do so by the user), and the final segment comprises both residual cruise and descent. For a given cruise segment, steady cruise is conducted at constant flight level and the distance traversed is numerically integrated as aircraft mass is reduced. The estimation of distance traversed for each cruise segment is computed using the closed form Breguet equation[35]. Choice of throttle setting is limited to two specific procedures: maximum cruise power afforded by the thrust model previously presented in Eq. (198), and partial power setting as per the rationale given in Eq. (245) required for optimal cruise performance. These facilitate optimal fuel usage (constrained maximum SAR and minimum fuel), maximum block speed, optimal time expended (constrained or minimum time) and intermediate flight techniques for payload-range and block time-fuel curve characteristics. Vehicles may exhibit an optimal cruise altitude that in some instances are lower than the maximum service ceiling attainable. Initiation of cruise performance at service ceiling and subsequent sequence of steps down in flight level are compared for relative improvements in SAR until the optimal cruise altitude is identified. Finally, the introduction of an additional criterion whereby block speed is maximised promotes iteration to lower flight levels, thus allowing for the identification of maximum block speed and minimum time flight techniques for payload-range and fixed sector mission respectively. OTPA defines maximum block speed and minimum time flight techniques as procedures comprising of CLB Mode H, MCRZ and DES Mode at optimal flight level, whereas, the maximum SAR and minimum fuel flight techniques always assume CLB Mode L, MRC (or other specific cruise) and DES Mode conducted at service ceiling (or optimal SAR altitude) and do not undergo any iterations flight levels unless inequality constraints such as a minimum cruise fraction violation require it to do so.

Where deemed necessary, the designer might wish to inspect for a residual P_s at given cruise speed, flight level and AUW; and this is quantified by assuming MCRZ throttle setting at the given conditions. Standard practise in industry is to assume 0.51 m/s (100 fpm), and for a conceptual design study this constraint may in fact be a fortuitous one. Regularly, in the actual operation of commercial aircraft, the residual P_s at cruise proves to be a more limiting scenario than P_s at climb (minimum RoC) or even the 1.3g to buffet limitations[146]. By virtue of adopting a residual P_s premise, the designer can have some semblance of confidence that buffet limited situations can be mostly avoided, hence promoting a strong likelihood the estimated performance will still remain as pertinent minimum goals whilst the aeroplane candidate is continually refined.

The diversion reserve is optimised as a maximum SAR technique and fixed sector distances are usually considered. Further reserve contingencies are accommodated through selection of an extended cruise time duration option as well as the possibility of assuming some fixed percentage of the total flight fuel. The algorithm facilitates inequality

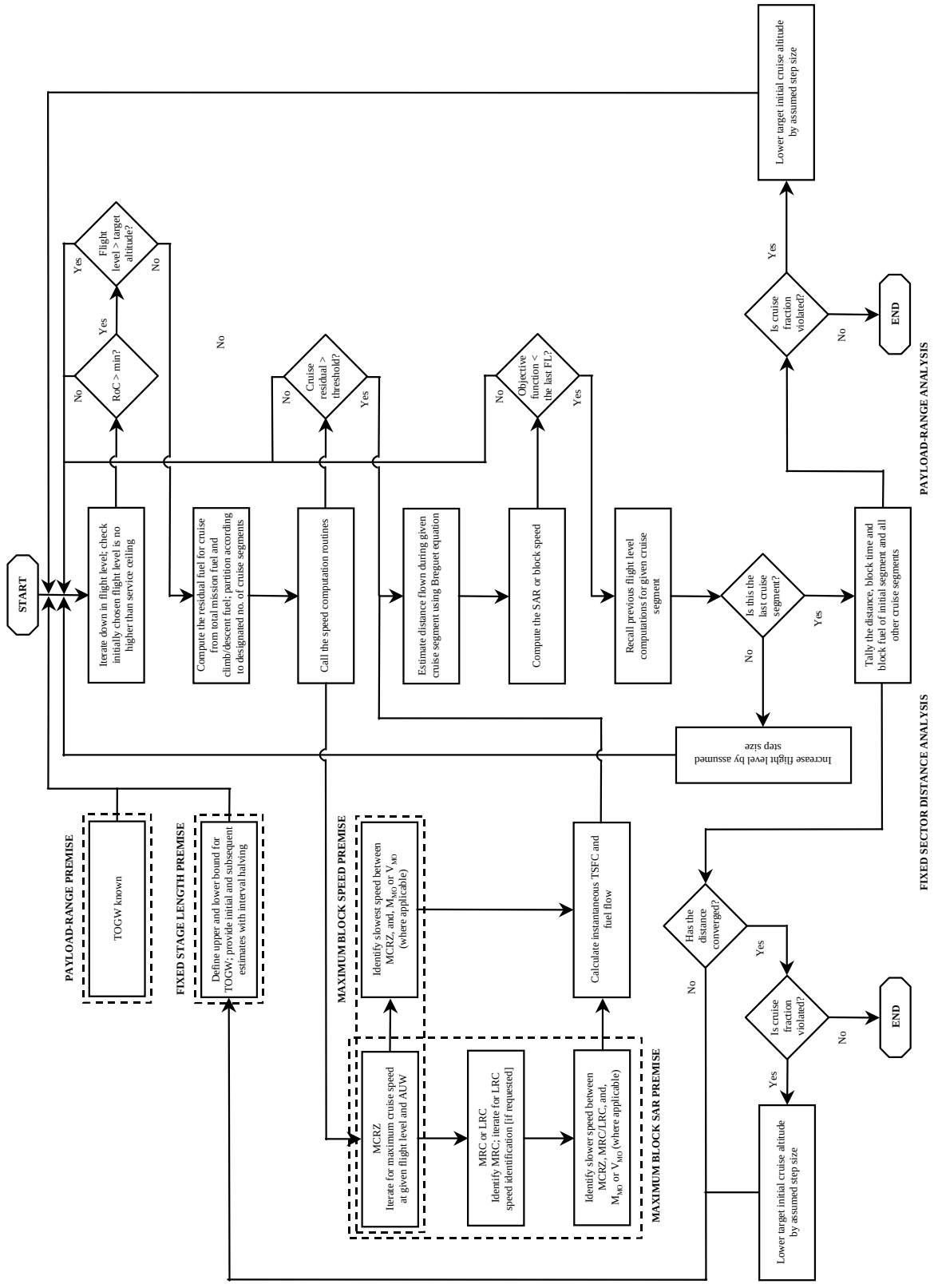

Figure 48. Flow chart depicting the algorithm construct of OTPA catering to both payload-range and fixed sector mission premise.

constraints defined as: a minimum cruise fraction to ensure cruise segments do not become too small and compromise passenger comfort; operational limitations imposed by structure, design weight thresholds and power plant; and, any other aircraft model, ATC or route structure limitations that require consideration. One such example of operational limitations includes adherence to the "odd/even" rule[‡‡‡] as stipulated in FAR 91.109 and FAR 91.121[147].

10.5 Comparison Between Estimated and Actual Aircraft Data for Integrated En route Performance

To establish an idea of what level of accuracy the OTPA algorithm generates, a number of regional, narrow-body and business aircraft payload-range characteristics were predicted and compared to known manufacturer data. The aircraft used for benchmarking purposes were: Boeing BBJ1[76] and B737-600[77]; Bombardier Aerospace Challenger CL-604[51], Global Express[64], CRJ200[79] and CRJ700[80]; Dassault Aviation Falcon 2000EX[52] and Falcon 900EX[53]; Embraer ERJ 145LR[84], Embraer 170[44] and Embraer 190[148]; and, Gulfstream Aerospace GIV-SP[89]. Note that where data was available, predicted performance was compared to the harmonic (maximum payload) range, maximum useful (maximum fuel load at MTOW) and maximum (ferry) range.

Each range was computed assuming a constrained maximum SAR objective at ISA, still air conditions, using derived drag polars based on methods outlined in Section 7,

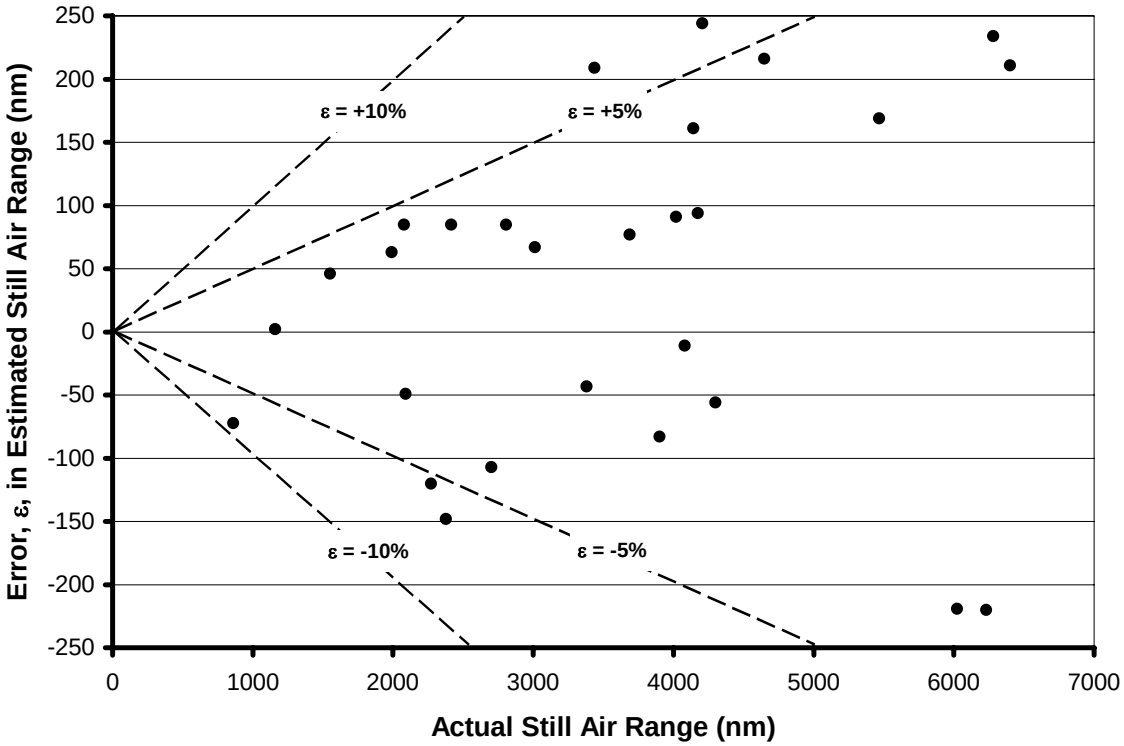

Figure 49. Comparison between known data and predicted ISA still air range performance of in-service aircraft using the conceptual operational control methods and OTPA algorithm.

[‡‡‡] This altitude convention is also commonly referred to as east bound and west bound flights.

intentionally predicted CLB Mode L based on the method described in Section 10.1.2, corresponding DES Mode as discussed in Section 10.2, and, cruise speed as indicated by each respective aircraft manufacturer. Also, in the absence of any flight profile information, the range prediction defaulted to an eastbound flight premise (the odd rule) with each step cruise altitude incremented by 4000 ft.

Results of OTPA's proficiency in estimating the range of widely varying aircraft types is presented in Figure 49 (above). Generally, if one approaches the estimation of range without any idea of operational control schedules and techniques, operational control theory and OTPA tend to produce predictions within a reasonable ±5% error splay. Even though an absolute error exceeding the ±100 nm threshold has occurred, in view of the intentional inferences used in the analysis, this fact illustrates that an encouraging array of results was generated.

intentionally blank

11 Stability and Control

Although all the other core disciplines are addressed with some element of detail during the conceptual design phase, one area of investigation that has traditionally lacked any form of sophisticated depth is stability and control. This circumstance is quite puzzling considering the unavoidable fact as Cook[14] states whilst citing the Wright brothers, "…stability and control comprised the single most critical requirement for flight…". Without question, most aircraft projects have experienced problems associated with vehicular flying qualities and pilot-in-the-loop response attributes, particularly those aircraft configured as powered (boosted), or otherwise, manual primary Flight Control Systems (FCS). The difficulties in achieving satisfactory qualities become even more pronounced when the powered FCS needs to be complemented by some form of manual reversion as well.

When discussing the stability and control attributes of an aircraft, two fundamental handling characteristics are cited as controllability and manoeuvrability. Controllability pertains to a quality that enables the pilot to initiate and subsequently maintain a manoeuvre. The primary concern of controllability is establishing a vehicular reaction one would normally expect to a given stick command, and then extending that attribute to an assessment of the ease or difficulty of maintaining such an initiated manoeuvre. Manoeuvrability alludes to the capability of a pilot-aircraft system to effect changes in the flight path, angular rates and speed of the aircraft. Other concerns such as time lag, overshoots and necessary compensation by the pilot during entry into a manoeuvre and maintenance of a steady-state acceleration, and return to normal flight come into consideration as well.

11.1 Methods and Criteria for Empennage Sizing

As stated, at the very early stages of conceptual design, little attention is given to the stability and control aspect. Historical trend sizing of the empennage and the control surfaces through a tail volume approach is usually deemed sufficient[2,3,4,5]. Briefly, the term "volume" actually refers to a product of quantities collectively described by the dimension L^3 and are specifically reference values associated with the aircraft being investigated. The horizontal tail volume coefficient is defined as

$$\overline{V}_h = \frac{S_{ht}\, l_{ht}}{S_W\, MAC} \tag{285}$$

where l_{ht} is the horizontal tail tail-arm, or the distance between the MAC quarter chords of the reference wing and horizontal stabiliser. Similarly, the vertical tail volume coefficient is given as

$$\overline{V}_v = \frac{S_{vt}\, l_{vt}}{S_W\, b} \tag{286}$$

and, l_{vt} is vertical tail tail-arm, or the distance between MAC quarter chords of the reference wing and vertical stabiliser. The MAC is defined to be[4]

$$MAC = \frac{2}{3} c_R \frac{\lambda^2 + \lambda + 1}{\lambda + 1} \tag{287}$$

As a general rule in industry, volume coefficients of $\overline{V}_h = 0.8$ and $\overline{V}_v = 0.08$ are assumed for all vehicles employing aft fuselage mounted engine arrangement, whereas, $\overline{V}_h = 1.0$ and $\overline{V}_v = 0.10$ are necessary requirements for underwing podded engine installations.

More ambitious methods of sizing beyond the scope of the tail volume approach requires identification of critical operational scenarios that traditionally have been used as a basis of sizing the empennage in the context of small to medium size commercial and business transport aircraft. The horizontal stabiliser design condition usually corresponds to the vehicle at a high AUW (corresponding to MLW), the c.g. at the most forward position and the designated V_{REF} of the aircraft and maximum flaps deflected. A supplemental sizing condition for the horizontal stabiliser probably also includes examination of the aircraft longitudinal Short Period (corresponding to CAP[‡‡‡149] > 0.28) characteristics at a light AUW and the c.g. at the most aft position. In contrast, the vertical tail is predominately dictated by field performance during OEI conditions and when the centre of gravity is most aft. The goal here would be to create a vertical tail planform definition and control surface authority such that V_{MC} limitations do not impart any undue influence for TOGWs heavier than the aeroplane's mid-weight. Another consideration for the vertical tail generally includes adequate authority for field performance during 30 KTS crosswinds. Finally, the ailerons cater to a case where the vehicle is able to turn away from a dead engine in 11 seconds (JAR) – it is quite evident that this consideration is usually beyond the scope of conceptual analysis capabilities. A more tangible requirement appropriate for initial to preliminary sizing is roll control surfaces should not draw upon more than two-thirds authority during OEI and at maximum crosswind conditions. It should be noted that the ailerons are usually sized assuming supplementary assistance by spoiler(ons). To expand upon this, a more detailed run-through of stability and control can be found in an array of knowledge accumulated by Mitchel[15], Perkins and Hage[16], Roskam[17,150], USAF Datcom[18], Etkin[151] and ESDU[152].

11.2 The Mitchell Computer Program

The Mitchell Code[15] was written in ICL FORTRAN and the primary function is to predict stability and control attributes of aircraft from geometry, aerodynamic qualities, propulsion effects and weight for given flight condition. The software does not permit an option to improve the stability and control characteristics of an aircraft candidate by indicating necessary changes to a given array of independent variables. The latest version of the Mitchell Code, called "MITCHELL2", was a product of the original source code authored by Mitchell in September 1973, with three subsequent modifications completed by Cranfield Institute of Technology until 1992.

The program consists of a driver routine directed by a single input file that calls necessary core functions and serves to generate a relatively detailed output file. Currently, a total of sixteen subroutines and six function segments conduct the following operations:

- Calculation of required geometric and parametric attributes;

‡‡‡ Known as Bihrle's Control Anticipation Factor (or Parameter) defined as the ratio of steady-state normal acceleration factor change to the AoA.

- Estimation of aerodynamic derivatives;
- Estimation of moments of inertia;
- Calculation of eigenvalues of the equations for longitudinal and lateral motions with controls fixed;
- Calculation of forced responses to certain disturbances at the specified flight condition; and,
- Calculation of limiting speeds for low-speed flight at sea level.

The input file contains information not only pertaining to the geometric attributes of the aircraft being analysed, but indication of what specific computational result is desired by the user. External geometry definitions of the aircraft being analysed must conform to a myriad of variables deemed necessary for MITCHELL2, and these are presented in Figure 50.

11.2.1 Aerodynamic Derivatives

The primary source of this data is from ESDU with some elements drawn from the USAF Datcom[18] handbook. The aerodynamic data are stored as polynomial coefficients that allow derivatives to be evaluated within a chosen range of aspect ratio (AR = 3.0 to 10.0), sweep angle (Λ_{Qchd} = 0° to 40°), taper ratio (λ = 0.20 to 1.00), etc. Investigations have shown the controls computed fixed longitudinal and lateral quantities and derivatives fall within ±5% of the data sheet value.

11.2.2 Moments of Inertia

Depending on the extent of available weight constituent information, two possibilities are available to the user in computing the three principal moments of inertia. If the weights of major components are known then a simplified version of the method outlined in the USAF Datcom[18], i.e. combination of the major components' inertia about their respective centres, is utilised. Alternatively, those instances where only a limited array of information is at hand, a simple method based on the radii of gyration in pitch, roll and yaw correlated to l_{fuse}, b, and $(l^2_{fuse} + b^2)^{1/2}$ respectively is suitable for all transport type aircraft. In both methods, the inclination of the principal axis of inertia can be read as data and the product of inertia calculated. Finally, if any or all three the principal moments of inertia are known, they can be read in directly together with the roll-yaw product of inertia.

11.2.3 Assumptions when Solving the Equations of Motion

The stability of the aircraft with fixed controls is determined by finding the eigenvalues of the determinants of the equations of motion after separating the lateral and longitudinal motions in the conventional manner.

The forced response of an aircraft to abrupt disturbances is calculated in a simplified manner to provide additional information on the handling characteristics. The quasi-static acceleration due to a change of incidence, n_z / α, is calculated for longitudinal motion. To derive the peak rolling acceleration, final steady roll rate and time to roll from +30° bank to –30° bank is evaluated based on a single degree-of-freedom response in roll to full aileron deflection (and full spoiler(on) extension if applicable).

The lateral response of an aircraft in three degrees-of-freedom to an abrupt disturbance is calculated from the equations of motion that constitutes the controls-fixed scenario. The only difference is the right hand side contains a definition of the disturbances. Four disturbances are considered: (1) step application of full aileron and spoiler(on); (2) a step application of full rudder; (3) a step reduction of the thrust of the outboard engine; and,

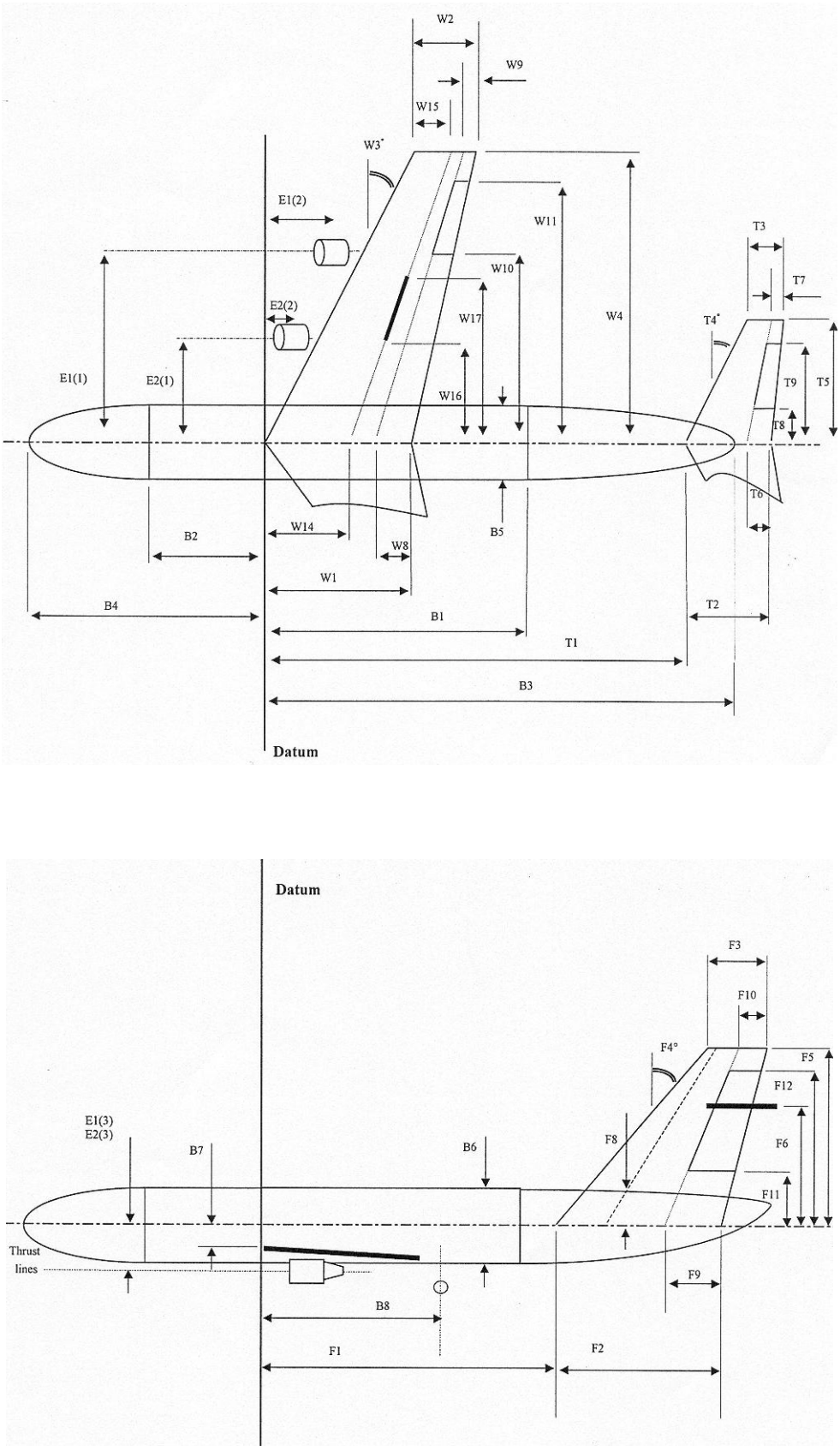

Figure 50. Basic geometric definition of aircraft required by Mitchell Code[15]; reproduced from a sketch congruous with the originally drafted version[153].

(4) a step side gust.

The program contains a subroutine to determine low-speed handling which includes the stalling speed and incidence, tail load and elevator angle at the stall, the nose-wheel lift speed with the tailplane set either to trim for climb or to as near the trim position as it can be moved, the V_{MC} limitation during engine failure, and the steady sideslip angle that can be held with either full rudder or 80% of full aileron and the corresponding crosswind component.

11.2.4 Conversion to the MATLAB Platform

To ensure maximum compatibility within a conceptual design software framework (to be presented in Section 14), the latest form of the original code dubbed "SCMITCH" was converted into the MATLAB Version 5.3 language. Although an alternative philosophy has been introduced in terms of how input data is supplied to the driver routine, the original functionality of directing analysis using a formatted input file has been retained, and is fully compatible with all versions of input files originally intended for the original FORTRAN application. By virtue of adopting the MATLAB platform, the new version of Mitchell Code permits the user of by-passing what is now considered to be redundant functionality, such as those relating to aircraft drag, vehicular low-speed aerodynamic characteristics including maximum lift, lift curve slope and aerodynamic coefficient and derivative information.

The SCMITCH system of routines comprises 26 M-files, of which one is specifically devoted to acting as an intermediary data exchange conduit. This application distinguishes the user's intention of executing all analysis from a single input file (thus requiring the complete gamut of computations), or from within an integrated MATLAB analysis environment. If the latter is selected the data exchange conduit is then tasked to ensure any geometric and/or aerodynamic information generated outside of the SCMITCH system is allocated to appropriate variables recognisable by SCMITCH. In perpetuating the basic construct and modular philosophy of the original Mitchell Code, a single driver routine directs all computations conducted by either all or most of the remaining 25 M-files. A flow chart that elucidates the sequencing of analysis with respect to primary functional routines is presented in Figure 51, and a list in alphabetical order identifying each of the 26 routines with a brief explanation is given below:

SCAERCE	Calculates the vehicular a.c.
SCAEROC	Calculates the neutral point (n.p.) and static margin (SM)
SCDOWNW	Calculates the downwash gradient
SCDRAWB	Drafts the parametric plots used to assess handling characteristics
SCELPWR	Calculates the lift curve slope for horizontal tail due to elevator
SCFLSPD	Calculates low-speed handling characteristics
SCFNA10	Calculates the lift curve slope of a two dimensional wing
SCFNA20	Calculates the a two dimensional lift curve slope with control deflection
SCFNPAC	Calculates the position of the a.c. on the wing
SCFNSAC	Calculates the shift of the a.c. by the fuselage and nacelles
SCFUNA1	Supplement to derive three dimensional lift curve slope of wing
SCGEOMT	Calculates the geometric properties of the aircraft
SCHANDL	Calculates the fixed controls stability, simplified forced response and three degrees-of-freedom lateral response
SCINDAT	Identifies how source data is to be acquired and allocates appropriate values to internal variable structure

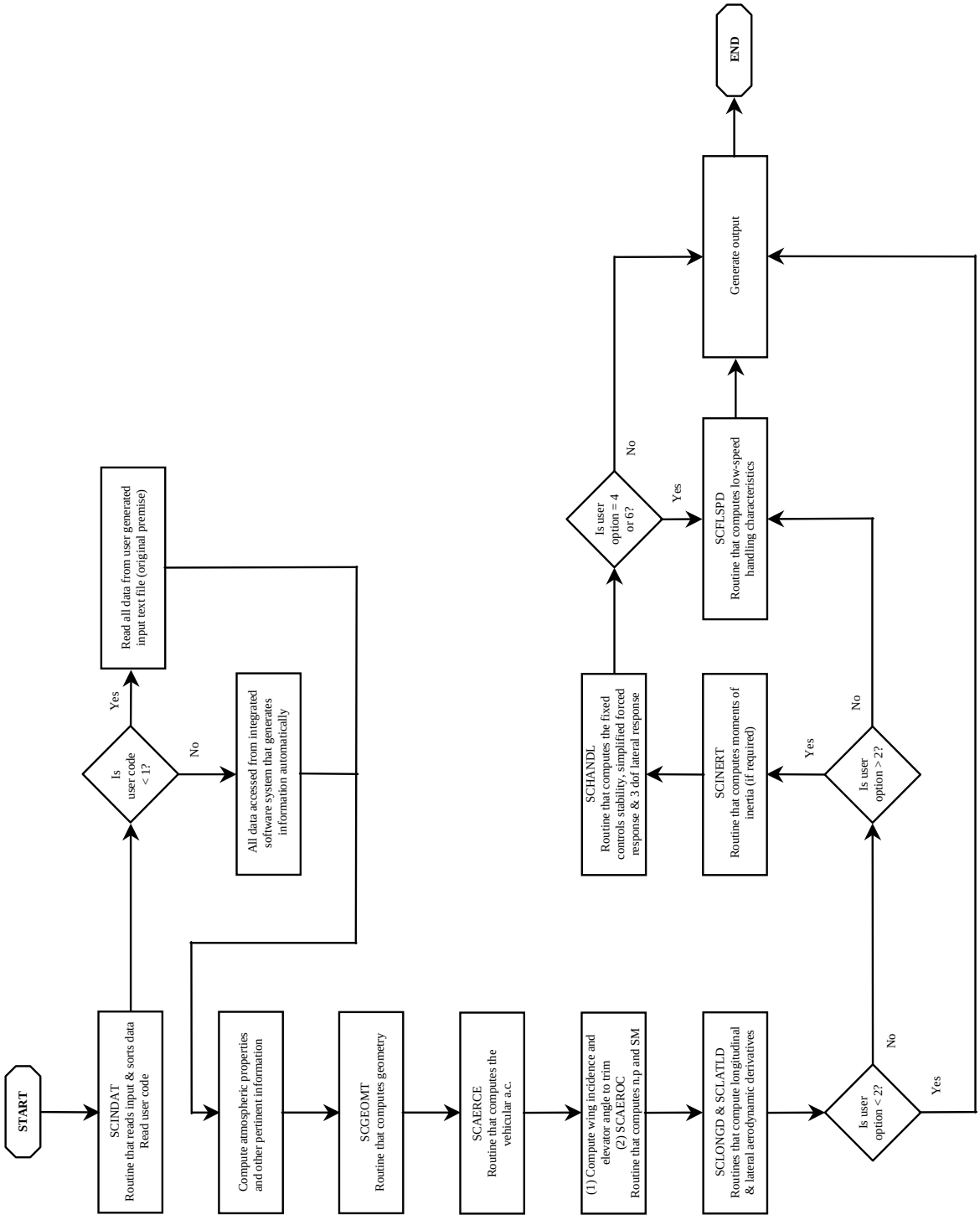

Figure 51. Flow chart depicting the algorithm construct of SCMITCH code for analysing stability and control attributes of an aircraft design candidate.

SCLATLD Calculates the lateral aerodynamic derivatives
SCLONGD Calculates the longitudinal aerodynamic derivatives
SCLPCAL Calculates the rolling moment due to rolling
SCLRCAL Calculates the rolling moment due to yawing
SCLVCAL Calculates the rolling moment due to sideslip

SCLZCAL	Calculates the rolling moment due to aileron deflection
SCLZSCL	Calculates the rolling moment due to application of spoilers
SCINERT	Calculates the principal moments of inertia of the aircraft
SCMITCH	Primary routine that directs all intermediary and core computations, and handles output
SCNRCAL	Calculates the yawing moment due to yaw
SCNVCAL	Calculates the yawing moment due to sideslip
SCRDPWR	Computes the rudder derivatives

11.3 Assessing the Suitability of Aircraft Design Candidates

One of the more difficult tasks associated with assessing the stability and control merits of a given aircraft design candidate is the esoteric nature of the results. For example, inspecting parametric values like undamped natural frequency, period, damping angle, damping ratio, time and number of cycles to half amplitude and logarithmic decrement does not necessarily imbue designers who are novices when it comes to the discipline of stability and control with a coherent appreciation of the mode that is being investigated.

In determining the flying qualities of an aircraft the pilot will assess the degree of acceptability and suitability of a given category of aircraft in an entirely subjective manner. Descriptive terms associated with a level of flying qualities such as a pilot might use have been formulated into a numerical rating process. The most widely known rating guide is the Cooper-Harper[154] scale as shown in Figure 52 and covers all phases of flight. Importance is placed upon the major decision terms, i.e. “controllable”, “acceptable” and “satisfactory”, and the pilot at each stage assesses whether the term has been met relative to the intended use of the aircraft. The best category is defined as “excellent, highly desirable” and is associated with a satisfactory level of pilot workload since the pilot has no need in compensating for any deficiencies in the manoeuvre performance of the aircraft.

The following sections detail a suggested procedure in ascertaining the feasibility (or otherwise) of a new aircraft design. In an attempt to familiarise the designer as to how the analysed vehicle fairs in accordance with the Cooper-Harper rating system, and primarily, in order to allay any confusion to what is satisfactory, the method employs predominantly a graphical approach. It is highlighted that not only will the charts to follow display examples of how one might establish the qualities of an aircraft for a given dynamic mode premise, but also, as denoted by a circle in the plots, serves to act as a validation (original sample input file accompanying MITCHELL2 code) for the SCMITCH system.

11.3.1 Longitudinal Short Period Mode

Short Period oscillation is a motion where the incidence, attitude and flight path angle of the aircraft change while airspeed remains constant. The motion can consequently be resolved into vertical translation and pitching components. One of the most difficult issues facing contemporary FCS design is the prevention of Pilot Involved Oscillation (PIO), sometimes known as Aircraft-Pilot Coupling (APC). This phenomenon is directly related to concurrent interaction between the human pilot, FCS and airframe dynamics. The goal of a new aircraft concept is to avoid susceptibility to PIO and there currently exist several studies wherein the PIO problem is being investgated[155]. Nonetheless, that does not detract from the fact all attempts should be made in avoiding such an eventuality as the design matures. In this instance, even a rudimentary attempt is deemed to be sound practise.

Substantial disagreement between results based on pilot ratings corresponding to Short Period damping and natural frequency has resulted in formulation of a multitude of parameters. Today, response to elevator input on the basis of the Short Period mode

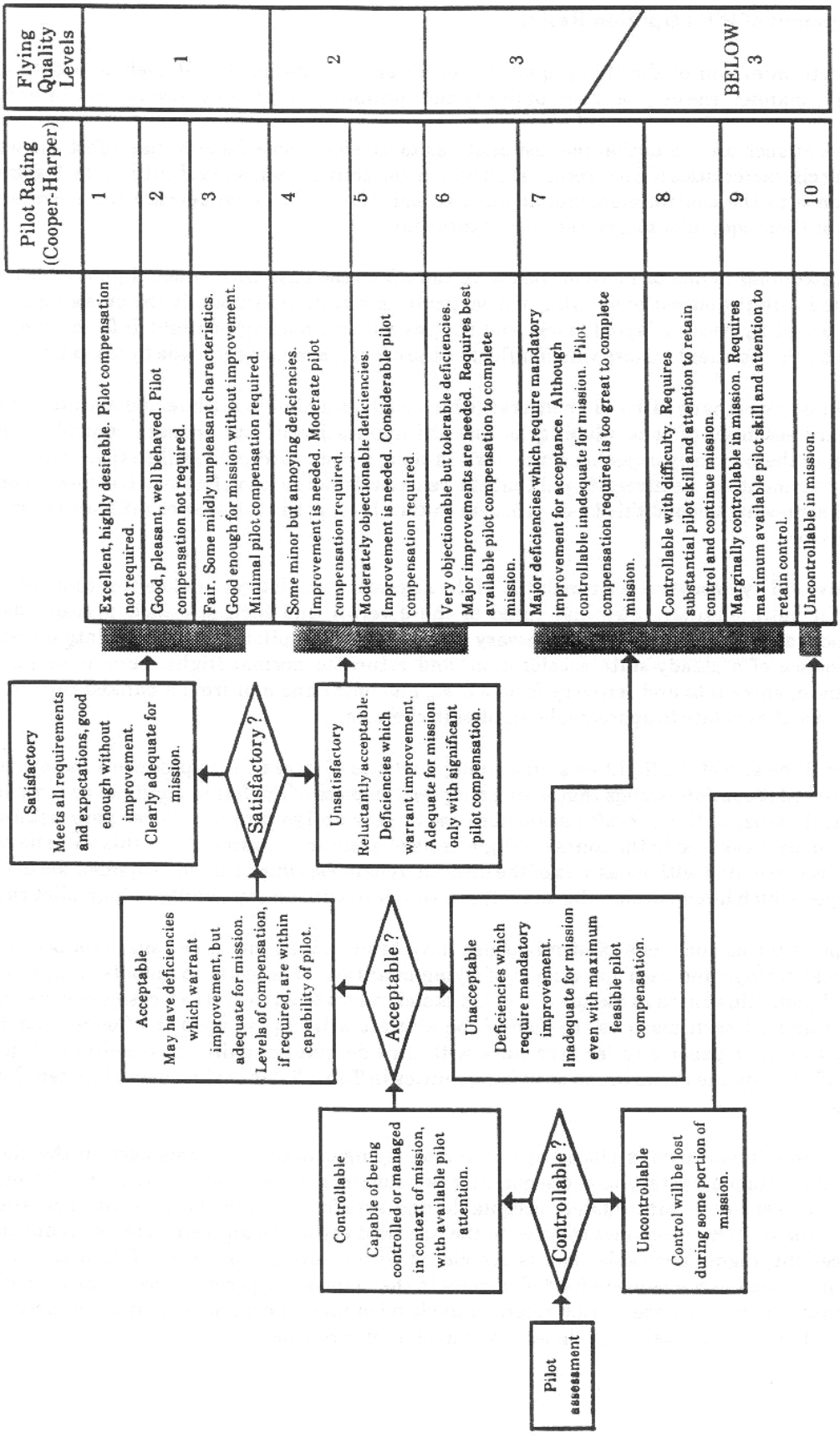

Figure 52. Qualitative pilot assessment rating of flying characteristics (Cooper-Harper[154]).

approximation yields the following quantifiable handling qualities:

1. time to peak pitch rate;
2. response time to steady pitch rate and steady normal accelerations;
3. ratio of peak to steady pitch rate;
4. initial pitch acceleration related to CAP;
5. pitch attitude dropback (overshoot); and,
6. flight path angle time delay.

Results of studies indicating the variation of frequency and damping have been charted into zones of qualitative pilot opinion[156]. Figure 53 shows a typical example of pilot opinion contours where zones of satisfactory, acceptable, poor and unacceptable are indicated. Also displayed are additional comments relating to anticipated response characteristics away from the zone that is ideal.

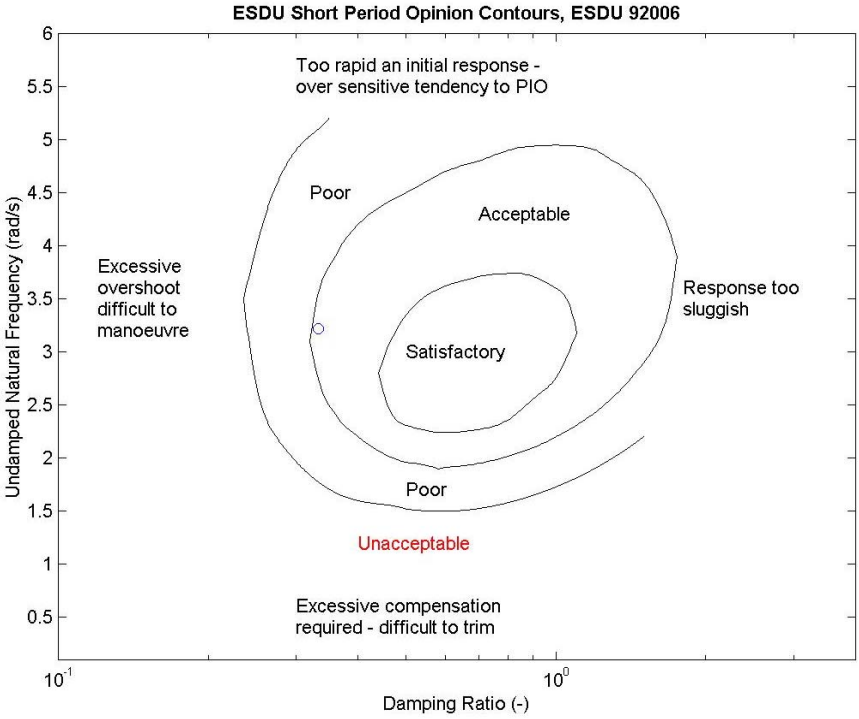

Figure 53. Longitudinal Short Period oscillation pilot opinion contours taken from ESDU[156].

Short Period frequency boundaries for acceptability[157,158] is shown in Figure 54 and boundaries are functions of the change of the steady-state normal acceleration factor per unit AoA (n_α). Figure 54 applies only to Phase C operations, namely, take-off, approach, overshoot and landing, which normally call for gradual manoeuvres and precise flight path control.

As a supplement to the presented charts, a final salient correlation (Figure 55) can be found between the dynamic mode period and time to damp to half amplitude based on criteria formulated by ICAO[159]. Lines of constant Cooper-Harper pilot ratings are also indicated in conjunction with a minimum threshold that also offers a qualitative description

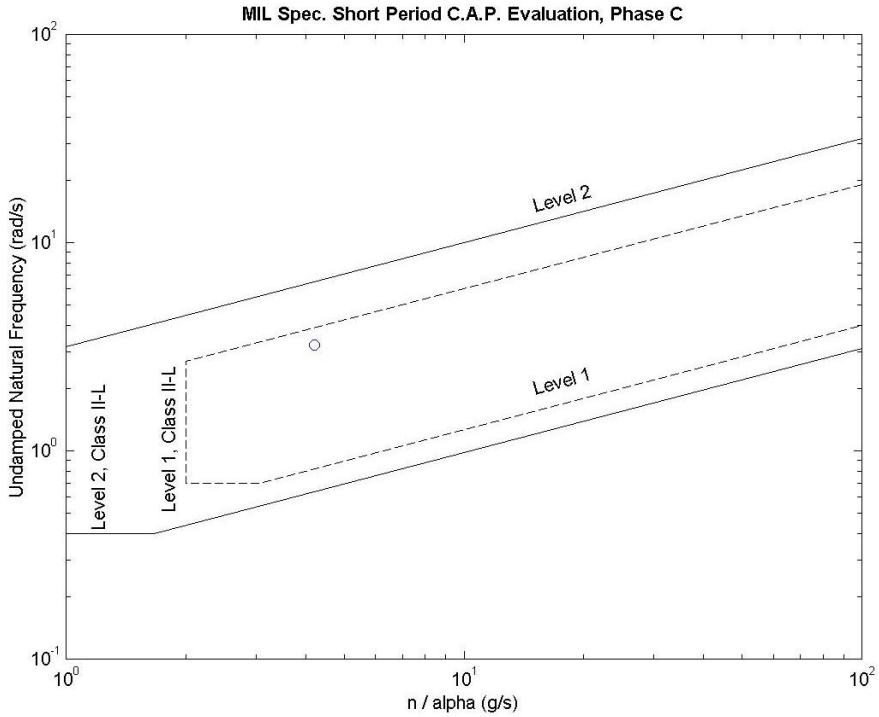

Figure 54. Short Period frequency characteristics, CAP evaluation; Category C Flight phase[157,158].

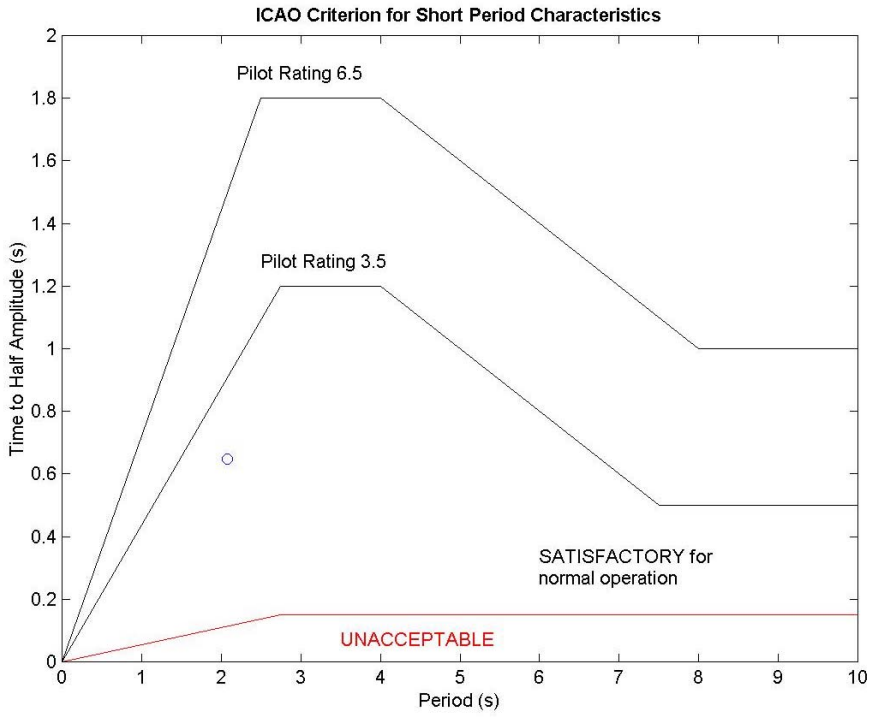

Figure 55. ICAO recommended Short Period mode characteristics[159].

of acceptability or otherwise.

11.3.2 Phugoid Mode

The Phugoid is a lightly damped low frequency oscillation in which an exchange of height and airspeed occurs at constant aircraft incidence. The pilot generally experiences little difficulty in controlling this motion when attitude is continually scrutinised. The significance of inspecting Phugoid characteristics relates primarily with the period of the oscillation: if the period is short, the degree to which monitoring the speed may become excessive, and thus, distract the pilot from attending to other more pressing tasks. A useful chart indicating acceptable Phugoid mode attributes can be found in Figure 56, the source of which originates from ICAO[160].

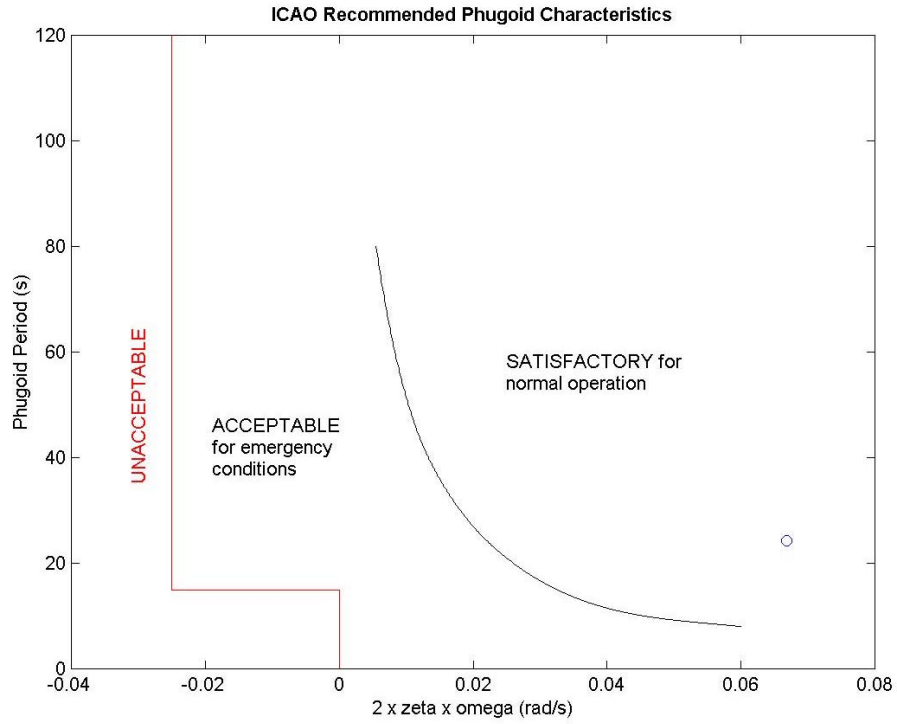

Figure 56. ICAO recommended Phugoid mode characteristics[160]; key: zeta = damping ratio, omega = undamped natural frequency.

11.3.3 Dutch-Roll Mode

The Dutch Roll mode is a short period oscillation having components in yaw, roll and sideslip. The period, the damping and an ancillary parameter, such as the amplitude ratio of bank to sideslip, which defines the degree to which the principal freedoms are coupled in this motion, can universally describe the Dutch Roll mode. For low-altitude flight, the problem is one of yawing and how expediently this can be damped out. In contrast, rolling usually predominates for high-speed aircraft operating at high altitudes.

Figure 57 and Figure 58 offer two perspectives in assessing the Dutch Roll characteristics of a new aircraft design proposal. Figure 57 originates from MIL-Spec[157,158] and correlates the damping ratio to the undamped natural frequency; also, a Level 1 flying quality (achievement of task without excessive pilot workload) is assumed. Two curves for

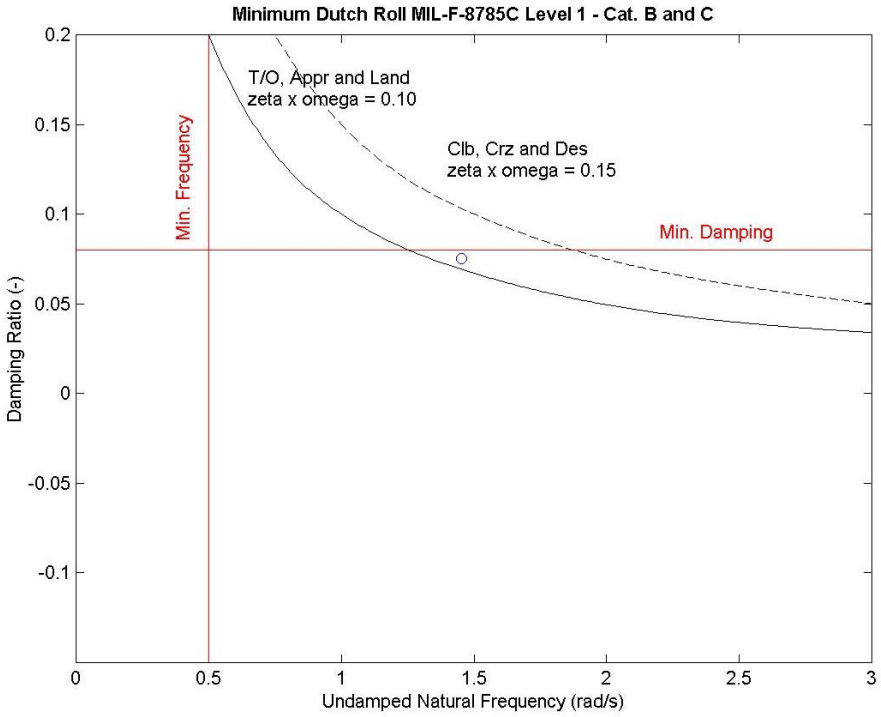

Figure 57. Minimum values of natural frequency and damping ratio for Dutch Roll oscillation[157,158].

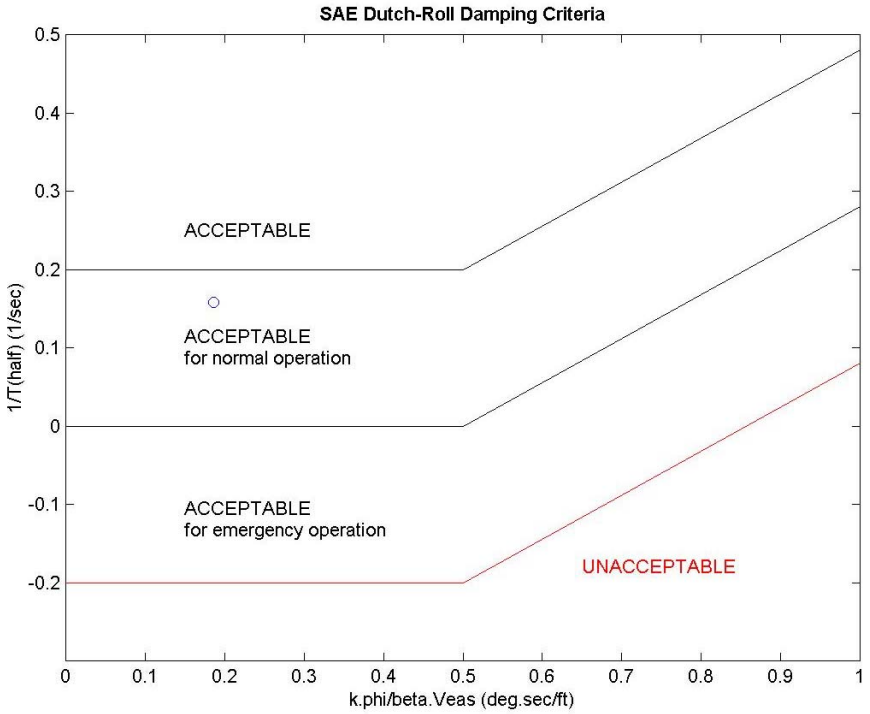

Figure 58. Dutch Roll damping criteria as stipulated by SAE[161]; key: k = κ, phi = ϕ and beta = β.

Category B (all aircraft classes) and C (Class II, medium weight, low to medium manoeuvrability) Flight Phases are plotted, thus denoting minimum criteria of acceptability for field and en route operational performance respectively.

Using standards stipulated by SAE[161], the inverse of time to damp to half amplitude ($1 / T_{1/2}$) is compared to an augmented amplitude ratio of bank to sideslip, or given as $57.3\ \kappa\ \phi / \beta\ V_{EAS}$, where ϕ is the bank angle and β is the sideslip angle, V_{EAS} represents equivalent airspeed expressed in ft/sec, and

$$\kappa = 1 + (0.4 - 1.60 \times 10^{-3} h)\ \Phi_{hcut} \tag{288}$$

with the impulse function $\Phi_{hcut} = \Phi$ (h,FL 250) invoking a reduction in the constant κ for altitudes less than FL 250.

11.3.4 Roll Mode

The predominant lateral controlling manoeuvre is rolling because it is used to keep the wings level in disturbances and for changing heading. An ideal roll would be one that involves pure roll response and achieves a steady-state rate of roll quickly. Pilot opinion boundaries for roll response is shown in Figure 59, where the maximum roll acceleration (p_{ss}) is shown versus the roll mode time constant (t_R). As an aid to enhancing cognisance of the implication each of the three boundaries lead to, Cooper-Harper ratings have been derived and indicated on the chart accordingly.

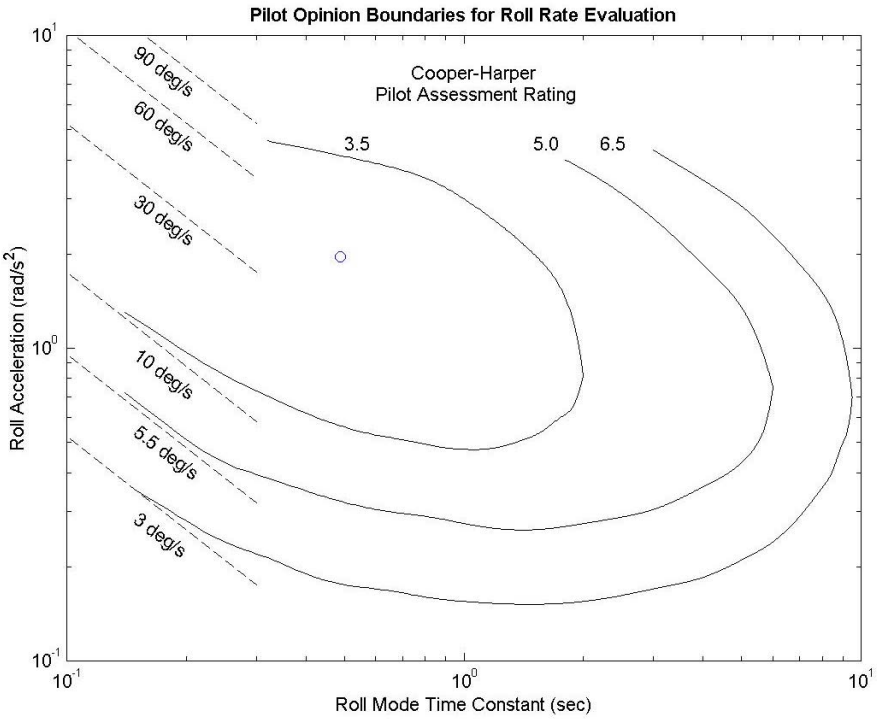

Figure 59. Roll response pilot opinion boundaries[156]; lines of constant Cooper-Harper pilot ratings also indicated.

intentionally blank

12 Direct Operating Cost, Profit-Return On Investment and Associated Optimal Flight Techniques

It is becoming increasingly important for designers of transport aircraft to be well versed in how commercial airline operators establish the feasibility of introducing new equipment types for fleet planning. Airline economics now dictate the need for more flexible commercial transports, thus invalidating the traditional approach of focusing on the design point specifications and giving little regard to off-design sensitivities. Even though the basic requirement of operational performance is scrutinised, airlines will consider in parallel the corresponding DOC, and more significantly, the P-ROI generated. In the context of this study, the profit generated is attributable to flying services, before income taxes, non-operating items such as retirement of property and equipment, affiliated companies and subsidies. There are in addition other considerations beyond the control of aircraft designers. These are issues related to product support, fleet commonality and mix that offers the best flexibility in seating and loading, long-standing and exclusive associations with particular airframe manufacturers, and the dynamic of internal politics. Notwithstanding these other factors, the cost and profit functions mentioned are often used as a rational basis for any future acquisition exercises. In view of this, it can be concluded that operational en route performance should be optimised with respect to the primary objectives of cost and profit and more importantly, it seems logical that both these aspects should be coupled in some manner, whereby it is possible to weigh the combined relative merits of different aircraft. Figure 60 offers a graphical perspective to assist in elucidating the interrelationship between vehicular attributes, operational performance, DOC and P-ROI, and, to serve as an outline for determining constituent working parameters, assumptions upon which the calculations are based, as well as the flow to produce the requisite objective and merit functions.

The effect of block speed (or time) variation results in markedly different block speeds when minimum fuel, minimum time, minimum DOC and maximum P-ROI are compared for fixed sector distances with given mission criteria[162]. These concepts, in part or collectively depending on the role of the vehicle, are integral for gauging the merits of new conceptual designs since they quantify operational flexibility. All operational aspects are considered in terms of potential objective functions that might exhibit dependence to flight technique. The merit of any given flight technique can be weighed from a proposal's block time-fuel curve summary. These curves represent for a given sector distance and mission criteria thresholds for minimum time as well as fuel, and, intermediate flight techniques yielding height-energy block fuel minima for fixed block times between these two extremes. Figure 61 shows a schematic interpretation of the typical block time-fuel summary.

12.1 Formulation of Models Adhering to a Continuous Function Concept

Since the block time-fuel summary is made up of a collection of different flight techniques, i.e. combinations of distinct climb, cruise and descent modes at specific flight level(s), the curve geometry is constructed through a combination of quasi-discrete and discrete points. The quasi-discrete portion of the curve is usually generated by a sole flight technique, commonly of highest speed schedule for climb, cruise and descent, in which flight level varies from the optimum altitude (unconstrained SAR maximum - SAR optimum) or service ceiling (constrained SAR maximum) to lower altitudes until the

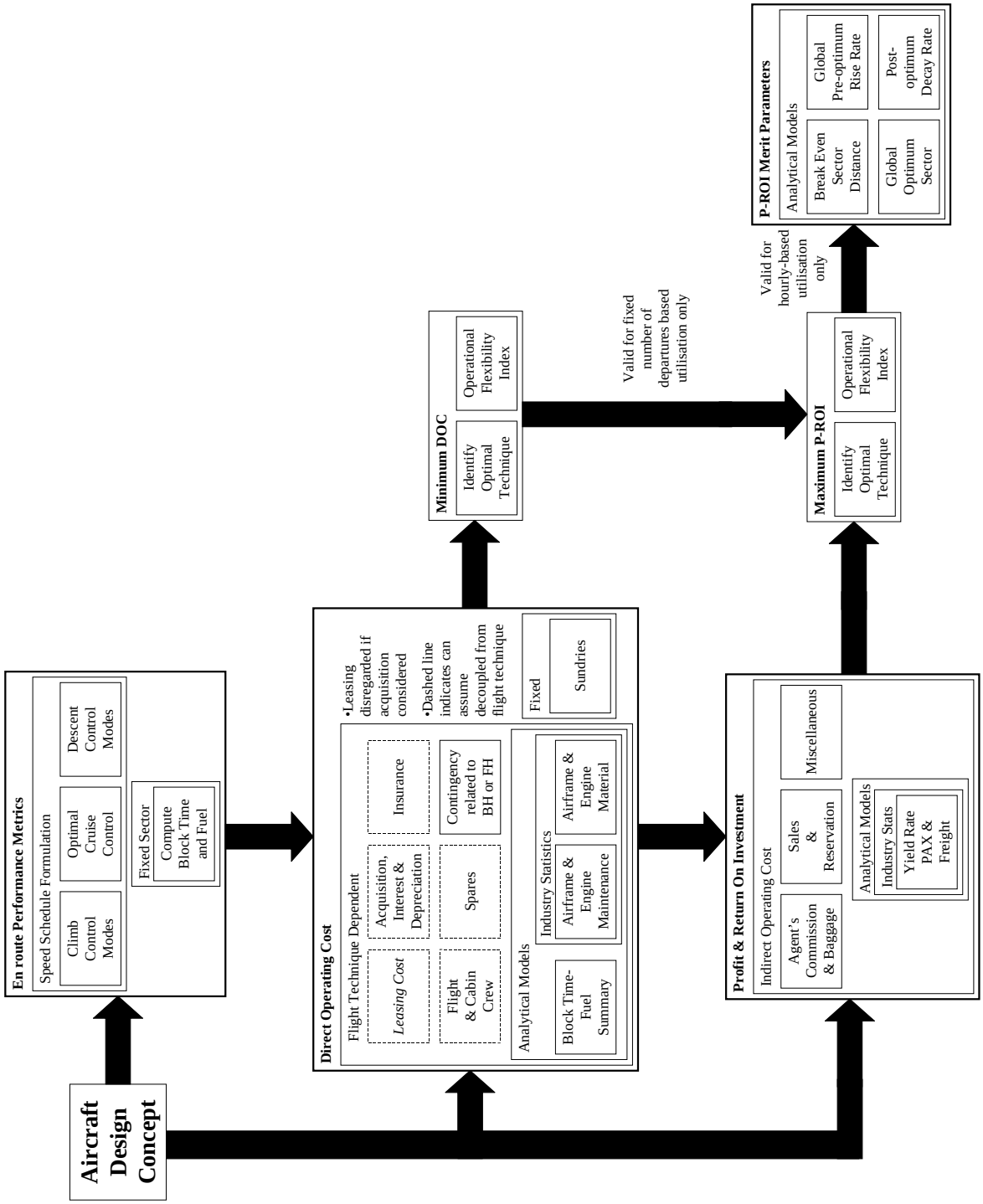

Figure 60. DOC and P-ROI computation and identification of corresponding optimal flight techniques procedure flowchart.

minimum time threshold is reached. The discrete points usually consist of intermediate to low climb and descent modes combined with intermediate to LRC and MRC speeds at optimal altitude or service ceiling. In addition, it should be noted, assuming the margin to buffet is not violated, instances might arise where the en route specific excess power is sufficient enough to employ step cruise procedures. This aspect of performance is very

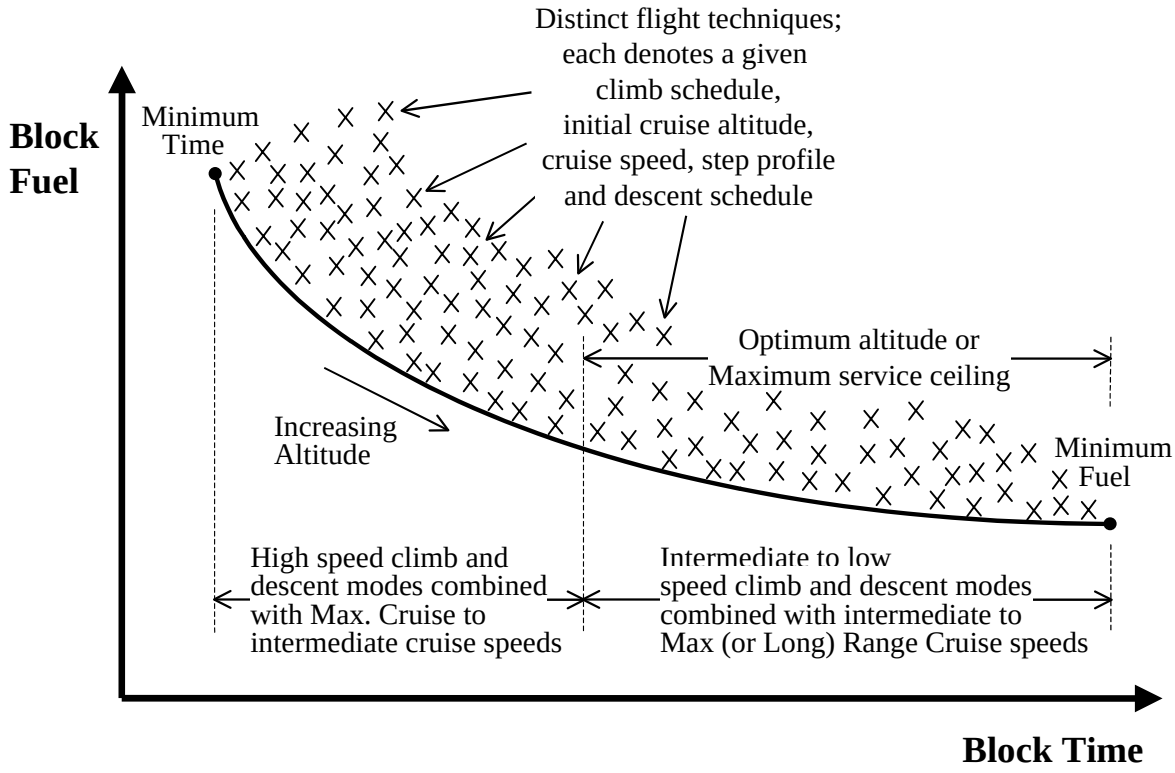

Figure 61. Typical block time-fuel summary for a given sector distance and mission.

difficult to predict with simplified expressions coupled to a general set of aircraft parameters, so as a consequence, is reliant upon batch calculations and comparison until a collection of points describing a distinct lower boundary is established.

It is evident the block time-fuel summary is rather complex and cannot be easily represented by an analytical expression which produces a continuous function with respect to block time. The failure of this option implies that another philosophy may be required to achieve the task. A hyperbolic function appears well suited to the curve definition exercise and a suggested model in the closed block time interval $[t_{mintime},t_{minfuel}]$ is presented here as

$$W_{fuel} = W_{f,min\,time}\left(1-k_1\right)\tanh\left[k_2\left(t_{min\,time}-t\right)\right] - W_{f,min\,fuel}\left(1-k_3\right)\tanh\left[k_4\left(t_{min\,fuel}-t\right)\right] + k_5 \tag{289}$$

where W_{fuel} is the block fuel for given block time, t, in the closed interval $[t_{mintime},t_{minfuel}]$, $W_{f,mintime}$ the block fuel for a minimum time flight technique, k_1 and k_2 constants which allow for the impact of different higher speed technique attributes to assorted combinations of intermediate schedules, $W_{f,minfuel}$ the block fuel for a minimum fuel flight technique, k_3 and k_4 constants which allow for the impact of different lower speed technique attributes to assorted combinations of intermediate schedules, and k_5 is an arbitrary constant. The suitability of Eq. (289) hinges on the ability of the function being differentiable, and thus giving scope for the identification of optimal flight techniques.

In order to facilitate the continuous function concept, two additional sets of models have been introduced. The first relates to maintenance cost, which itself must be partitioned into two tiers of dependency. Maintenance cost for systems that encompass air conditioning, auto flight, communications, electrical power, flight controls, fuel, hydraulic

power, instruments, lights, navigation, oxygen, nacelles and pylons, and windows were found dominated by proportionality with time. In contrast, equally split time-cyclic dependency and predominately cyclic maintenance cost constituents were associated with systems covering equipment and furnishings, ice and rain protection, landing gear, pneumatics, water and waste, APU, doors, fuselage, stabilisers and wings. One generally accepted approach involves the correlation of maintenance cost to average segment flight time for given sector distance; the flight hour cost should then be some function of flight time for a given mission, whereas, the associated cyclic cost should be considered as some proportion of the flight hour cost[163,164]. This deduction is based on the premise that influences of skill level, shop efficiency and learning curve would impart a significant contribution to both the time dependent and cyclic costs[164]. In view of these concepts, a maintenance-materiel cost model for the sample closed interval $[t_o,t_n]$ was derived to be

$$C_{MAIN} = c^{I}_{main}\, t + c^{II}_{main} \tag{290}$$

where

$$c^{I}_{main} = \left(c_{main} + \frac{\alpha_{main}}{t\left(t - t_{man}\right)^{(\beta_{main}-1)}} \right) \left(1 + k_{main}\right) \tag{291}$$

and

$$c^{II}_{main} = -c_{main} \left(1 + k_{main}\right) t_{man} \tag{292}$$

C_{MAIN} is the total maintenance cost, c_{main} is the flight time dependent maintenance cost denoting theoretically most efficient work practise or learning curve asymptote, α_{main} and β_{main} are constants of proportionality, t_{man} is the manoeuvre allowance (includes start-up, taxi-out and taxi-in) and k_{main} is a constant depicting the fraction of cyclic to time dependent costs. The second model relates to yield, which indicates a measure of ticket prices. For an assumed passenger load factor, λ, and sector distance, s, upon formulation of a feasible yield rate model, the total revenue per flight (Y_{SEC}) is proposed as

$$Y_{SEC} = y_1\, \lambda\, PAX\, s \left(1 + y_2\, \tanh\left[y_3 \left(s_{ref} - s\right)\right]\right) \tag{293}$$

where PAX is the maximum passenger capacity of the aircraft, s_{ref} is the reference stage length and y_n are constants of proportionality. Combined with the other standard cost methodologies available in literature[165], identification of cost minima and profit maxima coupled to variation of flight technique or block time can be ensured.

12.2 Solving for Optimal Flight Techniques

It is evident that any identified optimal flight technique will fall into one of two distinct categories: applicability for hourly-based reference time frame or fixed departures based utilisation. For a given reference time frame utilisation, optimum flight techniques were found to be governed by the conditions

$$\frac{dC_{DOCS}}{dt} = 0 \qquad \text{Min. DOC, hourly and fixed departures based utilisation} \tag{294}$$

$$\frac{dP}{dt} = \left(\frac{dP}{dN_S}\right)\left(\frac{dN_S}{dt}\right) \equiv \frac{dC_{DOCS}}{dt} = 0 \qquad \text{Max. P-ROI assuming fixed departures} \tag{295}$$

or

$$\left(\frac{\partial P}{\partial N_S}\right)_s = \left(\frac{\partial P}{\partial t}\right)_s \left(\frac{\partial t}{\partial N_S}\right)_s = 0 \qquad \text{Max. P-ROI, hourly based utilisation} \tag{296}$$

where C_{DOCS} is the DOC per sector mission, N_S is the number of sectors completed per given reference time frame and P is the P-ROI per sector mission or time frame. Both DOC and P-ROI optimal flight techniques can be categorised as constrained or unconstrained.

These conditions of optimality can be expressed algebraically as a more recognisable and tangible quantity, such as block time, in order to permit identification of the required climb, cruise and descent flight technique for optimality. Interestingly, the algorithm structures that solve for minimum DOC and maximum P-ROI block times ($t_{min\text{-}max}$) were found to be quite similar

$$t_{min-max} = t_{min\,time} + \frac{1}{k_2}\cosh^{-1}\sqrt{\frac{p_f\, W_{f,min\,time}\left(1-k_1\right) k_2}{\varpi}} \tag{297}$$

The only difference in Eq. (297) for minimum DOC and maximum P-ROI amounts to adoption of an alternate definition to what constitutes the residual function ϖ in the denominator. The optimal block time algorithm is given by a transcendental equation and can be solved numerically via simple iteration. Provided the inverse hyperbolic cosine function in Eq. (297) does not carry out operations on results less than unity (otherwise implies an unconstrained optimum) the hyperbolic function always aids in achieving quick convergence and the iterative scheme is inherently stable.

12.3 Operational Flexibility Index

One important requirement is to develop a useful tool in qualitatively assessing any penchant an aircraft has to flying faster in achieving economically optimal results. A parameter such as Cost Index[163,164] (CI) commonly used in operational circles does not imbue the analyst or designer with a true perspective of a given vehicle's operational flexibility, and also, a computed value of CI is not universally comparable between aircraft of varying scale and propulsion philosophy. One suggestion is to inspect the non-dimensional ratio of optimal block time against the minimum fuel and minimum time flight technique block time bandwidth. Since Eq. (297) is algorithm solving for optimal block time referenced to minimum time, a possibility now arises in the formulation of an OFI

$$OFI = \frac{\cosh^{-1}\sqrt{\frac{p_f\, W_{f,\min\,time}\,(1-k_1)k_2}{\varpi}}}{k_2\left(t_{\min\,fuel} - t_{\min\,time}\right)} \tag{298}$$

It is evident that a limitation arises due to the inverse hyperbolic cosine function; such an occurrence signifies that the optimal flight technique corresponds to minimum time flight, and can thus be considered equivalent to OFI = 0. In order to appreciate the extent of operational flexibility contemporary vehicles offer, typical values of OFI for various aircraft, economic objective function and utilisation assumptions are itemised below:

- DOC and P-ROI optimal hourly-based utilisation – OFI ≤ 0.15 for regional aircraft, and, OFI ≅ 0.75 for narrow and wide-bodies.
- DOC and P-ROI optimal fixed departures utilisation – OFI ≅ 0.20 for regional aircraft, and, OFI ≅ 0.90 for narrow and wide-bodies.

A design condition OFI value approaching zero denotes little or no scope for flexibility since it is congruous with minimum time flight techniques. Not only does this condition usually deny the possibility of achieving unconstrained optima, but also, implicitly dictates that all shorter-range operations will follow suit. Additionally, this circumstance is seen to be detrimental since the criterion of a higher engine rating flight technique may reduce the service life of the power plant. It does however, allow for longer-range mission capability without trading payload for fuel, but at an ever-increasing penalty of off-optimality as distance becomes longer. A maximum value of OFI = 1.00 at the design condition, akin to a minimum fuel technique, affords limited range of operational flexibility on the other end of the spectrum. Even though scope is given for the generation of unconstrained optima flight techniques for shorter sector distances, useful load limitations may not permit the opportunity of longer-range missions for a given payload. This would necessitate an exchange of payload for increased range thereby limiting the potential for revenue. A salient objective would be a design OFI = 0.50 for any prospective aircraft evaluation exercise. This will ensure avoidance of premature useful load limitations for longer sector distances, and importantly increase the likelihood of unconstrained optima for shorter distances. Finally, the penalties associated with off-optimal flight techniques commonly experienced in actual operation can be minimised.

12.4 An Alternative to the Traditional Long Range Cruise Speed Schedule Definition

Traditionally, LRC has been understood to be 99% (sometimes even 98%) of MRC SAR towards the faster end of the curve[3,38,136,142]. This practise is employed to trade increased speed capability for what is considered to be a relatively small penalty in fuel consumption rate. Indeed, after the inception of this rule-of-thumb procedure for en route performance analysis, it has now become a mainstay technique in industry circles. Of great interest here was to observe how this popular assumption measures up against speed technique formulation using economic criteria alone.

Initially, an objective function for what constitutes economical cruise must be formulated. One candidate is to use a fixed departures utilisation assumption. Not only is this a consistent basis of emulating actual operator scheduling, but also as outlined before, this premise theoretically generates optimal flight techniques slower than an hourly-based

utilisation. Even though CI represents a necessary magnitude of dW_{fuel} / dt that ensures cost optimality for any sector mission criteria, an approximate expression explicitly related to cruise speed and SAR can also be derived. Assuming a cruise fraction that is sufficiently large, thus neglecting the influence of climb and descent, it can be demonstrated[38] that

$$CI = \left|\frac{dW_{fuel}}{dt}\right| \approx \left| a_{sls}\, \theta^{1/2} \left(\frac{M}{SAR}\right)^2 \frac{dSAR}{dM} \right| \tag{299}$$

Figure 62 shows the degradation of SAR compared to the MRC datum for regional, narrow-body and wide-body twins using computed CIs of 10, 25 and 40 (such speed techniques are henceforth dubbed as Economical Long Range Cruise or ELRC) respectively. These values were based on a projected fuel price and known operator time dependent maintenance cost data. Note that a standard representation of CI assumes a value normalised by 100 lb/hr[163,164]. Upon comparison to a 1% reference line denoting the contemporary LRC assumption, it is observable that a large disparity between LRC and ELRC takes place. It is immediately evident that the SAR curve is quite flat for lower flight levels promoting even larger deviations from the conventional 1% degradation. However, for narrow and wide-bodies at typical cruise altitudes in excess of 29,000 ft where optimal cruise begins and subsequently does reside in the drag rise region, ELRC dictates speed schedules around 99.5% maximum SAR. Regional aircraft appear to reach a constant value of 97% maximum SAR at higher altitudes, and this is attributable to the fact drag rise effects are generally not prevalent.

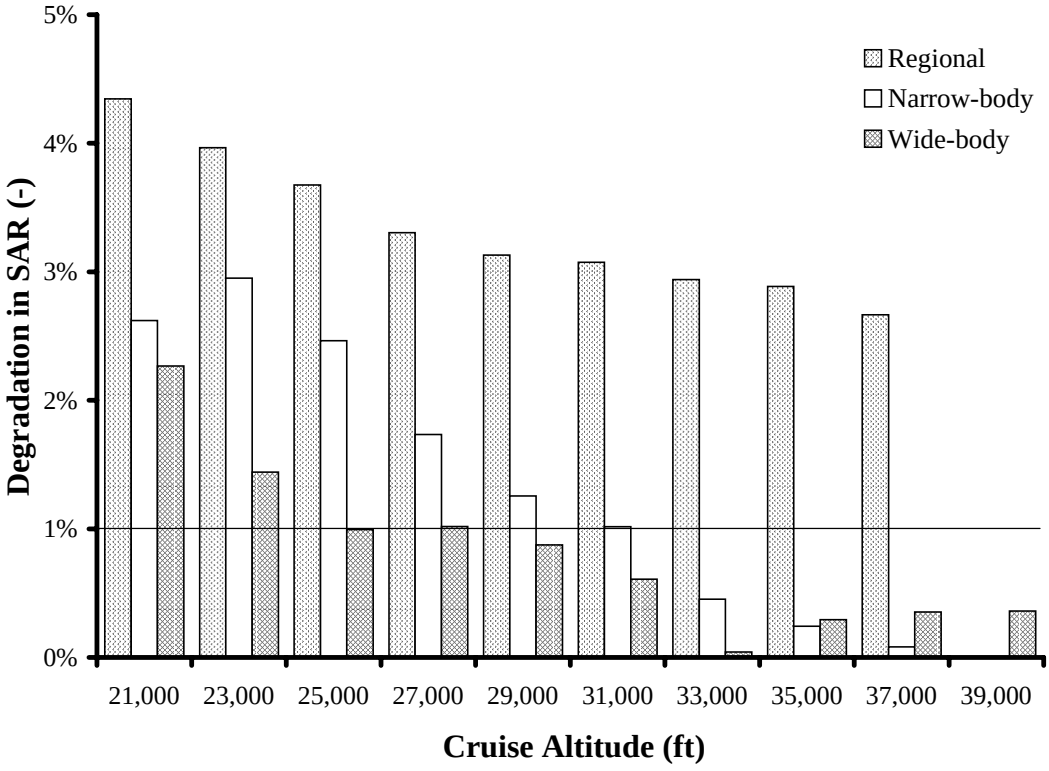

Figure 62. Degradation in SAR assuming traditional LRC (1% reference line) and ELRC compared to datum of MRC (fixed AUW, ISA, still air).

Upon perusal of Figure 62, for both twin narrow-body and wide-body equipment types, adopting the slower ELRC schedule as opposed to LRC amounts to almost a 1% integrated mission flight fuel reduction because the technique is closer to an optimal SAR condition. Correspondingly, the difference between LRC and ELRC equates to a speed reduction of approximately 5 KTAS at typical flight plan altitudes. Today, there exists a capacity for operators to soak the slight increase in flight time due to a slower speed – especially now that scheduled block times have been widened in order to improve on-time dependability and fuel prices are on the rise. For occasions where block times must be reduced due to sake of dependability, the ELRC method is congruous with a Flight Planning System (FPS) increased block speed iteration scheme since the starting point is slightly slower than traditional LRC in any case. In spite of the speed margin to MRC being rationalised upon application of an ELRC schedule for narrow and wide-bodies, the buffer is still greater than 5 KCAS. This is a margin commonly assumed for contemporary Flight Management Computer (FMC) en route operational software, and from an operational perspective the margin is not deemed prohibitive in terms of speed stability (excursions due to wind shift, turbulence, etc.) in maintaining the target level.

12.5 Merit Functions to Measure Relative Profit and Return On Investment

An interesting feature of the derivation for optimal P-ROI block times assuming hourly-based reference time frame utilisation is that these solutions are partial optima due to a co-dependence on block time and quantity of available seat-miles completed by the vehicle. Even though the hourly-based reference time frame utilisation can be considered idealistic compared to the more pragmatic assumption of a fixed number of sectors, it can provide valuable insight. One important conclusion is that the comparison of different equipment types for only one fixed sector is not a sound enough basis to rationalise the superiority of an aircraft over another. A practical application would be use of this approach as a work tool that aids in maximising utilisation of a given vehicle for existing markets. Another is the possibility of showing the relative merits associated with the introduction of new projected markets involving either variations in sector distance, or mission criteria, or both. A further review potential includes the possibility of conducting detailed competitor studies where economic flexibility can be weighed between the vehicles taken into consideration.

Since it has been shown that sector distance can be regarded as an independent variable, it would be of interest to evaluate the various merits of an output P-ROI response with respect to distance. An adequate model for representing the P-ROI coverage in the closed sector distance interval $[s_o,s_n]$ is presented here as

$$P = \left(\Phi_\alpha\, s - \Phi_\beta\right) e^{-\left(\Phi_\chi + \Phi_\delta\, s\right)} + \Phi_\varepsilon \tag{300}$$

The equation coefficients represent quantities that enable a possibility of evaluating the properties of a vehicle's flexibility in earning potential through a geometric interpretation. If the model given by Eq. (300) is actually taken into consideration as an open interval, say, $[s_{be}, \infty)$, or from break-even sector distance and upwards, one can identify uncanny similarities to a typical step response of stable linear control systems (see Figure 63) - in this particular instance, the reference input being sector distance and P-ROI the output. It contains a transient response due to sector distance which also includes tendency to approach an asymptote as sector distance becomes large and exceeds distances

constrained by useful load limitations (akin to steady state), and, a lower threshold where break-even occurs, or zero P-ROI at some sector distance value. Typical performance criteria can be formulated which characterises the transient response. These are proposed here as: break-even sector distance and corresponding pre-optimum P-ROI rise rate, the global P-ROI optimum and corresponding sector distance, measure of the post-optimum P-ROI decay rate and the magnitude of the model asymptote value. This can be achieved mostly through inspection of the first and second derivatives of Eq. (300).

The break-even sector distance is defined as the sector distance that creates a condition where the P-ROI is zero. Eq. (300) is in a form where an exact formula for solving P(s) = 0 is not available. By employing a suitable initial estimate, i.e. $s_i = s_o$, utilising Eq. (300) and corresponding first derivative in consort with Newton-Raphson produces

$$s_{be} = s_i - \frac{\Phi_\alpha s_i - \Phi_\beta + \Phi_\varepsilon e^{(\Phi_\chi + \Phi_\delta s_i)}}{\Phi_\alpha - \Phi_\delta (\Phi_\alpha s_i - \Phi_\beta)} \tag{301}$$

and the main criterion here is the break-even sector distance, s_{be}, should be minimised.

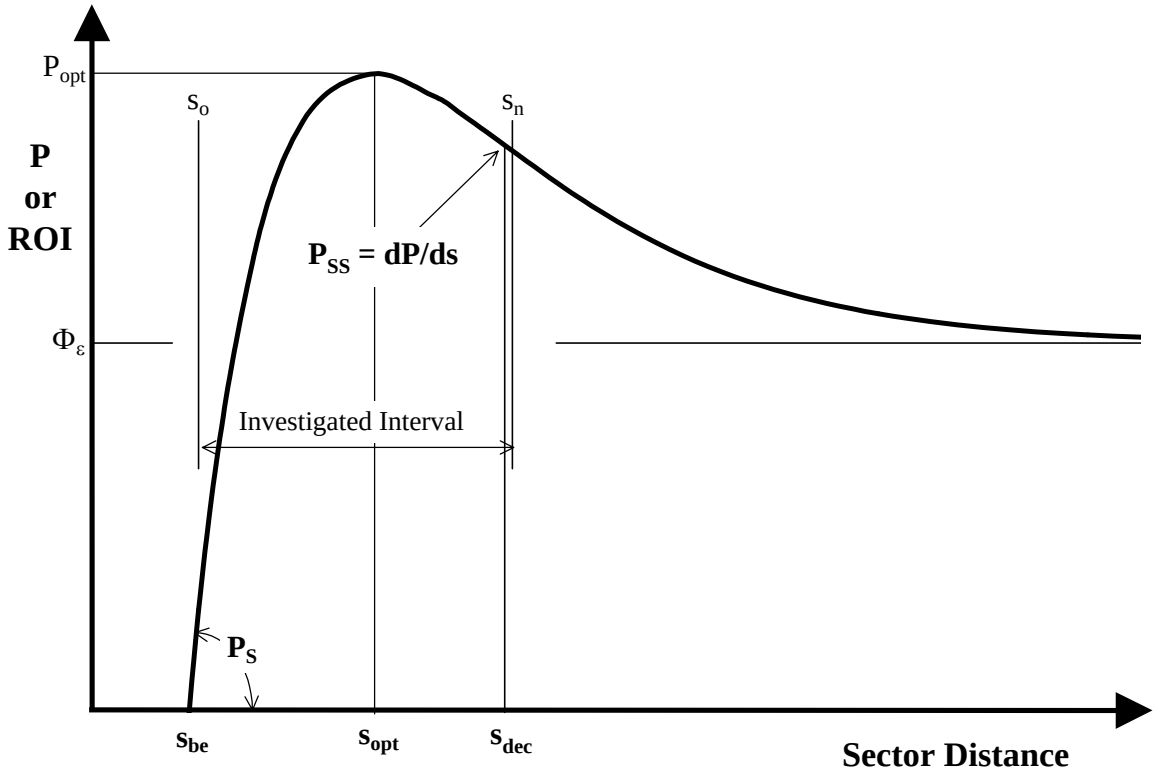

Figure 63. Typical sector distance response of P-ROI model assuming an hourly-based reference time frame utilisation.

P-ROI increases with greater sector distance for sector distances larger than break-even. The reciprocal of the rate P-ROI increase with respect to sector distance would give a measure of what increment in sector distance achieves a target increase in P-ROI before the global maximum threshold is crossed. An adequate representation of the pre-optimum P-ROI rise rate may be given by the instantaneous slope at the break-even sector distance via the definition found in Eq. (301)

$$P_S = \left[\left. \frac{dP}{ds} \right|_{s_{be}} \right]^{-1} = \frac{e^{\left(\Phi_\chi + \Phi_\delta s_{be}\right)}}{\Phi_\alpha - \Phi_\delta \left(\Phi_\alpha s_{be} - \Phi_\beta\right)} \tag{302}$$

P_S is a parameter expressed as distance covered per unit P-ROI and should be minimised.

Yet another fundamental observation that can be extracted from Eq. (300) is the identification of sector distances that yield global P-ROI maxima (P_{opt}). The distance where a P- ROI global optimum occurs is given by the first derivative of Eq. (300), hence

$$s_{opt} = \frac{\Phi_\beta}{\Phi_\alpha} + \frac{1}{\Phi_\delta} \tag{303}$$

Having s_{opt} as low as possible whilst simultaneously maximising P_{opt} would be the primary goal of any prospective vehicle or design proposal.

It is evident to see that P-ROI decreases with increasing sector distance once the P-ROI global optimum sector distance has been surpassed. The rate reduction in P-ROI with respect to sector distance conducted at the inflection point between the post-optimum transient and steady state responses is proposed here as a useful merit parameter. By utilising the second derivative of Eq. (300) and solving for sector distance at this inflection point

$$s_{dec} = \frac{\Phi_\beta}{\Phi_\alpha} + \frac{2}{\Phi_\delta} \tag{304}$$

and hence, the post-optimum decay rate is given by slope of the sector distance response

$$P_{SS} = \left. \frac{dP}{ds} \right|_{s_{dec}} = -\Phi_\alpha \exp\left(-\Phi_\chi - \frac{\Phi_\beta \Phi_\delta}{\Phi_\alpha} - 2 \right) \tag{305}$$

P_{SS} is a quantity that is always negative, therefore, it should be maximised in order to reduce the potential P-ROI loss rate per unit distance flown.

13 A Survey of Constrained Multi-objective Optimisation Methods

The purpose of any automated design software is to apply sizing algorithms to optimise the vehicular design towards one that satisfies the user-specified objectives. The traditional approach, particularly in industry, to conceptual design problems is to conduct simplified MVO exercises and then compare the collective outcome each set of design parameters has produced, such as MTOW or where sufficient sophistication is available DOCs. There is however, an inherent limitation to this process and as such are encountered easily, let alone addressing the question of conducting hyper-dimensional aircraft design problems, or X = {x(1),…,x(n)} where n > 20. The scope for this particular investigation was to take an inventory of optimisation methods and analytical tools and assemble those components showing the best attributes into a package. The primary considerations included a strong resilience to frequently settling in local minima and maximising the execution speed.

The increasing requirement for complexity of the aircraft system definition at the conceptual design phase has created extensive interest in MDO[166-168]. MDO is described as a methodology for the design of systems where the interaction between several disciplines must be considered, and where the designer can exercise a freedom to significantly affect the system performance in more than one discipline[169]. In the context of the aircraft conceptual design problem one example could be the active alteration of wing planform, in terms of not only a parametric sense but of tangible design variables like t/c, thus concurrently working with aerodynamic qualities and fuel volume in an effort to deliver a target level of performance. The MDO procedure is intended to work at the conceptual level by employing simple analysis tools and because of the simplicity of these tools, it is possible to integrate the various disciplinary analyses into a modular computer program and avoid tapping into an inordinate amount of computational resources accordingly.

13.1 Fundamentals of Multi-disciplinary Design Optimisation

Basically, the generalised MDO task can be condensed mathematically in the following manner:

Find a set of design variables, X, which will minimise

$$F(X) \tag{306}$$

which is subject to

$$g_j(X) \leq 0 \tag{307}$$

and

$$X_l(k) \leq X(k) \leq X_u(k) \tag{308}$$

for j = 1, …, n_{con} and k = 1, …, n_{dv}. The parameter, g, specifies the n_{con} inequality constraints. $X_l(k)$ and $X_u(k)$ refer to lower and upper bounds (side constraints) applied to each of the design variables respectively, and they are used to limit the region of search for the optimum.

In defining a formal optimisation problem, an objective function must be specified that is to be minimised for a design. When a point is reached such that no further decrease in the objective function can be obtained, the process is terminated.

Extending this simple basis to that of constrained multi-objective optimisation, the problem now is to minimise

$$F_i(X) \tag{309}$$

for $i = 1, \ldots, n_{fn}$ number of objectives subject to a series of constraints given by

$$g_j(X) \leq 0$$

as defined by Eq. (307). The entire design problem is linked to a set of design variables, such that each independent parameter is uniquely restricted to a set of side constraints, namely,

$$X_l(k) \leq X(k) \leq X_u(k)$$

for n_{dv} number of design variables. Since most of the methodologies available for optimisation analysis do not permit definition of constraints and side constraints formally in the mathematical construct, the fundamental goal here is to somehow condense all of these requirements and then transform it into a problem whereby a scalar-value function is minimised in order to arrive at the minimised form of the original objective vector[167].

13.1.1 Design Variables

Linear design variables denote a combination of local design variables and elemental properties that yield a factorable, linear relationship among the design variables and the elemental matrices. For a conceptual aircraft design problem, the design variables are generally considered to be non-linear, i.e. a combination of design variables and elemental properties does not yield a factorable relationship among the design variables and elemental matrices. This assumption can prove to be an added complexity for gradient based optimisation methods because mo analytical gradient matrices would be readily available and compel the use of finite difference methods to approximate the first derivative. This means that global sensitivity matrices need to be recomputed at each new design point as well. The ultimate goal should be to select a set of design variables that result in the least amount of parameters (to speed up convergence) and minimises the amount of complications with respect to the objective function topographies[22].

13.1.2 Constraints

Inequality constraints are applicable to either individual design variables, intermediary functional values called synthetic functions and objective functions dependent upon a given set of design variables. Typically, only a small number of constraints will affect the final design and it is necessary to exploit this fact to reduce the mathematical operation task and the effort required to compute constraint sensitivities. The basic concept is to retain only those constraints for the design task that are presupposed to play an active role in the design process. As a result, the selection of these critical constraints requires an element of subjective decision-making to build a consistent strategy in identifying the optimum.

13.1.3 Synthetic Functions

Synthetic functions can assume the role of either an objective function or constraint function during the course of optimisation. They are formed as mathematical combinations of analytical response, model characteristics or parametric representations. Examples of such functions can be lift-to-drag ratio, block SAR for a given sector mission scenario, initial cruise altitude, etc.

13.2 Selecting Optimisers Appropriate for the Conceptual Aircraft Design Problem

There are a number of key requirements candidate optimisers must meet in order to be incorporated into a dedicated MDO framework for conceptual design. The foremost requirement is the optimiser must be robust in the sense global minima of each objective function are consistently identified. The next important attribute is a question of computational time – an excessive amount of time is not desirable, especially within the context of a pre-design or highly simplified conceptual study. The final stipulation is ability for the optimiser to handle hyper-dimensional parameter spaces. Although the third requirement had been formally defined, it was considered more of a soft specification as opposed to the hard specifications imposed by the first and second requirements. Notwithstanding, the third specification minimum goal can also be interpreted as at least having the ability of handling optimisation problems spanning up to the hyper-dimensional design space. With regards to these criteria, a number of optimisers were reviewed. The final selection process involved examination of a comprehensive survey conducted by Van der Velden[19].

In Van der Velden's study, three groups of optimisation methods were investigated: evolution, downhill Simplex and gradient methods. Choosing the best candidates involved comparison of predefined array of merit functions specially formulated for the study. One metric supposed to represent speed was defined as the number of function calls required to find a global minimum plus time spent and lost by the designer restarting the algorithm when it becomes trapped in a local minimum. The other merit function describes robustness as the mean harmonic error of the most optimum objective normalised by the local optimum for a set of 24 randomly chosen start vectors.

A salient conclusion was the very fact it was deemed unwise to select any one of the methods as the "optimum optimiser" even though the kick-Simplex demonstrated reliability for so-called "rough" objective function topographies. In the end, only the evolution and the kick-Simplex methods proved to be reliable enough for application to MDO conceptual aircraft design problems. Van der Velden then proceeded to recommend the notion of "cocktails" or combinations of optimisers would be the most robust means of tackling the MDO problem.

One rapidly converging and robust strategy was cited as commencing the exercise with an evolution method, and then strategically switching over to a kick-Simplex algorithm towards the end of the process. It was further recommended that to estimate an optimal sequencing of optimisers and number steps per optimiser, each optimiser could be run in isolation, and thus allow one to determine an optimal sequence by identifying most rapid convergence for a given optimisation phase. It is fortunate that both the evolution-based and Simplex optimisers are available through OPTIM, an Optimisation Toolbox in the MATLAB computing environment, and two such working examples will be briefly reviewed here.

13.2.1 Evolutionary Computing – "GAOTv5" in MATLAB

Evolutionary computing comprises several methods for exploring solution spaces probabilistically based on the principles of natural evolution. Computer codes that embody this approach to searching for the optimum are called GA. The use of GA requires the determination of six fundamental issues:

1. chromosomes
2. selection function;
3. genetic operators making up the reproduction;
4. the creation of an initial population;
5. termination criteria; and,
6. the evaluation function.

GA begin with a random selection of chromosome strings and each chromosome string consists of numbers, or, in the context of an aircraft design problem, the array of independent variables. First, each chromosome in the population is tested for fitness. The fitness is simply how well the alleles in the chromosome solve the problem. A portion of the population is selected on a purely random basis. The only distinction is that the more a chromosome is fit, the more likely it is to be chosen. The selected chromosomes are then reproduced and each chromosome that is reproduced stands a small but finite chance of being mutated. After reproduction, a second probabilistic selection takes place. This set of chromosomes undergoes the process of crossover or exchange of genes. Finally, the population is culled back to a target population size. Here again the selection process is probabilistic with the fittest chromosomes standing a better chance of survival. The end result is a more fit population and a single chromosome providing a better solution than at the start. A more complete discussion of GA, including extensions and related topics can be found in texts authored by Davis[171], Goldberg[172], Holland[173] and Michalewicz[174]. GA display many distinct advantages. They are beneficial for instances where the coefficients need to be generated for a large number of variables and are applicable to a wide range of problems. A major disadvantage hinges on the fact that GA find near optimal solutions, which calls for additional tweaking of the model if the true global optimum is to be identified.

The evaluation function is called from the GA to determine the fitness of each solution string generated during the search. An evaluation function is unique to the optimisation of the problem at hand therefore, every time the GA is used for a different problem, an evaluation function must be developed to determine the fitness of the individuals. For any GA, a chromosome representation is needed to describe each individual in the population of interest. The representation scheme determines how the problem is structured in the GA and also determines the genetic operators that are used. Each individual or chromosome is made up of a sequence of genes from a certain alphabet. An alphabet could consist of binary digits (0 and 1), floating point numbers, integers, symbols (i.e., A, B, C, D), matrices, etc. One useful representation of an individual or chromosome for function optimisation involves genes or variables from an alphabet of floating point numbers with values within the variables upper and lower bounds. Michalewicz[174] has done extensive experimentation comparing real-valued and binary GAs and shows that the real-valued GA is an order of magnitude more efficient in terms of CPU time.

The selection of individuals to produce successive generations plays an extremely important role in a GA. A probabilistic selection is performed based upon the individual's fitness such that the better individuals have an increased chance of being selected. An

individual in the population can be selected more than once with all individuals in the population having a chance of being selected to reproduce into the next generation. There are several schemes for the selection process: roulette wheel selection and its extensions, scaling techniques, tournament, elitist models, and ranking methods[172,174].

Genetic operators provide the basic search mechanism of the GA. The operators are used to create new solutions based on existing solutions in the population. There are two basic types of operators: crossover and mutation. Crossover takes two individuals and produces two new individuals while mutation alters one individual to produce a single new solution. The application of these two basic types of operators and their derivatives depends on the chromosome representation used.

A GA capable of either using a floating point representation or a binary representation has been implemented as a MATLAB toolbox[175]. This toolbox provides a modular, extensible, portable algorithm in an environment rich in mathematical capabilities. The toolbox has been tested on a series of non-linear, non-convex, multi-modal functions. The algorithm has been implemented as a group of related MATLAB functions, named "GAOT", or Genetic Algorithms for Optimization Toolbox. This provides for easy extensibility, as well as modularity. The basic function is the GA function, which runs the simulated evolution. The program has been run successfully on a DecStation 3100, a DecStation 5000/25, Motorolla 604 and an HP 715.

The basic call to the GA function is given by the following MATLAB command

```
[x,endPop,bPop,traceInfo] = ga(bounds,evalFN,evalParams,params,...
                            startPop,termFN,termParams,selectFN,...
                            selectParams,xOverFNs,xOverParams,...
                            mutFNs,mutParams)
```

x is the best solution string, i.e. final solution, **endPop** (optional) is the final population, **bPop** (optional) is a matrix of the best individuals and the corresponding generation they were found, **traceInfo** (optional) is a matrix of maximum and mean functional value of the population for each generation. For the input parameters, **bounds** is a matrix of upper and lower bounds on the variables, **evalFN** is the evaluation function, **evalParams** (optional) is a row matrix of any parameters to the evaluation function defaults to [NULL], **params** (optional) is a vector of options, e.g. whether a binary or float version of the algorithm is to be employed, **startPop** (optional) is a matrix of solutions and their respective functional values. The starting population defaults to a randomly created population created with initialize, **termFN** (optional) is the name of the termination function which defaults to ['maxGenTerm'], **termParams** (optional) is a row matrix of parameters which defaults to [100], **selectFN** (optional) is the name of the selection function which defaults to ['normGeomSelect'], **selectParams** (optional) is a row matrix of parameters for the selection function which defaults to [0.08], **xOverFNs** (optional) is a blank separated string of the names of the cross-over functions which defaults to ['arithXover heuristicXover simpleXover'] for the float version and ['simpleXover] for the binary version. **XOverParams** (optional) is a matrix of the crossover parameters which default to [2 0;2 3;2 0] for the float version and [0.6] for the binary, **mutFNs** (optional) is a blank separated string of mutation operators which default to ['boundaryMutation multiNonUnifMutation nonUnifMutation unifMutation'] for the float version and ['binaryMutation'] for the binary version. **mutParams** (optional) is a matrix of mutation parameters which defaults to [4 0;6 100 3;4 100 3;4 0] for the float version and [0.05] for the binary.

GA performs the simulated evolution using the evalFN to determine the fitness of the solution strings. The GA uses the operators xOverFNs and mutFNs to alter the solution strings during the search.

The system maintains a high degree of modularity and flexibility as a result of the decision to pass the selection, evaluation and termination functions to the GA as well as a list of genetic operators. Thus, the base GA is able to perform evolution using any combination of selection, crossover, mutation, evaluation and termination functions that conform to the functional specifications as outlined below or can easily be used with the default parameters.

Operator Functions – Operators provide the search mechanism of the GA. The operators are used to create new solutions based on existing solutions in the population. There are two basic types of operators, crossover and mutation. Crossover takes two individuals and produces two new individuals while mutation alters one individual to produce a single new solution. The GA function calls each of the operators to produce new solutions. The function call for crossovers is as follows

```
[c1,c2] = crossover(p1,p2,bounds,params)
```

where **p1** is the first parent, **p2** is the second parent, **bounds** is the bounds matrix for the solution space and **params** is the vector of [current generation, operatorParams], where **operatorParams** is the appropriate row of parameters for this crossover/mutation operator. The first value of the operatorParams is frequency of application of this operator.

The mutation function call is similar, but only takes one parent and returns one child

```
[c1] = mutation(p1,bounds,params)
```

The crossover operator must take all four arguments, the two parents, the bounds of the search space, the information on how much of the evolution has taken place and any other special options required. The following GA for function optimisation operators are defined: uniform mutation, non-uniform mutation, multi-non-uniform mutation, boundary mutation, simple crossover, arithmetic crossover, and heuristic crossover. Uniform mutation randomly selects one variable and sets it equal to a uniform random number. Boundary mutation randomly selects one variable and sets it equal to either its lower or upper bound. Non-uniform mutation randomly selects one variable and sets it equal to a non-uniform random number. The multi-non-uniform mutation operator applies the non-uniform operator to all of the variables in the parent. Arithmetic crossover produces two complimentary linear combinations of the parents, Heuristic crossover produces a linear extrapolation of the two individuals and this is the only operator that utilizes fitness information.

Selection Function – The selection function determines which of the individuals will survive and continue on to the next generation. The GA function calls the selection function for each generation after all the new children have been evaluated to create the new population from the old one. The basic function call used in GA for selection is

```
[newPop] = selectFunction(oldPop,options)
```

where **newPop** is the new population selected, **oldPop** is the current population, and options is a vector for any other optional parameters such as Roulette Wheel, Normalized Geometric Select or Tournament.

Initialisation and Termination Functions – Initialisation of a population provides the GA a starting point and this is usually accomplished by generating random strings within the search space (this is the default behavior of the GA function). However, it is possible to "seed" the initial population with individuals, or generate solutions in some other form. The GA allows for this with the optional startPop parameter, which provides the GA with an explicit starting population. The termination function determines when to stop the simulated evolution and return the resulting population. The GA function calls the termination function once every generation after the application of all the operator functions and the evaluation function for the resulting children. The function call is the format:

```
done = terminateFunction(options,bestPop,pop)
```

where **options** is a vector of termination options the first of which is always the current generation. **bestPop** is a matrix of the best individuals and the respective generation it was found. **pop** is the current population.

13.2.2 Nelder-Mead Simplex Method – "fminsearch" in MATLAB

If n is the length of X, a simplex in n-dimensional space is characterized by the n+1 distinct vectors that are its vertices. In two-space, a simplex is a triangle; in three-space, it is a pyramid. At each step of the search, a new point in or near the current simplex is generated. The function value at the new point is compared with the function's values at the vertices of the simplex and, usually, one of the vertices is replaced by the new point, giving a new simplex. This step is repeated until the diameter of the simplex is less than the specified tolerance[176]. The MATLAB function "fminsearch" is a direct search method that does not use numerical or analytic gradients. It can often handle discontinuity, particularly if it does not occur near the solution, however, fminsearch may only give local solutions.

The MATLAB command fminsearch invokes the Simplex search method and for unconstrained non-linear optimisation problems endeavours to find the minimum of a scalar function of several variables, starting at an initial estimate. A call to this function looks something like

```
[x,fval] = fminsearch(fun,x0,options)
```

x is the best solution and **fval** is the value of the objective function "fun" at the solution. Input parameters include **fun**, which represents the function (M-file in the context of this optimisation problem) that shall be minimised near the starting vector x0. The parameter fun must return a scalar function value f evaluated at x when called with **feval**

```
f = feval(fun,x)
```

The **options** parameter is defined using the **optimset** function. **Display** sets the level of output information, i.e. **off** for no ouput, **iter** to show each iteration**,** or **final** to present the final output only. **MaxFunEvals** sets the maximum allowable number of function evaluations. **MaxIter** bounds the maximum number of iterations. **TolFun** defines the termination tolerance on the function value, and **TolX** relates to the termination tolerance.

13.2.3 Running a Sample Problem using a Cocktail Combination of GAOTv5 and fminsearch

After setting up a core driver routine that permits the so-called cocktail optimisation as a MATLAB M-file, it was considered prudent to examine the core functionality by bench-testing the code against a well-known objective function that displays quite complex topological features before incorporating it into any on-going aircraft design software development project. One suitable candidate was found to be the objective function used in Van der Velden's valuation of various optimisation methods[19]. The proposed non-linear transcendental objective function is given by

$$f = 1 + \sum_{i=1}^{n} \left(A_i - B_i \right)^2$$

where

$$A_i = \sum_{j=1}^{n} \left(a_{i,j} \sin \alpha_j + b_{i,j} \cos \alpha_j \right)$$

$$B_i = \sum_{j=1}^{n} \left(a_{i,j} \sin \beta_j + b_{i,j} \cos \beta_j \right)$$

and

$$\alpha = [1.0 \quad 2.0]$$

$$a = \begin{bmatrix} 0.5 & 1.0 \\ 1.5 & 2.0 \end{bmatrix} \qquad b = \begin{bmatrix} -2.0 & -1.5 \\ -1.0 & -0.5 \end{bmatrix}$$

where β represents the free variable. It was known from the outset that a minimum value of f is reached when $\beta = \alpha$.

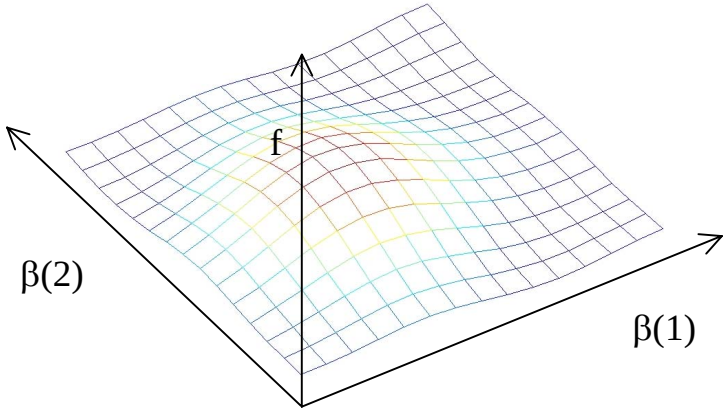

Figure 64. Objective function topography used to bench-test the MATLAB GAOTv5 and fminsearch cocktail optimiser algorithm.

Testing has found that the MATLAB algorithm produces a converged result. For the initial optimiser utilising a GA, assuming a termination operator of 100 generations, the best values for the free variables were $\beta(1) = 0.73896$ and $\beta(2) = 2.0147$ with corresponding objective function value of $f = 1.0002$. A change over to the Simplex search further refined these estimates to original target of $\beta(1) = 1.0000$ and $\beta(2) = 2.0000$ and corresponding objective function value of $f = 1.0000$. The Simplex algorithm had performed 38 iterations and 77 function calls before terminating the procedure based on a convergence tolerance of 10^{-5} set for both the free variables and objective function. Figure 64 above plots the sample non-linear transcendental objective function defined as produced by the MATLAB software.

13.3 Fashioning Non-linear Multi-objective Optimisation Problems into Manageable Forms

In the design of complex engineering systems, it is often a difficult task to select a single objective function, which will satisfy all of the desired requirements. Basically, the purpose here is to convert a constrained optimisation problem into an unconstrained one and then extend it to cover all multi-objective optimisation problems including inequality and side constraints. When employing optimisation techniques such as GA, no opportunity is available for the definition of inequality constraints, and for instances where the Simplex method is utilised, a further barrier is the absence of any means to even define the upper and lower bounds of side constraints. By transforming all of the objective functions into a condensed form of reduced (scaled) objective functions and subsequently appending this result to a set of constraints to generate one composite function, the result can then be utilised to search for an unconstrained minimum. A primary benefit of this method is the avoidance of separate optimisations for each objective, which is required by some optimisation methods.

To form a single composite function, one approach is to conduct a summation of each objective function weighted by a subjectively derived factor. An example of this is the utility function method[170,177]. The second is to solve the optimisation problem once for each single objective function and to use the resulting optimum objective function or design variable vector as a target, solving an additional optimisation to attain a suitable compromise. Examples of this method are the global criterion formulation, game theory approach, goal programming method and goal attainment method[170]. Any number of objective functions and constraints are combined using a special function to form a single composite function. This composite function is then used to solve the optimisation problem. Based on a significant survey and analysis conduct by Dovi and Wrenn[177], three of the most suitable methods for aircraft conceptual design analysis, namely, the Kreisselmeier-Steinhauser function, Global Criteria formulation and the Utility Function formulation, in redefining the multi-objective optimisation problem are briefly described below. Note that all of these methods produce feasible solutions in the design space, however, issues relating to ease of use including an ability of integrating complex computational algorithms with minimal inconvenience, data requirements, programming and computational efficiency compels the review of each of these approaches in an order of applicability.

13.3.1 Kreisselmeier-Steinhauser Function

The conversion from constrained to unconstrained problem is achieved using the Kreisselmeier-Steinhauser function[178,179], which is commonly referred to as the KS

method. The KS method combines one or more objective functions with all of the inequality constraints to form a single composite KS function. The original KS function[178] was first defined as an exponential function prone to numerical difficulties when composite function values were large. An alternate and more pragmatic definition is cited by Wrenn[179] as

$$KS(X) = f_{max} + \frac{1}{\rho} \ln \sum_{i=1}^{I} e^{\rho f_i(X) - f_{max}} \tag{310}$$

where f_{max} is the maximum value of the set of functions evaluated at X and taken to be constant, and $f_i(X)$ is a set of objective functions and constraints. The computed objective function now identified as DEMAND(X), and the constraint now identified as CAPACITY is typically fashioned to read as

$$g_j(X) = \frac{DEMAND(X)}{CAPACITY} - 1 \tag{311}$$

for upper bounded constraints, and,

$$g_j(X) = 1 - \frac{DEMAND(X)}{CAPACITY} \tag{312}$$

for lower limits imposed on the objective function in question. The scalar multiplier, ρ, is typically set between 5 and 200 and Figure 65 demonstrates the sensitivity of the scalar multiplier with respect to the KS function attributes. Larger values of ρ create a tendency for the KS function to be pulled in closer to the actual curve intersections with correspondingly less filleting thus describing the region of curve intersection more adequately.

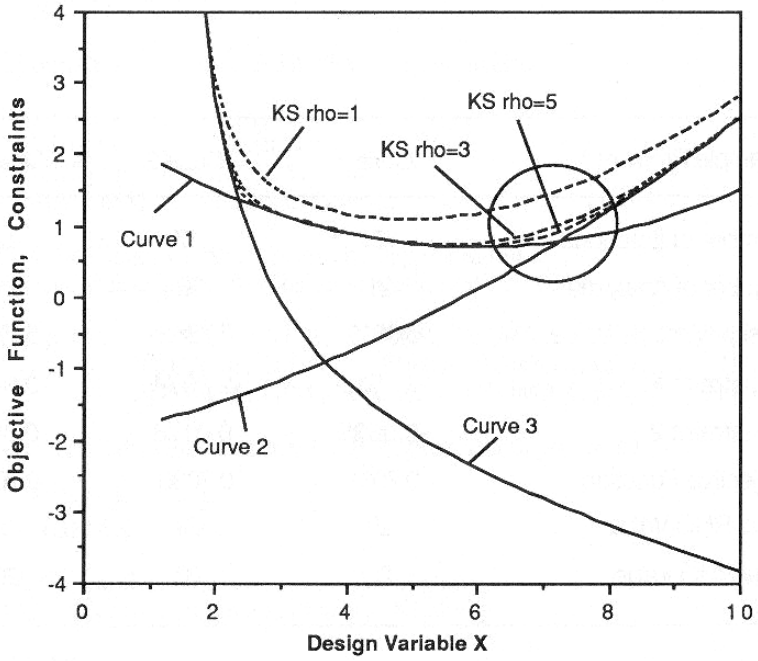

Figure 65. Example of KS function characteristics for various scalar multiplier, or ρ values[179].

To minimise oscillatory behaviour during the convergence process ρ will need to be augmented to cater for this circumstance. One approach is to set any oscillation threshold equal to the convergence threshold and a test it against the difference between i-2nd and the ith iterations. If the result is greater than the oscillation threshold then ρ is factored by 2. An additional check needs to be conducted to ensure that the new value of ρ does not exceed that of ρ_{max}.

Converting a constrained optimisation problem to an unconstrained one requires the combination of objective functions and constraints in some manner such that the resulting composite function can be minimised using any unconstrained optimisation technique. Once the constraints have been scaled, a modified objective function is then computed using

$$F_m^*(X) = \frac{F_m(X)}{F_m^0} - 1 - g_{max} \tag{313}$$

where F_m^0 is the value of the mth objective function at the beginning of an iteration, g_{max} is the maximum value of the set of inequality constraints evaluated at X and taken to be constant throughout the entire iteration, and $F_m^*(X)$ is the modified objective function and at the beginning of an iteration is equal to the negative of g_{max}. Each scaled and offset objective function is appended to the set of inequality constraints $g_j(X)$ to form a set of Q functions referred to $f_q(X)$ where Q comprises the total number of I objective functions and the number of J constraints

$$f_1(X) = F_1^*(X),\ f_2(X) = F_2^*(X),\ \ldots,\ f_I(X) = F_I^*(X)$$

$$f_{I+1}(X) = g_1(X),\ f_{I+2}(X) = g_2(X),\ \ldots,\ f_{I+J}(X) = g_J(X). \tag{314}$$

The functions are then combined to form a single continuous function using Eq. (310), thus representing an envelope of all objective functions and constraints in the optimisation problem. In keeping with Dovi and Wrenn's conclusions, the KS method is seen to be the most desirable for aircraft conceptual design problems due to it consistently demonstrating robust performance qualities.

13.3.2 Utility Function Formulation

In this formulation, a utility function $U_i(F_i)$ is defined for each objective function $F_i(X)$ depending on the importance of $F_i(X)$ compared to the other objective functions. Then a total or overall utility function $F^*(X)$ is defined as[170]

$$F^*(X) = \sum_{i=1}^{I} U_i(F_i) \tag{315}$$

The solution vector for X is then found by minimising the total utility function $F^*(X)$ subject to constraints $g_j(X)$. Introducing a scaling weight factor, w_i, associated with the ith objective function, a formulation to minimise Eq. (315) looks something like

$$F^*(X) = -\sum_{i=1}^{I} w_i F_i(X) \tag{316}$$

A penalty function can be incorporated to signify what amount of violation with respect to the constraints has occurred and re-direct the search accordingly. One such method is to include the composite objective function of Eq. (316) in a quadratic extended interior penalty function[177]. Stated in generalised form is given as

$$\tilde{F}(X, r_p) = F^*(X) - r_p \sum_{j=1}^{J} G_j(X) \tag{317}$$

with

$$G_j(X) = \left\{ \begin{array}{c} \dfrac{1}{g_j(X)} \\ \dfrac{2\varepsilon - g_j(X)}{\varepsilon^2} \end{array} \right\} \tag{318}$$

where ε is a transition parameter chosen by the designer. The term alongside $F^*(X)$ on the right hand side of Eq. (317) penalises the extended function with the influence of a penalty multiplier, r_p, initially estimated according to the type of problem being solved and successively made smaller until a constrained minimum is achieved.

13.3.3 Global Criteria Formulation

The optimum solution for X is found by minimising a pre-selected global criterion $F^*(X)$, therefore, the optimum solution for X is found by minimising[170]

$$F^*(X) = \sum_{i=1}^{I} \left\{ \frac{F_i^T(X) - F_i(X)}{F_i^T(X)} \right\}^p \tag{319}$$

subject to the constraint $g_j(X)$. The variable p is generally taken as 2, thus converting the problem into a sum of squares of the relative deviations of the individual objective functions from the target values $F_i^T(X)$ or the feasible ideal solutions. The performance function $F^*(X)$ can then be minimised using the KS method.

14 Aircraft Design Software Synthesis

A software system that is the culmination of all previously discussed modelling and analysis techniques and specifically designed to predict, visualise and assist in optimising conceptual aircraft designs with emphasis placed on user interactivity was developed for this research work. QCARD-MMI, or, Quick Conceptual Aircraft Research and Development, Version 2001, is an interactive MATLAB based conceptual design package, which allows the design of any gas-turbine commercial and business aircraft. Critical development objectives included acceleration of design response time with a significant increase in design freedom, accuracy and consistency of the results. The package affords a systematic and transparent process to not only conduct analyses with respect to geometry, weights, aerodynamics and performance profiles, but also facilitates coupling of the en route performance subspace to that of economic criteria as defined by DOC and P-ROI. The package through total user control can create, calculate and analyse 15 configurationally and/or parametrically distinct designs concurrently.

A variety of known regional aircraft were input and QCARD-MMI predictive powers were inspected against each respective vehicle's manufacturer PEH or its equivalent. As supported by evidence presented thus far, indications have shown very good agreement against published results with typical errors frequently falling within a bandwidth of ±5% for weight; engine performance - TSFC and thrust lapse; aerodynamics - total drag for AEO and OEI at low and high speed, maximum lift for clean wing and for given flap setting; and, operational performance - takeoff including minimum control speed limitations and initial climb, en route climbing, cruise, complete mission and landing. Additionally, QCARD-MMI methodology was benchmarked against GASP developed by NASA-Ames Research Centre[39,112,181,182].

This section serves as an introductory note to illustrate how the software is configured and subsequently presented to the designer. Opportunity is also given to succinctly explain the scope of functionality and how each of these subspaces being analysed integrate to produce the global multi-disciplinary conceptual aircraft model.

14.1 Introduction and Advantages of MATLAB

MATLAB from MathWorks Inc. of Massachusetts has established a growing reputation as one of the best contemporary numerical programming environments. MathWorks describes three central themes to MATLAB: to make the software easier to use; to extend the connections to other environments; and, to improve code generation tools.

MATLAB's programming language is a BASIC-like procedural language, which can be used interactively, or to write programs (stored as text "M-files") that MATLAB interprets while executing. Most MATLAB functions are actually M-files, and as such can be inspected and modified. They can also be compiled into C/C++ code either as "MEX-files" called at execution or stand-alone executables for other applications. Graphical output is generated during the program execution as a separate "Figure" window and offers a rather extensive array of capabilities, from plotting mathematical functions to generating complex surfaces or even reading in graphics images from external picture files.

In combination with the platform's popularity within both academic and industrial circles and the broad-ranging graphics capabilities combine to motivate MATLAB as being an ideal environment for developing the QCARD-MMI conceptual aircraft design package. Additionally, since there exists an expectation that QCARD-MMI will spawn new

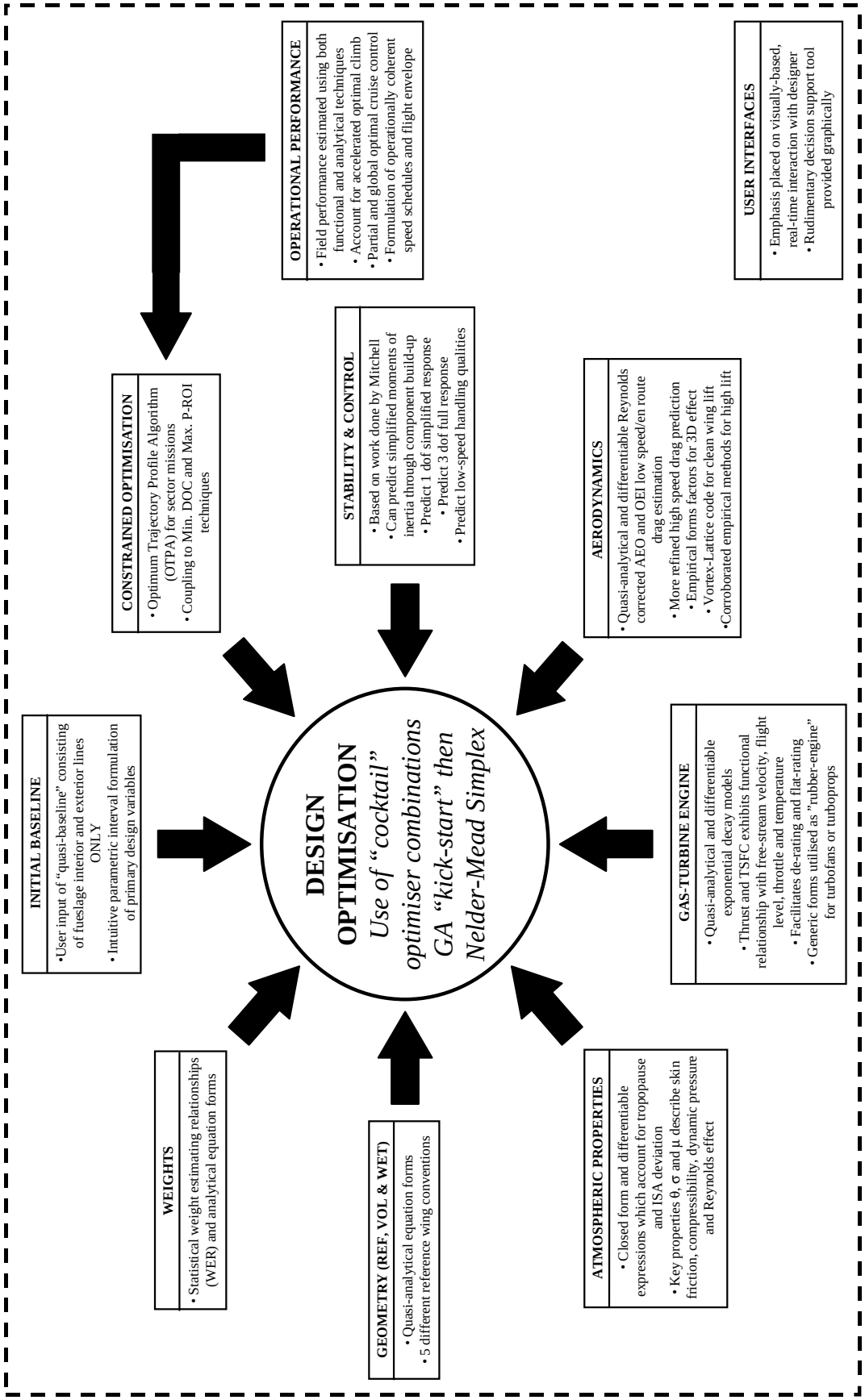

Figure 66. QCARD-MMI design synthesis system core subspace contributors.

upcoming versions, MATLAB is considered to be the most stable environment in terms of future availability and potential for further enhancements.

14.2 The QCARD System

QCARD is a modular code and a general understanding of the main analysis contributions to the overall system construct is offered in Figure 66 (previous page). The software essentially consists of four compartments, of which some aspects within each can be designated as being a concurrent participant, or when desired, processed in isolation.

The first level, data input, includes routines for data input of user defined baseline data, design and certification requirements, mission requirements, or any other constraint. Level two encompasses all functionality ranging from disciplinary analysis, parametric surveys, and a possibility of conducting basic MVO in conjunction with constrained optimisation analysis of a chosen synthetic function, e.g. identifying maximum block speed for given payload and sector distance. The third level alludes to output information and this aspect is addressed through a possibility of reviewing not only global objective function values, but also results of prominent synthetic functions and parametric quantities. When integrated with a series of engineering plots, the output information combines to produce a coherent design history of the given aircraft candidate for the user-in-the-loop. The final level concerns the induction of information necessary to facilitate complete execution of all analysis algorithms. This is achieved using empirical data, statistically derived correlations as well as some analytical methods to calculate needed parameters.

14.2.1 Launching the QCARD System

The QCARD software is executed by issuing the command “qroutin” in the MATLAB command window, upon which, the QCARD splash-screen will appear (Figure 67).

Figure 67. The QCARD-MMI introductory splash-screen when launching the system.

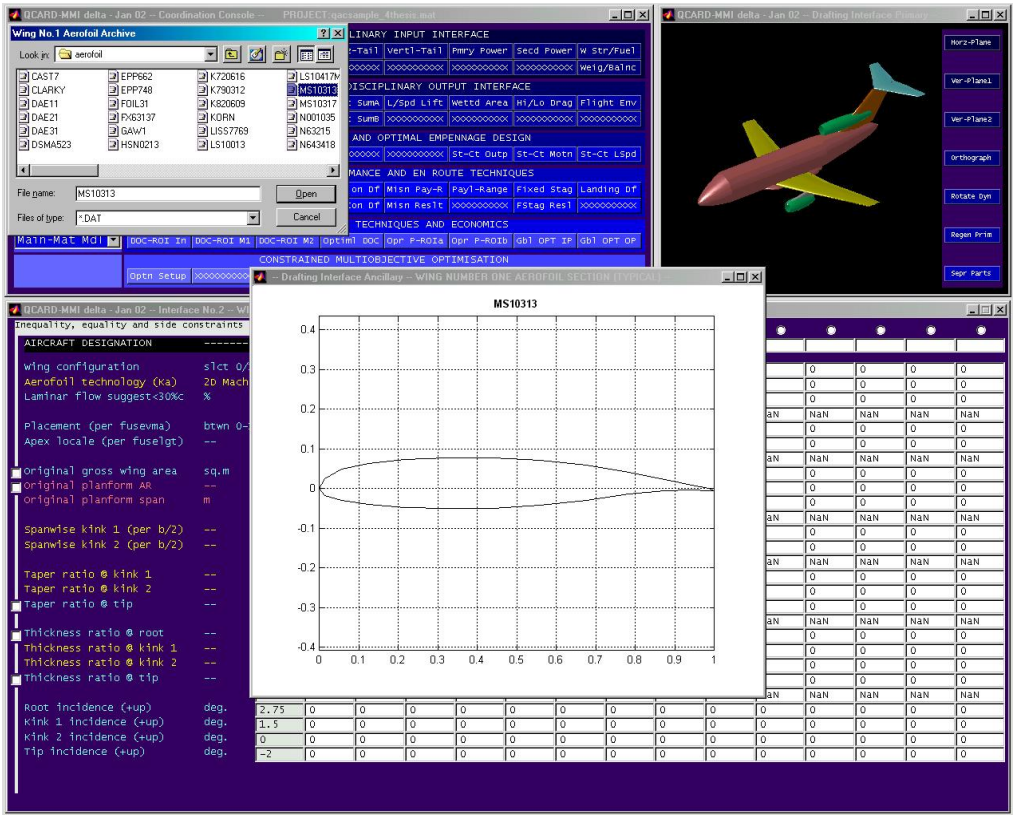

Figure 68. Definition of the aerofoil section for a wing in the QCARD synthesis system.

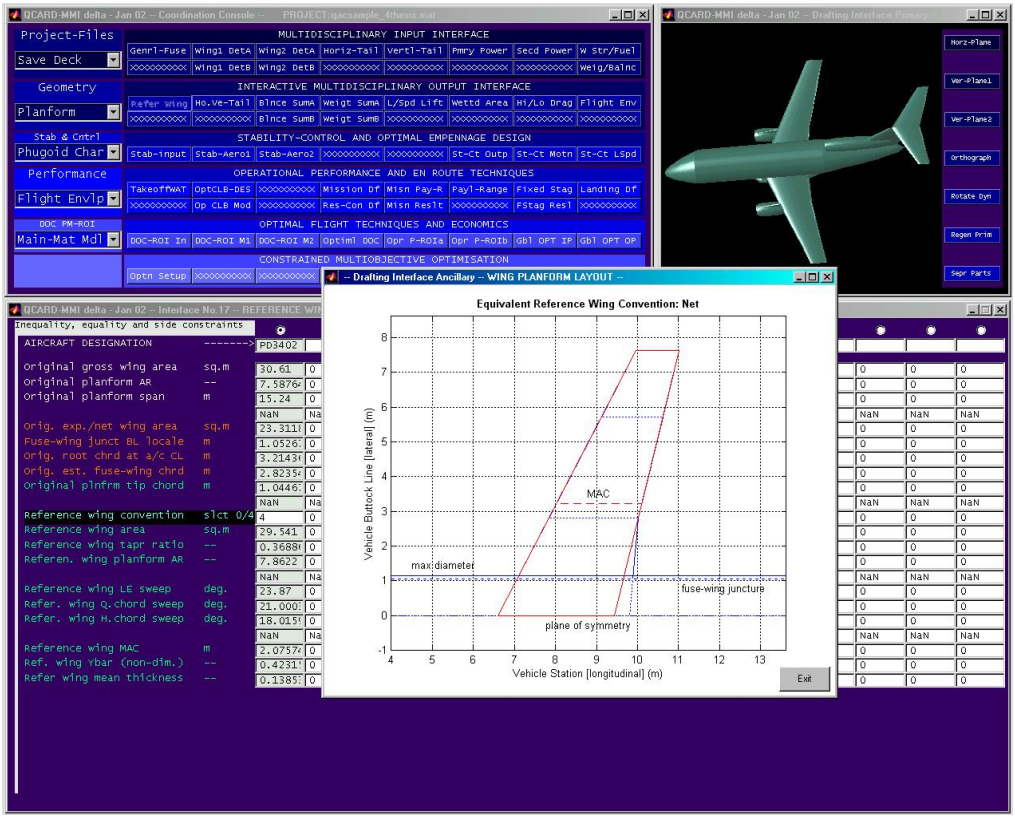

Figure 69. Inspection of the reference wing definition for a given design candidate.

14.2.2 Geometric Definition

QCARD-MMI is a fully interactive environment and as opposed to expending up to 1-4 man days deemed necessary for more sophisticated packages, permits a sufficiently comprehensive definition and subsequent synthesis of any new aircraft candidate within a couple of hours. The designer inputs all necessary information, and with each input action, observes in real-time the graphical outcome of that decision of allocating a particular value to a given design variable or design philosophy choice. Figure 68 and Figure 69 on the previous page respectively present examples of how the designer can define aerofoil geometry for a wing and inspect the resultant reference wing definition.

14.2.3 Total Drag

Drag calculations are partitioned into three distinct groups, namely, friction, vortex-induced and wave. Friction drag that is independent of lift is predicted using the component build-up method at a representative Mach number and altitude (generally LRC and next step below optimum altitude) and subsequently used to derive an equivalent characteristic length for off-reference conditions.

Figure 70 shows a typical wetted area breakdown and demonstrates an instance of many simplistic DSS tools; this particular one involving the integration of power plant.

Figure 71 presents a sample aerodynamics, power plant and vehicular en route performance summary that is instantaneously computed for a given ambient condition input by the designer. The plot shown in the centre of the screen-shot in Figure 71 represents a correlation between vehicular skin friction coefficient and total wetted area. This chart can be thought of as a basic DSS in assisting the designer to choose if a given aircraft design candidate is sufficiently realistic or if there is room for any improvement.

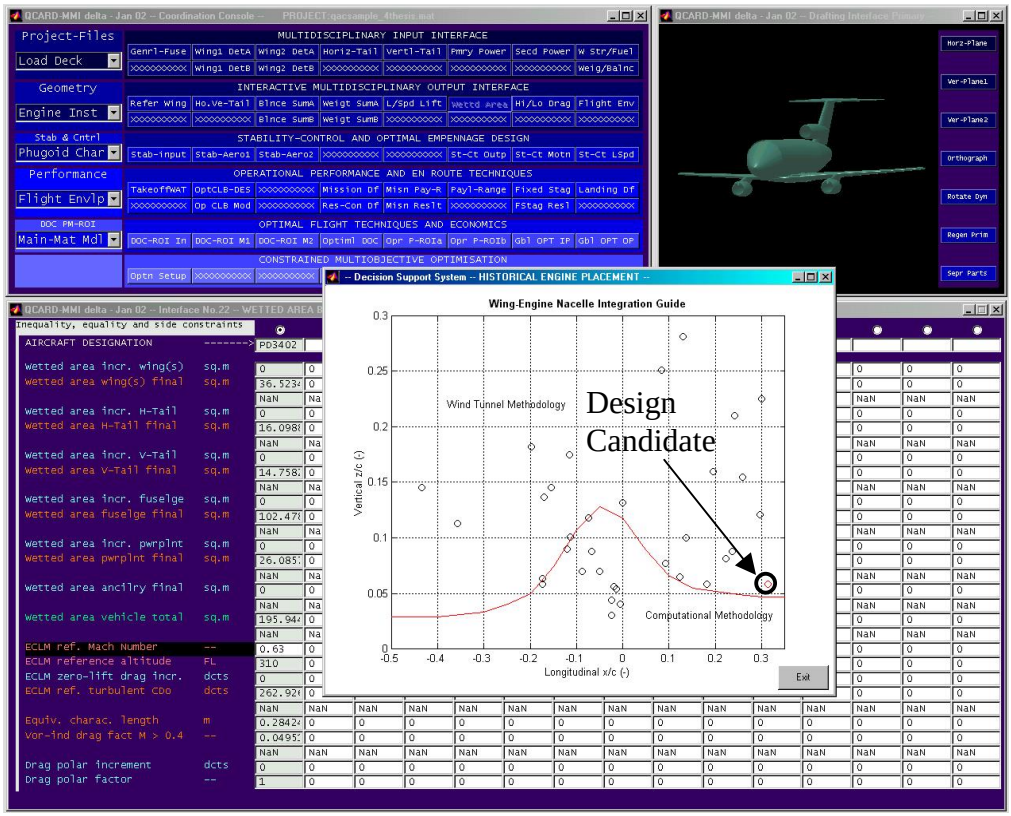

Figure 70. Rudimentary DSS through inspection of generalised nacelle location chart.

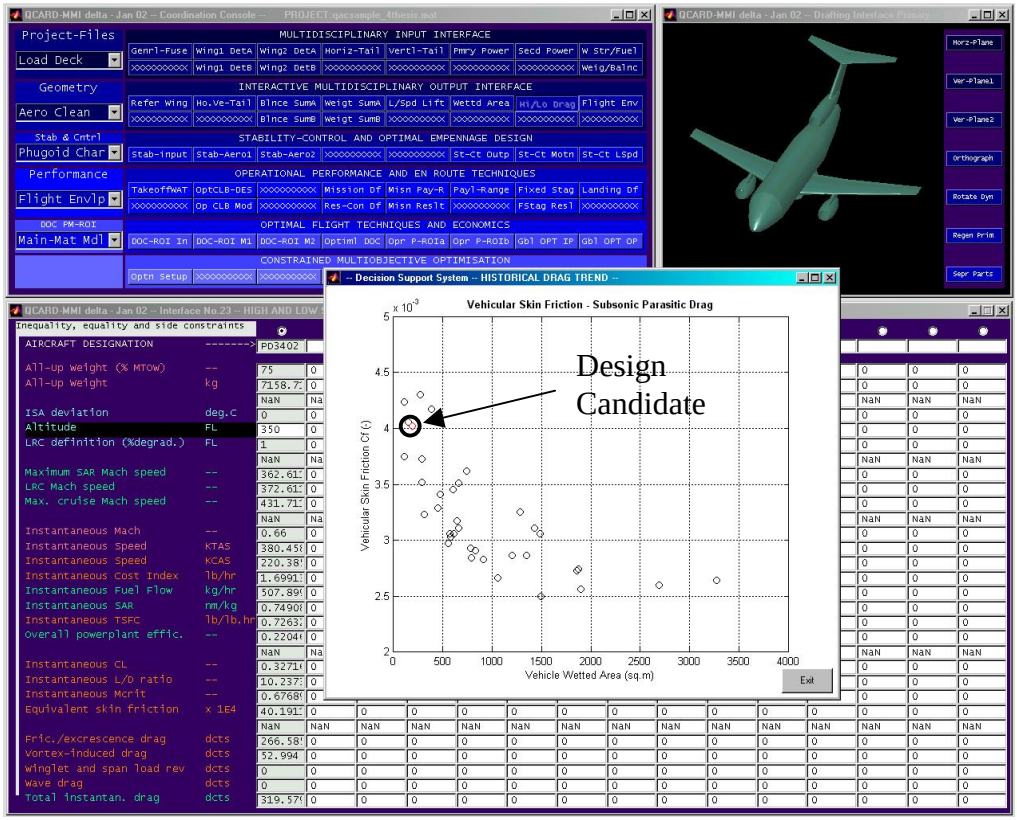

Figure 71. Gauging the relative aerodynamic merits of a chosen design candidate.

14.2.4 Maximum Lift

The clean wing maximum lift is computed for any original planform geometric definition using a MATLAB module developed by KTH called TORNADO[95]. The TORNADO software with a 3-dimensional VLM calculates aerodynamic properties of multi-wing designs that are swept (symmetric or otherwise skewed), tapered, cambered, twisted and cranked with dihedral. The interface (Figure 72) permits selection of either single-slotted, double-slotted of Douglas type and Fowler flap trailing edge high-lift arrangements in conjunction with the option to introduce contribution of a slat in the computations as well.

14.2.5 Propulsion

An engine model taken from previous work done by the author, based on the premise of exponential decay and proportional to variation of flight level and speed was expected to generate an adequate description of thrust lapse and TSFC variation. For accuracy, two distinct models describing takeoff-climb, and, maximum cruise thrust characteristics are employed. Linear performance deterioration models to account for effects of off-ISA temperature deviations are also considered.

14.2.6 Weight

Aircraft constituent weight estimates (Figure 73) of wings, vertical tail, fuselage, landing gear, avionics, electrical, hydraulic, ECS, anti-icing, APU and other equipment on board can be predicted. The maximum volume to house fuel offers the designer a notion of what maximum fuel load potential exists when considering a given aircraft design candidate's wing, centre, conformal fairing or aft fuselage tanks.

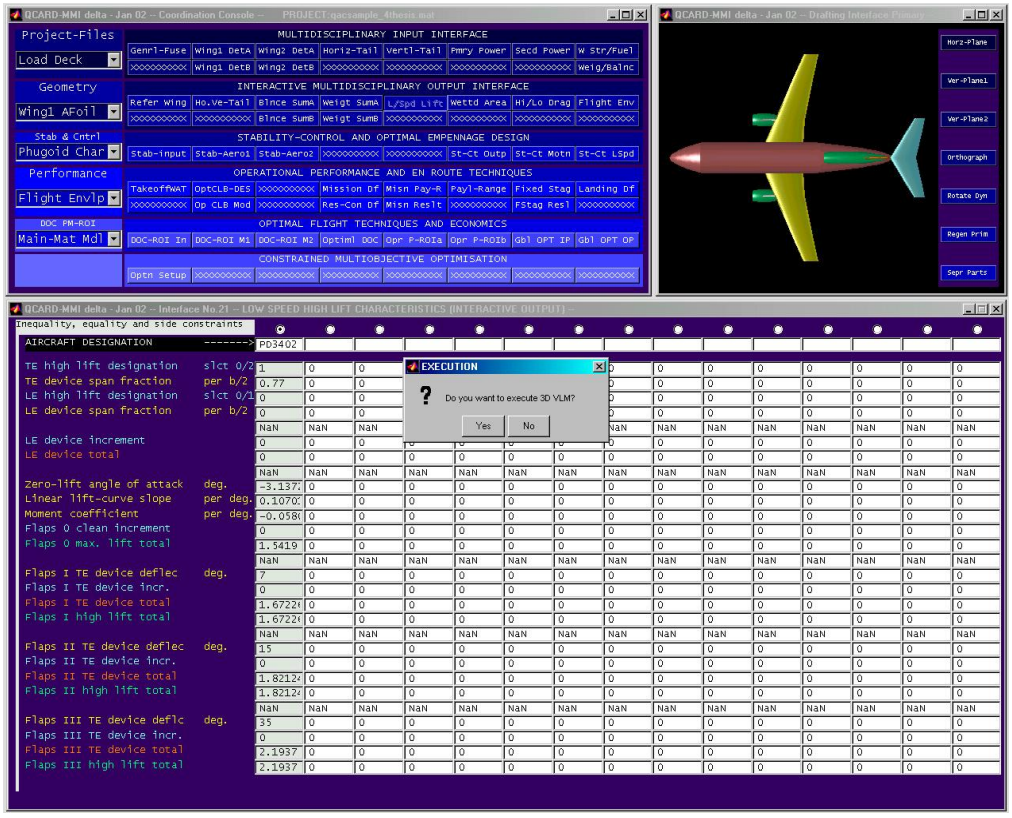

Figure 72. Maximum lift prediction for high-lift device deflection neutral or otherwise.

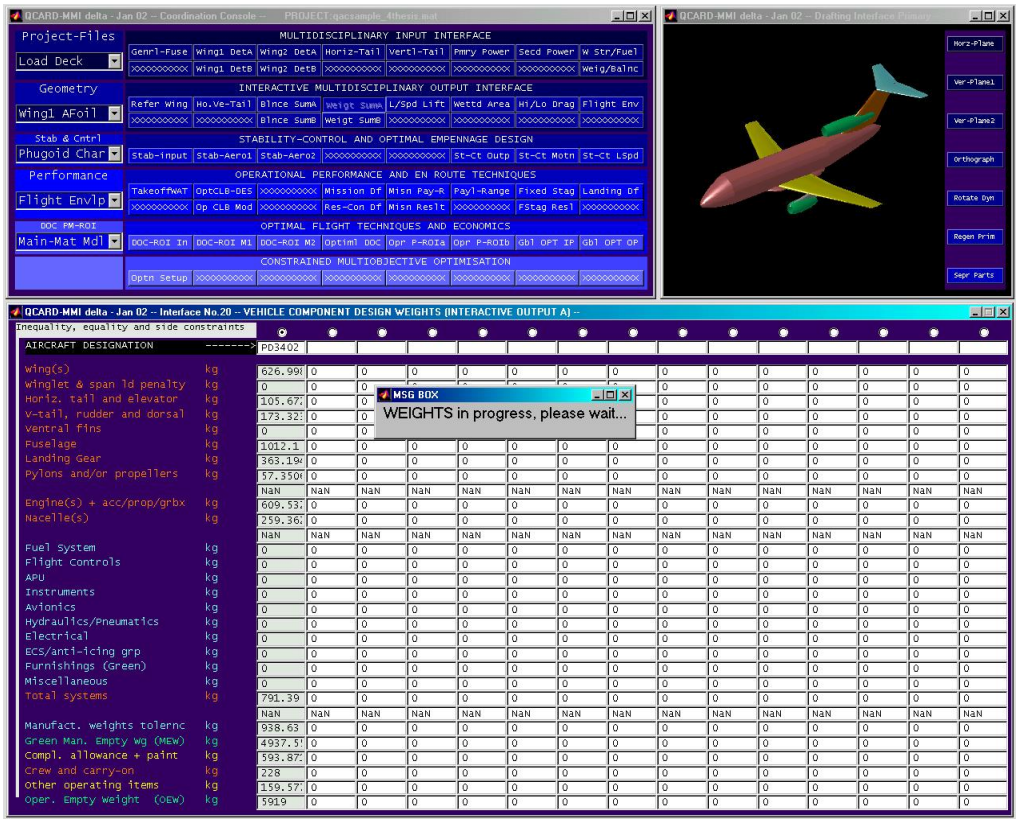

Figure 73. QCARD interface (executing) to predict the constituents' weight breakdown.

14.2.7 Performance Definitions

Field performance can be computed instantaneously for any given flap angle and ambient condition, i.e. whether airport pressure altitude or outside air temperature. Figure 74 shows one such BFL example where the three designated flap settings are automatically computed. An additional functionality that enables the designer to identify flap setting for minimum TOFL assuming minimum OEI climb gradient is also available.

The en route performance modules allow the designer to inspect operationally permissible performance control (automatically generated by QCARD or otherwise) in addition to optimal performance control. This freedom assists in formulating performance control close to the idealised scenario whilst adhering to the dictates due to operational relevance. Figure 75 elucidates this concept by showing a performance chart for CLB Mode L where the dashed line denotes the results of an optimal speed schedule and the solid line indicates the deviation from this ideal. Combining all of the separate performance control features enables definition of the flight envelope for a given aircraft design candidate; this is depicted in Figure 76.

The OTPA in QCARD-MMI utilises an interval halving numerical scheme with TOGW as the free variable for given flight level. The algorithm caters to a myriad of objective function evaluations, including unconstrained maximum SAR, constrained maximum SAR at given speed technique and unconstrained minimum time (maximum block speed) flight technique evaluation. For accuracy, a default of 5 segments including a user-defined step-cruise protocol is assumed for the entire mission profile. As a margin for establishing the validity of en route cruise speed minimum goals, a residual specific excess power can be imposed to identify the engine thrust limit, and can be utilised in lieu of an altitude capability assessment constrained by high-speed buffet. Finally, all en route mission computations conform to preset definitions of reserves and contingency policies. Alternatively, a unique set of reserves and contingency fuel can be defined according to the designer's wishes. Figure 77 demonstrates derived payload-range attributes adhering to maximum SAR and maximum block speed for an example aircraft design candidate.

14.2.8 Stability and Control

The stability and control modules permit the computation of aerodynamic derivatives, estimation of moments of inertia, forced responses to certain disturbances at a specified flight condition and identification of limiting speeds for low-speed flight. The designer has a choice as to how the aerodynamic derivatives shall be estimated. QCARD can either use results generated by the TORNADO[95] module or default to the Mitchell method[15]. A basic DSS facility is available to assess the feasibility of a given aircraft design through the inspection of parametric merit plots, an example of which is shown in Figure 78.

14.2.9 Economics

A comprehensive array of costing and profit assessment is facilitated here. The costing analysis comprises lease (if applicable), acquisition, insurance, crew, spares, time dependent contingency, maintenance, materials, fuel and sundries. When considered in consort with yield modelling, the system then proceeds to identify flight techniques, expressed equivalently as a block time and fuel, which correspond to some intended cost or profit objective optimality. For occasions where critical data is available but adequate modelling of sensitivities is not at hand, QCARD contains in-built sensitivity templates that require only minimal information. By supplying this minimum array of reference values, the ensuing computations work off the premise of scaling the sensitivity templates according to the designer specified data. Figure 79 presents a computed profit result.

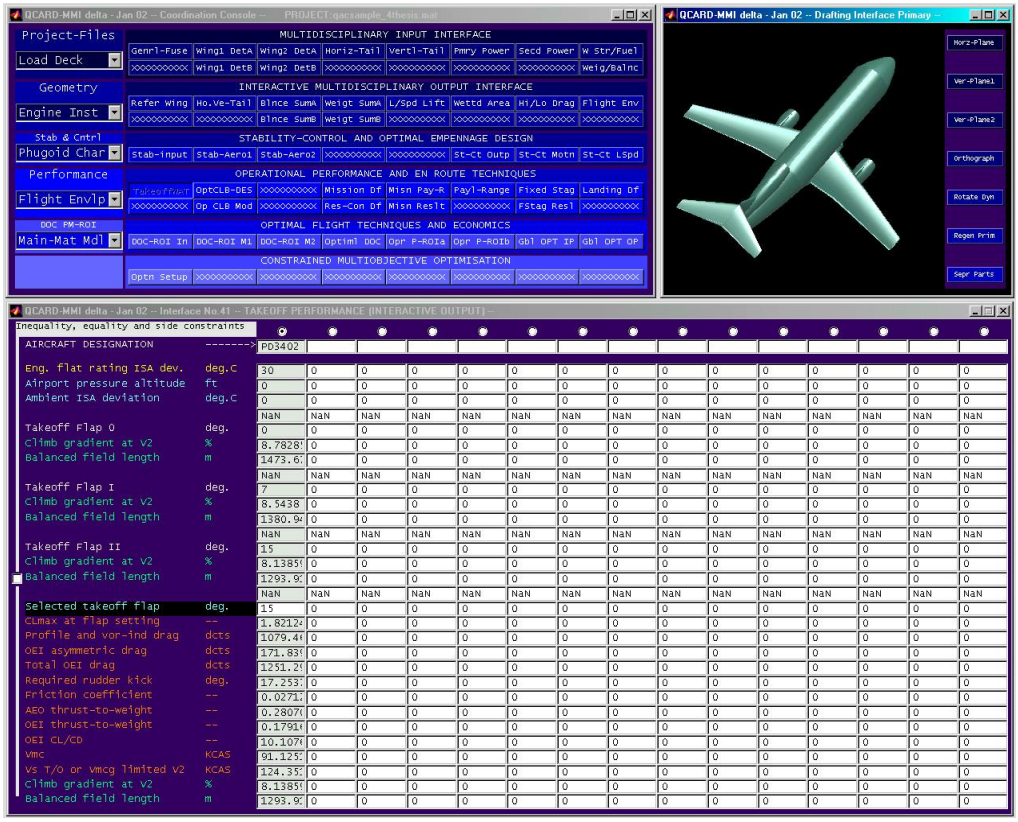

Figure 74. Instantaneous BFL estimation according to given flap and ambient conditions.

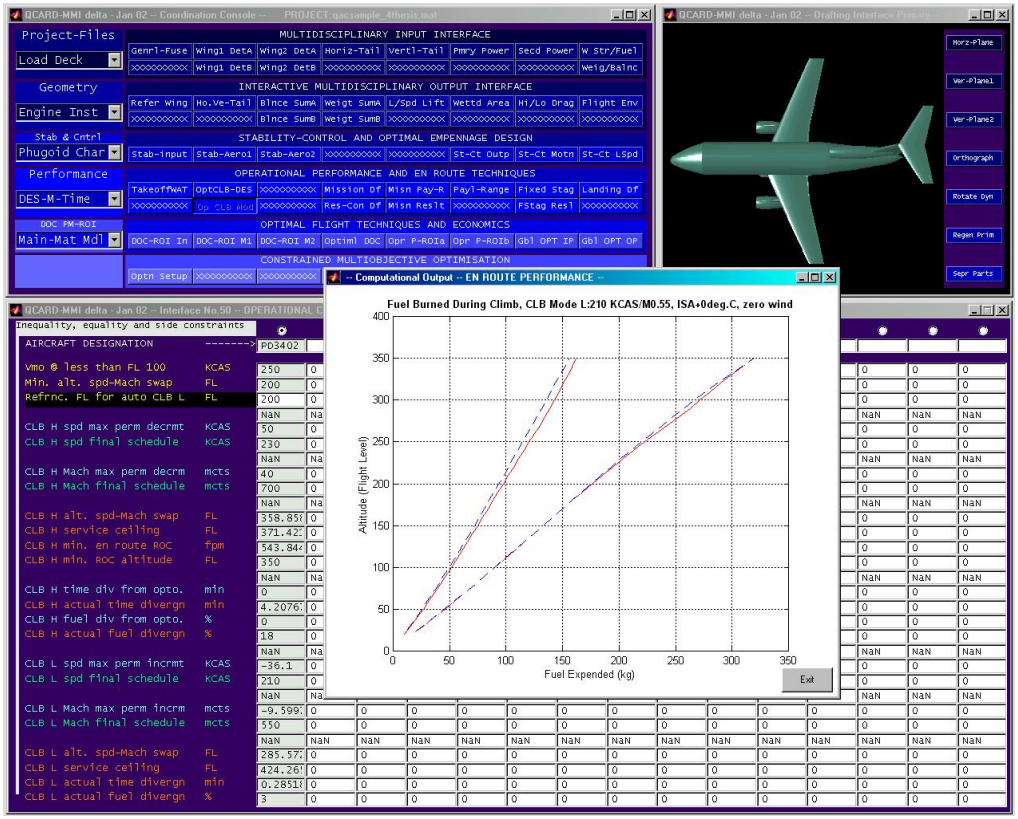

Figure 75. Examining and contrasting CLB Mode L against the optimal schedule results.

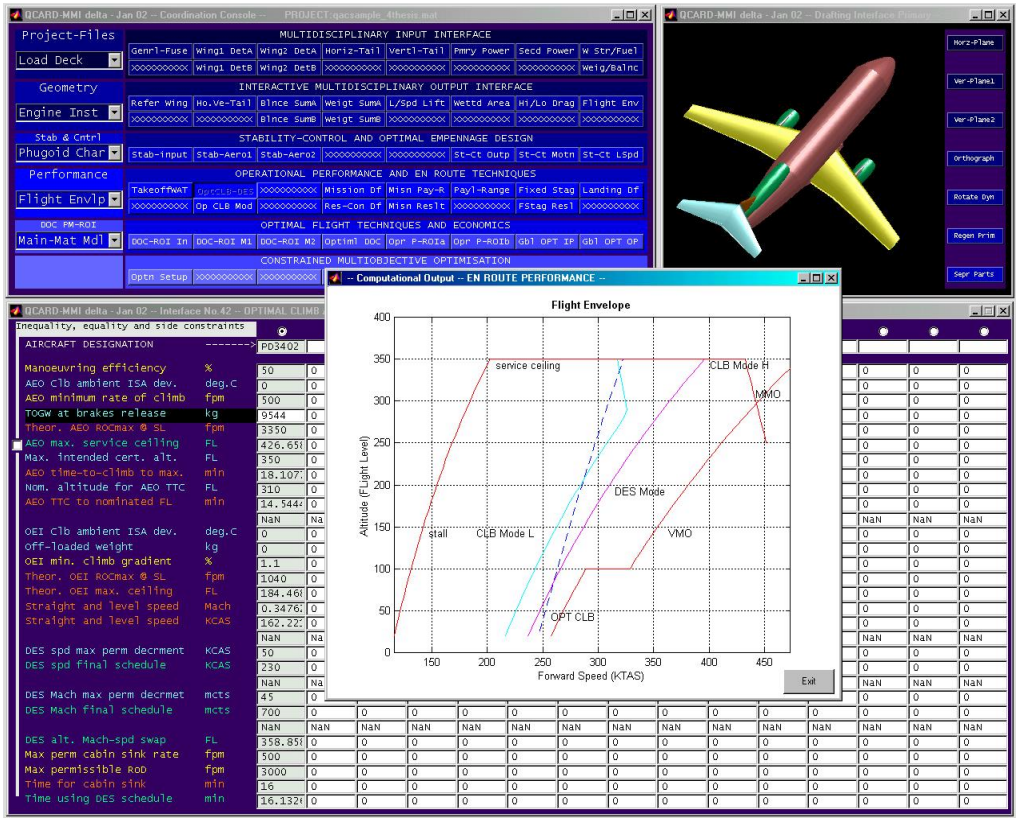

Figure 76. Flight envelope (including performance control) formulation and visualisation.

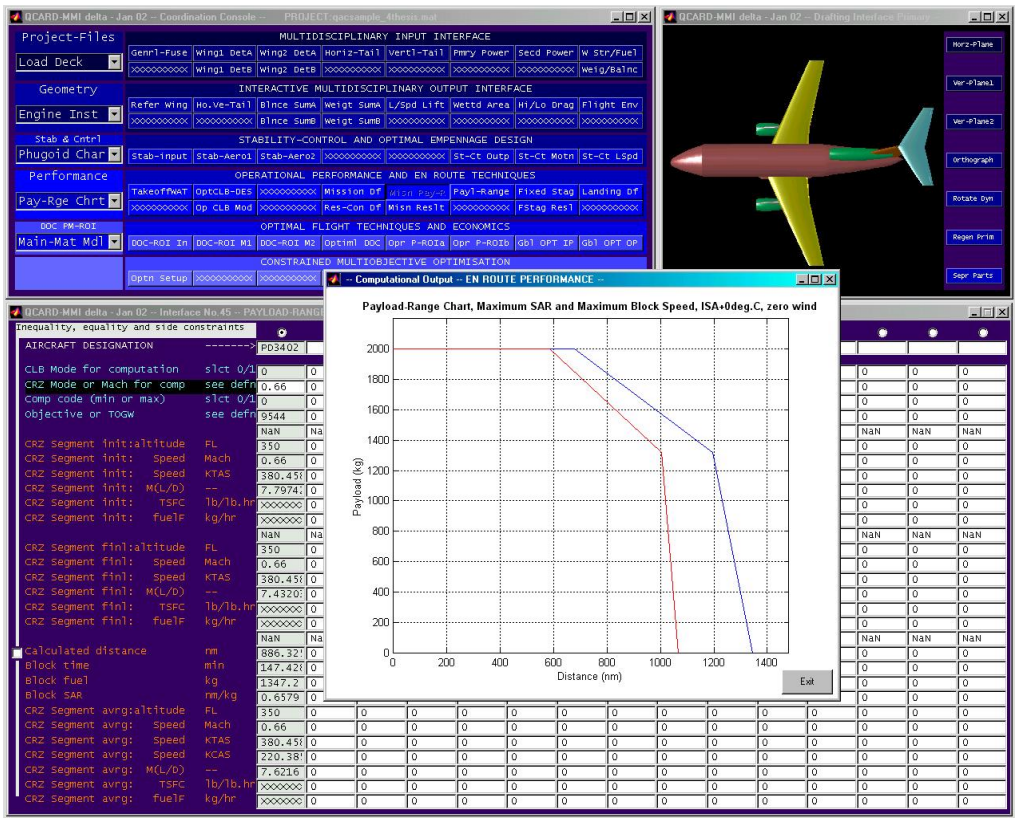

Figure 77. Example payload-range for maximum SAR and maximum block speed.

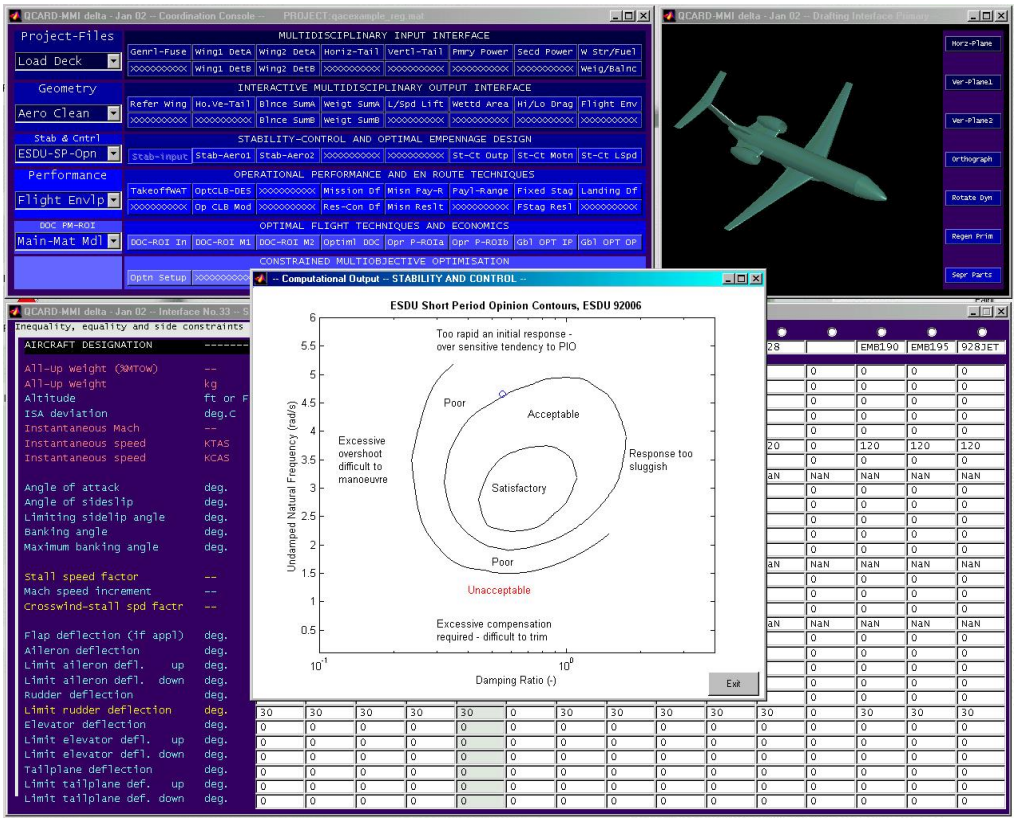

Figure 78. Examining the longitudinal Short Period contours for an aircraft design.

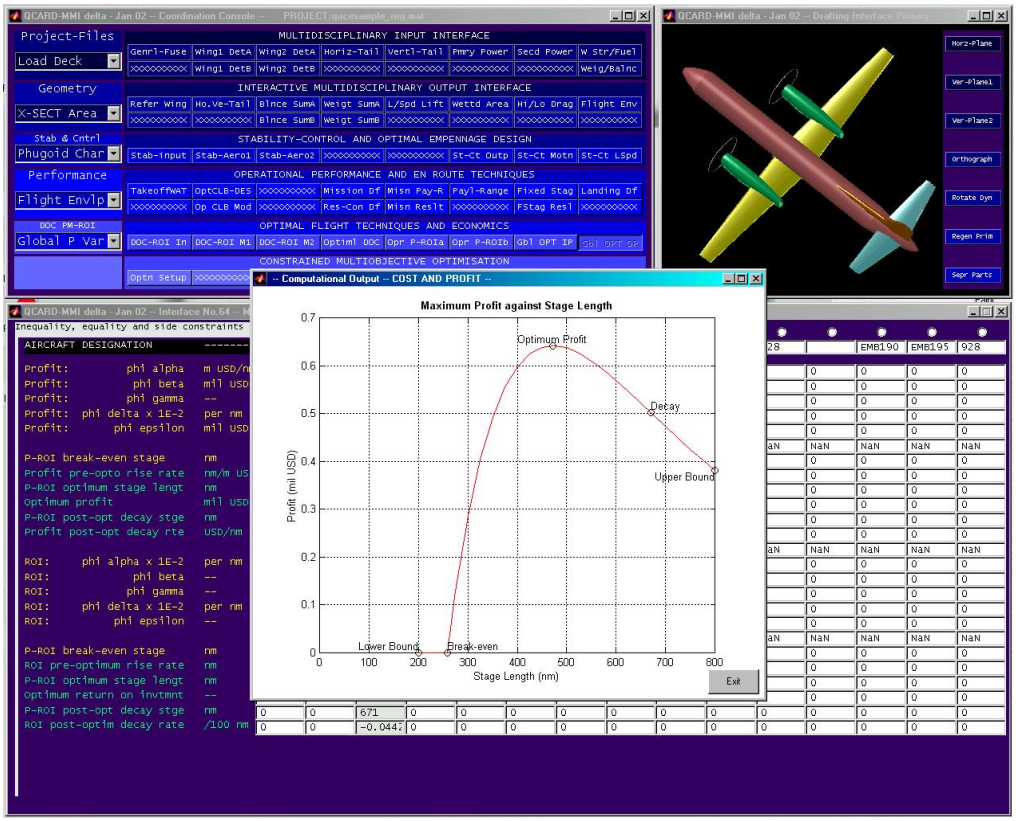

Figure 79. Predicting the maximum profit of an aircraft design using the QCARD system.

14.2.10 Constrained Multi-objective Optimisation

Facility (Figure 80) is given for the designer to conduct constrained multi-objective optimisation studies ranging in complexity from a few design variables up towards the hyper-dimensional design space. All of the side constraints, synthetic functions and the objective function variables are selected as the designer proceeds through each analysis module when defining the baseline aircraft. The choice of optimisers is limited to three: evolution method; Nelder-Mead Simplex search; and, a cocktail algorithm employing strategic utilisation of both the evolution method and Nelder-Mead Simplex search. Notwithstanding this limitation, scope is given to accommodate more optimisation methods and the interface module has been fashioned to easily incorporate addtional optimisers in the future. The designer can also exercise an option of "switching" on or off selected core analysis modules, and therefore constrain the optimisation problem even further.

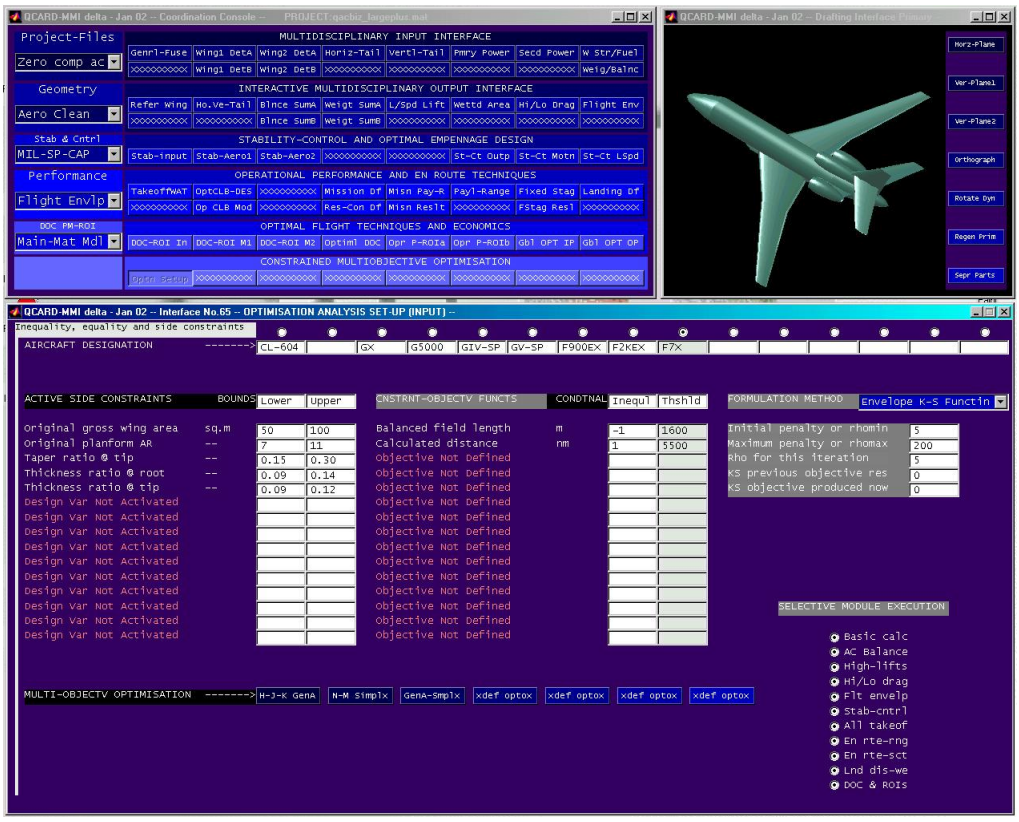

Figure 80. QCARD interface for constrained multi-objective optimisation analysis.

15 Aircraft Design Projects – Practical Demonstration of Prediction Methods and QCARD-MMI Software

Although an extensive amount of validation against known in-service commuter, regional, narrow-body and business aircraft data has been expended in establishing soundness of the presented methods, importance was subsequently placed on gauging how the design prediction theory and resulting software package QCARD-MMI would fair when applied to actual synthesis problems. It is highlighted that the purpose of this exercise was to not only demonstrate software capabilities, but more poignantly attention should be drawn to the actual design proposals themselves, i.e. the perception of new market niche possibilities, or the introduction of an alternate philosophy in aircraft configuration to fulfil atypical mission roles. Three new aircraft design projects were undertaken and they are itemised as follows:

- PD340-2, a 19 passenger turbofan commuter aircraft[112,181,182];
- PD340-3X, 31-34 passenger turbofan commuter aircraft[183]; and,
- TOLS-X, a Trans-Atlantic 19 passenger executive transport able to cruise at low supersonic speeds[184].

This section briefly presents these studies and each aircraft design review is covered by an overview of the aircraft mission role and purpose, an outline of the hard specifications, a synopsis of trade studies and MVO considerations, a design description, review of operational performance (includes operating economics where applicable), and a critical appraisal based on comparisons to in-service aircraft.

15.1 PD340-2

The PD340 project study was performed for Williams-Rolls Inc. with support from Saab Aerospace AB, Karlebo Aviation AB and KTH. The aim was to produce a new aircraft with a purchase price that would be considered non-prohibitive for current regional operators but with greatly enhanced speed and comfort. Furthermore, a focus on operational flexibility to accommodate non-stop service between cities with relatively low traffic and extended hub feed operations was also taken to be of primary concern. In order to achieve this, the use of the cost-effective, quiet and fuel-efficient Williams-Rolls Inc. FJ44-2A engines were incorporated from the outset.

15.1.1 PD340-2 Specifications

The hard specifications that were deemed necessary for the success of this proposal are defined below:

- The vehicle must accommodate at least 19 passengers with a 32 in. (813 mm) seat pitch and a typical fuselage cross-section that is similar to the Saab 340 and Saab 2000;
- BFL less than 4000 ft (1219 m) at ISA, sea level conditions;
- Effective operation at 5000 ft (1524 m) airport pressure altitude and at ISA+20°C conditions;
- Time to climb to typical cruise flight levels of around 15-20 minutes;
- Service ceiling not less than FL 350 and high-speed cruise not less than M0.70;

- Maximum range not less than 600 nm (1100 km) with typical US regional mission reserves and a full payload complement;
- Landing V_{REF} to be not greater than 110 KCAS at ISA, sea level conditions;
- A competitive break-even load upon comparison to current 19 seat turboprops;
- Maximise commonality with Saab 340 vehicle in order to reduce initial development and manufacturing cost; and,
- The vehicle shall be certified according to FAR 25 and JAR 25 transport category aircraft requirements.

15.1.2 PD340-2 Synopsis of Trade Studies and Optimisation

In this particular study, since the engine and configuration layout were set a priori, for a given wing thickness ratio and sweep, wing taper ratio and span were designated as primary free variables due to the design's philosophical stipulation of maximising commonality with the Saab 340 – in this instance, the wing torsion box geometry being the fundamental constraint. In view of this, a transcendental dimension equation for wing root chord dependent upon taper ratio and wingspan constrained by an already existing Saab 340 wing-fuselage interface was adhered to. It was surmised that this objective function sensitivity would be directly coupled to a corresponding resultant S_W. With variation of wing geometry, associated changes in MAC adjusted the empennage accordingly since approximate dimensioning was based on the premise of keeping each vertical and horizontal tail volume coefficients fixed. In the absence of reliable detailed data, cost can be considered as a direct function of airframe weight, therefore the MTOGW was minimised. A final plot that trades MTOGW against reference wing area for given performance characteristics was inspected and feasible configurations reviewed.

Various combinations of engine count, wing area, sweep angle and thickness were analysed to determine an acceptable trade-off between good field and en route performance. A myriad of possible performance constraint criteria to inspect for sensitivity and subsequently identify feasible solutions were reviewed. Stall speed at MLW (V_s), and, maximum range assuming maximum payload with 19 passengers (PAX) at 200 lb (91 kg) (Range 1 and Range 2) with conventional U.S. regional reserves of 100 sm (87 nm) alternate and 45 minutes hold were finally designated as primary constraint criteria because these displayed the greatest potential for compromise when trading MTOGW and S_W. Consequently, the selection process focused on maximising range, and, minimising time to climb as well as landing stall (or indirectly the required LFL) and BFL. In terms of the PD340 study, span and reference wing area were minimised to rationalise weight thereby acquisition cost, whereas in stark contrast, area and span needed to be maximised in order to minimise takeoff and landing distances and maximise range performance. To reconcile these conflicting effects, the requirements were plotted on one chart that allowed definition of a bounded geometric region in which freedom of selection existed. An example of the final simplified trade study for PD340-2 is given in Figure 81 and it can be discerned that the gross weight sensitivity indicated that approximately 29.5 m^2 (317 sq.ft) of wing area was appropriate.

15.1.3 PD340-2 Design Description

The vehicle is a tricycle, monoplane, low-winged tri-jet with two underwing podded and dorsal intake-tail engine mountings. It is pressurised and incorporates a T-tail empennage. The landing gear is retractable and each leg is twin wheeled. The vehicle accommodates a flight crew of two and an optional flight attendant. The standard

configuration accommodates a maximum of 19 PAX. The power plants utilised are Williams-Rolls Inc. FJ44-2A turbofans. The vehicle is designed to comply with FAR 25 U.S airworthiness regulations and the European JAR 25 rules. Figure 82 shows an artist's impression.

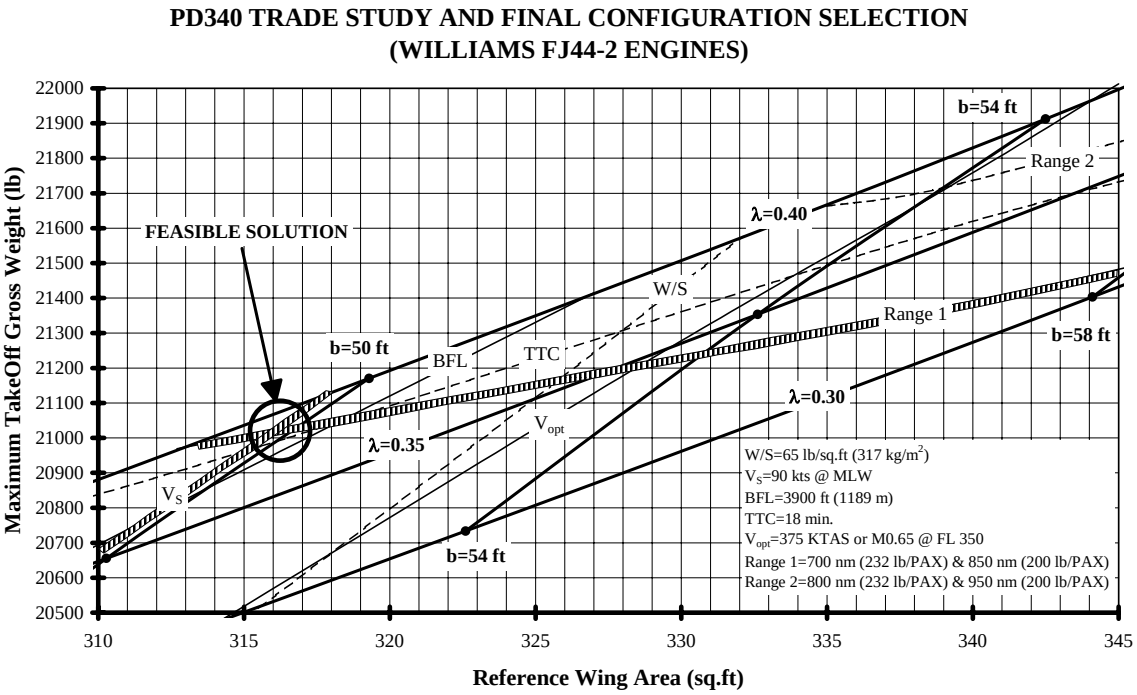

Figure 81. Final simplified selection process for PD340-2 turbofan commuter concept.

Figure 82. Artist's impression of the PD340-2 19 PAX regional turbofan transport.

Table 5 and Figure 83 present salient aircraft data and three-view of the PD340-2 respectively.

Weights		
Maximum Ramp Weight	21141 lb	9590 kg
Maximum Takeoff Weight	21041 lb	9544 kg
Maximum Landing Weight	20047 lb	9093 kg
Maximum Zero fuel Weight	17457 lb	7918 kg
Operational Empty Weight	13049 lb	5919 kg
Manufacturing Empty Weight	12525 lb	5681 kg
Maximum Payload	4408 lb	2000 kg
Maximum Usable Fuel	5186 lb	2352 kg
External Dimensions		
Overall span	50 ft	15.24 m
Height	19 ft 11 in.	6.07 m
Overall length	62 ft 11 in.	19.18 m
Fuselage Dimensions		
Length	54 ft 9 in.	16.69 m
External diameter	7 ft 7 in.	2.31 m
Wing Geometry		
Total area	317 sq.ft.	29.5 m^2
Aspect ratio	7.9	

Table 5 Weight and geometry data for the PD340-2 19 PAX turbofan commuter.

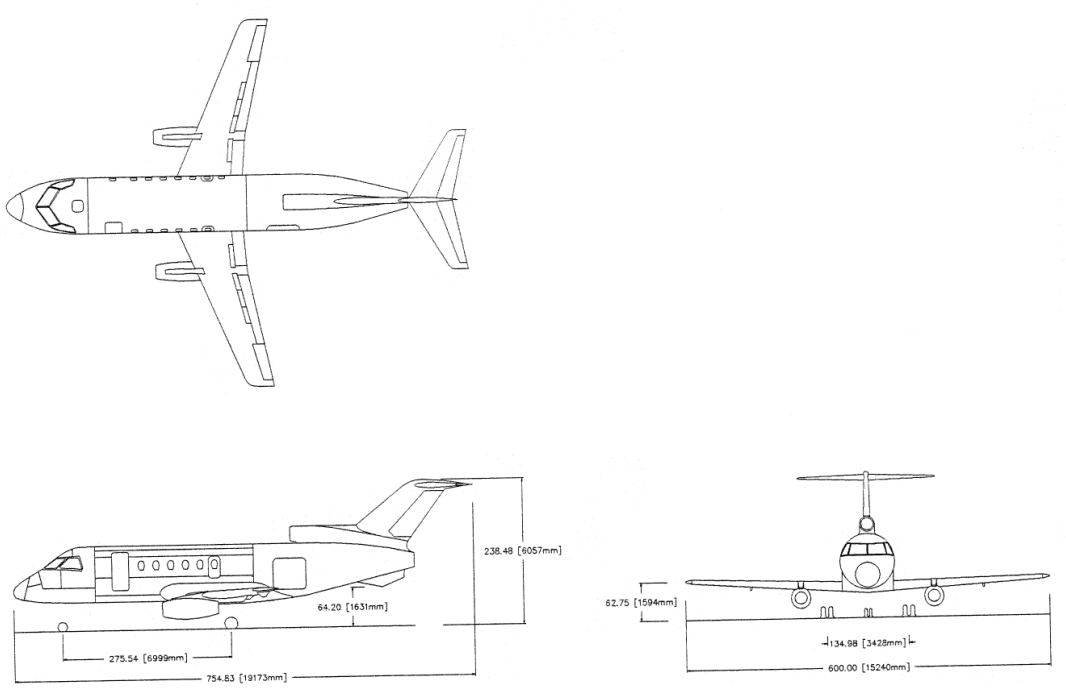

Figure 83. General arrangement of the PD340-2 19 PAX turbofan commuter aircraft.

The structure of the fuselage (Figure 84) consists of three major assemblies: front - nose with cockpit; centre - cabin; and, aft - rear section including the cargo compartment. Each section is spliced in a manner, which duplicates as much as possible the Saab 340's manufacture/assembly production tiers. With the exception of fore and aft sections, the fuselage is cylindrical with a 2.31 m (7 ft 7 in.) maximum diameter cross-section, and, the front and some of the centre as well as aft sections are utilised from the Saab 340 design.

Fuselage Structure commonality with Saab 340

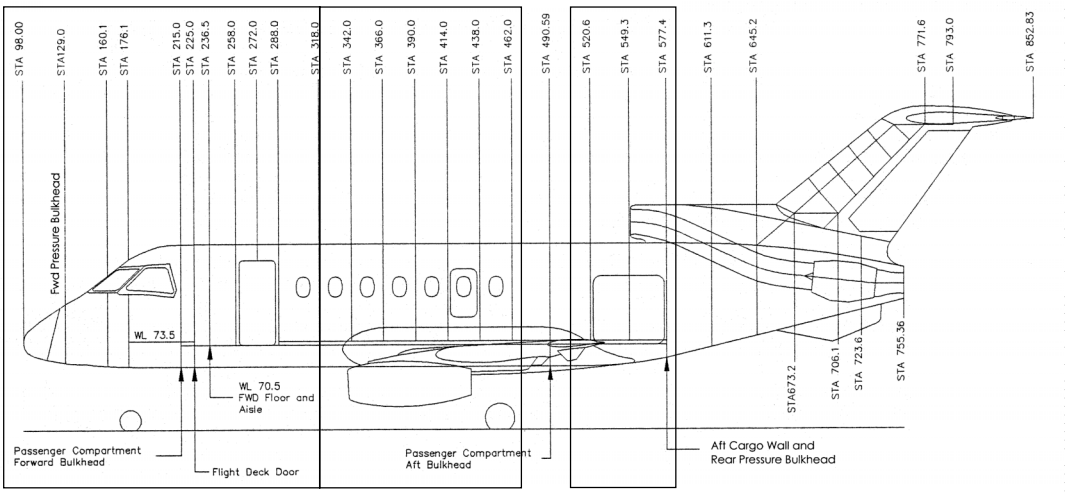

Figure 84. Fuselage structural arrangement and assemblies common to Saab 340 vehicle.

The PD340-2's wing thickness variation of 16% at the root to 12% near the tip, quarter-chord sweep of 21° and aspect ratio of 7.9 caters for typical cruise Mach numbers in the region of 0.70-0.75. The planform layout shows a distinct deviation away from the Saab 340 geometry, however, the modified super-critical MS(1)-0313 aerofoil section has been adopted from the Saab 340 and Saab 2000 designs. It was felt that well-established properties together with comprehensive experimental analysis base would aid in reducing initial research and development work.

15.1.4 PD340-2 Predicted Performance and Design Review

Figure 85 shows the predicted payload-range capabilities, whilst Table 6 summarises estimates of the major performance characteristics and compares these with current market equipment. It can be discerned that the 19 PAX regional/commuter market is basically a turboprop dominated one, and comparison of PD340-2 to these vehicles is based on data gathered from reference Business and Commercial Aviation[185]. PD340-2 appears to deliver a superior BFL of 1244 m (4082 ft) at ISA, sea level when compared to the Merlin 23 and Jetstream 31 vehicles. This indicates an improvement of 34% and 26% respectively. The only exceptions are Dornier 228 with 793 m (2600 ft) and Beech 1900D with 1139 m (3737 ft) giving approximately 36% and 9% shorter field lengths respectively. Furthermore, PD340-2 displays similar attributes even at hot/high conditions. The FAR/JAR landing field performance is estimated to be 1067 m (3502 ft) at ISA, sea level ambient conditions.

LRC and High Speed Cruise (HSC) show an appreciable difference between the PD340-2 and contemporary turboprops. LRC is 135 KTAS quicker than the fastest of the turboprops at maximum service ceiling and the maximum cruise speed capability has opened up a totally new regime of lower block times. A combined flight level and speed

increase promotes unconstrained cost and profit optimal flight technique formulation, therefore allowing for operational flexibility when ATC or route structure imposes off-optimal restrictions. In contrast, the slower and lower turboprops generally produce constrained optimal flight techniques, or a requirement of block times faster than the lower block time threshold physically permissible by the given vehicle. The direct consequence of this favourable performance is increased fuel consumption rate; however, as exemplified by SAR and PAX x SAR values close to or the lowest found in the survey. Nonetheless, a detailed DOC and annual profit analysis demonstrates that the higher fuel and other acquisition/maintenance related costs may be rationalised utilising turbofan technology through an increased productivity potential.

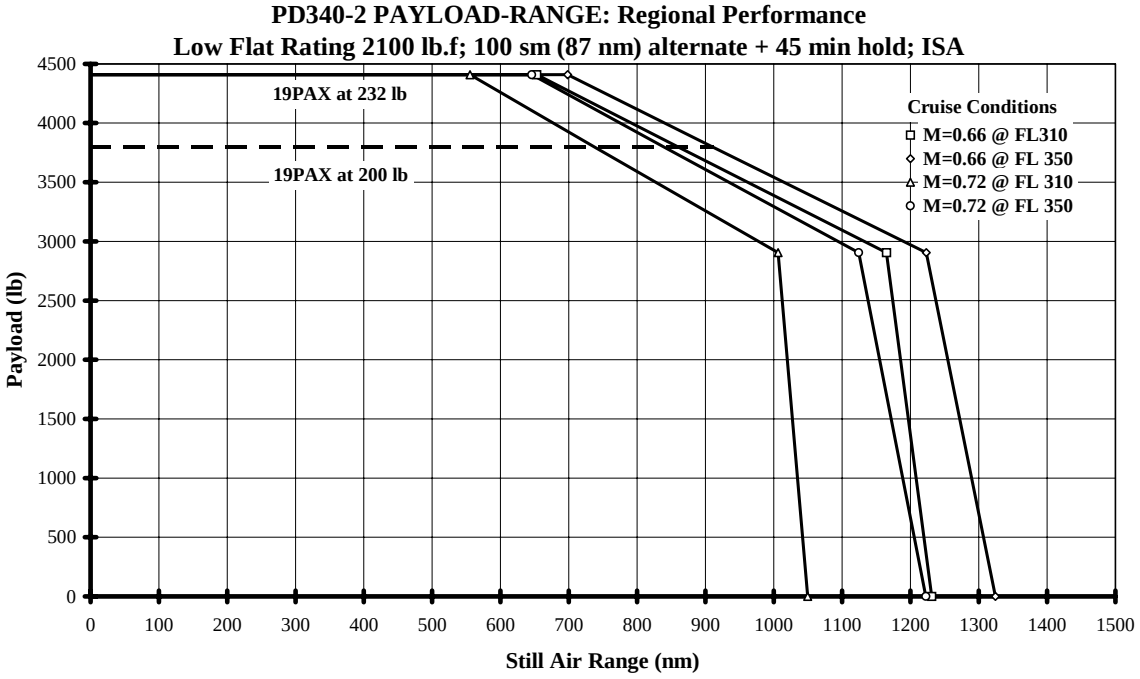

Figure 85. Payload-range envelope for PD340-2 19 PAX commuter turbofan transport.

Costing analysis has shown that an anticipated acquisition cost for PD340-2 would be around USD 6.0 million. This figure includes the total nominal manufacturing cost breakdown and a reasonable margin for future contractual negotiations. A cost and profitability model developed by Williams-Rolls Inc. was utilised in order to gauge the relative operational merits of PD340-2 against a typical 19 PAX turboprop competitor. The Metro 23 was chosen as the regional 19 PAX comparison basis because results for other competitors had demonstrated a close correlation to this aircraft.

Figure 86 illustrates the total normalised DOC with respect to maximum accommodation and stage length flown between PD340-2 and Metro 23. It should be noted that an 800 nm (1482 km) sector distance DOC result for the Metro 23 is not published even though the vehicle demonstrates no useful load limitations. Turboprop vehicles are considered less than attractive for stage lengths greater than 500 nm (926 km) due to prolonged block times with excessive noise and vibration leading to passenger discomfort. Using the sector DOC characteristics given above, an annual operating profit for given sector distance is presented in Figure 87. It can be discerned that the PD340-2 in terms of profitability exceeds that of the contemporary turboprops for stage lengths greater than

	PD340-2 Tri-jet	Dornier DO-228-212	Fairchild Merlin 23 SA-227-DC	Beech Executive BE-1900D	British Aerospace J31 BAe 3201
BFL (SL ISA) (ft)	4082	2600	5460	3737	5147
BFL (5000ft + 20°C) (ft)	6069	4500	6900	4977	6386
All Engines Operating ROC (fpm)	3431	1870	2320	2625	2240
One Engine Inop. ROC (fpm)	1059	440	580	675	450
AEO Service Ceiling	FL 350	FL 250	FL 252	FL 250	FL 250
OEI Service Ceiling	FL 164	FL 130	FL 115	FL 175	FL 100
Missions: 4PAX @ 200lb/PAX					
300nm					
Takeoff (ft)	2418	1800	3700	3193	3755
Block Time (hrs:mins)	0:53	1:22	1:04	1:08	1:13
Block Fuel (lb)	1301	1063	813	1029	810
Passenger Specific Range (nm/lb)	0.924	1.129	1.476	1.166	1.481
Flight Level	FL 350	FL 080	FL 160	FL 250	FL 250
600nm					
TO (ft)	2621	1900	3750	3271	3869
Block Time (hrs:mins)	1:35	2:40	2:07	2:12	2:24
Block Fuel (lb)	2214	2050	1523	1826	1478
PSR (nm/lb)	1.084	1.171	1.576	1.314	1.624
FL	FL 350	FL 080	FL 180	FL 250	FL 250
1000nm					
TO (ft)	2899	2120	3920	3378	4081
Block Time (hrs:mins)	2:35	4:24	3:36	3:38	3:59
Block Fuel (lb)	3398	3366	2277	2907	2362
PSR (nm/lb)	1.176	1.188	1.753	1.376	1.693
FL	FL 350	FL 080	FL 220	FL 250	FL 250
Productivity Missions					
275sm (239 nm)					
Stage/Fuel	2	2	3	2	2
PAX (@ 200 lb/PAX)	19	19	19	19	19
Engine Hours (hrs)	9.68	9.80	10.45	10.01	10.40
Total Fuel (lb)	13013	6602	7525	8174	6599
Total Trips	11	8	10	9	9
Seat Miles	57475	41800	52250	47025	47025
Block Speed (kts)	272	195	229	215	207
Mission Fuel (lb)	1183	825	752	908	733
Flight Level	FL 310	FL 100	FL 150	FL 240	FL 210
400sm (348 nm)					
Stage/Fuel	2		2	1	1
PAX	19		19	19	19
Engine Hours (hrs)	10.32		10.00	10.61	10.99
Total Fuel (lb)	13546		7181	8401	7031
Total Trips	9		7	7	7
Seat Miles	68400		53200	53200	53200
Block Speed (kts)	303		244	230	222
Mission Fuel (lb)	1505		1026	1200	1004
FL	FL 350		FL 160	FL 250	FL 210
800sm (695 nm)					
Stage/Fuel	1				
PAX	19				
Engine Hours (hrs)	9.79				
Total Fuel (lb)	13012				
Total Trips	5				
Seat Miles	76000				
Block Speed (kts)	355				
Mission Fuel (lb)	2602				
FL	FL 350				

Table 6. Parametric review of PD340-2 commuter against contemporary turboprops.

approximately 180 nm (333 km) and maintains this posture up to about 1000 nm (1852 km) with a global profit maximum occurring for distances of around 600 nm (1111 km). This profit crossover between PD340-2 and Metro 23 at 180 nm may not seem immediately evident if the normalised DOC comparison is considered in isolation.

The increased productivity potential (exemplified by Table 6 above) of the turbofan through increased block speed enables completion of a greater number of sector missions for given hourly based reference time frame utilisation compared to the much slower

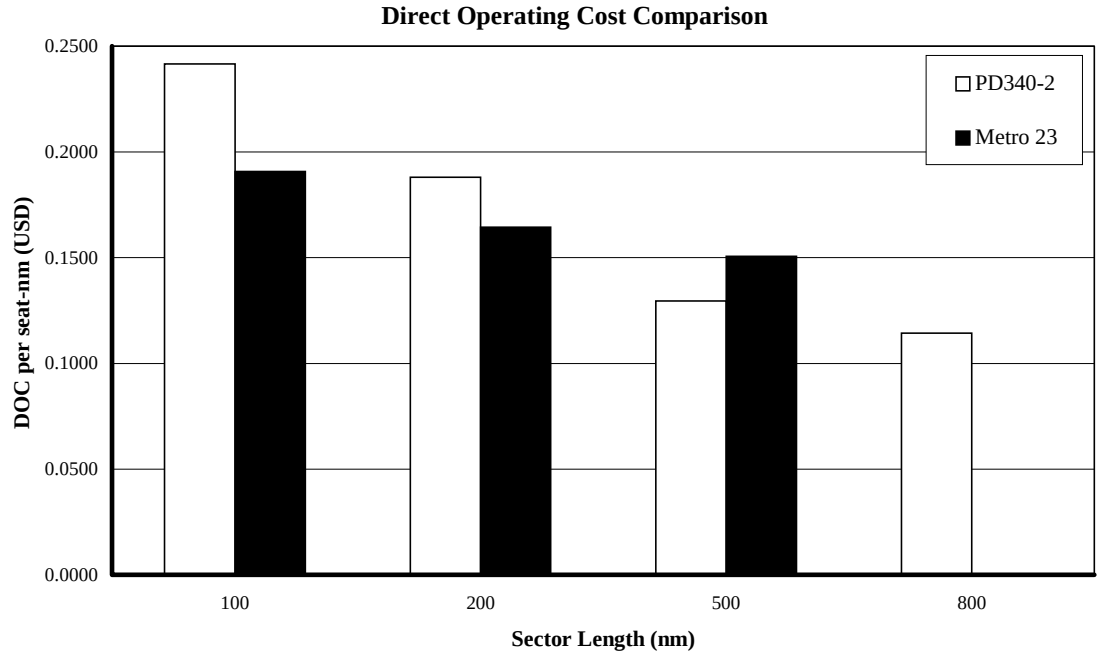

Figure 86. Direct Operating Cost per seat-nm comparison of PD340-2 to competition.

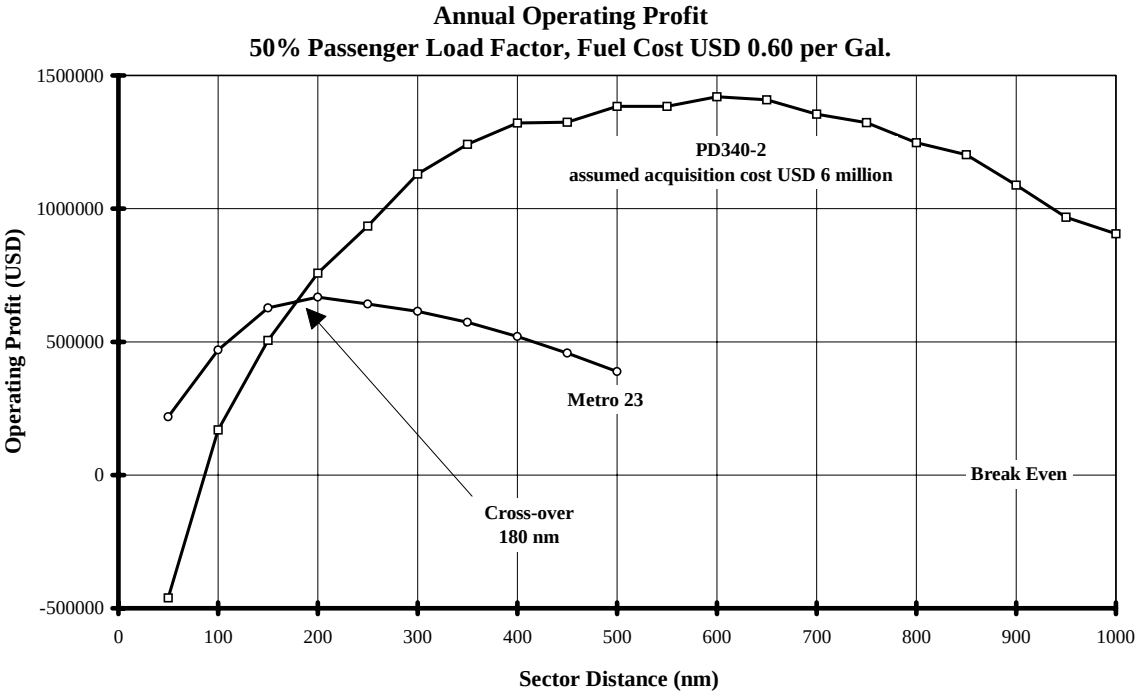

Figure 87. Annual operating profit comparison of PD340-2 to competition (50% load factor).

turboprop - thereby rationalising the impact of sector mission cost through reduction of the time related cost component. It must be duly noted that this study utilised a conservative

assumption of 50% passenger load factor. FAA[186] forecasts indicate that a 60% load factor for turbofans would be more attune to market realities; however, the lower load factor assumption has the advantage of enabling an equitable comparison between equipment by keeping the yield quantity the same regardless of power plant selection. Even though the acquisition cost for PD340-2 is approximately USD 1-2 million higher than it's ageing 19 PAX contemporaries, the regional turbofan's staid viability and extreme competitiveness demonstrates the potential for this design.

It was deemed early in the project that the final PD340-2 design not only conform to a unique set of specifications from the outset, but also, each decision whether philosophical or technical should be based on the premise of accommodating an ER variant as well as stretching the current 19 PAX vehicle to a 30-35 PAX version[183], hence giving the vehicle marketing flexibility and fulfilling objectives of creating a family concept. Initial studies show that the PD340-2 layout may permit an ER version. Considerable fuel increments can be available through the introduction of outboard wing tanks and a centre fuel tank. Projections show range performance may be enhanced by at least 500 nm (900 km) for given payload complements if an increased gross weight variant produced by the addition of this fuel increment to PD340-2's current MTOW is considered. By raising available thrust to the maximum flat rating threshold of 2300 lb.f (10.2 kN) per engine, this should assist in off setting excessive field and en route performance degradation, and indications show that PD340-2 ER would still exhibit competitive attributes upon comparison to contemporary turboprops.

The PD340-2 vehicle proposal is a concept that accommodates a maximum of 19 PAX and affords comfort through speed and spaciousness that is not paralleled in a contemporary regional/commuter market. The result was a regional workhorse that utilises turbofan technology without high costs; it is projected that new niche markets may be opened as a result of this and other similar proposals. The design has pivoted around the philosophy of derivative compatibility with the Saab 340, namely, fuselage including cross-section, partial aft structure and forward cabin, wing torsion box geometry, and, ancillary basic structural elements and principles. This has greatly assisted formulation of a current projected equipped price of around USD 6.0 million. A trade off of increased fuel flow denoted by lower SAR and PAX x SAR values compared to its turboprop counterparts was shown to be offset by reduction of time related costs due to the improved block time performance. The design has also demonstrated a significant degree of potential by allowing for an extended range variant, as well as, requiring only a moderate array of modifications to the basic 19 PAX vehicle configuration in order to produce a future 30-35 PAX version.

15.2 PD340-3X

In keeping with an economically feasible practise of generating new products from an existing baseline, efforts were now focused on the 30-35 PAX category of aircraft. It was recognised that unlike contemporary 50 PAX turbofan aircraft, the current offerings of Fairchild Dornier 328JET and Embraer ERJ 135 are not truly optimised vehicles, but are reconfigured versions with great emphasis placed on economic considerations of commonality. The most unfortunate consequence of this situation is that the contemporary 30-35 PAX turbofan has become quite limited in terms of operational flexibility, and large penalties with regards to the field-en route performance and design weight trade off have been incurred. The goal of this project was to create a commuter aeroplane capable of demonstrating greater operational flexibility whilst still retaining the family concept philosophy as well as possessing a competitive operating costs edge.

15.2.1 PD340-3X Specifications

After studying the current market the following specifications were adopted:

1. 30-35 seats at 32-31 inch seat pitch;
2. Engines to be new generation Williams FJ44-XX preliminary design fan with projected maximum sea level static thrust of 2850 lb.f. (12.68 kN);
3. JAR/FAR takeoff BFL of no greater than 5000 ft (1524 m) at ISA, sea level;
4. No climb restrictions on maximum takeoff gross weight for conditions up to and including ISA+30^{o}C and 5000 ft airport elevations;
5. The penalty in off-loaded weight from MTOW to be significantly lower than competition when clearing FL 160 during OEI en route climbs at ISA+20^{o}C conditions (driftdown proficiency);
6. Minimum range of about 500 nm with full payload assuming JAR OPS-1 reserves, and an emphasis placed on maximising multi-hop capability for typical sector mission segments;
7. Comparable block times for typical sector missions with operating costs equal to or better than direct competitors;
8. Flexibility for both standard and extended-range versions; and
9. A derivative of the 19 PAX PD340-2 tri-jet turbofan vehicle[112,181,182] with an emphasis placed on maximising commonality.

15.2.2 PD340-3X Synopsis of Trade Studies and Optimisation

The basic shape of the aircraft was already set because a specification to adhere to a family concept was proposed. The initial trade study involved inspection of different stretched fuselage layouts until both cargo and seating could be maximised with respect to general performance criteria and power plant used.

An example of the final trade study for PD340-3X STD is given in Figure 88. In this particular instance, since the power plant was already selected, MTOGW was traded against S_W with off-loaded fuel (maximum available fuel less some arbitrary fixed amount) as the additional primary sensitivity parameter. The S_W trade interval was not large due to a stipulation given by the specifications of utilising already existing structure: the PD340-2 wing imposed limitations on maximum span increase through introduction of a minimum permissible taper ratio threshold of $\lambda \geq 0.27$ set by the author. Even though guidelines for cost and profit optimisation were available, initial observations showed that fixed sector mission performance parameters like block time and block fuel did not alter by any great measure due to this small S_W interval thus not affording much scope for assessment of operational flexibility versus DOC and P-ROI. It was therefore postulated that cost would in this instance show an adequate measure of potential for profitability and was then in turn considered to be a direct function of airframe weight - this assumption having the additional benefit of minimising the effort expended for final selection.

The selection process for optimum MTOW and corresponding S_W necessitated a trade off between increases in range and OEI climb performance against minimising of BFL together with V_{REF}, or indirectly the required landing distance. Attention should be paid to the constraints shown in Figure 88. They represent maximum payload range (MPAY-R) assuming maximum SAR flight techniques and JAR OPS-1 reserves, lines of constant maximum attainable stage length (MT-MS) assuming minimum time flight techniques with various passenger mission requirements and JAR OPS-1 reserves, and finally, off loaded weight penalties from MTOGW associated with lines indicating clearance of FL 160 assuming ISA+20^{o}C conditions and OEI. The V_{REF} constraint lines were derived by

assuming each respective candidate completes a stage length of 200 nm from MTOGW at brakes release and finishes with a conservative landing gross weight based on fuel burned via minimum fuel techniques - in accordance with the multi-hop specification. The optimum reference wing area was chosen to be 31.8 m^2 (342 sq. ft), which corresponds to a predicted MTOW of 12950 kg (28550 lb) defined by the criterion that 1369 kg (3018 lb) of fuel is off-loaded from its respective maximum available fuel load of 2912 kg (6420 lb).

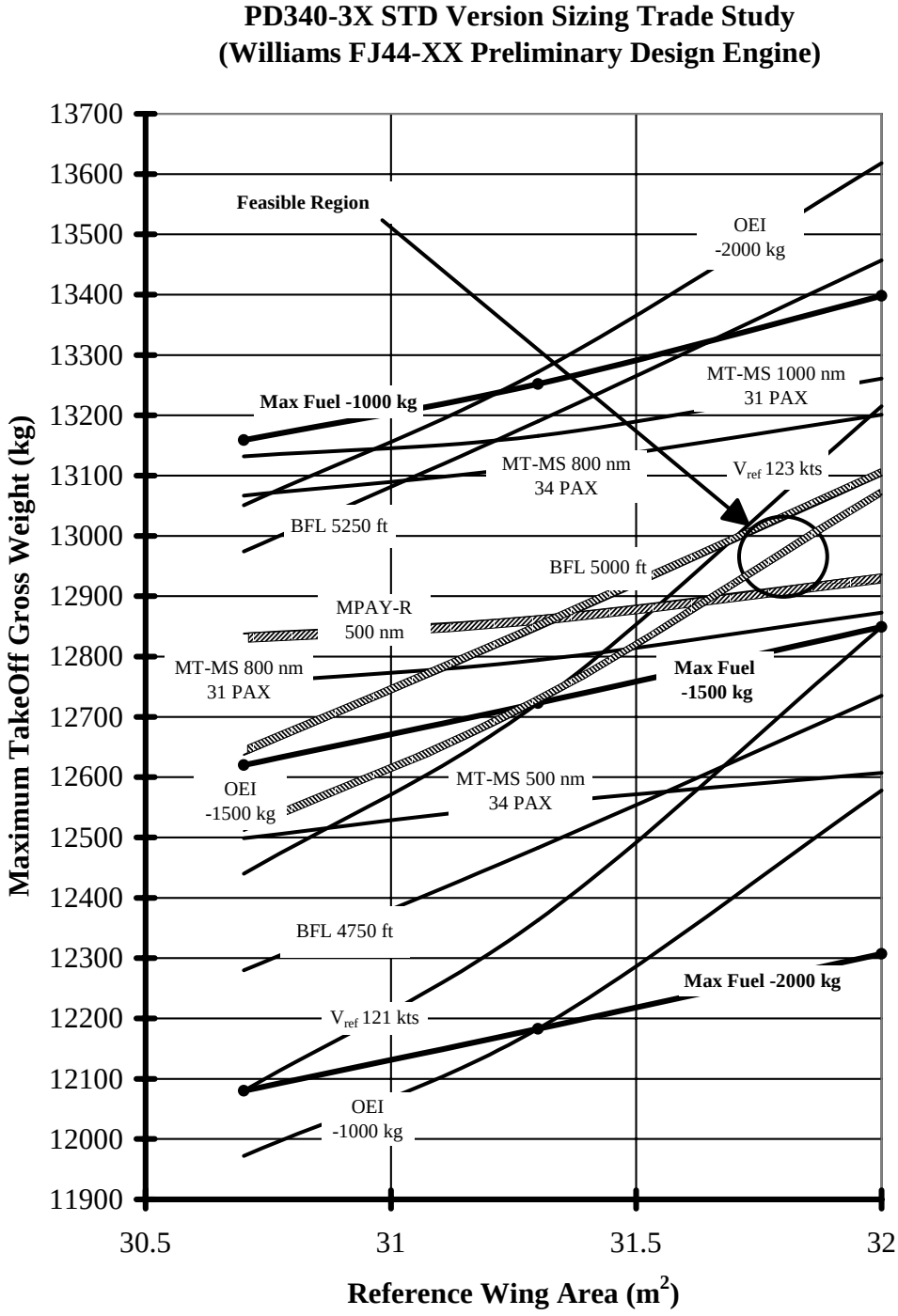

Figure 88. Trade study and final configuration selection for PD340-3X STD tri-jet regional transport.

15.2.3 PD340-3X Design Description

Since the already existing PD340-2 wing planform was utilised, subsequent low-level optimisation involved span increases with some modifications to wing tip geometry. Span was increased from the current 15.24 m (50 ft) to 17.88 m (58 ft 8 in.) with the original PD340-2 basic wing planform intact. The span increase gave a 9% wing area expansion (and greater maximum available fuel capacity) with associated increases in aspect ratio from 8.0 to 10.0 and flap as well as aileron span. A moderate sweepback combined with a relatively thick supercritical wing section profile enables cruise in the region of M0.70-0.75 while projected certification altitude remains at 35000 ft. The wing planform geometry was enhanced through the introduction of raked wing tips, which is envisaged to decrease vortex-induced drag at low speeds with the added advantage of offering some element of increased en route performance efficiency. The PD340-2's high lift system of double slotted Douglas type flaps were retained and are expected to deliver slightly higher lift increments when deployed for PD340-3X due to improved aerodynamic efficiency.

The fuselage cross section utilises the basic PD340-2 which was incidentally based on dimensions used for the Saab Aerospace Saab 2000 and Saab 340 vehicles. Forward and aft plugs permitted a fuselage structural stretch from the original 16.70 m (54 ft 9 in.) used for the 19 PAX to 19.20 m (63 ft) for the 31-34 PAX variant. There is space for 31 PAX at a comfortable 32 inch seat pitch, or alternately, 34 PAX can be seated at a 31 inch pitch. Due to the larger capacity of this vehicle, additional space was incorporated to the PD340-2's cargo hold resulting in an increase from 6.4 m^3 (226 cu. ft) to 8.3 m^3 (295 cu. ft). The nacelles were also modified since the fan is slightly larger and airflow requirements are higher. Projected increases in fan diameter with the Williams preliminary design FJ44-XX compared to PD340-2's already existing FJ44-2 installation are approximately 0.076 m (3 in.). This fortuitously requires no lengthening of the landing gear legs but the gear must accommodate increases in constituent weight due to overall increases in gross weight. The increase in empennage moment arm is produced by a fuselage stretch, and calculations have shown that no changes to the PD340-2's existing empennage are necessary to cope with both the larger wing and higher thrust ratings of PD340-3X.

Figure 89 gives a three-view representation while Table 7 summarises the predicted PD340-3X STD and PD340-3X ER weight, geometry and performance characteristics. It

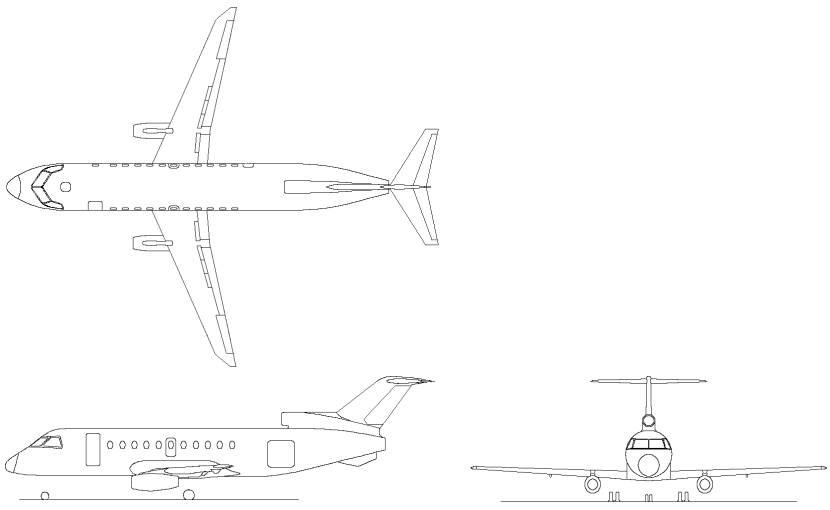

Figure 89. PD340-3X 31-34 PAX turbofan regional transport general arrangement.

	PD340-3X STD		PD340-3X ER	
Weights				
Maximum Takeoff Weight	12950 kg	28550 lb	13750 kg	30313 lb
Maximum Landing Weight	12436 kg	27416 lb	13224 kg	29154 lb
Maximum Structural Payload	3720 kg	8201 lb	3720 kg	8201 lb
Geometry				
Wing Span	17.9 m	58 ft 8 in.	17.9 m	58 ft 8 in.
Reference Wing Aspect Ratio	10.0		10.0	
Reference Wing Area	31.8 m^2	342 sq. ft	31.8 m^2	342 sq. ft
Fuselage Length	19.2 m	63 ft	19.2 m	63 ft
Fuselage Maximum Diameter	2.31 m	91 in.	2.31 m	91 in.
Performance (ISA) JAR/FAR 25				
Balance Field Length, s.l.	1507 m	4944 ft	1586 m	5203 ft
AEO Service Ceiling	FL 350		FL 350	
Typical Max. Cruise Speed	M0.72		M0.72	
Landing Field Length, s.l.	1480 m	4856 ft	1528 m	5013 ft

Table 7. Leading particulars for PD340-3X STD and PD340-3X ER commuter turbofan concept.

should be noted that the PD340-3X STD power plant thrust has been de-rated to a 2600 lb.f maximum static rating, whereas, the PD340-3X ER utilises the maximum flat rating of 2850 lb.f at ISA, s.l., available from Williams' FJ44-XX preliminary design engine.

15.2.4 PD340-3X Predicted Performance and Design Review

Figure 90 shows the predicted payload-range for both STD and ER versions of the aircraft. The chart curves are given for maximum SAR and maximum block speed flight techniques since this representation not only gives the maximum range capability but also an indication of the maximum fixed sector distance performance afforded by the vehicle for given mission payload and assuming minimum time flight techniques.

Comparison for typical sector missions of 34 PAX and stage length of 500 nm with JAR OPS-1 reserves policy and minimum time flight techniques in ISA still air show that PD340-3X is approximately 4 minutes slower than the ERJ 135 where the total block time for both aircraft is around 90 minutes. This performance is complemented by a significant reduction in block fuel – an estimated saving of around 30% can be achieved with a PD340-3X vehicle over its competitor. The TOGW required for completing this mission results in PD340-3X being approximately 4100 kg (9000 lb) lighter over ERJ 135, which exemplifies the projected lower airport charges through a MTOW review, and, the BFL comparison using these mission gross weights are also in favour of PD340-3X with field lengths of 1291 m (4236 ft) at s.l., ISA for standard and extended range versions assuming an initial takeoff flap setting of 20^o. This is approximately 6-7% shorter than ERJ 135 employing a 22^o takeoff flap setting at similar ambient conditions. A direct comparison to the 328JET shows that this vehicle is with a MCRZ of M0.66 slower in terms of block speed than both PD340-3X and ERJ 135 for fixed sector distances but is superior in terms of field length performance. No climb limitations on TOGW are imposed (assuming no field length limited unbalanced performance exists) for conditions up to ISA+35^{o}C and ISA+29^{o}C and 5000 ft airport pressure elevation for PD340-3X STD and PD340-3X ER

vehicles respectively. This makes for competitive performance even if the 328JET is characterised by exceptional field climb performance. The ERJ 135 is climb-limited for conditions above ISA+25^{o}C and 2500 ft airport pressure altitude. Combined with a target acquisition cost of USD 8.0 million, this design is seen to be an attractive as well as competitive alternative to the USD 14.0 million ERJ 135 and USD 13.0 million 328JET turbofan vehicles in the market.

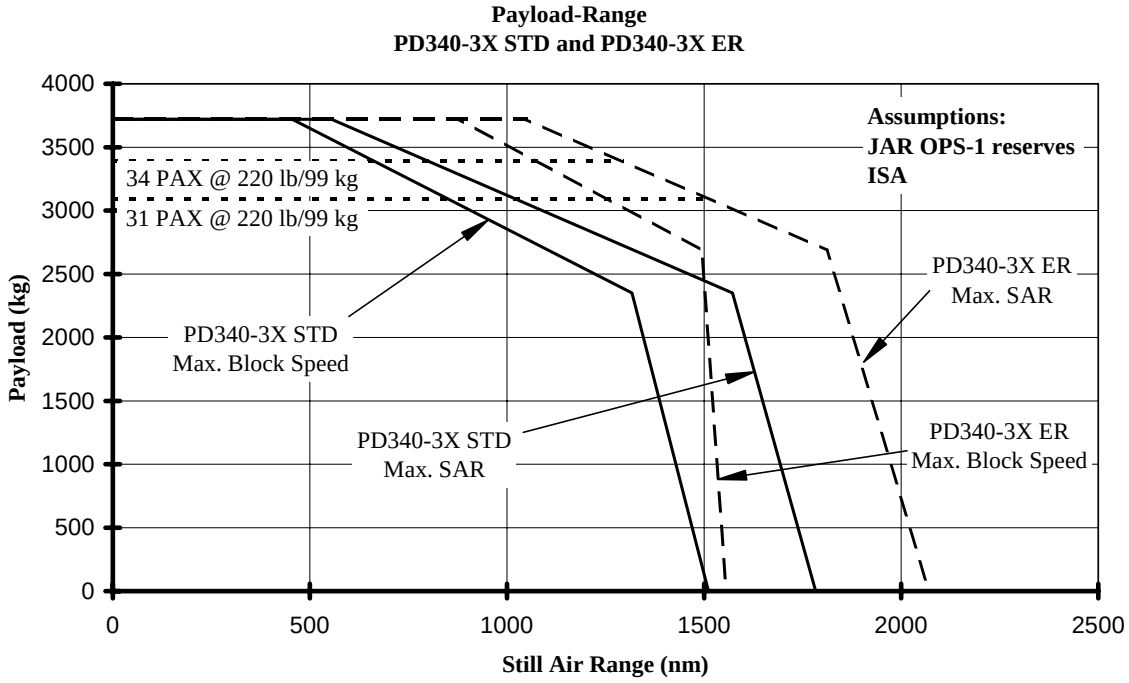

Figure 90. Payload-range envelope for PD340-3X STD and PD340-3X ER 31-34 PAX regional turbofan transports.

15.3 TOLS-X

The oblique wing concept has fallen in and out of favour over the latter half of the Twentieth Century. It gathered notoriety with Vogt's variable sweep oblique wing aircraft design proposal in the 1940s designated as the Blohm and Voss P202[187]. This unconventionally asymmetric aircraft design was one of the first concerted attempts to reconcile conflicting conditions of wing sweep optimality for low and high speed performance of an aerospace vehicle. Around the same period, Campbell and Drake[188] at NACA conducted experimentation on similar layouts. It was subsequently championed by Jones[189,190] who found interest in such a configuration because analysis and windtunnel testing indicated that elliptical oblique wings would provide minimum wave drag in supersonic flow.

Notwithstanding the potential offered by oblique wings, there exists a distinct absence of such aircraft in both the military and civilian operational arenas. From a programme perspective, it is potentially a large risk venture. Historically, difficulties have included the following: problems with low-speed aeroelastic divergence associated with a high aspect ratio, forward swept semi-wing; in the absence of a mature automatic control systems technology knowledge-base, the adequate handling of longitudinal and lateral motion coupling produced by the interaction of highly non-linear aerodynamic and inertial

moments; lack of rigid body and wing structural mode coupling; the drawback of having an obligatory wing pivot mechanism; and, the sense it is a highly exotic configuration.

Alternative configurations that challenge the traditional cantilevered single wing have also been examined. As a follow on from experimentation done by Olson and Selberg[191], studies by Rhodes and Selberg[192] showed that both closely coupled dual-wing and swept forward swept rearward (connected at the wingtip) systems exhibit aerodynamic advantages over single wing configurations. Another example of unconventional planform design is the strut-braced wing (SBW) and origins of this concept can be traced back to Pfenninger's research of a long-range transonic transport truss-braced wing study[193] done in the mid-1950s. Proponents of SBWs cite as a result of favourable interaction between structures, aerodynamics and propulsion, potential for higher aerodynamic efficiency and lower MTOW can be realised. Encouraging results from design studies of the 2010 SBW transonic transport completed by Virginia Polytechnic (Gundlach et al[194]) show a potential to shave up to 10% of MTOW defined by design mission requirements.

In view of the significant potential for performance enhancement and with due regard given to the difficulties discussed above, a new hybrid concept is proposed here which comprises two independent, fixed, oblique (or skewed) wings linked by a wing-pylon-engine bracing structural system (WPEBS). This configuration, coined as Twin Oblique Lifting Surfaces or TOLS (Figure 91), is intended to produce a new aircraft design perspective that will afford acceptable en route efficiency at high-transonic and low-supersonic speeds with an unconventional operational flexibility of satisfactory field performance and stalling characteristics.

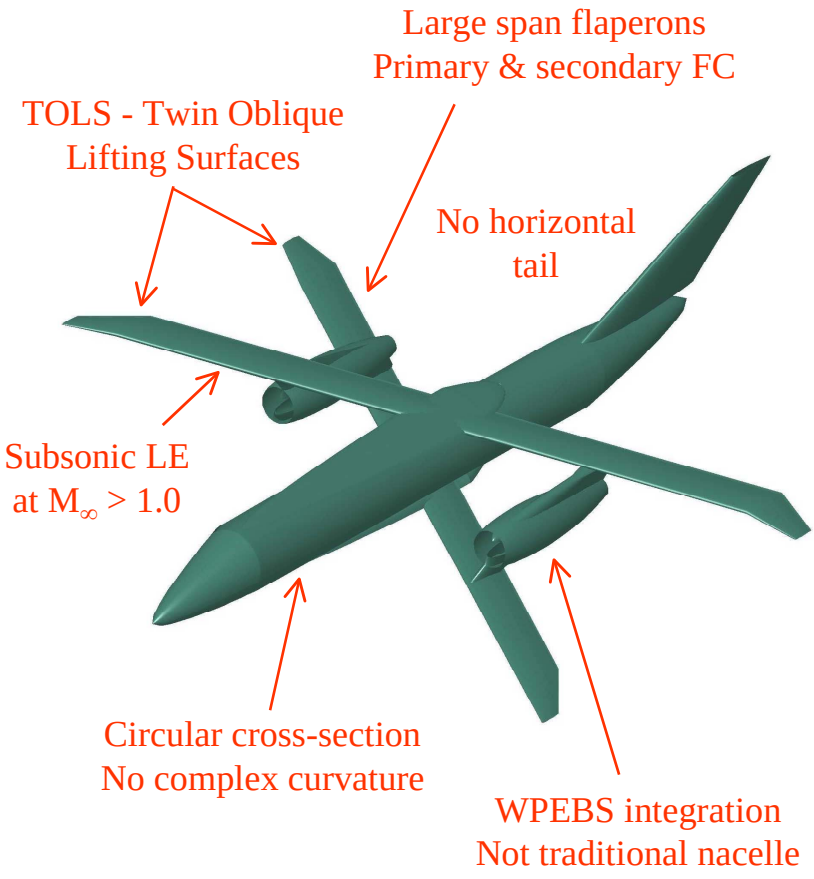

Figure 91. Introducing the Twin Oblique Lifting Surfaces (TOLS) configuration.

15.3.1 TOLS-X Specifications

A business jet aeroplane design must concurrently fulfil a number of requirements as dictated by today's discerning clientele: a premium on passenger comfort, a high degree of operational readiness and exceptional performance characteristics. After surveying current offerings, and re-defining the notion of contemporary business aircraft en route performance capabilities, the hard specifications were defined to be:

- The vehicle must accommodate at least 19 passengers seated with a 1.40 m (55 in.) pitch;
- TOFL less than 1830 m (6000 ft) at ISA, sea level conditions;
- Effective operation at 5000 ft (1524 m) airport pressure altitude and at ISA+20°C conditions;
- Initial cruise altitude of at least FL 470;
- Time to climb to typical bandwidth of cruise flight levels in around 15-25 minutes;
- Service ceiling not less than FL 510 and HSC Mach number not less than 1.20;
- Maximum range not less than 4000 nm (7408 km) at Typical Speed Cruise (TSC) of M0.95, and, 3500 nm (6482 km; this represents a westbound Trans-Atlantic flight between LHR and JFK with 85% probability winds) at MCRZ assuming NBAA IFR mission rules and reserves, and, a maximum passenger complement;
- Landing reference speed to be not greater than 135 KCAS at MLW and ISA, sea level conditions;
- A competitive en route SAR efficiency at TSC compared to similarly sized contemporary large and super-large business jets;
- Low parts count and relatively simple construction, avoidance of complex double curvature in fuselage geometry;
- Should fit into existing ATC patterns, and noise levels should comply to current version of yet to be ratified Chapter 4 definition;
- The vehicle shall be certified according to FAR 25 and JAR 25 transport category aircraft requirements.

15.3.2 TOLS-X Synopsis of Trade Studies and Optimisation

The design cycle began by establishing the fuselage size in isolation. The height, width and resulting fineness basically catered to providing ample volume in accommodating the necessary 1.40 m (55 in.) seat pitch for passengers. Ancillary attention was paid to minimizing frontal area as well as producing a lower $\text{Volume}^2/\text{Length}^4$ (or volume-reference length ratio) for minimum zero-lift and wave drag respectively. The width of the fuselage was also influenced by the requirement of allowing at least 610 mm (24 in.) of aisle width between passenger seats. Finally, consideration was also given to ensure space for landing gear, avionics, supporting systems and fuel was sufficient. The geometric layout of the fuselage was loosely based on the 50 PAX Saab 2000 high-speed turboprop[92]. Apart from catering to a higher pressure differential, the cylindrical cabin has mostly been retained, however, extensive modifications have been introduced to the forward fuselage to meet the requirements imposed by operating in the high transonic and low supersonic speed regime.

Even though this design study involves a hypothetical or "paper" engine the results derived from initial analysis were used to propose a plausible engine the market could conceivably design and manufacture. As expected, the engine optimisation process focused

on the cruise condition for sizing. Preliminary investigations showed a suitable engine should meet the following criteria:

- Target maximum static thrust of 71.2 kN (16000 lb.f) at sea level standard conditions;
- Cruise BPR of around 3.0 to reduce the thrust lapse rate at given speed and altitude;
- Overall Pressure Ratio (OPR) of at least 30 to keep the overall engine efficiency as high as possible;
- Relatively high engine Turbine Entry Temperature (TET) to maintain required specific thrust characteristics.

The BMW Rolls-Royce BR715 was identified as an ideal candidate for future derivative development work. The basic engine configuration can be retained but the requirement of an en route design BPR decrease from 4.8 to 3.0 will have with it an associative reduction in fan diameter from 1.53 m (60 in.) to approximately 1.25 m (49 in.). This had a beneficial effect of reducing the engine empty weight by almost 454 kg (1000 lb). The design point TSFC degrades somewhat from 0.63 at M0.76 and 35000 ft to approximately 0.73 at 45000 ft and M0.95. Operation at low supersonic speeds will reduce the possibility of maintaining an exceptionally high pressure recovery. Nonetheless, the axisymmetric intake was found to be satisfactory for speeds slower than M1.50. Providing due consideration is given to applying sharper lip geometry, the single normal shock wave of a pitot intake would yield only about a 2% reduction compared to the two-dimensional shock intake as cited by Whitford[195]. Also, this design ensures efficient structural shape for low duct weight and minimum wetted area for given stream-tube flow area.

The selection of aerofoil section thickness and general wing design characteristics were based on studies presented by Kroo[196]. Numerical optimisation techniques have shown that a t/c of up to 14.0% is acceptable for oblique wing design proposals. Indeed, Van der Velden and Torenbeek[197] have taken this notion further by employing a higher t/c of 15.0% for their supersonic oblique wing transport design. With respect to planform geometry design, taper ratio and wing twist needs to be selected such that unbalanced lift loads are avoided. This circumstance fortuitously gives scope to approximate the elliptical load distribution ideal as well.

A very limited scope of MVO was undertaken in this study. The objective here was to ascertain in a relatively quick manner if the TOLS configuration exhibits feasibility. Many of design variables were systematically bounded for the global optimisation process after formulating the best objective function result for that given sub-space. For example, once initial estimates yielded an idea of the most likely engine candidate dimensions and weight, a generic trade study between engine lateral coordinate wing placement and aircraft empty weight was examined. To assist in this process, weight relief factors were drawn from semi-analytical methods of contemporary transport aircraft wing weight estimation done by Torenbeek[12].

Various combinations of wing area, complementary wing skew angles, thickness and aspect ratio were analysed to determine an acceptable trade off between good field and en route performance. Each candidate MTOW design point was defined as one in which 19 PAX at 100 kg (220 lb) can be accommodated with maximum fuel load. A myriad of possible performance constraint criteria to inspect for sensitivity and subsequently identify feasible solutions were reviewed. The hard specification TOFL constraint of 1830 m (6000 ft) was initially found to be a limiting condition. Further scrutiny revealed the engine inoperative decision speed (V_1) should be considered as a primary parameter because a

combined effect of high wing loading and V_{MC} limitations produced reference speeds that became quite high. As an orthogonal delineation to the V_1 decision speed trade, two separate en route performance inequality constraints were examined: maximum PAX range at MCRZ speed technique, and, range with maximum payload assuming constrained maximum SAR technique at M0.95. The first choice, which proved to be the most limiting, of maximum range at MCRZ speed technique assuming a payload of 19 PAX at 100 kg (220 lb) each with NBAA IFR flight guidelines and reserves, 200 nm alternate and 30 minutes hold was finally designated as the primary en route constraint criterion. Consequently, the selection process focused on maximising range, and, minimising TOFL as well as lowering the V_1 take-off safety speed.

In terms of final selection in this study, thrust-to-weight (T/W) and wing loading (W/S) needed to be maximised in order to rationalise the gross weight, thereby theoretically reducing the equipped price. This is explained by the presence of a fixed power plant (hence thrust level) and the fact decreasing reference wing area allows less available space for fuel. In stark contrast, S_W and AR needed to be maximised (minimise W/S) in order to minimise takeoff and landing distances as well as the respective reference speeds. For given S_W, AR needed to be reduced to increase available fuel volume thence to maximise range performance. To reconcile these conflicting effects, the requirements were plotted on a series of charts that allowed definition of bounded geometric regions in which freedom of selection existed. An example of a simplified final T/W and W/S trade study for the high-performance executive transport is given in Figure 92. Note the final candidate for selection was subsequently given the designation of TOLS-X.

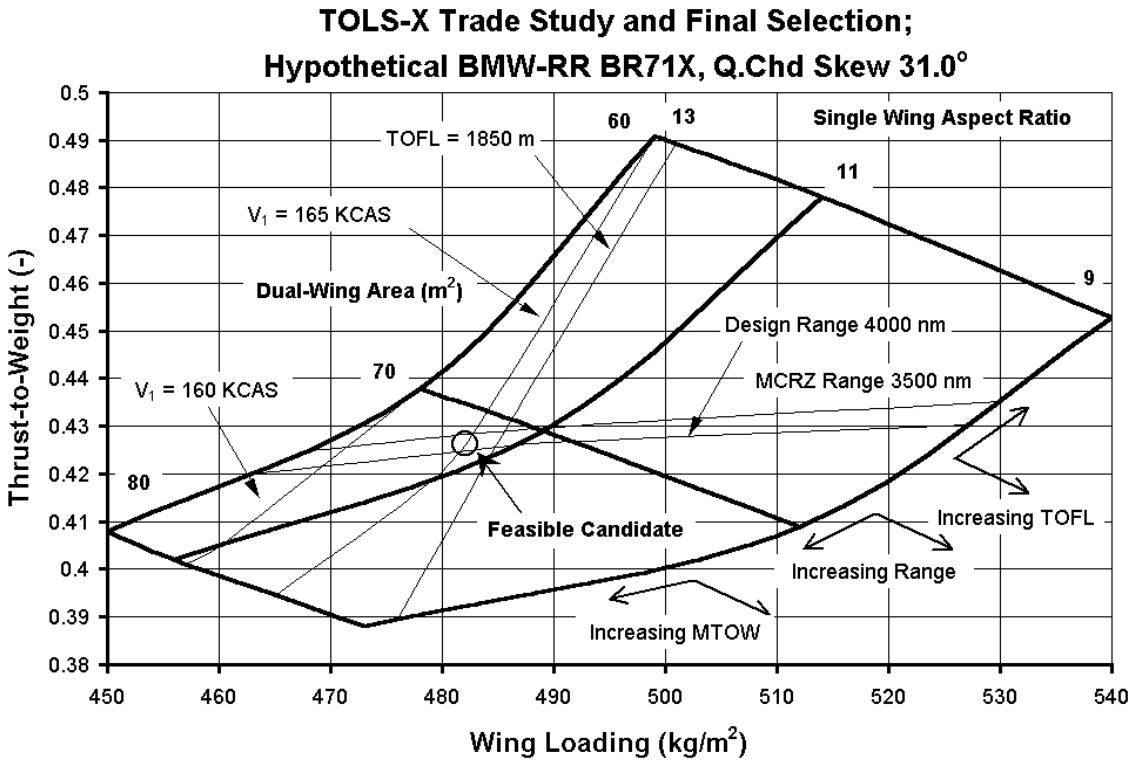

Figure 92. Simplified representation of final selection for TOLS-X design.

It can be discerned for an optimal wing skew of 31.0°, the T/W and W/S sensitivity study indicates that approximately 482 kg/m^2 (98.7 lb/sq.ft) and T/W of 0.426 are appropriate. This design candidate with MTOW equal to 34493 kg (76043 lb) and S_W of 71.6 m^2 (771 sq.ft) produces a vehicle which can operate out of runways less than 1830 m (6000 ft), and is capable of completing 3500 nm (6480 km) range at MCRZ speeds of up to M1.22.

15.3.3 TOLS-X Design Description

The TOLS-X vehicle is a tricycle, employs dual-winged planforms with relative skew, and, twin turbofan using podded engine installations connected with pylons between the upper and lower skewed planforms. The vehicle is pressurised and incorporates only a vertical tail for empennage. The landing gear is retractable and each leg is twin wheeled. The vehicle accommodates a flight crew of two and an optional flight attendant. The standard configuration seats a maximum of 19 passengers. The power plant is a medium BPR derivative of the BMW Rolls-Royce BR715 turbofan designated as BMW Rolls-Royce BR71X. It is projected the engines shall comply with the yet to be determined Chapter 4 noise levels. The vehicle shall be configured in a manner such that Extended Twin Operations (ETOPS) approval shall be granted with minimal modifications. The vehicle is designed to comply with FAR 25 U.S airworthiness regulations and the European JAR 25 rules. Table 8 supplies a synopsis of TOLS-X design weights, merit values and geometry data. Figure 93 shows a three view general arrangement of the TOLS-X high performance executive transport design.

Weights		
Maximum Ramp Weight	34593 kg	76264 lb
Maximum Takeoff Weight	34493 kg	76043 lb
Maximum Landing Weight	31000 kg	68343 lb
Maximum Zero Fuel Weight	20660 kg	45547 lb
Basic Operating Weight	17968 kg	39612 lb
Maximum Payload	2693 kg	5937 lb
Maximum Usable Fuel	14729 kg	32472 lb
Merit Parameters		
Wing loading	482 kg/m^2	98.7 lb/sq.ft
Thrust-to-weight	0.426	
External Dimensions		
Overall span	20.5 m	67 ft 2 in.
Height	7.48 m	24 ft 7 in.
Overall length	29.6 m	97 ft 1 in.
Fuselage Length	27.3 m	89 ft 6 in.
Fuselage External diameter	2.31 m	7 ft 7 in.
Wing Geometry		
Total reference area	71.6 m^2	771 sq.ft.
Reference wing aspect ratio	8.79	
Quarter chord skew	±31.0°	

Table 8. Design weights, merit values and geometry data for TOLS-X vehicle.

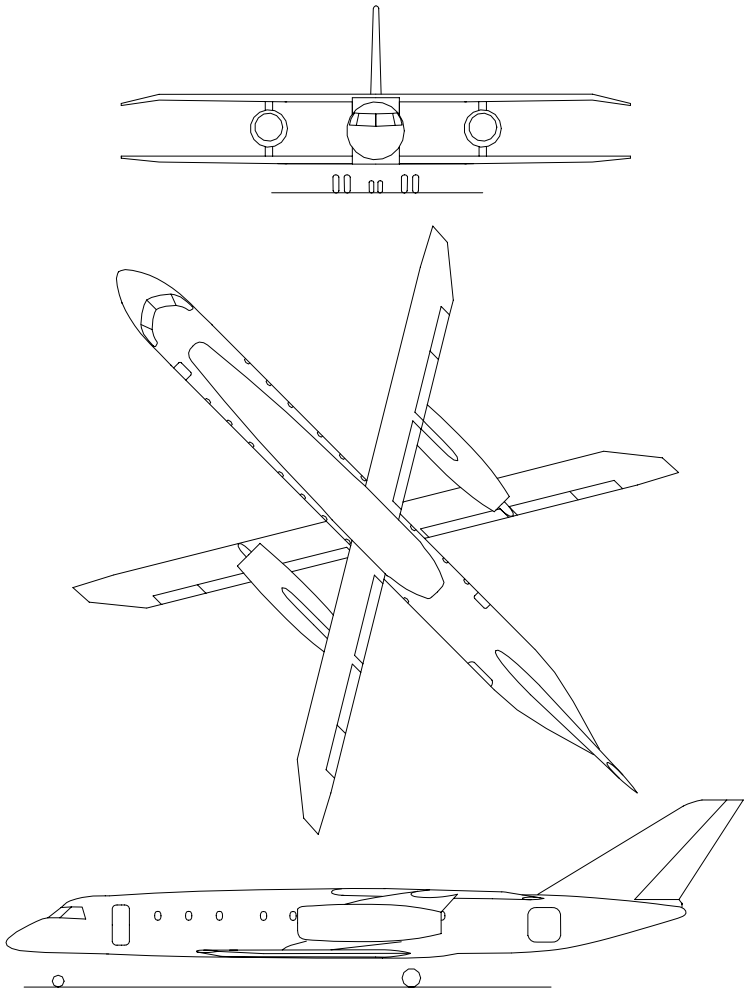

Figure 93. The TOLS-X high-performance executive transport general arrangement.

Longitudinal and lateral-roll control are produced by three distinct surfaces, namely, the upper and lower fixed skewed wings and the vertical tail. Each of the four semi-wings employ the use of three simple plain flaps tasked to act in the dual role of flaperon. The wing mounted flaperon relative chord length is 25% of the local swept wing chord. The maximum deflection is set at 30° TEU (-) and 75° TED (+). Symmetric flaperon deflection provides pitch control; while asymmetric deflection of the flaperons coordinated with rudder-assist provides roll control authority through an aileron to rudder interconnect. The flaperons are each a mono-spar structure hinged on four supports attached to the wing rear spar and collectively extend out to 80% of wing semi-span. The two most inboard flaperons that extend out to 65% semi-span also act as the secondary flight control surface group, i.e. high-lift arrangement, in-flight spoilers, speed-brakes and ground spoilers with interconnected controls to prevent asymmetric operation. The entire flaperon system acting as spoilers can be deployed in unison during rejected takeoff procedures and landing ground-roll.

The design is to be control-configured with longitudinal, roll and lateral control accomplished via a full 6 degrees-of-freedom Stability Augmentation System (SAS). TOLS-X flight control is to be a triplex fly-by-wire with two digital modes (a primary and backup) and an analog mode. This approach will assist handling qualities and shall negate any questions on how the onboard pilot will react to an asymmetric highly coupled aircraft.

The common primary and secondary control surfaces located on the wings will be simply flapped arrangements thus reducing complexity with an added benefit of allowing for a cleaner wing free of flap fairings and blisters.

The upper and lower wing structures are complete and continuous assemblies and interfaced to the fuselage top and belly by two reinforced frames. The structure accommodates flaperons or simple plain flaps, integral fuel tanks, one centre fuel tank and the main landing gear attachment assembly. Each wing structure consists of two spars, upper and lower skins, stringers and ribs. Air loads are carried by the front and rear spars that are located at 15% and 60% of local swept chord respectively. Each of the rear spars from outer wing to WPEBS interface, then towards the wing-fuselage interface closes out the flaperon bay and supports control systems therein. This spar also closes out the integral fuel tanks as well; the entire box beam encloses two distinct integral fuel tanks. The central wing torsion box consists of two beams that run in the same sense as wing skew. Aft of the lower wing planform centre wingbox, a box beam yielded from a Keelson and closed by a beam perpendicular to the fuselage contour houses the main landing gear as well as various equipment and systems. In a concerted effort to avoid undue sophistication for the sake of promoting improved dispatch reliability, reducing zero-lift drag increments incurred from flap supports; avoiding the structural complications of multi-track supports and extension mechanisms, and, the associative weight penalties of utilising chord extending leading edge and trailing edge flaps, the TOLS-X design utilizes a simple plain flap for high-lift. The array of flap settings available are designated as 0°, 15°, 30° and 60°.

The maximum cross-section area was derived from the cross-section area development plot generated by QCARD-MMI and is shown in Figure 94. Note that the stream tube area has been subtracted from the cross-sections, i.e. 10% of the nacelle inlet capture area was retained to account for an inlet mass-flow ratio of 0.90. Because wave drag is more a function of cross-section area than reference wing area, it is appropriate to consider the wave drag coefficient based on cross-section area. Figure 95 presents transonic aerodynamic performance of TOLS-X plotted against results obtained for military and experimental aircraft published by Jobe[198], and, Saltzman and Hicks[199]. The ordinate is referenced to maximum cross-section area from which the equivalent diameter is derived for the fineness ratio merit function on the abscissa. It is discernable that the TOLS-X configuration in keeping with satisfactory area-ruling practise exhibits quite desirable transonic wave drag traits; showing qualities in step with significantly older and aerodynamically efficient transonic configurations than contemporary military and experimental aircraft.

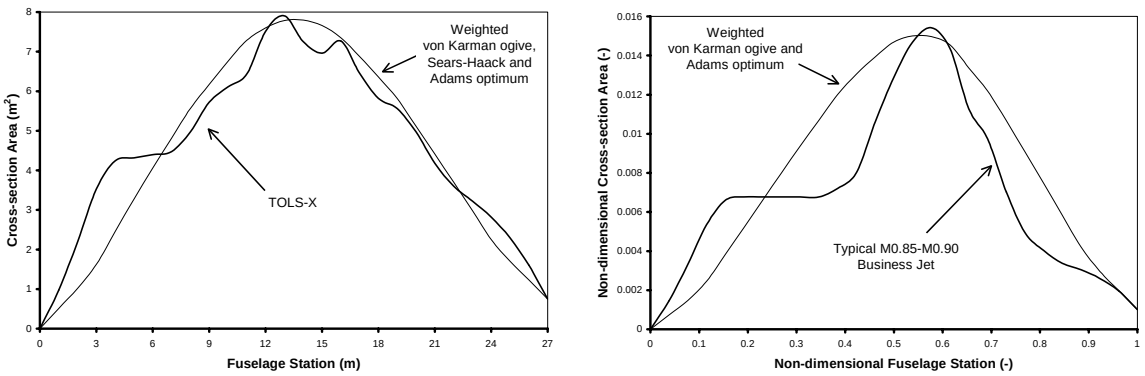

Figure 94. Cross-section area development plot of TOLS-X configuration (left) at sonic speed compared to contemporary high-speed business aircraft.

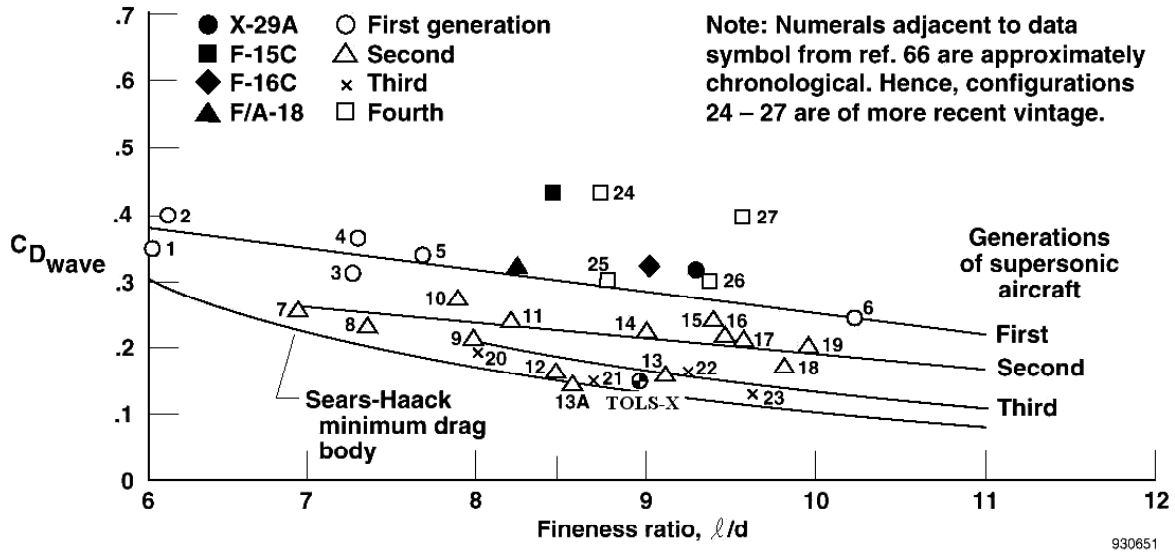

Figure 95. Historic correlation of wave drag sourced from Jobe[198], and, Saltzman and Hicks[199] compared to TOLS-X concept.

15.3.4 TOLS-X Predicted Performance and Design Review

At a typical commercial Trans-Atlantic operation altitude of FL 370, TOLS-X can achieve an operating LRC M*L/D (or aerodynamic efficiency merit function) value of 10.9; this figure is approximately 22% lower than contemporary single-aisle long-range transports flying at an LRC speed schedule of M0.80. If one considers a TOLS-X typical cruise speed technique of M0.95 (corresponding to an operating C_L of 0.475 at FL 470), M*L/D values close to 12.0 are predicted, and this contrasts as +12% over the single-aisle long-range transports flying at MCRZ speed schedule of M0.85 (12% slower). In addition, TOLS-X displays an M*L/D advantage of anywhere between +4% to +25% compared to the super-large business jets at M0.85. At a cruise speed of M1.22, M*L/D parity occurs between TOLS-X and super-large business jets at MCRZ. Even though, en route efficiency is somewhat lacking at contemporary business jet LRC speed schedules and altitudes, it is evident that TOLS-X is optimised specifically for missions above FL 410 and speeds greater than M0.90.

Figure 96 shows the predicted TOLS-X payload-range capabilities, whilst Table 9 summarises estimates of the major performance characteristics and compares these with current market equipment. Comparison of TOLS-X to these vehicles is based on technically analysed data taken from originally published marketing information[52,53,89].

Takeoff distance for TOLS-X is approximately 4-12% longer (maximum +192 m; +630 ft) compared to the F2000, F900EX and GIV-SP. This can be regarded as satisfactory because the hard specification limit of 1830 m (6000 ft) has not been violated. One unsavoury aspect of TOLS-X takeoff field performance is the reference speeds. A decision speed of 165 KCAS is quite fast, approximately +15 KCAS to +35 KCAS upon comparison to the large and super-large business jets. Further scrutiny showed this speed is equivalent to a B737-400 at Flaps 5, but since the TOLS-X V_2 speed does not violate an upper threshold exhibited by contemporary commercial transports, was considered to be within the realm of tacit acceptability. Nonetheless, one suggestion might be to investigate ways in reducing this without compromising the global design considerations. The landing distance at MLW is estimated to be 881 m (2890 ft) with corresponding landing field length equal to 1468 m (4820 ft) at ISA, sea level ambient conditions. TOLS-X displays

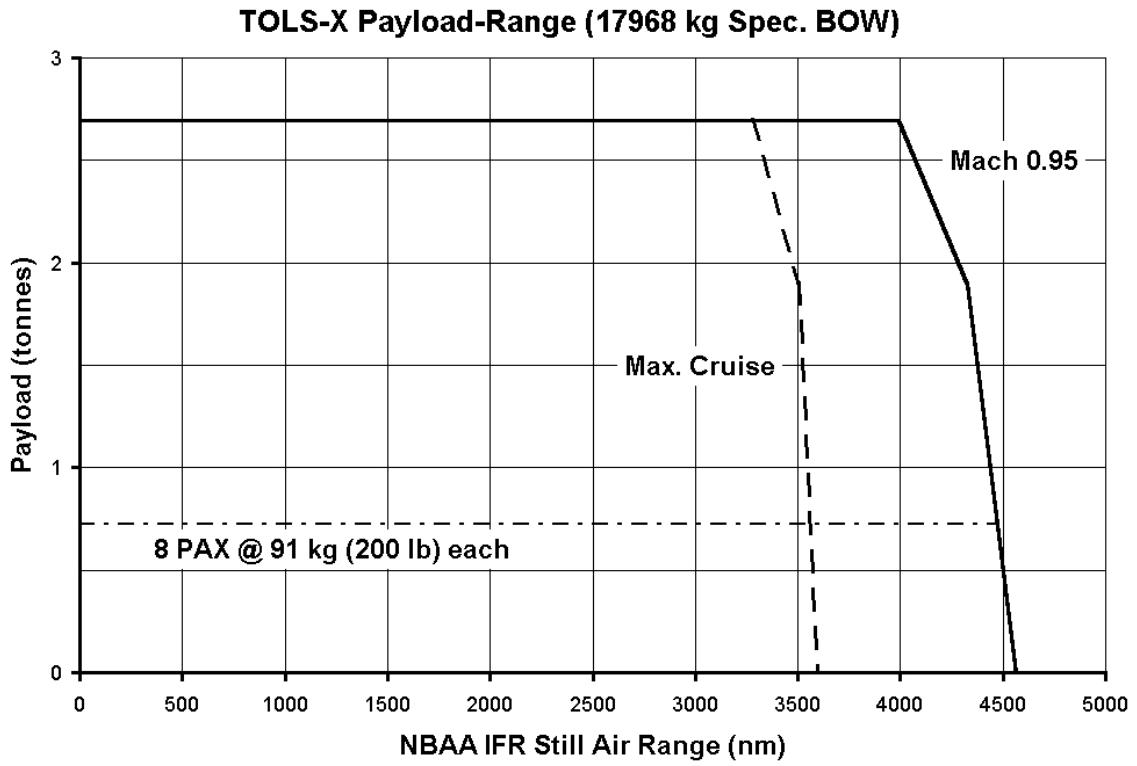

Figure 96. Payload-range envelope for TOLS-X business jet transport.

better attributes in this respect compared to the large and super-large business jets. A landing reference speed of 133 KCAS is another positive trait comparable to that of the F900EX. In view of the above analysis, it can be surmised intentions of producing a vehicle to conduct effective operations in and out of relatively short airfields has been realised with TOLS-X.

TOLS-X maximum rate of climb of 5340 fpm at sea level is around 30-56% higher than contemporary large and super-large business jets. Owing to the considerable amount of specific excess power available at maximum climb thrust, a 33% de-rate was invoked by setting the criterion TOLS-X should cruise initially at maximum service ceiling or FL 510 using CLB Mode H speed techniques. Notwithstanding the significant maximum climb thrust de-rate, this still translates into exceptional time-to-climb to altitude FL 370 and maximum service ceiling of FL 510 in 13 minutes and 23 minutes respectively assuming MTOW at brakes release. Even though TOLS-X frequently flies in the drag rise and divergence regime that promotes optimum (or maximum SAR) altitudes below the service ceiling, further increases in de-rate were disregarded to permit operator flexibility of slotting into higher altitudes if traffic congestion at lower airways becomes an issue.

LRC, TSC and HSC show an appreciable difference between the TOLS-X and contemporary large and super-large business jets. LRC is at least 75 KTAS and TSC (at M0.95) is 85 KTAS faster than the F900EX and GIV-SP business jets above the tropopause. The maximum cruise speed capability of up to +210 KTAS for TOLS-X has opened up a totally new regime of lower block times. It is evident that the Dassault Aviation range of aircraft display quite superior en route performance efficiency characteristics compared to TOLS-X; as exemplified by a greater than 50% better SAR (at 14% and 30% slower speeds for LRC and HSC respectively) of the F900EX. The GIV-SP

however, has SAR attributes more in-line with TOLS-X consistently demonstrating a +4% to +1% advantage but again at 14% and 30% slower speeds for LRC and HSC respectively. Even though the F900EX has more desirable en route burn attributes, TOLS-X has fulfilled the main objective of matching en route efficiency characteristics to a primary competitor, namely the GIV-SP, whilst permitting a marked increase in block speed performance.

	TOLS-X	Falcon 2000	Falcon 900EX	GIV-SP
External Length (m)	29.6	20.2	20.2	26.9
External Height (m)	7.48	7.07	7.56	7.44
Fuselage Diameter (m)	2.31	2.50	2.50	2.38
Engines	2 x RR-BMW BR71X	2 x CFE CFE738-1-1B	3 x Honeywell TFE731-60	2 x RR Tay Mk 611-8
Unit Output (kN)	71.2	26.3	22.3	61.6
Span [Excl. Winglets] (m)	20.5	19.3	19.3	23.2
Ref. Wing Area (m^2)	71.6	47.8	47.8	88.3
Ref. Aspect Ratio (-)	8.79	7.80	7.82	6.08
Q.Chd Sweep (deg.)	31.0	25.6	25.6	26.8
Wing loading (kg/m^2)	482	347	465	383
Thrust-to-Weight (-)	0.426	0.324	0.306	0.371
Cabin Seating Length (m)	14.0	5.73	7.70	7.77
Internal Height (m)	1.83	1.89	1.89	1.89
Max. Internal Width (m)	2.16	2.35	2.35	2.23
Cabin Floor Width (m)	1.70	1.92	1.92	1.68
Cabin Vol. Less Bagg. (m^3)	49.9	25.2	35.8	38.4
Baggage Volume (m^3)	5.35	3.80	3.60	4.79
MRW (kg)	34593	16647	22317	34020
MTOW (kg)	34493	16556	22226	33838
MLW (kg)	31000	14969	19051	29937
MZFW (kg)	20660	13000	14000	22226
Spec. BOW (kg)	17968	9730	11204	19278
BOW/MTOW (-)	0.521	0.588	0.504	0.570
Max Payload (kg)	2693	3270	2796	2948
Max Fuel (kg)	14729	5513	9526	13381
Payload @ Max Fuel (kg)	1896	1404	1588	1361
M_{MO} (Mach)	1.26	0.870	0.870	0.880
V_{MO} (KCAS)	440	370	370	340
Certified Ceiling (ft)	51000	47000	51000	45000
TOFL, sl ISA, MTOW (m)	1823	1760	1631	1661
LD, sl ISA, MLW (m)	881	953	1073	972
V_{REF} at MLW (KCAS)	133	122	132	149
CLB Schedule Initial Cruise Altitude (ft)	320KCAS/M0.80 51000	260KCAS/M0.75 41000	260KCAS/M0.72 39000	300KCAS/M0.75 41000
LRC Speed (Mach)	0.90	0.75	0.77	0.77
Max Cruise (Mach)	1.22	0.83	0.85	0.85
Range[(1)] @ LRC (nm)	4460	3110	4320	4125
SAR[(1)] @ LRC (nm/kg)	0.336	0.656	0.509	0.348
Range[(1)] @ MCRZ (nm)	3560	NA	3549	3200
SAR[(1)] @ MCRZ (nm/kg)	0.268	NA	0.417	0.271

[(1)] 8 PAX @ 200 lb per PAX, NBAA mission and IFR reserves.

Table 9. Parametric review of TOLS-X against contemporary large and super-large business jets.

The marked increase in block speed of TOLS-X does require a trade off in higher fuel flow as denoted by lower Specific Air Range (SAR) values compared to the smaller and lighter Dassault Aviation Falcon 2000 and Falcon 900EX business jets. However, upon comparison to an equivalent airframe in size and weight, such as the Gulfstream Aerospace GIV-SP, it was found that comparable SAR values are produced at speeds that are 17-44% faster. Irrespective of the dramatic increase in cruising speeds, effective field performance has been maintained and permits the original hard specification of operations in and out of relatively short airfields.

Various issues needed to be addressed with the TOLS design. One drawback was the greater structural weight of TOLS integrated with the WPEBS compared to a cantilevered single wing equivalent. It was appreciated from the outset that the TOLS configuration would possess some benefit from a structural efficiency perspective. Ideally, a piece-wise linear beam model would have been employed in estimating the bending material weight. Unfortunately, owing to an absence of this functionality, and even an equivalent conceptual method, possibilities of investigating for leaner structural weight was not realised. Regardless, the more conservative weight prediction may serve to allay any unforeseen problems concerning wing deformation due to upward bending.

The higher wing loading and modest lift increments at lower flap deflections using the assumed plain flapping arrangement translates into higher stall speeds and hence reference speeds during takeoff. Another disadvantage was an increase in zero-lift drag due to a significantly lower Reynolds number generated by the smaller local wing chords characteristic of TOLS configurations and a preliminary assumption of 5% chordwise laminarisation on wing surfaces only. This aspect can be enhanced with application of aerofoils specially optimised (such as modified HSNLF-1-0213 section) for low Reynolds number thus promoting further aft chordwise flow transition. Much work needs to be expended in further examining the area ruling characteristics and how this can be further improved upon. Also, interference effects produced by two wing planforms in close proximity to one another, which seems indicative of being a viscous problem, will need to be scrutinised using sophisticated numerical aerodynamic modelling techniques.

Trim for this configuration requires the equilibrium of six highly non-linear forces and moments. In view of the longitudinal and lateral motions being coupled, a good deal of research will need to take place on identifying optimal combinations of control surface deflection. One method is to decouple the dynamic modes so that handling quantities are similar to those of a conventional symmetric swept wing aircraft using special purpose control laws.

As a final note for improvement, since this particular investigation concentrated on a very limited scope of multivariate optimisation, it is suggested that application of MDO techniques would be an advantageous step. This procedure should realise the most efficient vehicular candidate when considering all the primary disciplines concurrently.

This investigation has shown the potential of the TOLS layout integrated with WPEBS for high-speed mission capability compared to the conventional wisdom of delta wing designs employed on all modern supersonic business jet proposals. It is granted the highly exotic nature of the TOLS configuration will be met with less than a favourable reaction from crews and passengers alike. It also is granted that by virtue of TOLS-X typically operating in the drag rise and divergence regime, this equates into a heightened sensitivity of performance[200] (whether an improvement or otherwise) to small differences between what is predicted in this to study to what might eventuate as the design is examined further. Notwithstanding these negative aspects, the results in this study demonstrate there exists a feasibility albeit at a very preliminary stage, and if the abovementioned areas of conservative assessment can be rationalised through future research, it is projected the TOLS layout may become even more of an appealing proposition.

intentionally blank

16 Summary and Conclusions

As a result of this comprehensive research effort, the major achievements are itemised as such:

(i) A method to formulate new project design specifications has been proposed in an effort to equip the designer with a tool that assists in making strategic technical decisions during the product development process. This is realised by integrating the widely known Productivity Index concept with the Airframer Paradigm multivariate model based on a build-up of component “costs” generated from a chosen set of aircraft design objectives.

(ii) A series of quasi-analytical expressions have been developed for atmospheric properties, geometry, weights, power plant, aerodynamics (including new methods to compute drag at high-transonic and supersonic speeds, and, drag reduction due to presence of winglet devices) and operational performance qualities coupled to Direct Operating Cost (DOC) and Profit or Return on Investment (P-ROI) objective functions. By introducing the notion of an impulse function, differentiable continuous expressions out of normally discrete processes have been produced, and also as a useful bi-product, an analytical tool to construct maximising and minimising functions has come to fruition. A comprehensive validation exercise has confirmed that the predictive powers of these models and associative theory to be consistent. Investigations have not only covered inspection of prediction adequacy for the stand alone equations, but by virtue of examining aircraft that vary significantly in scale and mission role, intended goals of formulating coherent objective function sensitivity with respect to free design variables has been achieved.

(iii) Presented conceptual design prediction methods focus on the generation of conventional transport aircraft configurations. However, scope has been given to accommodate more exotic deviations from conventional wisdom. Some element of flexibility is now afforded to define and subsequently analyse alternative configuration ideas with respect to fuselage and wing geometric design.

(iv) Operationally permissible climb and descent control formulation based on the vehicle’s characteristic unconstrained performance as a reference was produced. Climb schedules were categorised as two distinct techniques: a slow speed CLB Mode L, and faster CLB Mode H. CLB Mode L was postulated to be a speed schedule which is constructed by considering the vehicle’s theoretical accelerated optimal trajectory profile. Comparison of predicted fixed Calibrated Airspeed/Mach schedules to those of known designs found this premise to be valid. The conceptual CLB Mode H speed schedule determined from a dual criteria of climb thrust limitations in conjunction with appreciation of a design’s propensity to reduce DOC and increase P-ROI potential with block speed (or time) was observed and hence adopted. A single speed schedule for descent was chosen since small differences in state and time variables resulted, and, definition of the speed schedule was based on control variables of vehicular as well as cabin maximum rate of descent limitations. This potion of study also involved creation of the Optimum Trajectory Profile Algorithm (OTPA) aimed specifically at expediently computing integrated en route performance with multiple constraints as dictated by operational rules and guidelines.

(v) Presentation of a comprehensive treatment to identify optimal flight techniques with respect to DOC and P-ROI for given sector mission criteria and assumed reference

time frame utilisation has been developed. To facilitate this required the creation of a series of new models used to accurately simulate maintenance and material costs, block fuel expenditure and revenue. One salient conclusion from the derived DOC and P-ROI theory was hourly-based utilisation results in faster block speeds tending towards the minimum block time threshold, whereas, the fixed departures scenario yields a slower yet congruous flight technique optima requirement for DOC and P-ROI objectives. A new speed schedule definition called Economical Long Range Cruise (ELRC) was created to replace the traditional 99% maximum Specific Air Range (SAR) Long Range Cruise (LRC) speed. To complement this, a new merit function called Operational Flexibility Index (OFI) was derived to enable transparency of what en route operational qualities a given aircraft exhibits. Finally, merit parameters that give rise to the ability of sub-optimising for more desirable P-ROI characteristics were also presented.

(vi) An aircraft synthesis software system called QCARD-MMI, or, Quick Conceptual Aircraft Research and Development Version 2001, that amalgamates all the newly devised modelling and analysis techniques discussed in this treatise has been created. The software is an interactive MATLAB based package that permits the design of any gas-turbine commercial and business aircraft with functionality tailor-made for predicting, visualising and assisting the optimisation of conceptual aircraft designs in a highly interactive environment. Critical development objectives that have been achieved include acceleration of design response time with a significant increase in design freedom, accuracy and consistency of the results. Added enhancements to the software system included the introduction of stability and control analysis using the Mitchell code as a basis, and the facilitation of constrained multi-objective optimisation using evolution methods, the Nelder-Mead Simplex search or a “cocktail” of both.

(vii) Two turbofan regional conceptual aircraft designs using the theory have been presented. The first was a 19 passenger turbofan transport, PD340-2, aimed primarily at the commuter/regional market. It resulted in a vehicle that displays attributes of competitive field performance coupled with a capacity for much higher block speeds compared to contemporary turboprops and was found to deliver superior potential for profit as well. The design was given a significant degree of flexibility by allowing an extended range variant as well as fuselage stretch capabilities for a 30-35 PAX derivative. Based on the PD340-2 concept, the 31-34 PAX PD340-3X was pursued as a competitive alternative to contemporary 30-35 PAX turbofan vehicles in the market. Comparisons show the vehicle was much lower in acquisition cost whilst simultaneously possessing characteristics of competitive design weight, and, field and en route performance.

(viii) A third and final aircraft conceptual design project undertaken using the QCARD system was the design of TOLS-X, a new Trans-Atlantic 19 passenger executive transport able to cruise at low supersonic speeds. This particular project first introduced the concept of Twin Oblique Lifting Surfaces (TOLS) configuration and motivated aerodynamic suitability for high-transonic and low-supersonic operation. The proposal called for the integration of BR-71X engine, namely, a modified BMW Rolls-Royce BR-715 power plant conceived by the author as being suitable for up to low super-sonic operation. The TOLS-X design was characterised as being the largest cabin volume compared to contemporary large and super large business jets, and, was found to possess similar SAR efficiency to the Gulfstream GIV-SP at 17-44% faster speeds while having ability to operate out of typical corporate airfields.

17 Bibliography

[1]Torenbeek, E., "Synthesis of Subsonic Airplane Design", Delft University Press, the Netherlands, 1982.

[2]Bil, C., "Development and Application of a Computer-based System for Conceptual Aircraft Design", Delft University Press, The Netherlands, 1988.

[3]Obert. E., "Some Aspects of Aircraft Design and Aircraft Operation", Linkoping Institute of Technology (LiTH), Aircraft Design Lecture Series, Sweden, 1996.

[4]Raymer, D.P., "Aircraft Design: A Conceptual Approach", AIAA, 1989.

[5]Roskam, J., "Airplane Design", Part I through VIII, Roskam Aviation and Engineering Corporation, Kansas, 1990.

[6]Eason, E.D., Nystrom, G.A., Burlingham, A., Nelson, E.E., "Non-Hierarchic Multi-disciplinary Design of a Commercial Aircraft", AIAA-94-4302-CP, 1994, pp. 493-504.

[7]Erzberger, H., Lee H., "Characteristics of Constrained Optimum Trajectories with Specified Range", NASA Technical Memorandum 78519, Ames Research Centre.

[8]Simos D., Jenkinson L.R., "The Determination of Optimum Flight Profiles for Short-Haul Routes", Journal of Aircraft, Volume 22, No. 8, August 1985, pp. 669-674.

[9]Burt, M.E., "Weight Prediction for Wings of Box Construction", RAE Report No. Structures 186, 1955.

[10]Shanley, F.R., "Weight-strength Analysis of Aircraft Structures", Dover Publications Inc., New York, 1960.

[11]"Introduction to Aircraft Weight Engineering", (initial issue provided by Northrup Grumman Corporation), Society of Allied Weight Engineers, 1996.

[12]Torenbeek, E., "Development and Application of a Comprehensive, Design-sensitive Weight Prediction Method for Wing Structures of Transport Category Aircraft", Report LR-693, Delft University of Technology, Faculty of Aerospace Engineering, the Netherlands, September 1992.

[13]Den Braven, W., "A Description of Present-Day ATC, Its Shortcomings and Alternatives for Improvement", NRL Memorandum, VG-89-011, 1990.

[14]Cook, M.V., "The New Age of Flight Control", Aerogram, Vol. 9, No. 4, December 1999, pp. 9-13.

[15]Mitchell, C.G.B, "A Computer Programme to Predict the Stability and Control Characteristics of Subsonic Aircraft", TR 73079, Royal Aircraft Establishment, Procurement Executive, Ministry of Defence, September 1973.

[16]Perkins, C.D., Hage, R.E., "Airplane Performance Stability and Control", John Wiley and Sons, New York, 1949.

[17]Roskam, J., "Methods for Estimating Stability and Control Derivatives of Conventional Subsonic Airplanes", Roskam Aviation and Engineering Corporation, Kansas, 1971.

[18]"The USAF Stability and Control Digital Datcom, Volume II, Implementation of Datcom Methods", Technical Report AFFDL-TR-793032, Vol. II, McDonnell Douglas Astronautics Company, April 1979.

[19]Van der Velden, A., "The Global Aircraft Shape", presented at AGARD-FDP-VKI Special Course at VKI, Rhode-Saint-Genese, April 1994, pp. 9-1 to 9-11.

[20]Kafyeke, F., Abdo, M., Piperni, P., Laurendeau, E., "Challengees of Aircraft Design Integration", presented at the 3rd SST-CFD-Workshop internation Workshop on Numerical Simulation Technology for Design of Next Generation Supersonic Civil Transport, Tokyo, Japan, December 2001.

[21]Herendeen, D.L., Hoesly, R.L., Johnson, E.H., Venkayya, V.B., "ASTROS – An Advanced Software Environment for Automated Design", AIAA/ASME/ASCE/AHS 27th Structures, Structural Dynamics and Materials Conference, AIAA-86-0856, San Antonio, Texas, May 1986.

[22]Van der Velden, A., "Tools for Applied Engineering Optimisation", presented at AGARD-FDP-VKI Special Course at VKI, Rhode-Saint-Genese, April 1994, pp. 8-1 to 8-10.

[23]Simos, D., "Project Interactive Analysis and Optimization – PIANO version 3.8", Lissys Limited, 1990-2001.

[24]De Filippo, R., "ACSYNT User's Guide", Northrop Aircraft, 1983.

[25]Kroo, I., Takai, M., "A Quasi-Procedural, Knowledge-Based System for Aircraft Design", AIAA Paper 88-6502, 1988.

[26]Eaglesham, M.A., "A Decision Support System for Advanced Composites Manufacturing Cost Estimation", Ph.D. thesis, Industrial and Systems Engineering, Virginia Polytechnic Institute and State University, Blacksburg, Virginia, April 1998.

[27]Timmons, L.M., "Improving Business Jet Performance: The Mark Five Sabreliner", SAE Paper 790582, 1979.

[28]Norris, R., "Relative Value of Regional Airline Aircraft", Professional Pilot Magazine, 1999.

[29]Killingsworth, E.C., Jr., Wolz, R.R., "Requirements of Business Jet Aircraft", AIAA Paper 90-2038, 1990.

[30]Moghadam, A., Farsi, K., "Business Aircraft: Cost of Performance", AIAA Paper 95-3955, 1995.

[31]"Business Jet Market Map-1995", Aviation International News, May 1995, p. 46.

[32]McMasters, J.H., "Reflections of a Paleoaerodynamicist", AIAA Paper 84-2167 (Invited Paper), AIAA Second Applied Aerodyanmics Conference, August 1984.

[33]"Gulfstrean V-SP on Track to Fly Later This Year", Aviation Week & Space Technology, 30 April 2001, pp. 70-71.

[34]McCormick, B.W., "Aerodynamics, Aeronautics, and Flight Mechanics", John Wiley and Sons, 1979.

[35]Clancy, L.J., "Aerodynamics", Longman Scientific and Technical, 1975.

[36]"Geometrical Properties of Cranked and Straight Tapered Wing Planforms", Engineering Science Data Units (ESDU), 76003, Issued January 1976, Amendment A, October 1981.

[37]A320-200 Technical Description", 432 013/88, Issue 1, Airbus Industrie, March 1988.

[38]"Jet Transport Performance Methods", D6-1420, Seventh Edition, Boeing Flight Operations, Boeing Commercial Airplanes, May 1989.

[39]"GASP - General Aviation Synthesis Program", NASA CR 152303, January 1978.

[40]Rao, S.S., "Mechanical Vibrations", Second Edition, Addison-Wesley Publishing Company, 1990, pp. 37-45.

[41]de Vahl Davis, G., "Numerical Methods in Engineering and Science", Allen and Unwin Publishers Ltd., 1986.

[42]"A Method for the Solution of Certain Non-linear Problems in Least Squares", Q. Appl. Math., 11, pp. 164-168.

[43]"An Algorithm for Least Squares Estimation of Non-linear Parameters", J. Soc. Ind. Appli. Math., 2, p431-441, 1963.

[44]"ERJ 170", marketing brochure, now re-branded as Embraer 170, Embraer, May 2001.

[45]Thomas, Jr., G.B., Finney, R.L., "Calculus and Analytical Geometry", Seventh Edition, Addison-Wesley Publishing Company, 1988.

[46]"Saab 2000 Aerodynamic Design Data Book – Section 3 Geometry", 73ADS0014, Rev. B, Amendment B5, Saab Aircraft AB, March 1994.

[47]"Saab 340 Aerodynamic Design Data – Section 3 Geometry", 72ADS303, Rev. A, Saab Aircraft AB, September 1987.

[48]"Gulfstream 200 Product Specifications", Revision Applicability: Serial Numbers 040-059, Gulfstream Aerospace Corporation, September 2001.

[49]"Embraer Legacy", Business and Commercial Aviation, September 2001, pp. 56-63.

[50]"ERJ 145XR Speed-News Presentation", March 2002.

[51]"Type Specification Canadair Challenger Model CL600-2B16 Variant CL-604 Green Aircraft", RAD-604-100, Bombardier Inc., September 1993.

[52]"Falcon 2000EX EASy Aircraft Specification", DGT 81640, Dassault Aviation, February 2001.

[53]"Falcon 900EX Aircraft Specification", DGT 65157, Dassault Aviation, March 1998.

[54]Isikveren, A.T., "Methodology for Conceptual Design and Optimisation of Transport Aircraft", Report 98-8, Royal Institute of Technology (KTH), Department of Aeronautics, Sweden, 1998.

[55]"Aerospace Source Book", Aviation Week and Space Technology, January 12, 1998.

[56]"Jane's All the Worlds Aircraft", 1990-1991 through 2001-2002, Jane's Information Group Limited, 1990 through 2001.

[57]Svoboda, C., "Turbofan Engine Database as a Preliminary Design Tool", Aircraft Design 3 (2000) 17-31, Aircraft Design Journal, 2000.

[58]"AIAA Aerospace Design Engineers' Guide", Fourth Edition, AIAA, 1998.

[59]"Type Specification for the CL-601 Canadair Challenger with the General Electric CF34", RAD-601-100, Issue A, Bombardier Inc., August 1983.

[60]"Global Express Dimensional Data", MAA700-100, Revision NC, Bombardier Inc., September 1996.

[61]"CL-601 RJ Dimensional Data", MAA-601R110, Revision NC, Bombardier Inc., March 1988.

[62]"CRJ-700 Dimensional Data", MAA-BA670-124, Revision NC, Bombardier Inc., September 1998.

[63]"Type Specification for the Canadair SE", RAD-601R-126, Issue B, Bombardier Inc., April 1996.

[64]"Type Specification for the Global Express Aircraft Model No. BD-700-1A10", RAD-700-100, Issue C, Bombardier Inc., July 2000.

[65]Linnell, R., "Weight Estimation Methods", FKHV-1-RL790724:01, Saab AB, July 1979.

[66]Scott, P.W., Nguyen D., "The Initial Weight Estimate", SAWE Paper No. 2327, Index Category No. 11, MDC 96K0030, 55th International Conference of the Society of Allied Weight Engineers, Inc., June 3-5 1996.

[67]Niu, M.C.Y., "Airframe Structural Design", Lockheed Aeronautical Systems Company, Comilit Press Ltd.

[68]Federal Aviation Regulations (FAR), Vol. III, Part 25 – Airworthiness Standards: Transport Category.

[69]Abbott, I.H., Von Doenhoff, A.E, "Theory of Wing Sections", Dover Publications Inc., 1949.

[70]Ishimitsu, K.K., "Aerodynamic Design and Analysis of Winglets", AIAA Paper 76-940, 1976.

[71]Dees, P., Stowell, M., "737-800 Winglet Integration", SAE Paper 2001-01-2989, 2001 World Aviation Congress, September 2001.

[72]"SF340A Mass Properties Summary", SWEA-INFO Version 2.0 output, Saab Aerospace, November 1992.

[73]Danielsson, L., "FedEx Aircraft Estimated Weights", PDD-LD-97.052, Saab Aerospace, October 1997.

[74]"Aircraft Weight and Balance Control", Advisory Circular 120-27C, US Department of Transportation, Federal Aviation Administration, 17 October 1995.

[75]"Notional Weights (Standard Masses)", JAR OPS Chapter 4(E), 1994.

[76]"Model 737 BBJ and BBJ2 Airplane Charcateristics for Airport Planning", D6-58325-4, Boeing Commercial Airplane Group, December 2000.

[77]"737-600/700/800/900, Airplane Characteristics for Airport Planning", D6-58325-3, Boeing Commercial Airplane Group, April 1998.

[78]"Learjet 45 Model Specification", 00-RD-45.2.55, Bombardier Inc., July 1996.

[79]"Performance Data Canadair Regional Jet CF34-3B1 Engines (Metric)", MAA-601R-178, Bombardier Inc., June 1997.

[80]"Preliminary Performance Data for the Canadair Regional Jet Series 700", MAA-BA670-107, Revision C, Bombardier Inc., October 1998.

[81]"Type Specification for the Canadair Regional Jet Series 900", RAD-690-100, Revision NC, Bombardier Inc., December 1999.

[82]"Citation Excel Specification and Description", Cessna, September 1998.

[83]"Citation Sovereign Specification and Description", Revision B, Preliminary, Cessna, September 2001.

[84]"ERJ 145 Technical Description", TD 145/016, Contracts Dept., Embraer, December 1999.

[85]"Embaer 175", marketing brochure, Embraer, November 2001.

[86]"ERJ 190-200", marketing brochure, now re-branded as Embraer 195, Embraer, May 2001.

[87]"Fairchild Dornier 728 Specifications and Performance", marketing brochure, Fairchild Dornier, February 2002.

[88]"Fairchild Dornier 928 Specifications and Performance", marketing brochure, Fairchild Dornier, February 2002.

[89]"Gulfstream IV-SP Product Specifications", Revision Applicability: Serial Numbers 1460-1479, Gulfstream Aerospace Corporation, August 2001.

[90]"Gulfstream V-SP Product Specification", Gulfstream Aerospace Corporation, March 2001.

[91]"Saab 340B Leading Particulars", marketing brochure, Saab Aerospace, date not supplied.

[92]"Saab 2000 Type Specification", 73VPS0010, Revision F, Saab Aerospace, November 1996.

[93]Bertin, J.J., Smith, M.L., "Aerodynamics for Engineers", Prentice-Hall Inc., Englewood Cliffs, N.J., 1979.

[94]Moran, J., "Computational Fluid Dynamics", Weily & Sons, 1984.

[95]Melin, T., "A Vortex-Lattice MATLAB Implementation for Linear Aerodynamic Wing Applications", Masters thesis, Royal Institute of Technology (KTH), Department of Aeronautics, Sweden, December 2000.

[96]Pitts, W.C., Nielsen, J.N., Kaattari, G.E., "Lift and Centre of Pressure of Wing-body-tail Combinations at Subsonic, Transonic and Supersonic Speeds", NACA Technical Report 1307, 1954.

[97]Schaufele, R.D., Ebeling, A.W., "Aerodynamic Design of the DC-9 Wing and High-Lift System", Douglas Aircraft Div., McDonnell Douglas Corp., AIAA Paper No. 670846, 1967, pp 2575-2583.

[98]Obert, E., "Fourty Years of High-lift R&D – an Aircraft Manufacturer's Experience", Fokker Aircraft B.V., AGARD CP 505, September 1993, pp. (27)1-28.

[99]Chandrasekharen, R.M., Murphy, W.R., "Computational Aerodynamic Design of The Gulfstream IV Wing", Gulfstream Aerospace Corporation and Grumman Aerospace Corporation, Journal of Aircraft, Vol.22, No. 9, September 1985, pp. 797-801.

[100]Obert, E., "The Aerodynamic Development of the Fokker 100", ICAS Paper 88-6.1.2, 1988.

[101]Thibert, J.J., Reneaux, J., Moens, F., Preist, J., "ONERA Activities on High-lift Devices for Transport Aircraft", Aeronautical Journal, November 1995, pp. 395-411.

[102]Young, A.D., "The Aerodynamic Characteristics of Flaps", Aeronautical Research Council Reports and Memoranda, Ministry of Supply, United Kingdom, 1953.

[103]Pazmany, L., "Preliminary Design of the Pazmany PL-1 Laminar Airplane", December 1964.

[104]Isikveren, A.T., Khezri, R., Monti, A., Räisänen, S., "NGR-20/2C: 19PAX Regional Commuter Preliminary Design", KIF-95:4, Royal Institute of Technology (KTH), Department of Aeronautics, Sweden, May 1995.

[105]Nield, B.N., "An Overview of Boeing 777 High Lift Aerodynamic Design", Aeronautical Journal, November 1995, pp. 361-371.

[106]"FAA Model 60 Program Update", PVB:20310, Bombardier Inc. (originally Learjet), March 1992.

[107]"Falcon 2000 Technical Specification", DGT 39521 Issue 3, Dassault Aviation, January 1992.

[108]"Embraer RJ 135 Technical Description", TD-135/000, Embraer, November 1997.

[109]"ERJ 140", Marketing Brochure, Embraer, May 2001.

[110]"Fokker 70 Performance Information Rolls-Royce Tay Mk620 (metric units)", MM100/AA/F70/P.I.R.-M/Issue 2, Fokker Aircraft B.V., May 1993.

[111]"Fokker 100 Performance Information Rolls-Royce Tay Mk650 (imperial units)", MDAA/F100/RP-110 Issue 1, Fokker Aircraft B.V., January 1990.

[112]Isikveren, A.T., "The PD340-2 19 Passenger Turbofan Regional Transport – Feasibility Study", Report 98-5, Royal Institute of Technology (KTH), Department of Aeronautics, Sweden, 1998.

[113]"Saab 340 Aerodynamic Design Data – Section 6 Performance Basic Data", 72ADS303, Rev. A, Saab Aircraft AB, September 1987.

[114]"Saab 2000 Aerodynamic Design Data Book – Section 7 Performance Basic Data", 73ADS377, Rev. A, Saab Aircraft AB, February 1997.

[115]Eckert, E.R.G., "Engineering Relations for Friction and Heat Transfer to Surfaces in High Velocity Flow", Journal of the Aeronautical Sciences, Vol. 22, 1955, pp. 585-587.

[116]Poisson-Quinton, P., "From Wind Tunnel to Flight, the Role of the Laboratory in Aerospace Design", Journal of Aircraft, Volume 5, No. 3, May-June 1968, pp.193-214.

[117]Bulgubure, C., "Laminar Wing Design Applied to Business Jets", Aerodynamics Department, Dassault Aviation, conference unknown, Athens, September 1998.

[118] Boppe, C.W., "Aircraft Drag Analysis Methods", AGARD Report LS, May 1991.

[119]"British Aerospace 146/200 Performance Engineer's Manual", British Aerospace, July 1984.

[120]"Williams International – In-house GASP User's Guide", Revision 15, June 1995.

[121]Boeing Performance Software (BPS) database 37867B – B737-800 with CFM56-7 Series engines, Version 1.00, March 1998.

[122]Torenbeek, E., "Optimum Wing Area, Aspect Ratio and Cruise Altitude for Long Range Transport Aircraft", Report LR-775, Delft University of Technology, Faculty of Aerospace Engineering, The Netherlands, October 1994.

[123]Boppe, C.W., "CFD Drag Predictions for Aerodynamic Design", AGARD Report AR-256, 1989.

[124]Torenbeek, E., "On the Conceptual Design of Supersonic Cruising Aircraft with Subsonic Wing Leading Edges", Delft Progress Report 8 (1983), Delft University of Technology, Faculty of Aerospace Engineering, The Netherlands, November 1982, pp. 55-80.

[125]"Optimum Area Distribution and Associated Theoretical Transonic Drag-Rise for Aircraft at Zero Lift", Aircraft 02.03.02, Engineering Science Data Units, Issued September 1959, Amendment A, December 1982.

[126]Kuchemann, D., "The Aerodynamic Design of Aircraft", Pergamon Press Ltd., 1978.

[127]Jones, R.T., "The Minimum Drag of Wings in Frictionless Flow", ARC, Journal of Aero. Sciences, No. 18, pp. 75-81, 1951.

[128]"Winglet Benefits", Flight International, 1-7 May 1996, p. 31.

[129]Taylor, A.B., "Winglet and Long-Duct Nacelle Aerodynamic Development for DC-10 Derivatives", CTOL Transport Technology, NASA-CP-2036-PT-2, 1978, pp. 609-623.

[130]Da Costa, A.L., "Application of Computational Aerodynamics Methods to the Design and Analysis of Transport Aircraft", ICAS Proceedings B2, September 1978, pp. 261-269.

[131]Kuhlman, J.M., "Optimised Aerodynamic Design Process for Subsonic Transport Wing Fitted with Winglets", NASA CR-159180, December 1979.

[132]Anderson Jr., J.D., "Fundamentals of Aerodynamics", Second Edition, McGraw-Hill Inc., 1991.

[133]Head, M.R., "Flow Visualization II", Hemisphere Publishing Co., New York, 1982, pp. 399-403.

[134]"Learjet 60 Drag Model", Bombardier Inc., March 2002.

[135]"Global Express Flight Test Drag Model A/C 9004 Cruise Tests", Bombardier Inc., June 1999.

[136]Torenbeek, E., "Optimum Cruise Performance of Subsonic Transport Aircraft", Report LR-787, Delft University of Technology, Faculty of Aerospace Engineering, the Netherlands, March 1995.

[137]"Saab 340 Performance Course, 72ADS7101, Revision A, Saab Aerospace, March 1998.

[138]"Federal Aviation Regulations (FAR), Part 25 Airworthiness Standards: Transport Category Airplanes", Subpart B – Flight, FAR 25.105 Takeoff, US Department of Transportation.

[139]"Joint Aviation Requirements JAR-25 Large Aeroplanes", Subpart B – Flight Section 1, JAR 25.105 Takeoff, Civil Aviation Authority on behalf of Joint Aviation Authorities Committee.

[140]Page, R.K., "Performance Calculation for Jet-Propelled Aircraft", Journal of the Royal Aeronautical Society, Volume 51, 1947, pp. 440-450.

[141]Miller, L.E., "Optimal Cruise Performance", Engineering Notes, Journal of Aircraft, Volume 30, No. 3, May-June 1993, pp. 403-405.

[142]PAN-AM Flight Operations Manual, Revision 228, August 1988.

[143]Isikveren, A.T., "A Method to Identify Optimal Flight Techniques of Transport Aircraft", Report 98-7, Royal Institute of Technology (KTH), Department of Aeronautics, Sweden, 1998.

[144]Isikveren, A.T., "Identifying Economically Optimal Flight Techniques of Transport Aircraft", C-9699, AIAA Journal of Aircraft, issue pending, 2002.

[145]"Definitions and Inputs for Range and Direct Operating Cost Calculation", Appendix 1, G(T) 5656, Association of European Airlines, 1990.

[146]"American Airlines Flight Planning System User's Manual", Revision 5, American Airlines Flight Operations Engineering – En route Performance Engineering, August 1998.

[147]"Federal Aviation Regulations (FAR), Part 25 Airworthiness Standards: Transport Category Airplanes", Subpart B – Flight, FAR 91.109 and 91.121, US Department of Transportation.

[148]"ERJ 190-100", marketing brochure, now re-branded as Embraer 190, Embraer, May 2001.

[149]Bihrle, W., "A Handling Qualities Theory for Precise Flight Path Control", AFFDL-TR-65-198, June 1966.

[150]Roskam, J., "Airplane Dynamics and Automatic Flight Controls – Part I", Roskam Aviation and Engineering Corporation, Kansas, 1979.

[151]Etkin, B., "Dynamics of Atmospheric Flight", John Wiley and Sons, Inc., 1972.

[152]Engineering Science Aerodynamics Data Sheets, Engineering Science Data Unit, London.

[153]Amiree, R.A., "Interactive System for Aircraft Layout Using Object-Oriented Techniques", MSc thesis, Report 99-37, Royal Institute of Technology (KTH), Department of Aeronautics, Sweden, 1999.

[154]Cooper, G.E., Harper, R.P., "The Use of Pilot Rating in the Evaluation of Aircraft Handling Qualities", AGARD Report 567, April 1969.

[155]"Maradon, F., "Investgation of a Pilot Induced Oscillation During Landing of the Jetstream 100 Aircraft G-NFLC", College of Aeronautics, MSc thesis, Cranfield University, 1999.

[156]"A Background to the Handling Qualities of Aircraft", Engineering Science Data Units (ESDU), 92006, Issued March 1992.

[157]"Military Specification, Flying Qualities of Piloted Airplanes", MIL-F-8785C (USAF), 1980.

[158]"Military Standard, Flying Qualities of Piloted Airplanes", MIL-STD-1797 (USAF), 1987.

[159]"ICAO Airworthiness Technical Manual", pg. III-2-23.

[160]"ICAO Airworthiness Technical Manual", pg. III-2-26.

[161]"Design Objectives for Handling Qualities of Transport Aircraft", ARP4104, SAE Recommended Practice, Issued July 1988.

[162]Torenbeek, E., "Some Fundamental Aspects of Transport Aircraft Conceptual Design Optimisation", AGARD Symposium, September 1979, pp. (5)1-22.

[163]"Cost Index", Revised April 1990, Boeing Flight Operations Engineering, April 1990.

[164]"Cost Index", Performance Engineer Operations Course Notes, Vol. 1, Boeing Flight Operations Engineering, May 1997.

[165]Gogate, S.D., Pant, R.K., Arora, P., "Incorporation of Some Cost and Economic Parameters in the Conceptual Design Optimisation of an Air-Taxi Aircraft", AIAA Paper 94-4301-CP, pp. 443-453.

[166]Zang, T.A., Lawrence, L.G., "Multi-disciplinary Design Optimisation Techniques: Implications and Opportunities for Fluid Dynamics Research", AIAA Paper 99-3798, 30th AIAA Fluid Dynamics Conference, June-July 1999.

[167]Van der Velden, A., Kelm, R., Kokan, D., Mertens, J., "Application of MDO to Large Subsonic Transport Aircraft", AIAA Paper 2000-0844, 38th Aerospace Sciences Meeting & Exhibit, January 2000.

[168]Gern, F.H., Ko, A., Sulaeman, E., Gundlach, J.F., Kapania, R.K., "Multi-disciplinary Design Optimisation of a Transonic Commercial Transport with Strut-Braced Wing", Journal of Aircraft, Volume 38, No.6, November-December 2001, pp. 1006-1014.

[169]Sobieszczanski-Sobieski, J., Haftka, R.T., "Multi-disciplinary Aerospace Design Optimisation: Survey of recent Developments", AIAA paper 96-0711, 34th Aerospace Sciences Meeting and Exhibit, January 1995.

[170]Rao, S.S., "Multi-objective Optimisation in Structural Design with Uncertain Paramters and Stochastic Processes", AIAA Journal of Aircraft, November 1984, pp. 1670-1678.

[171]Davis, L., "The Handbook of Genetic Algorithms", Van Nostrand Reingold, New York, 1991.

[172]Goldberg, D., "Genetic Algorithms in Search, Optimisation and Machine Learning", Addison-Wesley, 1989.

[173]Holland, J., "Adaption in Natural and Artificial Systems", The University of Michigan Press, Ann Arbor, 1975.

[174]Michalewicz, Z., "Genetic Algorithms + Data Structures = Evolution Programs", AI Series, Springer-Verlag, New York, 1994.

[175]Houck, C.R., Joines, J.A., Kay, M.G., "A Genetic Algorithm for Function Optimisation: A MATLAB Implementation", North Carolina State University, 1996.

[176]Lagarias, J.C., J. A. Reeds, M.H. Wright, and P.E. Wright, "Convergence Properties of the Nelder-Mead Simplex Algorithm in Low Dimensions", May 1, 1997. To appear in the SIAM Journal of Optimisation.

[177]Dovi, A.R., Wrenn, G.A., "Aircraft Design for Mission Performance Using Non-linear Multi-objective Optimisation Methods", NASA CR-4328, Langley Research Centre, 1990.

[178]Kreisselmeier, G., Steinhauser, R., "Systematic Control Design by Optimising a Vector Performance Index", International Federation of Active Controls Symposium on Computer-Aided Design of Control Systems, Zurich, Switzerland, August 29-31, 1979.

[179]Wrenn, G., "An Indirect Method for Numerical Optimisation Using the Kreisselmeier-Steinhauser Function", NASA CR-4220, Langley Research Centre, March 1989.

[180]Cassis, J.H., Schmit, L.A., "On Implementation of the Extended Interior Penalty Function", International Journal for Numerical Methods in Engineering, Volume 10, 1976, pp. 3-23.

[181]Isikveren, A.T., "Design and Optimisation of a 19 Passenger Turbofan Regional Transport", SAE Paper 1999-01-5579, 1999 World Aviation Conference, October 1999.

[182]"Feasibility of Fanjet-Powered 19-Passenger Regional Aircraft – A Study Conducted by Williams International", Williams International, April 1997.

[183]Isikveren, A.T., "Methodology for Conceptual Design and Optimisation of Transport Aircraft", ICAS Paper 98-7.8.2, September 1998.

[184]Isikveren, A.T., "High-Performance Executive Transport Design Employing Twin Oblique Lifting Surfaces", SAE Paper 2001-01-3031, World Aviation Congress and Exposition, September 2001.

[185]"Review of Regional Airliners", Business and Commercial Aviation, May 1995 through 1998.

[186]FAA Aviation Forecasts, Fiscal Years 1995-2006, U.S. DOT, Federal Aviation Administration, FAA-APO-95-1.

[187]Taylor, J., Munson, K., "History of Aviation", Crown Publishers Inc., 1978.

[188]Campbell J.P., Drake, H.M., "Investigation of Stability and Control Characteristics of an Airplane Model with Skewed Wing in the Langley Free-Flight Tunnel", NACA TN 1208, 1945.

[189]Jones, R.T., "New Design Goals and a New Shape for the SST", Astronautics and Aeronautics, Volume 10, No.12, December 1972.

[190]Jones, R.T., Nisbet J.W., "Transonic Transport Wings – Oblique or Swept?", Astronautics and Aeronautics, January 1974.

[191]Olson E.C., Selberg, B.P., "Experimental Determination of Improved Aerodynamic Characteristics Utilising Biplane Wing Configurations", Journal of Aircraft, Vol. 13, April 1976.

[192]Rhodes, M.D., Selberg, B., "Dual Wing, Swept Forward Swept Rearward Wing, and Single Wing Design Optimisation For High Performance Business Airplanes", ICAS-82-1.4.2, 1982.

[193]Pfenninger, W., "Design Considerations of Large Subsonic Long Range Transport Airplanes with Low Drag Boundary Layer Suction," Northrop Aircraft, Inc., Report NAI-58-529 (BLC-111), 1958. (Available from DTIC as AD 821 759).

[194]Gundlach IV, J.F., Naghshineh-Pour, A., Gern, F., Tetrault, P.-A., Ko, A., Schetz, A., Mason, W.H., Kapania, B., Grossman, B., Haftka R.T. (University of Florida), "Multi-disciplinary Design Optimisation and Industry Review of a 2010 Strut-Braced Wing Transonic Transport", MAD 99-06-03, Department of Aerospace and Ocean Engineering, Virginia Polytechnic Institute and State University, June 1999.

[195]Whitford, R., "Design for Air Combat", Jane's Information Group Ltd., date not found.

[196]Kroo, I., "The Aerodynamic Design of Oblique Wing Aircraft", AIAA Paper 86-2624, October 1986

[197]Van der Velden, A.J.M, Torenbeek, E., "Design of a Small Oblique-Wing Transport Aircraft", Journal of Aircraft, Vol. 26, No. 3, March 1989.

[198]Jobe, C.E., "Prediction of Aerodynamic Drag", AFWAL-TM-84-203, Flight Dynamics Laboratory, Air Force Wright Aeronautical Laboratories, Wright-Patterson Air Force Base, OH 45433, July 1984.

[199]Saltzman, E.J., Hicks, J.W., "In-Flight Lift-Drag Characteristics for a Forward-Swept Wing Aircraft (and Comparisons with Contemporary Aircraft)", NASA Technical Paper 3414, December 1994.

[200]Goodmanson, L.T., "Transonic Transports", Astronautics and Aeronautics, November 1971, pp. 46-56.

intentionally blank

Appendix A – Abstract of Papers and Technical Papers

Paper I: Methodology for Conceptual Design and Optimisation of Transport Aircraft

This paper presents techniques for conducting and subsequently optimising new transport aircraft designs at the conceptual level with an emphasis placed on turbofan vehicles ranging in size from 19 to 100 passengers as well as business jets. The method is comprised of the discrete operations usually performed for a conventional (intuitive) design process but combines it with a non-hierarchic multidisciplinary optimisation philosophy. A new unified analytical treatment of the design problem is presented which utilises closed form solutions together with transcendental expressions. These methods cover: installed power plant modelling, high and low speed aerodynamics, minimum control speed limited balanced field estimation, and, the formulation of operational performance characteristics such as definition of speed schedules and techniques for payload-range/sector flight profile optimisation with regards to maximum specific range, minimum fuel, maximum block speed, minimum time, minimum direct operating cost and maximum return on investment. A design study has been performed with a spreadsheet-based version of the theory and methodology. With the aid of QCARD or Quick Conceptual Aircraft Research and Development, a new 31-34 passenger regional turbofan transport was presented with lower acquisition cost and competitive weight, field and en route performance attributes compared to its contemporaries.

Paper II: Design and Optimisation of a 19 Passenger Turbofan Regional Transport

During this study, the conceptual design of a 19 passenger turbofan transport aimed primarily at the regional/commuter market was synthesised. Final configuration selection was based on a method conceived by the author, which incorporates a hybrid of the conventional intuitive conceptual design process with overtones of a non-hierarchic multi-disciplinary optimisation philosophy. To ensure validity of the aforementioned design and optimisation algorithms, the General Aviation Synthesis Program (GASP) software developed by NASA-Ames Research Centre and subsequently refined by Williams-Rolls Inc. was used. In addition, attention was paid during the design sequence to minimise the alterations necessary for variants of the basic design, i.e. future extended range and stretched versions. The final proposal ended with a vehicle that displays marketing flexibility, competitive field performance, superior climb capability with significant increases in block speed, and more poignantly, higher potential for profit upon comparison to contemporary turboprops.

Paper III: High-Performance Executive Transport Design Employing Twin Oblique Lifting Surfaces

This paper presents a new Trans-Atlantic high performance executive transport suitability equipped to offer accommodation for 19 first class passengers. The unique feature of this conceptual design is application of Twin Oblique Lifting Surfaces or TOLS configuration. Minimum goals for the design included: similar maximum takeoff gross weight; satisfactory field performance; good stalling characteristics; and, competitive fuel burn qualities at high-transonic and low-supersonic speeds, i.e. M0.90-1.20, compared to contemporary M0.75-0.85 large and super-large business jets. The vehicle is to be powered by two medium by-pass derivative engines based on the BMW-Rolls Royce BR715 in an effort to maximize the likelihood of availability, ensure adequate en route performance efficiency and fulfilment of yet to be ratified Stage 4 noise compliance requirements.

Paper IV: Identifying Economically Optimal Flight Techniques of Transport Aircraft

A treatment of identifying optimal flight techniques for transport aircraft with respect to direct operating cost and profit or return on investment is derived for given sector mission criteria and assumed reference time frame utilisation. A series of models used to accurately simulate maintenance and materiel costs, block fuel expenditure and revenue have been introduced in order to force the direct operating cost, and, profit or return on investment expressions as continuous functions allowing for determination of their respective minima and maxima. The selection of utilisation (hourly or fixed number of sectors) per reference time frame was found to be an important precursor to what type of flight technique is to be expected. An hourly-based utilisation results in faster block speeds tending towards the minimum block time threshold of a given vehicle and sector mission, whilst, the fixed departures scenario yields a slower yet congruous flight technique optima requirement for direct operating cost and profit or return on investment objectives. Details are given to show how the methodology may be integrated for the purpose of conducting competitor reviews during fleet planning exercises, and also, how one may facilitate the optimisation of conceptual aircraft designs via inspection of some useful merit parameters.

Paper I

Methodology for Conceptual Design and Optimisation of Transport Aircraft

intentionally blank

METHODOLOGY FOR CONCEPTUAL DESIGN AND OPTIMISATION OF TRANSPORT AIRCRAFT

Askin T. Isikveren*, Research Scientist
Royal Institute of Technology (KTH), Stockholm, Sweden

Abstract

This paper presents techniques for conducting and subsequently optimising new transport aircraft designs at the conceptual level with an emphasis placed on turbofan vehicles ranging in size from 19 to 100 passengers as well as business jets. The method is comprised of the discrete operations usually performed for a conventional (intuitive) design process but combines it with a non-hierarchic multidisciplinary optimisation philosophy. A new unified analytical treatment of the design problem is presented which utilises closed form solutions together with transcendental expressions. These methods cover: installed power plant modelling, high and low speed aerodynamics, minimum control speed limited balanced field estimation, and, the formulation of operational performance characteristics such as definition of speed schedules and techniques for payload-range/sector flight profile optimisation with regards to maximum specific range, minimum fuel, maximum block speed, minimum time, minimum direct operating cost and maximum return on investment. A design study has been performed with a spreadsheet-based version of the theory and methodology. With the aid of QCARD or Quick Conceptual Aircraft Research and Development, a new 31-34 passenger regional turbofan transport was presented with lower acquisition cost and competitive weight, field and en route performance attributes compared to its contemporaries.

Introduction

Contemporary conceptual design methodology primarily focuses on a variety of closed form expressions to enable prediction of aircraft geometry, weight, aerodynamics and field-en route performance. Simplifications are generally introduced through the basic first order assumption or otherwise complexity is avoided through empirical means. Applicability of these methods is not questioned but the equations are concerned mainly with idealised performance of transport aircraft as opposed to the reality of various operational criteria. Issues of minimum control speed limited field performance, speed schedule formulation for climb, cruise and descent modes, fixed sector mission performance and associated optimal cost and profit flight techniques are not generally addressed. Studies have shown that the predictive powers of these methods display reasonable accuracy but objective function sensitivity to a generalised array of design parameters is left wanting when the notion of operational criteria is incorporated into the process.

Attempts have been made through the introduction of complex computer algorithms and multivariate optimisation (MVO) techniques like Quadratic Sequential Programming, Latin Squares, Decomposition, etc. in conjunction with calculus of variations and finite element theory, but unfortunately rather than truly achieving the goal of creating a market orientated competitive design, the sole end becomes an optimised mathematical model with no real reflection placed upon realistic operational concerns.

The purpose of this paper is to consider a middle ground between generalist first order minimalism and more complex higher order MVO with emphasis still placed on simplicity but not at the expense of objective functionality and operational applicability. A number of revised as well as a variety of new methods are presented for calculation and subsequent design optimisation. These are validated against known aircraft designs as well as demonstrated with an actual small turbofan regional transport example.

Conceptual Design Prediction Methods

Concept of An Impulse Function

A traditional conceptual study revolves around analysis that is predominately discrete in nature. This can become quite cumbersome and impractical especially when typical conceptual design performance assessments even at the most elementary level can consist of hundreds or even thousands of point calculations, each requiring an instantaneous estimate. Additionally, this philosophy denies the possibility of conducting analytical performance optima identification via single expression algorithms, thereby, in an effort to reduce complexity it compels the use of coarser numerical integration procedures or closed form approximations prone to large errors.

By introducing the concept of an impulse function or approximate unit step, normally discrete procedures of analysis can be transformed into continuous differentiable

* Aircraft Performance Engineer, American Airlines.
Formerly employed by Saab Aircraft AB.
Graduate Member RAeS.

equations. The impulse function is mathematically approximated here as

$$\Phi(f, f_s) = k_1 + k_2 \tanh[k_3(f - f_s)] \qquad (1)$$

where the coefficients k_n represent values which assist in modelling an idealised unit step, and, the variables f and f_s are the tested and critical values respectively. For example, $\Phi(10,20)$ results in 0 or conversely $\Phi(20,10)$ is 1. This idea can be extended for identification of maxima or minima between quantities as well. A maximising function can be produced via the associative rule

$$\Phi_{max}(a,b) = a\Phi(a,b) + b\Phi(b,a) \qquad (2)$$

whereas, a minimising function is of the form

$$\Phi_{min}(a,b) = a\Phi(b,a) + b\Phi(-b,-a) \qquad (3)$$

for the tested values a and b.

Atmospheric Modelling

It has been demonstrated temperature decreases linearly with altitude while the atmospheric hydrostatic relation equates density ratio lapse as some exponential function of temperature ratio[15]. These relations hold true up to the troposphere, and when surpassed, temperature remains approximately constant with increasing flight level up to about 70000 ft or the lower part of the stratosphere. This altitude can be considered as an upper threshold of flight level well in excess of those frequented by contemporary subsonic transport aircraft. By incorporating an impulse function to mimic commencement of the tropopause [$\Phi_{trop}=\Phi(h,FL\ 361)$], the lapse rates for temperature (θ) and density (σ) ratio as a function of flight level (h) and International Standard Atmosphere temperature deviation (ΔISA) can be adequately modelled via

$$\theta = 1 + \frac{\kappa\Phi_{trop}\left(k_1^{\theta}h + k_2^{\theta}\right) + k_3^{\theta}\Delta ISA - h}{\kappa} \qquad [FL\ 0,\ FL\ 700] \qquad (4)$$

and

$$\sigma = \frac{\theta_{ISA}\sigma_{ISA}}{\theta} \qquad [FL\ 0,\ FL\ 700] \qquad (5)$$

where

$$\sigma_{ISA} = \theta_{ISA}^{4.2561} + \Phi_{trop}\left(k_1^{\sigma}\ln h + k_2^{\sigma}\right) \qquad [FL\ 0,\ FL\ 700] \qquad (6)$$

For instance, the coefficients k_1^{θ}=6.900 x 10^{-4} per FL, k_2^{θ}=-0.2480, k_3^{θ}=5.046 FL/^{o}C, k_1^{σ}=-0.4398, k_2^{σ}=2.583 and κ=1454 FL would be used in order to model the atmosphere for given temperature deviation from ISA.

Another physical quantity important for the calculation of Reynolds number used for drag prediction is the ratio of sonic velocity to kinematic viscosity (a/ν) at given flight level. Investigations have shown adequate results can be obtained via a third order polynomial curve fit.

Aircraft Weight Estimation

Constituent weight estimation is based on statistical fits of current production aircraft, and together with estimates for useful load, the sum of these constitutes the aircraft Maximum Takeoff Weight (MTOW). As is the case with most weight prediction methods in literature[18,24], more refined estimates based on statistical equations through sophisticated regression analysis become transcendental algorithms characterised by relatively small and partially self cancelling errors with accuracies of the order of 5-10%. Studies showed this to be somewhat true for specific methods but were found to be wanting in many instances when adequate objective function sensitivity for rather advanced trade studies are desired. The final weight estimation algorithm adopted by the author involves a hybrid transcendental approach with Linnell's[14] parametric description used for major components in conjunction with additional methods requiring fidelity from more specific parameters related to performance and geometry. By adopting Scott and Nguyen's[20] notion of two functional weight groups, a basis can be laid for derivation of the aircraft Operational Empty Weight (OEW). Since the sum of fuel and payload or useful load can be regarded as both a variable to optimise and the objective function, a third functional weight group is now introduced - leading to a combination of all three for MTOW.

The first functional weight group comprises of fuselage, wing, empennage and landing gear constituents and are derived via trend equations produced by Linnell. An adequate parametric representation of the relationship between applied loads, geometric shape and configuration choice was achieved with modifications made by the author to most of the trend coefficients. Since Linnell had allowed for an objective function sensitivity of dynamic pressure to structure, a direct coupling between fuselage structural weight and a design candidate's speed envelope or primarily V_{MO} speed were incorporated and together with the introduction of a limit manoeuvre-gust load parameter concept proposed by the author, this is envisaged to possess a consistent objective function sensitivity to a wide scope of the design parameters.

The second functional group designated as fixed equipment weight are estimated using a variation of the method given by Scott and Nguyen. The fixed weight is referred by Scott and Nguyen to be a "constant weight" because it is assumed to be related to passenger capacity, and hence, constant during the conceptual sizing process. The variation of a linear constant weight coefficient models the impact of fuselage size to fixed equipment and it can be quickly surmised that this parameter is specific to each respective manufacturer. The power plant and installation weight including contributions made by nacelles and pylons is based on a logarithmic statistical regression produced by the author. The sample size covered 66 different gas turbine engines produced by 7 manufacturers and each varying in maximum sea level static thrust capability between 8.5 kN (1900 lb.f) to 118 kN (26500 lb.f).

The third and final function group consists of weights characterised by ancillary geometric and philosophical

considerations. These encapsulate estimation of available fuel weight with or without a centre tank, and, contingency design maximum payload-OEW allowances. Maximum available fuel weight estimation was developed from a statistical correlation to wing geometry presented by Torenbeek[24] but was later modified by the author to reflect more contemporary data. Further algebraic extensions to this basic model were incorporated in order to facilitate more realistic fuel increments produced by introduction of a centre tank - this was considered important since many vehicles are frequently offered as standard or extended range versions. A philosophical decision of artificially increasing the desired maximum payload by some factor to create a contingency buffer for unexpected OEW penalties incurred during preliminary design is often considered in practise and is therefore also facilitated. To round off this functional group, an advanced technology multiplier to account for weight reduction possibilities of aircraft empty weight is also available. This parameter first proposed by Scott and Nguyen represents the progress of weight reduction over the last four decades with emphasis placed on vehicles with an average entry-into-service year (YEIS) of 1975.

Power Plant Installation

The attributes of a gas turbine power plant are primarily dependent upon the effect of pressure ratio, altitude and free-stream velocity. The instantaneous production of thrust relies generally upon an engine's thermal efficiency in conjunction with variations in disc loading. The compression ratio is achieved partly by the inlet (ram pressure) generated by elevated mass flow at increased velocities but mostly through the compressor itself thus making pressure ratio engine specific. In view of this, an approximate engine model proportional to variation of flight level (h) and velocity (V) would be expected to generate an adequate description of thrust lapse.

By assuming this lapse rate decays exponentially, an approximation of instantaneous thrust can be proposed as

$$T = T_{oi}\left[1+\exp\left\{-\left(k_1+k_2h\right)T_{oi}\right\}\right] k_3\exp\left\{-k_4h-k_5v\exp\left(-k_6h\right)\right\} \quad (7)$$

where T is the instantaneous available thrust, T_{oi} is the installed maximum sea level static thrust and k_n are constants of proportionality. Eqn 7 is applicable for normal takeoff, maximum takeoff with auxiliary power reserve (APR), maximum climb and maximum continuous thrust ratings. A distinct maximum cruise thrust prediction method was also developed and is of the form

$$T = T_{oi}\left[1+\exp\left\{-\left(k_1+k_2h\right)T_{oi}\right\}\right] k_3 \exp\left\{-k_4h-v\left[k_5+k_6\exp\left(-k_7h\right)\cos\left(\frac{\pi}{4}+k_8h\right)\right]\right\} \quad (8)$$

It can be observed that incorporation of an engine rating parameter for universal modelling which accommodates both takeoff/climb and maximum cruise has been dispensed with. takeoff/climb ratings are usually associated with lower vehicular subsonic speeds, whereas, maximum cruise with considerably higher ones, and because present day gas turbine overall power plant efficiencies exhibit strong variation with Mach number particularly in the transonic regime[22] i.e. free-stream Mach numbers greater than approximately 0.65, this condition denies adequate regression qualities - and therefore compels distinction from one another. Furthermore Eqn 8 need not be in an easily differentiable form for steady cruise analysis, whereas, as it will be demonstrated later Eqn 7 must.

Thrust specific fuel consumption (TSFC or c) is also a function of overall power plant efficiency[22] and Mach number. Scope was given for the creation of a unified analytical treatment of instantaneous TSFC prediction so a single expression that accounts for not only Mach number, but variations in engine rating was pursued.

$$c = \left\{k_1h^{-k_2}\left(\frac{T}{T_{oi}}\right)^{\left(k_3h+k_4\right)}\right\}M + \left(k_5h+k_6\right)\left(\frac{T}{T_{oi}}\right)+k_7h+k_8 \quad (9)$$

A linear performance deterioration model (k_θ) to account for the effects of temperature deviations from ISA (T_d) when calculating instantaneous available thrust or even TSFC may be incorporated via

$$k_\theta = 1 \pm k_1\Phi\left(T_d, T_c\right) \quad (10)$$

where T_c is the critical ISA deviation for flat rating.

These expressions do not permit direct sensitivities to bypass ratio, pressure ratio or turbine entry temperature because such a facility was deemed too detailed for this level of analysis. Investigations have shown that adequate representation of these parameters are produced through correlation of lapse coefficients to the maximum static thrust rating of a given engine. In this way generic turboprop and turbojet models can be created through regression thereby giving good representation of expected overall power plant efficiency without altering the inherent structure of the model itself. Due to the structure of the instantaneous thrust and TSFC models, they offer the opportunity of delivering relatively accurate predictions of thrust and fuel flow when a statistical regression for specific power plants are done, and additional consideration to temperature deviations from ISA standard atmosphere and bleed losses can be incorporated when desired. If available, Reynolds number variation and other installation effects may be introduced thus allowing for accurate prediction, otherwise a generic model would possess the inherent capability of being utilised as a rubber engine for comprehensive sensitivity studies. Also, these functional forms are differentiable via

logarithmic differentiation with respect to independent parameters, which have a direct physical consequence i.e. flight level and velocity, thus allowing for a rather comprehensive scope of performance optimisation possibilities.

Low-Speed and En route Aerodynamic Modelling

Lift Prediction

The clean wing maximum lift is derived from an algorithm developed by the author[12,13] with a source database constructed utilising MIT's TODOR Vortex-Lattice software for a gamut of typical transport aircraft aspect ratio, taper ratio, root chord incidence and dihedral. Each generic planform was subsequently modified for a desirable lift distribution through wing tip wash out. High lift produced by flap and slat deflection are estimated based on methods presented by Young[25]. This reference uses empirical correlation from assorted accumulated data and predicts with reasonable accuracy the aerodynamic characteristics of high lift devices. Combined with a wide variety of device choice for estimation this was found to be most suitable.

The final combined method accounts for effects due only to wing aspect ratio, taper ratio as well as quarter chord sweep and does not consider wing section thickness and camber in an effort to reduce complexity. Abbott and Von Doenhoff[1] show that for the interval of mean wing thicknesses commonly employed for modern day transport aircraft, the variation of sectional maximum lift characteristics is generally small except for thickness ratios less than 12 percent and the effects of increasing camber to wing section increased lift becomes less significant for thicknesses greater than 12 percent. Additionally, scale effects due to Reynolds number for thickness ratios between 12 to 24 percent were experimentally found to be nearly independent of thickness ratio. It is felt that wing geometry trades via mean wing section thickness would be more influential in terms of structural efficiency, available fuel capacity and en route compressibility drag rather than drastically alter, for example, field performance by a small incremental change in lift.

Low-Speed and En route Drag Prediction

When formulating predicted drag polars at the conceptual level, it is common practise to neglect variations in Reynolds number and centre of gravity location reducing the analysis to a narrow band of what is considered as the typical scenario. This approach suffers from great inconsistencies when variations in drag occur with Mach number at low subsonic speeds or in particular when compressibility effects become significant. After careful review of the impact each simplification has to the final result, a different approach to drag estimation was created by the author, which introduces the influence of Reynolds number but retains the previous assumption of negligible contributions due to centre of gravity. The goal was to establish a single algorithm (combined drag model, or, CDM) that covers the entire spectrum of operation for transport aircraft whilst still maintaining a good degree of accuracy. Furthermore, an additional stipulation of differentiability for subsequent performance optimisation purposes was also pursued.

Vortex-induced drag estimation for field and en route regimes together with other sources such as profile drag increments from flap deflection, roughness, excrescences, interference and three dimensional effects are treated by traditional empirical models[17,18,24], but have been adjusted where required.

A common method for determining the zero-lift drag of aircraft components is an assumption that the constituent's friction drag is equivalent to a flat plate having the same wetted area and characteristic length. In this way, the preliminary stage of complete vehicular zero-lift drag estimation may be accomplished by summation of these individual components. By creating a hybrid approach where the component build-up method is benchmarked against a standardised closed form expression, economy of effort can be achieved without incurring excessive degradation in predictive powers.

A tool for estimating zero-lift drag (C_{Do}) is the friction coefficient equation based on experimentation done by Eckert[4] which accounts for fully turbulent flow and compressibility effects. By assuming an appropriate reference condition of Mach number and flight level, the component build-up method may be employed and a characteristic equivalent length (l_ε) for the entire vehicle can be derived from its equivalent skin friction coefficient - a quantity commonly used for aircraft comparison exercises. This equivalent characteristic length may in turn be reintroduced into Eckert's Equation and solved for any other Mach number (M) and flight level (h) combinations the aeroplane encounters, viz.,

$$C_{Do}\big|_{M,h} \cong \frac{A(\ln 10)^b}{\left[\ln\left\{Ml_\varepsilon\left(\frac{a}{\nu}\right)\right\}\right]^b\left[1+cM^2\right]^d}\frac{S_{wet}}{S_w} \qquad (11)$$

where, a, represents the sonic velocity and ν the kinematic viscosity at flight level, S_{wet} is the total wetted area of the vehicle, S_w is the reference wing area, and constants A, b, c and d are coefficients of proportionality derived by Eckert.

In an effort to theoretically gauge the magnitude of inherent errors produced by this approach, the equivalent characteristic length method (ECLM) expression was reconfigured as an error function and resultant equivalent skin friction errors were observed for a range of contemporary regional transport and business jet Reynolds number regimes. For a typical en route Reynolds number of 1.5×10^6 based on vehicular characteristic length, errors of -24% in the equivalent characteristic length correspond to a +5% overestimation of equivalent skin friction or total zero-lift drag. Conversely, for the same Reynolds number, a -5% underestimation of zero-lift drag is tolerated by a +33% error in equivalent characteristic length. This result shows the resilience of ECLM.

Compressibility effects on drag are commonly described by arbitrary mathematical models because much of what

is known about the mixed flow regime is largely experimental. At the conceptual level they generally do not adequately account for the dependence of drag divergence Mach number on design parameters like instantaneous lift coefficient, wing sweep, mean wing thickness and type of airfoil geometry but are estimated with simple empirical increments. As an alternative, Torenbeek[23] offers a variation of Korn's Equation[2] to quantify the limits of wing section performance. After some manipulation[12] of the modified Korn's Equation, the critical Mach number (M_{cr}) can be estimated as

$$M_{cr} = \left\{ \frac{1}{\cos\Lambda}\left[M_{ref} - \frac{1}{10}\left(\frac{C_L}{\cos^2\Lambda} \right)^{3/2} - \left(\frac{t/c}{\cos\Lambda} \right) \right] \right\} - \Delta M \qquad (12)$$

where Λ is the wing quarter chord sweep, C_L the instantaneous lift produced by the wing, t/c is the mean wing thickness ratio, M_{ref} is an empirical wing section technology factor and ΔM is an empirical representation of the relationship between M_{cr} and divergence Mach number (M_{DD}). In order to produce a continuous function concept for compressibility drag (ΔC_{Dcomp}), the critical Mach number threshold can be flagged by an approximate impulse function [$\Phi_{Mcr}=\Phi(M,M_{cr})$] and combining this with an empirical drag rise model given by Torenbeek[24] this yields

$$\Delta C_{Dcomp} = \Phi_{Mcr}\,\Delta C_{DD}\left[1 + \Phi_{Mcr}\left(\frac{M - M_{cr}}{\Delta M} - 1 \right) \right]^n \qquad (13)$$

thus making the expression differentiable for all Mach numbers.

The one engine inoperative (OEI) condition appears to be mostly disregarded in conceptual design literature. It is usually classified as a preliminary design problem[18,24] because yawing and rolling considerations become rather complex in nature since these must be trimmed out by primarily the rudder and then aileron. Drag due to engine windmilling, airframe sideslip, incremental changes in normal force induced and profile drag from control surface deflection, asymmetric slipstream effects and lift distribution reconfiguration producing vortex-induced contributions all combine to complicate matters. By examining the exact approach, a number of valid simplifications may be incorporated in order to reduce the scope of detailed information required whilst retaining strong predictive powers and objective function sensitivity with respect to the design variables.

Studies have shown that many of these constituent contributors can be neglected with the exception of induced and profile drag generated by rudder deflection. Figure 1 demonstrates the pertinent forces and moments once this simplification is introduced. It is assumed that the vertical tail utilises a symmetric profile and all rudder deflections during asymmetric flight will be below stall, thus, from linear thin aerofoil theory, the rudder deflection (δ_r) required for equilibrium of the OEI asymmetric condition is given by

$$\delta_r = \frac{2y_{eng}\left(D_{wm} + T_{op}\right)}{\rho v^2 S_{vt} C_{L\alpha}\,\tau\eta l_{vt}} \qquad (14)$$

where y_{eng} is the moment arm from fuselage center line (assumed centre of gravity location) to the critical and windmilling engines, D_{wm} is the drag produced by the windmilling engine and is estimated using empirical methods, T_{op} is the instantaneous available thrust produced by the critical engine at velocity V, S_{vt} is the vertical tail reference area, $C_{L\alpha}$ is the lift-curve slope characteristic of the vertical tail, τ is the flap effectiveness factor, η is a correction which accounts for the effects of viscosity and l_{vt} is the vertical tail moment arm. It is highlighted that $C_{L\alpha}$ estimates are adjusted for aspect ratio with the Helmbold Equation[15] and effects of sweep by a first order cosine relation[24]. From this basis, the possibility of accounting for the influence of minimum control speed limitations on field length and climb performance can be introduced at the conceptual level, and, the method for predicting this aspect of operational performance is discussed with greater detail in the section to follow.

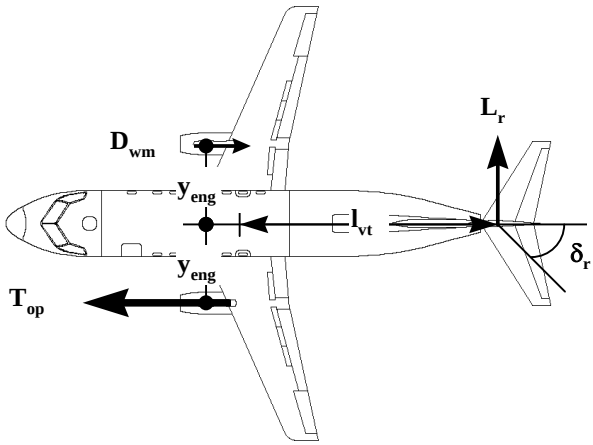

FIGURE 1 - Simplification of forces and geometric considerations during the asymmetric thrust condition.

By summing the forces and moments in Figure 1 and quantifying rudder deflection from Eqn 14, the incremental drag contribution produced by OEI asymmetric condition (ΔC_{DOEI}) is therefore given by

$$\Delta C_{DOEI} = \frac{2\left[D_{wm} + \left(D_{wm} + T_{op}\right)\frac{y_{eng}}{l_{vt}}\tan\delta_r \right]}{\rho V^2 S_w} \qquad (15)$$

This relation is not only applicable for low speed field performance drag prediction, but can also be utilised for climb out analysis as well: specifically in relation to OEI maximum attainable flight level and driftdown

proficiency trade studies at ISA and more importantly off-ISA conditions.

Field Performance

Takeoff and landing field length prediction can become quite complex if one approaches the problem via integral methods. Many alternatives for the estimation of field performance exist in current literature. Rather than opt for new algorithms, existing methods found in literature were utilised but with some enhancements introduced by the author.

Torenbeek[24] offers a useful equation in functional form which correlates the field length performance of similar aircraft and this serves as an adequate first order approximation.

$$BFL = \left(\frac{0.863}{1+2.3\Delta\gamma_2}\right)\left(\frac{W_{to}/S_W}{\rho g C_{L_2}} + h_{to}\right)\left(\frac{1}{T/W_{to}-\mu'} + 2.7\right) + \frac{\Delta s_{to}}{\sqrt{\sigma}} \quad (16)$$

where $\gamma_2=T/W-C_D/C_L$ is the instantaneous OEI climb gradient of the vehicle at the 35 ft (10.7 m) screen height threshold (h_{to}), $\Delta\gamma_2$ is γ_2 less the minimum second segment climb gradient permitted by airworthiness authorities, W_{to}/S_w is the wing loading at Takeoff Gross Weight (TOGW), T/W_{to} is mean thrust-weight for the takeoff run, C_{L2} is the instantaneous lift coefficient at V_2 speed, μ' is the coefficient of friction during acceleration and Δs_{to} is the inertia distance. The asymmetric drag-lift ratio is calculated based on the most limiting condition when taking the stall speed factored (V_2/V_S) and the minimum control (V_{MC}) speeds into consideration. The V_{MC} can be derived by rearranging Eqn 14 and solving for an instantaneous velocity when maximum permissible rudder deflection occurs (i.e. $\delta=\delta_{max}$) - the resultant transcendental equation thereby deriving minimum control speed on the ground which is also treated as an approximation of minimum control speed in the air. In this way, an objective function sensitivity with engine thrust line location as well as thrust generation potential to balanced field length performance can be established and hence locate any stationary point thresholds.

The landing segment can be separated into three portions of operation: approach, flare and the ground roll. The method presented by McCormick[15] offers an opportunity of not only producing reliable predictions but is comprehensive enough for adequate objective function sensitivity. The flare is assumed to be a circular arc and approach speed is constant throughout the flare. After touchdown, delay time allowances are made for reconfiguring the vehicle from landing to braking, and finally, the ground roll is simply defined as a continuous deceleration where upon the magnitudes of all relevant variables are evaluated at the root mean square of touch down speed. Approach and landing climb minimum control speed thresholds have been disregarded in this instance since these scenarios are usually not limiting at ISA, sea level conditions although exceptions may occur where positive engine thrust levels are significant in some vehicles.

The coefficient of friction for acceleration and braking is estimated using linear fits with lift-drag ratio (takeoff) and root mean square touchdown speed (landing) respectively. Additional refinements through introduction of spoiler actuation and thrust reversing capability modelled by empirical methods are also available to enable regulatory flexibility (JAR or FAR) as well as demonstrate performance improvement possibilities.

En route Performance Assessment

Operational Limitations

Appropriate formulation of the flight envelope is essential for maximising the en route performance capabilities of any respective aircraft and many regulatory guidelines exist for its definition[24]. The problem here is to create a set of simplistic rules that allows for accurate envelope construction without unduly restricting the vehicle's unconstrained predicted performance. The flight envelope usually consists of four distinct boundaries, three of which are defined by speed thresholds related to stall (V_S), buffeting and emergency dive (M_{MO}), and, a combined consideration of manoeuvre-gust loads and maximum dynamic pressure (V_{MO}). The remaining boundary is an upper threshold of flight level derived from simultaneous appreciation of climb thrust limitations, maximum cabin pressure differential and occasionally buffeting. The derivation of these boundaries is commonly performed using extrapolated wind tunnel data to full-scale and subsequently verified with flight-testing. Initial prediction methods can become mathematically quite extensive which do not easily lend themselves to simplification or otherwise lose significant precision in the process. For example buffeting is characterised by breaks in C_L-α, c_m-α or c_x-α curves and emergence of pressure divergence on any of the lifting surfaces or fuselage - this poses a daunting challenge from the analytical point of view. By tackling this problem through the basic conceptual design philosophy of implicit minimum goal success, a useful empirical method may be developed that adequately defines the flight envelope without the need for more esoteric aerodynamic modelling. This approach uses the information already available from an investigated vehicle's unconstrained predicted performance and correlates this to a database of previous observations collected from known designs.

Initially, the stall speed is trivially calculated as an aerodynamic minimum speed with power off. The upper flight level boundary can be derived from known climbing performance of the vehicle with some attention paid to performance and structural limits - this matter is clarified further in the section to follow. By assuming that buffet onset and minimum buffet margin violation can be avoided, the maximum projected service ceiling for certification can then be predicted. The V_{MO} and M_{MO} placard speeds are set using known maximum cruise thrust limited performance for a pre-designated minimum

flight weight (MFLW) vehicle configuration with adjustments incorporated from statistical bias. The MFLW can be defined by assuming some percentage of the vehicle's MTOW: this figure may be obtained from comparisons made with Performance Engineer Handbooks (PEH) of other known designs or equivalently estimated by assuming an All-Up Weight (AUW) equal to the sum of OEW and 25% of the Maximum Fuel Weight (MFW). Thereafter, the maximum cruise speed threshold can be obtained assuming equilibrium of forces in horizontal flight for given MFLW at a specified interval of flight levels commonly assumed to be between FL 150 and FL 300 in order to maximise en route performance flexibility. This speed variation with flight level is in fact hyperbolic, however using the same reasoning for Eqn 19, a transformation of speed as an exponential function of flight level can be introduced and appropriate placard speeds can then be predicted based on statistical regression from a database derived from other aircraft.

For example, if a design proposal is to be inspected for its predicted V_{MO}/M_{MO} boundaries, maximum cruise speed (V_{mcr}) for flight levels h_1 and h_2 assuming MFLW are investigated, and correspondingly plotted as free variables of calibrated air speed (CAS) and Mach, thus a cross plot similar in form to Figure 2 can be established. It is evident that Mach number tends to increase with increasing flight level whereas CAS increases with reduction in flight level. By considering these curves as potential M_{MO} and V_{MO} candidates respectively and introducing the "20-80" rule, the vehicle's V_{MO}/M_{MO} boundary can be predicted. The 20-80 rule is actually an interval which disregards 20% of the slower CAS and faster Mach speed portions of the investigated flight level interval and was derived empirically. One drawback is that the method does not facilitate a multiple V_{MO}/M_{MO} boundary definition, however the approach is simple, promotes synergistic utilisation of primary conceptual calculation algorithms and validation has shown it to be relatively accurate.

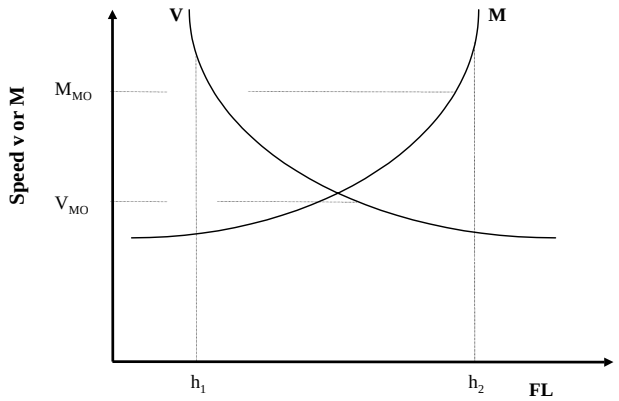

FIGURE 2 - Identification of V_{MO}/M_{MO} flight envelope boundary using "20-80" rule.

Climb and Descent Control Formulation

Neglecting flight path-angle dynamics and effects of wind, the point mass equation of motion for accelerated flight in the vertical plane is

$$\frac{dh}{dt} = \frac{(T - D)V}{\left[1 + \frac{V}{g}\frac{dV}{dh}\right]W} \qquad (17)$$

where dh/dt is the instantaneous climb rate, T, D, and W are instantaneous available thrust, total drag and AUW at forward velocity V, and the final component accounts for accelerated climbs. Operational conventions dictate a definition of flight level that gives reasonable measure of maximum operating height potential for an aircraft whilst simultaneously fulfilling legitimate considerations of attaining this height in reasonable time. A well tempered conceptual climb control formulation for any prospective aircraft should therefore weigh the attributes of maximum rate of climb (ROC) and minimum time to climb optimal trajectories and create a final approximate trajectory which would be used for the definition of a maximum service ceiling or flight envelope upper threshold. Since ROC is proportional to specific excess power, satisfying the condition

$$\frac{\partial[(T - D)V]}{\partial V} = 0 \qquad (18)$$

and subsequently rearranging as a transcendental function would allow identification of optimal instantaneous forward speeds at given flight level and AUW since available thrust and total drag have been previously defined as continuous differentiable functions. If speed profile is plotted as an optimal climb trajectory is generated, the resultant locus shows strong hyperbolic tendencies with flight level. This circumstance unfortunately requires an integral approach or its common approximate numerical alternative. Conversely, if flight level can be regarded as a free variable against optimal forward speed, it is evident that this transformation promotes an approximate exponential progression to mimic the profile. Consequently, if two reference flight levels can be selected which minimise the error incurred when weight loss due to fuel burn is neglected, i.e. rate change of speed with respect to flight level does not vary greatly between each reference flight level, an adequate approximation for the locus of forward speed of an optimal climb trajectory covering the entire flight level envelope can be constructed. For example, at reference flight levels h_1 and h_2, the corresponding instantaneous forward speeds V_{h1} and V_{h2} can be expressed as

$$V_{h_1} = k_1 e^{k_2 h_1} \quad \text{and} \quad V_{h_2} = k_3 e^{k_4 h_2} \qquad (19)$$

and after solving these simultaneous equations for constants of proportionality k_n, a single closed form expression can approximate an optimal climb trajectory forward speed at given flight level. A conceptual service ceiling estimate would require two distinct profiles based on the premises of idealised acceleration-free and accelerated climb scenarios in order to derive a realistic optimal accelerated climb trajectory (see Figure 3). A splay resulting from these distinct schedules are then constructed and subsequently compared for a resultant closer approximation to the actual accelerated climb

profile. The original accelerated climb is initially approximated via an analytical approach, which traces a path of speed loci where lines of constant height-energy are tangential to curves of specific excess power. However, this procedure is not sufficient enough for final optimal trajectory definition because it assumes that potential and kinetic energy can be interchanged instantaneously and without loss thereby yielding speed schedules with optimistically higher velocities. The final speed profile constitutes a predicted vehicular maximum service ceiling, but is only regarded as an upper limit the vehicle is capable of fulfilling. This in turn does not necessarily constitute the aeroplane's final service ceiling because other considerations of operational flexibility and structural limitations, which are mostly based on an intuitive trade, must be taken into consideration.

It is common practise to assign two distinct climb modes or more specifically speed schedules for climb control by means of fixed CAS and Mach speeds. The advantages with faster speed schedules are that they create possibilities in conducting further time, cost or profit function optimisation, or more importantly opportunities in constraining previously unconstrained optima compared to single speed schedules because faster climb speed schedules (designated here as CLB Mode H) encourage cruise "soaking"[12] or the exchange of cruise distance for climb which leads to significant block time reductions - this especially being the case for regional type sector missions. Furthermore, a slower climb speed schedule (CLB Mode L) enables closer adherence to fuel optimal procedures during climb thereby enhancing range capability. In this way, CLB Mode L and CLB Mode H speed schedule definitions are formulated with respect to optimal climb trajectory profile state and time function adherence and designated divergence criteria respectively.

It is common practise to neglect weight loss due to fuel burn, however, the effect of weight loss on trajectory becomes important in two respects: a greater degree of operational flexibility through higher ceiling capability may be afforded if an optimal trajectory for block time, cost or profit functions are denied i.e. air-traffic control (ATC) or route structure, and, greater scope for improvements in efficiency of fuel load burned for range can be achieved or at least traded for feasibility. By introducing a fuel burn model via exponential extrapolation, not only can better approximations for actual time, distance and fuel burn be modelled as the trajectory is generated for given speed schedule from an initial TOGW, but occasionally, valid predicted performance enhancements may be exploited.

Descent speed schedule definitions are mostly treated in the same way as climb with CAS, permissible vehicular as well as cabin maximum rate of descent (ROD) as the control variables. In this instance multiple descent modes are disregarded in favour of one DES Mode owing to small differences in the state and time variables.

Optimal Cruise Control Identification

The objective here is to derive a single expression to instantaneously derive optimal cruise conditions at constant flight level. For an accurate assessment of maximum specific range (SAR), optimisation should focus on the control variables of speed, flight level and overall power plant efficiency[22]. At the conceptual level it is customary however to introduce a critical assumption that thrust specific fuel consumption is independent of throttle setting together with large variations in Mach number for the sake of simplicity. Since the structure of the thrust specific fuel consumption model presented earlier facilitates these dependencies, a single expression algorithm can be formulated to identify the condition for optimal cruise performance.

The need for throttle setting (T/T_o) can be determined a priori and incorporated in the following manner

$$\frac{\partial(T/T_o)}{\partial V} \equiv \frac{\partial(D/T_o)}{\partial V} \equiv \frac{1}{T_o}\frac{\partial D}{\partial V} \qquad (20)$$

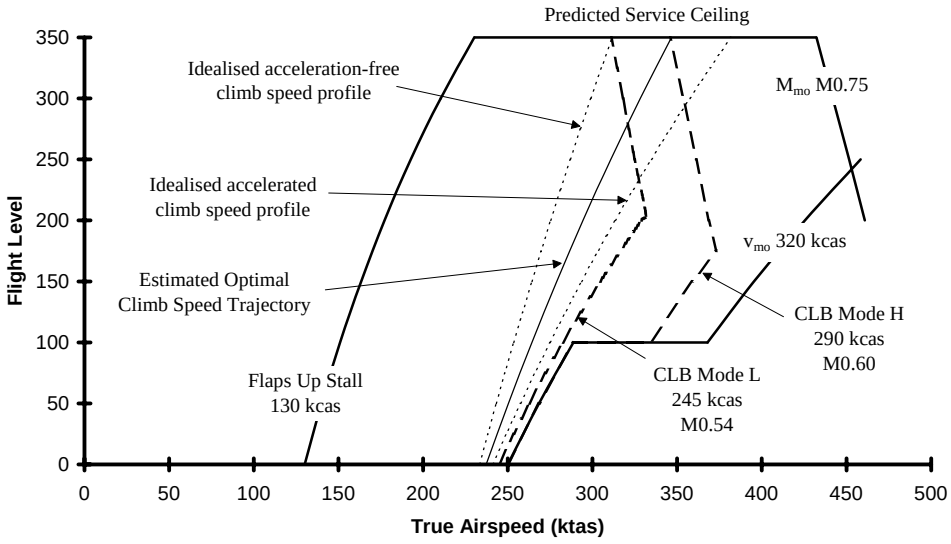

FIGURE 3 - Example optimal climb trajectory, climb control speed schedule and flight envelope definitions.

where the total drag D consists of zero-lift, induced and compressibility contributions and hence dispensing with the need for a partial power thrust model. By employing Miller's[16] logarithmic differentiation of the Breguet equation with respect to speed and introducing the additional control variable of throttle setting, the generalised criteria for maximum specific range speed (V_{opt}) at flight level h is given by

$$V_{opt} = \left\{ \frac{1}{c}\left(\frac{\partial c}{\partial M}\right)_h \left(\frac{\partial M}{\partial V}\right)_h + \left[\frac{1}{cT_o}\left(\frac{\partial c}{\partial [T/T_o]}\right)_h + \frac{1}{D}\right]\left(\frac{\partial D}{\partial V}\right)\right\}^{-1} \quad (21)$$

where c is the thrust specific fuel consumption. It can be observed that this transcendental expression is comprehensive enough to offer a thorough treatment of identifying not only partial and global cruise performance optima but has the flexibility of finding such solutions below the drag rise and more importantly identification of optima within the transonic regime as well. In order to inspect for consistency of these unconstrained solutions against operational limitations, comparison to the thrust limited speed, maximum operating limit speed and maximum operating limit Mach number at flight level are also considered via a minimising function, viz.

$$V_h^* = \Phi_{min}\left\{\Phi_{min}\left(V_{opt}, V_{mcr}\right), \Phi_{min}\left(V_{MO}, M_{MO}\right)\right\} \quad (22)$$

where the maximum cruise speed threshold at flight level is simply obtained assuming equilibrium of forces in horizontal flight.

En route Operational Performance and Flight Profile Optimisation

The optimum trajectory-profile algorithm (OTPA) analyses a three-phase flight in which interactions between climb, steady cruise and descent are considered in order to allow for inspection of objective function sensitivities against the collective influence imposed by a general set of design variables. Rather than attempt to approach this problem via a fully blown calculus of variations[7] or even its simplified version[21], the idea was to create algebraic functions which can adequately describe the constituent known trajectories, thence combine all segments in order to construct an assumed trajectory and optimise for any state or time function. Cost and subsequent profitability functions together with their inherent sub-optimisation possibilities are also considered but are presented in the next section of this paper.

During climb and descent it customary to correlate distance travelled, time elapsed and fuel expended as free variables against an instantaneous TOGW or AUW and flight level. A transformation using the assumption that AUW, time elapsed and fuel expended (all denoted by variable λ_h) are monotonic functions of distance travelled at a particular flight level (d_h) can be expressed as

$$d_h = \exp\left(\frac{\lambda_h - k_2}{k_1}\right) \Leftrightarrow \lambda_h = k_1 \ln(d_h) + k_2 \quad (23)$$

An impulse function for Eqn 23's flight level dependent coefficients (k_n) give instantaneous values of otherwise free variables, thereby, enabling a solution for trajectory optimisation through known distance and flight level.

Steady cruise is conducted at constant flight level and depending on the accuracy desired the distance traversed may be numerically integrated as aircraft mass is reduced, however, experience has shown using Eqn 22 or maximum cruise speed at an average cruise AUW is sufficient enough for a good approximation. The possibility of examining intermediate CAS for steady cruise has been disregarded since these scenarios are perceived to be inconsequential with regards to a design proposal's operational and cost objective functionality. Instead, a choice of throttle setting limited to two particular procedures, i.e. maximum cruise power afforded by the thrust model previously presented in Eqn 8 and partial power setting (as per the rationale given in Eqn 20) required for optimal cruise performance, is given in order to facilitate optimal fuel usage (maximum SAR and minimum fuel), maximum block speed, optimal time expended (minimum time) and intermediate flight techniques for payload-range and block time-fuel curve characteristics.

OTPA begins with an initial flight level assumption of maximum service ceiling. For reasons of computational speed and simplicity, the algorithm utilises an interval halving numerical scheme with climb distance as the free variable - an upper and lower climb distance interval at flight level can be derived when MTOW and MFLW are assumed respectively. Based on this premise, other pertinent parameters such as the fuel expended to clear flight level, time elapsed to climb and TOGW are quantified for the interval mid-point. The first iteration assumes an initial beginning of descent (BOD) AUW to be the sum of OEW, payload and fixed fuel reserves which then permits an estimate of available fuel for cruise. The scheme then proceeds until satisfaction of either of the two conditions arises: (a) fuel weight balance occurs for payload-range, or, (b) distance balance occurs for fixed sector missions. Holding can be defined via a pre-selected minimum drag or fixed speed schedule for given flight level and time duration and is initially quantified from an AUW comprising of OEW, payload and diversion reserves. The diversion reserve is formulated using the iterative scheme discussed above but only considers a minimum fuel flight technique since fixed sector distances are usually considered. Further reserve contingencies may be accommodated through selection of an extended cruise time duration option as well as the possibility of assuming some fixed percentage of the total flight fuel. The algorithm facilitates inequality

constraints of: a minimum cruise fraction to ensure cruise segments do not become too small and compromise passenger comfort; operational limitations imposed by structure, design weight thresholds and power plant; and, any other aircraft model, ATC or route structure limitations that require consideration.

The introduction of an additional criterion whereby block speed is maximised promotes iteration to lower flight levels thus allowing for the identification of maximum block speed and minimum time flight techniques for payload-range and fixed sector mission respectively. A presentation with payload-range block speed maximised can be useful for objective function sensitivity studies where the designer may wish to trade the merits of a particular design candidate's maximum attainable sector mission stage length for given mission payload against other potential configurations or even compare results against known competitor aircraft performance. After intensive investigations it was decided that a pre-selected speed schedule combination for given distance, time and fuel variable optimisation would offer a tangible reduction in algorithm complexity without any undue compromises in accuracy. OTPA defines maximum block speed and minimum time flight techniques as procedures comprising of CLB Mode H, maximum cruise (MCR) and DES Mode at optimal flight level, whereas, the maximum SAR and minimum fuel flight techniques always assume CLB Mode L, maximum range cruise (MRC) and DES Mode conducted at service ceiling and do not undergo any flight level iterations unless inequality constraints such as a minimum cruise fraction violation require it to do so.

Direct Operating Cost, Return On Investment and Associated Optimal Flight Techniques

The effect of block speed (or time) variation results in markedly different block speeds when minimum fuel, minimum time, minimum direct operating cost (DOC) and maximum return on investment (ROI) are compared for fixed sector distances with given mission criteria. These concepts, in part or collectively depending on the role of the vehicle, are integral for gauging the merits of new conceptual designs since they quantify operational flexibility. Even if the problem is reduced to the first order level, non-linearities still predominate, hence, not affording the designer clues to what variables exert strong influences. Other options include the use of MVO algorithms which deny the designer control over the final trade consideration of optimal solution versus feasibility. The idea is to utilise a standardised array of models which are universally consistent and are empirically derived for each trade study investigated by the designer.

All operational aspects are considered in terms of potential objective functions that might exhibit dependence to flight technique. Indeed, the problem of speed schedule formulation with respect to optimal operational performance could even be considered here but is not generally dealt with in this phase of design: it is felt that such an investigation should belong to the realm of refined sizing such as the initial phases of preliminary design work or product operational performance improvement programmes for existing vehicles.

The merit of any given flight technique can be weighed from a proposal's block time-fuel curve summary. These curves represent for a given sector distance and mission criteria thresholds for minimum time as well as fuel, and, intermediate flight techniques yielding height-energy block fuel minima for fixed block times between these two extremes. Since the block time-fuel summary is made up of a collection of different predetermined speed schedules and flight techniques, i.e. distinct climb, cruise and descent modes at a specific flight level, the curve geometry is constructed through a combination of quasi-discrete and discrete points indicative of high and intermediate-low speed techniques. One may conclude that the block time-fuel summary is a complex function that cannot be easily represented by an analytical expression coupled to a general set of aircraft parameters; in fact to achieve this goal the calculus of variations[7] approach must be employed and this is unfortunately not a viable option for conceptual work. The failure of this option implies that another philosophy may be required: a model using hyperbolic functions appears well suited to the curve definition exercise and for a given sector mission is suggested here as

$$W_{fuel} = W_{f,\min time}(1-k_1)\tanh\left[k_2\left(t_{\min time}-t\right)\right] - W_{f,\min fuel}(1-k_3)\tanh\left[k_4\left(t_{\min fuel}-t\right)\right] + k_5 \qquad (24)$$

where W_{fuel} is block fuel in the closed block time interval $[t_{mintime}, t_{minfuel}]$, $W_{f,mintime}$ the block fuel for a minimum time flight technique, k_1 and k_2 constants which allow for the impact of different higher speed technique attributes to assorted combinations of intermediate schedules, $W_{f,minfuel}$ the block fuel for a minimum fuel flight technique, k_3 and k_4 constants which allow for the impact of different lower speed technique attributes to assorted combinations of intermediate schedules, and k_5 is an arbitrary constant. Investigations have shown the non-linear coefficients in Eqn 24 cannot be explicitly related to a specialised set of design variables or expressed as consistent continuous functions of variables like for example sector distance, but, this function is differentiable and more poignantly allows for the identification of optimal flight techniques.

In order to facilitate the continuous function concept, two additional models are introduced. A maintenance-material cost model for the sample closed interval $[t_o, t_n]$

$$c_{main,fhr} = c_{main} + \frac{\alpha_{main}}{\left(t - t_{man}\right)^{\beta_{main}}} \qquad (25)$$

where $c_{main,fhr}$ is the total maintenance time dependent cost, c_{main} is the flight time dependent maintenance cost denoting theoretically most efficient work practise or learning curve asymptote, α_{main} and β_{main} are constants of proportionality, t_{man} is the manoeuvre allowance and t is

block time. A yield model indicating a measure of ticket prices (Y_{sec}) with respect to stage length s is presented as

$$Y_{SEC} = y_1 \lambda \, PAX \, s \left\{1 + y_2 \tanh\left[y_3 \left(s_{ref} - s\right)\right]\right\} \quad (26)$$

where λ is passenger load factor for given sector mission, PAX is the maximum passenger capacity of the aircraft, s_{ref} is the reference stage length and y_n are constants of proportionality. Combined with the other standard cost methodologies available in literature[10,11], identification of cost minima and profit maxima coupled to variation of flight technique or block time can be ensured.

For a given reference time frame utilisation, optimum flight techniques were found to be governed by the conditions

$$\frac{dC_{DOCS}}{dt} = 0 \qquad \text{Min. DOC, hourly and fixed departures based utilisation}$$

$$\frac{dP}{dt} \equiv \frac{dC_{DOCS}}{dt} = 0 \qquad \text{Max. ROI assuming fixed departures}$$

$$\left(\frac{\partial P}{\partial N_S}\right)_S = 0 \qquad \text{Max. ROI, hourly based utilisation} \quad (27)$$

where C_{DOCS} is the DOC per sector mission, N_S is the number of sectors completed per given reference time frame and P is the ROI per sector mission or time frame. Both DOC and ROI optimal flight techniques are categorised as constrained or unconstrained[11]. The constrained condition denotes a flight technique yielding block times within the closed interval $[t_{mintime}, t_{minfuel}]$, whereas, the unconstrained condition signifies a requirement of block times faster than the lower block time threshold physically permissible by a given vehicle. Pertinent conclusions drawn from this study concern the relationship of cost and profit optimal flight techniques to one another. An hourly-based utilisation theoretically results in distinct flight technique optima for minimum cost and maximum ROI. The ROI optima are characterised by faster block speeds than cost optimal ones because of a co-dependence on block time and the quantity of aircraft seat-miles completed by the vehicle. A fixed number of sectors utilisation assumption reduces the sensitivity of time related costs to flight technique, and thus, minimise the significance of this component compared to the fuel expended. This situation produces block speed optima appreciably slower than those assuming an hourly-based reference time frame utilisation. Furthermore, the fixed departures assumption theoretically creates a condition where both cost optimal and profit optimal flight techniques coincide with one another. Since an hourly based reference time frame utilisation results in partial ROI optima for specific sector distances, this implies the existence of a global optimum at some specific stage length and block time. An ROI model was developed in order to identify this condition. The model is proposed as

$$P = \left(\Phi_\alpha s - \Phi_\beta\right) \exp\left\{-\Phi_\chi - \Phi_\delta s\right\} + \Phi_\varepsilon \quad (28)$$

between the lower and upper stage length thresholds of the surveyed interval $[s_o, s_n]$. Fortunately, this information can be exploited for ensuring profit earning flexibility for future transport aircraft design proposals. If the model given above is actually taken into consideration as an open interval, for example, $[s_{be}, \infty)$ or from break even stage length and upwards, one can identify uncanny similarities to a typical step response of stable linear control systems as exemplified by Figure 4. Subsequently, a collection of merit parameters which give rise to the ability of sub-optimising for more desirable ROI characteristics can be formulated from the model's own intrinsic behaviour. Break even stage length (s_{be}) and corresponding pre-optimum ROI rise rate (P_S), the ROI global optimum (P_{opt}) and corresponding stage length (s_{opt}), the post-optimum ROI decay rate (P_{SS}) together with the magnitude of the model's asymptote value (Φ_ε) are suggested as a logical sequence of guidelines when conducting new conceptual aircraft designs or even detailed competitor reviews.

Prediction Method Effectiveness

In order to validate the methodology effectiveness and relative simplicity, a spreadsheet based software package called QCARD or Quick Conceptual Aircraft Research and Development was designed. A wide variety of known regional aircraft were input and QCARD's predictive powers were inspected against each respective vehicle's manufacturer PEH or its equivalent. The aircraft used for this validation exercise were: the 19 PAX PD340-2[13]; 37 PAX Embraer RJ135[5]; 50 PAX Saab 2000[19], Embraer RJ145[6] and Canadair RJ100[3]; 70 PAX Fokker 70[8]; and 100 PAX Fokker 100[9] vehicles.

The known drag performance characteristics of the Saab 2000 were available to validate the predictive powers of CDM. Figure 5 shows the agreement between CDM calculations and the flight test drag polars - it can be discerned that a ±5% maximum error bandwidth was produced for Saab 2000's entire flight envelope.

Although the overall drag polars produced by CDM show good agreement to flight test data in the operational envelope, validation for objective function sensitivity of the drag constituents was not conducted due to the lack of disseminated flight test results. By inspecting for regimes well outside Saab 2000's operational Mach number and lift coefficient envelope, deviations in the total drag were quantified and qualitatively reviewed for relevant conclusions. At relatively low free stream Mach numbers and lift coefficients approximately 1.5 times higher than maximum operational values, and for Mach numbers in excess of the vehicle's M_{MO} boundary, errors of between +2 to +5% resulted. against published results with typical errors frequently falling within a bandwidth of ±5% for

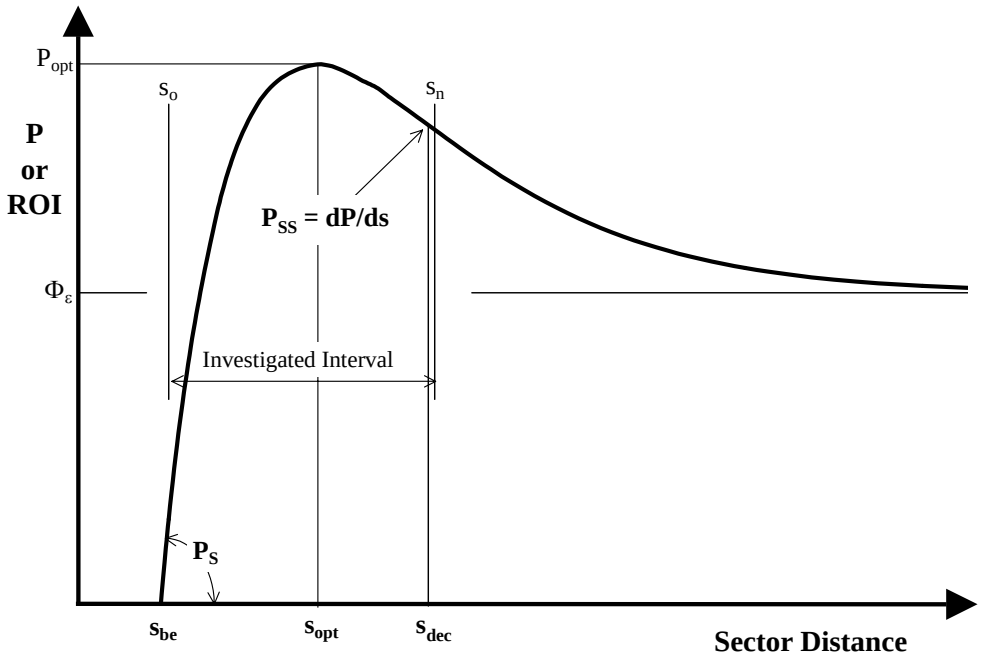

FIGURE 4 - Typical stage length response of ROI assuming an hourly-based reference time frame utilisation.

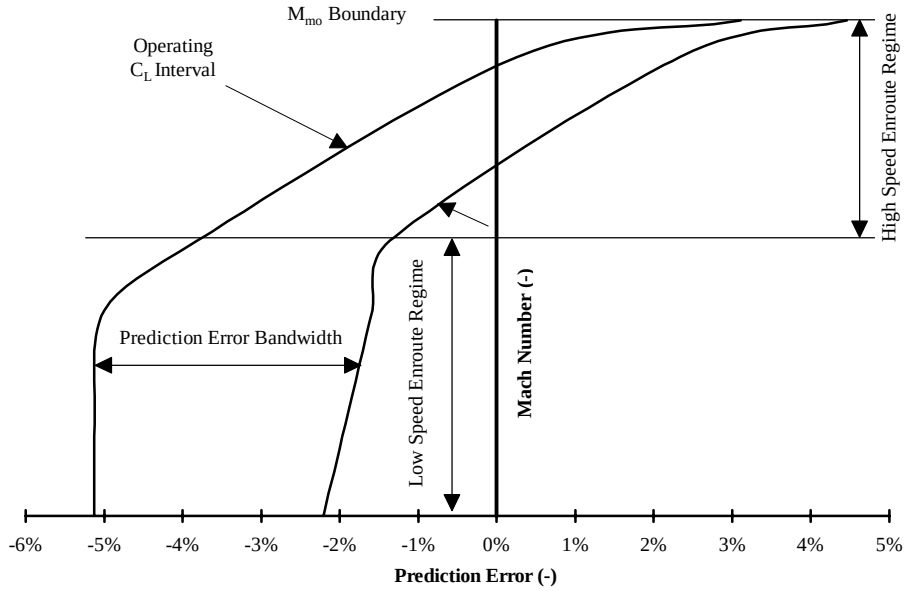

FIGURE 5 - CDM predictions against flight test drag polars for the Saab 2000, en route configuration.

weight, aerodynamics and performance. Additionally, the against published results with typical errors frequently falling within a bandwidth of ±5% for weight, aerodynamics and performance. Additionally, the QCARD package was also utilised for two Saab Aircraft AB conceptual design studies and these exercises verified the accuracy of field-en route performance and OTPA trajectory-profile generation algorithms previously discussed.

Aircraft Optimisation

The General Approach

Since it has been shown that computational effort has been minimised without undue loss of detail and precision in the result, it is suggested that an approach, which rids the designer of expending energy in formulating baselines or an initial balanced aircraft design, would be prudent. By reducing almost all configuration related analysis to a baseline fuselage exterior and interior layout or “quasi-initial baseline”

formulation, this leaves the technical judgement process to consider what arbitrary array of independent variables are to be varied and by what arbitrary interval quantities. Rather than improving on a known baseline candidate, the identification of a region of feasibility enables the designer to choose through intuition what configuration would suitably fulfil the specifications, or conversely, permit transparency by giving the opportunity of assessing the benefits that arise when initial specifications are relaxed. The interdependencies between free variables with regard to overall design sensitivity can become somewhat easier to interpret if the dependent variable is expressed as a tangible quantity, for example as operational performance, design weights, cost, profit, etc. instead of traditional intermediary mainstays like drag, lift coefficient or aspect ratio.

Conceptual Aircraft Design Problem

Growing public apprehension has created a preference for turbofan aircraft to assume the traditional regional role supported by turboprops. The market also has increasing interest in small regional jets not only to enlarge the catchment area in the hub and spoke system but more importantly to create possibilities of entering a new direct services market or avoiding congested hubs, thereby filling new niche markets of mid-length and long thin routes abandoned by major airlines. The pundits had forecast a radical shift away from turboprops for the 50-seater category and current indications show this to be accurate; as spectacularly exemplified by the successes of Canadair Regional Jet CRJ100 and Embraer RJ145.

In view of these events, the focus is now concentrated on the 30-35 passenger category with the introduction of Dornier Do328-300 and Embraer RJ135 vehicles. Unlike their 50-passenger turbofan counterparts these aeroplanes are not truly optimised vehicles but are reconfigured versions with great emphasis placed on economic considerations of commonality. The most unfortunate consequence of this situation is that the contemporary 30-35 passenger turbofan has become quite limited in terms of operational flexibility and large penalties with regards to the field-en route performance and design weight trade off have been incurred. The goal of this project is to create a regional commuter aeroplane capable of demonstrating greater operational flexibility whilst still retaining the family concept philosophy as well as possessing a competitive operating costs edge.

After studying the current market the following specifications were formulated:

1. 30-35 seats at 32-31 inch seat pitch;
2. Engines to be new generation Williams FJ44-XX preliminary design fan with projected maximum sea level static thrust of 2850 lb.f. (12.68 kN);
3. JAR/FAR takeoff balanced field length of no greater than 5000 ft (1524 m) at ISA, sea level;
4. No climb restrictions on maximum takeoff gross weight for conditions up to and including ISA+30^{o}C and 5000 ft airport elevations;
5. The penalty in off-loaded weight from MTOW to be significantly lower than competition when clearing FL 160 during OEI en route climbs at ISA+20^{o}C conditions (driftdown proficiency);
6. Minimum range of about 500 nm with full payload and an emphasis placed on maximising multi-hop capability for typical sector mission segments;
7. Comparable block times for typical sector missions with operating costs equal to or better than direct competitors;
8. Flexibility for both standard and extended-range versions; and
9. A derivative of the 19 PAX PD340-2 tri-jet turbofan vehicle[13] with an emphasis placed on maximising commonality.

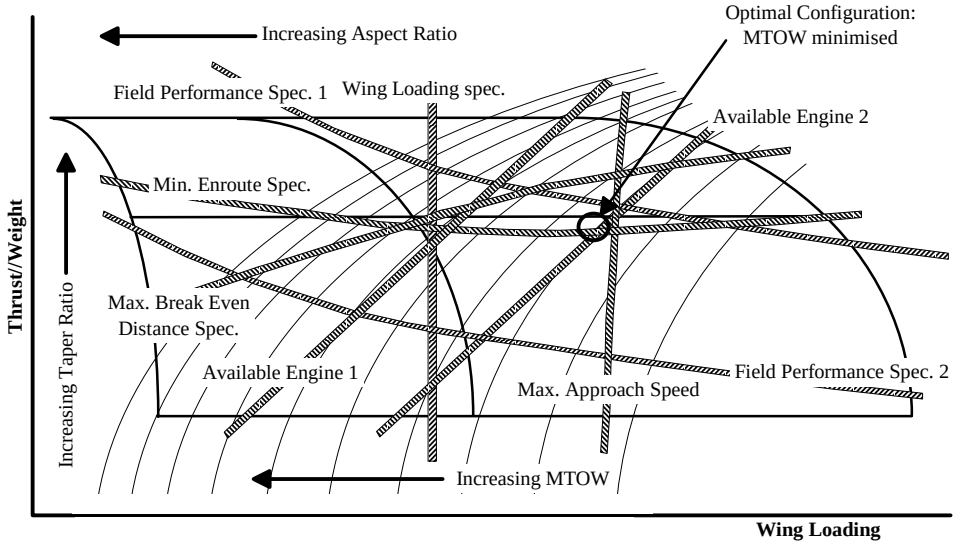

FIGURE 6 - Example of typical arbitrary free variable sensitivity study and subsequent identification of optimal configuration.

Initial Design and Sensitivity Analysis

The basic shape of the aircraft was already set because a specification to adhere to a family concept was proposed. The initial trade study involved inspection of different stretched fuselage layouts until both cargo and seating could be maximised with respect to general performance criteria and power plant used.

An example of the final trade study for PD340-3X STD is given in Figure 7. In this particular instance, since the power plant was already selected, Maximum Takeoff Gross Weight (MTOGW) was traded against reference wing area with off-loaded fuel (maximum available fuel less some arbitrary fixed amount) as the additional primary sensitivity parameter. The reference wing area trade interval was not large due to a stipulation given by the specifications of utilising already existing structure: the PD340-2 wing imposed limitations on maximum span increase through introduction of a minimum permissible taper ratio threshold of $\lambda \geq 0.27$ set by the author. Even though guidelines for cost and profit optimisation were available, initial observations showed that fixed sector mission performance parameters like block time and block fuel did not alter by any great measure due to this small reference wing area interval thus not affording much scope for assessment of operational flexibility versus DOC and ROI. It was therefore postulated that cost would in this instance show an adequate measure of potential for profitability and was then in turn considered to be a direct function of airframe weight - this assumption having the additional benefit of minimising the effort expended for final selection. The selection process for optimum MTOW and corresponding wing reference area necessitated a trade off between increases in range and one engine inoperative (OEI) climb performance against minimising of balanced field length (BFL) together with the landing reference speed (V_{REF}), or, indirectly the required landing distance. Attention should be paid to the constraints shown in Figure 7. They represent maximum payload range (MPAY-R) assuming maximum SAR flight techniques and JAR OPS-1 reserves, lines of constant maximum attainable stage length (MT-MS) assuming minimum time flight techniques with various passenger mission requirements and JAR OPS-1 reserves, and finally, off loaded weight penalties from MTOGW associated with lines indicating clearance of FL 160 assuming ISA+20^{o}C conditions and OEI. The V_{REF} speed constraint lines were derived by assuming each respective candidate completes a stage length of 200 nm from MTOGW at brakes release and finishes with a conservative landing gross weight based on fuel burned via minimum fuel techniques - in accordance with the multi-hop specification. The optimum reference wing area was chosen to be 31.77 m^2 (342 sq. ft), which corresponds to a predicted MTOW of 12950 kg (28550 lb) defined by the criterion that 1369 kg (3018 lb) of fuel is off-loaded from its respective maximum available fuel load of 2912 kg (6420 lb).

Design Description

As discussed, the already existing PD340-2 wing planform was utilised and subsequent optimisation involved span increases with some modifications to wing tip geometry. Span is increased from the current 15.24 m (50 ft) to 17.88 m (58 ft 8 in.) with PD340-2's basic wing planform intact. The span increase gives a 9% wing area expansion (and 8% greater maximum available fuel capacity) with associated increases in aspect ratio from 8 to 10 and flap as well as aileron span. A moderate sweepback combined with a relatively thick supercritical wing section profile enables cruise Mach numbers in the region of 0.70-0.75 while projected certification altitude remains at 35000 ft. The wing planform geometry has been enhanced through the introduction of raked wing tips, which is envisaged to decrease induced drag at low speeds with the added advantage of reducing wetted area to a smaller extent. The PD340-2's high lift system of double slotted Douglas type flaps have been retained and are expected to deliver slightly higher ΔC_L when deployed for PD340-3X due to improved aerodynamic efficiency.

The fuselage cross section has not been altered from the basic PD340-2 which was incidentally based on dimensions used for the Saab 2000 and Saab 340 vehicles. The structure itself has been stretched from the original 16.70 m (54 ft 9 in.) used for the 19 PAX to 19.20 m (63 ft) for the 31-34 PAX variant. There is space for 31 passengers at a comfortable 32 inch seat pitch, or alternately, 34 passengers can be seated at a 31 inch pitch. Due to the larger capacity of this vehicle, additional space has been incorporated to the PD340-2's cargo hold resulting in an increase from 6.4 m^3 (226 cu. ft) to 8.3 m^3 (295 cu. ft).

The nacelles have also been modified since the fan is slightly larger and airflow requirements are higher. Projected increases in fan diameter with the Williams preliminary design FJ44-XX compared to PD340-2's already existing FJ44-2 installation are approximately 0.076 m (3 in.). This fortuitously requires no lengthening of the landing gear legs but the gear must accommodate increases in constituent weight due to overall increases in gross weight.

The increase in empennage moment arm is produced by a fuselage stretch, and calculations have shown that no changes to the PD340-2's existing empennage are necessary to cope with both the larger wing and higher thrust ratings of PD340-3X.

Predicted Performance and Design Review

Figure 8 (previous page) gives a three-view representation while Table 1 summarises the predicted PD340-3X STD and PD340-3X ER weight, geometry and performance characteristics. It should be noted that the PD340-3X STD power plant thrust has been derated to a 2600 lb.f maximum static rating, whereas, the PD340-3X ER utilises the maximum flat rating of 2850 lb.f at ISA, s.l., available from Williams' FJ44-XX preliminary design engine.

Figure 9 shows the predicted payload-range for both

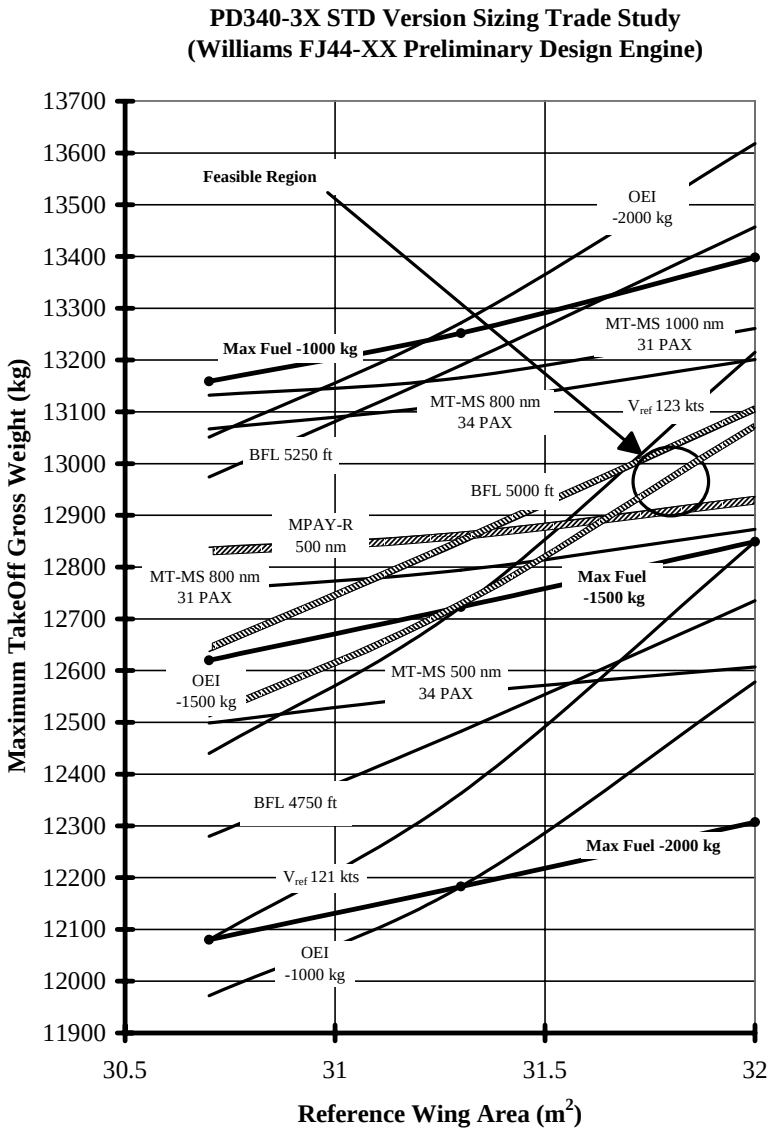

FIGURE 7 - Trade study and final configuration selection for PD340-3X STD tri-jet regional transport.

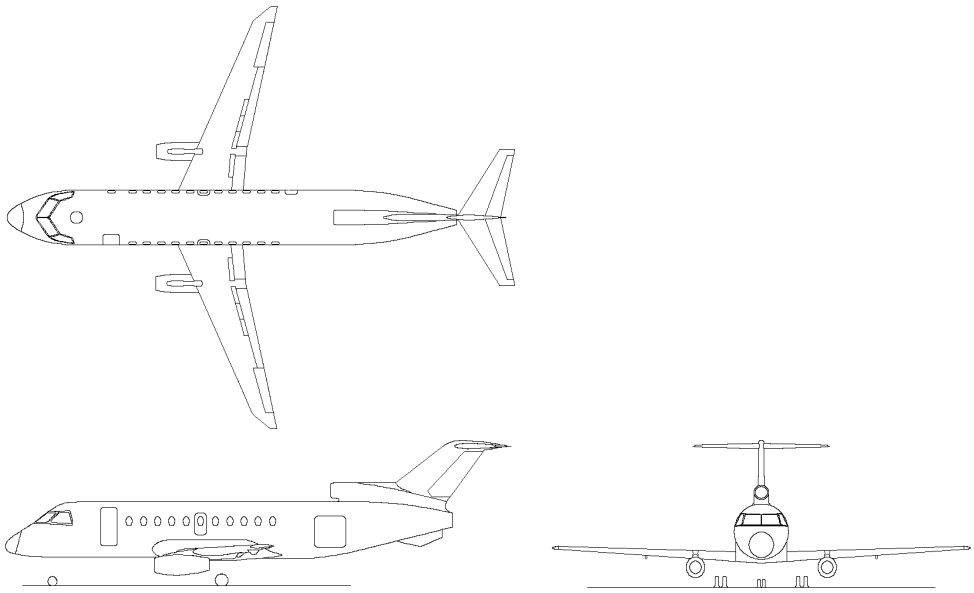

FIGURE 8 - PD340-3X 31-34 PAX regional tri-jet general arrangement.

	PD340-3X STD		PD340-3X ER	
Weights				
Maximum Takeoff Weight	12950 kg	28550 lb	13750 kg	30313 lb
Maximum Landing Weight	12436 kg	27416 lb	13224 kg	29154 lb
Maximum Structural Payload	3720 kg	8201 lb	3720 kg	8201 lb
Geometry				
Wing Span	17.88 m	58 ft 8 in.	17.88 m	58 ft 8 in.
Reference Wing Aspect Ratio	10.0		10.0	
Reference Wing Area	31.77 m^2	342 sq. ft	31.77 m^2	342 sq. ft
Wing Quarter Chord Sweep	21°		21°	
Wing Aerofoil Section	root	16%	MS(1)-0313 (mod)	
	tip	12%	supercritical	
Fuselage Length	19.20 m	63 ft	19.20 m	63 ft
Fuselage Maximum Diameter	2.31 m	91 in.	2.31 m	91 in.
Performance (ISA)				
JAR/FAR 25				
Balance Field Length, s.l.	1507 m	4944 ft	1586 m	5203 ft
AEO Service Ceiling	FL 350		FL 350	
OEI Ceiling	FL 173		FL 191	
Typical Max. Cruise Speed	M0.72		M0.72	
JAR/FAR 25 Landing Distance				
without OEI braking	1480 m	4856 ft	1528 m	5013 ft
with OEI braking	1294 m	4245 ft	1341 m	4350 ft

TABLE 1 - Data for PD340-3X STD and PD340-3X ER.

standard and extended range versions of the aircraft. The chart curves are given for maximum SAR and maximumblock speed flight techniques since this representation not only gives the maximum range capability but also an indication of the maximum fixed sector distance performance afforded by the vehicle for given mission payload and assuming minimum time flight techniques. Comparison for typical sector missions of 34 PAX and stage length of 500 nm with JAR OPS-1 reserves policy and minimum time flight techniques in ISA still air show that PD340-3X is approximately 4 minutes slower than the Embraer RJ135 where the total block time for both aircraft is around 1 1/2 hours. This performance is complemented by a significant reduction in block fuel - an estimated saving of around 30% can be achieved with PD340-3X over its competitor. The TOGW required for completing this mission results in PD340-3X being approximately 4100 kg (9000 lb) lighter over RJ135, which exemplifies the projected lower airport charges through a MTOW review, and, the BFL comparison using these mission gross weights are also in favour of PD340-3X with field lengths of 1291 m (4236 ft) at s.l., ISA for standard and extended range versions assuming an initial takeoff flap setting of 20°. This is approximately 6% shorter than RJ135 employing a 22° takeoff flap setting at similar ambient conditions. Direct comparison to Do328-300 could not be conducted owing to the lack of reliable detailed data, however, early indications show that this vehicle is slower in terms of block speed than both PD340-3X and RJ135 for fixed stage lengths but is superior in terms of field length performance. No climb limitations on MTOGW are imposed (assuming no field length limited unbalanced performance exists) for conditions up to ISA+35°C and ISA+29°C and 5000 ft airport pressure elevation for PD340-3X STD and PD340-3X ER vehicles respectively. This makes for competitive performance even if the Do328-300 is characterised by exceptional field climb performance. The RJ135 is climb limited for conditions above ISA+25°C and 2500 ft airport pressure altitude. Combined with a target acquisition cost of USD 7-8 million, this design is seen to be an attractive as well as competitive alternative to the contemporary 30-35 PAX turbofan vehicles in the market.

Conclusions

It has been demonstrated that conceptual design of modern transport subsonic aircraft need not be relegated for the sake of a reduction in complexity to the realm of first order closed expressions or coarser numerical integration procedures which are prone to large errors and poor objective function sensitivity against a generalised set of design parameters. By combining many of the discrete operations usually performed for a conventional design process with the single solution philosophy,

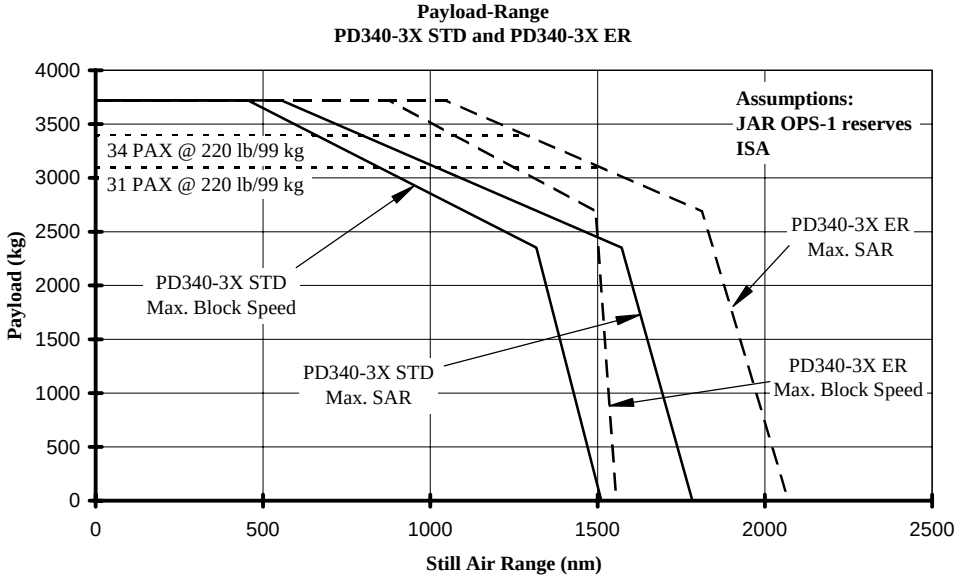

FIGURE 9 - Payload-range envelope for PD340-3X STD and PD340-3X ER 31-34 PAX regional turbofan transport.

designers can utilise both the intuitive and non-hierarchic approach to create a powerful method that dispenses with the need for MVO techniques. By adopting an attitude more attune to actual operational considerations, the methodology presented through transcendental functions has surpassed the closed form expression in complexity somewhat. Notwithstanding, the spreadsheet based software QCARD or Quick Conceptual Aircraft Research and Development which embodies this theory has demonstrated an appreciable reduction in programming complexity usually required for MVO whilst affording the designer complete control at all steps of the process and confronting them with issues of realistic operational concern. To demonstrate the accuracy of the method, seven known aircraft designs ranging in size from 19 to 100 passengers were input and subsequently validated its predictive powers. A 31-34 PAX turbofan regional transport was designed and optimised in order to demonstrate the speed and comprehensiveness of the method and resulted in a vehicle that can be regarded as a competitive proposal against its contemporaries.

References

[1]Abbott, I.H., Von Doenhoff, A.E, ”Theory of Wing Sections”, Dover Publications Inc., 1949.

[2]Boppe, C.W., ”CFD Drag Predictions for Aerodynamic Design”, AGARD Report AR-256, 1989.

[3]Canadair Regional Jet Performance Data, Model CL-601R, MAA-601R107F, Issue F, Bombardier, February 1993.

[4]Eckert, E.R.G., ”Engineering Relations for Friction and Heat Transfer to Surfaces in High Velocity Flow”, Journal of the Aeronautical Sciences, Vol. 22, 1955, pp. 585-587.

[5]Embraer RJ135 Technical Description, TD-135/000, November 1997.

[6]EMB145 Technical Description, TD-145/009, January 1997.

[7]Erzberger, H., Lee H., ” Characteristics of Constrained Optimum Trajectories with Specified Range”, NASA Technical Memorandum 78519, Ames Research Center.

[8]Fokker 70 Performance Information Rolls-Royce Tay Mk620 (metric units), MM100/AA/F70/P.I.R.-M/issue 2, Fokker Aircraft B.V., May 1993.

[9]Fokker 100 Performance Information Rolls-Royce Tay Mk650 (imperial units), MDAA/F100/RP-110 Issue 1, Fokker Aircraft B.V., January 1990.

[10]Gogate, S.D., Pant, R.K., Arora, P., ”Incorporation of Some Cost and Economic Parameters in the Conceptual Design Optimisation of an Air-Taxi Aircraft”, AIAA-94-4301-CP, pp. 443-453.

[11]Isikveren, A.T., ”A Method to Identify Optimal Flight Techniques of Transport Aircraft”, Report 98-7, Royal Institute of Technology, Department of Aeronautics, Sweden, 1998.

[12]Isikveren, A.T., ”Suggested Procedures in Conceptually Predicting Structural Weight and Low-Speed/Enroute Aerodynamics and Performance Attributes of Transport Aircraft”, Report 98-6, Royal Institute of Technology, Department of Aeronautics, Sweden, 1998.

[13]Isikveren, A.T., ”The PD340-2 19 Passenger Turbofan Regional Transport-Feasibility Study”, Report 98-5, Royal Institute of Technology, Department of Aeronautics, Sweden, 1998.

[14]Linnell, R., ”Weight Estimation Methods”, FKHV-1-RL790724:01, Saab AB, July 1979.

[15]McCormick, B.W., ”Aerodynamics, Aeronautics, and Flight Mechanics”, John Wiley and Sons, 1979.

[16]Miller, L.E., ”Optimal Cruise Performance”, Engineering Notes, Journal of Aircraft, Vol. 30, No. 3, May-June 1993, pp. 403-405.

[17]Obert, E., ”Some Aspects of Aircraft Design and Aircraft Operation”, Lecture Series, Sweden, 1996.

[18]Raymer, D.P., ”Aircraft Design: A Conceptual Approach”, American Institute of Aeronautics and Astronautics, 1989.

[19]Saab 2000/AE2100A Performance Engineers’ Handbook Metric Version, Revision B, 73ADS0394, Saab Aircraft AB, October, 1996.

[20]Scott, P.W., Nguyen D., ”The Initial Weight Estimate”, SAWE Paper No. 2327, Index Category No. 11, MDC 96K0030.

[21]Simos D., Jenkinson L.R., ”The Determination of Optimum Flight Profiles for Short-Haul Routes”, Journal of Aircraft, Vol. 22, No. 8, August 1985, pp. 669-674.

[22]Torenbeek, E., ”Optimum Cruise Performance of Subsonic Transport Aircraft”, Report LR-787, Delft University of Technology, Faculty of Aerospace Engineering, The Netherlands, March 1995.

[23]Torenbeek, E., ”Optimum Wing Area, Aspect Ratio and Cruise Altitude for Long Range Transport Aircraft”, Report LR-775, Delft University of Technology, Faculty of Aerospace Engineering, The Netherlands, October 1994.

[24]Torenbeek, E., ”Synthesis of Subsonic Airplane Design”, Delft University Press, The Netherlands, 1982.

[25]Young, A.D., ”The Aerodynamic Characteristics of Flaps”, Aeronautical Research Council Reports and Memoranda, Ministry of Supply, United Kingdom, 1953.

intentionally blank

Paper II

Design and Optimisation of a 19 Passenger Turbofan Regional Transport

intentionally blank

1999-01-5579

Design and Optimisation of a 19 Passenger Turbofan Regional Transport

Askin T. Isikveren*, Research Scientist
Royal Institute of Technology (KTH), Stockholm, Sweden

ABSTRACT

During this study, the conceptual design of a 19-passenger turbofan transport aimed primarily at the regional/commuter market was synthesised. Final configuration selection was based on a method conceived by the author that incorporates a hybrid of the conventional intuitive conceptual design process with overtones of a non-hierarchic multi-disciplinary optimisation philosophy. To ensure validity of the aforementioned design and optimisation algorithms, the General Aviation Synthesis Program (GASP) software developed by NASA-Ames Research Centre and subsequently refined by Williams-Rolls Inc. was used. In addition, attention was paid during the design sequence to minimise the alterations necessary for variants of the basic design, i.e. future extended range and stretched versions. The final proposal ended with a vehicle that displays marketing flexibility, competitive field performance, superior climb capability with significant increases in block speed, and more poignantly, higher potential for profit upon comparison to contemporary turboprops.

INTRODUCTION

Historically, 19 passenger turboprops have dominated the small commuter and regional segment of aircraft with 80 seats or less. Federal Aviation Administration[2] (FAA) forecasts project a diminishing of the 19-seat market, however, it must be borne in mind that this conjecture assumes characteristics of short range and slower speeds will always hold true.

Combined with growing public apprehension, it is felt that market demand would increase substantially if an economical and fast 19 seat turbofan aircraft were to be introduced. This notion is reinforced by the spectacular success of 50 seat turbofans which grew from virtually zero in 1994, and, the emergence of 30-35 seat jet aircraft today; the introduction of turbofan technology into an even smaller seat category is projected to have a similar impact. Furthermore, it is surmised that such vehicles would not only replace the current turboprop fleet through operator trade-up in engine technology, but market expansion is envisioned through promotion of hub by-pass or the creation of new routes by linking secondary hubs in an effort to avoid hubs congested by large carrier operations.
Smaller regional aircraft design involves close attention to cost and weight sensitive factors that differ somewhat from larger passenger aircraft. These factors include: turbofan construction, weight and its relation to acquisition cost; design simplification for low tooling and production costs; aerodynamic design for inherent stability in an effort to avoid artificial stabilisation and damping; sensitivity to engine placement as it affects weight and balance, moment of inertia and drag; optimum wing loading and aspect ratio; a requirement for lower noise and emissions than for larger aircraft; and, freedom from ground support equipment. In order to expedite the feasible solution identification process, which is characterised by this multi-faceted and sometimes conflicting set of requirements, a new approach to addressing the conceptual design problem is considered. The idea combines many of the discrete operations that are usually performed for a conventional design process and hybridises this with a single solution philosophy.

The aim was to produce a new aircraft† with a purchase price that would be considered non-prohibitive for current regional operators but with greatly enhanced speed and comfort. Furthermore, a focus on operational flexibility to accommodate non-stop service between cities with relatively low traffic and extended hub feed operations was also taken to be of primary concern. In order to achieve this, the use of the cost-effective, quiet and fuel-efficient Williams-Rolls Inc. FJ44-2A engines were incorporated from the outset.

To round off the study, a validation of the final design

* Aircraft Performance Engineer, American Airlines.
Formerly employed by Saab Aircraft AB.
Graduate Member RAeS.

† PD340 project study performed for Williams-Rolls Inc. with support from Saab Aerospace AB, Karlebo Aviation AB and KTH.

was conducted using the General Aviation Synthesis Program[3] software developed by NASA-Ames Research Centre. This served to substantiate the author's design method techniques via confirmation of purported weights and performance attributes predicted for the 19-passenger turbofan transport.

DESIGN SPECIFICATION

The hard specifications that were deemed necessary for the success of this proposal are defined below.

- The vehicle must accommodate at least 19 passengers with a 32 in. (813 mm) seat pitch and a typical fuselage cross-section that is similar to the Saab 340 and Saab 2000;
- Balanced field length less than 4000 ft (1219 m) at ISA, sea level conditions;
- Effective operation at 5000 ft (1524 m) airport pressure altitude and at ISA+20°C conditions;
- Time to climb to typical cruise flight levels of around 15-20 minutes;
- Service ceiling not less than FL 350 and high-speed cruise Mach number not less than 0.70;
- Maximum range not less than 600 nm (1111 km) with typical regional mission reserves and a full payload complement;
- Landing stall speed to be not greater than 90 KCAS at ISA, sea level conditions;
- A competitive break-even load upon comparison to current 19 seat turboprops; and
- Maximise commonality with Saab 340 vehicle in order to reduce initial development and manufacturing cost;
- The vehicle shall be certified according to FAR 25 and JAR 25 transport category aircraft requirements.

In addition to these requirements, a soft specification was set to provide for a voluminous cargo hold, i.e. a target total volume which matched the Beech 1900D's allocation of 11.8 cu.ft (0.334 m^3) per passenger.

AIRCRAFT OPTIMISATION

GENERAL METHODOLOGY AND FINAL SELECTION

Conventional methods of design and optimisation involve formulation of a baseline or initial balanced aircraft design and a subsequent iterative analysis of variations from that given design point until satisfaction of all performance requirements are simultaneously achievable. The end result is presumably the best possible compromise but this subjective process requires the expenditure of many man-hours.

Rather than approach conceptual design in the traditional manner, the idea is to formulate unique procedural optimisation methods by selecting dynamically free-variables perceived to show strong objective function sensitivity. Consequently, the technical judgement process is reduced to the identification of an arbitrary array of independent variables and associated intervals of values for investigation. Rather than improving on a known baseline candidate, this leads to identification of a final feasible solution which not only fulfils imposed performance criteria, but definition of compromises which are tolerated by structural, operational and economic limitations.

The interdependencies between free variables with regard to overall design sensitivity can become somewhat easier to interpret if the dependent variable is expressed as a tangible quantity, for example as operational performance, design weights, cost, profit, etc. instead of traditional intermediary mainstays like drag, lift coefficient or aspect ratio. Furthermore, the approach permits transparency for the designer not generally afforded by complex dedicated conceptual design and optimisation programs by enabling an assessment of the benefits that arise when specifications are relaxed. Another direct advantage is that not only does the designer have freedom to observe the trade off required for various performance traits, but it also delivers a detailed aerodynamic and geometric result when the final configuration is chosen.

METHODOLOGY SPECIFIC TO THIS PROJECT

After extensive research, the investigator makes conjectures of what parameters will have the greatest impact or sensitivity with respect to the scope of the design project at hand. This can take the form of trade studies between thrust-weight and wing loading for a rubber engine approach or a multitude of other types of presentations in accordance with required procedural methods for solution, which in turn are dependent upon the initial assumptions.

In this particular study, since the engine and configuration layout were set a priori, for a given wing thickness ratio and sweep, wing taper ratio and span were designated as primary free variables due to the design's philosophical stipulation of maximising commonality with the Saab 340 - in this instance, the wing torsion box geometry being the fundamental constraint. In view of this, a transcendental dimension equation (Eqn. 1) for wing root chord dependent upon taper ratio and wingspan constrained by an already existing Saab 340 wing-fuselage interface was adhered to. A schematic in Figure 1 geometrically interprets this constraint criterion and this in turn can be analytically expressed as

$$c_R = c_{wf} - \frac{d_{wf}\left(\lambda c_R - c_{wf}\right)}{b - d_{wf}} \qquad (1)$$

where b is the vehicle span, d_{wf} is the fuselage geometric chord at the wing-fuselage juncture, c_{wf} is the wing chord at the wing-fuselage juncture, λ is the reference wing taper ratio and c_R is the resultant

reference wing root chord.

It was surmised that this objective function sensitivity would be directly coupled to a corresponding resultant reference wing area. With variation of wing geometry, associated changes in the mean aerodynamic chord (MAC) adjusted the empennage accordingly since approximate dimensioning was based on the premise of keeping each vertical and horizontal tail volume coefficients fixed. In the absence of reliable detailed data, cost can be considered as a direct function of airframe weight, therefore the Maximum Takeoff Gross Weight (MTOGW) was minimised. A final plot, which trades MTOGW against reference wing area for given performance characteristics was inspected and feasible configurations reviewed. A spreadsheet based conceptual design and mission analysis code developed by the author[5,6] was used to perform the required parametric calculations.

Various combinations of engine count, wing area, sweep angle and thickness were analysed to determine an acceptable trade off between good field and en route performance. A myriad of possible performance constraint criteria to inspect for sensitivity and subsequently identify feasible solutions were reviewed. Stall speed at Maximum Landing Weight (V_S), and, maximum range assuming maximum payload with 19 passengers (PAX) at 200 lb (91 kg) (Range1 and Range 2) with conventional U.S. regional reserves of 100 sm (87 nm) alternate and 45 minutes hold were finally designated as primary constraint criteria because these displayed the greatest potential for compromise when trading MTOGW and reference wing area.

Consequently, the selection process focused on maximising range, and, minimising time to climb as well as landing stall (or indirectly the required landing distance) and balanced field length. In terms of the PD340 study, span and reference wing area were minimised to rationalise weight thereby acquisition cost, whereas in stark contrast, area and span needed to be maximised in order to minimise takeoff and landing distances and maximise range performance. To reconcile these conflicting effects, the requirements were plotted on one chart that allowed definition of a bounded geometric region in which freedom of selection existed. An example of the final simplified trade study for PD340-2 is given in Figure 2 and it can be discerned that the gross weight sensitivity indicated that approximately 317 sq.ft (29.5 m^2) of wing area was appropriate.

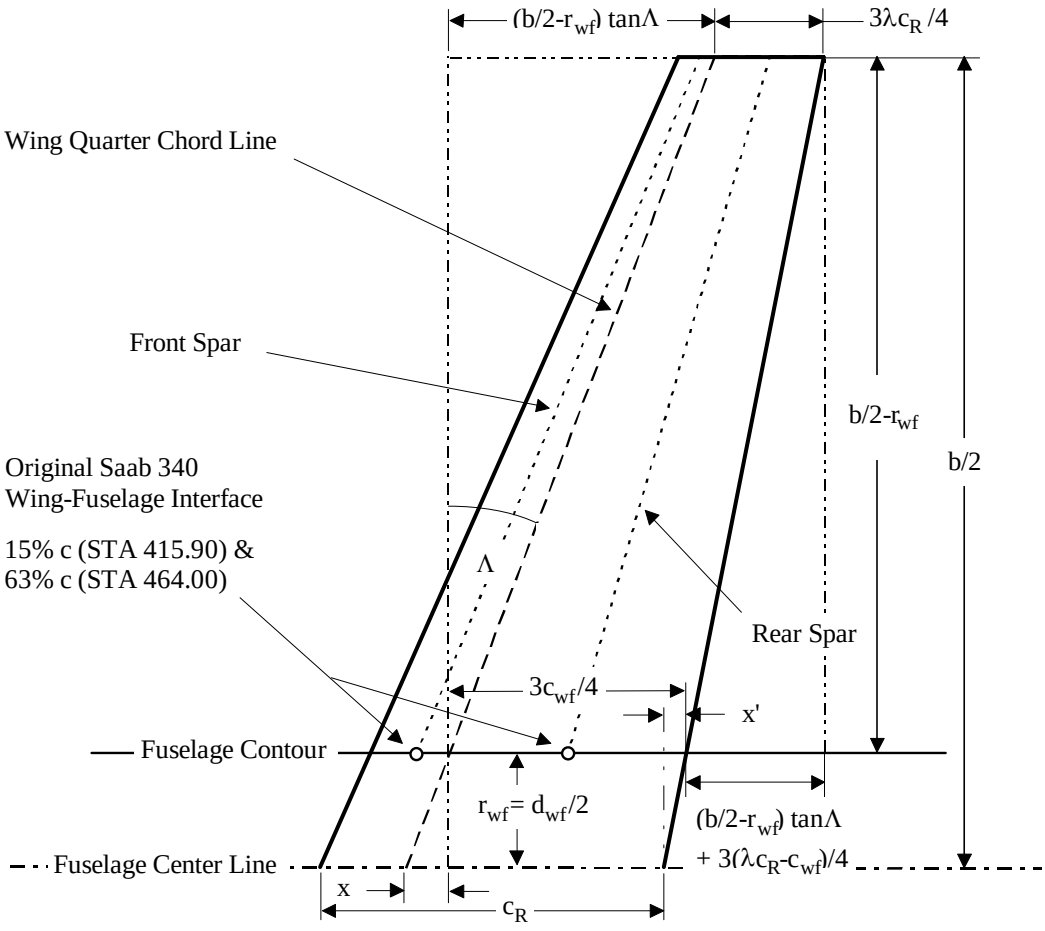

Figure 1 - Definition of wing geometry with Saab 340 wing torsion box constraint imposed.

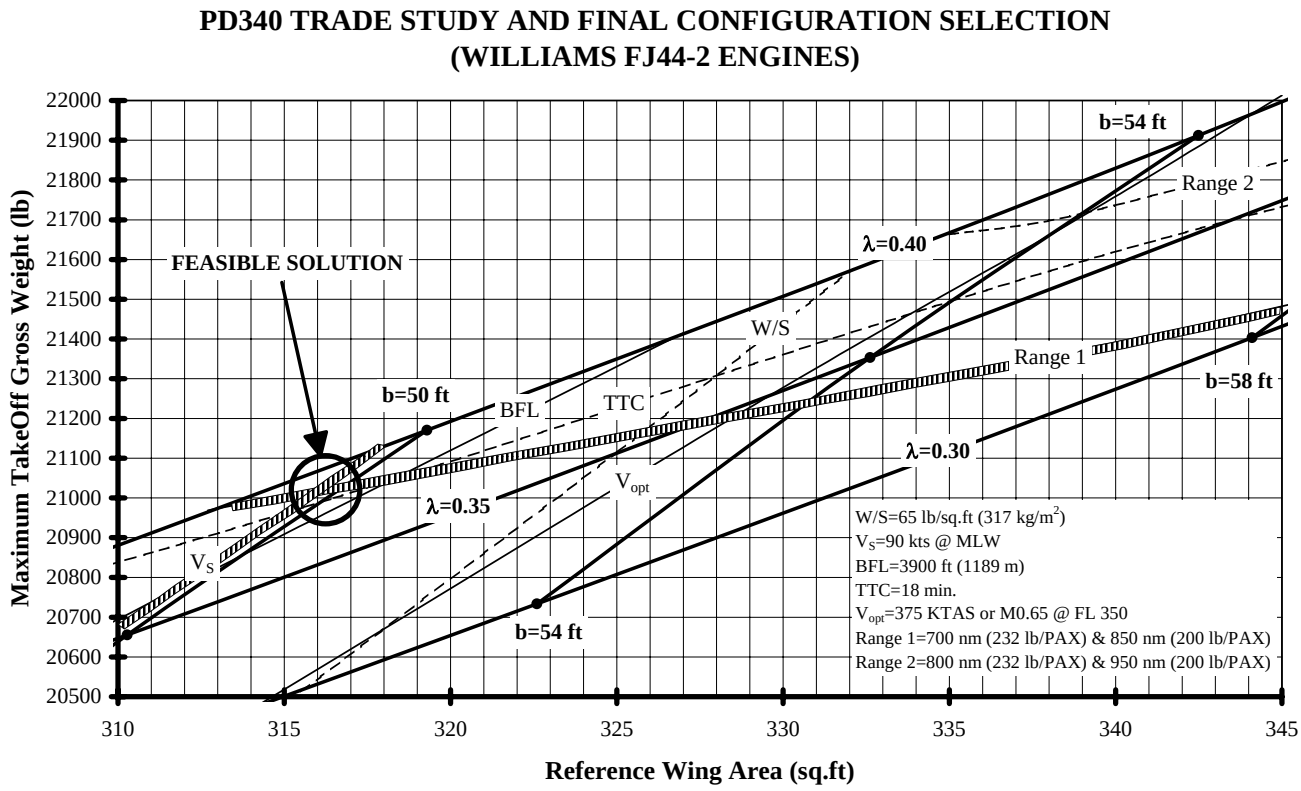

Figure 2 - Final simplified selection for PD340-2 vehicle.

DESIGN DESCRIPTION

The vehicle is a tricycle, monoplane, low-winged tri-jet with two underwing podded and dorsal intake-tail engine mountings. It is pressurised and incorporates a T-tail empennage. The landing gear is retractable and each leg is twin wheeled. The vehicle accommodates a flight crew of two and an optional flight attendant. The standard configuration accommodates a maximum of 19 passengers. The power plants utilised are Williams-Rolls Inc. FJ44-2A turbofans. The vehicle is designed to comply with FAR 25 U.S airworthiness regulations and the European JAR 25 rules. Figure 3 shows an artist's impression.

Figure 3 - PD340-2 19 PAX regional turbofan transport.

Table 1 and Figure 4 present salient aircraft data and three-view of the PD340-2 respectively.

A Further detailed presentation and analysis of the design can be obtained from reference 4.

Weights		
Maximum Ramp Weight	21141 lb	9590 kg
Maximum Takeoff Weight	21041 lb	9544 kg
Maximum Landing Weight	20047 lb	9093 kg
Maximum Zero fuel Weight	17457 lb	7918 kg
Operational Empty Weight	13049 lb	5919 kg
Manufacturing Empty Weight	12525 lb	5681 kg
Maximum Payload	4408 lb	2000 kg
Maximum Usable Fuel	5186 lb	2352 kg
External Dimensions		
Overall span	50 ft	15.24 m
Height	19 ft 11 in.	6.07 m
Overall length	62 ft 11 in.	19.18 m
Wheel base	23 ft	7.01 m
Wheel track11 ft 3 in.	3.43 m	
Fuselage Dimensions		
Length	54 ft 9 in.	16.69 m
External diameter	7 ft 7 in.	2.31 m
Wing Geometry		
Total area	317 sq.ft.	29.5 m^2
Aspect ratio7.9		
Horizontal Tail Geometry		
Span	19 ft	5.79 m
Area	82.3 sq.ft.	7.7 m^2
Vertical Tail Geometry		
Area	59.4 sq.ft.	5.5 m^2

Table 1 - Weight and geometry data for PD340-2 vehicle.

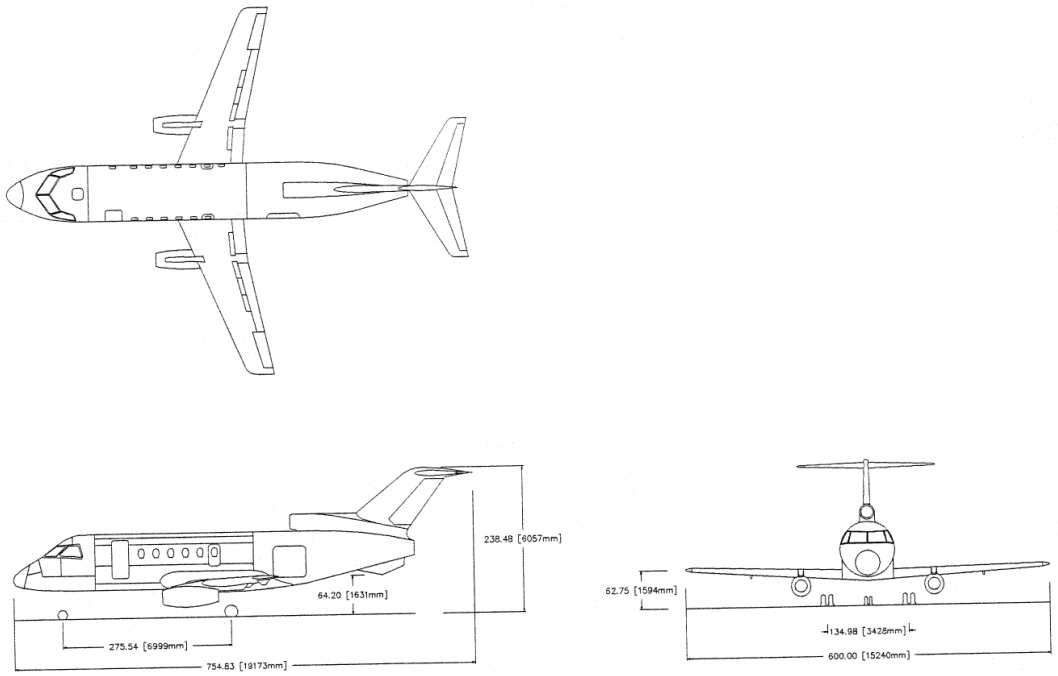

FIGURE 4 - PD340-2 general arrangement.

Fuselage Structure commonality with Saab 340

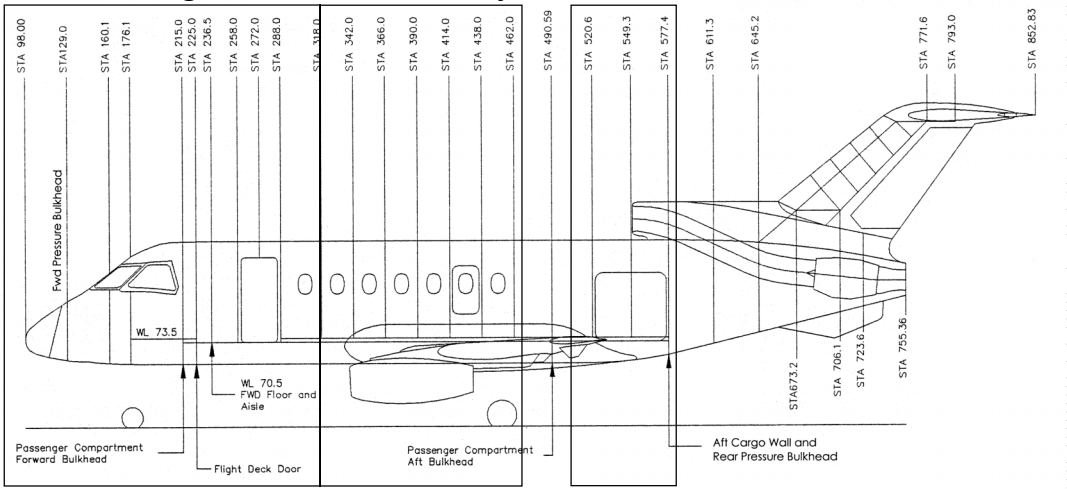

Figure 5 - Fuselage structural arrangement and assemblies common to Saab 340 vehicle.

GENERAL OVERVIEW

Fuselage

The structure of the fuselage (Figure 5) consists of three major assemblies: front - nose with cockpit; centre - cabin; and, aft - rear section including the cargo compartment. Each section is spliced in a manner, which duplicates as much as possible the Saab 340's manufacture/assembly production tiers.

With the exception of fore and aft sections, the fuselage is cylindrical with a 7 ft 7 in. (2.31 m) maximum diameter cross-section, and, the front and some of the centre as well as aft sections are utilised from the Saab 340 design. The front section is comprised of the radome, nose landing gear attachments, electronics/avionics, the hydraulic bay and pilot compartment. The centre section constitutes the passenger and/or cargo cabin including windows, emergency exits, overhead baggage racks, stowage compartments and cargo or seat attachments/rails. Plug type doors are standard. The centre cabin is divided into top, bottom and two side panels. These single piece panels consist of an outer skin to which the required doublers and stringers are bonded. The primary floor supporting structure is defined by continuous longitudinal beams (extruded stiffeners with continuous "C" shaped geometry) connected to frames by crossbeams. The floor is capable of withstanding a maximum floor loading of 150 lb/sq.ft (732 kg/m^2). Two special reinforced frames are incorporated for wing interface. Space has been provided below the floor and within the region of the

wing-fuselage attachment fairing for systems and equipment installation. The aft section is comprised of a baggage compartment; empennage supporting structure which includes reinforced frames to provide support for the mounting of the second (centre) engine; rear pressure bulkhead; and, compartments for ancillary electrical/electronic systems. The compartment terminates just past the bay door aft bulkhead. The baggage compartment floor area and volume are 37.2 sq.ft (3.46 m^2) and 226 cu.ft (6.40 m^3) respectively and can withstand a maximum permissible load of 1356 lb (615 kg).

The fuselage maximum pressure differential of 7.5 psi (51.7 kPa) allows maintenance of a sea level cabin pressure up to an altitude of 18493 ft (5637 m). The pressurised area is confined by a flat bulkhead located forward of the flight deck and a flat rear bulkhead located aft of the baggage compartment and forward of the second engine installation. In the region cut by the wing, the pressurised area maintains integrity by way of a pressure floor above the wing carry-through.

Interior Arrangement

The pressurised vessel of the fuselage includes the cockpit, passenger cabin and baggage compartment. The cockpit accommodates a crew of two. The layout of the cabin permits 19 passengers to be accommodated in dual seats to the right of the aisle and single seats to the left with a seat pitch of 32 in. (813 mm), and, a flight attendant can also be accommodated.

Overhead baggage bins running the full length of the passenger cabin are installed above the dual seats. Provision is also made for a stowage/closet compartment and/or galley located aft of the cabin on the left hand side of the aisle. The toilet is located at the front of the cabin. A baggage compartment with approximately 226 cu.ft (6.40 m^3) of volume is located rear of the cabin and the compartment provides space for an optional catering trolley.

The main door, 63 in. x 27 in. (1.60 m x 0.69 m) with sill height of 67 in. (1.70 m), is located on the left side of the fuselage front section to permit crew and passengers to have access to the cabin. Two emergency exits 36 in. x 20 in. (0.91 m x 0.51 m) are located over the wing. Access to the baggage compartment is from the left side of the rear fuselage through an up-and-over baggage bay door with dimensions of 52 in. x 53 in. (1.32 m x 1.35 m). Seats are of the type employed on the Saab 2000 vehicle. Figure 6 elucidates the interior arrangement of the cabin with 19 seats, toilet, and, wardrobe and galley.

Wing

The PD340-2's wing thickness variation of 16% at the root to 12% near the tip, quarter-chord sweep of 21° and aspect ratio of 7.9 caters for typical cruise Mach numbers in the region of 0.70-0.75. The planform layout shows a distinct deviation away from the Saab 340 geometry, however, the modified super-critical MS(1)-0313 aerofoil section has been adopted from the Saab 340 and Saab 2000 designs. It was felt that well-established properties together with comprehensive experimental analysis base would aid in reducing initial research and development work.

The wing structure (Figure 7) is an assembly of left and right hand panels spliced at the aircraft centre line and interfaced to the fuselage belly by two reinforced frames. The structure accommodates double-slotted flaps, ailerons, spoilers, integral fuel tanks and the main landing gear attachment assembly. The wing main structure is comprised of two spars, upper and lower skins, stringers and ribs. Air loads are carried by the front and rear spars, which are located at 15% and 63% chord respectively. The rear spar from wingtip to

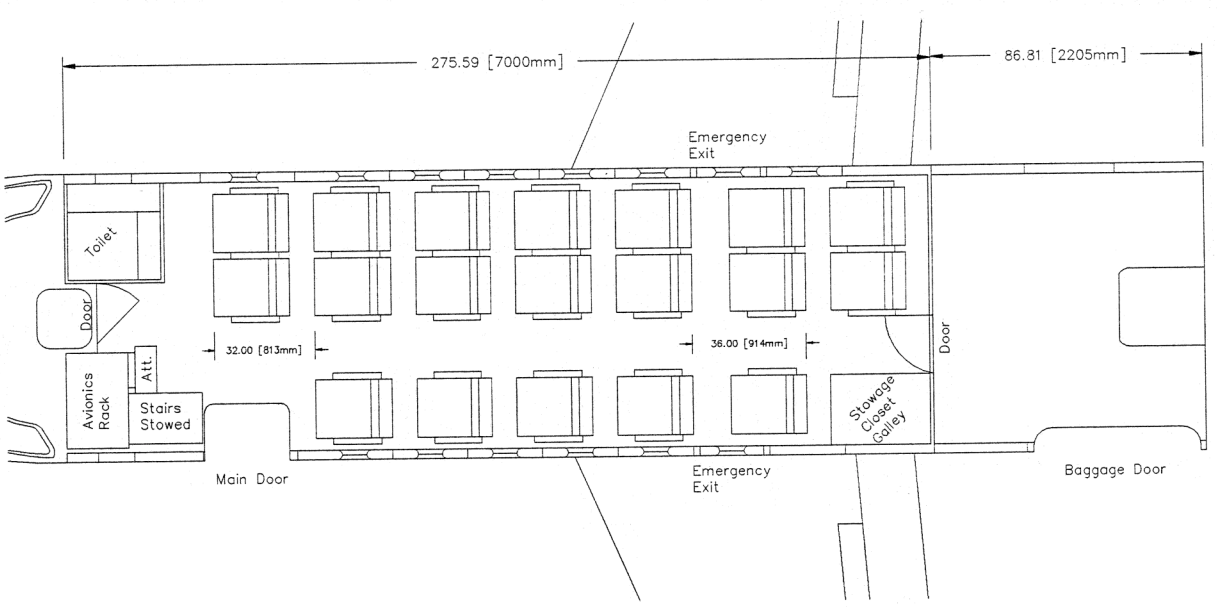

Figure 6 - PD340-2 standard interior for 19 PAX layout.

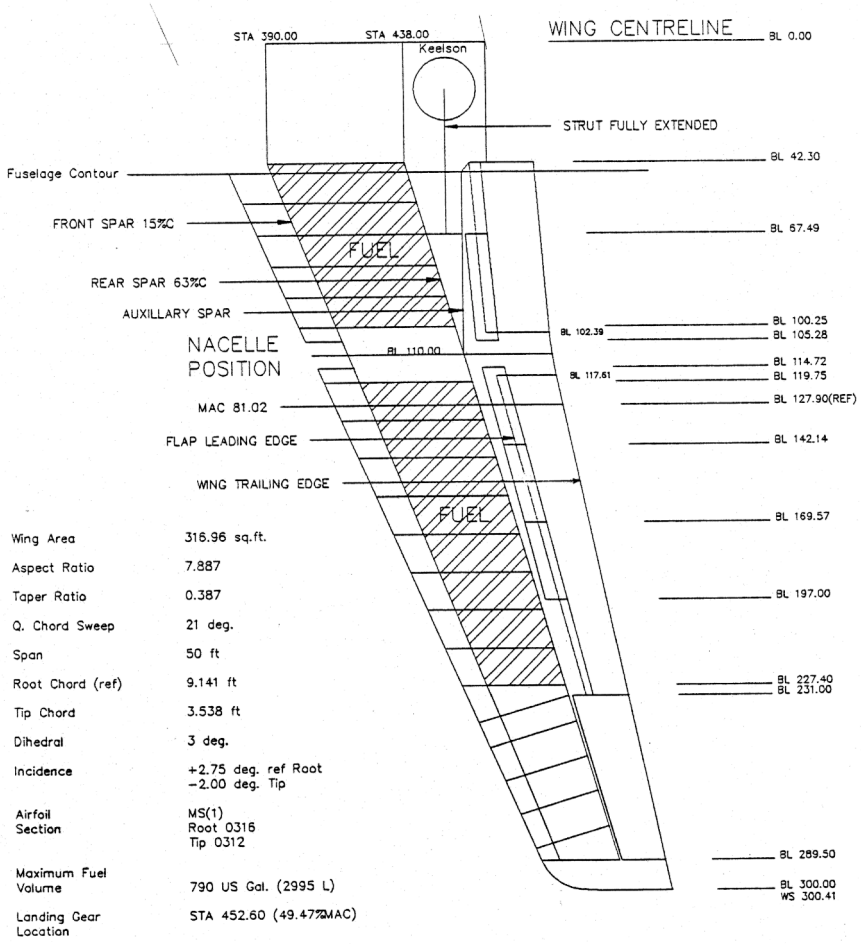

Figure 7 - Wing structural arrangement.

pylon/wing interface closes out the flap bay and supports control systems therein. The spar is continued from this interface to the wing/fuselage attachment. It provides hard points for the main landing gear and closes out integral fuel tanks. An auxiliary spar, or Yehudi is also incorporated for closing out the inboard flap bay and supporting inboard spoilers.

The entire box beam encloses two distinct integral fuel tanks. The central wing torsion box consists of two beams that run perpendicular to the fuselage contour. An additional box beam yielded from a Keelson and closed by a beam perpendicular to the fuselage contour (upon which is attached the previously mentioned Yehudi) houses the main landing gear as well as various equipment and systems.

The wing leading edges are detachable parts, made of metal in order to facilitate hot air to be supplied via these assemblies for anti-icing purposes. The ailerons are a mono-spar structure hinged on four supports attached to the wing rear spar. The spoilers and speed brakes consist of four carbon-fibre panels per semi-wing and are each hinged at three stations and hydraulically actuated at the centre hinge locale. Roll-spoilers are operable in flight and the entire spoiler system can be deployed in unison during landing ground-roll.

Flaps

The high lift arrangement consists of simple externally hinged, hydraulically actuated double slotted flaps. Each flap consists of two panels and the respective vanes are made retractable for small flap deflections, making the flapping mechanism effectively single slotted when desired. One hinge is located at the wing/fuselage contour juncture, and another at the pylon/wing interface wing station. A hinge is also located at the outboard end of the outer flap segment. The latter hinge is made compatible to the wing contour as much as possible - which turns out to be permissible with the modified MS(1)-0313 section geometry. The inboard flap segment requires one actuator while the outboard segment employs independent actuation to avoid binding in the tracks: therefore three bell cranks are planned in each semi-wing.

Empennage

The empennage is a ”T” configuration with the horizontal stabiliser mounted on top of the vertical fin. This places the tailplane above the jet efflux and increases moment arm due to sweepback of the fin.

The variable incidence horizontal tail consists of a stabiliser and elevators. The horizontal stabiliser is a

single structural component attached to the top of the vertical fin. It has two spars with inboard, mid and outboard ribs. The two inboard ribs accommodate the stabiliser-fin attachment fittings. The tailplane structure is complemented by surface covers that are integrally stiffened, and a honeycomb bonded structure is utilised. The leading edge is of aluminium construction housing a bleed air anti-ice assembly. The stabiliser pivots about bearings housed in the support structure at the top of the fin rear spar. A jack arm in the centre of the horizontal stabiliser is connected to and driven by a variable incidence jackscrew extending from mounting plates at the top of the fin front spar. Separate left and right hand elevators are hinge mounted on the horizontal stabiliser.

A vertical fin and rudder constitutes the vertical tail. The vertical tail structure consists of two spars and integrally stiffened panels and a honeycomb-bonded structure is utilised. The rudder comprises of one segment and is supported by two hinges with self-aligning bearings attached to the rear of the vertical stabiliser. The rudder is metallic with ribs, reinforced skin and two spars.

Undercarriage

The landing gear is a tricycle type arrangement consisting of two main gear assemblies mounted at the root of each wing, and a nose gear mounted on the forward fuselage beneath the flight deck. Extension and retraction is hydraulically actuated and electrically controlled. The nose gear retracts forward into the nose gear bay while the main gears retract sideward into the main landing gear bay. For the main landing gear, either a trailing arm or cantilever design shall be adopted. All shock absorbers are of the oleo-pneumatic type, and each gear strut is equipped with two wheels. Positive mechanical locks are provided on both the up and down positions. Unlocking is performed hydraulically in normal mode. The main gears are equipped with two power operated brake assemblies that provide anti-skid performance. The nose gear has a hydraulically powered steering system with shimmy damping and is steerable ±60°.

Engines

The power plant installation consists of three FJ44-2A turbofans configured in a tri-jet layout, i.e. two underwing podded and one tail mounted S-duct arrangement that support thrust-reversing capability.

Each underwing podded installation is a nacelle-pylon arrangement in which the pylon provides redundant support. The pylon has two spars (longerons) - upper and lower major bulkheads, and is attached to the wing at four primary points through the use of two mid-spar fittings, an upper link and a diagonal brace (drag strut). Each nacelle installation clears the ground by 24 in. (610 mm) and is an engine break away design: break between the engine pod and pylon interface by means of a shear-off structure is achieved by the application of ”fuse” bolts at the attachment points for shear-failure at a defined load.

The tail mounted torque box serves as mounting points for both the empennage and second engine installation. The entire structure consists of reinforced frames that follow the contour of the vertical stabiliser and is stiffened with stringers. The forward and aft torque box bulkheads used for engine mounting are complemented by the addition of an aft lightweight fairing with a vertical fillet from the engine nozzle to the rudder lower platform.

Fuel Tanks and System

Fuel is stored in integral wing tanks and the projected maximum usable fuel capacity is 774 US Gal (2930 L). Baffles in each tank restrict fuel sloshing, limit centre of gravity shifts with changes in aircraft attitude. Access doors to the fillers are installed in the upper wing panels. Gravity refuelling is made possible via these fillers. A pressure refuelling capability is provided on the wing lower surface. Gravity de-fuelling is accomplished via dump valves installed on the wing tanks’ lower surface. Fuel is supplied to each engine by an engine driven integral fuel pump. A DC electrically powered positive displacement pump in each fuel tank is provided for redundancy.

Environmental Control System

Pressurisation and air-conditioning for the flight deck, cabin and cargo hold are provided by bleed air from the engines. The system is operated through two air cycle packs located in the wing/fuselage fairing. Conditioned air is supplied from the air cycle packs by separate lines to the flight deck and cabin. Air-conditioning is provided on the ground either by an external ground connection or from the second engine (tail), which acts as a synergistic auxiliary power unit (APU).

Flight Control System

The flight control system comprises ailerons, elevator and rudder, flight and ground spoilers, flaps and variable incidence tailplane. Control is segmented into primary and secondary systems. The primary control surfaces are mechanically actuated by conventional floor mounted control columns and adjustable rudder pedals complemented by cables, pulleys, bellcranks and rods. The elevator and aileron control paths are redundant and the control path is duplicated where required. A gust lock system is also provided and is operable from the flight deck. Trim tabs (to be incorporated later) on all surfaces are controlled by redundant electromechanical actuators.

Upon examination of the secondary flight controls, each semi-wing has inboard and outboard externally hinged double slotted flaps of Douglas type extending from the fuselage to the aileron. Two pairs of spoiler surfaces, for lateral control and lift dumping, are

hydraulically actuated and electrically commanded. Each spoiler surface is driven by a single hydraulic actuator. When the surfaces are not deployed, the retract chamber of the actuators are pressurised. A mechanical locking device is provided in the retract position of the actuators to avoid spoiler opening following a loss of hydraulic pressure supply. The spoiler surfaces deploy automatically in unison during landing. The vehicle is equipped with a stall prevention system to limit high angles of attack that could result in a stall condition. A two-pronged protection system consisting of a stick-shaker and a stick-pusher shall be employed.

Electrical and Hydraulic System

Basic electrical power sources are starter generators, auxiliary generators, inverters and batteries. A 28 V ground power receptacle allows the use of external power sources for ground operation and engine starting. The second engine can be used as an APU and its own generator is used to provide electrical power to assist engine starts if a ground power unit (GPU) is not available.

The hydraulic system consists of a power and distribution section that operates the landing gear, wheel brakes (inboard/outboard wheels having separate supplies), nose wheel steering, flap actuation, spoiler actuation and emergency landing gear extension. The system is driven by an engine driven pump as well as an electric motor driven pump. The hydraulic power section equipment including pump, reservoirs, accumulators and supply manifold are placed in the hydraulic accessory compartment in the nose section.

Flight Deck, Avionics and Equipment

The flight deck has accommodation for two crewmembers and an observer. The windows give a field of vision in excess of the recommendations in SAE 580B. An allocation of the latest avionics used on the Saab 2000 vehicle is available here including a FADEC system to monitor flight which will aid in reducing pilot workload as well as fuel burn.

Ice and Rain Protection

Ice protection is provided for the wing and horizontal stabiliser leading edges, windshields, engine inlets and air-data sensors. Anti-icing of wing and stabiliser leading edges is accomplished by means of a bleed-air system similar to that used on larger jets - no de-icing boots are used. The windshield panels are electrically anti-iced while windshield and side panels are defogged by conditioned air. Electrically driven windshield wipers are also installed. The vehicle employs a bleed-air anti-icing system for nacelle intake lips and critical regions of the S-duct are electrically anti-iced. The pitot heads and static ports are electrically heated as well as the sensors for outside air temperature and angle of attack.

VEHICULAR INTEGRATION HIGHLIGHTS

Underwing Podded Engine

In any transport aircraft development, considerable effort is needed in properly integrating underwing engine nacelles such that interference drag effects can be minimised and the detrimental effects a nacelle-pylon system imparts on the wing's lift capability is reduced. The final underwing nacelle placement relative to the wing can be examined in Figure 8.

Notwithstanding the above-mentioned criteria, a closely coupled nacelle-pylon-wing philosophy was of reducing wetted area due to the minimisation of pylon size, hence drag. As a final affirmation of the closely coupled nacelle-pylon-wing proposal, the relationship between the fan exhaust stream and the wing trailing

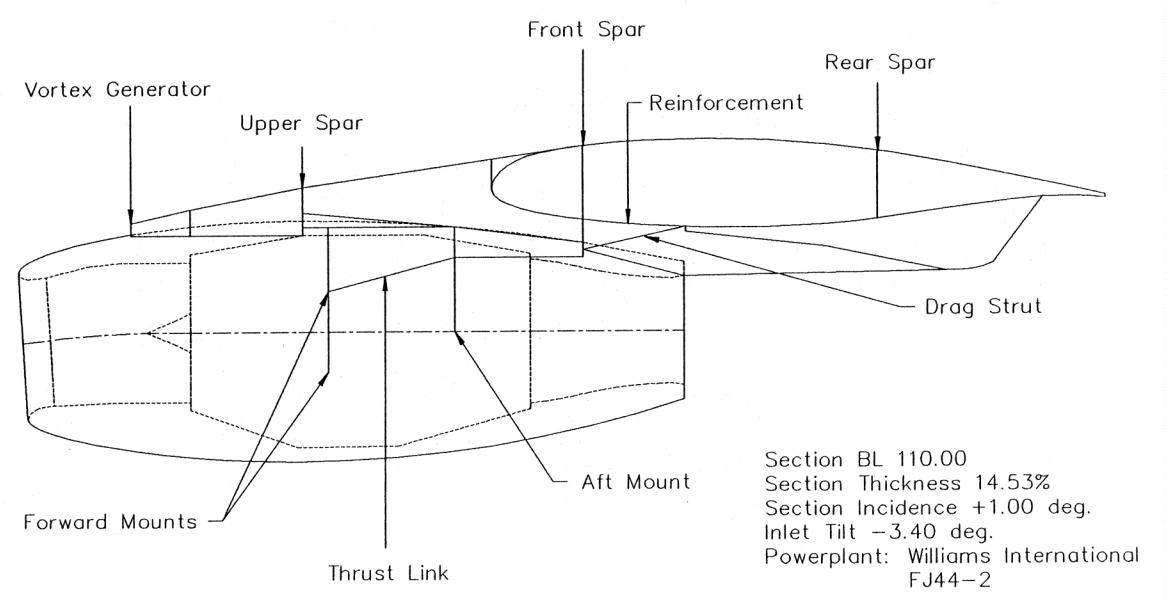

Figure 8 - Underwing podded engine installation.

edge were examined. Early indications show that propulsive losses and incremental drag increases due to scrubbing are considered minimal. Additionally, the nacelle-pylon arrangement was placed in a spanwise station corresponding to the wing planform trailing edge break. This was enacted in order to take advantage of a postulated high concentration of vorticity shed due to a large variation in wing planform geometry.

As an initial guess of aligning the nacelle with local flow, a 3^{o} inlet face planar tilt was employed to align the inlet to the incoming flow-field, which will have upwash. This was considered in lieu of future streamline tracing techniques for the conceptual design phase and to minimise contouring of the nacelle and pylon arrangement with respect to the wing streamline. If contouring is indeed required, consideration will probably be required for the inboard to lower quadrant of the nacelle to fit the wing streamlines about 10% chord ahead of the wing, so that the inboard side of the nacelle emulates the natural wing flow in order to avoid local normal shock formation.

Avoiding Foreign Object Damage (FOD)

Jet engines are sensitive to ingestion of many types of debris. Apart from bird-strike, it is necessary to ensure that gravel, slush, mud, snow and ice thrown up by the landing gear cannot enter into inlets or other critical components of the propulsive installation. To provide reasonable assurance in the conceptual phase that a proposed installation is not prone to landing gear FOD, a survey of the relative locations of engine inlets and landing gears on existing aircraft together with their angular relationships were examined.

The literature survey indicated that the angle between nose gear and the inboard side of an inlet in plan view should be at least 31° - the PD340-2 final layout angle was measured to be 32°. The second criterion against FOD is the angle between the nose gear and upper lip of the inlet in side view; PD340-2's angle of 15° meets the parametric study minimum of 10°. Notwithstanding, an option of utilising special deflectors on the nose gear for operation on gravel runways should be available for future use.

Single Engine Dorsal Intake

Since a design requirement was to employ Williams FJ44-2A engines, thrust-weight trades during the design process indicated that a tri-jet configuration would be the most suitable way of achieving minimum performance goals. As a result, possible solutions that adequately integrate a third engine were considered. An extensive review of each respective installations' relative merits found that the dorsal intake described by an S-duct had lower drag characteristics and lower weight compared to its straight duct counterpart. There are penalties of duct losses, which is detrimental to any pressure recovery efforts for maximising thrust, but it was surmised that by applying a relatively weak S-duct, minimisation of these problems could be achieved. Freedom in tilting the engine to a maximum of 6° while maintaining axial flow from the nozzle enables reduction of the fuselage total length at the expense of minimal losses in thrust. Finally, this installation also has the inherent benefit of allowing some structural synergism in the aft fuselage region of the vehicle - any weight penalty incurred from the use of a T-tail arrangement may be offset from application of this philosophy.

Ventral Fins

Two ventral fins have been added to the aft portion of PD340-2's fuselage for the purposes of fulfilling requirements imposed by tip-back angle and stability. It was found that ventral fins even with associated wetted area penalties were more feasible than compromising an already synergistic structural layout of the aft fuselage structure, empennage and engine. Additional benefits of possibly avoiding the need of a stability augmentation system through stall protection, inherent improved directional stability at high Mach numbers and altitudes, increased dutch-roll damping, and, properties that tend to prevent high angles of sideslip, makes the ventral fin a very good candidate for selection. Nominally, an angle of 25° to the vertical, and a location that ensures adequate engine access/removal was considered to be a good initial layout.

PERFORMANCE SYNOPSIS

Figure 9 shows the predicted payload-range capabilities, whilst Table 2 summarises estimates of the major performance characteristics and compares these with current market equipment. It can be discerned that the 19 PAX regional/commuter market is basically a turboprop dominated one, and comparison of PD340-2 to these vehicles is based on data gathered from reference 1.

PD340-2 appears to deliver a superior balanced field length of 4082 ft (1244 m) at ISA, sea level when compared to the Merlin 23 and Jetstream 31 vehicles. This indicates an improvement of 34% and 26% respectively. The only exceptions are Dornier 228 with 2600 ft (793 m) and Beech 1900D with 3737 ft (1139 m) giving approximately 36% and 9% shorter field lengths respectively. Furthermore, PD340-2 displays similar attributes even at hot/high conditions. The FAR/JAR landing field performance is estimated to be 3502 ft (1067 m) at ISA, sea level ambient conditions.

The competition’s rate of climb (ROC) has been surpassed considerably. Even though the PD340-2 is a turbofan aircraft that cruises at altitudes 10000 ft plus higher than turboprops, a climb time to typical flight level FL 310 and maximum service ceiling FL 350 of 14.3 and 18.4 minutes respectively from MTOW at brake release demonstrates yet another very competitive attribute.

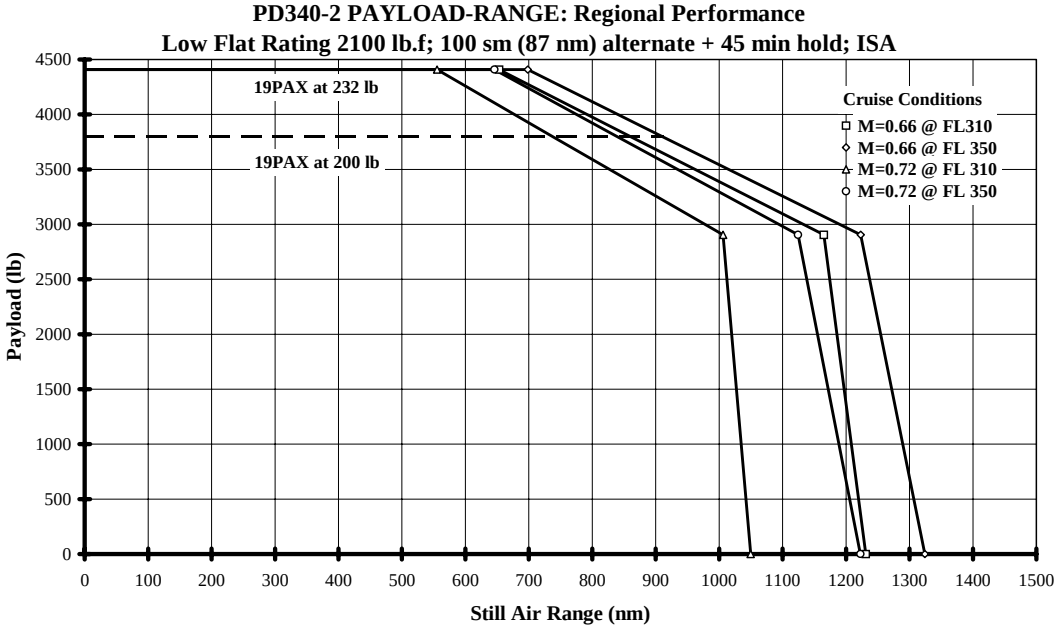

Figure 9 - Payload-range envelope for PD340-2 19 PAX regional turbofan transport.

	PD340-2 Tri-jet	Dornier DO-228-212	Fairchild Merlin 23 SA-227-DC	Beech Executive BE-1900D	British Aerospace J31 BAe 3201
BFL (SL ISA) (ft)	4082	2600	5460	3737	5147
BFL (5000ft + 20°C) (ft)	6069	4500	6900	4977	6386
All Engines Operating ROC (fpm)	3431	1870	2320	2625	2240
One Engine Inop. ROC (fpm)	1059	440	580	675	450
AEO Service Ceiling	FL 350	FL 250	FL 252	FL 250	FL 250
OEI Service Ceiling	FL 164	FL 130	FL 115	FL 175	FL 100
Missions: 4PAX @ 200lb/PAX					
300nm					
Takeoff (ft)	2418	1800	3700	3193	3755
Block Time (hrs:mins)	0:53	1:22	1:04	1:08	1:13
Block Fuel (lb)	1301	1063	813	1029	810
Passenger Specific Range (nm/lb)	0.924	1.129	1.476	1.166	1.481
Flight Level	FL 350	FL 080	FL 160	FL 250	FL 250
600nm					
TO (ft)	2621	1900	3750	3271	3869
Block Time (hrs:mins)	1:35	2:40	2:07	2:12	2:24
Block Fuel (lb)	2214	2050	1523	1826	1478
PSR (nm/lb)	1.084	1.171	1.576	1.314	1.624
FL	FL 350	FL 080	FL 180	FL 250	FL 250
1000nm					
TO (ft)	2899	2120	3920	3378	4081
Block Time (hrs:mins)	2:35	4:24	3:36	3:38	3:59
Block Fuel (lb)	3398	3366	2277	2907	2362
PSR (nm/lb)	1.176	1.188	1.753	1.376	1.693
FL	FL 350	FL 080	FL 220	FL 250	FL 250
Productivity Missions					
275sm (239 nm)					
Stage/Fuel	2	2	3	2	2
PAX (@ 200 lb/PAX)	19	19	19	19	19
Engine Hours (hrs)	9.68	9.80	10.45	10.01	10.40
Total Fuel (lb)	13013	6602	7525	8174	6599
Total Trips	11	8	10	9	9
Seat Miles	57475	41800	52250	47025	47025
Block Speed (kts)	272	195	229	215	207
Mission Fuel (lb)	1183	825	752	908	733
Flight Level	FL 310	FL 100	FL 150	FL 240	FL 210
400sm (348 nm)					
Stage/Fuel	2		2	1	1
PAX	19		19	19	19
Engine Hours (hrs)	10.32		10.00	10.61	10.99
Total Fuel (lb)	13546		7181	8401	7031
Total Trips	9		7	7	7
Seat Miles	68400		53200	53200	53200
Block Speed (kts)	303		244	230	222
Mission Fuel (lb)	1505		1026	1200	1004
FL	FL 350		FL 160	FL 250	FL 210
800sm (695 nm)					
Stage/Fuel	1				
PAX	19				
Engine Hours (hrs)	9.79				
Total Fuel (lb)	13012				
Total Trips	5				
Seat Miles	76000				
Block Speed (kts)	355				
Mission Fuel (lb)	2602				
FL	FL 350				

Table 2 - Parametric review of PD340-2 against contemporary turboprops.

Long range and high speed cruise show an appreciable difference between the PD340-2 and contemporary turboprops. Long range cruise is 135 KTAS quicker than the fastest of the turboprops at maximum service ceiling and the maximum cruise speed capability has opened up a totally new regime of lower block times. A combined flight level and speed increase promotes unconstrained cost and profit optimal flight technique formulation, therefore allowing for operational flexibility when air-traffic control (ATC) or route structure imposes off-optimal restrictions. In contrast, the slower and lower turboprops generally produce constrained optimal flight techniques, or a requirement of block times faster than the lower block time threshold physically permissible by the given vehicle.

The direct consequence of this favourable performance is increased fuel consumption rate; however, as exemplified by specific and passenger specific range values close to or the lowest found in the survey. Nonetheless, a detailed Direct Operating Cost (DOC) and annual profit analysis demonstrates in the section to follow that the higher fuel and other acquisition/maintenance related costs may be rationalised utilising turbofan technology through an increased productivity potential.

For individual sector missions, at 275 sm (239 nm; 443 km) stage lengths, PD340-2 equals all competitors' capability of conducting 2 such legs with the one tank of fuel - the only exception being Merlin 23 which yields 3 legs; PD340-2's 400 sm (348 nm; 644 km) sector is characterised by 2 legs - which equals the highest turboprop value produced by Merlin 23; and, a distinct advantage of PD340-2 is an ability to complete 800 sm (695 nm; 1287 km) sector missions which is not generally afforded by any of the turboprops in this survey. Even though PD340-2 has matched multi-hop potential, it surpasses the competition in terms of the number of trips that can be achieved in a typical 14-hour day profile for all sectors. Competitive multi-hop capability combined with the highest productivity for a given day's utilisation elucidates the feasibility of the PD340-2 proposal.

ECONOMICS

Costing analysis has shown that an anticipated acquisition cost for PD340-2 would be around USD 5-6 million. This figure includes the total nominal manufacturing cost breakdown and a reasonable margin for future contractual negotiations. A cost and profitability model developed by Williams-Rolls Inc. was utilised in order to gauge the relative operational merits of PD340-2 against a typical 19 PAX turboprop competitor. The Metro 23 was chosen as the regional 19 PAX comparison basis because results for other competitors had demonstrated a close correlation to this aircraft. The Williams-Rolls model calculations addressed cost constituent contributions of fuel usage, flight crew, maintenance, lease, hull insurance, spares and sundry expenses related to vehicle utilisation.

Figure 10 illustrates the total normalised DOC with respect to maximum accommodation and stage length flown between PD340-2 and Metro 23. It should be noted that an 800 nm (1482 km) sector distance DOC result for the Metro 23 is not published even though the vehicle demonstrates no useful load limitations. Turboprop vehicles are considered less than attractive for stage lengths greater than 500 nm (926 km) due to prolonged block times with excessive noise and vibration leading to passenger discomfort.

Using the sector DOC characteristics given above, an annual operating profit for given stage length is presented in Figure 11. It can be discerned that the PD340-2 in terms of profitability exceeds that of the contemporary turboprops for stage lengths greater than approximately 180 nm (333 km) and maintains this posture up to about 1000 nm (1852 km) with a global profit maximum occurring for distances of around 600 nm (1111 km). This profit cross-over between PD340-2 and Metro 23 at 180 nm may not seem immediately evident if the normalised DOC comparison is considered.

The increased productivity potential (exemplified by Table 2) of the turbofan through increased block speed enables completion of a greater number of sector missions for given hourly based reference time frame utilisation compared to the much slower turboprop - thereby rationalising the impact of sector mission cost through reduction of the time related cost component. It must be duly noted that this study utilised a conservative assumption of 50% passenger load factor. FAA[2] forecasts indicate that a 60% load factor for turbofans would be more attune to market realities; however, the lower load factor assumption has the advantage of enabling an equitable comparison between equipment by keeping the yield quantity the same regardless of power plant selection. Even though the acquisition cost for PD340-2 is approximately USD 1-2 million higher than its ageing 19 PAX contemporaries, the regional turbofan's staid viability and extreme competitiveness demonstrates the potential for this design.

VALIDATION OF CONCEPTUAL SIZING METHOD

The General Aviation Synthesis Program[3] (GASP), a digital computer program developed by NASA-Ames Research Centre, is a complex conceptual design tool for the aircraft designer who has to investigate the interaction among various disciplines. The program has several subroutines to carry out the analysis within each discipline, and a control routine which provides the user flexibility in calling any subroutine at any stage is available. Initial conceptual design and optimisation procedures for PD340 involved simpler first order analysis techniques created by the author[5,6]. This had inherent advantages of producing quick results for detailed sensitivity studies as well as being flexible by enabling the use of predetermined constraint criteria, which frequently proves to be cumbersome with dedicated conceptual design

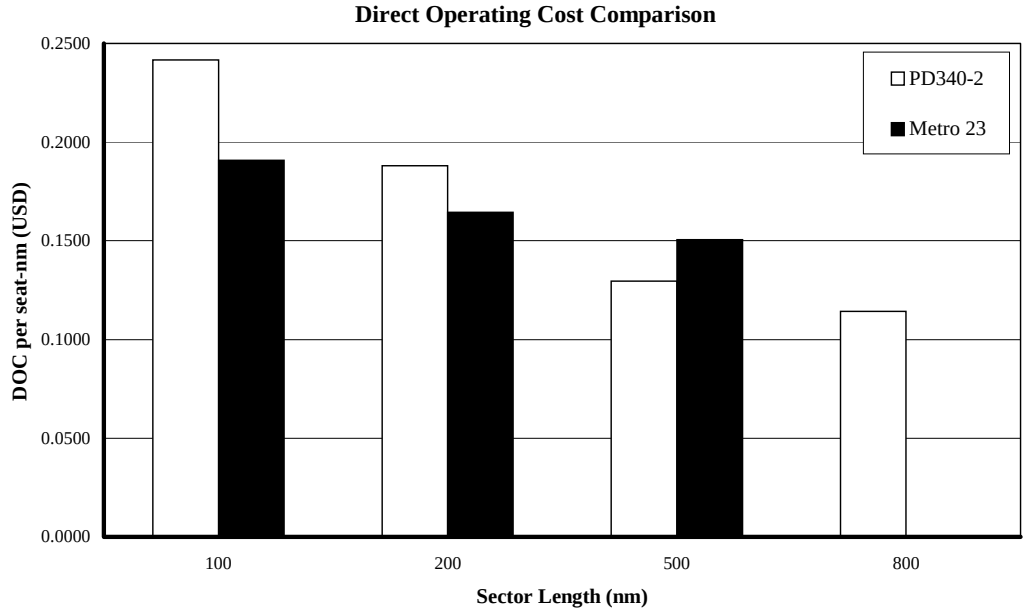

Figure 10 - Direct Operating Cost per seat-nm comparison of PD340-2 to competition.

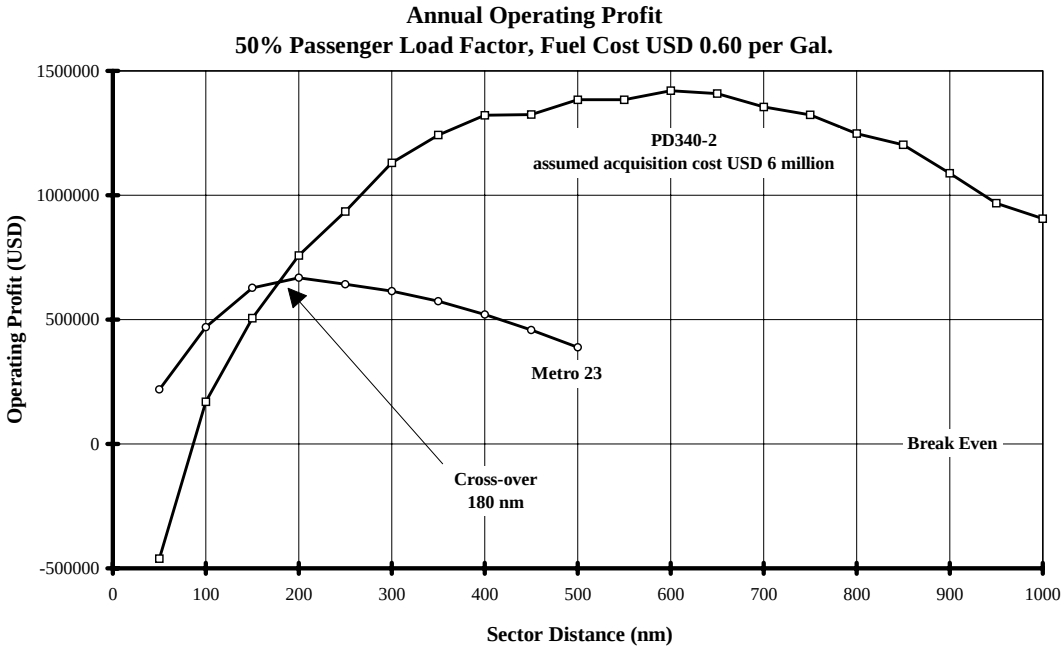

Figure 11 - Annual operating profit comparison of PD340-2 to competition (50% load factor).

analysis codes.

MTOW prediction variances between GASP and the author's first order method were fortuitously minor - in the order of less than 1%. Detailed investigation of the constituents' weight prediction showed some discrepancies between GASP and the author's method, however, deviations were mostly associated with constituents that did not have great influence on MTOW.

The author's method allowed for a limited scenario for field performance prediction. Balanced field length equal to 3920 ft (1195 m) was calculated for an initial 15° flap setting and assuming the highest flat rating of 2300 lb.f (10.2 kN) per engine at ISA, sea level conditions. This was postulated to model the final de-rated (2100 lb.f; 9.4 kN) and flap deflection optimised result close to the hard specification of 4000 ft balanced field length. GASP estimated balanced field length to be 4082 ft (1244 m) at the low flat rating and optimised flap setting of 25° at ISA and sea level conditions which denotes a variance of +4.1% against the author's assumptions. Even though the low flat rating had exceeded the maximum permissible stipulated by PD340's hard specifications, a

parametric review found that this figure was still very competitive against existing turboprop performance.

The initial time to climb to FL 350 from MTOW brakes release at ISA, sea level of 18 minutes was calculated by GASP to be 18.4 minutes which represents a -2.2% deviation and considered to be most satisfactory. GASP's calculated optimum cruise speed of 380 KTAS at FL 350 compares favourably with the author's estimate of 389 KTAS yielding a deviation of +2.4%.

FURTHER DERIVATIVE COMPATIBILITY

It was deemed early in the project that the final PD340-2 design not only conform to a unique set of specifications from the outset, but also, each decision whether philosophical or technical should be based on the premise of accommodating an extended range (ER) variant as well as stretching the current 19 PAX vehicle to a 30-35 PAX version[6], hence giving the vehicle marketing flexibility and fulfilling objectives of creating a family concept.

Initial studies show that the PD340-2 layout may permit an extended range version. Considerable fuel increments can be available through the introduction of outboard wing tanks and a centre fuel tank. Projections show range performance may be enhanced by at least 500 nm (900 km) for given payload complements if an increased gross weight variant produced by the addition of this fuel increment to PD340-2's current MTOW is considered. By raising available thrust to the maximum flat rating threshold of 2300 lb.f (10.2 kN) per engine, this should assist in off setting excessive field and en route performance degradation, and indications show that PD340-2 ER would still exhibit competitive attributes upon comparison to contemporary turboprops.

By further utilising analysis tools employed for the basic design, various ideas were incorporated in the 19 PAX design formulation which focused on maximising commonality for a 30-35 PAX stretched version of PD340-2. Initially, it was recognised that the fuselage exterior and interior layouts required no radical shift away from the basic geometry presented in this paper. Projections show the fuselage would require a stretch of around 10 ft (3 m) whilst no other aspect of exterior and structural geometry, such as the fore and aft, need revision. Preliminary estimates indicate the basic planform of PD340-2 can cater for a larger PAX version through span (wing tip) extensions alone. This aspect is considered crucial because the already existing wing torsion box and wing structure including choice of high-lift device can be retained. Nacelle modifications are postulated to be at best moderate, with calculated increases in fan diameter of around 2-3 in. (50-75 mm) in order to accommodate slightly higher airflow requirements associated with a predicted necessary maximum sea level static thrust increase of 25%.

Undesirable alterations to improve nacelle ground clearance minima are not envisaged for the landing gear legs but increases in constituent weights due to an overall increase in gross weight are anticipated. Finally, an increase in moment arm produced by a fuselage stretch fortuitously does not require any modifications to the PD340-2's existing empennage layout even though a larger wing and higher thrust rating must be incorporated.

CONCLUSION

The PD340-2 vehicle proposal is a concept that accommodates a maximum of 19 passengers and affords comfort through speed and spaciousness that is not paralleled in a contemporary regional/commuter market. The result was a regional workhorse that utilises turbofan technology without high costs; it is projected that new niche markets may be opened as a result of this and other similar proposals. The design has pivoted around the philosophy of derivative compatibility with the Saab 340, namely, fuselage including cross-section, partial aft structure and forward cabin, wing torsion box geometry, and, ancillary basic structural elements and principles. This has greatly assisted formulation of a current projected equipped price of around USD 5-6 million. It has been shown that the author's own method of final configuration synthesis was valid by confirmation of predicted results using NASA-Ames Research Centre's conceptual design program GASP. In terms of regional performance, PD340-2 sits comfortably in the realm of a turboprop-dominated market. Competitive field performance coupled with much higher cruise speed capability is clearly in this proposal's favour. A trade off of increased fuel flow denoted by lower specific and passenger specific range values compared to its turboprop counterparts was shown to be offset by reduction of time related costs due to the improved block time performance. The design has also demonstrated a significant degree of potential by allowing for an extended range variant, as well as, requiring only a moderate array of modifications to the basic 19 PAX vehicle configuration in order to produce a future 30-35 PAX version.

ACKNOWLEDGMENTS

This project could not have been possible without the assistance of many individuals and organisations. The following people are recognised for their support.

Williams-Rolls Inc.
Ed Lays
Dr. Gary Ludwig
Paul K. Meyer
Ronald P. Schwedland
Bruce E. Wilcox

Saab Aerospace AB
Bengt V. Andersson
Ingemar Arvidsson
Lennart Danielsson
Ulf Edlund
Tord Jonsson
Krister Karling
Lars Kinell
Tommy Nygren

Royal Inst. of Tech. (KTH)
Prof. Arthur Rizzi

Karlebo Aviation AB
Göran Berg

REFERENCES

1. Business and Commercial Aviation, Review of Regional Airliners, May 1995-1998.
2. FAA Aviation Forecasts, Fiscal Years 1995-2006, U.S. DOT, Federal Aviation Administration, FAA-APO-95-1.
3. GASP - General Aviation Synthesis Program, NASA CR 152303, January 1978.
4. Isikveren, A.T., ”The PD340-2 19 Passenger Turbofan Regional Transport - Feasibility Study”, Report 98-5, Royal Institute of Technology, Department of Aeronautics, Sweden, 1998.
5. Isikveren, A.T., ” Methodology for Conceptual Design and Optimisation of Transport Aircraft”, Report 98-8, Royal Institute of Technology, Department of Aeronautics, Sweden, 1998.
6. Isikveren, A.T., ”Methodology for Conceptual Design and Optimisation of Transport Aircraft”, ICAS 98-7.8.2, September 1998.

ADDITIONAL SOURCES

1. Abbott, I.H., Von Doenhoff, A.E., ”Theory of Wing Sections”, Dover Publications, 1959.
2. Archer, Prof. R.D., ”Aircraft Propulsion Notes”, University of New South Wales, Australia, 1991.
3. Clancy, L.J., ”Aerodynamics”, Longman Scientific & Technical, 1975.
4. Currey, N., ”Aircraft Landing Gear Design: Principles and Practises”, AIAA, 1988.
5. Gillette, W.B., ”Nacelle Installation Analysis for Subsonic Transport Aircraft”, AIAA Paper 77-102.
6. In-House GASP Users' Guide, Williams-Rolls Inc., 1994 Update.
7. Isikveren, A.T., Khezri, R., Monti, A., Räisänen, S., ”NGR-20/2C: 19PAX Regional Commuter Preliminary Design”, KIF-95:4, Royal Institute of Technology, Department of Aeronautics, Sweden, May 1995.
8. Ljungström, O., ”Transport Aircraft Systems Synthesis”, Lidingö, Sweden, April 1973.
9. McCormick, B.W., ”Aerodynamics, Aeronautics and Flight Mechanics”, John Wiley & Sons, 1979.
10. McGhee, R.J., Beasley, W.D., ”Low Speed Aerodynamic Characteristics of a 13 Percent Thick Medium-Speed Airfoil Designed for General Aviation Applications”, NASA Technical Paper 1498, 1979.
11. Megson, T.H.G., ”Aircraft Structures”, Edward Arnold, 1990.
12. Niu, M.C.Y., ”Airframe Structural Design”, Conmilit Press Ltd., 1989.
13. Perkins, C.D., Hage, R.E., ”Airplane Performance, Stability and Control”, John Wiley & Sons, 1953.
14. Raymer, D.P., ”Aircraft Design: A Conceptual Approach”, AIAA Educational Series, 1992.
15. Roskam, Dr. J., ”Airplane Design”, Vol. I-VII, 1986.
16. Roskam, Dr. J., ”Airplane Dynamics & Automatic Flight Controls”, Part I, 1979.
17. Saab 340 Aerodynamic Design Data, Section 3 & 6, Report 72AD0303, Saab Aerospace AB, 1992.
18. Saab 2000 Type Specification, 73VPS010, Revision F, Saab Aerospace AB, November 1996.
19. Schaufele, R.D., Ebeling, A.W., ”Aerodynamic Design of the DC-9 Wing and High-Lift System”, Douglas Aircraft Div., McDonnell Douglas Corp., AIAA Paper No. 670846, 1967.
20. Schippers, K.A., ”Cowl Design Methodology”, D6-41800 TN (unreleased), Boeing Airplane Company.
21. Snyder, S.F., Voorhees, G.C., Heinrich A.M., Baisden, D.N., ”Conceptual Design of Single Turbofan Powered Light Aircraft”, Gates Learjet Corporation/AMES/NASA, March 1977.
22. Torenbeek, E., ”Synthesis of Subsonic Airplane Design”, Delft University Press, 1988.
23. Young, A.D., ”The Aerodynamic Characteristics of Flaps”, Aeronautical Research Council, Technical Report No. 2622, 1953.
24. Representation of Drag in Aircraft Performance Calculations, ESDU Data Sheets: 81026, 1981.

intentionally blank

Paper III

High-Performance Executive Transport Design Employing Twin Oblique Lifting Surfaces

intentionally blank

High Performance Executive Transport Design Employing Twin Oblique Lifting Surfaces

Askin T. Isikveren
Department of Aeronautics
Royal Institute of Technology (KTH)

ABSTRACT

This paper presents a new Trans-Atlantic high performance executive transport suitability equipped to offer accommodation for 19 first class passengers. The unique feature of this conceptual design is application of Twin Oblique Lifting Surfaces or TOLS configuration. Minimum goals for the design included: similar maximum takeoff gross weight; satisfactory field performance; good stalling characteristics; and, competitive fuel burn qualities at high-transonic and low-supersonic speeds, i.e. M0.90-1.20, compared to contemporary M0.75-0.85 large and super-large business jets. The vehicle is to be powered by two medium by-pass derivative engines based on the BMW-Rolls Royce BR715 in an effort to maximize the likelihood of availability, ensure adequate en route performance efficiency and fulfilment of yet to be ratified Stage 4 noise compliance requirements.

INTRODUCTION

The oblique wing concept has fallen in and out of favour over the latter half of the Twentieth Century. It gathered notoriety with Vogt's variable sweep oblique wing aircraft design proposal in the 1940s designated as the Blohm and Voss P202[1]. This unconventionally asymmetric aircraft design was one of the first concerted attempts to reconcile conflicting conditions of wing sweep optimality for low and high speed performance of an aerospace vehicle. Around the same period, Campbell and Drake[2] at NACA conducted experimentation on similar layouts. It was subsequently championed by Jones[3,4] who found interest in such a configuration because analysis and windtunnel testing indicated that elliptical oblique wings would provide minimum wave drag in supersonic flow.

Notwithstanding the potential offered by oblique wings, there exists a distinct absence of such aircraft in both the military and civilian operational arenas. From a programme perspective, it is potentially a large risk venture. Historically, difficulties have included the following: problems with low-speed aeroelastic divergence associated with a high aspect ratio, forward swept semi-wing; in the absence of a mature automatic control systems technology knowledge-base, the adequate handling of longitudinal and lateral motion coupling produced by the interaction of highly non-linear aerodynamic and inertial moments; lack of rigid body and wing structural mode coupling; the drawback of having an obligatory wing pivot mechanism; and, the sense it is a highly exotic configuration.

Alternative configurations that challenge the traditional cantilevered single wing have also been examined. As a follow on from experimentation done by Olson and Selberg[5], studies by Rhodes and Selberg[6] showed that both closely coupled dual-wing and swept forward swept rearward (connected at the wingtip) systems exhibit aerodynamic advantages over single wing configurations. They found the low drag of multi-surfaces were due to a combination of two and three dimensional drag reductions, tailoring the three dimensional drag for the swept forward swept rearward design, and improved structural efficiency through connection thus permitting higher aspect ratios.

Another example of unconventional planform design is the strut-braced wing (SBW) and origins of this concept can be traced back to Pfenninger's research of a long-range transonic transport truss-braced wing

study[7] done in the mid-1950s. Proponents of SBWs cite as a result of favourable interaction between structures, aerodynamics and propulsion, potential for higher aerodynamic efficiency and lower Maximum Takeoff Weight (MTOW) can be realised. Encouraging results from design studies of the 2010 SBW transonic transport completed by Virginia Polytechnic (Gundlach et al[8]) show a potential to shave up to 10% of MTOW defined by design mission requirements.

In view of the significant potential for performance enhancement and with due regard given to the difficulties discussed above, a new hybrid concept is proposed here which comprises two independent, fixed, oblique (or skewed) wings linked by a wing-pylon-engine bracing structural system (WPEBS). This configuration, coined as Twin Oblique Lifting Surfaces or TOLS (Figure 1), is intended to produce a new aircraft design perspective that will afford acceptable en route efficiency at high-transonic and low-supersonic speeds with an unconventional operational flexibility of satisfactory field performance and stalling characteristics.

Figure 1. Introducing the TOLS configuration.

Even though commercial aviation and the charter industry provide transportation at more competitive rates for the upper echelon of customers, they have proven to be both inefficient and unreliable. Due to a growing dissatisfaction with commercial airliner services, there are strong indications demand will shift towards business aviation. There are some newly emerging business and corporate aviation concepts to improve affordability and quality of contemporary air travel. Today, prospective customers can choose from five distinct methods of owning or chartering business jets:

- Traditional ownership – outright ownership and complete responsibility for operation;
- New and used fractional ownership – allotment of time based on a given fractional ownership of a new or used business jet;
- Branded charter – privately owned fleet of similarly outfitted business jets offering chartered service;
- "By-the-seat" charter – chartered seats sold in scope similar to commercial operators; and,
- Business airline charter – regularly scheduled flights using business jets between city pairs deemed profitable.

Traditional business jet ownership is the most dependable means of travel, but comes at an appreciable expense. As a result, the charter services and fractional ownership have demonstrated to be schemes attracting the majority of commercial aviation customers as well as enticing clientele who would normally not purchase business jets to consider fractional ownership. In view of the great potential of growth, a new conceptual aircraft design targeting this market niche is taken to be a potentially lucrative venture.

UNIQUE CONCEPTUAL DESIGN PREDICTION INFERENCES FOR THE TOLS CONFIGUATION

Almost all conceptual design synthesis methods rely on empirical or handbook methods based on datasets of similar aircraft. In effect, the analysis methods assume a level of weights, aerodynamics and performance within the bounds of the aircraft survey dataset. With regards to the unconventional nature associated with TOLS configurations, a series of unique conceptual design prediction algorithms must be formulated in order to ensure consistent account of weight and aerodynamics, and to establish minimum goals with confidence. The main considerations that ideally would be reviewed for study of this unique configuration are addressed below.

WING WEIGHT RELIEF – With respect to SBWs, Gundlach et al[8] reason the vertical force of the strut produces a shear force discontinuity along the wing span creating a break in the bending moment slope, thus reducing the magnitude of bending moment inboard of the strut. Also, the strut vertical offset generates a favourable moment that creates a spanwise bending moment curve discontinuity further alleviating the bending moment inboard of the strut. For SBWs, this condition translates into a significant rationalisation of weight and thus allows for thinner wing sections promoting a decrease in zero-lift and transonic wave drag. It also gives scope to decrease vortex-induced drag via an increase in wing aspect ratio; combining to yield an improved aerodynamic efficiency.

Even though TOLS configurations employ dual-wing planforms skewed in opposite sense to each other, a legitimate parallel to SBWs and the associative benefits therein can be drawn. The WPEBS system which links individual oblique lifting surfaces is akin to the bracing effect produced by an offset strut – in this context, the offset strut height being equivalent to each of the four engine pylon heights.

INTERFERENCE DRAG DUE TO WING-ENGINE-PYLON BRACING SYSTEM – To quantify the interference drag between the wings and WPEBS intersections, a combination of form factors[9] and a wing-strut interference drag model developed using Computational Fluid Dynamics (CFD) techniques by Tetrault (reproduced in the 2010 SBW transonic transport study by Gundlach et al[8]) was employed. Tetrault shows the wing-strut interference drag (ΔC_{Dint}) model is best described utilising a hyperbolic fit to the CFD results because interference drag was found to vary inversely with arch radius (or offset strut height), viz.

$$\Delta C_{D\,int} = \frac{18}{h_{os}} \qquad (1)$$

where h_{os} is the offset strut height in feet, and, ΔC_{Dint} is expressed in drag counts.

For the final TOLS configuration selected in this study, a total increment of drag due to dual-wings, WPEBS and empennage interference effects was predicted to be 40 drag counts, or, typically 10% of the total en route drag. This contrasts as proportionately 2-3 times greater constituent contribution compared to contemporary subsonic transport aircraft.

MULTIPLANE VORTEX-INDUCED DRAG – The shortcoming of contemporary reference wing definition conventions (ESDU, Boeing Wimpress, Airbus Gross and Net) is an inadequacy to appropriately and consistently represent multi-surface wing designs. These methods are only suited to the single cantilevered wing premise, thus producing a geometric to aerodynamic qualities disconnect. One objective was to derive an expression that quantifies the TOLS equivalent reference wing aspect ratio (AR_E) with consistency so that the vortex-induced drag factor to be used for ensuing calculations can be based directly on the geometric attributes of an equivalent single reference wing.

To address this requirement, a starting point is Prandtl's "two-surface" vortex-induced drag equation as presented by Kendall[10]. Prandtl indicates that, "The total [induced] drag (of a multi-surface) consists of the sum of all the separate drag and of as many mutual drags as there are combinations of the wings in twos". For speeds greater than M0.40 and with no account of compressibility effects, the elliptically loaded two-surface vortex-induced drag factor equation can be related to an analytical expression derived by Obert[11]:

$$\frac{dC_D}{dC_L^2} = \frac{1}{\pi S_W}\left[\frac{S_1^2}{b_1^2} + 2\sigma\frac{S_1 S_2}{b_1 b_2} + \frac{S_2^2}{b_2^2}\right] \equiv \frac{\alpha}{\pi AR_E} + \beta \qquad (2)$$

where Prandtl's mutual drag factor σ accounts for gap effect as presented by Kerber and can be found in Durand[12], S and b are the constituent area and span respectively for wings 1 (lower) and 2 (upper), S_W is the reference wing area, and, α and β are coefficients of proportionality equal to 1.05 and 0.0070 respectively as derived by Obert.

To round off, Munk's stagger theorem states no change in the vortex-induced drag will occur due to longitudinal location as long as the surface loads remain unchanged. This means Prandtl's mutual drag factor may be applied to any multi-surface configuration without any consideration given to the longitudinal location of the semi-wing surfaces relative to each other.

DESIGN SPECIFICATIONS

A business jet aeroplane design must concurrently fulfil a number of requirements as dictated by today's discerning clientele: a premium on passenger comfort, a high degree of operational readiness and exceptional performance characteristics. High passenger comfort levels are paramount since the cabin living volume can act as an executive office or conference room. Also, a business jet is viewed as an aid to saving time and increasing productivity, and so, dispatch-reliability should be maintained at very high levels. Superior performance attributes afford a great deal of operational flexibility. The ability of operating in and out of relatively short airfields, of expediently climbing to cruising altitudes above inclement weather or avoiding congested airways altogether, and cruising at significantly faster speeds than conventional aircraft at comparable en route efficiencies would all combine to produce a vehicle with unmatched appeal.

In view of the mission role discussed above, the hard specifications that were deemed necessary for the success of this proposal are defined below.

- The vehicle must accommodate at least 19 passengers seated with a 1.40 m (55 in.) pitch;
- Takeoff field length less than 1830 m (6000 ft) at ISA, sea level conditions;
- Effective operation at 5000 ft (1524 m) airport pressure altitude and at ISA+20°C conditions;
- Initial cruise altitude of at least FL 470;
- Time to climb to typical bandwidth of cruise flight levels in around 15-25 minutes;
- Service ceiling not less than FL 510 and High-Speed Cruise (HSC) Mach number not less than 1.20;
- Maximum range not less than 4000 nm (7408 km) at Typical Speed Cruise (TSC) of M0.95, and, 3500 nm (6482 km; this represents a westbound Trans-Atlantic flight between LHR and JFK with 85% probability winds) at Maximum Cruise (MCRZ) assuming NBAA IFR mission rules and reserves, and, a maximum passenger complement;
- Landing reference speed to be not greater than 135 KCAS at Maximum Landing Weight (MLW) and ISA, sea level conditions;

- A competitive en route Specific Air Range (SAR) efficiency at TSC compared to similarly sized contemporary large and super-large business jets;
- Low parts count and relatively simple construction, avoidance of complex double curvature in fuselage geometry;
- Should fit into existing Air Traffic Control (ATC) patterns, and noise levels should comply to current version of yet to be ratified Chapter 4 definition;
- The vehicle shall be certified according to FAR 25 and JAR 25 transport category aircraft requirements.

In addition to these, a soft specification was set to provide for a suitable cargo hold, i.e. a target total volume of 0.28 m^3 (10 cu.ft) per passenger.

DESIGN PREAMBLE

FUSELAGE DESIGN – The design cycle began by establishing the fuselage size in isolation. The height, width and resulting fineness basically catered to providing ample volume in accommodating the necessary 1.40 m (55 in.) seat pitch for passengers. Ancillary attention was paid to minimizing frontal area as well as producing a lower $Volume^2/Length^4$ (or volume-reference length ratio) for minimum zero-lift and wave drag respectively. The width of the fuselage was also influenced by the requirement of allowing at least 610 mm (24 in.) of aisle width between passenger seats. Finally, consideration was also given to ensure space for landing gear, avionics, supporting systems and fuel was sufficient. The geometric layout of the fuselage was loosely based on the 50 PAX Saab 2000 high-speed turboprop[13]. Apart from catering to a higher pressure differential, the cylindrical cabin has mostly been retained, however, extensive modifications have been introduced to the forward fuselage to meet the requirements imposed by operating in the high transonic and low supersonic speed regime.

ENGINE SIZING AND SELECTION – Even though this design study involves a hypothetical or “paper” engine using methods conceived by the author[14] and investigations made by Svoboda[15], the results derived from initial analysis were used to propose a plausible engine the market could conceivably design and manufacture. As expected, the engine optimisation process focused on the cruise condition for sizing. Preliminary investigations showed a suitable engine should meet the following criteria:

- Target maximum static thrust of 71.2 kN (16000 lb.f) at sea level standard conditions;
- Cruise By-Pass Ratio (BPR) of around 3.0 to reduce the thrust lapse rate at given speed and altitude;
- Overall Pressure Ratio (OPR) of at least 30 to keep the overall engine efficiency as high as possible;
- Relatively high engine Turbine Entry Temperature (TET) to maintain required specific thrust characteristics.

The BMW Rolls-Royce BR715 is identified as an ideal candidate for future derivative development work. With the current configuration of 1 fan, 2 boosters, 10 compressors, 2 low pressure turbines and 3 high-pressure turbines, the basic layout can be retained but the requirement of an en route design BPR decrease from 4.8 to 3.0 will have with it an associative reduction in fan diameter from 1.53 m (60 in.) to approximately 1.25 m (49 in.). This has a beneficial effect of reducing the engine empty weight by almost 454 kg (1000 lb). The design point Thrust Specific Fuel Consumption (TSFC) degrades somewhat from 0.63 at M0.76 and 35000 ft to approximately 0.73 at 45000 ft and M0.95.

Operation at low supersonic speeds will reduce the possibility of maintaining an exceptionally high pressure recovery. Nonetheless, the axisymmetric intake was found to be satisfactory for speeds slower than M1.50. Providing due consideration is given to applying sharper lip geometry, the single normal shock wave of a pitot intake would yield only about a 2% reduction compared to the two-dimensional shock intake as cited by Whitford[16]. Also, this design ensures efficient structural shape for low duct weight and minimum wetted area for given stream-tube flow area.

EMPENNAGE SIZING – With variation of wing geometry and placement, associated changes to the empennage were made accordingly. Approximate dimensioning was based on the inequality constraint of keeping the vertical tail volume coefficient greater than or equal to 0.090.

AEROFOIL AND PLANFORM GEOMETRY – The selection of aerofoil section thickness and general wing design characteristics were based on studies presented by Kroo[17]. Numerical optimisation techniques have shown that a wing thickness (t/c) of up to 14.0% is acceptable for oblique wing design proposals. Indeed, van der Velden and Torenbeek[18] have taken this notion further by employing a higher t/c of 15.0% for their supersonic oblique wing transport design. With respect to planform geometry design, taper ratio and wing twist needs to be selected such that unbalanced lift loads are avoided. This circumstance fortuitously gives scope to approximate

the elliptical load distribution ideal as well.

DESIGN PREDICTION

SYNTHESIS CODE – To perform the required parametric calculations, the QCARD-MMI software package developed by Royal Institute of Technology (KTH) Department of Aeronautics was utilised. QCARD-MMI, or Quick Conceptual Aircraft Research and Development Version 2001, is a MATLAB based computer program and embodies the quasi-analytical

conceptual design prediction methods developed by the author[14]. The system places an emphasis on assisting the user to interactively draft, predict and optimise coherently during the conceptual aircraft design generation process.

A variety of known regional aircraft were input and QCARD-MMI predictive powers were inspected against each respective vehicle's manufacturer Performance Engineers' Handbook (PEH) or its equivalent. Indications have shown very good agreement against published results[9] with typical errors frequently falling within a bandwidth of ±5% for weight; engine performance - TSFC and thrust lapse; aerodynamics - total drag for All Engines Operational (AEO) and One Engine Inoperative (OEI) at low and high speed, maximum lift for clean wing and for given flap setting; and, operational performance - takeoff including minimum control speed limitations and initial climb, en route climbing, cruise, complete mission and landing. Additionally, QCARD-MMI methodology was benchmarked against the General Aviation Synthesis Program (GASP) developed by NASA-Ames Research Centre[19]. To ascertain consistency of the high-speed aerodynamics and engine thrust-burn modules, QCARD-MMI was tested on a supersonic design completed by van der Velden and Torenbeek[18] and was found to be in good agreement in the high transonic and low supersonic regime. The only significant discrepancy was observed in the friction drag component with a conservative prediction of +24%.

The points to follow outline the prediction algorithm methodology for a select array of core disciplines analysed by QCARD-MMI.

Drag – Drag calculations are partitioned into three distinct groups, namely, friction, vortex-induced and wave. Friction drag that is independent of lift is predicted using the component build-up method at a representative Mach number and altitude (generally Long Range Cruise [LRC] and optimum altitude) and subsequently used to derive an equivalent characteristic length for off-reference conditions. This approach is coined Equivalent Characteristic Length Method (ECLM) and a full treatment can be found in the author's previous work[9]. This component also accounts for interference, 3-dimensional effects, roughness and excrescences using the conventional form factor approach. The vortex-induced drag is calculated using an analytical expression derived by Obert[11], which approximates vortex-induced drag factors computed for a wide variety of commercial transport aircraft. Wave drag accounts for the presence of significant compressibility effects. The Critical Mach number (M_{CR}) is approximated with the Korn equation[20] modified to include simple sweep theory with adjustments made using empirical data given by Obert[11]. The total wave drag is estimated using the zero-lift and lift related components (representing geometric difference) from the total drag equation for supersonic cruise drag given by Jones[21]. Using this as a basis, an exponential drag rise and divergence model originating from Torenbeek's[22] proposed algebraic structure is dynamically constructed employing empirical guidelines for drag divergence properties presented by Raymer[23].

Maximum Lift – The clean wing maximum lift is computed for any original planform geometric definition using a MATLAB module developed by KTH called TORNADO[24]. The TORNADO software with a 3-dimensional Vortex-Lattice Method (VLM) calculates aerodynamic properties of multi-wing designs that are swept (symmetric or otherwise skewed), tapered, cambered, twisted and cranked with dihedral. Unlike the classical VLM approaches, TORNADO models the wake coming off the trailing edge of every lifting surface as flexible and changing shape according to the flight state considered. With a distorting wake, non-linear effects such as the interaction of multiple surfaces can be simulated more consistently.

Since the primary assumption of any VLM is linearity, the prediction of maximum lift coefficient (C_{Lmax}) is taken from empirical data describing the relative increment of C_L with change in angle of attack between the beginning of lift non-linearity and C_{Lmax}. Even though thickness effects are neglected, the slope of the mean camber surface is accommodated. Camber data is sourced from a comprehensive aerofoil library compiled for another MATLAB based program developed by KTH called PABLO[25] (low-speed aerofoil analysis using one-way coupled inviscid and boundary layer model). High-lift produced by flap and slat deflection is estimated based on methods presented by Young[26]. This reference uses empirical correlation from assorted accumulated data and predicts with adequate accuracy the aerodynamic characteristics of high lift devices.

Propulsion – An engine model taken from previous work done by the author[14], based on the premise of exponential decay and proportional to variation of flight level and speed was expected to generate an adequate description of thrust lapse and TSFC variation. For accuracy, two distinct models describing takeoff-climb, and, maximum cruise thrust characteristics are employed. Linear performance deterioration models to account for effects of off-ISA temperature deviations are also considered. Since these expressions do not permit direct sensitivities to more pertinent working parameters like BPR and OPR, a new hybrid model was developed to include this aspect using research compiled by Svoboda[15].

Weight – Aircraft constituent weight estimates of wings, vertical tail, fuselage, landing gear, avionics, electrical, hydraulic, environmental control system (ECS), anti-icing, auxiliary power unit (APU) and other equipment on board were obtained with the aid of methods developed by Linnell[27], Scott and Nguyen[28] and the author[14]. Formulae to account for weight relief due to presence of fixed masses on the wing (to be discussed in the Optimisation section) were also

introduced into the MTOW transcendental algorithm. Owing to the absence of a consistent conceptual prediction method, wing weight estimation for this study did not include account of the TOLS configuration structural efficiency due to WPEBS inter-wing connection. This produced a prediction almost 8% greater than that of a single wing with the same area, aspect ratio and strength.

Estimates for engine weight, and, complement of pylons and nacelles were obtained using methods detailed by the author[14]. A completion allowance of 2170 kg (4785 lb) was predicted from estimated interiors for contemporary large and super-large business jets. This figure did not intentionally include a crew rest area (saving almost 400 kg; 880 lb) as standard since it was assumed almost all missions would be completed within an 8-hour duty cycle.

Weight of fuel is estimated using a quasi-analytical procedure developed by the author. The integral wing and centre tanks are described by a series of truncated pyramid geometries with adjustments made to reconcile an over-estimated volume compared to the more elliptical face of aerofoil sections. Elliptic paraboloids more accurately describe volume encased by the forward fuselage fairing and saddle tanks. The aft fuselage auxiliary tank is simply predicted assuming a cylinder with segment cutout bounded by the circular cross-section and chord. All tank volume constituents were further reduced in volume to account for presence of structure based on recommendations made by Torenbeek[22].

Performance Definitions – A series of guidelines were adhered to when evaluating the operational performance attributes of each design candidate. Since the design engine sizing requirements for this exercise was understood to focus on en route cruise, it was surmised that both takeoff and climbing performance would still be acceptable even with a significant amount of engine de-rate for each of these two mission phases. The takeoff performance was defined using engine de-rate for normal takeoff thrust, with no facility for Automatic Power Reserve (APR), as a free variable. The selection of an appropriate de-rate level was based on one that yielded a minimum (twin engine) OEI second segment climb gradient of 2.4% at takeoff flaps of 30°, an airport pressure altitude of 5000 ft, ISA+20°C ambient conditions and MTOW at brakes release. A philosophically similar set of criteria were also employed for AEO en route climbing; in this instance, maximum climb thrust de-rate for the engines was determined by a vehicle candidate clearing FL 510 with residual climb rate of 300 fpm at the fastest forward speed technique assuming ISA still air and MTOW at brakes release.

The Optimum Trajectory-Profile Algorithm (OTPA) in QCARD-MMI utilises an interval halving numerical scheme with climb distance as the free variable for given flight level. The algorithm caters to a myriad of objective function evaluations, including unconstrained maximum SAR, constrained maximum SAR at given speed technique and unconstrained minimum time (maximum block speed) flight technique evaluation. For accuracy, a default of 5 segments is assumed for the entire mission profile. In this particular study, each of the numerically integrated en route mission computations was limited to a maximum of three cruise-steps to simulate actual operational procedures. As a margin for establishing the validity of en route cruise speed minimum goals, a residual of 100 fpm was imposed to identify the engine thrust limit. Even though consideration for altitude capability constrained by high-speed buffet (1.3g margin) is important, owing to the lack of a coherent conceptual method to determine this aspect, experience dictated that engine thrust limited altitude would be the most likeliest of constraints for the interim. Finally, all en route mission computations adhered to flight techniques, reserves and contingency policies stipulated by NBAA IFR guidelines including 200 nm alternate and 30 minutes hold.

DESIGN OPTIMISATION

A very limited scope of multivariate optimisation was undertaken in this study. The objective here was to ascertain in a relatively quick manner if the TOLS configuration exhibits feasibility. Many of design variables were systematically bounded for the global optimisation process after formulating the best objective function result for that given sub-space. For example, once initial estimates yielded an idea of the most likely engine candidate dimensions and weight, a generic trade study between engine lateral coordinate wing placement and aircraft empty weight was examined. To assist in this process, weight relief factors were drawn from semi-analytical methods of contemporary transport aircraft wing weight estimation done by Torenbeek[29].

CANDIDATE SELECTION – Various combinations of wing area, complementary wing skew angles, thickness and aspect ratio were analysed to determine an acceptable trade off between good field and en route performance. Each candidate MTOW design point was defined as one in which 19 PAX at 100 kg (220 lb) can be accommodated with maximum fuel load. A myriad of possible performance constraint criteria to inspect for sensitivity and subsequently identify feasible solutions were reviewed.

The hard specification takeoff field length (TOFL) constraint of 1830 m (6000 ft) was initially found to be a limiting condition. Further scrutiny revealed the engine inoperative decision speed (V_1) should be considered as a primary parameter because a combined effect of high wing loading and minimum control speed (V_{MC}) limitations produced reference speeds that became quite high. As an orthogonal delineation to the V_1 decision speed trade, two separate en route performance inequality constraints were examined: maximum PAX range at MCRZ speed technique, and, range with maximum payload

assuming constrained maximum SAR technique at M0.95. The first choice, which proved to be the most limiting, of maximum range at MCRZ speed technique assuming a payload of 19 PAX at 100 kg (220 lb) each with NBAA IFR flight guidelines and reserves, 200 nm alternate and 30 minutes hold was finally designated as the primary en route constraint criterion. Consequently, the selection process focused on maximising range, and, minimising takeoff field length as well as lowering the V_1 takeoff safety speed.

In terms of final selection in this study, thrust-to-weight (T/W) and wing loading (W/S) needed to be maximised in order to rationalise the gross weight, thereby theoretically reducing the equipped price. This is explained by the presence of a fixed power plant (hence thrust level) and the fact decreasing reference wing area allows less available space for fuel. In stark contrast, reference wing area and aspect ratio needed to be maximised (minimise W/S) in order to minimise takeoff and landing distances as well as the respective reference speeds. For given reference wing area, aspect ratio needed to be reduced to increase available fuel volume thence to maximise range performance. To reconcile these conflicting effects, the requirements were plotted on a series of charts that allowed definition of bounded geometric regions in which freedom of selection existed. An example of a simplified final T/W and W/S trade study for the high-performance executive transport is given in Figure 2. Note the final candidate for selection was subsequently given the designation of TOLS-X.

It can be discerned for an optimal wing skew of 31.0°, the T/W and W/S sensitivity study indicates that approximately 482 kg/m^2 (98.7 lb/sq.ft) and T/W of 0.426 are appropriate. This design candidate with MTOW equal to 34493 kg (76043 lb) and reference wing area of 71.6 m^2 (771 sq.ft) produces a vehicle which can operate out of runways less than 1830 m (6000 ft), and is capable of completing 3500 nm (6480 km) range at MCRZ speeds of up to M1.22.

AIRCRAFT DESIGN DESCRIPTION

OVERVIEW - The TOLS-X vehicle is a tricycle, employs dual-winged planforms with relative skew, and, twin turbofan using podded engine installations connected with pylons between the upper and lower skewed planforms. The vehicle is pressurised and incorporates only a vertical tail for empennage. The landing gear is retractable and each leg is twin wheeled. The vehicle accommodates a flight crew of two and an optional flight attendant. The standard configuration seats a maximum of 19 passengers. The power plant is a medium BPR derivative of the BMW Rolls-Royce BR715 turbofan designated as BMW Rolls-Royce BR71X. It is projected the engines shall comply with the yet to be determined Chapter 4 noise levels. The vehicle shall be configured in a manner such that Extended Twin Operations (ETOPS) approval shall be granted with minimal modifications. The vehicle is designed to comply with FAR 25 U.S airworthiness regulations and the European JAR 25 rules. Table 1 supplies a synopsis of TOLS-X design weights, merit values and geometry data. Figure 3 (overleaf) shows a three view general arrangement of the TOLS-X high performance executive transport design.

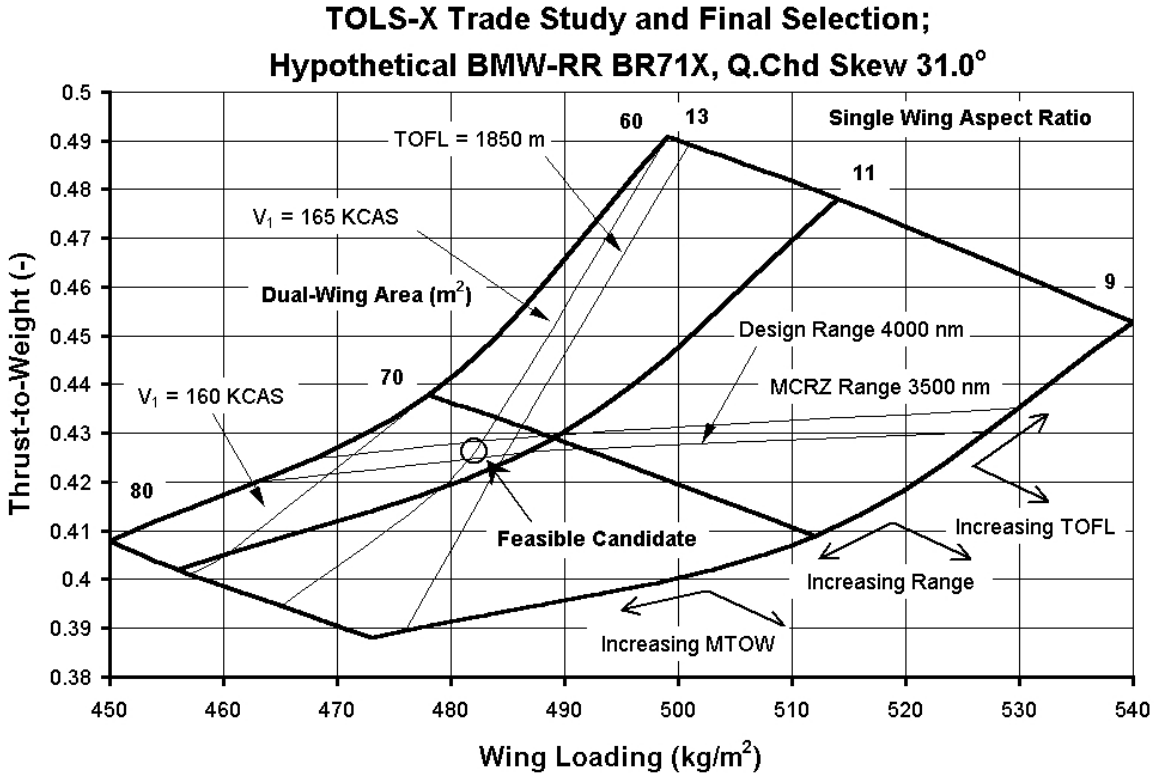

Figure 2. Simplified representation of final selection for TOLS-X design.

Table 1. Design weights, merit values and geometry data for TOLS-X vehicle.

Weights		
Maximum Ramp Weight	34593 kg	76264 lb
Maximum Takeoff Weight	34493 kg	76043 lb
Maximum Landing Weight	31000 kg	68343 lb
Maximum Zero Fuel Weight	20660 kg	45547 lb
Basic Operating Weight	17968 kg	39612 lb
Maximum Payload	2693 kg	5937 lb
Maximum Usable Fuel	14729 kg	32472 lb
Merit Parameters		
Wing loading	482 kg/m^2	98.7 lb/sq.ft
Thrust-to-weight	0.426	
External Dimensions		
Overall span	20.5 m	67 ft 2 in.
Height	7.48 m	24 ft 7 in.
Overall length	29.6 m	97 ft 1 in.
Wheel base	14.2 m	46 ft 7 in.
Wheel track2.74 m	9 ft	
Fuselage Dimensions		
Length	27.3 m	89 ft 6 in.
External diameter	2.31 m	7 ft 7 in.
Wing Geometry		
Total reference area	71.6 m^2	771 sq.ft.
Reference wing aspect ratio	8.79	
Quarter chord skew	±31.0°	
Vertical Tail Geometry		
Area	15.0 m^2	162 sq.ft.

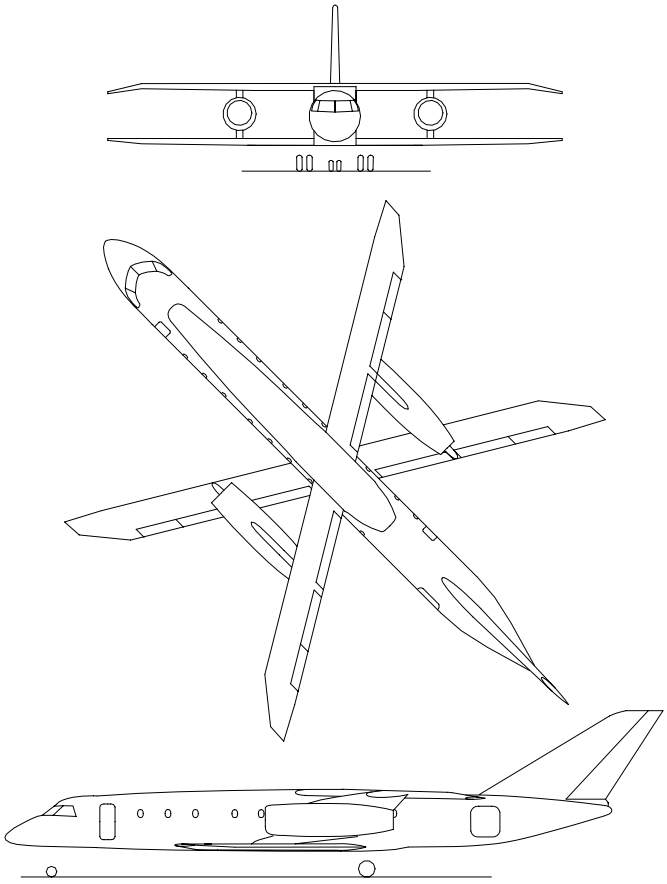

Figure 3. TOLS-X general arrangement.

INTERIOR ARRANGEMENT – The pressurised vessel of the fuselage includes the cockpit, passenger cabin and baggage compartment. The cockpit accommodates a crew of two. Facility for one flight attendant is also to be available.

The standard layout of the cabin permits 19 passengers to be accommodated in sleeper-seats arranged 9 rows to extends out to 1.83 m (72 in.) when fully reclined and with the footrest deployed.

Overhead baggage bins running the entire seating length of the passenger cabin are installed on the starboard side. Provision is also made for a forward stowage and closet compartment located starboard, and galley located aft of the cabin on the port side of the aisle. The toilet is located at the front of the cabin. The standard cabin allows no provision for a crew rest area since almost all TOLS-X missions will last less than 8 hours in duration. A baggage compartment with approximately 5.35 m^3 (189 cu.ft) of volume is located rear of the cabin. Figure 4 elucidates the interior arrangement of the cabin with 19 seats, toilet, stowage-wardrobe and galley.

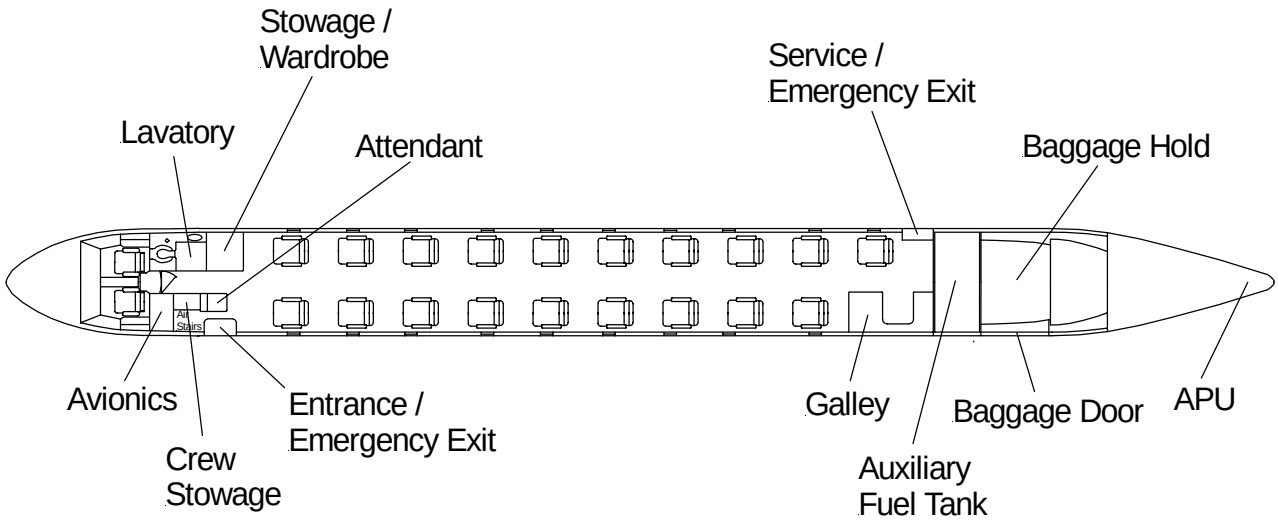

Figure 4. TOLS-X standard interior for 19 PAX.

The main door, 1.60 m x 0.69 m (63 in. x 27 in.) with sill height of 1.68 m (66 in.), is located on the port side of the fuselage front section to permit crew and passengers to have access to the cabin. An aft, starboard service door, 1.22 m x 0.61m (48 in. x 24 in.) permits unobstructed passage to the galley. Access to the baggage compartment is only from the port side of the rear fuselage section through an up-and-over baggage bay door with dimensions 1.32 m x 1.35 m (52 in. x 53 in.).

WING CHARACTERISTICS – The wing t/c variation of 15.0% at the root and 12.0% near the tip, complementary wing quarter chord skew of ±31.0° and reference wing aspect ratio of 8.79 generates an optimal speed schedule which varies between M0.80-0.98 at altitudes above FL 410. Each skewed wing is separated by almost one fuselage diameter or non-dimensional gap (with respect to local wing chord) of 1.06, hence, based on results posted by Rhodes and Selberg[6], flow blockage effects are not surmised to be significant. The wing thickness distribution assists in housing more volume for fuel, and, promotes structural efficiency thus rationalising weight and increasing stiffness.

The wing profile is designed for high-speed natural laminar flow (HSNLF)[30], and tentatively chosen to be HSNLF-1-0213, with a t/c of approximately 14.8% at each semi-wing MAC spanwise locale. Built-in wing washout was designed to optimise the wing lift distribution for low-speed flight (to assist the control-configured system in promoting satisfactory stall progression) with consideration given to minimising penalties incurred to high-speed aerodynamic qualities. The semi-wings have no leading edge devices and high-lift is effected by two panels of simple plain flaps, or flaperons, that extend out to 65% of each wing semi-span. High-speed buffet and flutter problems are not envisaged at faster speed flight since the bow shock wave emanating from the forward fuselage does not coincide with the forward TOLS wingtips until approximately M1.26. To assist in minimising the detrimental effects in this regime, modifications are envisaged for the TOLS-X wing such that the leading edge becomes akin to (more rounded nose) super-critical wing sections.

CONTROL SURFACES – Longitudinal and lateral-roll control are produced by three distinct surfaces, namely, the upper and lower fixed skewed wings and the vertical tail. Each of the four semi-wings employ the use of three simple plain flaps tasked to act in the duplicitous role of flaperon. The wing mounted flaperon relative chord length is 25% of the local swept wing chord. The maximum deflection is set at 30° TEU (-) and 75° TED (+). Symmetric flaperon deflection provides pitch control; while asymmetric deflection of the flaperons coordinated with rudder-assist provides roll control authority through an aileron to rudder interconnect. It would be desirable to minimize out-of-trim rolling moments on each of the oblique wings - for this reason some amount of positive and negative dihedral for the upper and lower planforms respectively have been considered at the wingtips.

FLIGHT CONTROL SYSTEM – The design is to be control-configured with longitudinal, roll and lateral control accomplished via a full 6 degrees-of-freedom Stability Augmentation System (SAS). This approach will assist handling qualities and shall negate any questions on how the onboard pilot will react to an asymmetric highly coupled aircraft. Vehicular manoeuvring and trim is to be effected with differential combinations of aileron and flap deflection (flaperons). Each upper and lower semi-wing will have three segment flaperons. The common primary and secondary control surfaces located on the wings will be simply flapped arrangements thus reducing complexity with an added benefit of allowing for a cleaner wing free of flap fairings and blisters.

For each upper and lower wing planforms, application of a TOLS configuration avoids the problem of pronounced aerodynamic centre (a.c.) shifting since wing chords are not as large as conventional symmetric swept layouts. Also, due to the fact lift produced by each respective forward and aft semi-wing panel is countered in a complementary fashion, a collective a.c. locale forward of the aft-swept semi-wing panels is fortuitously established. For oblique wing aircraft, aerodynamic coupling of the pitch, roll and yaw axes produces a condition where trim in roll predominates with increasing angle of attack. This effect also has a tendency of influencing the pitching moment and the asymmetric lift is also responsible for a yawing effect as well. With TOLS configurations, a less pronounced result of simultaneous disturbances around pitch, roll and yaw is expected since the four semi-wing panels will collectively offset each other. It is emphasized that aerodynamic coupling due to the asymmetric layout of the upper and lower wing in side-view will still be an issue but is postulated to be at a more manageable (therefore at more easily solvable) level.

TOLS-X flight control is to be a triplex fly-by-wire with two digital modes (a primary and backup) and an analog mode. Trim for this configuration requires the equilibrium of six highly non-linear forces and moments. In view of the longitudinal and lateral motions being coupled, a good deal of research will need to take place on identifying optimal combinations of control surface deflection. One method is to decouple the dynamic modes so that handling quantities are similar to those of a conventional symmetric swept wing aircraft. With respect to oblique wing aircraft designs, Kroo[17] indicates that several approaches to address this control law definition problem are under investigation. One area of research suggested by Kroo is to compile data about the correlation of aerodynamic coupling to handling qualities and pilot ratings. In principle, the results and conclusions drawn from these studies would be

relevant to aircraft employing TOLS configurations.

In an attempt to exploit benefits from control-configured vehicles, a possibility exists to reduce structural weight via manoeuvre load alleviation. For vehicles operating in the transonic speed regime and for those having high aspect ratio wings, this function reduces the wing root bending moment by re-orienting the spanwise lift distribution so that the magnitude of outboard loading is minimized. This effect is achieved by scheduling the flaperon deflections in a relative manner using advanced control laws. A technology factor to reflect benefits associated with manoeuvre load alleviation was not employed for this particular study.

EMPENNAGE – The empennage consists of a single surface vertical tail with no provision given for a horizontal stabiliser. A vertical fin and rudder constitutes the vertical tail. The rudder comprises one segment, is supported by two hinges attached to the rear of the vertical stabiliser and the deflection range is 30° for both TE left (+) and TE right (-). The vertical tail has an aspect ratio of 1.0 and taper ratio of 0.35. With a quarter chord sweep of 48°, increased moment arm due to sweepback of the fin is beneficially generated.

UNDERCARRIAGE – The landing gear is a tricycle type arrangement consisting of two main gear assemblies mounted on the fuselage lower portion just aft of the lower oblique wing root centre-section, and a nose gear mounted on the forward fuselage beneath the flight deck. Extension and retraction is hydraulically actuated and electrically controlled. The nose gear retracts forward into the nose gear bay while the main gears shall retract rearward into the main landing gear bay located in the fuselage fairing aft of the lower oblique wing. For the main landing gear, a trailing arm design shall be adopted. All shock absorbers are of the oleo-pneumatic type, and each gear strut is equipped with two wheels. The main gears shall be equipped with two power operated carbon brake assemblies that provide anti-skid performance. The nose gear shall have a hydraulically powered steering system with shimmy damping.

STRUCTURAL DESIGN – Fore and aft variation of the TOLS planforms distributes volume uniformly with that of the fuselage thus negating the need for fuselage cross-section reduction and complex double curvature. The skewed wingbox structure is to become continuous between regions close to the wingtips, and, both upper and lower assemblies shall be mated to the fuselage in one piece. Individual ribs and other sub-assemblies such as constituents that make up the wingtips are to be duplicated as much as possible. Advantages include greater parts commonality between each of the four semi-wing panels and much simpler construction compared to symmetrically swept aircraft wings.

Fuselage – The structure of the fuselage consists of three major assemblies: front - nose with cockpit; centre - cabin; and, aft - rear section including the aft fuselage auxiliary fuel tank and cargo compartment. With the exception of fore and aft sections, the fuselage is cylindrical with a 2.31 m (7.6 ft) maximum diameter cross-section.

The front section comprises the radome, nose landing gear attachments, electronics/avionics, the hydraulic bay and pilot compartment. The centre section constitutes the passenger cabin including windows, entrance/emergency exits, overhead baggage racks, stowage compartments and seat attachments. Plug type doors are standard. The floor is capable of withstanding a maximum floor loading of 732 kg/m^2 (150 lb/sq.ft). Two specially reinforced frames are to be incorporated for upper and lower wing interface. Space has been provided below the floor and within the region of the wing-fuselage attachment fairing for fuel storage as well as systems and equipment installation, and, landing gear housing. The aft section consists of: a rear pressure bulkhead; auxiliary fuel tank; baggage compartment; compartments for ancillary electrical/electronic systems; and, empennage supporting structure. The baggage compartment floor area and volume are 2.55 m^2 (27.5 sq.ft) and 5.35 m^3 (189 cu.ft).

The fuselage maximum pressure differential is 64.2 kPa (9.3 psi). The pressurised area is confined by a flat bulkhead located forward of the flight deck and a flat rear bulkhead located forward of the aft fuselage auxiliary fuel tank. In the regions cut by the upper and lower wings, the pressurised area maintains integrity by way of a pressure floor and ceiling outside the wing

carry-through sections.

Wing – The upper and lower wing structures are complete and continuous assemblies and interfaced to the fuselage top and belly by two reinforced frames. The structure accommodates flaperons or simple plain flaps, integral fuel tanks, one centre fuel tank and the main landing gear attachment assembly. Each wing structure consists of two spars, upper and lower skins, stringers and ribs. Air loads are carried by the front and rear spars that are located at 15% and 60% of local swept chord respectively. Each of the rear spars from outer wing to WPEBS interface, then towards the wing-fuselage interface closes out the flaperon bay and supports control systems therein. This spar also closes out the integral fuel tanks as well; the entire box beam encloses two distinct integral fuel tanks. The central wing torsion box consists of two beams that run in the same sense as wing skew. Aft of the lower wing planform centre wingbox, a box beam yielded from a Keelson and closed by a beam perpendicular to the fuselage contour houses the main landing gear as well as various equipment and systems.

The wing leading edges are detachable parts, made of metal and facilitate anti-icing. The flaperons are each a mono-spar structure hinged on four supports attached to the wing rear spar and collectively extend out to

80% of wing semi-span. The two most inboard flaperons that extend out to 65% semi-span also act as the secondary flight control surface group, i.e. high-lift arrangement, in-flight spoilers, speed-brakes and ground spoilers with interconnected controls to prevent asymmetric operation. The entire flaperon system acting as spoilers can be deployed in unison during rejected takeoff procedures and landing ground-roll.

Aeroelasticity – A structural divergence problem or lack of structural stiffness of the forward semi-wings (lower wing to port and upper wing to starboard) was initially surmised by the author as causing greatest potential for difficulties with TOLS configurations. However, Jones and Nisbet[31] have shown analytically and experimentally that due to lift load alleviation during rolling motion when the forward wing is deflected, oblique wing aircraft could be flown at speeds faster than the clamped divergence speed without instability. This result established the notion that structural divergence for TOLS would probably be a mute point in relation to the other primary consideration of upward bending for instance.

Wing deformation demonstrates the importance of bending for the forward semi-wings since there exists a direct influence on wing aerodynamic qualities and formulation of a consistent control system protocol suitable for the entire flight envelope. The undesirable traits of this phenomenon are postulated as being minimised by virtue of the WPEBS integration. A somewhat reduced cantilever ratio from the WPEBS juncture point to each of the four respective wingtips is perceived as countering any weight penalties incurred compared to the equivalent cantilevered wing premise. As another avenue to improve structural efficiency, consideration might be given to aeroelastic tailoring[31]. This would involve entertaining the notion of employing carbon fibre materials technology for TOLS-X even though this particular study adheres to application of metal alloys only.

FUEL TANKS AND SYSTEM – Similar to the Gulfstream G200, Embraer Legacy, Bombardier CL-604 Challenger, Dassault F900EX and Bombardier Global Express business jets, fuel is stored in multiple cells within the wing and fuselage. Locales include: an integral tank in the lower wing centre section (capacity 867 litres; 229 USG); one in each of the four semi-wings (totalling 5712 litres; 1509 USG); saddle and underfloor tanks forward of the lower wing centre-section (capacity of 8564 litres; 2262 USG); and, an auxiliary tank located aft of the fuselage (3223 litres; 851 USG); the projected maximum usable fuel capacity is 18366 litres (4851 USG). All auxiliary tanks located in the fuselage were required to supplement the four wing fuel tanks, which were too small to hold more than 31% of required fuel. To improve balance and loadability, a selective fuel management system shall be incorporated.

To limit centre of gravity shifts with changes in aircraft attitude and restrict fuel sloshing, wing ribs act as integrated baffles in each wing tank. Access doors to the fillers are installed in upper wing panels for each semi-wing. Gravity refuelling is made possible via these fillers. A single point pressure refuelling facility is located rear of the aft fuselage auxiliary tank. Gravity de-fuelling is accomplished via dump valves installed on the wing tanks' lower surface. Fuel is to be supplied to each engine by an engine driven integral fuel pump. A DC electrically powered positive displacement pump in each fuel tank is to be provided for redundancy.

PROPULSION SYSTEM - The power plant installation consists of two hypothetical BMW Rolls-Royce BR71X turbofans and is a derivative based on the BMW Rolls-Royce BR715 turbofan. The engines are to be flat-rated to ISA+20°C ambient conditions. The nacelles are located at 42% semi-span and do facilitate thrust-reversing capability. Each podded installation is a pylon-nacelle-pylon arrangement in which the pylon provides redundant support. Each pylon has two spars (longerons) - upper and lower major bulkheads, and is attached to the wing at four primary points through the use of two mid-spar fittings, an upper link and a diagonal brace (drag strut). Each nacelle adopts a long ducted shape, measures 5.70 m (18.7 ft) in length and is vertically aligned between each upper and lower wing stations such that the pylon heights are congruent.

AERODYNAMIC DESIGN QUALITIES

High-lift Characteristics – In a concerted effort to avoid undue sophistication for the sake of promoting improved dispatch reliability, reducing zero-lift drag increments incurred from flap supports; avoiding the structural complications of multi-track supports and extension mechanisms, and, the associative weight penalties of utilising chord extending leading edge and trailing edge flaps, the TOLS-X design utilizes a simple plain flap for high-lift. The array of flap settings available for field performance is designated as 0°, 15°, 30° and 60°.

Experimental data had shown that this arrangement is characterized by an optimum flap deflection angle of 60° and an optimum flap chord ratio of approximately 0.25. The TORNADO VLM module within QCARD-MMI software package was executed to set minimum goals for TOLS-X high-lift performance. For a takeoff flap setting of 30º, the incremental contribution was estimated to be ΔC_{L30} = 0.51. Similarly, for a landing flap setting of 60°, a ΔC_{L60} of 1.03 resulted, thus giving a predicted maximum lift coefficient of 2.26. The landing C_{Lmax} compares favourably with contemporary large and super-large business jets; the TOLS-X minimum goal is approximately 0.09 or 4% less than the best performing high-lift configuration employing both double slotted trailing edge flaps and leading edge slats. Notwithstanding comparable lift coefficients between TOLS-X and contemporary business jets with flaps deployed, one undesirable trait is the higher wing loading does translate into somewhat higher stalling speeds and hence reference speeds.

Subsonic En route Drag – The greatest disadvantage TOLS configurations have is a noticeable zero-lift drag penalty – attributable to shorter wing chords being approximately half of single wing vehicles. This generates a lower magnitude of Reynolds number and in conjunction with a very preliminary assumption of 5% chordwise flow transition for wing surfaces only, a correspondingly higher value of skin friction results. In this study, TOLS-X was predicted to produce a vehicular skin friction coefficient of between 0.0040 and 0.0042, which can be considered to be towards the much higher threshold of modern transport aircraft. Even though the possibility was not thoroughly investigated in this study, it is highlighted that using HSNLF aerofoil sections designed specifically for a lower Reynolds number operation to draw out the extent of chordwise laminarisation could reduce such a drag penalty.

Transonic Wave Drag Increment – The difference in zero-lift drag coefficient between the fastest Mach number and the Critical Mach (M_{CR}; where compressibility effects become significant) is defined as transonic wave drag. Figure 5 shows the breakdown of drag constituents for M0.80, M0.95 and M1.20 forward speeds. M_{CR} was found to occur around M0.73 for an operational C_L range of between 0.3-0.5. This value is similar to the M_{CR} speeds found on contemporary turbofan transport designs employing the now mainstay super-critical wing sections. Based on wing reference area, the total wave drag coefficient (volume and lift dependent) increment at M1.20 was predicted to be 146 counts. The maximum cross-section area was derived from the cross-section area development plot generated by QCARD-MMI and is shown in Figure 6 above. Note that the streamtube area has been subtracted from the cross-sections, i.e. 10% of the nacelle inlet capture area was retained to account for an inlet mass-flow ratio of 0.90.

Because wave drag is more a function of cross-section area than reference wing area, it is appropriate to consider the wave drag coefficient based on cross-section area. Figure 7 presents transonic aerodynamic performance of TOLS-X plotted against results obtained for military and experimental aircraft published by Jobe[33], and, Saltzman and Hicks[34]. The ordinate is referenced to maximum cross-section area from which the equivalent diameter is derived for the fineness ratio merit function on the abscissa. It is discernable that the TOLS-X configuration in keeping with satisfactory area-ruling practise exhibits quite desirable transonic wave drag traits; showing qualities in step with significantly older and aerodynamically efficient transonic configurations than contemporary military and experimental aircraft.

Lift-to-Drag Ratio and Aerodynamic Efficiency – Figure 8 shows the variation of lift-to-drag (L/D) with Mach number for three operating lift coefficients of 0.3, 0.4 and 0.5. A bounded speed range is presented for each operating C_L and this is attributable to limitations in instantaneous gross weight as dictated by the TOLS-X vehicular definition.

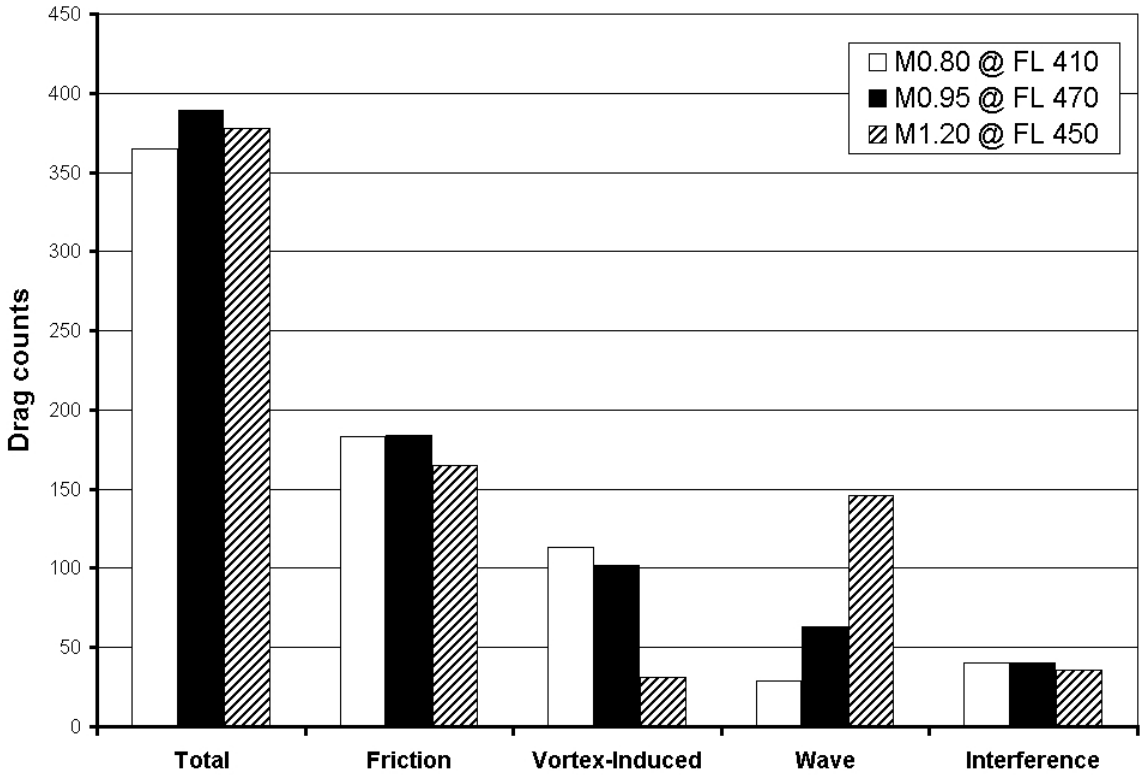

Figure 5. Total and constituent breakdown of TOLS-X drag at various cruise speeds (85% MTOW).

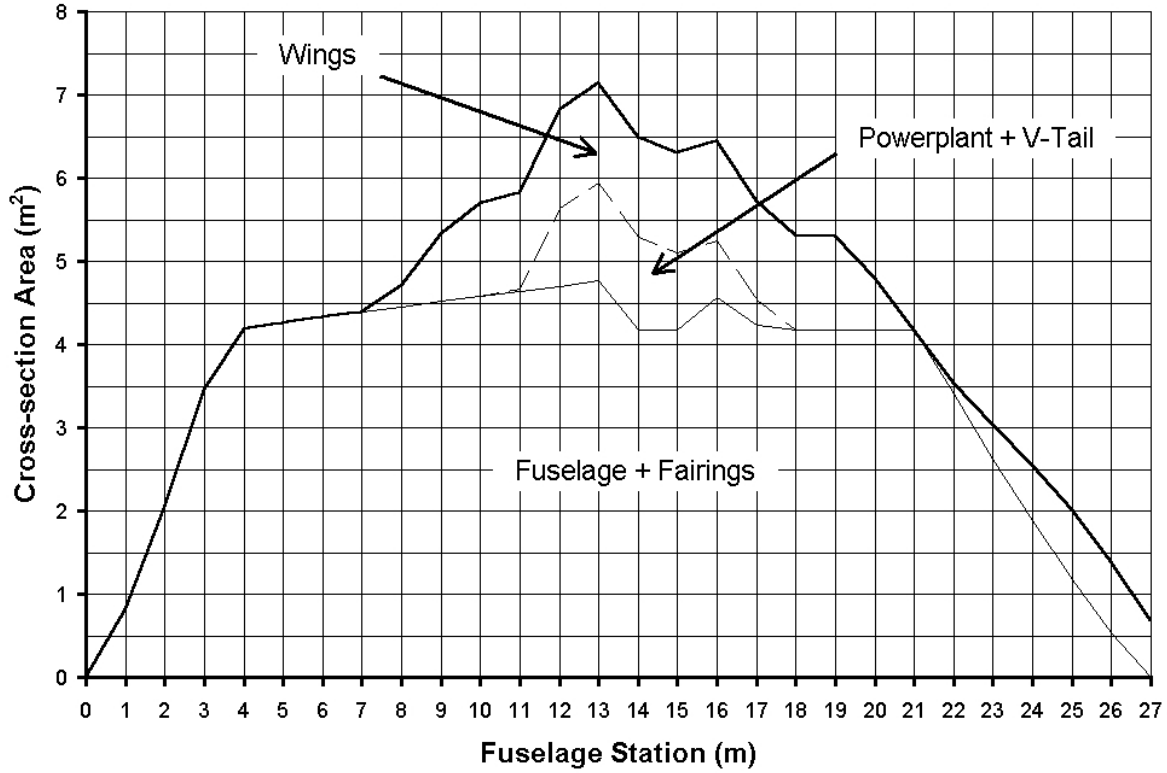

Figure 6. Cross-section area development plot of TOLS-X configuration at sonic speed.

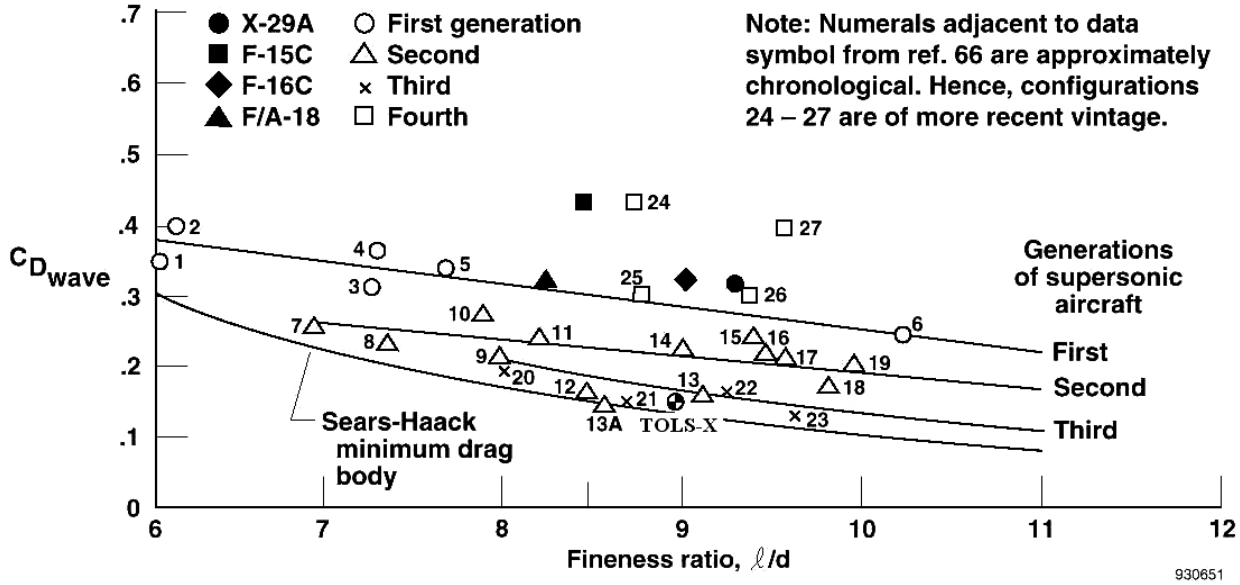

Figure 7. Historic correlation of wave drag sourced from Jobe[33], and, Saltzman and Hicks[34] compared to TOLS-X concept.

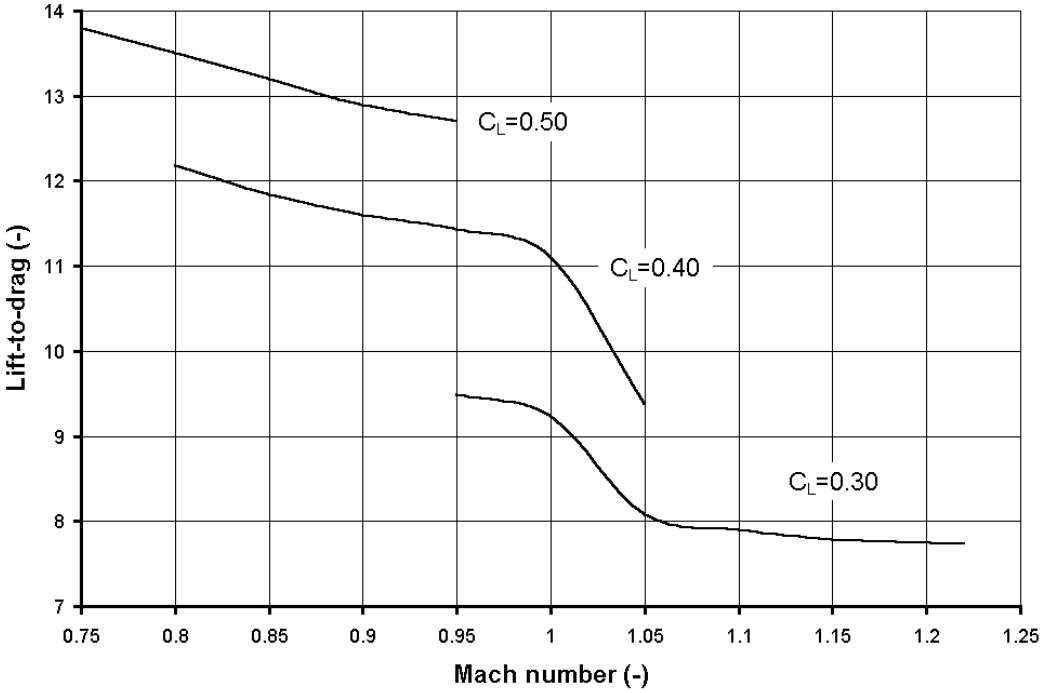

Figure 8. Variation of L/D ratio with Mach number for operating lift coefficients of 0.3, 0.4 and 0.5.

At a typical commercial Trans-Atlantic operation altitude of FL 370, TOLS-X can achieve an operating Long Range Cruise (LRC) M*L/D (or aerodynamic efficiency merit function) value of 10.9; this figure is approximately 22% lower than contemporary single-aisle long-range transports flying at an LRC speed schedule of M0.80. If one considers a TOLS-X typical cruise speed technique of M0.95 (corresponding to an operating C_L of 0.475 at FL 470), M*L/D values close to 12.0 are predicted, and this contrasts as +12% over the single-aisle long-range transports flying at MCRZ speed schedule of M0.85 (12% slower). In addition, TOLS-X displays an M*L/D advantage of anywhere between +4% to +25% compared to the super-large business jets at M0.85. At a cruise speed of M1.22, M*L/D parity occurs between TOLS-X and super-large business jets at MCRZ. Even though, en route efficiency is somewhat lacking at contemporary business jet LRC speed schedules and altitudes, it is evident that TOLS-X is optimised specifically for missions above FL 410 and speeds greater than M0.90.

FLIGHT ENVELOPE, PERFORMANCE SYNOPSIS AND COMPETITIVE ANALYSIS – The unique aerodynamic design behind TOLS and WPEBS integration allows for a much broader flight envelope compared to contemporary large and super-large business jets. Flight at FL 510 and speeds up to M1.26 (723 KTAS) are achievable. The flight envelope is presented in Figure 9.

Figure 10 shows the predicted TOLS-X payload-range capabilities, whilst Table 2 summarises estimates of the major performance characteristics and compares these with current market equipment. Comparison of TOLS-X to these vehicles is based on technically analysed data taken from originally published marketing information.

Cabin – TOLS-X cabin and baggage volume is the biggest in the class of large and super-large business jets. The gross cabin volume less baggage is superior by at least 30%, and the baggage compartment is at least 11% larger than competitor aircraft. The 190-220 mm (7-9 in.) difference in maximum internal and floor width between Dassault products and Gulfstream GIV-SP and the TOLS-X design produced in this study indicates the superiority of F2000 and F900EX in terms of cabin cross-section.

Takeoff and Landing – Takeoff distance for TOLS-X is approximately 4-12% longer (maximum +192 m; +630 ft) compared to the F2000, F900EX and GIV-SP. This can be regarded as satisfactory because the hard specification limit of 1830 m (6000 ft) has not been violated. One unsavoury aspect of TOLS-X takeoff field performance is the reference speeds. A decision speed of 165 KCAS is quite fast, approximately +15 KCAS to +35 KCAS upon comparison to the large and super-large business jets. Further scrutiny showed this speed is equivalent to a B737-400 at Flaps 5, but since the TOLS-X V_2 speed does not violate an upper threshold exhibited by contemporary commercial transports, was considered to be within the realm of tacit acceptability. Nonetheless, one suggestion might be to investigate ways in reducing this without compromising the global design considerations. The landing distance at MLW is estimated to be 881 m (2890 ft) with corresponding landing field length equal to 1468 m (4820 ft) at ISA, sea level ambient conditions. TOLS-X displays better attributes in this

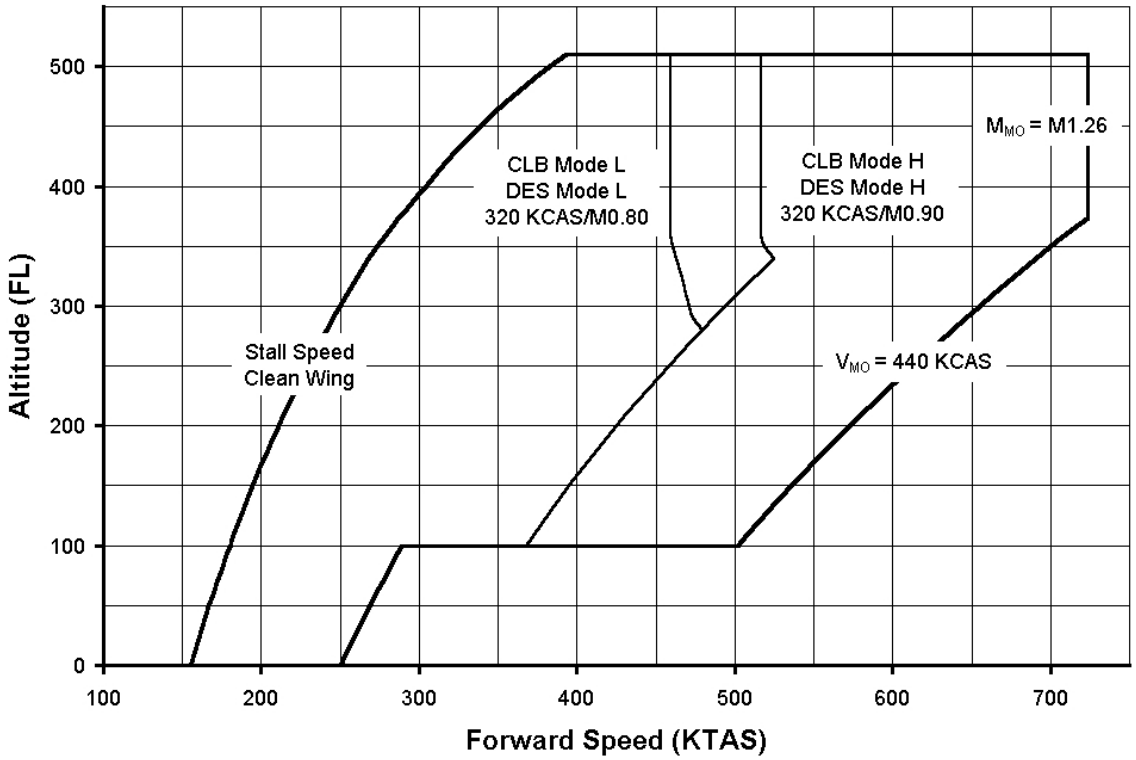

Figure 9. Flight envelope for TOLS-X business jet transport.

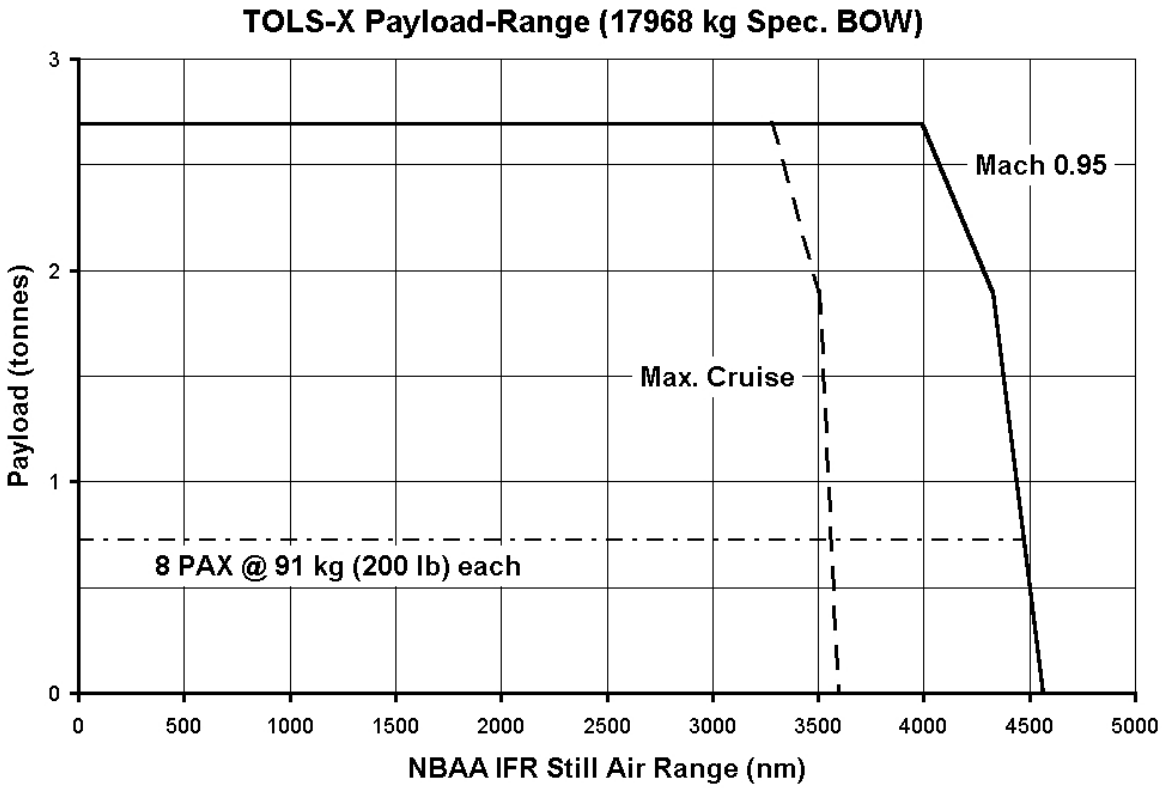

Figure 10. Payload-range envelope for TOLS-X business jet transport.

Table 2. Parametric review of TOLS-X against contemporary large and super-large business jets.

	TOLS-X	Falcon 2000	Falcon 900EX	GIV-SP
External Length (m)	29.6	20.2	20.2	26.9
External Height (m)	7.48	7.07	7.56	7.44
Fuselage Diameter (m)	2.31	2.50	2.50	2.38
Engines	2 x RR-BMW BR71X	2 x CFE CFE738-1-1B	3 x Honeywell TFE731-60	2 x RR Tay Mk 611-8
Unit Output (kN)	71.2	26.3	22.3	61.6
Span [Excl. Winglets] (m)	20.5	19.3	19.3	23.2
Ref. Wing Area (m^2)	71.6	47.8	47.8	88.3
Ref. Aspect Ratio (-)	8.79	7.80	7.82	6.08
Q.Chd Sweep (deg.)	31.0	25.6	25.6	26.8
Wing loading (kg/m^2)	482	347	465	383
Thrust-to-Weight (-)	0.426	0.324	0.306	0.371
Cabin Seating Length (m)	14.0	5.73	7.70	7.77
Internal Height (m)	1.83	1.89	1.89	1.89
Max. Internal Width (m)	2.16	2.35	2.35	2.23
Cabin Floor Width (m)	1.70	1.92	1.92	1.68
Cabin Vol. Less Bagg. (m^3)	49.9	25.2	35.8	38.4
Baggage Volume (m^3)	5.35	3.80	3.60	4.79
MRW (kg)	34593	16647	22317	34020
MTOW (kg)	34493	16556	22226	33838
MLW (kg)	31000	14969	19051	29937
MZFW (kg)	20660	13000	14000	22226
Spec. BOW (kg)	17968	9730	11204	19278
BOW/MTOW (-)	0.521	0.588	0.504	0.570
Max Payload (kg)	2693	3270	2796	2948
Max Fuel (kg)	14729	5513	9526	13381
Payload @ Max Fuel (kg)	1896	1404	1588	1361
M_{MO} (Mach)	1.26	0.870	0.870	0.880
V_{MO} (KCAS)	440	370	370	340
Certified Ceiling (ft)	51000	47000	51000	45000
TOFL, sl ISA, MTOW (m)	1823	1760	1631	1661
LD, sl ISA, MLW (m)	881	953	1073	972
V_{REF} at MLW (KCAS)	133	122	132	149
CLB Schedule Initial Cruise Altitude (ft)	320KCAS/M0.80 51000	260KCAS/M0.75 41000	260KCAS/M0.72 39000	300KCAS/M0.75 41000
LRC Speed (Mach)	0.90	0.75	0.77	0.77
Max Cruise (Mach)	1.22	0.83	0.85	0.85
Range[(1)] @ LRC (nm)	4460	3110	4320	4125
SAR[(1)] @ LRC (nm/kg)	0.336	0.656	0.509	0.348
Range[(1)] @ MCRZ (nm)	3560	NA	3549	3200
SAR[(1)] @ MCRZ (nm/kg)	0.268	NA	0.417	0.271

(1) 8 PAX @ 200 lb per PAX, NBAA mission and IFR reserves.

respect compared to the large and super-large business jets. A landing reference speed of 133 KCAS is another positive trait comparable to that of the F900EX. In view of the above analysis, it can be surmised intentions of producing a vehicle to conduct effective operations in and out of relatively short airfields has been realised with TOLS-X.

Climb – TOLS-X maximum rate of climb of 5340 fpm at sea level is around 30-56% higher than contemporary large and super-large business jets. It is common practise to assign at least two distinct climb modes, or more specifically, two different speed schedules for climb control that complements cruising techniques. A slow climb speed technique (CLB Mode L) and faster climb speed schedules (CLB Mode H) are also formulated with regards to optimal climb trajectory profile state and time function adherence and designated divergence criteria respectively. Owing to the considerable amount of specific excess power available at maximum climb thrust, a 33% de-rate was invoked by setting the criterion TOLS-X should cruise initially at maximum service ceiling or FL 510 using CLB Mode H speed techniques. Notwithstanding the significant maximum climb thrust de-rate, this still translates into exceptional time-to-climb to altitude FL 370 and maximum service ceiling of FL 510 in 13 minutes and 23 minutes respectively assuming MTOW at brakes release. Even though TOLS-X frequently flies in the drag rise and divergence regime that promotes optimum (or maximum SAR) altitudes below the service ceiling, further increases in de-rate were

disregarded to permit operator flexibility of slotting into higher altitudes if traffic congestion at lower airways becomes an issue.

Cruise – LRC, TSC and HSC show an appreciable difference between the TOLS-X and contemporary large and super-large business jets. LRC is at least 75 KTAS and TSC (at M0.95) is 85 KTAS faster than the F900EX and GIV-SP business jets above the tropopause. The maximum cruise speed capability of up to +210 KTAS for TOLS-X has opened up a totally new regime of lower block times. It is evident that the Dassault range of aircraft display quite superior en route performance efficiency characteristics compared to TOLS-X; as exemplified by a greater than 50% better SAR (at 14% and 30% slower speeds for LRC and HSC respectively) of the F900EX. The GIV-SP however, has SAR attributes more in-line with TOLS-X consistently demonstrating a +4% to +1% advantage but again at 14% and 30% slower speeds for LRC and HSC respectively. Even though the F900EX has more desirable en route burn attributes, TOLS-X has fulfilled the main objective of matching en route efficiency characteristics to a primary competitor, namely the GIV-SP, whilst permitting a marked increase in block speed performance.

CONCLUSION

The TOLS-X vehicle proposal is an executive jet concept that accommodates a maximum of 19 passengers and affords excellent comfort through speed, spaciousness and amenities not paralleled by contemporary large and super-large business jets. This business/corporate jet works off a contemporary turbofan technology level, i.e. by virtue of being a derivative of the BMW Rolls-Royce BR715. The marked increase in block speed of TOLS-X does require a trade off in higher fuel flow as denoted by lower Specific Air Range (SAR) values compared to the smaller and lighter Dassault F2000 and F900EX business jets. However, upon comparison to an equivalent airframe in size and weight, such as the Gulfstream GIV-SP, it was found that comparable SAR values are produced at speeds that are 17-44% faster. Irrespective of the dramatic increase in cruising speeds, effective field performance has been maintained and permits the original hard specification of operations in and out of relatively short airfields.

Various issues needed to be addressed with the Twin-Oblique Lifting Surfaces (TOLS) design. One drawback was the greater structural weight of TOLS integrated with the wing-pylon-engine bracing structural system (WPEBS) compared to a cantilevered single wing equivalent. It was appreciated from the outset that the TOLS configuration would possess some benefit from a structural efficiency perspective. Ideally, a piece-wise linear beam model would have been employed in estimating the bending material weight. Unfortunately, owing to an absence of this functionality, and even an equivalent conceptual method, possibilities of investigating for leaner structural weight was not realised. The higher wing loading and modest lift increments at lower flap deflections using the assumed plain flapping arrangement translates into higher stall speeds and hence reference speeds during takeoff. Another disadvantage was an increase in zero-lift drag due to a significantly lower Reynolds number generated by the smaller local wing chords characteristic of TOLS configurations and a preliminary assumption of 5% chordwise laminarisation on wing surfaces only. This aspect can be enhanced with application of aerofoils specially optimised (such as modified HSNLF-1-0213 section) for low Reynolds number thus promoting further aft chordwise flow transition. As a final note for improvement, since this particular investigation concentrated on a very limited scope of multivariate optimisation, it is suggested that application of Multi-disciplinary Design Optimisation (MDO) techniques would be an advantageous step. This procedure should realise the most efficient vehicular candidate when considering all the primary disciplines concurrently.

This paper has shown the potential of the TOLS layout integrated with WPEBS for high-speed mission capability compared to the conventional wisdom of delta wing designs employed on all modern supersonic business jet proposals. It is granted the highly exotic nature of the TOLS configuration will be met with less than a favourable reaction from crews and passengers alike. Notwithstanding this negative aspect, it must be highlighted that unless a radical shift in vehicle configuration design is entertained, significant strides in performance will not come to fruition - not even incremental increases in speed up to the high transonic to low supersonic regime. The results in this study demonstrate there exists a feasibility, and if the abovementioned areas of conservative assessment can be rationalised through future research, it is projected the TOLS layout will become even more of an appealing proposition.

REFERENCES

1. Taylor, J., Munson, K., “History of Aviation”, Crown Publishers Inc., 1978.
2. Campbell J.P., Drake, H.M., “Investigation of Stability and Control Characteristics of an Airplane Model with Skewed Wing in the Langley Free-Flight Tunnel”, NACA TN 1208, 1945.
3. Jones, R.T., “New Design Goals and a New Shape for the SST”, Astronautics and Aeronautics, Vol. 10, No.12, December 1972.
4. Jones, R.T., Nisbet J.W., “Transonic Transport Wings – Oblique or Swept?”, Astronautics and Aeronautics, January 1974.
5. Olson E.C., Selberg, B.P., “Experimental Determination of Improved Aerodynamic Characteristics Utilising Biplane Wing Configurations”, Journal of Aircraft, Vol. 13, April 1976.

6. Rhodes, M.D., Selberg, B., “Dual Wing, Swept Forward Swept Rearward Wing, and Single Wing Design Optimisation For High Performance Business Airplanes”, ICAS-82-1.4.2, 1982.
7. Pfenninger, W., “Design Considerations of Large Subsonic Long Range Transport Airplanes with Low Drag Boundary Layer Suction,” Northrop Aircraft, Inc., Report NAI-58-529 (BLC-111), 1958. (Available from DTIC as AD 821 759).
8. Gundlach IV, J.F., Naghshineh-Pour, A., Gern, F., Tetrault, P.-A., Ko, A., Schetz, A., Mason, W.H., Kapania, B., Grossman, B., Haftka R.T. (University of Florida), “Multidisciplinary Design Optimisation and Industry Review of a 2010 Strut-Braced Wing Transonic Transport”, MAD 99-06-03, Department of Aerospace and Ocean Engineering, Virginia Polytechnic Institute and State University, June 1999.
9. Isikveren, A.T., ” Methodology for Conceptual Design and Optimisation of Transport Aircraft”, Report 98-8, Royal Institute of Technology, Department of Aeronautics, Sweden, 1998.
10. Kendall, E.R., “The Minimum Induced Drag, Longitudinal Trim and Static Longitudinal Stability of Two-Surface and Three-Surface Airplanes”, AIAA-84-2164, 1984.
11. Obert. E., “Some Aspects of Aircraft Design and Aircraft Operation”, Lecture Series, Sweden, 1996.
12. Durand, W.F., “Aerodynamic Theory”, Vol. V, January 1943.
13. Saab 2000 Type Specification, 73VPS010, Revision F, Saab Aerospace AB, November 1996.
14. Isikveren, A.T., ”Methodology for Conceptual Design and Optimisation of Transport Aircraft”, ICAS 98-7.8.2, September 1998.
15. Svoboda, C., “Turbofan Engine Database as a Preliminary Design Tool”, Aircraft Design 3 (2000) 17-31, Aircraft Design Journal, 2000.
16. Whitford, R., “Design for Air Combat“, Jane’s Information Group Ltd., date not available.
17. Kroo, I., “The Aerodynamic Design of Oblique Wing Aircraft”, AIAA Paper 86-2624, October 1986
18. van der Velden, A.J.M, Torenbeek, E., “Design of a Small Oblique-Wing Transport Aircraft”, Journal of Aircraft, Vol. 26, No. 3, March 1989.
19. Isikveren, A.T., ”The PD340-2 19 Passenger Turbofan Regional Transport- Feasibility Study”, Report 98-5, Royal Institute of Technology, Department of Aeronautics, Sweden, 1998.
20. Mason, W.H., “Analytical Models for Technology Integration in Aircraft Design”, AIAA-90-3262-CP, 1990.
21. Jones, R.T., “The Oblique Wing – Aircraft Design for Transonic and Low Supersonic Speeds”, Acta Astronautica, Vol. 4, Pergammon Press, 1977.
22. Torenbeek, E., ”Synthesis of Subsonic Airplane Design”, Delft University Press, 1988.
23. Raymer, D.P., ”Aircraft Design: A Conceptual Approach”, AIAA Educational Series, 1992.
24. Melin, T., “A Vortex-Lattice MATLAB Implementation for Linear Aerodynamic Wing Applications”, Masters Thesis, Royal Institute of Technology, Department of Aeronautics, Sweden, December 2000.
25. Wauquiez, C., Rizzi, A., “PABLO – Potential Flow Around Airfoils with Boundary Layer coupled One-way”, Royal Institute of Technology, Department of Aeronautics, Sweden, 1999.
26. Young, A.D., ”The Aerodynamic Characteristics of Flaps”, Aeronautical Research Council, Technical Report No. 2622, 1953.
27. Linnell, R., “Weight Estimation Methods”, FKHV-1-RL790724:01, Saab AB, July 1979.
28. Scott, P.W., Nguyen D., ”The Initial Weight Estimate”, SAWE Paper No. 2327, Index Category No. 11, MDC 96K0030.
29. Torenbeek, E., “Development and Application of a Comprehensive, Design-sensitive Weight Prediction Method for Wing Structures of Transport Category Aircraft”, Report LR-693, Delft University of Technology, Faculty of Aerospace Engineering, The Netherlands, October 1994.
30. Sewall, W.G., McGhee, R.J., Viken, J.K., Waggoner, E.G., Walker, B.S., Millard, B.F., “Wind tunnel results for a high-speed, natural laminar-flow airfoil designed for general aviation aircraft”, NASA-TM-87602, NASA Langley Research Centre, November 1985.
31. Jones, R.T., Nisbet J.W., “Aeroelastic Stability and Control of an Oblique Wing”, The Aeronautical Journal of the Royal Aeronautical Society, August 1986.
32. Weisshaar, T., Zeiler, T., “Dynamic Stability of Flexible Forward Swept Wing Aircraft”, Journal of Aircraft, December 1983.
33. Jobe, C.E., “Prediction of Aerodynamic Drag”, AFWAL-TM-84-203, Flight Dynamics Laboratory, Air Force Wright Aeronautical Laboratories, Wright-Patterson Air Force Base, OH 45433, July 1984.
34. Saltzman, E.J., Hicks, J.W., “In-Flight Lift-Drag Characteristics for a Forward-Swept Wing Aircraft (and Comparisons with Contemporary Aircraft)”, NASA Technical Paper 3414, December 1994.

ADDITIONAL SOURCES

1. Abbott, I.H., Von Doenhoff, A.E., ”Theory of Wing Sections”, Dover Publications, 1959.
2. Clancy, L.J., ”Aerodynamics”, Longman Scientific & Technical, 1975.
3. Currey, N., ”Aircraft Landing Gear Design: Principles and Practises”, AIAA, 1988.
4. Gillette, W.B., ”Nacelle Installation Analysis for Subsonic Transport Aircraft”, AIAA Paper 77-102.
5. Graham, A., Jones, R.T., Boltz, F., “An Experimental Investigation of Three Oblique Wing and Body Combination at Mach Numbers Between 0.6 and 1.4”, NASA TM X-62256, April 1973.
6. McCormick, B.W., ”Aerodynamics, Aeronautics and Flight Mechanics”, John Wiley & Sons, 1979.

7. Nelms, Jr., W.P., “Applications of Oblique-Wing Technology – An Overview”, AIAA Paper 76-943, September 1976.
8. Niu, M.C.Y., ”Airframe Structural Design”, Conmilit Press Ltd., 1989.
9. Roskam, Dr. J., ”Airplane Design”, Vol. I-VII, 1986.
10. Schippers, K.A., ”Cowl Design Methodology”, D6-41800 TN (unreleased), Boeing Airplane Company.
11. Tipton, B.J., Dudley E.S., “The Preliminary Design Analysis of a Unique Semi-Tailless Aircraft Configuration”, AIAA Paper 952053, 1995.

ACRONYMS AND ABBREVIATIONS

a.c.	Aerodynamic centre
AEO	All Engines Operational
BOW	Basic Operating Weight
BPR	By-Pass Ratio
CFD	Computational Fluid Dynamics
CLB Mode H	Climb Mode High speed technique
CLB Mode L	Climb Mode Low speed technique
FAR	Federal Aviation Regulations
FL	Flight Level
HSC	High-Speed Cruise
HSNLF	High-Speed Natural Laminar Flow
IFR	Instrument Flight Rules
JAR	Joint Airworthiness Regulations
KTH	Royal Institute of Technology (KTH), Stockholm, Sweden
LD	Landing distance
LRC	Long Range Cruise
MCRZ	Maximum Cruise
MLW	Maximum Landing Weight
MRW	Maximum Ramp Weight
MTOW	Maximum Takeoff Weight
MZFW	Maximum Zero-Fuel Weight
NACA	National Advisory Committee for Aeronautics
NBAA	National Business Aviation Association
OEI	One Engine Inoperative
OPR	Overall Pressure Ratio
PAX	Passengers
SAR	Specific Air Range
SBW	Strut-Braced Wing
TE	Trailing Edge
TED	Trailing Edge Down
TEU	Trailing Edge Up
TOFL	Takeoff field length
TOLS	Twin Oblique Lifting Surfaces
TSC	Typical Speed Cruise
TSFC	Thrust Specific Fuel Consumption
USG	U.S. gallons
VLM	Vortex-Lattice Method
WPEBS	Wing-Pylon-Engine Bracing Structural system

intentionally blank

Paper IV

Identifying Economically Optimal Flight Techniques of Transport Aircraft

intentionally blank

Identifying Economically Optimal Flight Techniques of Transport Aircraft

Askin T. Isikveren*
Royal Institute of Technology (KTH), Stockholm, Sweden

A treatment of identifying optimal flight techniques for transport aircraft with respect to direct operating cost and profit or return on investment is derived for given sector mission criteria and assumed reference time frame utilisation. A series of models used to accurately simulate maintenance and materiel costs, block fuel expenditure and revenue have been introduced in order to force the direct operating cost, and, profit or return on investment expressions as continuous functions allowing for determination of their respective minima and maxima. The selection of utilisation (hourly or fixed number of sectors) per reference time frame was found to be an important precursor to what type of flight technique is to be expected. An hourly-based utilisation results in faster block speeds tending towards the minimum block time threshold of a given vehicle and sector mission, whilst, the fixed departures scenario yields a slower yet congruous flight technique optima requirement for direct operating cost and profit or return on investment objectives. Details are given to show how the methodology may be integrated for the purpose of conducting competitor reviews during fleet planning exercises, and also, how one may facilitate the optimisation of conceptual aircraft designs via inspection of some useful merit parameters.

Nomenclature

a_{sls} = sonic speed at ISA sea level standard conditions
BH = block hour
C_{ACQ} = aircraft acquisition cost and interest payable per sector (taking residual value into account becomes equivalent to depreciation cost)
C_{CONB} = block time related contingency cost per sector
C_{CONF} = flight time related contingency cost per sector
C_{CREW} = crew salary cost per sector
C_{DOCS} = direct operating cost per sector and given flight technique
C^{I}_{DOCS} = explicit time related direct operating cost component
C^{II}_{DOCS} = explicit fuel related direct operating cost component
C^{III}_{DOCS} = fixed direct operating cost component
C_{FUEL} = fuel cost for a given flight technique and sector
CI = Cost Index
C_{INS} = total insurance payable per sector
C_{LEASE} = lease cost per sector
C_{MAIN} = maintenance cost per sector and given flight technique
C_{MAT} = materiel cost per sector and given flight technique
C_{MISC} = miscellaneous indirect operating cost component per sector
C_{PAX} = passenger related indirect operating cost component per sector
C_{SALES} = sales and reservation related indirect operating cost component per sector
C_{SPARES} = spares inventory cost per sector
C_{SUND} = total sundries cost per sector
C_{TOCS} = total operating cost for given sector and flight technique
c_{acint} = aircraft acquisition cost and interest payable per reference time frame
c_{acres} = aircraft residual value per reference time frame
c_{conb} = block time related contingency cost per block hour
c_{conf} = flight time related contingency cost per flight hour
c_{crew} = crew salary cost per reference time frame
c_{grh} = ground handling charges incurred per sector
c_{hins} = hull insurance payable per reference time frame
c_{land} = landing fees incurred per sector
c_{lease} = lease cost per reference time frame
c_{main} = flight time dependent maintenance cost denoting theoretically most efficient work practise
$c_{main,CYC}$ = total cyclic maintenance cost per sector
$c_{main,FH}$ = total flight time dependent maintenance cost
$\dot{c}^{c}_{main}$ = total maintenance cost derivative with respect to block time
$\dot{c}^{p}_{main}$ = total maintenance cost derivative with respect to number of sectors completed per reference time frame utilisation
c^{I}_{main} = flight time related maintenance cost component
$\overline{c}^{I}_{main}$ = approximate flight time related maintenance cost component deemed independent of segment flight time
c^{II}_{main} = fixed maintenance cost component
$\overline{c}^{II}_{main}$ = fixed maintenance cost component assuming approximate flight time related maintenance cost
c_{mat} = flight time dependent materiel cost denoting theoretically most efficient work practise
c^{I}_{mat} = flight time related materiel cost component
$\overline{c}^{I}_{mat}$ = approximate flight time related materiel cost component deemed independent of segment flight time
c^{II}_{mat} = fixed materiel cost component
$\overline{c}^{II}_{mat}$ = fixed materiel cost component assuming approximate flight time related materiel cost
c_{misc} = additional [direct operating] costs and fees incurred per sector
c_{nav} = navigation fees incurred per sector
c_{pins} = passenger and/or distance related insurance rate
c_{spint} = spares inventory acquisition cost and interest payable per reference time frame

* Ph.D. Candidate, Department of Aeronautics, Division of Aerodynamics. Member RAeS. Current position as Conceptual Design Engineer, Bombardier Aerospace, Montreal, Canada. Former positions included: Performance Engineer, SAAB Aircraft, Sweden, and Aircraft Performance Engineer, American Airlines, Fort Worth, Texas, USA.

c_{spres} = spares inventory residual value per reference time frame
FH = flight hour
HLI = Hie Latency Index
k_{main} = constant depicting fraction of maintenance cyclic to maintenance flight time dependent cost
k_{mat} = constant depicting fraction of materiel cyclic to materiel flight time dependent cost
k^{I}_{IOC} = proportion of total yield that accounts for C_{PAX} indirect operating cost component
k^{II}_{IOC} = proportion of total direct operating cost that accounts for C_{MISC} indirect operating cost component
k^{III}_{IOC} = cost coefficient used for C_{SALES} indirect cost component
k^{IV}_{IOC} = fixed cost coefficient that accounts for C_{MISC} indirect operating cost component
k_1 = constant depicting the impact of higher speed technique attributes to assorted combinations of intermediate speed schedules with respect to block fuel for a given sector
k_2 = constant depicting the impact of higher speed technique attributes to assorted combinations of intermediate speed schedules with respect to block fuel for a given sector
k_3 = constant depicting the impact of slower speed technique attributes to assorted combinations of intermediate speed schedules with respect to block fuel for a given sector
k_4 = constant depicting the impact of slower speed technique attributes to assorted combinations of intermediate speed schedules with respect to block fuel for a given sector
k_5 = constant required for regression between block time (abscissa) and expended block fuel (ordinate) for a given sector
M = Mach number
N_s = number of sectors completed per reference time frame
OFI = Operational Flexibility Index
P = profit or return on investment (denoted by prime) attributable to flying services for given sector mission and reference time frame, before income taxes, non-operating items such as retirement of property and equipment, affiliated companies and subsidies
PAX = number of passengers
P_{opt} = profit or return on investment (denoted by prime) global maximum
P_S = pre-optimum profit or return on investment (denoted by prime) rise rate
P_{SEC} = profit for given sector mission and flight technique
P_{SS} = post-optimum profit or return on investment (denoted by prime) decay rate
p_f = price of fuel per unit weight
RPM = revenue passenger-miles
SECT = sector
s = sector distance for given mission
s_{be} = break-even sector distance where profit or return on investment is zero
s_{dec} = reference sector distance where the post-optimum profit or return on investment (denoted by prime) decay rate is measured
s_i = initial estimate for break-even sector distance numerical scheme
s_n = upper sector distance threshold of the surveyed sector distances
s_o = lower sector distance threshold of the surveyed sector distances
s_{opt} = sector distance where profit or return on investment (denoted by prime) global maximum occurs
s_{ref} = reference sector distance used for yield modelling
T_u = total reference time frame utilisation
t = block time for given sector and flight technique
t_a = turn-around time
t_{man} = time allowance for start-up, taxi-out and taxi-in
$t_{maxP\text{-}ROI}$ = optimal profit or return on investment block time for a given sector mission
$t_{mincost}$ = cost optimal block time for given sector mission
$t_{minfuel}$ = block time required to complete a sector mission resulting in the lowest possible block fuel
$t_{mintime}$ = lowest possible block time required to complete a sector mission
t_n = block time equal to the upper applicable threshold of a regressed maintenance cost model
t_o = block time equal to the lower applicable threshold of a regressed maintenance cost model
W_{fuel} = block fuel required to complete a sector mission for a given flight technique
$W_{f,minfuel}$ = lowest possible block fuel required to complete a sector mission
$W_{f,mintime}$ = block fuel required to complete a sector mission in the lowest possible block time
Y_{SEC} = total revenue for a given sector mission
y_1 = yield generated at a reference sector distance
y_2 = constant depicting yield variation with sector distance
y_3 = constant depicting yield variation with sector distance
α_{main} = constant coupling maintenance flight hour cost to segment flight time
α_{mat} = constant coupling materiel flight hour cost to segment flight time
β_{main} = potential regression parameter accounting for segment flight time influence on maintenance flight hour cost
β_{mat} = potential regression parameter accounting for segment flight time influence on materiel flight hour cost
Φ_α = linear sector distance gradient coefficient in profit or return on investment (denoted by prime) response model
Φ_β = linear sector distance constant in profit or return on investment (denoted by prime) response model
Φ_χ = exponential constant in profit or return on investment response model
Φ_δ = exponential sector distance coefficient in profit or return on investment response model
Φ_ε = coefficient representing the asymptotic behaviour in the profit or return on investment (denoted by prime) response model
λ = passenger load factor for given sector mission
θ = temperature lapse ratio
ϖ = adjusted cost differential with respect to block time or profit differential with respect to number of sectors completed per reference time frame
ϖ' = adjusted ancillary profit differential with respect to number of sectors completed per reference time frame

Introduction

It is becoming increasingly important for designers of transport aircraft to be well versed in how commercial airline operators establish the feasibility of introducing new equipment types for fleet planning. Airline economics now dictate the need for more flexible commercial transports, thus invalidating the traditional approach of focusing on the design point specifications and giving little regard to off-design sensitivities. One well-known example of this philosophy is the act of overly simplifying the procedural aspects of en route performance to one universally applicable Mach number or "Standard" Mach - commonly designated as the Long Range Cruise speed. Even though the basic requirement of operational performance is scrutinised, airlines will consider in parallel the corresponding Direct Operating Cost (DOC), and more significantly, the Profit or Return on Investment (P-ROI) generated. In the context of this study, the profit generated is attributable to flying services, before income taxes, non-operating items such as retirement of property and equipment, affiliated companies and subsidies. There are in addition other considerations beyond the control of aircraft designers. These are issues related to product support, fleet commonality and mix that offers the best flexibility in seating and loading, long-standing and exclusive associations with particular airframe manufacturers, and the dynamic of internal politics. Notwithstanding these other factors, the cost and profit functions mentioned are often used as a rational basis for any future acquisition exercises. In view of this, it can be concluded that operational en route performance should be optimised with respect to the primary objectives of cost and profit and more importantly, it seems logical that both these aspects should be coupled in some manner, whereby it is possible to weigh the combined relative merits of different aircraft.

A complete mission flight profile trajectory as depicted in Fig.1 consists of three consecutive segments: climb, cruise and descent. Each segment is subject to transversality conditions that are additional and depend on the end point constraints of state variables[1], thus the entire flight must be analysed as a global problem wherein the links between all the phases are considered concurrently. Unique and constant values of Calibrated (or Indicated) Airspeed (CAS), or Mach number, for corresponding throttle setting are indicative of each phase with strategic switches in CAS/throttle effected during the flight in accordance with procedures detailed in a flight plan.

A sector mission is the operation of an aircraft from the end of initial climb to the end of descent, with both nodes corresponding to a height of 1500 ft pressure altitude. Flight time and flight fuel include allowances required for takeoff, initial climb, approach and landing. The block time and block fuel includes additional allowances for start-up, taxi-out and taxi-in. The notion of flight and block definitions does not include any distance credit. Each sector mission analysis will have with it an associated reserve fuel that is carried to destination. Reserve fuel is a contingency allocation usually consisting of: an alternate or diversion flight over a designated distance; operation in a holding pattern for a specified duration and given altitude; possibly a contingency fuel proportional to the flight fuel expended to complete the sector mission; and where required, contingency fuel to cater for an extended flight of given duration and flight technique.

It is common practise to assign at least two distinct climb modes, or more specifically, two different speed schedules for climb control each consisting of a fixed CAS and Mach speed. The advantage with a faster climb speed schedule occurs for cruise fractions (ratio between cruise distance and sector distance) less than around 0.80 (or sector distance ≤ 1000 nm) where possibilities in conducting further time, cost or profit function optimisation can take place[3]. To elaborate, opportunities might arise in generating an unconstrained optima which was previously constrained using a single speed schedule premise, because faster climb speed schedules (designated here as CLB Mode H) encourage "cruise soaking", or the exchange of cruise distance for climb which leads to block time reductions - this especially being the case for regional type sector missions.

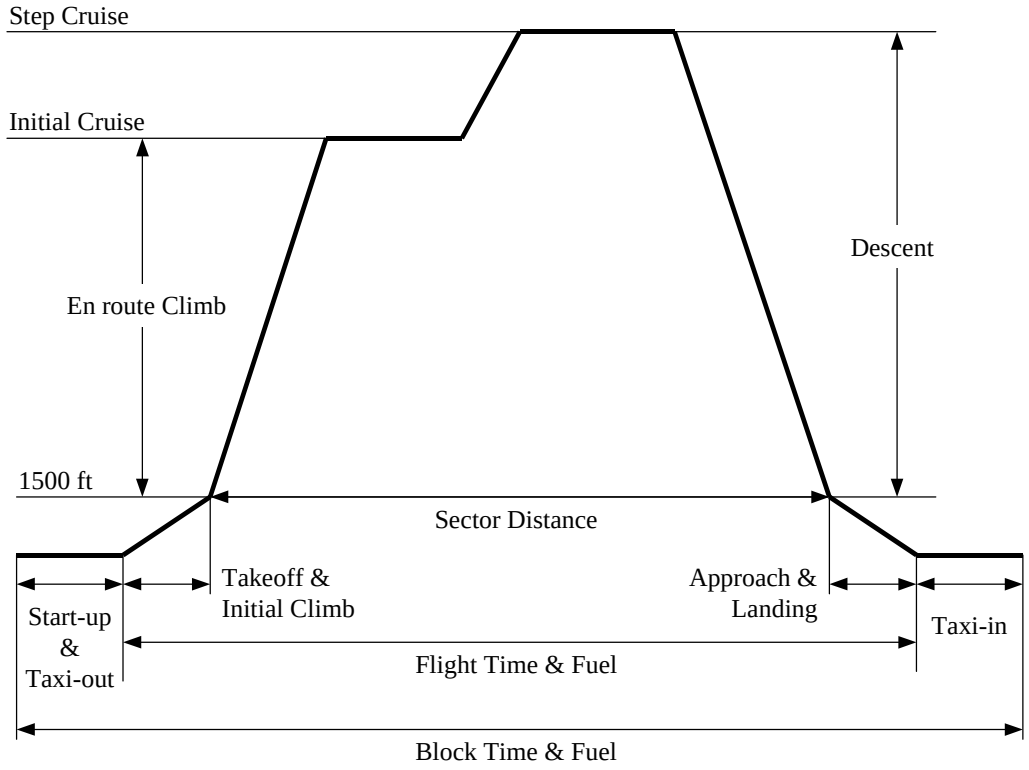

Fig. 1 – Flight profile as defined by Association of European Airlines (AEA)[2].

A slower climb speed schedule (CLB Mode L) enables closer adherence to fuel optimal procedures during climb, thereby enhancing range capability. In this way, CLB Mode L and CLB Mode H speed schedule definitions are formulated with respect to optimal climb trajectory profile state and time function adherence and designated divergence criteria respectively. Normally, one would describe speed schedules for descent much in the same way as was previously mentioned for climb control. Three options are usually available: rate of descent (ROD) as a control variable, a Mach/CAS schedule as the control variable, and, Mach/CAS speed schedule as the control variable with ROD used as the ancillary constraint.

Block speed (sector distance divided by block time) variation for a given reference time frame utilisation (total operating or block hours for a given period of time, e.g. per annum) results in markedly different speeds when optimal fuel usage (minimum fuel), optimal time expended (minimum time), minimum DOC, and, maximum P-ROI are compared for fixed sector distances and mission criteria (Torenbeek[4]). Identification of these speeds enables the formulation of optimal flight techniques or a formal definition of flight operational procedures consisting of distinct climb, cruise and descent modes at a suitable flight level(s).

The DOC consists of three major contributors - two of which are interrelated. The first and second designated as a flight technique source consist of time and fuel costs in which changes in block speed induce corresponding changes in cost of time and fuel relative to the speed increment. Moreover, the time related cost may also be sensitive to the influence of variations in reference time frame utilisation, which measures the productivity or number of sectors completed for given period of a vehicle. The third, independent of flight technique refers to an operating cost that is not proportional to the economic value of speed or utilisation, but is related to the act of completing a sector mission, hence is considered fixed.

Common practise among aircraft manufacturers is to only compare DOC between vehicles of varying productivity capabilities, which can on occasions be a questionable basis. There are instances, namely the way in which aircraft utilisation is defined, where the P-ROI objective might emphasise the importance of block speed yielding a condition for economic optimality incongruous with minimum DOC. Fundamentally, P-ROI should be viewed as the most comprehensive of all the objective function criteria usually considered for commercial aircraft design proposals and competitor analyses, but has been neglected in the past because of the added complexity in computing such results. Primary contributors to P-ROI include a multi-faceted trade-off between revenue and Total Operating Cost (TOC) constrained by the influence of productivity for a given reference time frame as well as the quantity of available seat-miles completed therein.

The purpose of this paper is to derive expressions for the DOC, TOC and P-ROI of a given aircraft and sector mission criteria, and to propose a method in which it is possible to

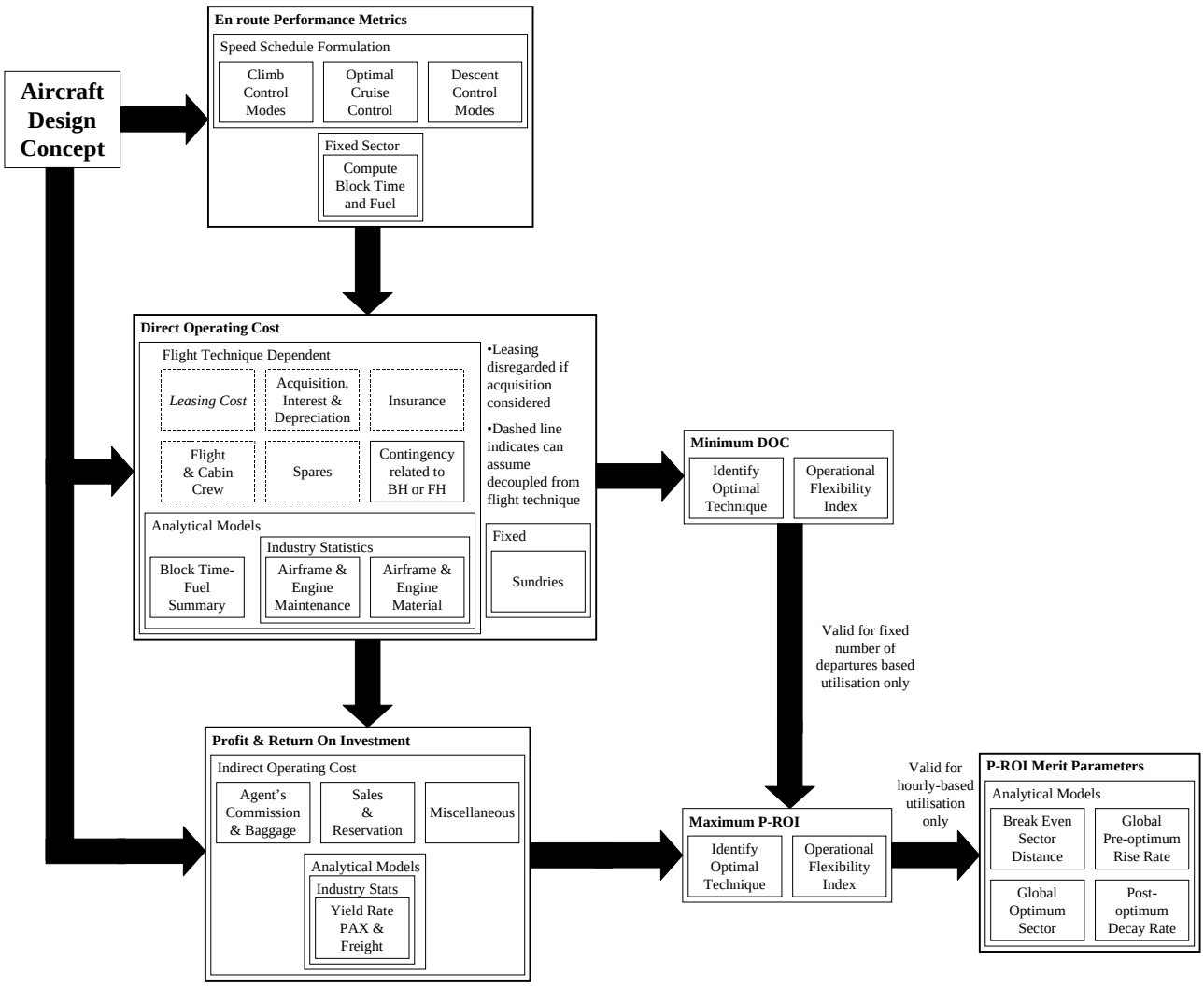

Fig. 2 – DOC and P-ROI computation procedure flowchart.

identify the associated economically optimal flight techniques. The final aim is to extend this knowledge further by offering an array of tangible merit functions related to operational performance and economics for the purpose of coupling these subspaces into the traditional conceptual aircraft design optimisation process. Fig. 2 offers a graphical perspective to assist in elucidating the interrelationship between vehicular attributes, operational performance, DOC and P-ROI, and, to serve as an outline for determining constituent working parameters, assumptions upon which the calculations are based, as well as the flow to produce the requisite objective and merit functions. This interdependent yet concurrent process will be described with detail in the sections to follow.

Utilisation for Given Reference Time Frame

The myriad of cost and revenue expressions to be presented shall become normalised to a per sector mission basis in order to afford a measure of effectiveness against a given flight technique. This is achieved by first allocating an assumed utilisation over a period of time, for example one year, and then consequently expressing it as an equivalent number of sectors. Aircraft utilisation is governed by: the ratio of flight time to the ground time spent loading and unloading the vehicle; any airport restrictions on night flying; and, the frequency of operations as dictated by public demand throughout the diurnal and seasonal cycles. In any traffic system, the initial planned goal is to fly the aircraft as much as possible. The number of sectors per reference time frame for a given sector mission and flight technique is simply computed by dividing the total number of operating hours of utilisation by the summation of single mission block and turn around times, thus

$$N_S = \frac{T_u}{t + t_a} \tag{1}$$

For instances where utilisation is assumed to be in block hours (BH), the turn around time t_a is taken to be zero. Typically, industry practise is to assume the utilisation or T_u of commercial aircraft to vary between 2000-4000+ BH per annum with the lower bound of this interval akin to regional aircraft usage and the upper bound characteristic of long-range equipment. The utilisation assumption is very important as it can influence both the productivity and cost attributes of airline operation. To assist in deciding an appropriate T_u, the Association of European Airlines (AEA)[2] suggest using

$$T_u = \frac{3750}{t + t_a}\, t \tag{2}$$

The declaration of T_u as presented in Eq. (2) implies utilisation is proportional to block time, hence is a function of flight technique. A quick sensitivity analysis shows the variation between upper and lower bounds would not exceed ±10%, thus leading one to conclude that a philosophy of setting T_u as fixed to simplify matters is also acceptable. Otherwise in either case, the methods of identifying economically optimal flight techniques to follow are equally applicable regardless of the nature of assumed utilisation – when using Eq. (2), the only stipulation is T_u must be computed dynamically before proceeding with the algorithm.

Another alternative is to assume a fixed number of departures; which means the parameter N_S may be expressed as a quantity independent of flight technique. It shall be shown later that this assumption produces significantly different optima compared to an hourly-based utilisation.

Direct Operating Cost

A number of techniques for the calculation of DOC are reported in literature[2,4,5,6,7]. The flight technique dependent costs for a given sector mission are those including lease (if applicable), aircraft acquisition and interest due to the initial cost, aircraft and passenger insurance (consisting of both flight technique dependent and independent components), air crew, spares inventory, aircraft maintenance, aircraft materiel, and fuel consumption. The costs incurred independent of flight technique include navigation, landing and handling charges. The cost components outlined here are all with respect to an hourly-based reference time frame utilisation assumption, i.e. different flight techniques employed for a given sector mission result in variations of block time, and hence, the number of sectors achievable corresponding to cost variations per sector flown. In contrast, a fixed departures utilisation assumption will modify the basis for account of the time dependent cost constituents. This aspect is to be discussed after the hourly-based utilisation optimal flight technique scheme has been derived.

Flight Technique Dependent Costs

These are costs related to aircraft specific operational performance attributes and mission requirements. This section intentionally includes aircraft ownership related costs as constituents that can be coupled to flight technique, however, it is highlighted that many DOC studies produced by airframe manufacturers[7,8,9] work off the premise of Cash DOCs or costs not related to aircraft ownership.

Aircraft Lease Cost

A contractual agreement by which the owner of the vehicle allows another party to use it for a specified time in return for a settled hire rate. Normalising this cost from reference time frame to a sector basis produces

$$C_{LEASE} = \frac{c_{lease}}{T_u}\left(t + t_a\right) \tag{3}$$

where c_{lease} is expressed as currency units per reference time frame (CU/RTF) and C_{LEASE} as currency units per sector (CU/SECT). It should be duly noted that the by-product of leasing means concepts like acquisition and interest payable for a depreciation period are neglected for ensuing DOC calculations.

Aircraft Acquisition, Interest Cost and Depreciation

This cost relates to the initial capital outlay and repayment of the interest invested for aircraft procurement. Depreciation is the allocation of the aircraft initial cost over the operating life of the aircraft. The total aircraft acquisition cost and interest payable (taking residual value into account becomes equivalent to depreciation cost) per sector (CU/SECT) is expressed as

$$C_{ACQ} = \frac{c_{acint} - c_{acres}}{T_u}\left(t + t_a\right) \tag{4}$$

Aircraft and Passenger Insurance Cost

During its operational life, the aircraft is to be insured. This is commonly known as hull insurance. A supplementary cost associated with the insurance of passengers is a function of both the number of passengers and/or the distance covered by the aircraft. For an assumed passenger load factor and sector distance, this contribution becomes

$$C_{INS} = \frac{c_{hins}}{T_u}\left(t + t_a\right) + c_{pins}\ \lambda\ PAX\ s \qquad (5)$$

where c_{hins} has units of CU/RTF, c_{pins} in currency units per available seat-mile (CU/ASM) and C_{INS} in CU/SECT.

Crew Cost

The crew cost includes salary of the pilots and the cabin crew. If c_{crew} is defined in CU/RTF

$$C_{CREW} = \frac{c_{crew}}{T_u}\left(t + t_a\right) \qquad (6)$$

C_{CREW} then is expressed in CU/SECT.

Aircraft Spares Inventory

Spares ownership involves initial investment with an added burden of interest payable on the capital for procurement as well as allocation of the initial cost over the operating life of the vehicle. The spares allowance is usually assumed as being some percentage of aircraft purchase price with adjustments made for interest and residual value. If the total spares inventory acquisition cost and interest payable (CU/RTF) and the residual value of the spares inventory (CU/RTF) are considered concurrently, the total spares inventory cost per sector (CU/SECT) is

$$C_{SPARES} = \frac{c_{spint} - c_{spres}}{T_u}\left(t + t_a\right) \qquad (7)$$

Contingency Costs Related to Flight Technique

Additional cost sources that have a direct coupling to block and flight time can be accounted for under the guise of contingency. For example, the cost of oil consumption may be introduced via this parameter by adjusting the volumetric cost with the volumetric requirement per block or flight hour and thence the total cost per hour. Other instances where costs are gauged on an hourly basis may be employed here. One typical example occurs when crew wages and penalty rates instead of fixed salaries are applicable.

A block hour dependent cost is simply

$$C_{CONB} = c_{conb}\ t \qquad (8)$$

where the contingency cost per block hour (CU/BH) is normalised into a contingency cost per sector (CU/SECT).

Correspondingly, flight hour dependent costs become

$$C_{CONF} = c_{conf}\left(t - t_{man}\right) \qquad (9)$$

where the contingency cost per sector (CU/SECT) is the product of contingency cost per flight hour (CU/FH) and the difference between block time and allowances for start-up, taxi-out and taxi-in.

Aircraft Maintenance Cost

It has been demonstrated that the maintenance cost consists of time dependent and cyclic components[2,6,8,9]. As a matter of interest, a survey completed by Boeing Commercial Airplanes[8] enables one an insight to the relative sensitivity of constituent aircraft systems cost to time dependent and cyclic airframe maintenance cost components. Maintenance cost for systems that encompass air conditioning, auto flight, communications, electrical power, flight controls, fuel, hydraulic power, instruments, lights, navigation, oxygen, nacelles and pylons, and windows were found dominated by time dependency. In contrast, equally split time-cyclic dependency and predominately cyclic maintenance cost constituents were associated with systems covering equipment and furnishings, ice and rain protection, landing gear, pneumatics, water and waste, auxiliary power unit (APU), doors, fuselage, stabilisers and wings. One generally accepted approach involves the correlation of maintenance cost to average segment flight time for given sector distance; the flight hour cost should then be some function of flight time for a given mission, whereas, the associated cyclic cost should be considered as some proportion of the flight hour cost[8]. This deduction is based on the premise that influences of skill level, shop efficiency and learning curve would impart a significant contribution to both the time dependent and cyclic costs[9]. Fig. 3 and Fig. 4 below demonstrate this notion with relative cost for regional, narrow-body and wide-body aircraft.

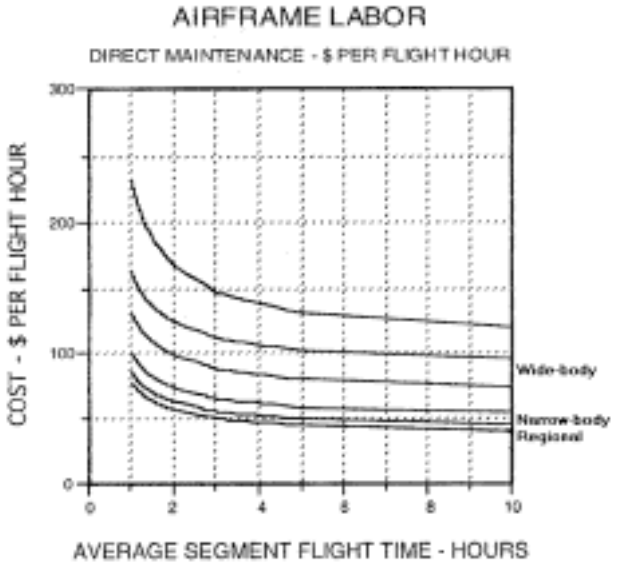

Fig. 3 – Variation of airframe time related maintenance cost with average segment flight time for various aircraft categories[9].

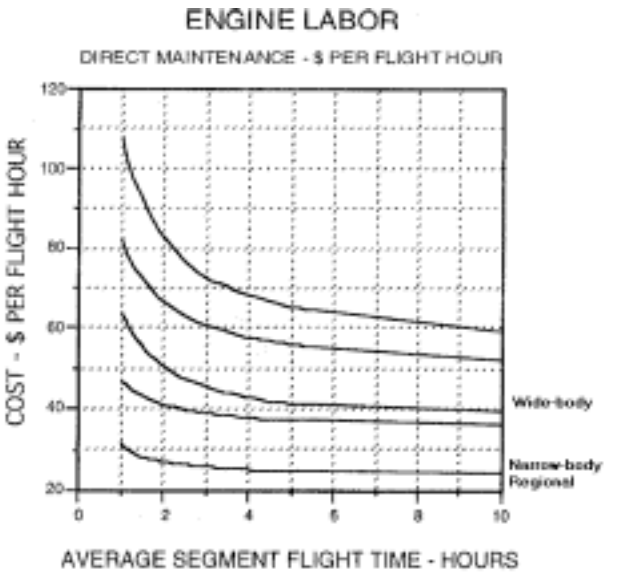

Fig. 4 – Variation of propulsion time related maintenance cost with average segment flight time for various aircraft categories[9].

An all-purpose model for flight hour related costs in the closed flight time interval $[t_o,t_n]$ is here proposed as

$$c_{main,FH} = c_{main} + \frac{\alpha_{main}}{(t - t_{man})^{\beta_{main}}} \quad (10)$$

and associated cyclic costs as

$$c_{main,CYC} = k_{main}\, c_{main,FHR} \quad (11)$$

where the total maintenance time dependent cost component (CU/FH) in Eq. (10) consists of c_{main} the portion of the cost that is flight time dependent and theoretically the most efficient work practise or learning curve asymptote, α_{main} a constant coupling the influence of segment flight time to the flight hour cost, and, β_{main} a potential regression fit. The cyclic maintenance cost (CU/FH) given by Eq. (11) is assumed to be proportional to the maintenance time dependent cost via k_{main} a constant depicting the fraction of cyclic to time dependent costs.

The parameters within the maintenance cost rate expressions given above must be adjusted for changes in price level against the base statistical survey. This means the differences between nominal and current direct labour rates for a supposed burden as well as the influence of inflation should already be taken into account. The cyclic maintenance cost has been assumed to be some proportion of the total maintenance flight hour cost, which may not be convenient in some cases. Instances where the cyclic component is considered to be a fixed quantity regardless of flight technique may be so classified under "Sundries". The procedure basically requires a definition that $k_{main} = 0$ and the subsequent cost entered as a miscellaneous source.

It will be necessary to manipulate the combined influences of Eq. (10) and Eq. (11) algebraically into a form more conducive for ease of differentiation with respect to block time. It can be demonstrated[3] that the total maintenance cost once coupling between flight hour cost and average segment flight time are established in conjunction with the cyclic constituent, can be alternatively expressed as

$$C_{MAIN} = c^{I}_{main}\, t + c^{II}_{main} \quad (12)$$

where

$$c^{I}_{main} = \left(c_{main} + \frac{\alpha_{main}}{t\,(t - t_{man})^{(\beta_{main}-1)}} \right)(1 + k_{main}) \quad (13)$$

and

$$c^{II}_{main} = -c_{main}\,(1 + k_{main})\, t_{man} \quad (14)$$

Recognising that maintenance cost consists of individual airframe and propulsion contributions; the total cost can be tallied

$$C_{MAIN} = \left(c^{I}_{amain} + c^{I}_{pmain}\right) t + c^{II}_{amain} + c^{II}_{pmain} \quad (15)$$

where the subscripts "a" and "p" denote airframe and propulsion components respectively, and, C_{MAIN} is now the total maintenance cost per sector (CU/SECT).

The propulsion maintenance cost can be manipulated to reflect a variation in takeoff thrust policies together with any alterations made to en route maximum climb and cruise thrust ratings. Generally, the influence of thrust rating would be built into the model attributes of Eq. (10) from actual cost data simulating the particular configuration. In addition, investigations have demonstrated that the influence of airplane cruise speed is minimal with respect to propulsion maintenance costs[8]. In fact, the flight time dependent engine component overhaul is theoretically less expensive when the aircraft is operated at faster speeds. Concurrently, this cost rationalisation is offset by virtue of operating at a higher thrust level, hence making redundant any consideration of throttle on cost. Those occasions where the effect of thrust rating or throttle setting must be considered, the k_{main} constant can be adjusted accordingly, thereby simulating this sensitivity from a modelled baseline.

It is important to note that the cost levels used in such analysis should represent mature (stabilised) airframe and engine maintenance[2,7]. The moment a new aircraft is placed into operation, the airframe and engine maintenance costs increase at asynchronous rates from an initial low level, reach a common plateau of maturity after five to seven years of operation and revert back to a steady increase, albeit at a less pronounced rate, due to effects imparted by age. This is a key assumption because data show the maturity factor between airframe and engine converges during this interval[7], thereby giving scope for simplification. The total cost estimate given by Eq. (15) requires a detailed array of reliable statistical correlation. One may resort to an approximate expression[10,11,12,13,14,15] under the proviso apt estimates of $c_{amain,FH} = \overline{c_{amain}}$ and $c_{pmain,FH} = \overline{c_{pmain}}$ are substituted for Eq. (10).

$$C_{MAIN} = \left(\bar{c}^{I}_{amain} + \bar{c}^{I}_{pmain}\right) t + \bar{c}^{II}_{amain} + \bar{c}^{II}_{pmain} \quad (16)$$

Aircraft Materiel Cost

The expression for total materiel costs can be derived a priori based on the conclusions drawn in the maintenance cost model and a premise that both maintenance and materiel costs may be combined in the one expression[2,6,8,9]. By employing the rationale given for Eq. (10) and Eq. (11), and rearranging the collective influence into a form suitable for differentiation, the general model for time related costs in the closed interval $[t_o,t_n]$ is proposed as

$$c^{I}_{mat} = \left(c_{mat} + \frac{\alpha_{mat}}{t\,(t - t_{man})^{(\beta_{mat}-1)}} \right)(1 + k_{mat}) \quad (17)$$

and the cyclic contributor also becomes

$$c^{II}_{mat} = -c_{mat}\,(1 + k_{mat})\, t_{man} \quad (18)$$

which is similar to the form of Eq. (13) and Eq. (14). As with Eq. (15), both combine to produce the total materiel cost per sector

$$C_{MAT} = \left(c^{I}_{amat} + c^{I}_{pmat}\right) t + c^{II}_{amat} + c^{II}_{pmat} \quad (19)$$

Again, the subscripts "a" and "p" denote airframe and propulsion components respectively. This total cost estimate will also require a detailed array of reliable statistical correlation, however, one may resort to an approximation[10,11,12,13,14,15] under the proviso apt estimates of $c_{amat,FH} = \overline{c_{amat}}$ and $c_{pmat,FH} = \overline{c_{pmat}}$ are used.

$$C_{MAT} = \left(\bar{c}^{I}_{amat} + \bar{c}^{I}_{pmat}\right) t + \bar{c}^{II}_{amat} + \bar{c}^{II}_{pmat} \quad (20)$$

This cost has been intentionally separated from the total direct maintenance so that facility is given for instances where cost between maintenance and materiel are deemed mutually exclusive. A common assumption is to consider spares allowances as a fixed proportion of aircraft price[2,13,14,15]; this contingency is offered under the "Aircraft Spares Inventory" classification.

Fuel Cost

As was discussed earlier in this treatise, a complete mission trajectory is subject to transversality constraints that are additional and depend on end point constraints. This means that for small enough cruise fractions, the influence of climb and descent may have a significant impact towards block fuel compared to that of cruise alone. The first step in estimating the total fuel cost for a given sector distance is to formulate a block time-fuel summary. These curves are derived from various combinations of speed schedules and flight trajectories thus encompassing techniques for minimum time, minimum fuel, and, intermediate schedules of height-energy-block fuel minima for fixed block times between these two extremes. Fig. 5 shows a generic interpretation of the typical block time-fuel summary.

Since the block time-fuel summary is made up of a collection of different flight techniques, i.e. combinations of distinct climb, cruise and descent modes at specific flight level(s), the curve geometry is constructed through a combination of quasi-discrete and discrete points. The quasi-discrete portion of the curve is usually generated by a sole flight technique, commonly of highest speed schedule for climb, cruise and descent, in which flight level varies from the optimum altitude (unconstrained specific air range maximum - SAR optimum) or service ceiling (constrained SAR maximum) to lower altitudes until the minimum time threshold is reached. The discrete points usually consist of intermediate to low climb and descent modes combined with intermediate to Long Range Cruise (LRC) and Maximum Range Cruise (MRC) speeds at optimal altitude or service ceiling. In addition, it should be noted, assuming the margin to buffet is not violated, instances might arise where the en route specific excess power is sufficient enough to employ step cruise procedures. This aspect of performance is very difficult to predict with simplified expressions coupled to a general set of aircraft parameters, so as a consequence, is reliant upon batch calculations and comparison until a collection of points describing a distinct lower boundary is established.

It is evident the block time-fuel summary is rather complex and cannot be easily represented by an analytical expression which produces a continuous function with respect to block time. The failure of this option implies that another philosophy may be required to achieve the task. A hyperbolic function appears well suited to the curve definition exercise and a suggested model in the closed block time interval $[t_{mintime}, t_{minfuel}]$ is presented here as

$$W_{fuel} = W_{f,min\,time}\left(1-k_1\right)\tanh\left[k_2\left(t_{min\,time}-t\right)\right] - W_{f,min\,fuel}\left(1-k_3\right)\tanh\left[k_4\left(t_{min\,fuel}-t\right)\right]+k_5 \qquad (21)$$

where $W_{f,mintime}$ is the block fuel for a minimum time flight technique, k_1 and k_2 constants which allow for the impact of different higher speed technique attributes to assorted combinations of intermediate schedules, $W_{f,minfuel}$ the block fuel for a minimum fuel flight technique, k_3 and k_4 constants which allow for the impact of different slower speed technique attributes to assorted combinations of intermediate schedules, and k_5 is a constant. Since the "k" properties are intended to represent vehicular en route performance attributes related to aerodynamic and propulsion characteristics, extensive investigations were conducted in order to ascertain if expressions could be developed to quantify their respective magnitudes. Results hitherto indicate these coefficients cannot easily be related to a specialised set of design parameters or even expressed as consistent continuous functions of variables like for example sector distance. This unfortunate circumstance is attributable to the complex nature associated with block time-fuel curve creation, therefore, the only recourse is to model the collectivised interdisciplinary result and weigh the relative sector mission merits of one complete aircraft against another.

By letting p_f be defined as the price of fuel per unit weight

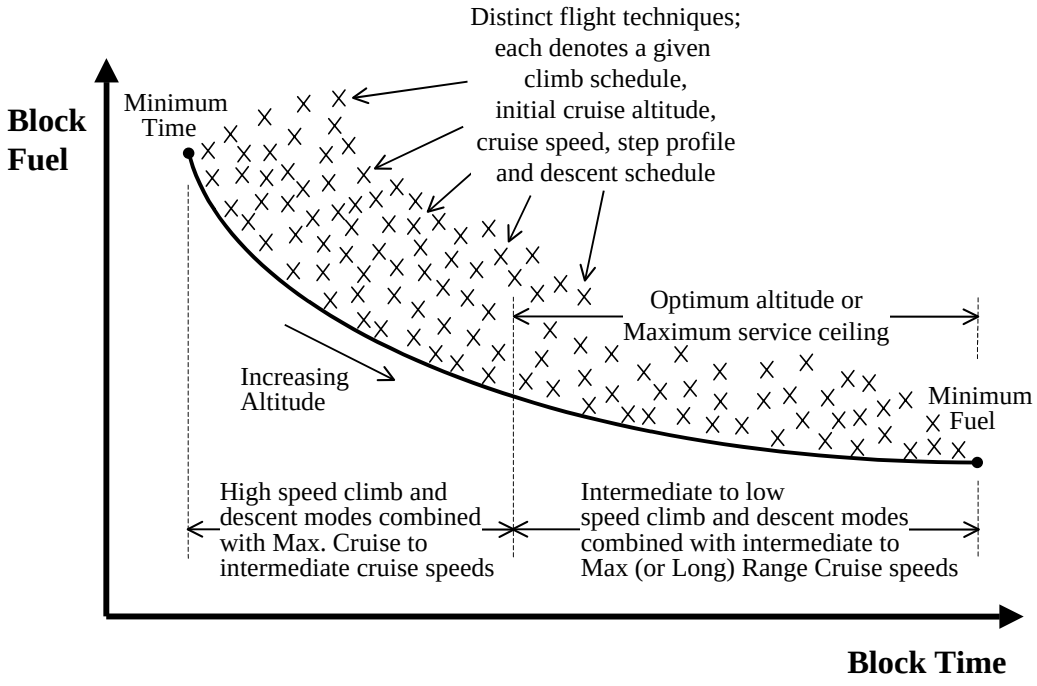

Fig. 5 – Typical block time-fuel summary for a given sector distance and mission.

$$C_{FUEL} = p_f \left(W_{f,\min time}(1-k_1)\tanh\left[k_2\left(t_{\min time}-t\right)\right] - W_{f,\min fuel}\left(1-k_3\right)\tanh\left[k_4\left(t_{\min fuel}-t\right)\right]+k_5\right) \quad (22)$$

the total fuel cost per sector (CU/SECT) can be calculated.

Sundries

Sundries entail costs not exclusively related to flight operational characteristics, i.e. those parameters that are not strictly functions of block time. These can consist of landing fees, navigational and ground handling charges – which incidentally, vary from country to country. These costs are primarily related to aircraft gross weight, sector distance and payload complement, thus can be considered constant for fixed sector distances. Other costs having no direct coupling to time and not addressed here may then be categorised as miscellaneous costs. The above said contributors to the total sundries cost collectively are summed as

$$C_{SUND} = c_{land} + c_{nav} + c_{grh} + c_{misc} \quad (23)$$

Direct Operating Cost for a Given Sector Mission

Upon summation of the previously mentioned cost constituents related to flight operational, aircraft, as well as sector specific aspects, the total DOC for a given sector mission and flight technique becomes

$$C_{DOCS} = \left[C_{LEASE}\right] + C_{ACQ} + C_{INS} + C_{CREW} + C_{SPARES} + C_{CONB} + C_{CONF} + C_{MAIN} + C_{MAT} + C_{FUEL} + C_{SUND} \quad (24)$$

By substituting the array of itemised cost constituents presented previously into Eq. (24), the total DOC assuming an hourly-based reference time frame utilisation becomes quite convoluted. To further analyse an expanded form of Eq. (24) in a coherent manner, a more palatable structure should be developed. An option is to partition C_{DOCS} into time dependent, fuel dependent (which is also a function of time) and ancillary parts

$$C_{DOCS} = C^{I}_{DOCS} + C^{II}_{DOCS} + C^{III}_{DOCS} \quad (25)$$

One practise is to evaluate the relative merits of a given aircraft design by assuming a fixed number of departures or sector missions per reference time frame. The implication is that utilisation dependent parameters like total ownership and crew salary are no longer coupled to variations in flight technique or block time. An assumed reference time frame utilisation expressed in hours has the inherent characteristic of continually varying the number of possible sectors completed per reference time frame with flight technique or block time. An identification of minimum DOC chiefly involves maximising the number of sectors completed per reference time frame, thus emphasising higher speed flight techniques. In this instance, the fixed departures assumption has a weaker criterion for maximising number of sectors; the proportion of time dependent cost is less significant compared to the fuel cost and thus is expected to result in slower cost optimal block speeds.

Yield Rate and Revenue

The yield rate is an indicator of the market in which the airline operates. This quantity is a measure of ticketing prices assumed as some function of available seat-miles. One salient characteristic any representation of yield must have is recognition there is tendency towards an asymptotic value for longer sector distances (see Fig. 6), thus reflecting the reducing trend for the operator cost per available seat-mile[6,7,13,14,15], or an appreciation that unit costs for short-haul operations are higher than those of longer-range flights.

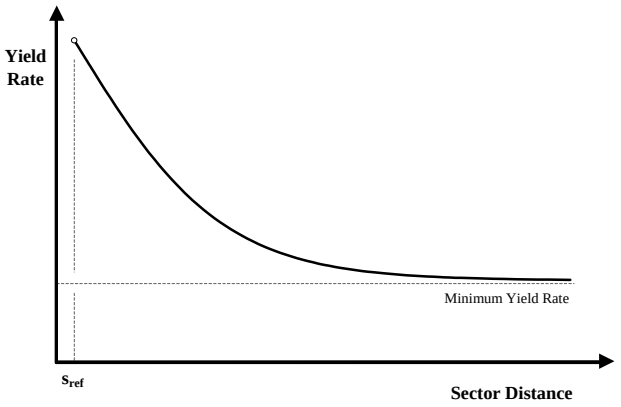

Fig. 6 – Variation of yield rate with sector distance for model formulation purposes.

The total income generated for a given flight is defined as the revenue. For an assumed passenger load factor and sector distance, upon formulation of a feasible yield rate model, the total revenue per flight becomes

$$Y_{SEC} = y_1 \lambda\, PAX\, s\left(1 + y_2 \tanh\left[y_3\left(s_{ref} - s\right)\right]\right) \quad (26)$$

where y_1 is the yield at the reference sector distance in currency units per available seat-mile (CU/ASM), y_2 (dimensionless) and y_3 (per nm) are constants depicting the impact of longer sector distances to the yield rate, and, s_{ref} is the reference sector distance (nm). As a supplement to the treatment given above, the commercial transportation of scheduled and non-scheduled freight adheres to a similar edict; the yield rate would still be modelled using Eqn. (26), but expressed in currency units per load tonne-mile instead of available seat-miles.

The Indirect Operating Cost

The Indirect Operating Costs (IOC) are related to the general operation of an airline. These components comprise advertising, ticketing, sales, reservations, administration, and passenger services. Most studies employ a very crude estimate between total indirect to direct costs of 1:1, which proves to be too simplistic since this ratio is reliant upon the type of market in which the airline operates. For example, carriers servicing mature markets generally have higher IOC:DOC compared to low cost airlines because of much higher passenger services and marketing costs. Thus, it is intended that a more detailed model for these costs should be employed. The information to follow proposes more realistic associations of these additional cost components.

Agent's Commission and Excess Baggage

This incurred cost is dependent upon the volume of paying customers, it can be deduced that a cost model in units of CU/SECT proportional to the total revenue would be applicable,

$$C_{PAX} = k^{I}_{IOC}\, Y_{SEC} \quad (27)$$

where k^{I}_{IOC} is a constant representing some factor of Y_{SEC} for per sector (CU/SECT).

Sales and Reservation

By assuming a coupling to the total number of revenue passenger-miles, this indirect cost contribution (CU/SECT) due to sales and reservation becomes

$$C_{SALES} = k_{IOC}^{III}\ \lambda\ PAX\,s \tag{28}$$

where k_{IOC}^{III} is a cost function factor in relation to the quantity of available seat-miles (CU/ASM).

Miscellaneous Indirect

This entry can be considered as a contingency cost (advertising, passenger handling, administration, etc.) not covered by any other formal definitions. The miscellaneous indirect costs also can be regarded as a reflection of an airliner's efficiency. Since it has been elucidated above there are occasions where it is desirable to consider the indirect proportional to the direct cost, the supposition is the effectiveness of a carrier with respect to this cost constituent can be represented by a compound function of sector distance (or a direct function of sector DOC) and a fixed component. By letting k_{IOC}^{II} be defined as a constant depicting the fraction of miscellaneous indirect cost to the DOC for a given sector mission, and, k_{IOC}^{IV} as an incremental cost contribution independent of all sources

$$C_{MISC} = k_{IOC}^{II}\ C_{DOCS} + k_{IOC}^{IV} \tag{29}$$

the miscellaneous IOC component has units of CU/SECT.

Total Operating Cost for a Given Sector Mission

The TOC per sector is the sum of the DOC and IOC. Upon substitution of all constituents and grouping the result, obtain

$$C_{TOCS} = k_{IOC}^{I}\ Y_{SEC} + \left(1 + k_{IOC}^{II}\right) C_{DOCS} + k_{IOC}^{III}\ \lambda\ PAX\,s + k_{IOC}^{IV} \tag{30}$$

Profit and Return On Investment

The profit for a given sector mission and flight technique is given by the difference between revenue and TOC,

$$P_{SEC} = Y_{SEC} - C_{TOCS} \tag{31}$$

By assuming a generalised total utilisation of N_S sectors per given reference time frame, total profit P is

$$\begin{aligned} P = {} & N_S \left(1 - k_{IOC}^{I}\right) Y_{SEC} \\ & - N_S \left[\left(1 + k_{IOC}^{II}\right) C_{DOCS} + k_{IOC}^{III}\ \lambda\ PAX\ s + k_{IOC}^{IV}\right] \end{aligned} \tag{32}$$

where N_S is substituted by Eq. (1) or Eq. (2) if an hourly-based utilisation is assumed, otherwise, becomes a pre-supposed fixed number of sectors for the arbitrary reference time frame considered. It is expected that the identification of profit optimal flight techniques will not depend on the total ownership and crew salary. This is evident because the profit calculated above applies for the entirety of the reference time frame in question, therefore is not anticipated to impart any influence since it has become decoupled from aircraft productivity.

It is sound practise for any airline to gauge the relative economic feasibility of potential equipment types by comparing a ratio calculated as the difference between revenue and TOC normalised by the initial investment cost in vehicle acquisition. The ROI (P') can be algebraically expressed as

$$P' = \frac{P}{c_{acint}} \tag{33}$$

Since the profit result is simply normalised by c_{acint} (here not equivalent to the depreciation cost) in order to derive ROI, the profit optimal flight technique algorithm to follow is equally applicable for identification of maximum ROI as well. It should be observed that even though conditions for P-ROI optimality are identical, divergent conclusions about the feasibility of an equipment type against another might arise, i.e. by virtue of comparisons using absolute currency units versus a non-dimensional result.

Flight Technique Optimisation for Given Mission

It is evident that any identified optimal flight technique will fall into one of two distinct categories: applicability for hourly-based reference time frame or fixed departures based utilisation. It would be of interest to see if the qualitative conjectures drawn earlier about the differences between these two utilisation premises will eventuate after analytical scrutiny.

Cost Optimal Flight Technique Identification

It has been shown previously that the total DOC is basically a function of block time, thus to accomplish the task of identifying an optimal cost flight technique depends primarily on solving for a block time that yields minimum cost. An optimum condition is defined by the criterion

$$\frac{dC_{DOCS}}{dt} = 0 \tag{34}$$

Hourly-based Reference Time Frame Utilisation

For minimum cost, a block time is selected that minimises C_{DOCS}. By setting the derivative of the total DOC per sector mission equal to zero and upon manipulation an interim result becomes

$$p_f\ W_{f,min\,time}\left(1 - k_1\right) k_2\, sech^2\left[k_2\left(t_{min\,time} - t\right)\right] = \varpi \tag{35}$$

where ϖ consists of the remaining variables on the right hand side of the differential of Eq. (25), namely,

$$\begin{aligned} \varpi\big|_{DOC} = {} & c_{conb} + c_{conf} + \dot{c}_{main}^{c} + \dot{c}_{pmain}^{c} + \dot{c}_{amat}^{c} + \dot{c}_{pmat}^{c} \\ & + p_f\ W_{f,min\,fuel}\left(1 - k_3\right) k_4\, sech^2\left[k_4\left(t_{min\,fuel} - t\right)\right] \\ & + \frac{\left[c_{lease}\right] + c_{acint} - c_{acres} + c_{hins} + c_{crew} + c_{spint} - c_{spres}}{T_u} \end{aligned} \tag{36}$$

The total maintenance cost contribution is given by examining the rate of change of Eq. (15) with respect to block time

$$\dot{c}_{main}^{c} = \frac{dC_{MAIN}}{dt} = \left(c_{main} - \frac{\left(\beta_{main} - 1\right)\alpha_{main}}{\left(t - t_{man}\right)^{\beta_{main}}}\right)\left(1 + k_{main}\right) \tag{37}$$

This expression can be considered generic, hence, applicable for both airframe and propulsion related cost modelling, and also, includes scope to partition the materiel cost in a similar fashion.

Thus, the block time required for a minimum cost flight operation is

$$t_{min\,cost} = t_{min\,time} + \frac{1}{k_2}\cosh^{-1}\sqrt{\frac{p_f\ W_{f,min\,time}\left(1-k_1\right)k_2}{\varpi\big|_{DOC}}} \tag{38}$$

The optimal cost block time is given by a transcendental equation and can be solved numerically via simple iteration. Provided Eq. (38) passes the Hie Latency Test (to be discussed afterwards), the hyperbolic function always aids in achieving quick convergence and the iterative scheme is inherently stable.

Fixed Departures Based Utilisation

Since N_S is considered to be a fixed quantity here, it was observed that the total ownership and crew salary would be uncoupled from flight technique and hence block time. Under the pretext of Eq. (24), the parameter ϖ in Eq. (35) becomes

$$\varpi\big|_{DOC} = c_{conb} + c_{conf} + \dot{c}^{c}_{main} + \dot{c}^{c}_{pmain} + \dot{c}^{c}_{amat} + \dot{c}^{c}_{pmat} + p_f\ W_{f,min\,fuel}\left(1-k_3\right)k_4\,\mathrm{sech}^2\left[k_4\left(t_{min\,fuel}-t\right)\right] \tag{39}$$

with the corresponding optimal block time found after substitution into Eq. (38).

Derivation of Cost Index

Upon inspection, it can be readily seen that Eq. (25) may be expressed in the form

$$C_{DOCS} = C^{I}_{DOCS} + p_f\ W_{fuel} + C^{III}_{DOCS} \tag{40}$$

where each component is the time related, fuel and fixed costs respectively. Differentiation of C_{DOCS} with respect to block time and upon application of the condition for optimality, namely Eq. (34), gives

$$\frac{dC_{DOCS}}{dt} = \frac{d}{dt}C^{I}_{DOCS} + p_f\frac{dW_{fuel}}{dt} = 0 \tag{41}$$

Or conversely, the condition for cost optimal flight technique occurs when

$$\left.\frac{dW_{fuel}}{dt}\right|_{min\,cost} = -\frac{\dot{C}^{I}_{DOCS}}{p_f} \tag{42}$$

where, for an hourly-based utilisation

$$\dot{C}^{I}_{DOCS} = c_{conb} + c_{conf} + \dot{c}^{c}_{main} + \dot{c}^{c}_{pmain} + \dot{c}^{c}_{amat} + \dot{c}^{c}_{pmat} + \frac{\left[c_{lease}\right] + c_{ac\,int} - c_{acres} + c_{hins} + c_{crew} + c_{sp\,int} - c_{spres}}{T_u} \tag{43}$$

otherwise, for fixed departures becomes

$$\dot{C}^{I}_{DOCS} = c_{conb} + c_{conf} + \dot{c}^{c}_{main} + \dot{c}^{c}_{pmain} + \dot{c}^{c}_{amat} + \dot{c}^{c}_{pmat} \tag{44}$$

By defining a Cost Index or CI as the rate of change of block fuel per unit block time, obtain

$$CI = \left|-\frac{\dot{C}^{I}_{DOCS}}{p_f}\right| \tag{45}$$

It now becomes possible to examine the relative merits of a given procedural flight technique to the theoretical optimum. In fact, CI describes a gradient magnitude (unit block fuel per unit block time) coinciding with the point where minimum cost occurs on a block time-fuel summary, and advantageously, is independent of sector distance, the mission characteristic of payload and ambient conditions. This parameter shows consistency with the CI definition for fixed departures utilisation found elsewhere in literature[8,9].

Profit and Return On Investment Optimal Flight Technique Identification

For maximum P-ROI, a flight technique is selected that maximises P (or P'). For a given sector mission this condition is governed by the following criterion

$$\left(\frac{\partial P}{\partial N_S}\right)_s = \left(\frac{\partial P}{\partial t}\right)_s\left(\frac{\partial t}{\partial N_S}\right)_s \tag{46}$$

Eq. (46) holds true for instances where the reference time frame total utilisation is expressed in operating or block hours. It can be surmised, since the number of sectors per given reference time frame is dependent upon flight technique, the variable t or block time shall impart a corresponding rate change in P steadily increasing until a maximum stationary point is reached. This represents a partially constrained optimum because the P-ROI expression actually imposes dual criteria that is not only flight technique dependent for given sector mission, but as a consequence, is a function of the number of available seat-miles, thus implying the existence of a global optimum at an appropriate sector distance. It is envisaged that the condition for optimal P-ROI will produce a lower block time requirement compared to its cost optimal counterpart, or faster flight techniques that tend more towards the minimum time threshold.

Alternatively, if a fixed number of departures for the given reference time frame is considered, the quantity N_S is no longer coupled to flight technique hence defining maximum P-ROI via the condition where minimum DOC occurs. This can be substantiated algebraically through manipulation of Eq. (46) into the form shown.

$$\frac{dP}{dt} = \left(\frac{dP}{dN_S}\right)\left(\frac{dN_S}{dt}\right) \equiv \frac{dC_{DOCS}}{dt} = 0 \tag{47}$$

Since a measure of P-ROI becomes dependent on the level of DOC for given block time, maxima identification results in a condition where maximum P-ROI is synonymous with minimum DOC.

Hourly-based Reference Time Frame Utilisation

By applying the partially constrained optimum condition given by Eq. (46) to the definition for P-ROI in Eq. (32),

$$p_f\ W_{f,min\,time}\left(1-k_1\right)k_2\,\mathrm{sech}^2\left[k_2\left(t_{min\,time}-t\right)\right] = \varpi \tag{48}$$

where ϖ consists of the remaining variables on the right hand side of the differential of Eq. (32).

Further scrutiny of ϖ allows for one possible simplification to be in the form of a quotient

$$\varpi\big|_{P-ROI} = \frac{\varpi'}{\left(1+k_{TOC}^{II}\right)\left(t+t_a\right)} \tag{49}$$

with the variable located in the numerator defined as

$$\begin{aligned}\varpi' = &\left(1-k_{IOC}^{I}\right) y_1 \lambda\ PAX\ s\left(1+y_2\tanh\left[y_3\left(s_{ref}-s\right)\right]\right)\\ &-\left[\left(1+k_{IOC}^{II}\right)\left\{c_{pins}\,\lambda\ PAX\ s - c_{conf}\ t_{man} - \left(c_{conb}+c_{conf}\right)t_a\right.\right.\\ &+\dot{c}_{amain}^{p}+\dot{c}_{pmain}^{p}+\dot{c}_{amat}^{p}+\dot{c}_{pmat}^{p}+p_f\ W_{fuel}\\ &-p_f\ W_{f,min\,fuel}\left(1-k_3\right)k_4\left(t+t_a\right)sec\,h^2\left[k_4\left(t_{min\,fuel}-t\right)\right]\\ &\left.\left.+c_{land}+c_{nav}+c_{grh}+c_{misc}\right\}+k_{IOC}^{III}\ \lambda\ PAX\ s+k_{IOC}^{IV}\right]\end{aligned} \tag{50}$$

One important piece of information gleaned upon perusal of Eq. (50) is that aircraft ownership and crew salary have now become uncoupled from the P-ROI optima identification process.

Unique nomenclature to represent rate change of maintenance cost with respect to number of sectors completed for a given hourly based reference time frame utilisation was derived to be

$$\begin{aligned}\dot{c}_{main}^{p} = \frac{\partial C_{MAIN}}{\partial N_S} &= -c_{main}\left(t_{man}+t_a\right)\\ &+\frac{\alpha_{main}}{\left(t-t_{man}\right)^{\beta_{main}}}\left[\beta_{main}\left(t+t_a\right)-\left(t_{man}+t_a\right)\right]\end{aligned} \tag{51}$$

This expression can be considered generic, hence, applicable for both airframe and propulsion related cost modelling, and also, includes scope to partition the materiel cost in a similar fashion.

Now, the block time required for a maximum P-ROI operation is given by

$$t_{max\,PM-ROI} = t_{min\,time} + \frac{1}{k_2}\cosh^{-1}\sqrt{\frac{p_f\,W_{f,min\,time}\left(1-k_1\right)k_2}{\varpi\big|_{PM-ROI}}} \tag{52}$$

As for optimal cost, the maximum P-ROI block time is given by a transcendental equation of similar form but additionally influenced by revenue, an IOC component and turn around time contributors within the ϖ transient. Once again, the above can be solved numerically via simple iteration. Eq. (52) must also adhere to rules governed by the Hie Latency Test (to be discussed afterwards).

Fixed Departures Based Reference Time Frame Utilisation

As shown previously, Eq. (46) gives the partially constrained optimal block time for hourly-based utilisation. Based on this premise, it was shown thereafter via Eq. (47) that a maximum P-ROI flight technique for fixed departures based reference time frame utilisation would be equivalent to a cost optimal procedure - thus the solution is given by Eq. (52) but with a revised definition of ϖ in Eq. (49)

$$\begin{aligned}\varpi\big|_{P-ROI} \equiv \varpi\big|_{DOC} = &\,c_{conb}+c_{conf}+\dot{c}_{main}^{c}+\dot{c}_{pmain}^{c}+\dot{c}_{amat}^{c}+\dot{c}_{pmat}^{c}\\ &+p_f\ W_{f,min\,fuel}\left(1-k_3\right)k_4\,sec\,h^2\left[k_4\left(t_{min\,fuel}-t\right)\right]\end{aligned} \tag{53}$$

Hie Latency Index

Owing to the form of Eq. (38) and Eq. (52), it can be deduced that a limitation of the inverse hyperbolic cosine function occurs for cases where the variables within the functions collectively produce numbers less than unity. This condition is analogous to a situation where an unconstrained DOC minimum or P-ROI maximum simply does not exist therefore implying that only the quickest flight technique (minimum time) is applicable.

The concept of a Hie Latency Test (HLT) is presented here as a hypothesis based testing procedure helping to identify the abovementioned circumstance. For DOC and P-ROI optima regardless of reference time frames, the Hie Latency Index (HLI) is defined as

$$HLI = \frac{p_f\ W_{f,min\,time}\left(1-k_1\right)k_2}{\varpi} \tag{54}$$

where ϖ conforms to definitions based on the type of reference time frame utilisation and cost-profit modelling premise. The HLT is then governed by the following criteria:

HLI > 1	a unique solution other than minimum time Flight technique exists (unconstrained optima)
HLI ≤ 1	minimum time flight technique is ONLY applicable (constrained optima)

It is emphasised that the HLT must be conducted whilst assuming minimum time flight technique block times.

For HLIs less than or equal to unity, the absence of an unconstrained DOC or P-ROI optimal flight technique is viewed as being unfavourable. Such a result implies block speeds faster than the lowest block time threshold physically permissible by the given vehicle is required in order to attain a true DOC or P-ROI optimum. Additionally, no operational flexibility is afforded when Air Traffic Control (ATC) or route structure impose off-optimal restrictions. Therefore, whenever scrutiny of en route performance is conducted, the objective of any operationally balanced design should be avoidance of such a situation – particularly for short-haul missions where there is a propensity for faster block speeds.

Operational Flexibility Index

The HLT is a useful tool in qualitatively assessing any penchant an aircraft has to flying faster in achieving economically optimal results. However, this parameter does not imbue the analyst or designer with a true perspective of a given vehicle's operational flexibility, and, as is the case with CI, a computed value of the HLI parameter is not universally comparable between aircraft of varying scale and propulsion philosophy. One suggestion is to inspect the non-dimensional ratio of optimal block time against the minimum fuel and minimum time flight technique block time bandwidth. Since Eq. (38) and Eq. (52) are algorithms solving for optimal block time referenced to minimum time, a possibility now arises in the formulation of an Operational Flexibility Index (OFI)

$$OFI = \frac{\cosh^{-1}\sqrt{HLI}}{k_2\left(t_{min\,fuel}-t_{min\,time}\right)} \tag{55}$$

It is evident that a limitation arises for HLI values less than unity in Eq. (55) because of the trigonometric properties displayed by hyperbolic cosine functions: cosh x varies from $-\infty$ to +1 to $+\infty$ and cosh 0 = 1. Notwithstanding, such an occurrence signifies that the optimal flight technique corresponds to minimum time flight and can thus be considered equivalent to OFI = 0. In order to appreciate the extent of operational flexibility contemporary vehicles offer, typical values of OFI for various aircraft, economic objective function and utilisation assumptions are itemised below:

- DOC and P-ROI optimal hourly-based utilisation – OFI ≤ 0.15 for regional aircraft, and, OFI ≅ 0.75 for narrow and wide-bodies.
- DOC and P-ROI optimal fixed departures utilisation – OFI ≅ 0.20 for regional aircraft, and, OFI ≅ 0.90 for narrow and wide-bodies.

A design condition OFI value approaching zero denotes little or no scope for flexibility since it is congruous with minimum time flight techniques. Not only does this condition usually deny the possibility of achieving unconstrained optima, but also, implicitly dictates that all shorter-range operations will follow suit. Additionally, this circumstance is seen to be detrimental since the criterion of a higher engine rating flight technique may reduce the service life of the power plant. It does however allow for longer-range mission capability without trading payload for fuel, but at an ever-increasing penalty of off-optimality as distance becomes longer.

A maximum value of OFI = 1.00 at the design condition, akin to a minimum fuel technique, affords limited range of operational flexibility on the other end of the spectrum. Even though scope is given for the generation of unconstrained optima flight techniques for shorter sector distances, useful load limitations may not permit the opportunity of longer-range missions for a given payload. This would necessitate an exchange of payload for increased range thereby limiting the potential for revenue.

A salient objective would be a design OFI = 0.50 for any prospective aircraft evaluation exercise. This will ensure avoidance of premature useful load limitations for longer sector distances, and importantly increase the likelihood of unconstrained optima for shorter distances. Finally, the penalties associated with off-optimal flight techniques commonly experienced in actual operation can be minimised.

Economical Long Range Cruise

Traditionally, LRC has been understood to be 99% (sometimes even 98%) of MRC SAR towards the faster end of the curve[16,17,18,19]. This practise is employed to trade increased speed capability for what is considered to be a relatively small penalty in fuel consumption rate. Indeed, after the inception of this rule-of-thumb procedure for en route performance analysis, it has now become a mainstay technique in industry circles. It would be of interest to see how this popular assumption measures up against speed technique formulation using economic criteria alone.

Initially, an objective function for what constitutes economical cruise must be formulated. One candidate is to use a fixed departures utilisation assumption. Not only is this a consistent basis of emulating actual operator scheduling, but also as outlined before, this premise theoretically generates optimal flight techniques slower than an hourly-based utilisation. Even though CI represents a necessary magnitude of dW_{fuel}/dt that ensures cost optimality for any sector mission criteria, an approximate expression explicitly related to cruise speed and SAR can also be derived. Assuming a cruise fraction that is sufficiently large, thus neglecting the influence of climb and descent, it can be demonstrated[16] that

$$CI = \left|\frac{dW_{fuel}}{dt}\right| \approx \left| a_{sls}\, \theta^{1/2} \left(\frac{M}{SAR}\right)^2 \frac{dSAR}{dM} \right| \qquad (56)$$

Fig. 7 shows the degradation of SAR compared to the MRC datum for regional, narrow-body and wide-body twins using computed CIs of 10, 25 and 40 (such speed techniques are henceforth dubbed as Economical Long Range Cruise or ELRC) respectively. These values were based on a projected fuel price and known operator time dependent maintenance cost data. Note that a standard representation of CI assumes a value normalised by 100 lb/hr[8,9]. Upon comparison to a 1% reference line

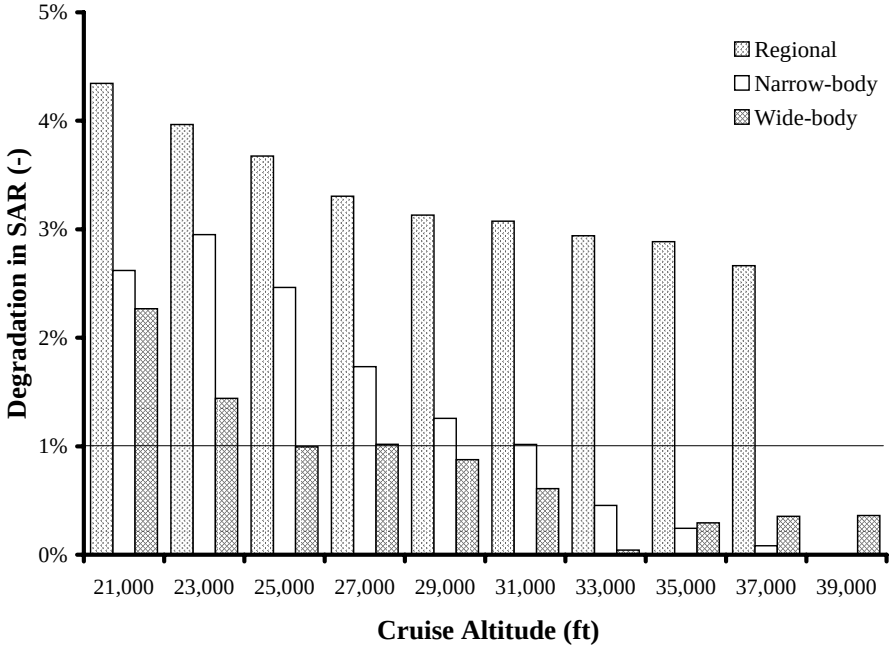

Fig. 7 – Degradation in SAR assuming traditional LRC (1% reference line) and ELRC compared to datum of MRC (fixed all-up weight, ISA, still air).

denoting the contemporary LRC assumption, it is observable that a large disparity between LRC and ELRC takes place. It is immediately evident that the SAR curve is quite flat for lower flight levels promoting even larger deviations from the conventional 1% degradation. However, for narrow and wide-bodies at typical cruise altitudes in excess of 29,000 ft where optimal cruise begins and subsequently does reside in the drag rise region, ELRC dictates speed schedules around 99.5% maximum SAR. Inspection of Eq. (56) lends support to this phenomenon. If one appreciates that dSAR/dM measurably increases in magnitude when flying within the drag rise at fixed CI and altitude, the resulting speed schedule candidate must be reconciled towards MRC. Regional aircraft appear to reach a constant value of 97% maximum SAR at higher altitudes, and this is attributable to the fact drag rise effects are generally not prevalent. Upon perusal of Fig. 7, for both twin narrow-body and wide-body equipment types, adopting the slower ELRC schedule as opposed to LRC amounts to almost a 1% integrated mission flight fuel reduction because the technique is closer to an optimal SAR condition. Correspondingly, the difference between LRC and ELRC equates to a speed reduction of approximately 5 KTAS at typical flight plan altitudes. Today, there exists a capacity for operators to soak the slight increase in flight time due to a slower speed – especially now that scheduled block times have been widened in order to improve on-time dependability and fuel prices are on the rise. For occasions where block times must be reduced due to sake of dependability, the ELRC method is congruous with a Flight Planning System (FPS) increased block speed iteration scheme since the starting point is slightly slower than traditional LRC in any case. In spite of the speed margin to MRC being rationalised upon application of an ELRC schedule for narrow and wide-bodies, the buffer is still greater than 5 KCAS. This is a margin commonly assumed for contemporary Flight Management Computer (FMC) en route operational software, and from an operational perspective the margin is not deemed prohibitive in terms of speed stability (excursions due to wind shift, turbulence, etc.) in maintaining the target level.

Merit Functions to Measure Relative Profit and Return On Investment

An interesting feature of the derivation for optimal P-ROI block times assuming hourly-based reference time frame utilisation is that these solutions are partial optima due to a co-dependence on block time and quantity of available seat-miles completed by the vehicle. Fig. 8 shows typical variation of P-ROI against block time for a variety of sector distances. Important facets of this representation include a distinct P-ROI global optimum, and, the existence of a break-even sector distance corresponding to an associative block time.

Even though the hourly-based reference time frame utilisation can be considered idealistic compared to the more pragmatic assumption of a fixed number of sectors, it can provide valuable insight. One important conclusion is that the comparison of different equipment types for only one fixed sector is not a sound enough basis to rationalise the superiority of an aircraft over another. A practical application would be use of this approach as a work tool that aids in maximising utilisation of a given vehicle for existing markets. Another is the possibility of showing the relative merits associated with the introduction of new projected markets involving either variations in sector distance, or mission criteria, or both. A further review potential includes the possibility of conducting detailed competitor studies where economic flexibility can be weighed between the vehicles taken into consideration. The section to follow suggests such guidelines via the introduction of an P-ROI model which can enable association between aircraft performance qualities to the model's geometric attributes and thus enable procedural methods of sub-optimising for more desirable P-ROI characteristics.

Method for Comparison of Contemporary Vehicles and Review of Aircraft Designs

A comprehensive method in identifying optimal flight techniques with respect to DOC and P-ROI enables the analyst to quantify the earning potential for given vehicles and mission criteria. Since it has been shown that sector distance can be

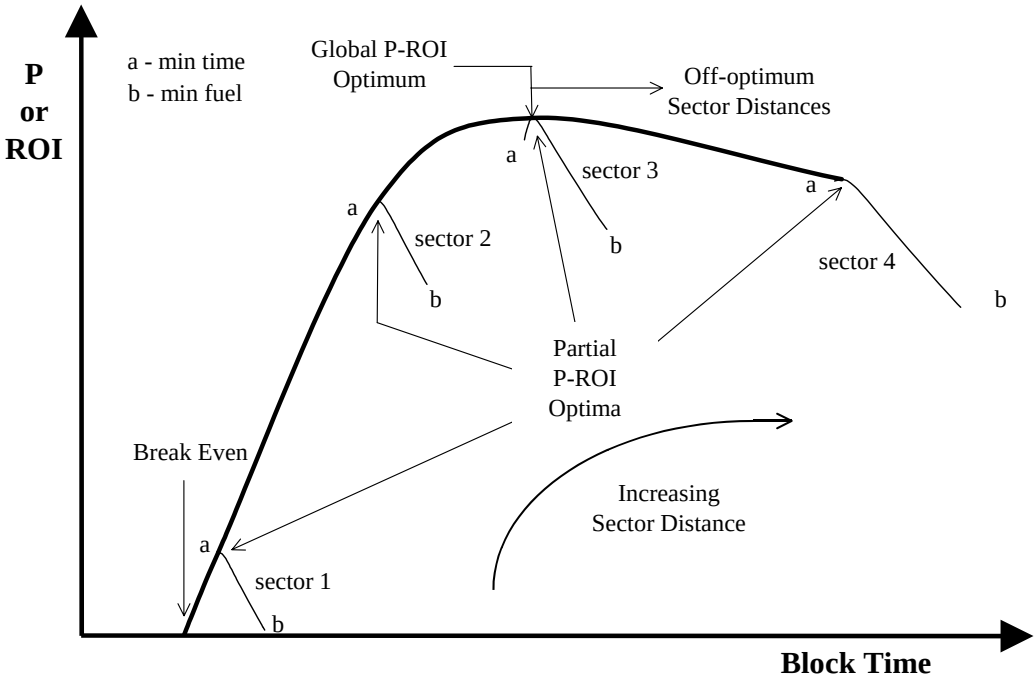

Fig. 8 – Typical P-ROI versus block time summary for a variety of sector distances assuming an hourly-based reference time frame utilisation.

regarded as an independent variable, it would be of interest to evaluate the various merits of an output P-ROI response with respect to distance. An adequate model for representing the P-ROI coverage in the closed sector distance interval $[s_o,s_n]$ is presented here as

$$P = \left(\Phi_\alpha\, s - \Phi_\beta\right) e^{-\left(\Phi_\chi + \Phi_\delta\, s\right)} + \Phi_\varepsilon \qquad (57)$$

where both P and P' are applicable for the basic structure of Eq. (57).

The equation coefficients represent quantities that enable a possibility of evaluating the properties of a vehicle's flexibility in earning potential through a geometric interpretation. If the model given above is actually taken into consideration as an open interval, say, $[s_{be}, \infty)$ or from break-even sector distance and upwards, one can identify uncanny similarities to a typical step response of stable linear control systems (see Fig. 9) - in this particular instance, the reference input being sector distance and P-ROI the output. It contains a transient response due to sector distance which also includes tendency to approach an asymptote as sector distance becomes large and exceeds distances constrained by useful load limitations (akin to steady state), and, a lower threshold where break-even occurs, or zero P-ROI at some sector distance value.

Typical performance criteria can be formulated which characterises the transient response. These are proposed here as: break-even sector distance and corresponding pre-optimum P-ROI rise rate, the P-ROI global optimum and corresponding sector distance, measure of the post-optimum P-ROI decay rate and the magnitude of the model asymptote value. This can be achieved mostly through inspection of the first and second derivatives of Eq. (57).

Break-even Sector Distance

The break-even sector distance is defined as the sector distance that creates a condition where the P-ROI is zero. Eq. (57) is in a form where an exact formula for solving P(s) = 0 is not available. The Newton-Raphson method would be a suitable way of approximating such solutions, and this iterative numerical method is projected to give an answer very close to the actual result in a single step with an apt initial estimate such as the lower threshold of the surveyed sector distances, i.e. $s_i = s_o$. Using Eq. (57) and corresponding first derivative in consort with Newton-Raphson produces

$$s_{be} = s_i - \frac{\Phi_\alpha\, s_i - \Phi_\beta + \Phi_\varepsilon e^{\left(\Phi_\chi + \Phi_\delta\, s_i\right)}}{\Phi_\alpha - \Phi_\delta\left(\Phi_\alpha\, s_i - \Phi_\beta\right)} \qquad (58)$$

The break-even sector distance, s_{be}, should ideally be minimised.

Pre-Optimum Profit and Return on Investment Rise Rate

P-ROI increases with greater sector distance for sector distances larger than break-even. The reciprocal of the rate P-ROI increase with respect to sector distance would give a measure of what increment in sector distance achieves a target increase in P-ROI before the global maximum threshold is crossed. An adequate representation of the pre-optimum P-ROI rise rate may be given by the instantaneous slope at the break-even sector distance via the definition found in Eq. (58)

$$P_S = \left[\left.\frac{dP}{ds}\right|_{s_{be}}\right]^{-1} = \frac{e^{\left(\Phi_\chi + \Phi_\delta\, s_{be}\right)}}{\Phi_\alpha - \Phi_\delta\left(\Phi_\alpha\, s_{be} - \Phi_\beta\right)} \qquad (59)$$

P_S (or P'_S) is a quantity expressed as distance covered per unit P-ROI and should be minimised.

The Global Profit and Return on Investment Optimum Sector Distance

Yet another fundamental observation that can be extracted from Eq. (57) is the identification of sector distances that yield global P-ROI maxima (P_{opt} or P'_{opt}). The distance where a P-ROI global optimum occurs is given by the first derivative of Eq. (57), hence

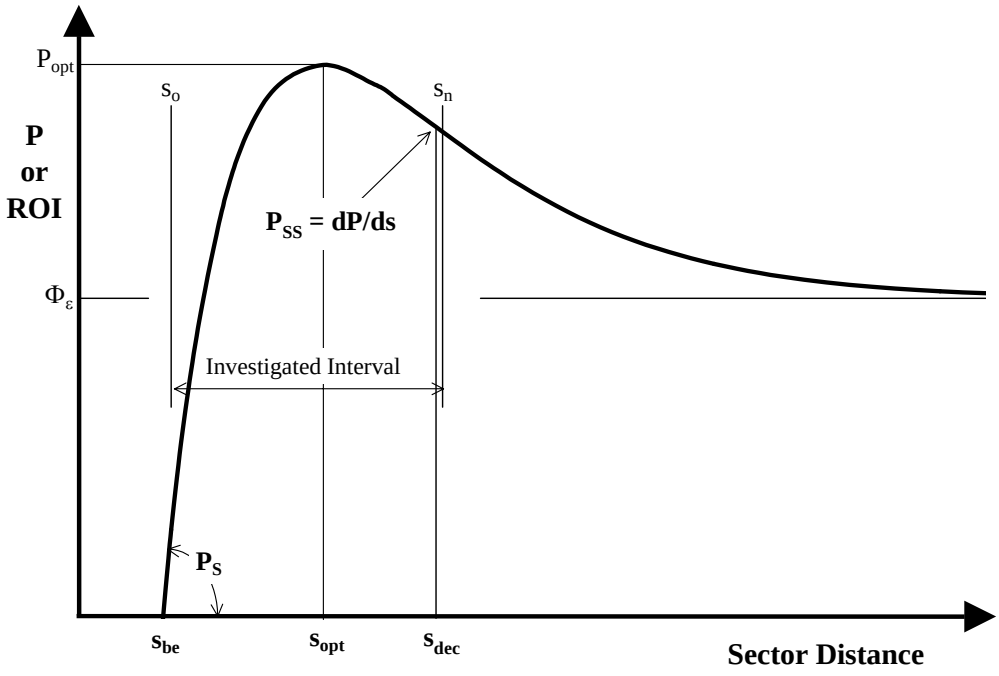

Fig. 9 – Typical sector distance response of P-ROI model assuming an hourly-based reference time frame utilisation.

$$s_{opt} = \frac{\Phi_\beta}{\Phi_\alpha} + \frac{1}{\Phi_\delta} \tag{60}$$

Having s_{opt} as low as possible whilst simultaneously maximising P_{opt} (or P'_{opt}) would be the primary goal of any prospective vehicle or design proposal.

Post-Optimum Profit and Return on Investment Decay Rate

It is evident to see that P-ROI decreases with increasing sector distance once the P-ROI global optimum sector distance has been surpassed. The rate reduction in P-ROI with respect to sector distance conducted at the inflection point between the post-optimum transient and steady state responses is proposed here as a useful merit parameter. By utilising the second derivative of Eq. (57) and solving for sector distance at this inflection point

$$s_{dec} = \frac{\Phi_\beta}{\Phi_\alpha} + \frac{2}{\Phi_\delta} \tag{61}$$

Hence, the post-optimum decay rate is given by slope of the sector distance response

$$P_{SS} = \left.\frac{dP}{ds}\right|_{s_{dec}} = -\Phi_\alpha \exp\left(-\Phi_\chi - \frac{\Phi_\beta \Phi_\delta}{\Phi_\alpha} - 2\right) \tag{62}$$

P_{SS} (or P'_{SS}) is a quantity that is always negative, therefore, it should be maximised in order to reduce the potential P-ROI loss rate per unit distance flown.

Worked Example for Regional Equipment

An illustration of the presented methods will be given for two turbofans and a high-speed turboprop of equal maximum accommodation. The analysis to follow is based on aircraft covering sector distances between 200 and 800 nm within the European operational environment, employing a JAR OPS-1 reserves fuel policy (30 min. hold at 1500 ft pressure altitude, 100 nm diversion and includes 5% trip fuel) and a complement of 60% load factor (maximum accommodation has intentionally not been divulged) at 99 kg each per PAX.

En route Performance

This survey consists of basic block time-fuel summaries derived from batch calculations subsequently stripped of those flight techniques not describing the lower bound of height-energy-block fuel minima for fixed block times. The parameters derived via non-linear regression techniques are presented in Tab. 1.

Cost and Yield Modelling

Primary assumptions were as follows:

Ownership Period:	10 years
Aircraft and Spares Inventory Interest:	10%
Aircraft and Spares Inventory Residual Value:	40%
Spares Ownership:	15%
Hull Insurance:	1%
Total Ownership per year:	
Turbofan 1	USD 2.87 m
Turbofan 2	USD 2.63 m
Turboprop	USD 2.23 m
Fuel Cost:	USD 0.60/USG
Flight Crew (Pilots and F/A):	$250 per BH
Annual Utilisation:	Fixed at 2500 Op. hrs
Turn Around Time:	30 minutes

Sundry expenses that include navigation, landing and handling charges that are fixed for each sector mission are itemised in Tab. 2

Tab. 1 – Block time-fuel summaries derived for three regional equipment types completing 200 nm to 800 nm sector distances (JAR OPS-1 rules).

Vehicle/ Sector	$W_{f,mintime}$ (kg)	k_1 (-)	k_2 (per min)	$t_{mintime}$ (min)	$W_{f,minfuel}$ (kg)	k_3 (-)	k_4 (per min)	$t_{minfuel}$ (min)	k_5 (kg)
Turbofan 1									
200 nm	863	0.912	0.723	40.4	736	1.483	0.0203	47.5	812
350 nm	1360	0.881	1.164	59.4	1057	2.050	0.0128	69.1	1215
500 nm	1866	0.849	0.817	78.2	1376	1.659	0.0160	91.5	1657
800 nm	2727	0.841	0.377	115.9	2033	1.876	0.00680	137.5	2467
Turbofan 2									
200 nm	772	0.928	1.468	43.0	679	1.480	0.0192	49.2	734
350 nm	1244	0.821	0.932	63.4	966	1.472	0.0161	70.8	1188
500 nm	1727	0.788	1.130	83.8	1268	1.835	0.00810	94.7	1633
800 nm	2203	0.874	0.514	125.0	1887	0.825	-0.00740	141.9	2165
Turboprop									
200 nm	705	0.974	1.726	46.8	600	1.909	0.0183	55.5	618
350 nm	1116	0.851	0.397	70.9	874	1.361	0.0165	85.8	1041
500 nm	1531	0.835	0.328	95.1	1155	1.371	0.0136	116.7	1408
800 nm	2362	0.827	0.248	143.5	1724	1.405	0.00981	178.0	2132

Tab. 2 – Synopsis of various sundry expenses incurred for three regional equipment completing 200 nm to 800 nm sector distances.

Sector Distance (nm)	Sundry Cost (USD) Turbofan 1	Turbofan 2	Turboprop
200	672	640	671
350	781	743	779
500	890	846	888
800	1108	1052	1104

Maintenance Model

A maintenance cost model conforming to the time dependent and cyclic constructs given by Eq. (10) and Eq. (11) in USD per FH for the Turboprop is approximated as

$$c_{main} = 90.3 + \frac{168.1}{(t - t_{man})^{0.827}}$$

where an allowance of t_{man} = 10 min. is common to all aircraft in this survey. In accordance with vehicular configuration and size, the Turboprop maintenance cost model was factored using k_{main} = 0.02 and k_{main} = 0.055 to formulate the Turbofan 2 and Turbofan 1 constituents costs respectively.

Yield and Revenue Model

Using the basic form given in Eq. (26), the yield and revenue model for this study is

$$Y_{SEC} = 0.5180\,\lambda\,PAX\,s\left(1 + 0.5283\tanh\left[0.001489\left(86.88 - s\right)\right]\right)$$

where, λ, the passenger load factor in this analysis being 60%, PAX is the maximum vehicular passenger capacity, and s, the sector distance varied between 200 and 800 nm.

Indirect Operating Cost Models

To complete the basis for ensuing P-ROI calculations, the following ancillary cost models were used to simulate the total operating cost, i.e. DOC + IOC

Agent's commission & excess baggage:	11% of yield
Sales & reservations office:	USD 0.004169/RPM
Other indirect:	14% of DOC

Synopsis of the Flight Technique Optima

Tab. 3, Tab. 4 and Tab. 5 give an overview of the cost and profit optimal flight techniques associated with the vehicles investigated in this survey.

Nota bene: The following nomenclature applies to the tabulations below

Header Information

CLB	climb	CRZ	cruise	DES descent
FL	flight level (100s ft)			

Specifics

H	high	M	medium
CLB	only one mode	DES	only one mode
MCR	max. cruise	INTER	intermediate cruise

A perspective on the operational flexibility of Turbofan 1, Turbofan 2 and the Turboprop is given in Fig. 10, Fig. 11 and Fig. 12 respectively. Except for shorter sector distances, i.e. less than 350-500 nm, the OFI of each vehicle resides between an interval of 0.05 to 0.10 for minimum DOC and maximum P-ROI assuming an hourly-based utilisation; the fixed based departures premise elevates OFI values to around 0.20. With respect to an ideal of OFI = 0.50, both these sets of values are considered to possess unfavourable tendencies towards the faster block speed procedure - limiting opportunities of minimising the penalty incurred when operating at slower off-optimal flight techniques.

As an exemplar of the flight technique results, Fig. 13 supplies a graphical interpretation using computed optimal block times for a given objective on each Turbofan 1, Turbofan 2 and Turboprop characteristic block time-fuel curves assuming

Tab. 3 – Flight technique breakdown for P-ROI global optima assuming an hourly-based reference time frame utilisation.

Vehicle	Sector	CLB Mode	CRZ Mode	DES Mode	Init. CRZ FL	Technique
Turbofan 1		H	MCR	H	250	Min Time[a]
Turbofan 2	**200 nm**	CLB	MCR	DES	230	Min Time[a]
Turboprop		H	MCR	H	230	Min Time[a]
Turbofan 1		H	MCR	H	330	Intermediate
Turbofan 2	**350 nm**	CLB	MCR	DES	330	Intermediate
Turboprop		H	MCR	H	240	Min Time[a]
Turbofan 1		H	MCR	H	350	Intermediate
Turbofan 2	**500 nm**	CLB	MCR	DES	350	Intermediate
Turboprop		H	MCR	H	240	Min Time[a]
Turbofan 1		H	MCR	H	350	Intermediate
Turbofan 2	**800 nm**	CLB	MCR	DES	360	Intermediate
Turboprop		H	MCR	H	260	Intermediate

[a] **Constrained partial optima**

Tab. 4 – Flight technique breakdown for DOC optima assuming an hourly-based reference time frame utilisation.

Vehicle	Sector	CLB Mode	CRZ Mode	DES Mode	Init. CRZ FL	Technique
Turbofan 1		H	MCR	H	250	Min Time[a]
Turbofan 2	**200 nm**	CLB	MCR	DES	250	Intermediate
Turboprop		H	MCR	H	230	Min Time[a]
Turbofan 1		H	MCR	H	330	Intermediate
Turbofan 2	**350 nm**	CLB	MCR	DES	330	Intermediate
Turboprop		H	MCR	H	240	Min Time[a]
Turbofan 1		H	MCR	H	350	Intermediate
Turbofan 2	**500 nm**	CLB	MCR	DES	350	Intermediate
Turboprop		H	MCR	H	270	Intermediate
Turbofan 1		H	MCR	H	370	Intermediate
Turbofan 2	**800 nm**	CLB	MCR	DES	370	Intermediate
Turboprop		H	MCR	H	290	Intermediate

[a] Constrained partial optima

Tab. 5 – Flight technique breakdown for DOC and ROI optima assuming a fixed departures based reference time frame utilisation.

Vehicle	Sector	CLB Mode	CRZ Mode	DES Mode	Init. CRZ FL	Technique
Turbofan 1		L	INTER	H	280	Intermediate
Turbofan 2	**200 nm**	CLB	INTER	DES	250	Intermediate
Turboprop		M	MCR	H	250	Intermediate
Turbofan 1		H	MCR	H	350	Intermediate
Turbofan 2	**350 nm**	CLB	MCR	DES	360	Intermediate
Turboprop		M	INTER	H	310	Intermediate
Turbofan 1		H	MCR	H	370	Intermediate
Turbofan 2	**500 nm**	CLB	MCR	DES	360	Intermediate
Turboprop		M	INTER	H	310	Intermediate
Turbofan 1		L	INTER	H	370	Intermediate
Turbofan 2	**800 nm**	CLB	INTER	DES	370	Intermediate
Turboprop		M	INTER	H	310	Intermediate

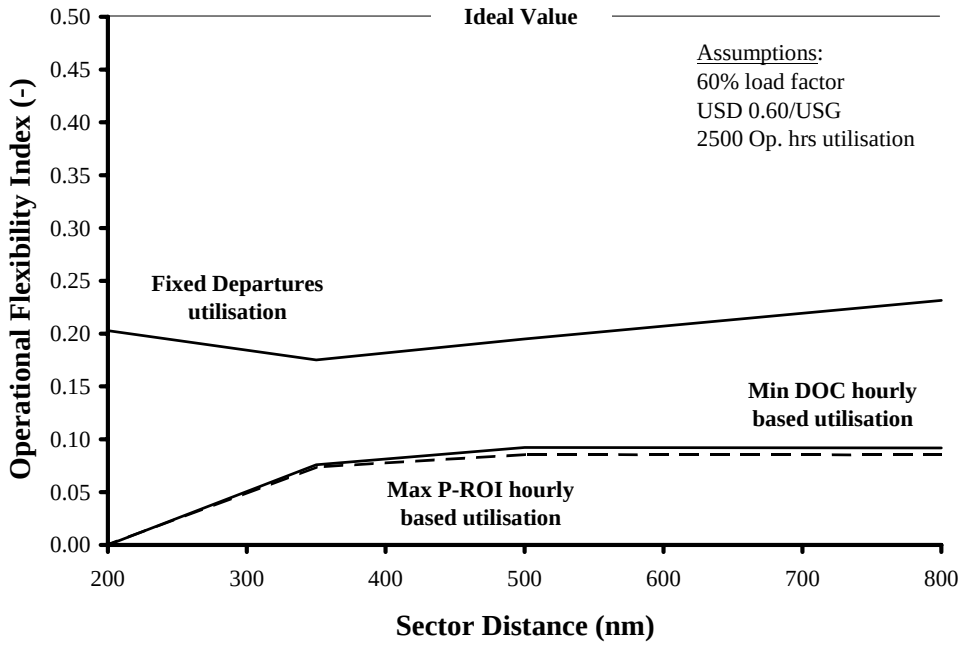

Fig. 10 – OFI values corresponding to optimal flight techniques assuming an hourly-based as well as fixed departures based utilisation for Turbofan 1 vehicle.

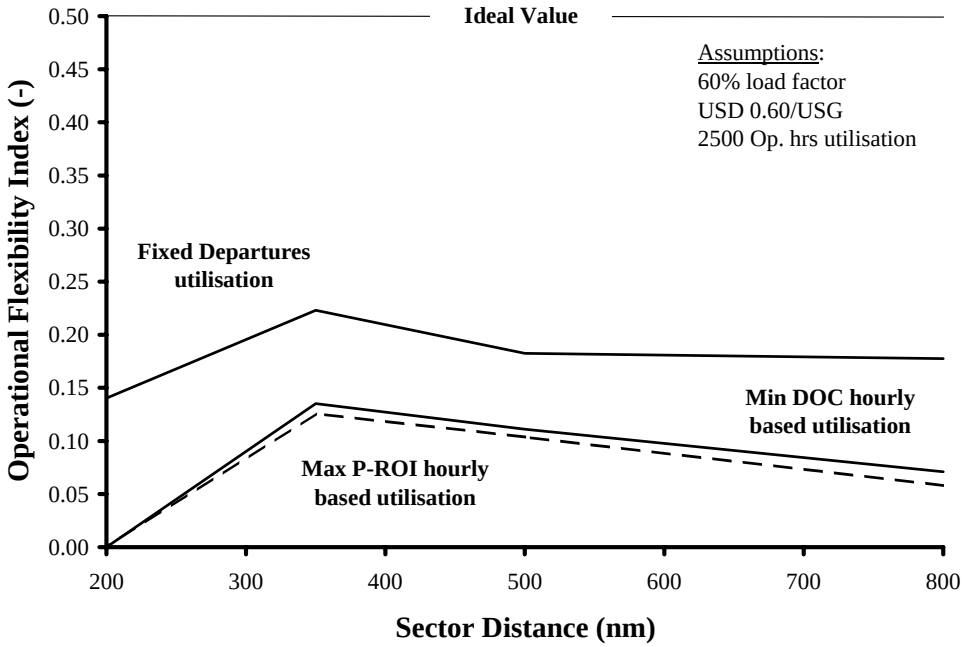

Fig. 11 – OFI values corresponding to optimal flight techniques assuming an hourly-based as well as fixed departures based utilisation for Turbofan 2 vehicle.

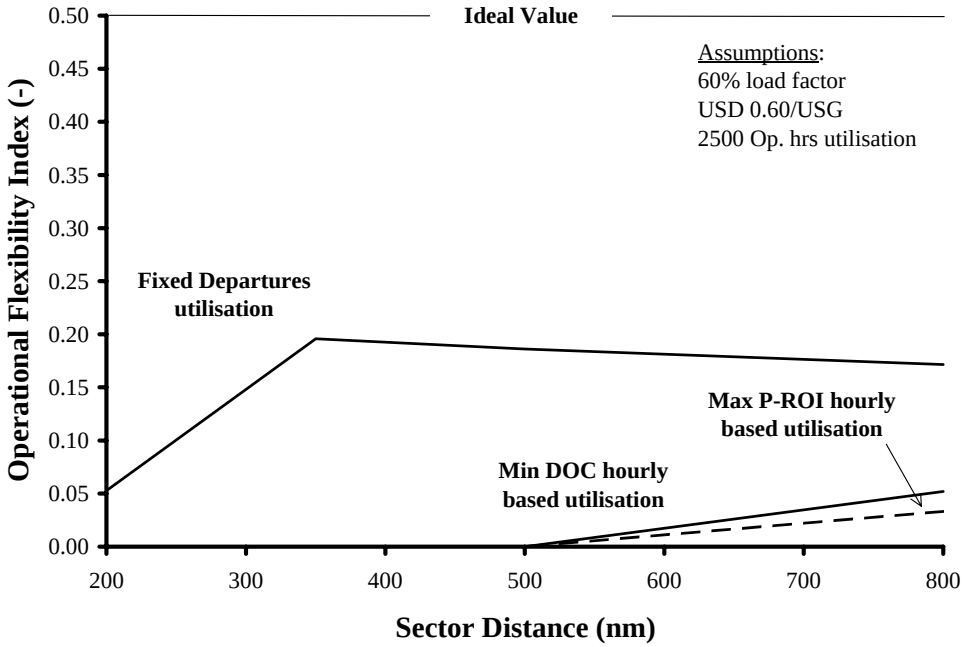

Fig. 12 – OFI values corresponding to optimal flight techniques assuming an hourly-based as well as fixed departures based utilisation for Turboprop vehicle.

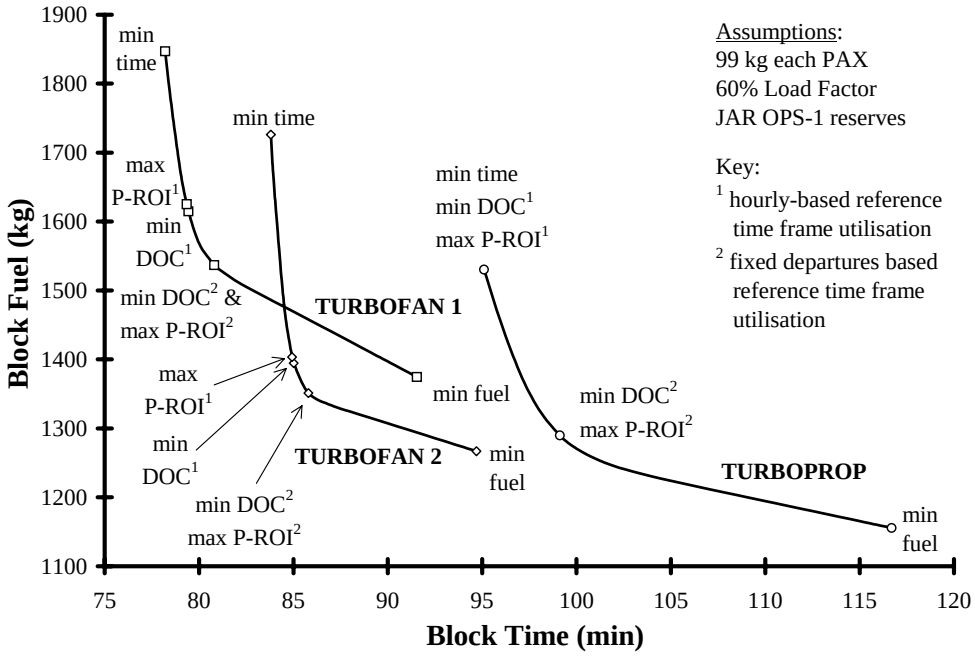

Fig. 13 – Block time-fuel summary for three regional equipment types completing 500 nm sector distances.

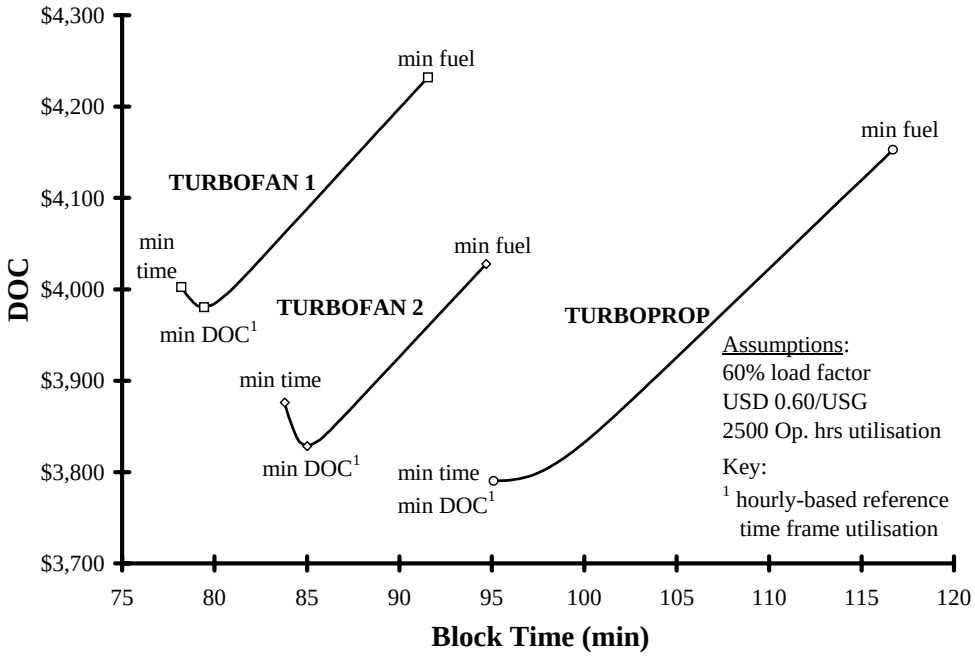

Fig. 14 – DOC variation with flight technique for three regional equipment types completing 500 nm sector distances.

a 500 nm sector mission. Within Fig. 13, the minimum fuel point is characterised by a constrained maximum SAR flight technique, i.e. the slowest forward speed climb mode, LRC (instead of MRC) en route speed, optimum altitude profile and the slowest forward speed for descent mode. Correspondingly, the minimum time node is congruous with the fastest block speed achievable for given sector distance, i.e. where no fuel limitation is imposed, the flight technique consists of the fastest forward speed climb mode, MCR en route speed, an altitude profile generating the fastest ground speed and the fastest forward speed for descent mode. The appeal of turbofan aircraft is quite apparent when comparing block times for minimum time and minimum fuel between Turbofan 1, Turbofan 2 and the Turboprop. As an indication of the speed difference, it is discernable in Fig. 13 that a minimum time flight technique for the Turboprop is equivalent in time to Turbofan 2's minimum fuel technique.

Competitive Analysis Between Regional Equipment

Fig. 14 (above) shows the relative DOC variation with block time and minimum DOC for Turbofan 1, Turbofan 2 and Turboprop vehicles assuming a sector distance of 500 nm and an hourly- based reference time frame utilisation. It is evident that most of the cost optimal flight techniques are indicative of the unconstrained optima condition with the exception of the Turboprop, wherein a constrained optimum applies, i.e. HLI ≤ 1 or minimum time flight technique. The Turboprop exhibits superiority in terms of minimum DOC achievable compared to

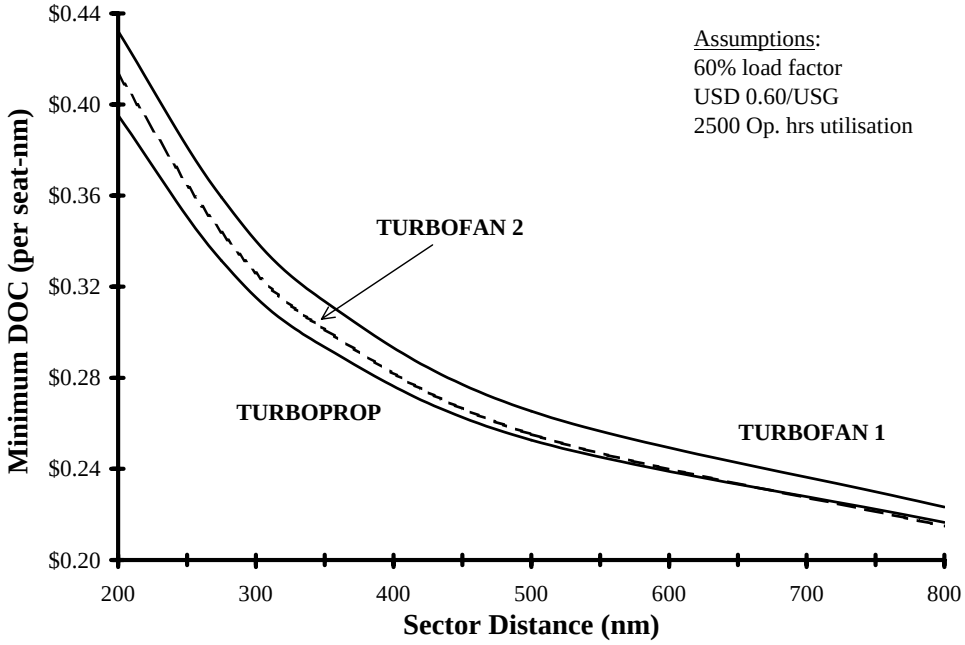

Fig. 15 – Minimum DOC against sector distance for three regional equipment types.

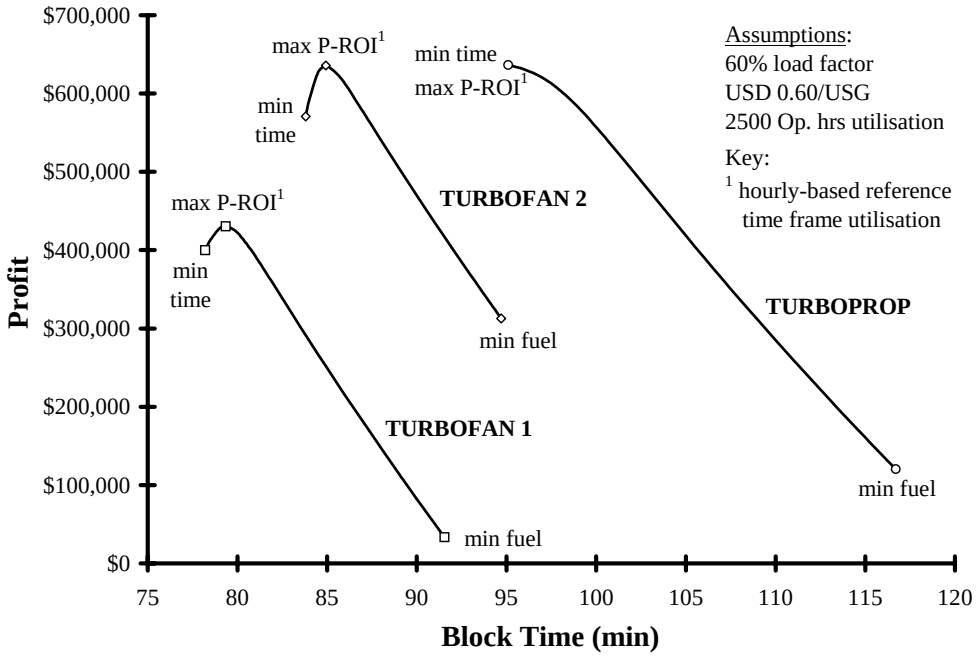

Fig. 16 – Profit per annum variation with flight technique for three regional equipment types completing 500 nm sector distances.

Turbofan 2, which can be regarded as the next closest rival, and over Turbofan 1.

In order to gauge how well the Turboprop performs against Turbofan 1 and Turbofan 2 in terms of DOC for a variety of sector missions, Fig. 15 (above) presents computed minimum DOCs per seat-nm for all three regional equipment. The Turboprop maintains a cost effective posture up to a sector distance of approximately 650 nm, at which point Turbofan 2 exhibits a marginal advantage.

Whilst assuming an hourly-based reference time frame utilisation, Fig. 16 (above) shows the variation of annual profit with block time and identifies the partial profit optima for a sector distance of 500 nm. The profit optimal flight techniques are indicative of somewhat slightly lower block times (faster block speeds) compared to their cost optimal counterparts. Turbofan 1 and Turbofan 2 are characterised by partially unconstrained optima, except for the Turboprop, where a partially constrained optimal flight technique is dictated.

Fig. 17 gives a graphical assessment of the annual potential for profit between Turbofan 1, Turbofan 2 and Turboprop vehicles for sector distances up to 800 nm. Visual inspection of this diagram qualitatively shows Turbofan 2's slender margin of superiority over the Turboprop with respect to the global maximum profit value.

Alternatively, by employing the analytical model given in Eq. (57), the parameters derived for the vehicles investigated can be found in Tab. 6.

Upon review of the primary merit quantities shown in Tab.

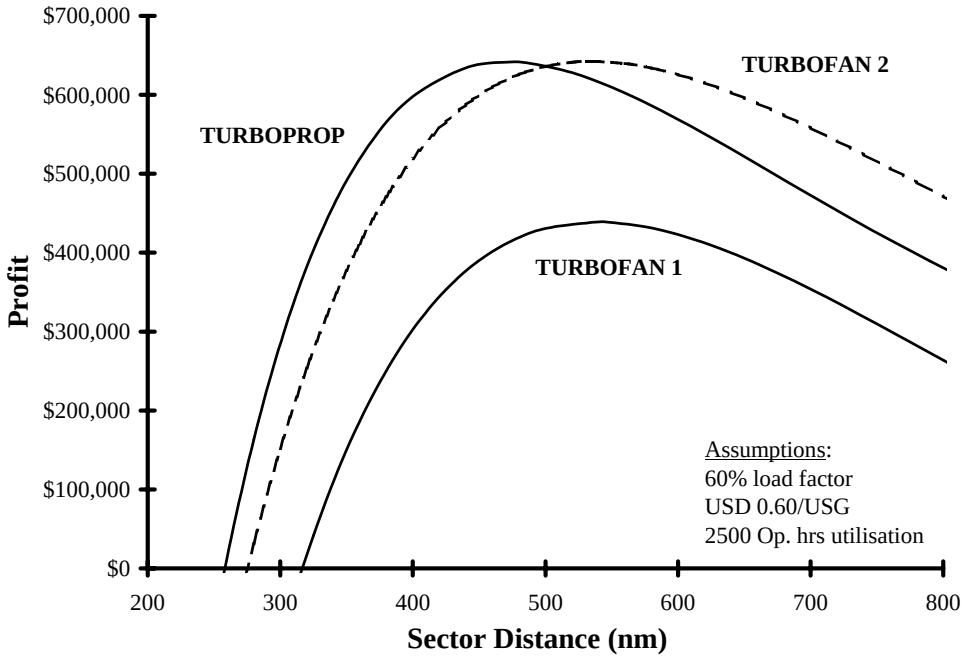

Fig. 17 – Maximum profit per annum against sector distance for three regional equipment types.

Tab. 6 – Tabulation of P-ROI regression coefficients and merit parameters for three regional equipment types.

Objective	Parameter		TURBOFAN 1	TURBOFAN 2	TURBOPROP
P	Φ_α	m USD/nm	0.01012	0.01013	0.01061
P	Φ_β	m USD	2.854	2.825	2.889
P	Φ_χ	(-)	-0.7061	-0.6520	-0.9862
P	Φ_δ	per nm	0.003896	0.003899	0.005019
P	Φ_ε	m USD	-0.2068	0.2349	0.1104
P-ROI	s_{be}	nm	317	275	258
P	P_s	nm/m USD	194	148	120
P-ROI	s_{opt}	nm	539	535	472
P	P_{opt}	m USD	0.439	0.642	0.641
P	P_{ss}	USD/nm	-925	-888	-981
ROI	Φ'_α	per nm	0.003522	0.003858	0.004788
ROI	Φ'_β	(-)	0.9932	1.076	1.304
ROI	Φ'_ε	(-)	-0.07197	0.008942	0.04982
ROI	P'_s	nm	556	390	266
ROI	P'_{opt}	(-)	0.153	0.245	0.290
ROI	P'_{ss}	per 100 nm	-0.0322	-0.0338	-0.0443

6, it can be seen that Turbofan 2 has the highest and best value of P_{SS} or post-optimum P-ROI degradation characteristics even though the Turboprop generates higher profit for sector distances less than around 500 nm. Advantages of the Turboprop vehicle over its counterparts are a P_s or profit rise rate of 120 nm/million USD and s_{be}, or break-even sector distance value of 258 nm. Also, the Turboprop appears to have the most desirable P-ROI global optimum sector distance as exemplified by comparison of s_{opt} values for Turbofan 1, Turbofan 2 and Turboprop of 539 nm, 535 nm and 472 nm respectively. Notwithstanding the positive attributes of the Turboprop vehicle's optimal P-ROI stage length, Turbofan 2's value of P_{opt} being the largest and Φ_ε which is at least twice as large the closest competitor, combined with previously mentioned qualities, signifies this vehicle's superior nature in terms of potential for generating profit and concludes the review as being the better acquisition.

As an interesting after-thought, if one ignores the absolute value of profit but instead examines ROI in isolation (Tab. 6 and Fig. 18), it is evident the Turboprop demonstrates superior attributes. This circumstance can be explained by the relatively inexpensive acquisition price of turboprop vehicles in the contemporary market, thus generating a proportionately higher return on investment. Even though this aspect might be construed as a lucrative outcome, the analyst or designer must recognise the significant trade-off in block speed for sector distances greater than 350 nm. This fundamental characteristic therefore ratifies the widely held notion that turboprops are well

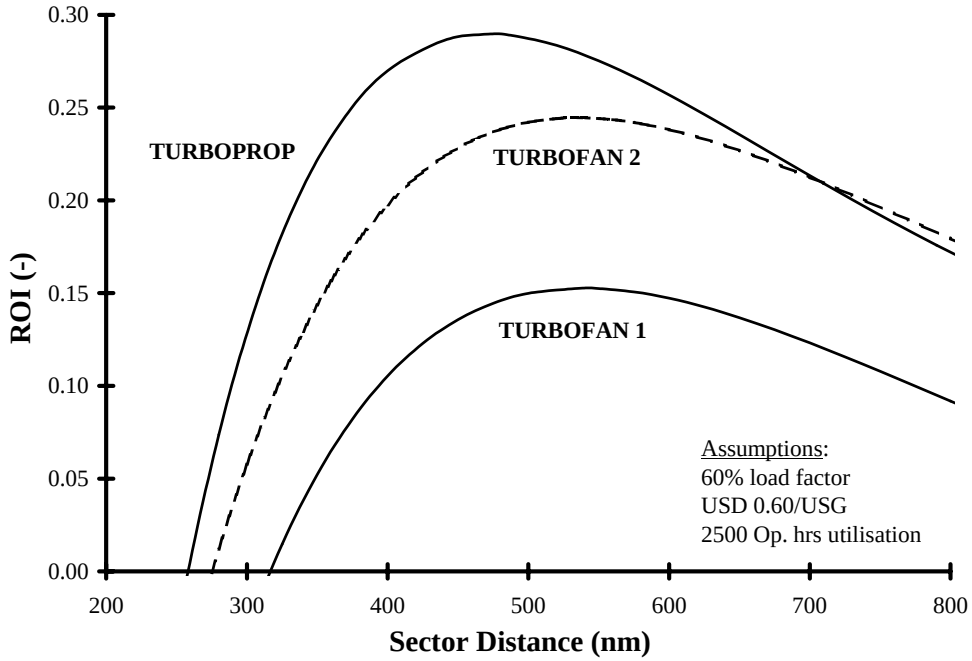

Fig. 18 – ROI against sector distance for three regional equipment types.

suited for shorter sector distance missions only.

Conclusion

This paper outlines a systematic methodology to identify a given sector distance mission flight techniques, or an operational protocol consisting of a specific climb speed schedule, initial cruise altitude, cruise speed schedule, step-cruise profile and descent speed schedule, which produce minimum DOC and maximum P-ROI. All cost and yield relationships can be manipulated to suit most contemporary calculation procedures, giving scope of incorporating a specialised routine into conceptual design mission analysis software.

Some pertinent conclusions drawn from this study concern the relationship of cost and profit optimal flight techniques to one another. An hourly-based reference time frame utilisation results in distinct flight technique optima for minimum DOC and maximum P-ROI. The P-ROI optima are characterised by faster block speeds than cost optimal ones because of a co-dependence on flight time and the quantity of available seat-miles completed by the vehicle. Also, the hourly-based utilisation resulted in partial P-ROI optima for different sector distances, which implied the existence of a global optimum at some specific sector distance and block time. This fact illustrates that comparison of distinct equipment types for only one fixed sector is not a sound enough basis to rationalise the superiority of one aircraft over another. A fixed number of sectors utilisation assumption reduces the sensitivity of time related costs to flight technique and thus reduces the significance of this component compared to the fuel expended. This situation produces block speed optima appreciably slower than those assuming an hourly-based utilisation. Furthermore, the fixed departures assumption creates a condition where both cost optimal and profit optimal flight techniques coincide with one another.

A new speed schedule definition called Economical Long Range Cruise (ELRC) was created to replace the traditional 99% maximum specific air range (SAR) Long Range Cruise (LRC) speed. It was motivated by the fact that not only is the 99% maximum SAR premise inconsistent with cost and profit optimality, but an alternative of simply assuming some other fixed degradation in SAR does not suffice either. It was found that Cost Index (CI) is the most suitable method in defining ELRC for the entire gamut of transport aircraft categories available today. To complement this, a merit function called Operational Flexibility Index (OFI) was derived to enable transparency of what en route operational qualities a given aircraft exhibits.

Merit parameters that give rise to the ability of sub-optimising for more desirable P-ROI characteristics were also formulated. Break-even sector distance (s_{be}) and corresponding pre-optimum P-ROI rise rate (P_S), the P-ROI global optimum (P_{opt}) and corresponding sector distance (s_{opt}), the post-optimum P-ROI decay rate (P_{SS}) together with the magnitude of the asymptote value (Φ_ε) were suggested as a logical set of guidelines when conducting new conceptual aircraft designs or detailed competitor reviews.

References

[1]Bryson, A.E., Jr., and Ho, Y-C., "Applied Optimal Control", Blaisdell, Waltham, Mass., Chapter 2, 1969.

[2]"Definitions and Inputs for Range and Direct Operating Cost Calculation", Appendix 1, G(T) 5656, Association of European Airlines, 1990.

[3]Isikveren, A.T., "A Method to Identify the Optimal Flight Techniques of Transport Aircraft", Report 98-7, Royal Institute of Technology (KTH), Department of Aeronautics, Sweden, 1998.

[4]Torenbeek, E., "Some Fundamental Aspects of Transport Aircraft Conceptual Design Optimisation", AGARD Symposium, September 1979, pp. (5)1-22.

[5]Gogate, S.D., Pant, R.K., and Arora, P., "Incorporation of some Cost and Economic Parameters in the Conceptual Design Optimisation of an Air-Taxi Aircraft", AAIA-94-4301-CP, pp. 443-453.

[6]Holkeri, J., "Analysis of the Operational Costs of some New Regional Airlines", Master of Science Thesis, Royal Institute of Technology (KTH), Department of Aeronautics, Sweden, 1988.

[7]Van Bodegraven, G., "Commercial Aircraft DOC Methods", AIAA 90-3224, September 1990.

[8]"Cost Index", Rev Apr 90, Boeing Flight Operations Engineering, April 1990.

[9]"Cost Index", Performance Engineer Operations Course Notes, Vol. 1, Boeing Flight Operations Engineering, May 1997.

[10]"Saab 340 Estimated Maintenance Cost Summary, Scheduled and Unscheduled, USD per flight hour", Saab Aircraft Division, 1990.

[11]"Saab 2000 Estimated Maintenance Cost Summary, Scheduled and Unscheduled, USD per flight hour", Saab Aircraft Division, 1990.

[12]Brochure for Fokker 50 and Fokker 50-200, Fokker Aircraft B.V., May 1988.

[13]"Dash 8 series 100, The Leaders' Choice", Boeing Canada de Havilland Division, May 1988.

[14]"Dash 8 series 300, The Leaders' Choice", Boeing Canada de Havilland Division, January 1989.

[15]"Saab 340 versus Competitive 30-40 Seaters - A Reference Guide", Saab Aircraft International Ltd., Saab Aerospace AB, January 1993.

[16]"Jet Transport Performance Methods", D6-1420, Seventh Edition, Flight Operations Engineering, Boeing Commercial Airplanes, May 1989.

[17]Obert. E., "Some Aspects of Aircraft Design and Aircraft Operation", Linkoping Institute of Technology (LiTH), Aircraft Design Lecture Series, Sweden, 1996.

[18]PAN-AM Flight Operations Manual, Rev.228, August 1988.

[19]Torenbeek, E., "Optimum Cruise Performance of Subsonic Transport Aircraft", Report LR-787, Delft University of Technology, Faculty of Aerospace Engineering, March 1995.

Additional Sources

[1]Erzberger, H., and Lee, H., "Characteristics of Constrained Optimum Trajectories with Specified Range", NASA TM-78519, Ames Research Centre.

[2]Jacobson, A.L., and Tsubaki, C.M., "Economics in New Commercial Aircraft Design", AIAA 86-2667, 1986.

[3]Jacobson, A.L., and Murphy, D.G., "The Designer's Impact on Commercial Aircraft Economics", ICAS-88.1.7.1, 1988.

[4]Miller, L.E., "Optimal Cruise Performance", Journal of Aircraft, Engineering Notes, Vol. 30, No. 3, May-June 1993, pp. 403-405.

[5]Raymer, D.P., "Aircraft Design: A Conceptual Approach", AIAA Educational Series, 1992.

[6]Simos, D., and Jenkinson, L.R., "The Determination of Optimum Flight Profiles for Short-Haul Routes", Journal of Aircraft, Vol. 22, No. 8, August 1985, pp. 669-674.

[8]Torenbeek, E., "Synthesis of Subsonic Airplane Design", Delft University Press, 1988.